ARPA/TIO-71-11

WORKING PAPER

COPIES OF PAPERS PRESENTED AT WOOD'S HOLE CONFERENCE ON SEISMIC DISCRIMINATION

VOLUME 1

SPONSORED BY ADVANCED RESEARCH PROJECTS AGENCY

20 - 23 JULY 1970

This document contains unedited copies of papers presented at the conference. Any views expressed in the papers of this conference are those of the authors and are not to be construed as reflecting the official opinions or policy of the Department of Defense or any agency of the Federal Government.

WORKING PAPER

DISCLAIMER NOTICE

THIS DOCUMENT IS THE BEST QUALITY AVAILABLE.

COPY FURNISHED CONTAINED A SIGNIFICANT NUMBER OF PAGES WHICH DO NOT REPRODUCE LEGIBLY.

TABLE OF CONTENTS

Evernden, Jack F.
Opening presentation ARPA symposium on seismic discrimination

Aki, K.
Theoretical M_s-m_b relation for small magnitudes

Solomon, S., Ward, R., and Toksöz, N.
Earthquake and explosion magnitudes: the effect of lateral variation of seismic attenuation

Syed, Atiq Reported by William Stauder
Effect of regional correction on the value of m_b

Capon, J.
Analysis of long-period noise at LASA

Mack, H.
Twenty to eighty second period characteristics of nuclear explosions recorded at LASA

Savino, J.
Long-period earth noise and the detection of and discrimination between earthquakes and underground explosions

Smith, S.W.
Long period earth noise

Toksöz, M.
Crustal effects on long period chirp filters

Capon, J.
Analysis of Rayleigh wave multipath propagation at LASA

Ward, P.
A high gain, broad-band, long-period seismic experiment

Block, B.
Report on a new broad band vertical accelerometer

Herrin, E., Sorrells, G., and McDonald, J.
A digital acquisition system for geophysical data and some preliminary results

TABLE OF CONTENTS (Cont'd.)

Sykes, L.
Review of recent research at Columbia University on the discrimination of underground explosions from earthquakes

Aki, K. and Tsai, Yi-Ben
Comparison of SH waves from large and small explosions

Molnar, P.
Spectral Differences of Seismic Waves from Earthquakes and underground nuclear explosions

Tsai, Y. and Aki, K.
Amplitude spectra of surface waves from small earthquakes and underground explosions

Lieberman, R.
Some remarks on the use of relative excitation of surface waves to discriminate between earthquakes and underground explosions

Lacoss, R.
Teleseismic surface wave detection and utilization with a single large array

OPENING PRESENTATION

ARPA SYMPOSIUM ON SEISMIC DISCRIMINATION

Woods Hole, Massachusetts

By

Jack F. Evernden

Collaborators (P. Pomeroy, J. Savino, L. Sykes, T. McEvilly)

I will begin the presentation with a short review of the presently documented identification capability. This review will be based upon several figures published by myself. These figures are used because they easily come to hand. Sole use of such figures does not imply that the capability shown by these figures can not be discussed in large part by the data of other investigators. Subsequent to this review, I shall present data on several remaining identification problems and give a few opinions on what course further investigations should take. I will not attempt at this time to review all aspects of the topics to be discussed in the next few days.

We should preface the remarks that are to follow with the statement that any conclusions drawn from the data presented are ours alone, and are not to be construed as those of the U.S. Government. In fact differences of opinion over interpretation of some points to be discussed do exist among American seismologists. As will be seen, the data presented are only suggestive of some of the functional relationships between M_S and m_b measurements for a limited suite of earthquakes and explosions. These research results cannot be interpreted as necessarily indicative of universal relationships. In fact, it is known that occasional earthquakes of m_b 5 and less do have parameters disagreeing markedly with the trends of average relationships to be shown here, such occasional earthquakes having M_S:m_b values similar to those of the available suite of explosion signatures.

As regards review of present state-of-the-art, primary consideration must be given to determination of depth of focus and measurement of ratio of long period to short period energy. As regards depth of focus, it can be said categorically that a capability to determine depth of focus to an accuracy of 5 km would be tantamount to having a near total identification capability for earthquakes and explosions. Our capability today is not nearly that high and only becomes even approximately that after diligent effort in analysis or by availability of data of a unique type. Improvement of estimates of depth attainable by routine use of P data does not yield depth determination of adequate quality, particularly for events recorded by only a handful of stations, for achieving the screening of events required for application of long period criteria. Improvements in that routine capability for determining depth of focus are easily obtained if sufficient analytical data are available.

The master event concept has proven highly useful in improving depth determinations for events in the Kamchatka/Kurils area and should be applicable in other regions. Figure 1 indicates the set of master events that were used in demonstration of the usefulness of the master event concept. Figure 2 presents data on the quality of depth determination available by use of that concept. The figure indicates the difference in depth calculated by use of master events and depth determination by use of pP for events of magnitude 4.5 or greater. It seems that depth determinations by use of master events appear to be randomly distributed around the pP depth. The standard deviation of master control depths relative to the pP depth was

16 kilometers for events having a station at 30° or less. In many regions such a capability for depth determination is adequate to allow application of long period criteria.

An improvement upon the master event concept is the determination of depth by use of an estimate of event origin time based upon measurements of the S-P interval at a near station.

Figure 3 illustrates the degree of agreement achieved between S-P computed depths and pP depths. If deep focus events (i.e., those of depth greater than 100 kilometers) are ignored, depth determination by S-P are markedly better than those by use of master events. However, use of S-P as a control of depth requires a station near enough to detect short period both S and P, and near enough to allow estimates of origin time valid to one or two seconds. It must always be remembered that our discussions here are to be based upon development of techniques applicable to magnitude 4 or thereabouts. A station having a gain of approximately 250,000 should see S and P from a magnitude 4 event within approximately 15° of the station.

It would certainly be desirable to develop additional techniques for determination of depth, i.e., to more effectively analyze seismograms in terms of measurement of multiple depth phases. Hopefully, much more will be said on this matter later in our discussions.

Figure 4 presents data on the AR criterion as applied to both earthquakes and explosions. The earthquakes used are shallow focus earthquakes occurring in Asia during 1965, depth of focus of events having been established by master events where possible. There seems to be clear separation of the AR values of earthquakes and explosions. As normalized for magnitude there appears to be no dependence of the criterion value upon m_b value for either earthquakes or explosions.

Note that earthquakes having AR values within less than 1 magnitude of the largest values for explosions satisfied either one or both of the S and AL criteria.

Figure 5 presents AL data (i.e., AR-type data based on Love waves) for the same general set of earthquakes as Figure 4. Note that essentially a full order of magnitude discrimination is achieved between the explosions and earthquakes.

Figure 6 presents long period S data for the same events. In this case also there appears to be a full order of magnitude or better discrimination between earthquakes and explosions. Therefore, by use of these three long period criteria as applied to shallow focus earthquakes from Asia during 1965 for events of magnitude 4 3/4 or greater, essentially an order of magnitude discrimination was achieved between the parameters of these earthquakes and those of Asian and American explosions.

Therefore, I think it is safe to say that the general problem of discriminating between earthquakes and explosions at magnitude 4 3/4 and greater is clearly solvable at a very high level of confidence by use of adequate depth criteria and by use of long period criteria

discussed. The problems then remaining are: a) the occasional event that fails to satisfy the criteria indicated above, at least at our present level or capability of applying those criteria; b) applicability of these criteria at magnitudes below 4 3/4; and, c) assuming applicability of these or similar cirteria, establishment of the distance range at which the significant data required for identification can be obtained.

As regards the latter point, two general ideas should be pursued: (1) the determination of the parameters characterizing an optimum detecting site, both for long and short period waves; and, (2) establishment of the threshold of the amplitude of wave detectable at such sites including evaluation of the additional gains achievable by either ordered or random arrays of seismometers. Both of these points are to be discussed during the next few days. I will only briefly note that work already published indicates significant signal to noise gain is achievable both for long period body wave and surface waves by use of arrays of seismometers.

Figure 7 indicates the improvements of S/N ratio obtainable when an 8-element array in Arizona was steered for a long period P signal from Komandorski earthquake.

Figure 8 indicates that steering of a United States-wide 11-element long period array achieved clear detection of long period P wave of that event when the P wave was not detected on any single instrument. Similar investigations of the S wave have indicated high coherence across large areas. Therefore, significant signal noise gains ($\sqrt{n}$ by the array and appreciably by bandpass filtering) can be achieved in the detection of both long period S and P by use by such arrays.

Figure 9 illustrates the matched filter concept as applied to the data of a single LASA element. A distinct signal-to-noise improvement was obtained.

Figure 10 indicates the signal-to-noise gain achieved by use of both match filtering and steering of the LASA long period array. The signal, essentially undetected on individual instruments, was detected at appreciable S/N ratio.

Figure 11 is a similar figure, the data however being comprised of both LASA and LRSM match filtered signals. Again the clear signal at high signal to noise ratio was detected on the steered beam. Therefore, single station detection capability by visual analysis is not a complete measure of ultimate capability of detection of long period waves.

Applicability of depth determination criteria to events of magnitude 4 simply requires building stations adequate to detect signals of small events at teleseismic distances. The existence and demonstrated capability of the TFSO array indicate that the required capability can be achieved by small arrays at carefully selected sites. Large arrays at less carefully selected sites can achieve a comparable

capability. Therefore, determination of depth of focus for magnitude 4 events by use of short period data is simply a matter of building the necessary stations.

As regards the second point, mentioned above, i.e., the applicability of long period criteria for events of magnitude below 4 3/4, I shall now present a large body of data on this point.

Figure 12 presents world-wide data on M_S and m_b versus cumulative number of events (N_C). It is seen on that figure that M_S versus log N_C is a straight line from M_S 7 1/2 to M_S 5 1/4 and below. The open circles are the data presented by Gutenberg and Richter in 1939. The open and closed squares are data compiled by Texas Instruments for the years 1960 and 1963. The absolute levels of activity seem somewhat different in 1960- 1963 and in the period covered by Gutenberg. However, the three lines are parallel. The closed circles are m_b world-wide data as published by the Coast and Geodetic Survey on their preliminary Determination of Epicenter lists.

The points to be noted here is the convergence of the m_b:M_S lines in the magnitude range m_b 5 1/4 and their essential parallelism from magnitude 5 1/4 towards lower magnitudes.

Though Figure 12 does not extend below magnitude 5, the extensive compilation of regional seismicity data published recently indicates that the slope of the M_S versus log N_C and m_b versus log N_C curves for different regions of the world range over the same values. Therefore, the parallelism of the M_S versus N_C and m_b versus N_C curves of Figure 12 continues to lower magnitudes. The parallelism of these two curves immediately implies that an M_S versus m_b plot of these data would yield a 1 to 1 slope of the M_S:m_b curves at m_b < 5 1/4 with divergency of M_S and m_b curves at higher magnitudes. In fact, if the entire body of Figure 12 were converted to an M_S versus m_b figure, it would look essentially identical to the M_S:m_b plots usually published.

I feel that this is a convincing argument as regards the relationship between M_S and m_b at small magnitudes. However, others are not so convinced and so I will now present data providing direct measurements of M_S and m_b for numerous earthquakes and explosions.

The first body of data to be inspected were obtained for United States earthquakes and explosions by use of LRSM data. Figures 13 through 17 indicate the type of data used, i.e., individual determinations of m_b and M_S at various LRSM stations. On Figures 13 through 17 plotted M_S values are calculated according to a 1.66 log Δ law. It is seen on each of the figures that the observed Rayleigh wave data do not agree with that law. They agree much more closely with a log Δ law for $\Delta \leq 25°$.

Figure 13 is for HANDCAR, Figure 14 for an earthquake in southern Idaho, Figure 15 is an earthquake off the coast of California, Figure 16 is for the explosion MISSISSIPPI, Figure 17 is for an

earthquake in Baja California. We could have presented a figure showing a similar behavior of the surface waves of an earthquake from Missouri. Therefore, the law describing variation of amplitude of Rayleigh waves with distance in the United States for epicenter distance of 25° or less has an approximately log Δ dependence rather than 1.66 log Δ. All M_S values of Figure 18 have been calculated based upon a log Δ law for Δ 25° or less, the coefficient in the equation being selected so as to agree with the standard Russian law at 25°. Another possible point to be noted before going further is that the M_S measurements made for explosions within the United States are made generally at periods of 10 - 12 seconds, while those for earthquakes are made at 17-19 seconds. As will be demonstrated shortly, M_S values for explosions are a pronounced function of the period at which the measurements are made.

Figure 18 then presents M_S versus m_b data on both United States explosions and earthquakes in the magnitude range m_b 6 to 4. Part of the data were compiled by me while the remainder were published by Basham. Since he followed the identical procedures for calculating both m_b and M_S that I used, the data can be plotted on the same figure. It is apparent on that figure that the M_S versus m_b mean lines describing M_S versus m_b for both earthquakes and explosions are parallel down to magnitude 4 and have slopes of approximately 1.2. In both cases, if the data beyond magnitude 5 1/2 were deleted from the figures, slopes of approximately 1.0 would be obtained. Two points should be mentioned. First, is that the degree of separation of earthquakes and explosion values is small in this figure. However, this figure is not intended to describe an optimum parameter of discrimination but rather to indicate the functional relation of M_S versus m_b for small explosions and earthquakes. The dependence of M_S on period for explosions results in much greater separation of the M_S:m_b values if consideration is limited to 20 second waves. The second point to be mentioned relative to Figure 18 is that, for events of magnitude less than 4, there appears to be an intermingling of explosions and earthquake values. This, of course, is exactly what happened near magnitude 5 before careful determination of M_S and m_b was achieved. It is my feeling that the mixing of explosion and earthquake values below magnitude 4 on Figure 18 may not be indicative of the source behavior but rather inadequacy of the data, i.e., low signal to noise ratio on the few records available.

The strong dependence of M_S on Rayleigh wave period is demonstrated on Figure 19. Here are given individual station M_S values as observed in the United States for surface waves of the RULISON event, the M_S values at distance of less than 25° being calculated according to the log Δ law in the upper right hand corner of the figure. This law still does not adequately describe the data of RULISON. If the only data used are data obtained beyond 20°, the M_S value for RULISON at 10 seconds is approximately 4.55. The limited data available suggested that the M_S value at 20 seconds is 3.8 or lower.

Figure 20 presents curves based on numerous explosions and illustrates the dependence of M_S on Rayleigh wave period for NTS

explosions. It appears that for explosions at NTS there is approximately 1.1 M_S differential between values computed at 10-12 seconds and values computed at 20 seconds. There is approximately .9 M_S differential between M_S values at 20 seconds and at 50 seconds. We will return to this figure later to discuss the significance of RULISON, LONG SHOT, and MILROW data. The last two figures clearly support the statement made earlier that Figure 18 does not constitute an indication of the optimum M_S versus m_b discriminant possible for United States earthquakes and explosions. It only serves to indicate the functional relationship of M_S and m_b for these events, the measurements being made at 10-12 seconds for explosions because these are the periods of dominant energy on the seismograms and because the characteristics of the crust and upper mantle of the United States is such as to give small dispersion from 10-20 seconds.

In order to determine if the convergence of M_S:m_b values for explosions and earthquakes at small magnitudes on Figure 18 is due to low signal-to-noise ratio or due to signal type, one must obtain data at a signal-to-noise ratio adequate to investigate the former possibility. Thus, the data of Figure 21 were obtained at such a range that this condition could be fulfilled to below m_b 4. The data of Figure 21 were obtained at Berkeley on NTS explosions and on earthquakes which were at essentially the same distance from Berkeley as is NTS. Again, measurements were made at the dominant period on the records. Thus the explosion data were taken at periods of approximately 10 seconds while earthquake data were at long periods. It would seem that there is no convergence of mean lines for explosion and earthquake data down to magnitude 3 3/4, i.e., to the limit of the detection capability of the Berkeley station. It is of interest to note on this figure that both the earthquakes and collapse events following NTS explosion have M_S:m_b values similar to those of earthquakes. This makes it quite clear that the spectral characteristics of explosions are influenced by the explosion itself and are not conditioned solely by the depth of explosion.

Figure 22 presents data on M_S versus m_b for a few earthquakes and explosions, the M_S values being computed based on 20 second surface waves. It is clear that the discrimination between explosions and earthquakes is improved over that in Figure 18.

Another discriminant that has been developed recently is to take the spectral energy ratio of Love and Rayleigh waves to short period P waves, this quantity being plotted versus m_b. Figure 23 presents a few such data for USSR earthquakes and presumed explosions. As would be expected from the data of Figure 22, this energy discriminant has a 2 order of magnitude discrimination between earthquakes and presumed explosions. The immediate reason for presenting this figure at this time is the fact that for events below magnitude 5 1/4 there appears to be a minimum value of the energy ratio for earthquakes. At first presentation of this figure, this behavior seemed anomalous. However, the interpretation now appears obvious. That is, if for events of m_b less than 5 1/2 the ratio of M_S to m_b approaches

one, this spectrum ratio discriminant has a fixed value.

Figure 24 presents similar data for a few U.S. earthquakes and explosions. Again, the ratio values appear to have the same minimum value for events of less than m_b 5 1/4.

I will now present a few figures based on M_S (20) values determined by a single instrument in the Ogdensburg mine and teleseismic m_b values determined by a network of stations. These data will help to establish the M_S:m_b relationship for earthquakes relative to M_S:m_b relationship for explosions and will provide data on the threshold of detection of the Ogdensburg instruments.

On each figure, the events plotted are those either for which surface waves were observed at Ogdensburg or those on which the high gain records were available but no signals were detected. Depths of all events, at least the best estimate of the depths of all events, are indicated. Open symbols are for events of unknown depth or with depth of less than 35 kilometers. Closed symbols are for events of 35 kilometers or greater, this last category being divided into those events with depths of 35 to 75 kilometers and those with depths of greater than 75 kilometers. Triangles indicate events for which no surface waves were detected on the high gain records at Ogdensburg. The noise level on the Ogdensburg records is generally 2 to 3 millimeters. The dashed lines on each figure indicate the equivlant M_S (20) values at Ogdensburg for events from the indicated regions. Signal values plotted between the two dashed lines indicate measured signals. Triangles plotted within that band indicate events for which the signal could be asserted to be present but not measurable as to amplitude. Triangles plotted below the two millimeter line indicate events for which no surface waves were detected at Ogdensburg. The line labeled NTS is the M_S(20) versus m_b curve for NTS explosions as observed in Eastern United States.

Figure 25 is for events on the Mid-Atlantic Ridge of the North Atlantic. These data extend to and below m_b 4 and indicate parallelism of the M_S:m_b curves for explosions and earthquakes (and thus a 1:1 ratio of M_S and m_b changes for events of m_b < 5 1/2).

Figure 26 is for earthquakes of Central America. Data extends in this case to and below magnitude 4.

Figure 27 is for earthquakes in Mexico and Guatemala. Data again extend to below m_b 4 and parallelism is indicated.

Figure 28 is for Peru and suggests parallelism.

Figure 29 presents data taken from a series of slides of the type just presented. It indicates the m_b threshold for high probability of detection of surface waves of shallow focus earthquakes from numerous areas by visual inspection of Ogdensburg's records. The last column indicates the db gain required over that of visual inspection to attain a high probability of detection for surface waves of m_b 4 earthquakes. The tabulation suggests that a 10 db gain over that attained by visual inspection of the Ogdensburg records

suffice for detection of surface waves of m_b 4 earthquakes at epicentral distances of several thousand kilometers.

The data just presented suggest that the M_S:m_b relationship for small magnitude earthquakes has a slope of approximately 1.0, i.e., it is parallel to that of explosions. In addition, these data suggest that the discriminating power of the standard long period discriminants is probably as great at magnitude 4 as at magnitude 5.

Another point to be briefly discussed is the spectral amplitude functions of the surface waves of earthquakes and explosions.

Figure 30 presents vertical component velocity spectral data for 4 NTS explosions. All four explosions were on Pahute Mesa. The great degree of similarity of these 4 spectra is quite remarkable.

Figure 31 presents similar data for BENHAM and for the BENHAM collapse. The major and important point to be recognized on this figure is that the spectral density for BENHAM is controlled in large part by the explosion and not entirely by the depth of focus. If depth of focus were the sole controlling parameter the spectrum of BENHAM collapse would be essentially identical to that of BENHAM itself. This is obviously not the case, the collapse having much more long period energy. The character and explanation of BENHAM data must be sought in the explosion phenomenon. The data do suggest that a characteristic of explosions, at least NTS explosions, is a high ratio of short period surface wave energy to long period energy.

Figure 32 presents data obtained at Ogdensburg on the spectrum amplitudes of NTS explosions and other explosions. It seems that for NTS explosions there is several fold decrease in amplitude between the 20 and 50 seconds waves. There is a full 10-fold decrease in amplitude between 20 and 50 seconds. The one event studied from Semipalatinsk shows only a two-fold decrease in amplitude between 20 and 44 seconds.

Figures 33 and 34 present relative amplitude versus period data for numerous earthquakes at various distances as observed at Ogdensburg. The data are grouped by epicentral distance and the data for all events are normalized to 20 second amplitude. The increase in distance is correlated with an increase in the m_b values. The ratio of 50 to 20 seconds amplitude is highly variable from earthquake to earthquake on these figures. The mean value of the 20-50 second ratio is approximately two, i.e., distinctly less than for NTS explosions. In addition, it can be seen that the 20-50 second ratio does not appear distance dependent but rather independent of distance, thus implying independence of the 20-50 second ratio of m_b values.

Figure 35 presents data on the amplitude of 100 second Rayleigh waves versus M_S values based on 20 second Rayleigh waves. The figure indicates that the ratio of 20 second to 100 second surface waves for earthquakes is essentially independent of magnitude from M_S 5 to M_S 9. The data suggest that discrimination between earthquakes and

explosions may be distinctly improved by basing the surface wave measurments on periods of 40 seconds or greater. A specific example of this contrast in signal type is presented in Figure 36. This figure presents amplitude ratio of Rayleigh wave spectra from GASBUGGY and a nearby earthquake of comparable m_b magnitude. The amplitude ratio of 10 second Rayleigh waves of the earthquake and explosion in approximately 1, while the equivalent ratio for waves of 50 second period is 20 or greater.

Figures 37, 38, and 39 present somewhat more detailed data than were presented on Figures 33 and 34. On Figure 37 are data for Aleutian events only. In this case the data are not normalized to 20 seconds. The long dash lines indicate the M_S versus m_b relationship if amplitudes of ground motion are the same for all periods. The lines of short dashes indicate approximate threshold of measurement of surface waves at Ogdensburg for earthquakes from the Aleutians. These data suggest that for events from the Aleutian Islands the 20 - 50 second ratio is approximately 2 with individual events showing high variability from this value. The shape of the spectral amplitude curve does not appear to be magnitude dependent.

Figure 38 presents similar data for events from Mexico and Guatemala. In this case the data extends to smaller magnitudes than do the Aleutian data. Similarity in shape of the spectral amplitude curve for small and large magnitudes is observed. For these events the mean value of the 20-50 second ratio is approximately 1. For data obtained at Ogdensburg, nearly all events for which 30 seconds was observed had measurable 40 second waves. Visual inspection of the records did not allow as frequent measurement of 50 second waves. Whether this is real aspect of the surface waves (doubtful) or whether it is an aspect of either dispersion or noise level was not determined at the time of the measurements.

Figure 39 presents similar data for events of the Kurils. On this figure the data of the several events are coded according to the same depth of focus symbols used on earlier figures. It seems that for events with depths of 35 km or greater, the 20-50 second ratio is markedly less than the average for events having depth of less than 35 kilometers. Reference to the $M_S(20)$ data of Kuril Islands (data not presented) indicates that those having high 20-50 second ratios on Figure 39 are those events having extremely high $M_S(20)$ values, i.e., the shallow focus events. The reason for these very high 20-50 second ratio for shallow focus events may reside in the type of faulting associated with Kuril earthquakes or possibly in high generation of first higher mode Rayleigh waves. The data presented do suggest that proper use of broad band long period data should increase discrimination capability between earthquakes and explosions. The data presented suggest that detection of 40 second waves at Ogdensburg is comparable to that for 20 second waves. If this be so, several advantages accrue, one being that propagating microseismic noise at 40 seconds is essentially non-existent or at least below present detection levels. If sites can be found and occupied which have very

low non-propagating atmospheric-induced noise, detection capability of 40 second Rayleigh waves should be distinctly better than that of 20 second surface waves.

Finally, I would like to make a suggestion as to the explanation of the observed regional dependence of M_S:m_b relationship.

In a recent paper (Evernden, 1970) it was pointed out that P amplitudes in Eastern United States (EUS) are, on the regional average, three times as high as in the Western United States (WUS). In another soon-to-be-published paper, (Evernden and Clark, Part II) details of this phenomenon are presented. It is shown that there exists a direct correlation between the 1-cycle noise level and the amplitude of P teleseismic signals. If consideration is limited to granite or equivalent sites, there is a linear relation between log amplitude and log noise level such that a tenfold change in noise level implies on the average a 2 1/2-fold change in P amplitude (Figure 40 of this paper). Available data indicate that a greater than 4-fold change in P amplitude can occur as a correlate of a 10-fold change in amplitude of normal 1-cycle noise (note on Figure 40 the high signal levels on both granite and sediments in the North Dakota-Ontario area). In the papers cited above, it was shown that the amplitude of P waves generated by SALMON (exploded in Mississippi) and GNOME (exploded in New Mexico) become more consistent with data for explosions at Nevada Test Site (NTS) when interpreted on the basis of the regional variation of P amplitude established by use of earthquake data. The suggestion made was that this P amplitude change is due to dissipation in the upper mantle or lower crust and thus should effect equally both down-going and upgoing P waves.

In Evernden, 1970, the relation between yield and magnitude (m_b) for NTS explosions was presented, the magnitudes being determined by use of data or by calibration against data obtained at stations at teleseismic distances from NTS in Eastern United States. It was there shown that 40 kiloton (RULISON yield) explosions in hard rock (granite or welded tuff or "equivalent") or water-saturated rock would if exploded at NTS generate P-wave signals of approximately magnitude 5.3.

Figure 41 is based upon the data of numerous NTS explosions. It presents the relation between m_b values, M_S values, and periods of surface waves used for the M_S measurement. The evidence of Rayleigh wave amplitude being a strong function of Rayleigh wave period for explosions is obvious, the dependence of M_S upon period being much greater than explainable by the period difference itself.

On the same figure are plotted M_S values for RULISON. At all periods, the RULISON M_S:m_b point plot above the NTS line, implying either a low m_b value or high M_S values for RULISON. On the same figure are data points for LONG SHOT and MILROW, the two explosions on Amchitka. For these, the M_S:m_b points are below the NTS values, implying either high m_b values or low M_S values relative to NTS explosions.

Note on Figure 41 that the observed m_b values for RULISON (approximately 5.0 as observed in EUS) is distinctly below that predicted by NTS explosions as observed in EUS while the average magnitude of LONG SHOT (6.05) and MILROW (6.6) as observed at calibrated stations in the EUS and WUS are distinctly greater than predicted from NTS data. (These magnitudes for LONG SHOT and MILROW are distinctly above the world-wide average m_b values). If, for all three events, one uses observed M_S values and calculates predicted m_b values from NTS versus yield data, the resultant points plot on Figure 2 very near the mean NTS M_S versus m_b curves. This suggests that the observational data for these three events are characterized by abnormal m_b values, not abnormal M_S values (relative to NTS explosions).

As was shown in Evernden and Clark (op. cit), noise levels in Nevada on hard rock are around 5 mμ, becoming as high as 10 mμ at some stations while noise levels in Colorado and Idaho can be as low as 1 - 1-5 mμ. The station at Durango, Colorado had the lowest mean P wave signal amplitude of all stations studied. Figure 1 would suggest that a .25 magnitude divergence between NTS and Colorado explosions would be expected as a correlate of their differing noise levels and locations. A .25 magnitude increase in the observed RULISON m_b magnitude makes RULISON M_S:m_b data consistent with NTS data.

Though NTS noise levels and P amplitudes are high relative to Colorado, they are low relative to stations in EUS. If the correlation between mantle/crustal characteristics affecting P amplitude are tectonically related as suggested earlier, they probably should be correlated with mean elevation. Therefore, it would not be surprising if P waves or explosions in Amchitka suffered less attenuation in the crust or upper mantle of that region than do signals of NTS explosions. The high m_b values of LONG SHOT and MILROW may then be explained on the same fundamental basis as the low m_b values for RULISON.

Another important feature of the yield versus m_b and M_S versus m_b data remains to be noted. Figure 42 presents the yield versus magnitude (m_b) curve for explosions in "hard-rock" as observed in EUS from events occurring at NTS. If the curve is considered as more probably a curved line rather than two intersecting straight lines, the dashed segment of the curve would be considered as more nearly correct. It is obvious that the yield versus m_b curve is strongly curved in the region of 40 - 200 kt (i.e., m_b 5 - 5 3/4). On Figure 41 was presented the M_S (20 sec) versus m_b curve for NTS explosions, the curve being strongly curved in the region m_b 5 - 5 3/4. In fact, if these two curves, yield versus m_b and M_S versus m_b, are superimposed and properly scaled (1 M_S unit equals 1 unit change in log yield), it will be observed that the two curves are of identical shape. The curvature of the yield versus m_b curve then must be expressive of the same factor as is the curvature of the M_S versus m_b curve and is probably the result of the differing spectral density characteristics of large and small explosions. Unfortunately, one of us missed a vital reference in this regard when writing the note cited about (Everden, 1970). N. Haskell (Haskell, 1967), by use of Werth's reduced

displacement potentials, developed a theory predicting the spectral density contrasts of large and small explosions in hard rock. If his theory is converted into a predicted log amplitude (at 1 sec) versus yield curve which is then normalized to the NTS curve at 10 kt, the result is the series of squares on Figure 42. It is obvious that Haskell essentially exactly predicted the observations, the critical observations actually being obtained subsequent to publication of his paper. Thus, it seems that the curvature of the hard rock observed yield versus m_b curve is explained as a spectral density phenomenon and its exact shape results from the band pass used for short period instruments.

The similarity in shape of the M_S versus m_b and yield versus m_b curves means, of course, that the log yield versus M_S curve is nearly a straight line at all yields and M_S values yet observed. Figure 43 is a demonstration of the fact that this is indeed true. Note particularly on this figure that, whereas on the NTS yield versus m_b figure (Figure 42) RULISON had an m_b value below that predicted for NTS while LONG SHOT and MILROW had m_b values above those predicted by use of the NTS curve, on Figure 4 all of these explosions plot within the statistical scatter of the NTS data. Thus the figure confirms that the regional dependence of M_S versus m_b is a result of perturbation of the m_b value, not the M_S value. Thus, the hard rock curve of Figure 43 is nearly a universal curve applicable to all regions. It is true that much of the reduced displacement potential curve used by Haskell has an assumed shape, particularly at long periods. It might be appropriate to state that Figure 43 demonstrates that the short period portion of the spectral density curves of small and large explosions are as predicted by Haskell though it does not demonstrate the detailed shape used by Haskell is correct at all periods (i.e., behavior of spectral density curve for periods of greater than 2 or 3 seconds is not established, only the behavior of the ratio of amplitudes at 1 and 20 seconds is as predicted by Haskell).

Some of the scatter of Figure 43 may result from the fact that the mean period of M_S measurement for all events were scaling was required based on Figure 41 was not at 10-12 seconds. However, the assumption that all observations were at 10-12 seconds (as most of them certainly were) is sufficient to prove the point addressed.

The arguments above suggest that yield is better determined by surface waves than by body waves, i.e., regional factors influencing P wave amplitude have less effect on 20 second Rayleigh waves and the greater slope of the M_S versus yield curve at high yields makes yield estimates less sensitive to an error in M_S values than to an error in m_b value. At yields of greater than 100 kt, an 0.3 error in m_b means greater than a three-fold error in yield determination while an equivalent error in the M_S determination means only a two-fold error in yield determination. Systematic differences in m_b induced by local factors can lead to errors in yield estimate of factors of 5 or greater if the NTS m_b versus yield curve is directly used.

Also, statistical scatter of M_S values is generally less than for m_b values. The application of the NTS yield versus m_b curve to other regions at small magnitude (i.e., at magnitudes below those for which surface waves are measurable at teleseismic distances) is possible subsequent to an explosion large enough to generate detectable surface waves. The NTS yield versus m_b curve can be normalized to this new region by establishing the yield versus m_b correlation at high yields, the universal yield versus M_S curve having given the yield while observations have given the m_b. The shape of the yield versus m_b curve is medium-controlled and should be the same from region to region. Thus, after calibration on the basis of a large explosion, valid estimates of yields of small events by use of yield versus m_b is possible.

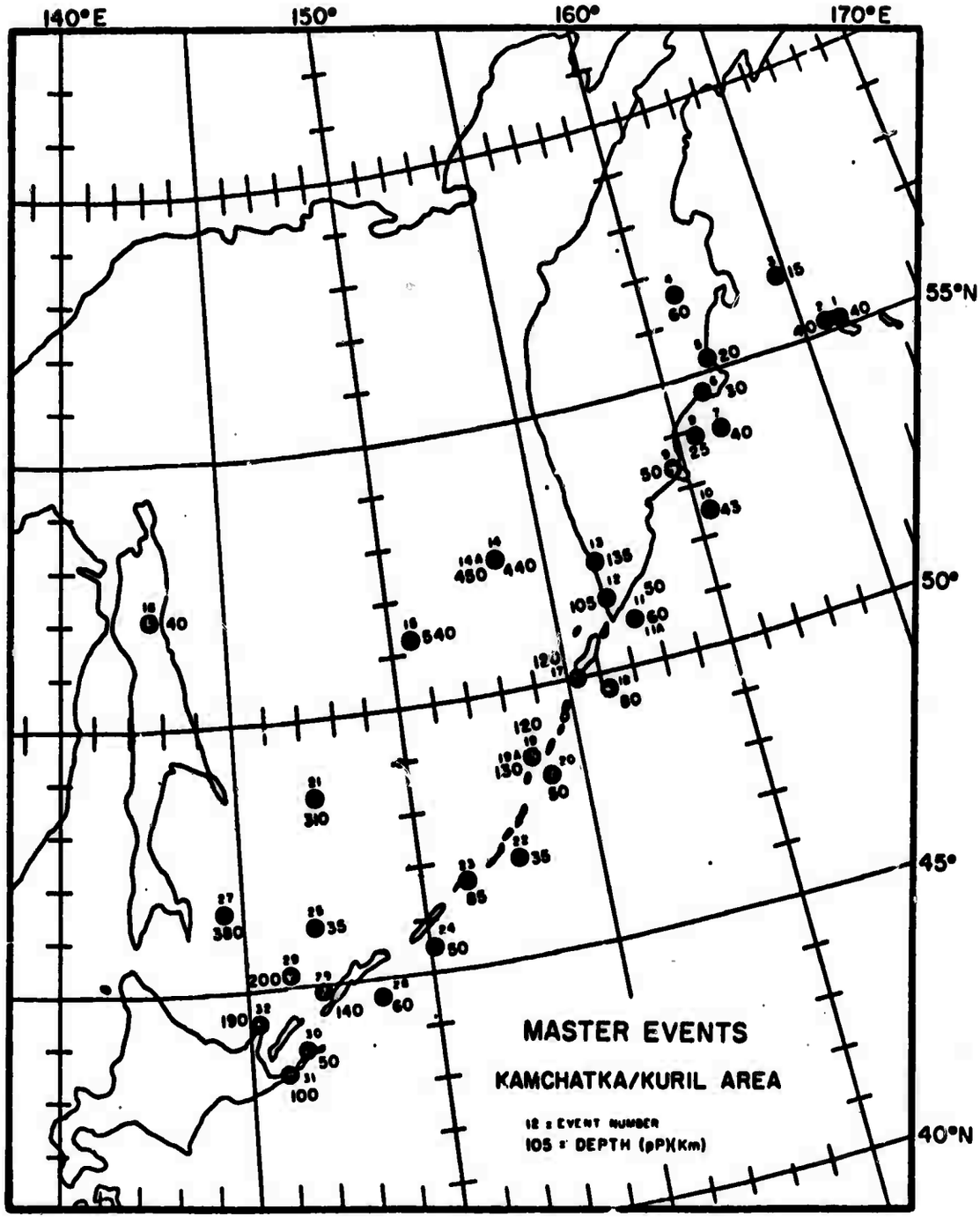
140°E
150°
160°
170°E
55°N
50°
45°
40°N
MASTER EVENTS
KAMCHATKA/KURIL AREA
12 = EVENT NUMBER
105 = DEPTH (pP)(Km)

Figure 1.

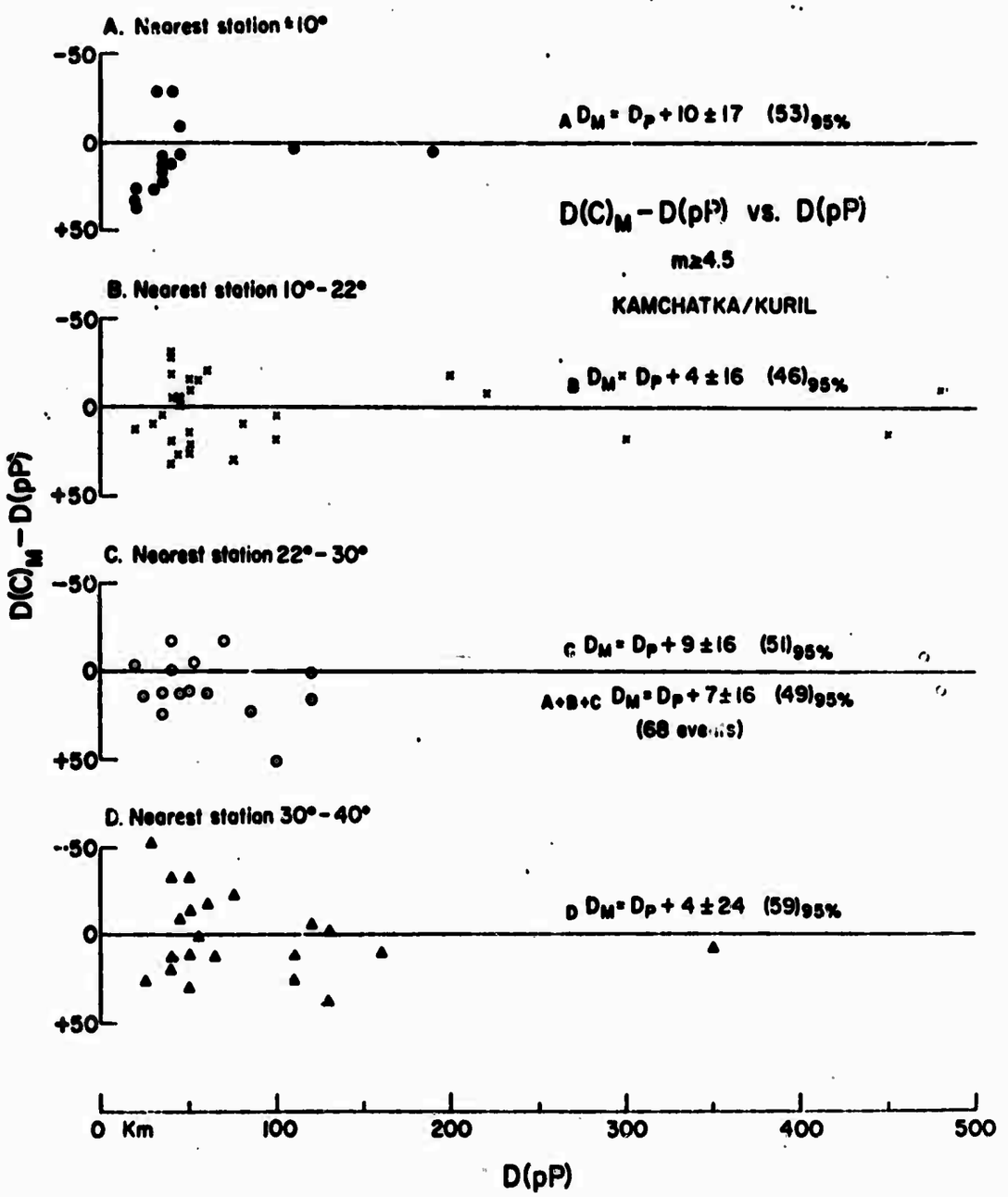
A. Nearest station ≤10°
-50
0
+50
A DM = DP + 10 ± 17 (53)95%
D(C)M − D(pP) vs. D(pP)
m≥4.5
KAMCHATKA/KURIL
B. Nearest station 10°-22°
B DM = DP + 4 ± 16 (46)95%
C. Nearest station 22°-30°
C DM = DP + 9 ± 16 (51)95%
A+B+C DM = DP + 7 ± 16 (49)95%
(68 events)
D. Nearest station 30°-40°
D DM = DP + 4 ± 24 (59)95%
D(C)M − D(pP)
0 Km
100
200
300
400
500
D(pP)

Figure 2.

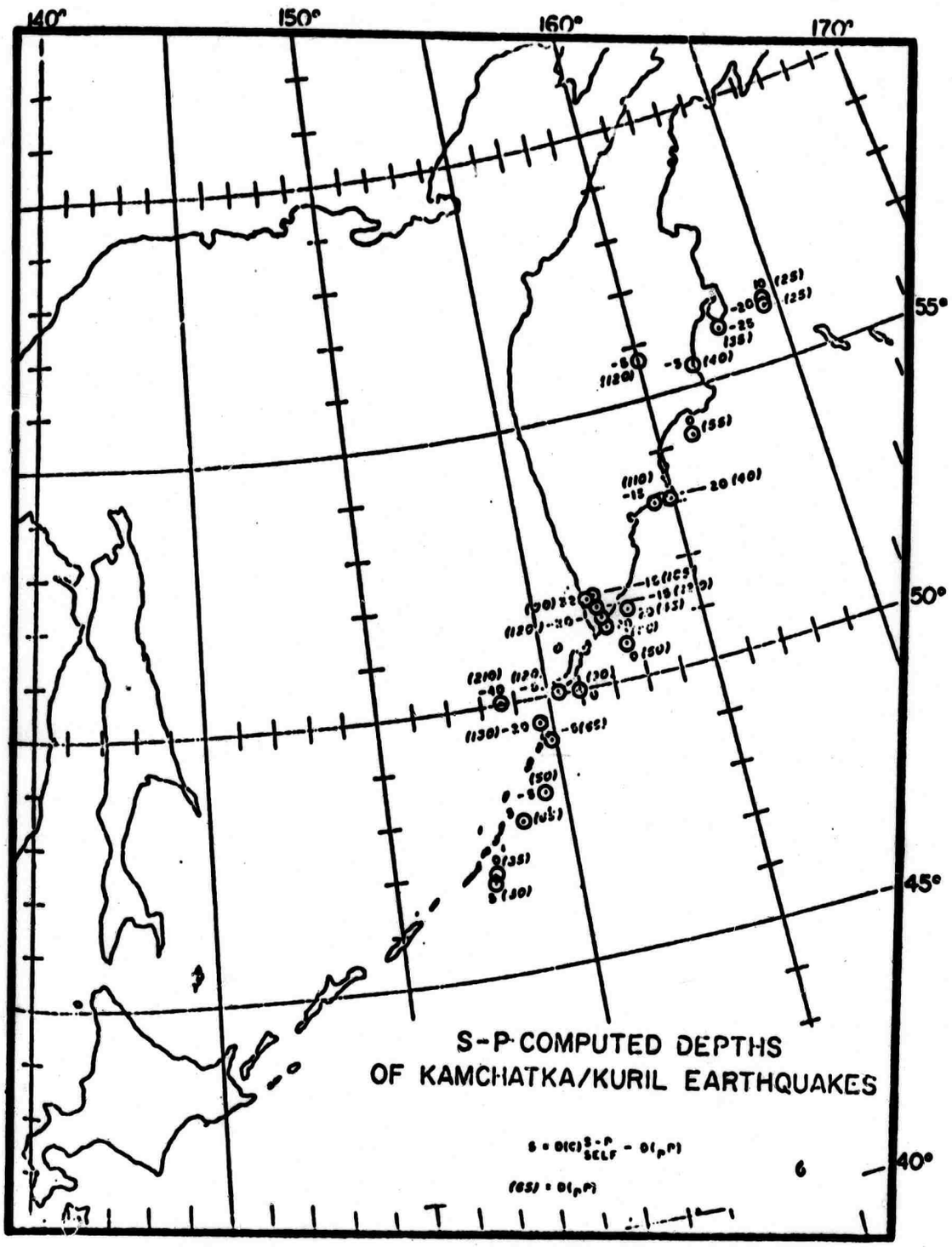
140°
150°
160°
170°
55°
50°
45°
40°
S-P COMPUTED DEPTHS
OF KAMCHATKA/KURIL EARTHQUAKES

Figure 3.

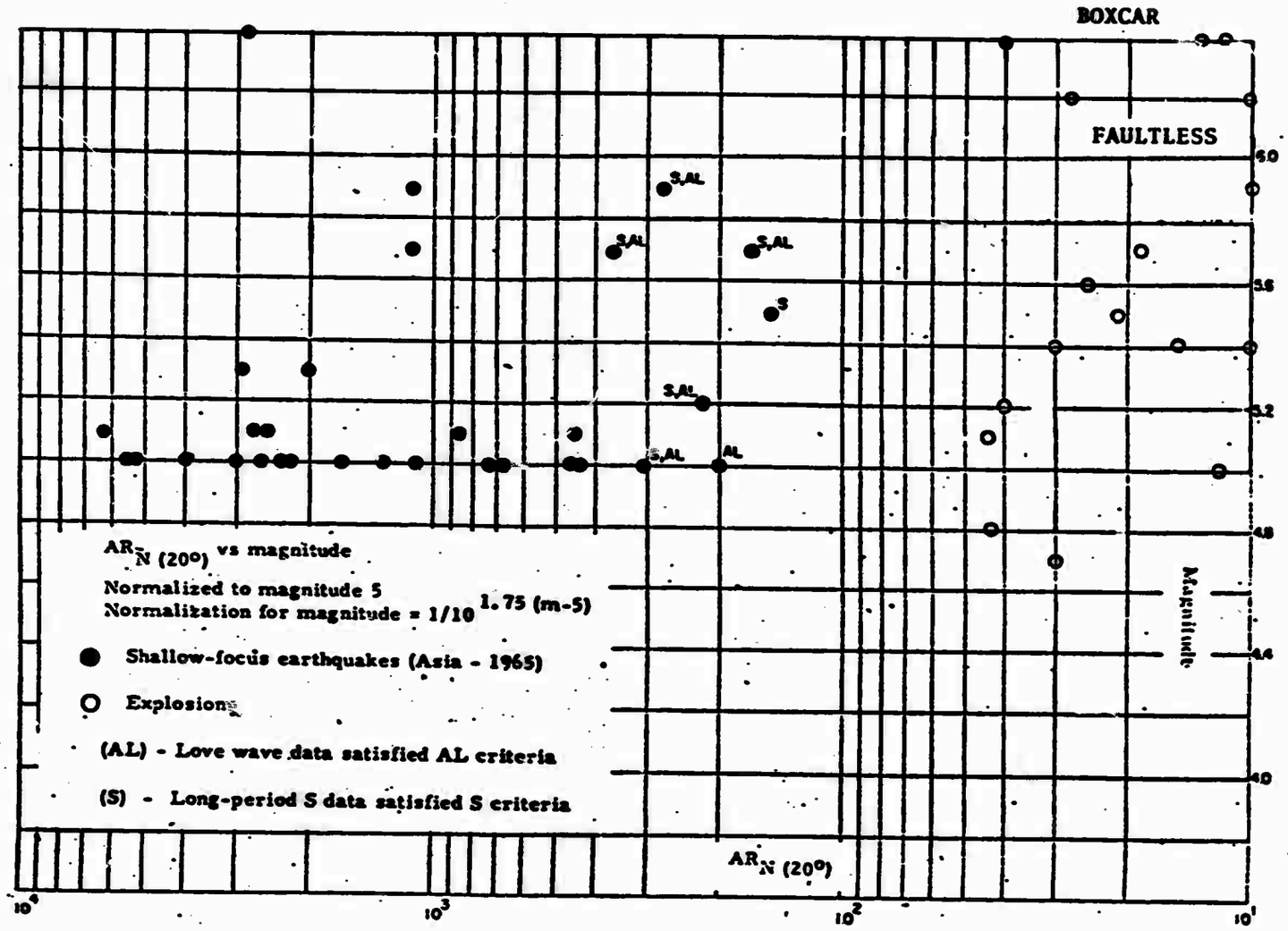
BOXCAR
FAULTLESS
6.0
5.6
5.2
4.8
4.4
4.0
Magnitude
S,AL
S,AL
S,AL
S
S,AL
S,AL
AL
AR_N (20°) vs magnitude
Normalized to magnitude 5
Normalization for magnitude = $1/10^{1.75\,(m-5)}$
Shallow-focus earthquakes (Asia - 1965)
Explosions
(AL) - Love wave data satisfied AL criteria
(S) - Long-period S data satisfied S criteria
AR_N (20°)
10^4
10^3
10^2
10^1

Figure 4.

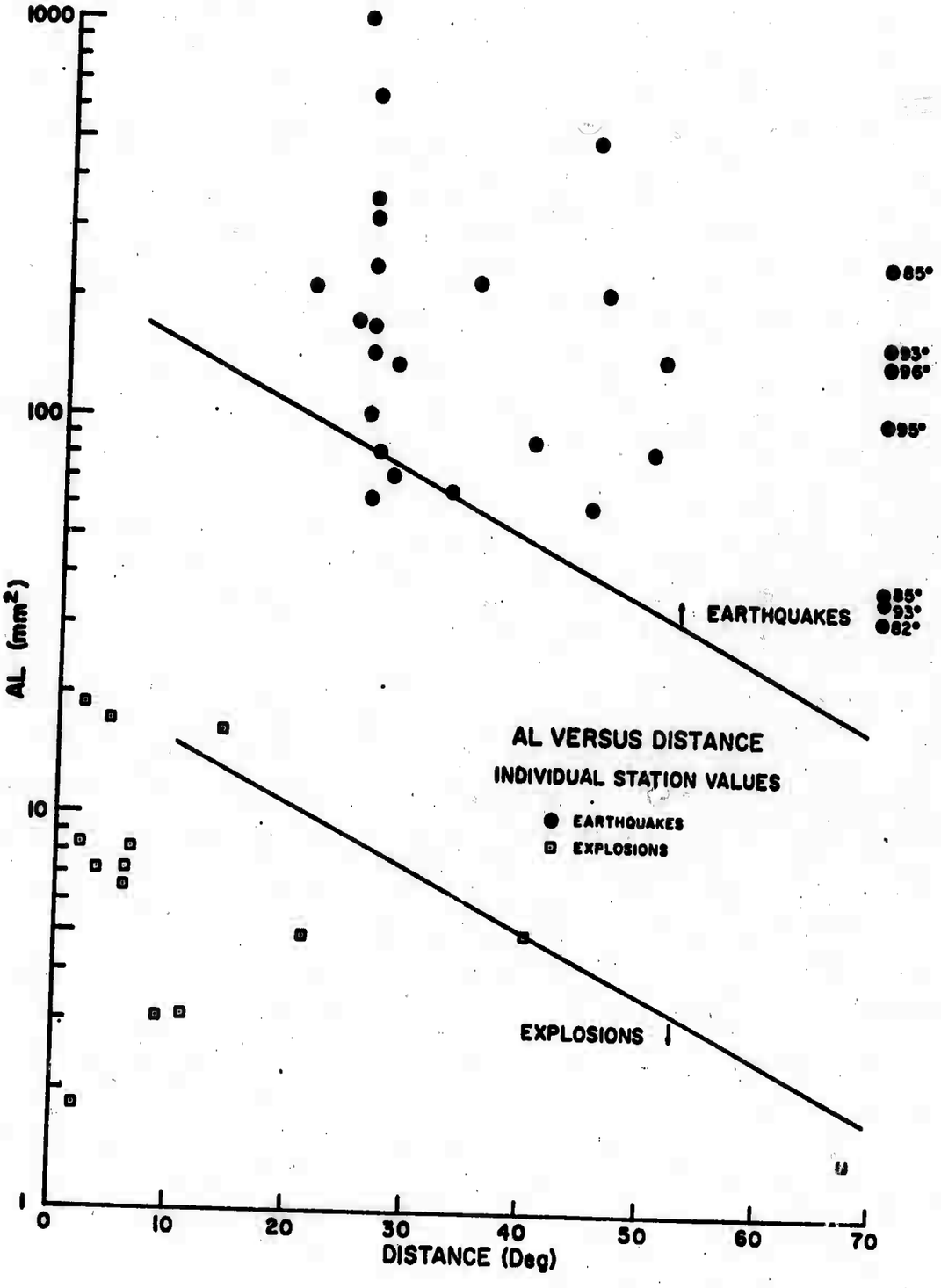
1000
100
10
1
AL (mm²)
0
10
20
30
40
50
60
70
DISTANCE (Deg)
85°
93°
96°
95°
85°
93°
82°
EARTHQUAKES
AL VERSUS DISTANCE
INDIVIDUAL STATION VALUES
EARTHQUAKES
EXPLOSIONS
EXPLOSIONS

Figure 5.

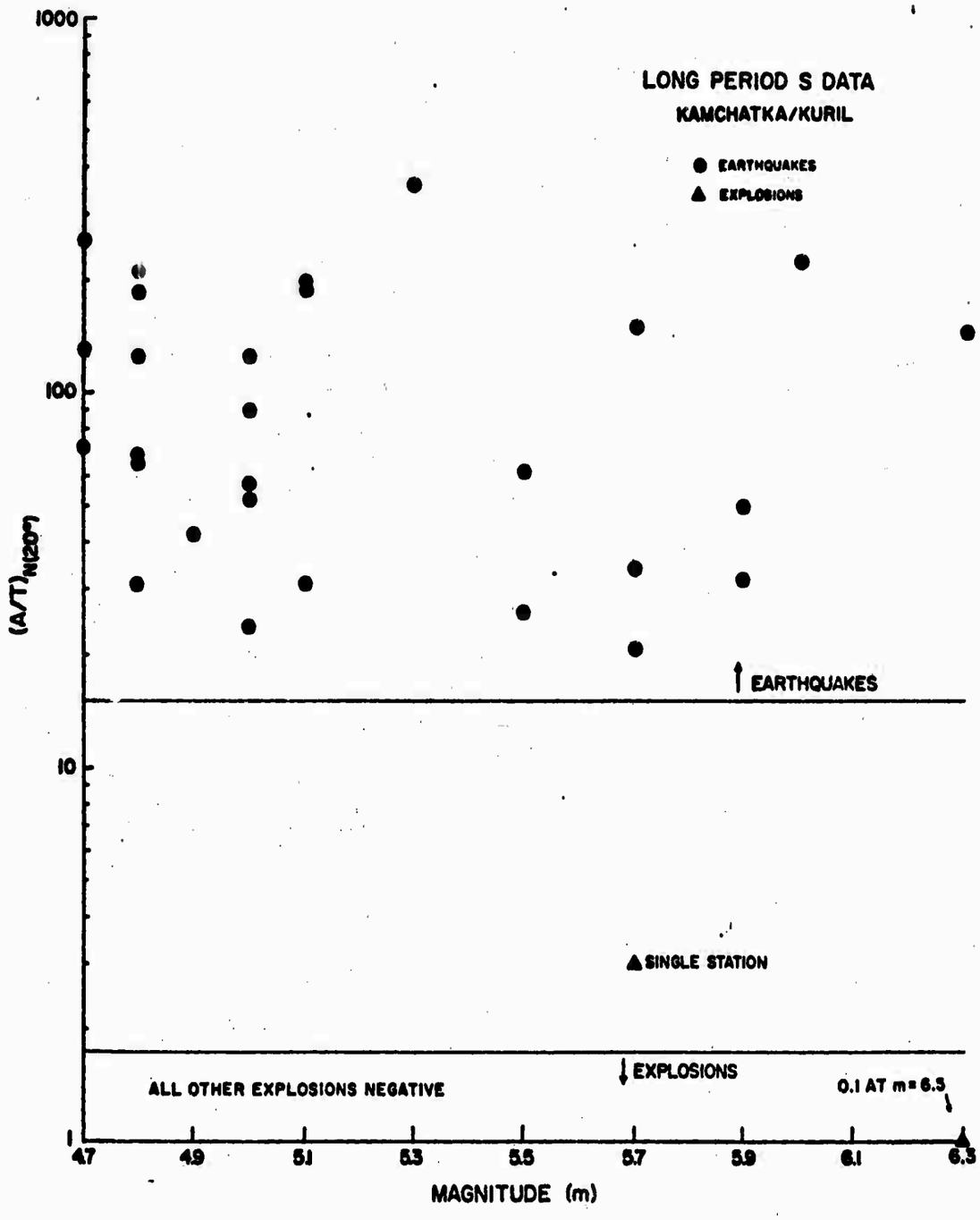
LONG PERIOD S DATA
KAMCHATKA/KURIL
EARTHQUAKES
EXPLOSIONS
1000
100
10
1
(A/T)N(20°)
EARTHQUAKES
SINGLE STATION
EXPLOSIONS
ALL OTHER EXPLOSIONS NEGATIVE
0.1 AT m = 6.5
4.7
4.9
5.1
5.3
5.5
5.7
5.9
6.1
6.3
MAGNITUDE (m)

Figure 6.

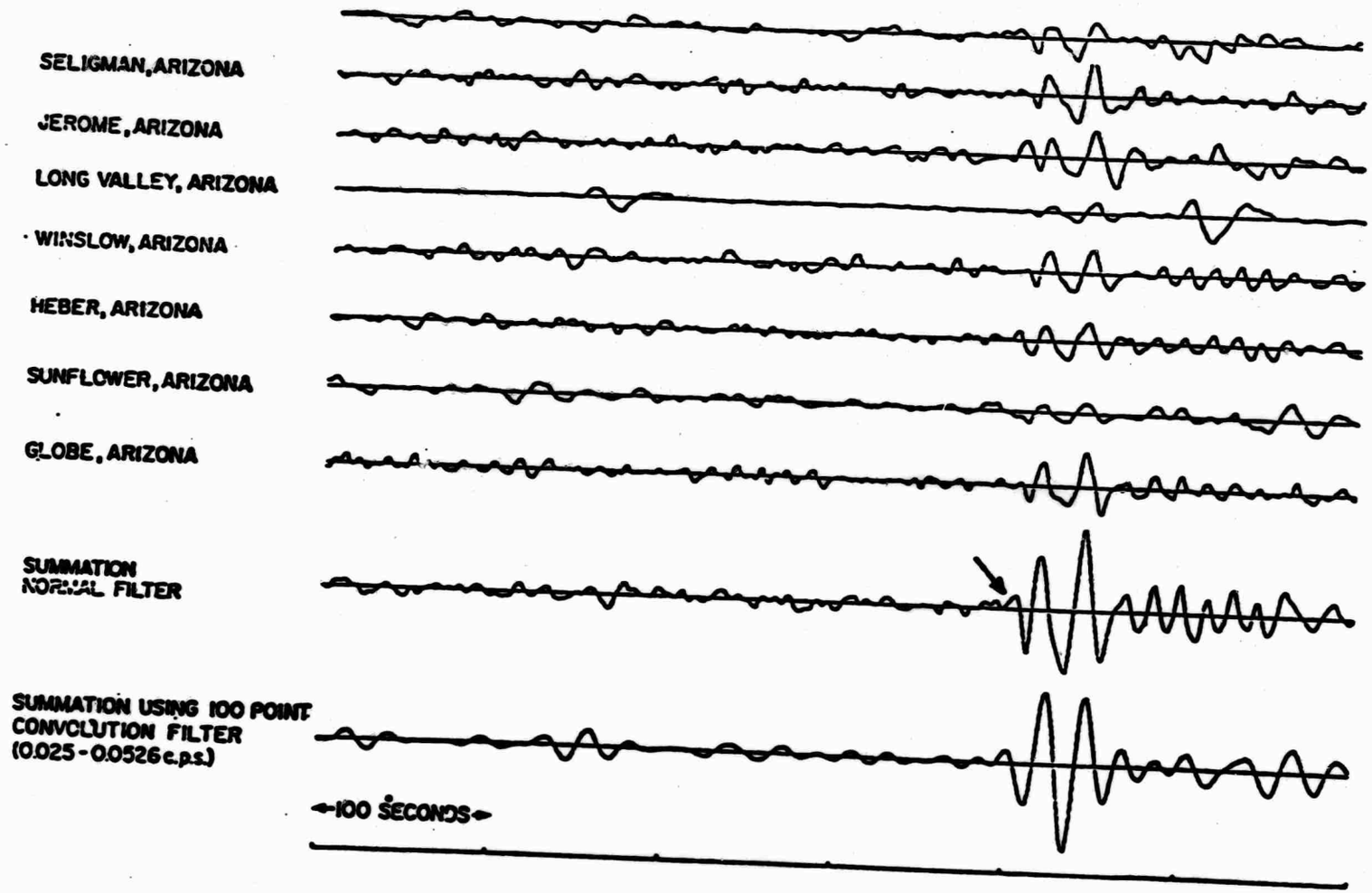

LONG PERIOD P WAVE
BEAM STEERING OF LONG PERIOD ARRAY

Figure 7.

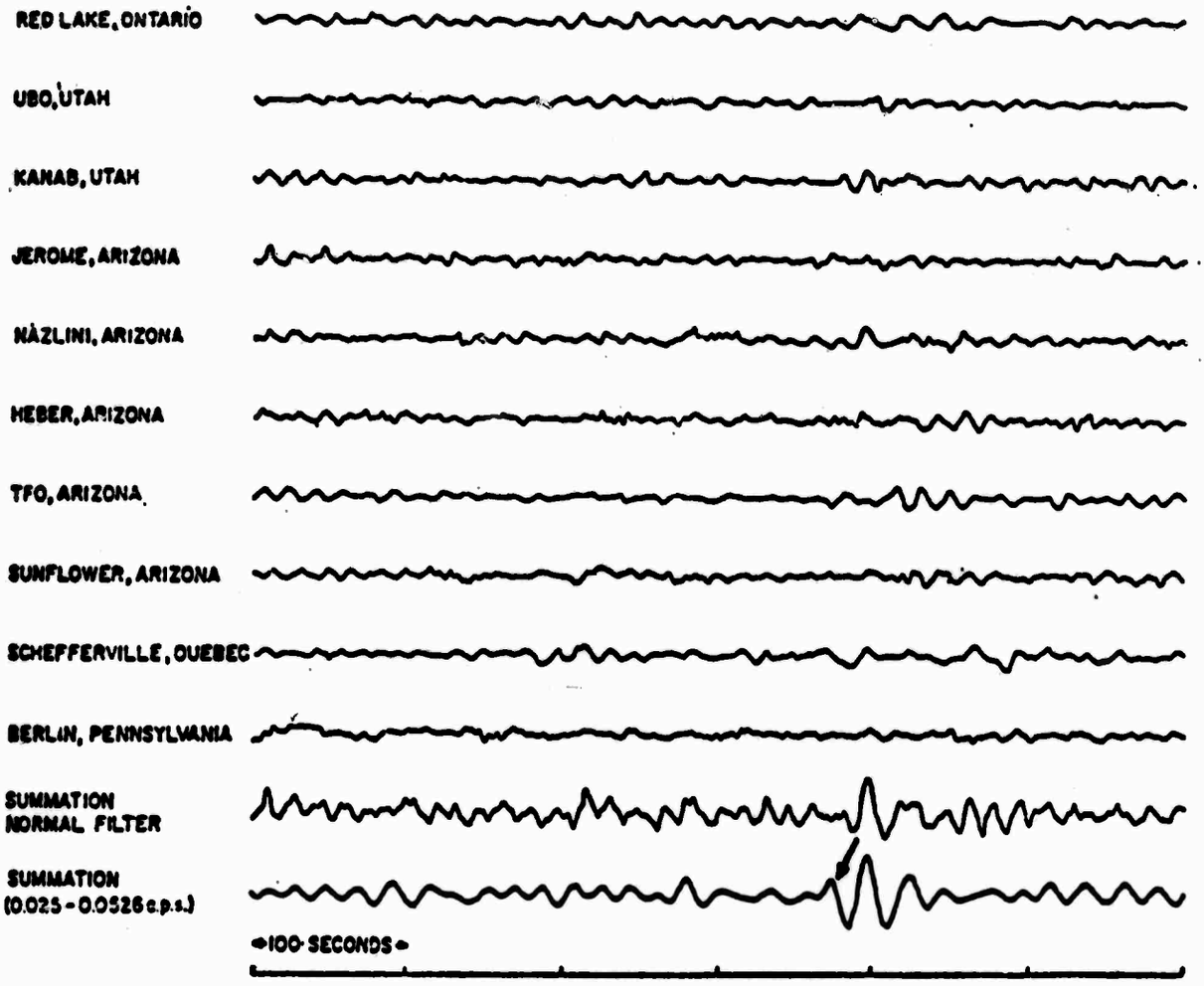

LONG PERIOD P WAVE
BEAM STEERING OF LONG PERIOD ARRAY

Figure 8.

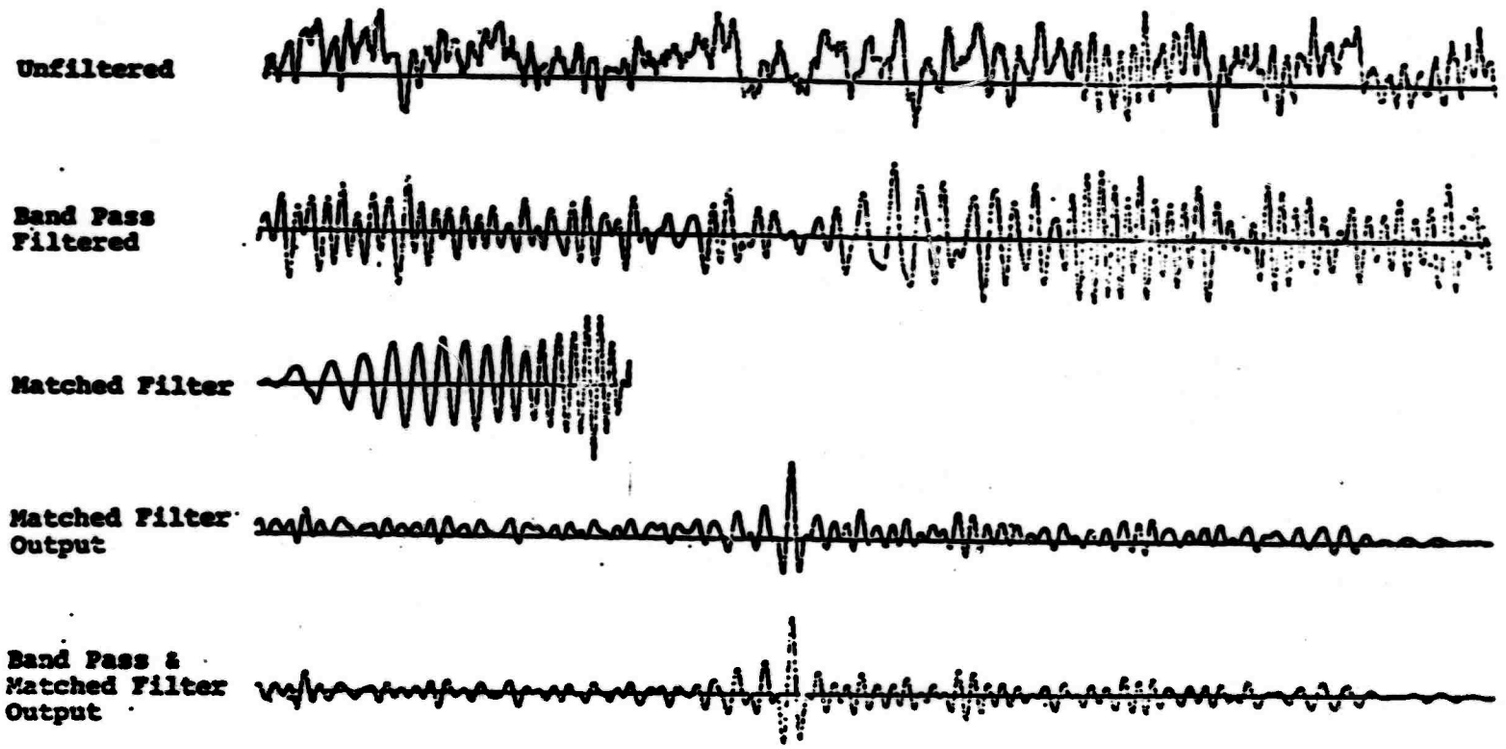

Comparison of Several Signal Enhancement Procedures For A Single LASA Element (E1 - LPZ)

Figure 9.

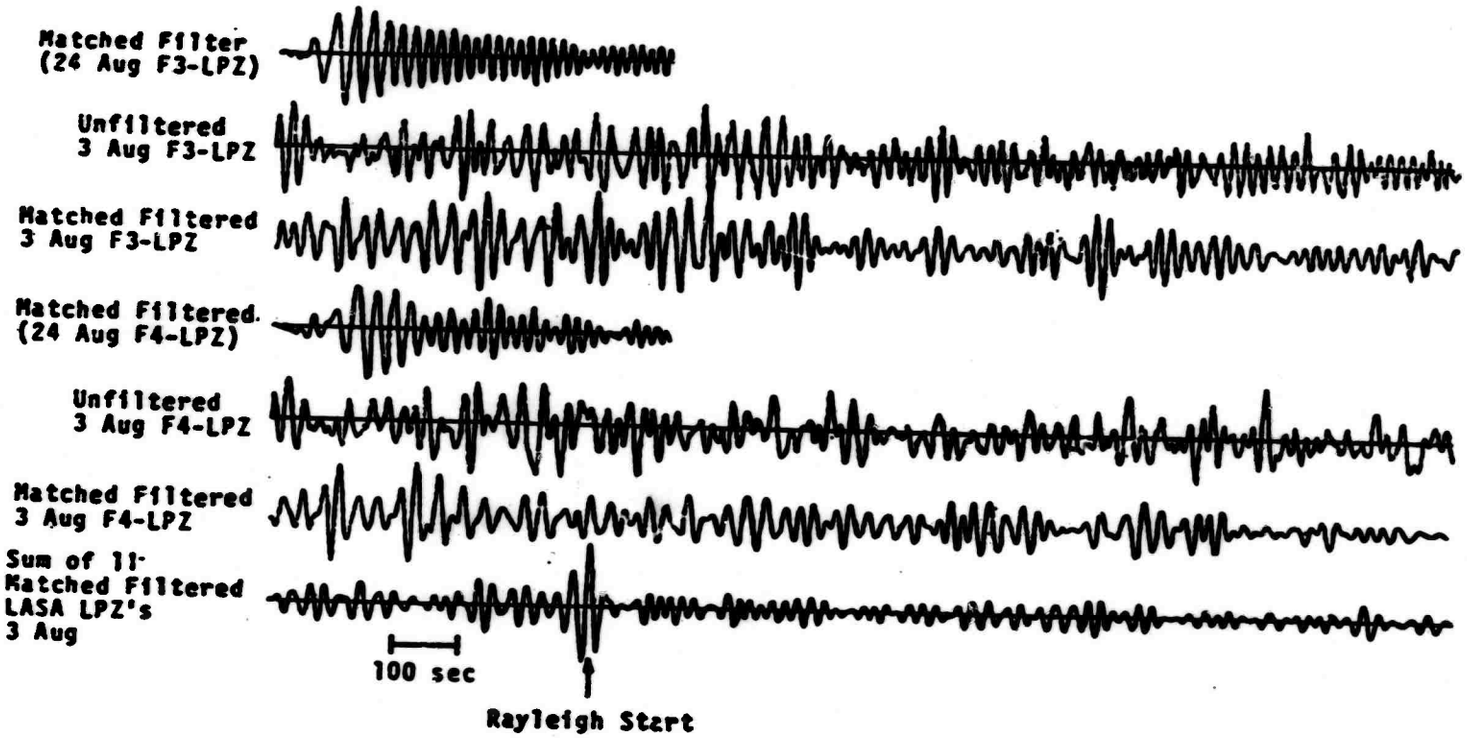

Event of 3 August 1968. LASA LPZ Rayleigh waves, matched filtered with signals from event of 24 August 1968. Sum of LASA matched filtered signals.

Figure 10.

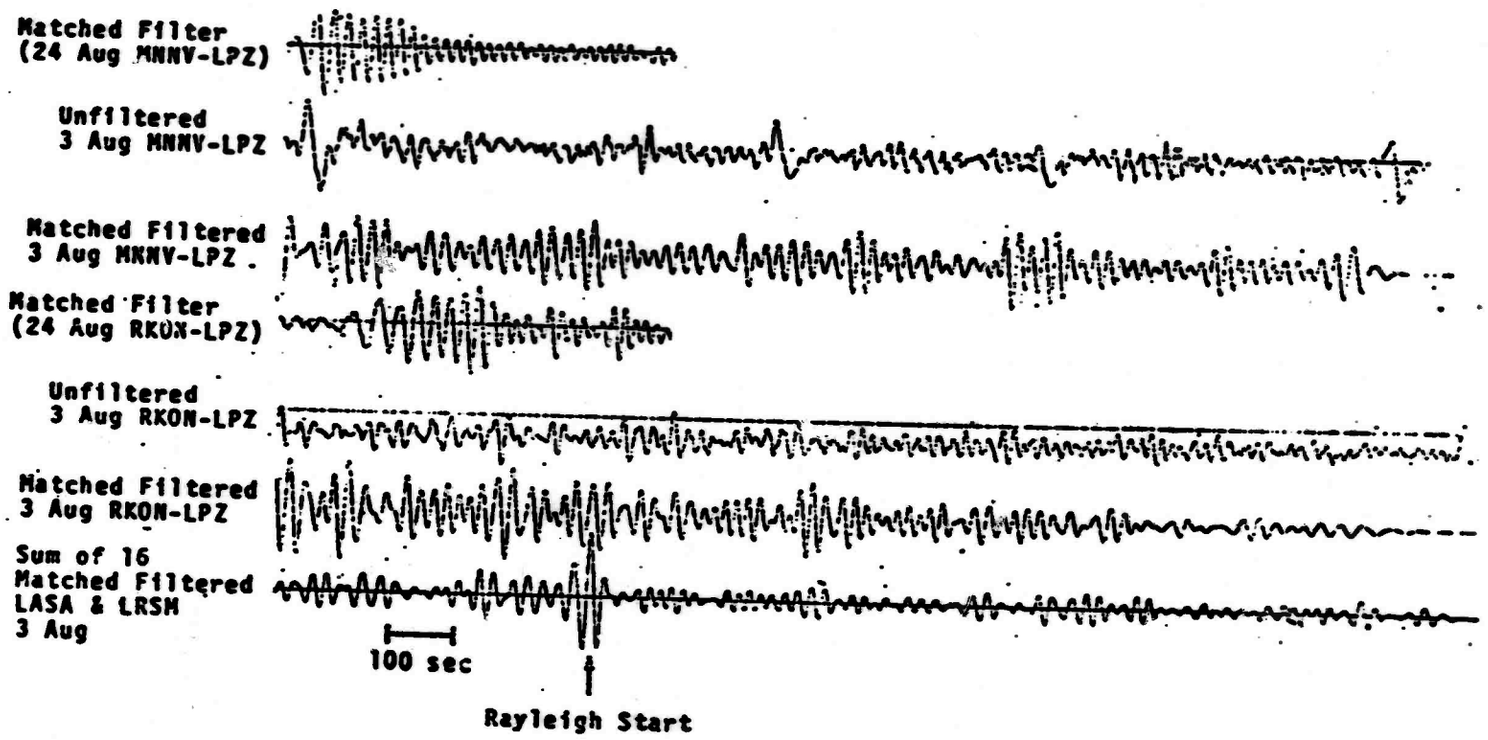

Event of 3 August 1968. LRSM LPZ Rayleigh waves, matched filtered with signals from event of 24 August 1966. Sum of LASA and LRSM matched filtered signals.

Figure 11.

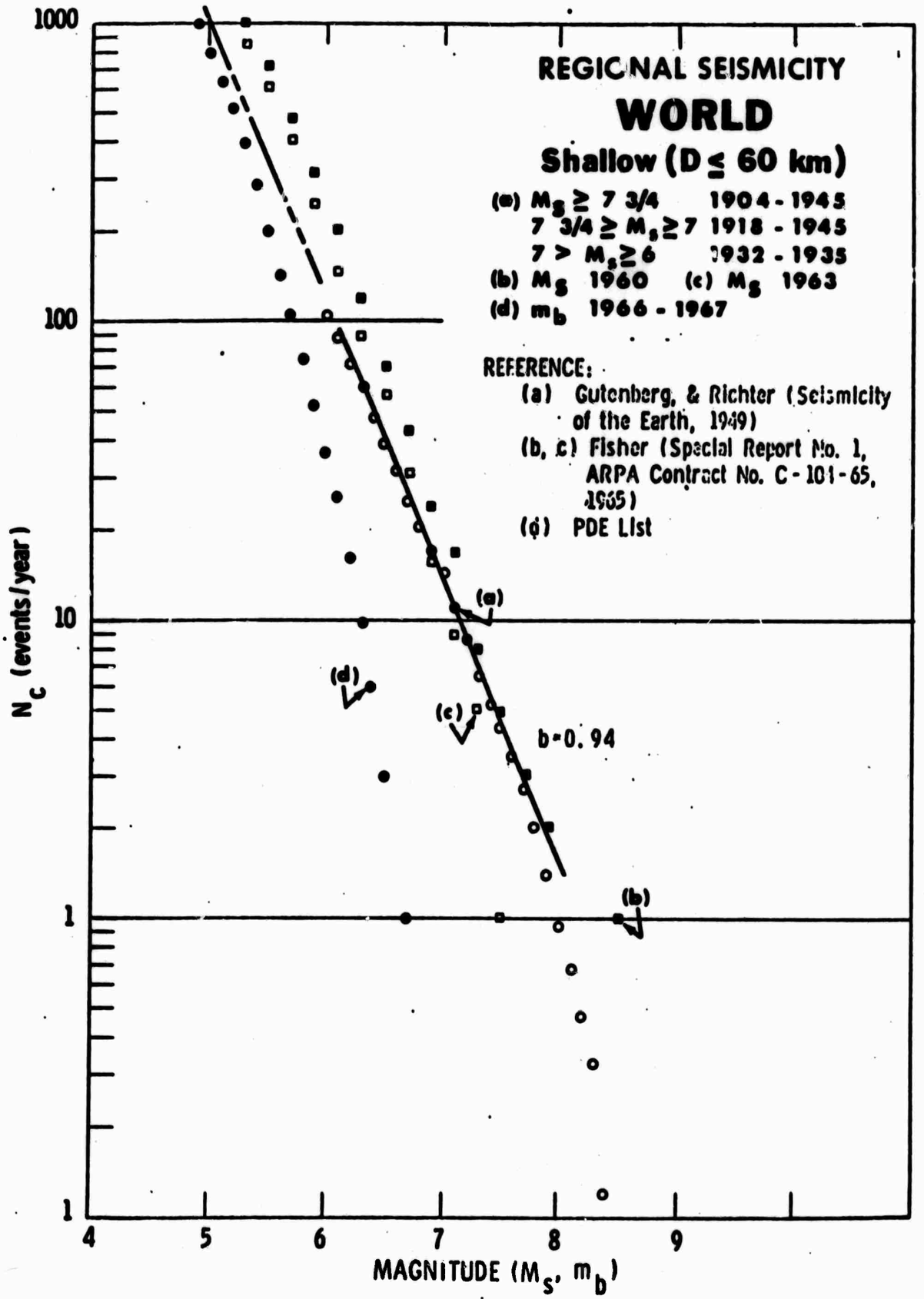
REGIONAL SEISMICITY
WORLD
Shallow (D ≤ 60 km)
(a) $M_s \geq 7\ 3/4$ 1904 - 1945
$7\ 3/4 \geq M_s \geq 7$ 1918 - 1945
$7 > M_s \geq 6$ 1932 - 1935
(b) M_s 1960 (c) M_s 1963
(d) m_b 1966 - 1967
REFERENCE:
(a) Gutenberg, & Richter (Seismicity of the Earth, 1949)
(b, c) Fisher (Special Report No. 1, ARPA Contract No. C-101-65, 1965)
(d) PDE List
b=0.94
(a)
(b)
(c)
(d)
1000
100
10
1
1
4
5
6
7
8
9
N_c (events/year)
MAGNITUDE (M_s, m_b)

Figure 12.

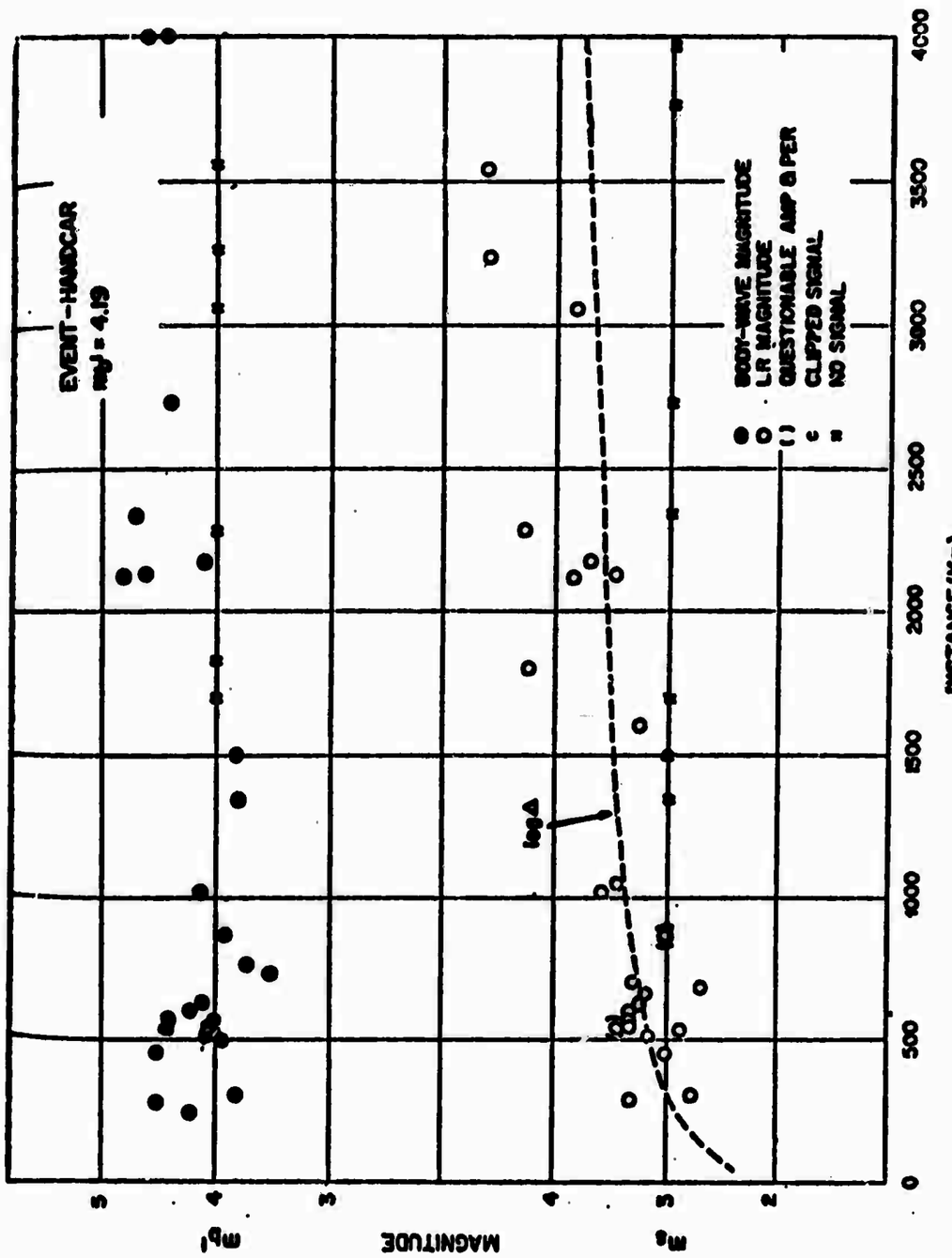
EVENT-HANDCAR
mbl = 4.19
BODY-WAVE MAGNITUDE
L.R MAGNITUDE
( ) QUESTIONABLE AMP & PER
C CLIPPED SIGNAL
N NO SIGNAL
log A
MAGNITUDE
DISTANCE (Km)
0
500
1000
1500
2000
2500
3000
3500
4000
5
4
3
4
3
2

Figure 13.

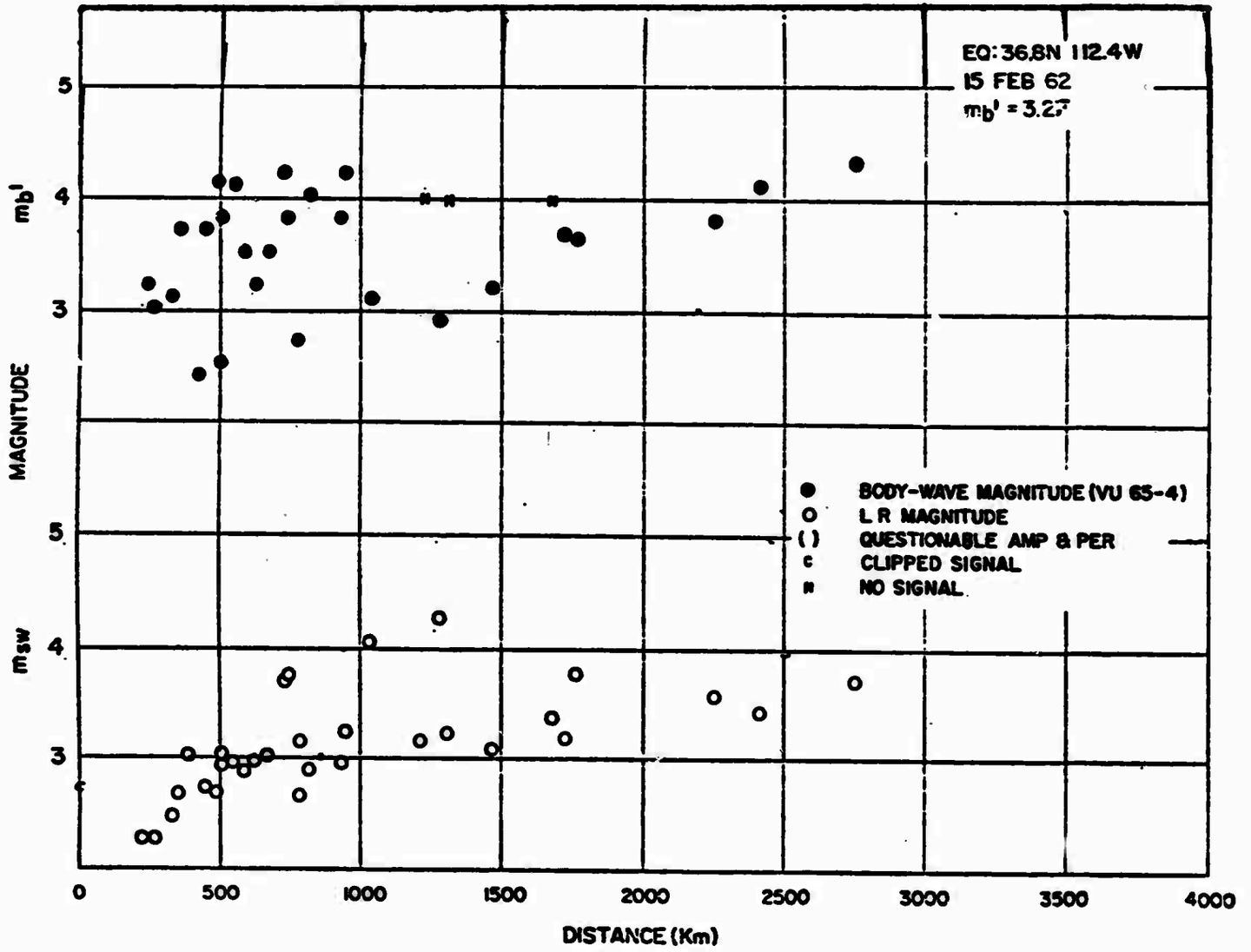
EQ: 36.8N 112.4W
15 FEB 62
mb' = 3.2?
MAGNITUDE
mb'
msw
5
4
3
5
4
3
0
500
1000
1500
2000
2500
3000
3500
4000
DISTANCE (Km)
BODY-WAVE MAGNITUDE (VU 65-4)
L R MAGNITUDE
( ) QUESTIONABLE AMP & PER
c CLIPPED SIGNAL
n NO SIGNAL

Figure 14.

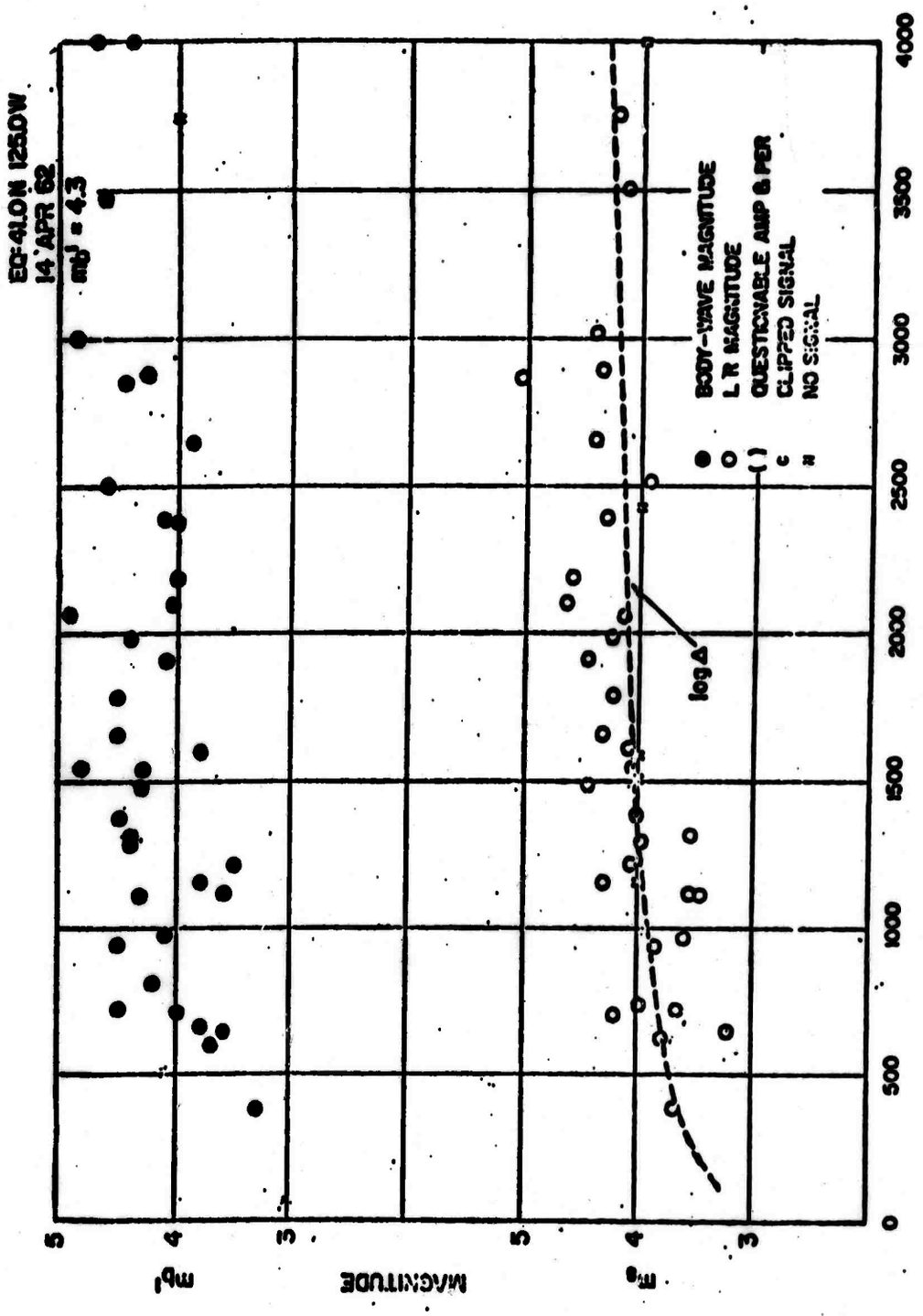
EDF-4 LON 125.0W
14 APR 62
mb = 4.3
BODY-WAVE MAGNITUDE
L R MAGNITUDE
QUESTIONABLE AMP & PER
CLIPPED SIGNAL
NO SIGNAL
log A
MAGNITUDE
DISTANCE (Km)
0
500
1000
1500
2000
2500
3000
3500
4000
3
4
5

Figure 15.

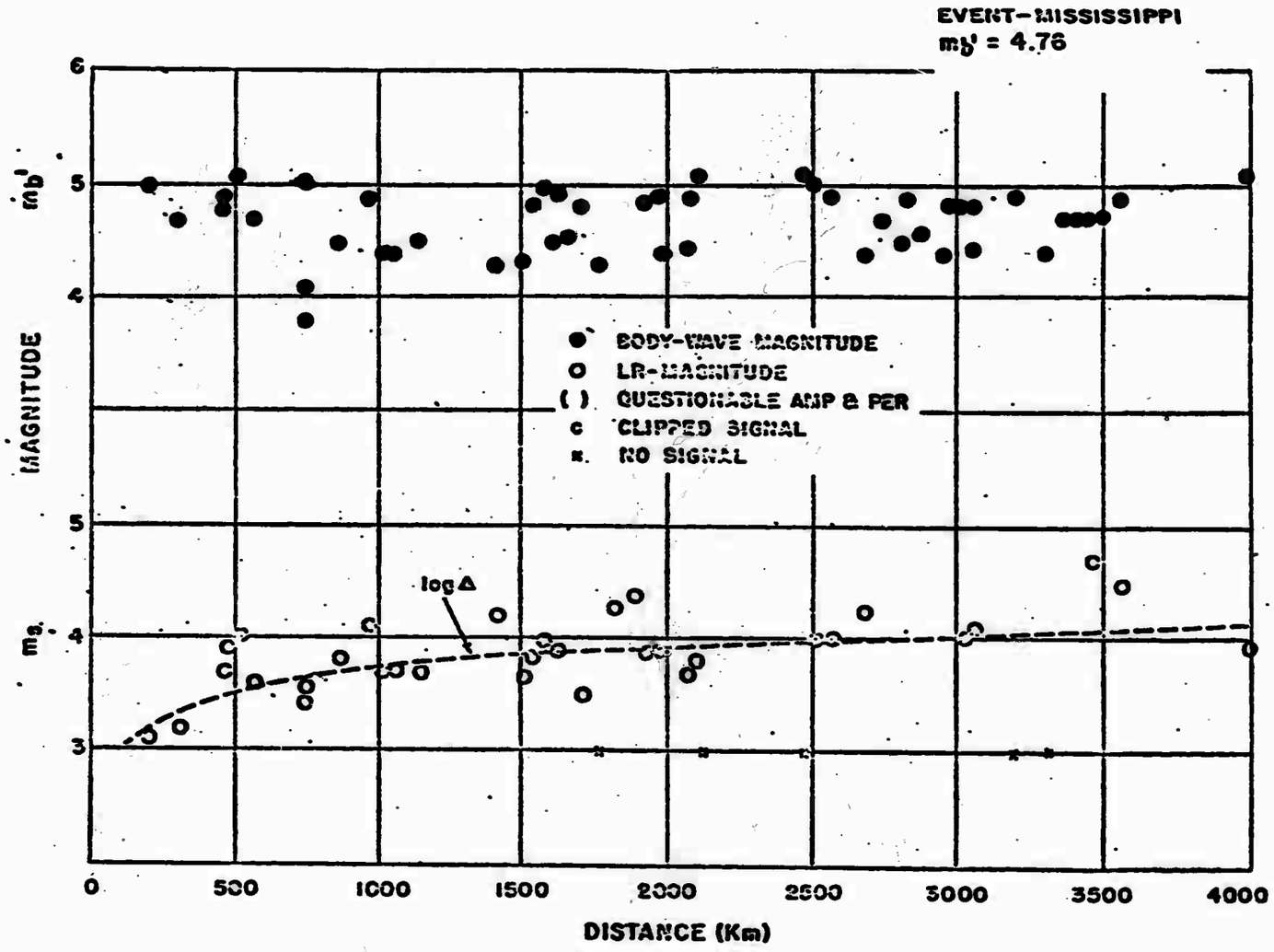
EVENT-MISSISSIPPI
mb' = 4.76
MAGNITUDE
mb'
ms
log Δ
BODY-WAVE MAGNITUDE
LR-MAGNITUDE
( ) QUESTIONABLE AMP & PER
c CLIPPED SIGNAL
x NO SIGNAL
6
5
4
5
4
3
0
500
1000
1500
2000
2500
3000
3500
4000
DISTANCE (Km)

Figure 16.

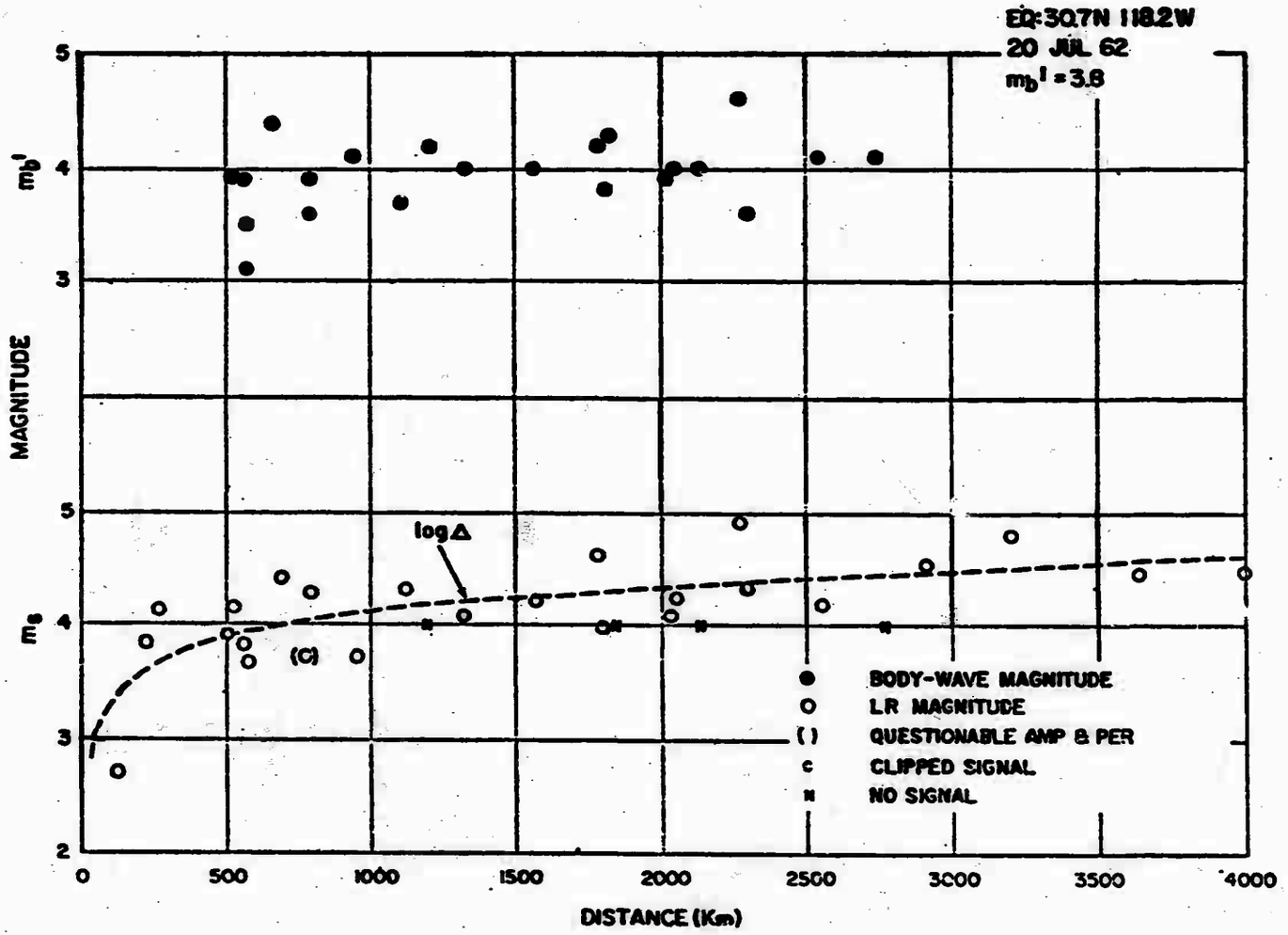
EQ:30.7N 118.2W
20 JUL 62
m_b^1 = 3.8
MAGNITUDE
m_b^1
m_s
log Δ
(C)
BODY-WAVE MAGNITUDE
LR MAGNITUDE
( ) QUESTIONABLE AMP & PER
c CLIPPED SIGNAL
n NO SIGNAL
DISTANCE (Km)
0
500
1000
1500
2000
2500
3000
3500
4000
2
3
4
5

Figure 17.

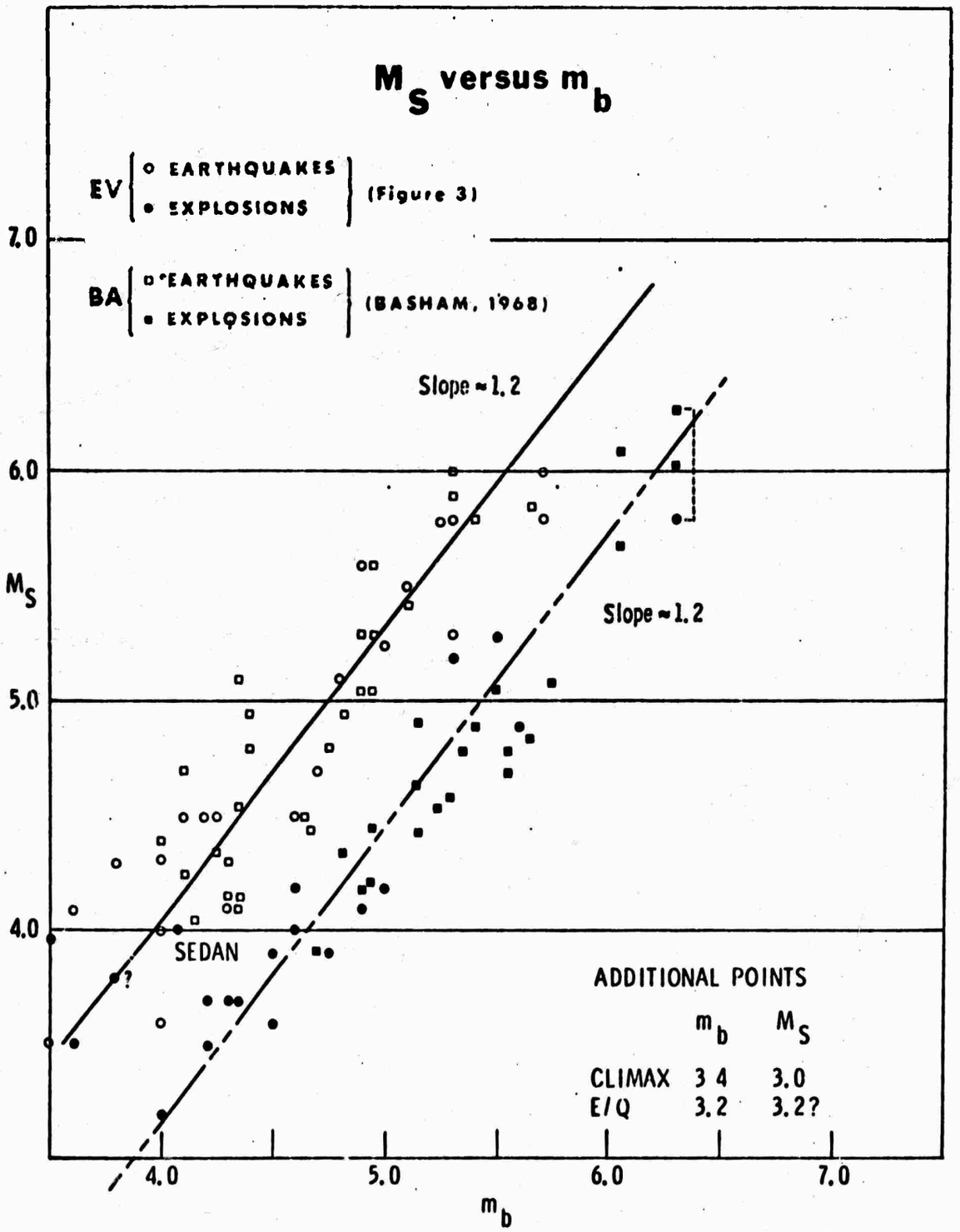
M_S versus m_b
EV
EARTHQUAKES
EXPLOSIONS
(Figure 3)
BA
EARTHQUAKES
EXPLOSIONS
(BASHAM, 1968)
Slope ≈ 1.2
Slope ≈ 1.2
SEDAN
?
ADDITIONAL POINTS
m_b M_S
CLIMAX 3.4 3.0
E/Q 3.2 3.2?
7.0
6.0
5.0
4.0
M_S
4.0
5.0
6.0
7.0
m_b

Figure 18.

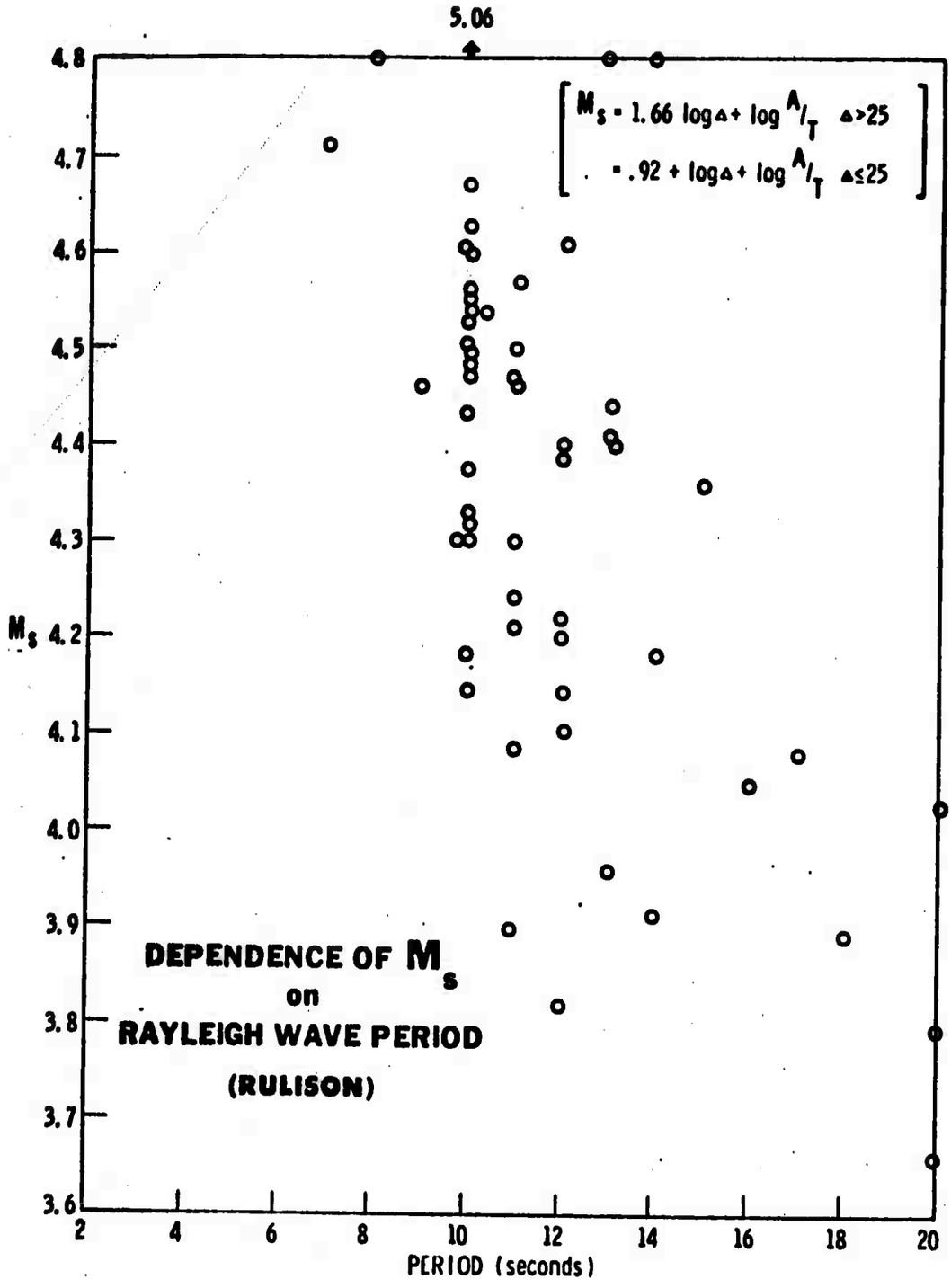
5.06
$M_S = 1.66 \log\Delta + \log A/T \quad \Delta > 25$
$= .92 + \log\Delta + \log A/T \quad \Delta \leq 25$
DEPENDENCE OF M_S
on
RAYLEIGH WAVE PERIOD
(RULISON)
M_S
4.8
4.7
4.6
4.5
4.4
4.3
4.2
4.1
4.0
3.9
3.8
3.7
3.6
2
4
6
8
10
12
14
16
18
20
PERIOD (seconds)

Figure 19.

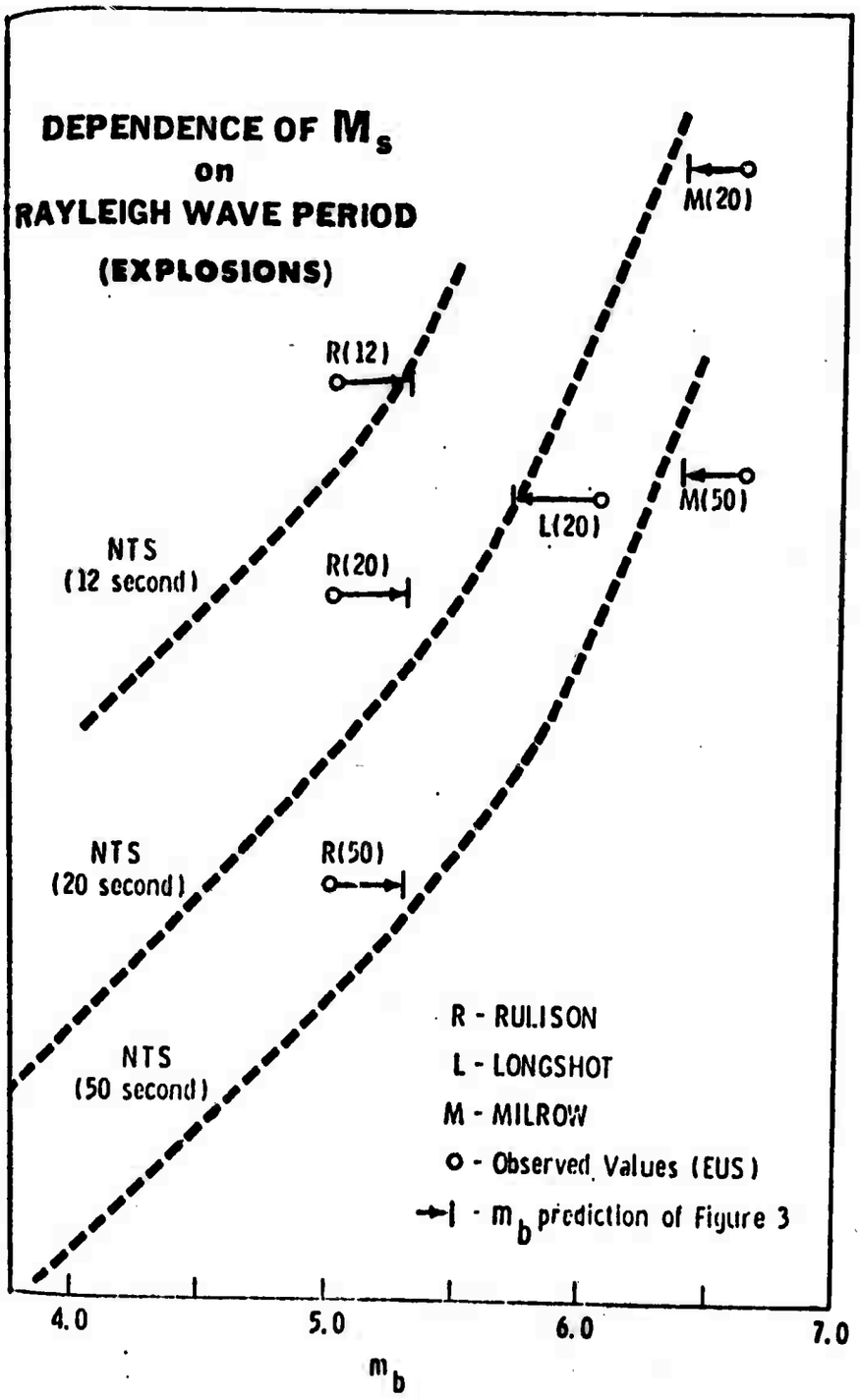
DEPENDENCE OF M_s
on
RAYLEIGH WAVE PERIOD
(EXPLOSIONS)
R(12)
M(20)
L(20)
M(50)
R(20)
NTS
(12 second)
R(50)
NTS
(20 second)
NTS
(50 second)
R - RULISON
L - LONGSHOT
M - MILROW
o - Observed Values (EUS)
→| - m_b prediction of Figure 3
4.0
5.0
6.0
7.0
m_b

Figure 20.

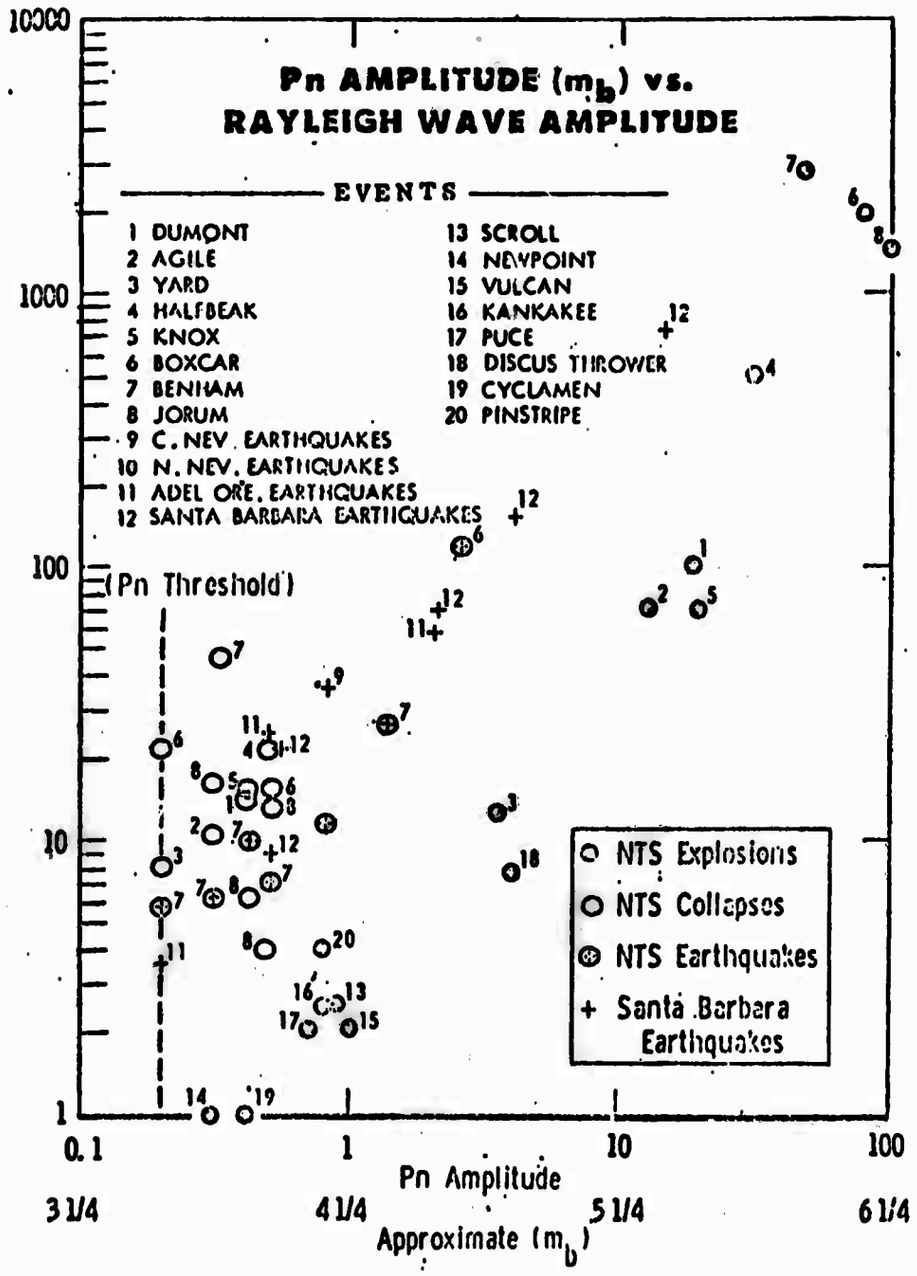

Data obtained at Berkely, California
Measured on Records Filtered 10-30 Seconds
Period - Maximum normally in 12-15 Seconds
period range.

Figure 21.

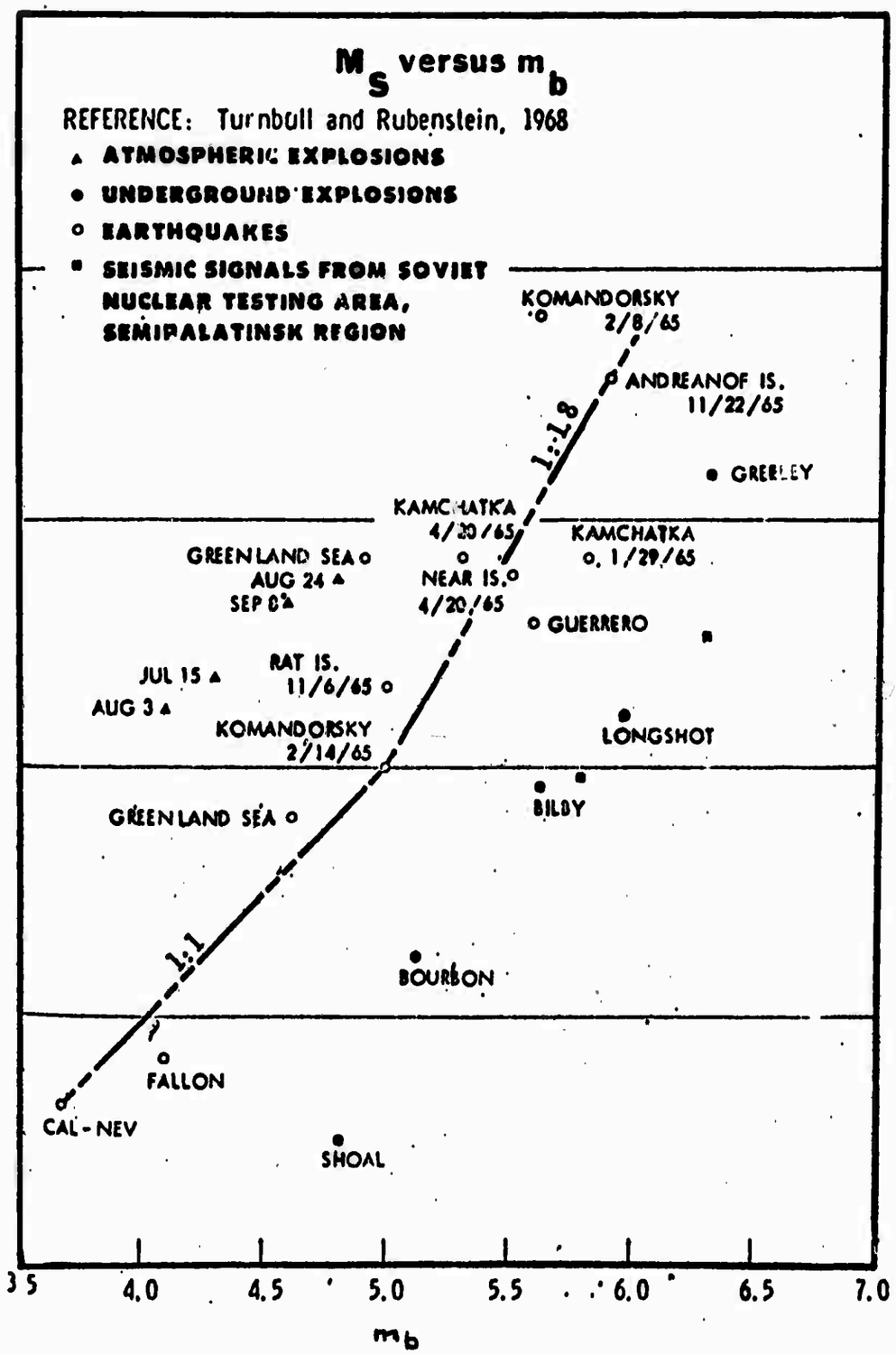
M_S versus m_b
REFERENCE: Turnbull and Rubenstein, 1968
ATMOSPHERIC EXPLOSIONS
UNDERGROUND EXPLOSIONS
EARTHQUAKES
SEISMIC SIGNALS FROM SOVIET NUCLEAR TESTING AREA, SEMIPALATINSK REGION
KOMANDORSKY 2/8/65
ANDREANOF IS. 11/22/65
1:1.8
GREELEY
KAMCHATKA 4/20/65
KAMCHATKA 1/29/65
GREENLAND SEA
AUG 24
SEP 0
NEAR IS. 4/20/65
GUERRERO
RAT IS. 11/6/65
JUL 15
AUG 3
KOMANDORSKY 2/14/65
LONGSHOT
BILBY
GREENLAND SEA
1:1
BOURBON
FALLON
CAL-NEV
SHOAL
3.5
4.0
4.5
5.0
5.5
6.0
6.5
7.0
m_b

Figure 22.

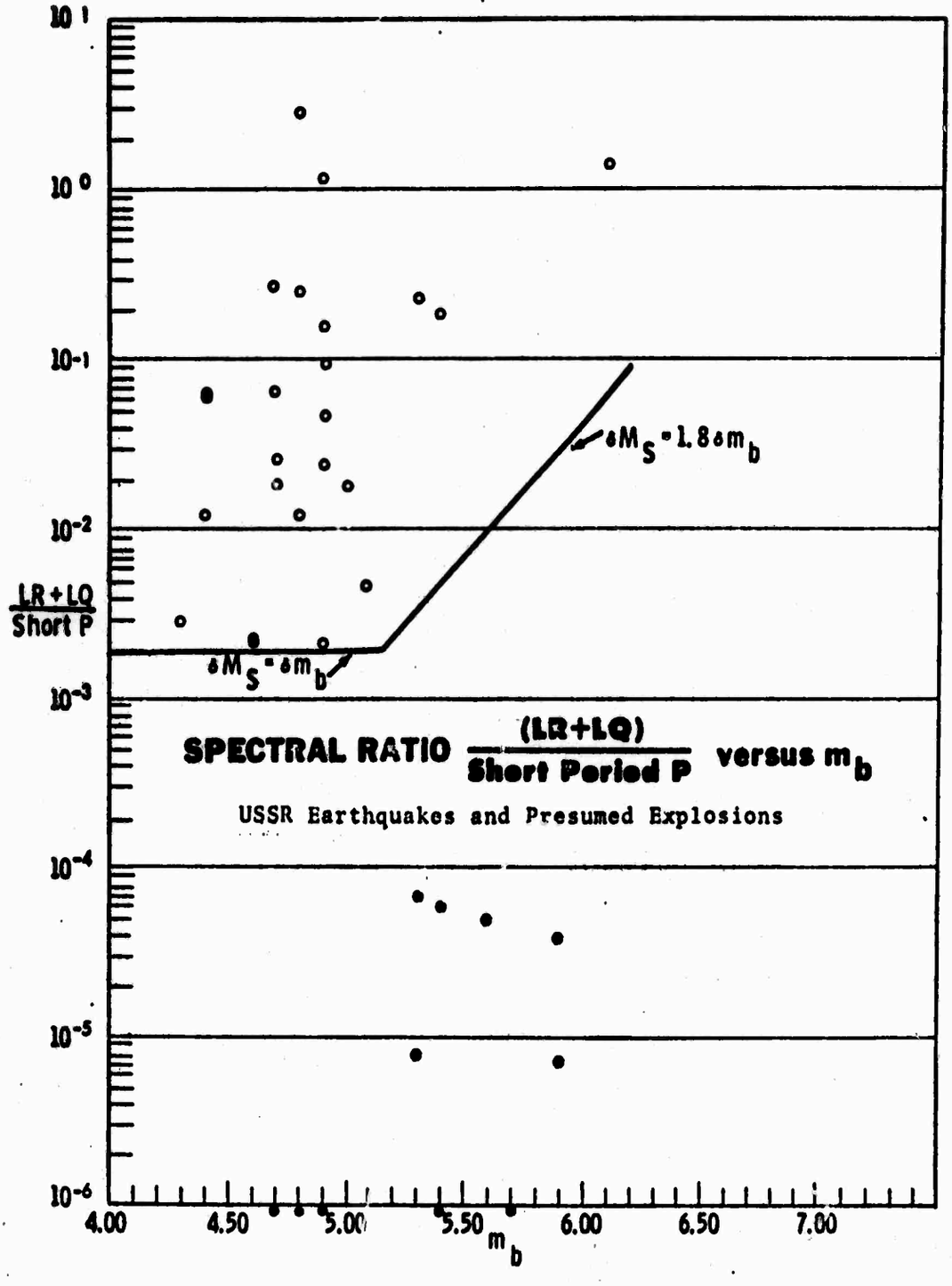
10 1
10 0
10-1
10-2
10-3
10-4
10-5
10-6
LR+LQ
Short P
δMS = 1.8δmb
δMS = δmb
SPECTRAL RATIO (LR+LQ) / Short Period P versus mb
USSR Earthquakes and Presumed Explosions
4.00
4.50
5.00
5.50
6.00
6.50
7.00
mb

Figure 23.

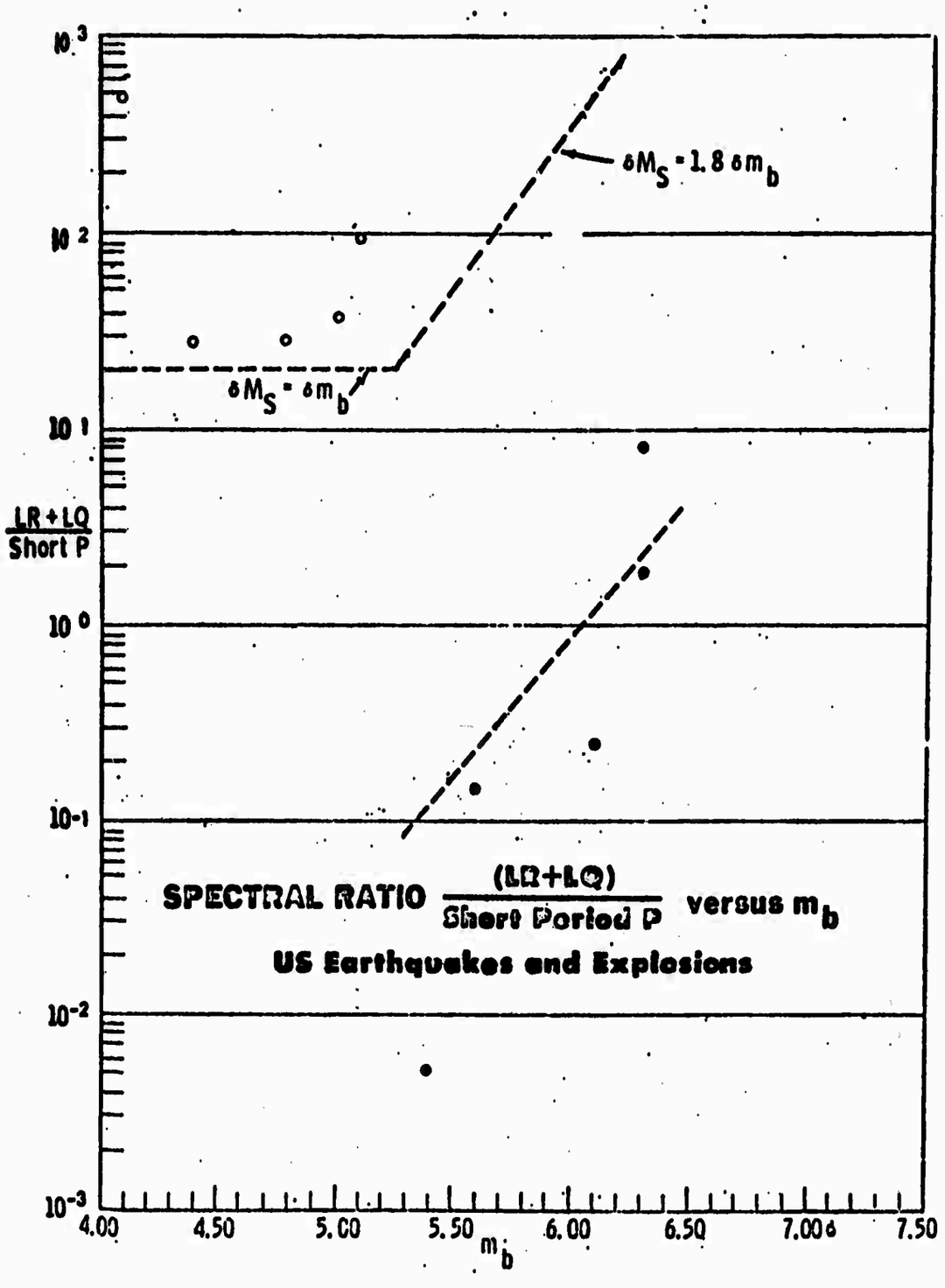
10^3
10^2
10^1
10^0
10^{-1}
10^{-2}
10^{-3}
$\delta M_S = 1.8\,\delta m_b$
$\delta M_S = \delta m_b$
LR+LQ / Short P
SPECTRAL RATIO (LR+LQ) / Short Period P versus m_b
US Earthquakes and Explosions
4.00
4.50
5.00
5.50
6.00
6.50
7.00
7.50
m_b

Figure 24.

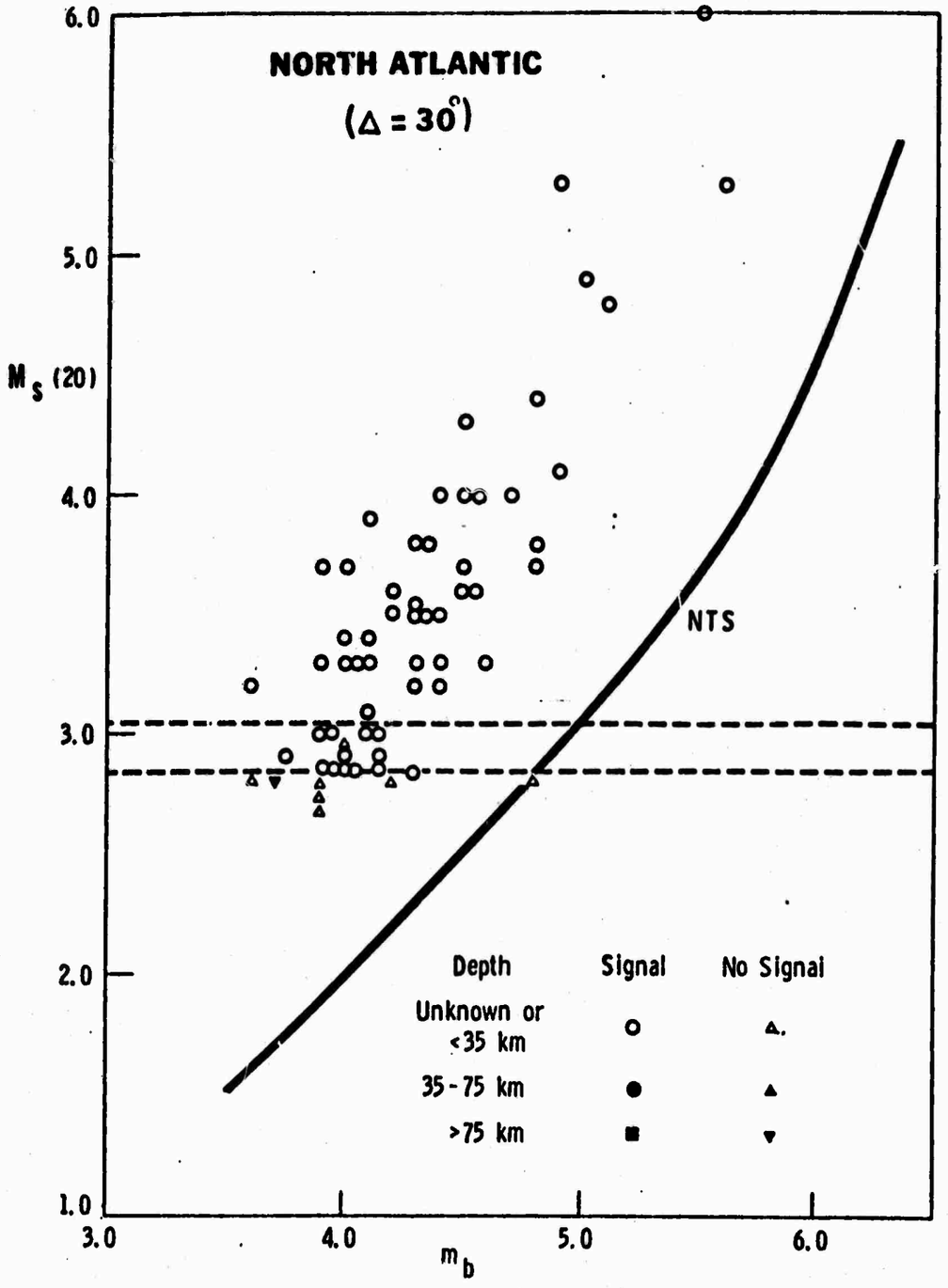
NORTH ATLANTIC
(Δ = 30°)
NTS
Depth
Signal
No Signal
Unknown or <35 km
35 - 75 km
>75 km
6.0
5.0
4.0
3.0
2.0
1.0
M_S (20)
3.0
4.0
5.0
6.0
m_b

Figure 25.

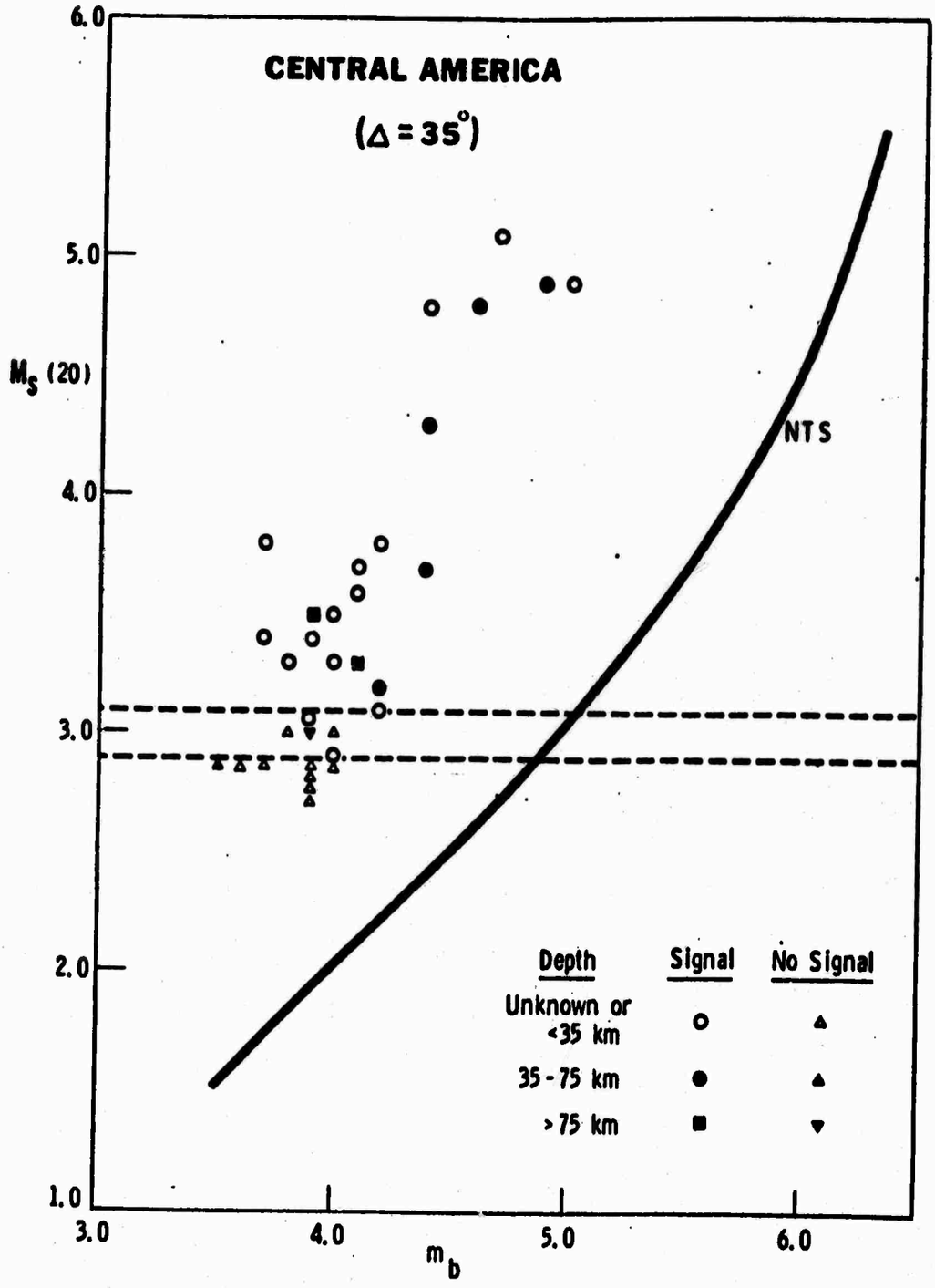
CENTRAL AMERICA
(Δ = 35°)
NTS
M_S (20)
m_b
6.0
5.0
4.0
3.0
2.0
1.0
3.0
4.0
5.0
6.0
Depth
Signal
No Signal
Unknown or <35 km
35 - 75 km
> 75 km

Figure 26.

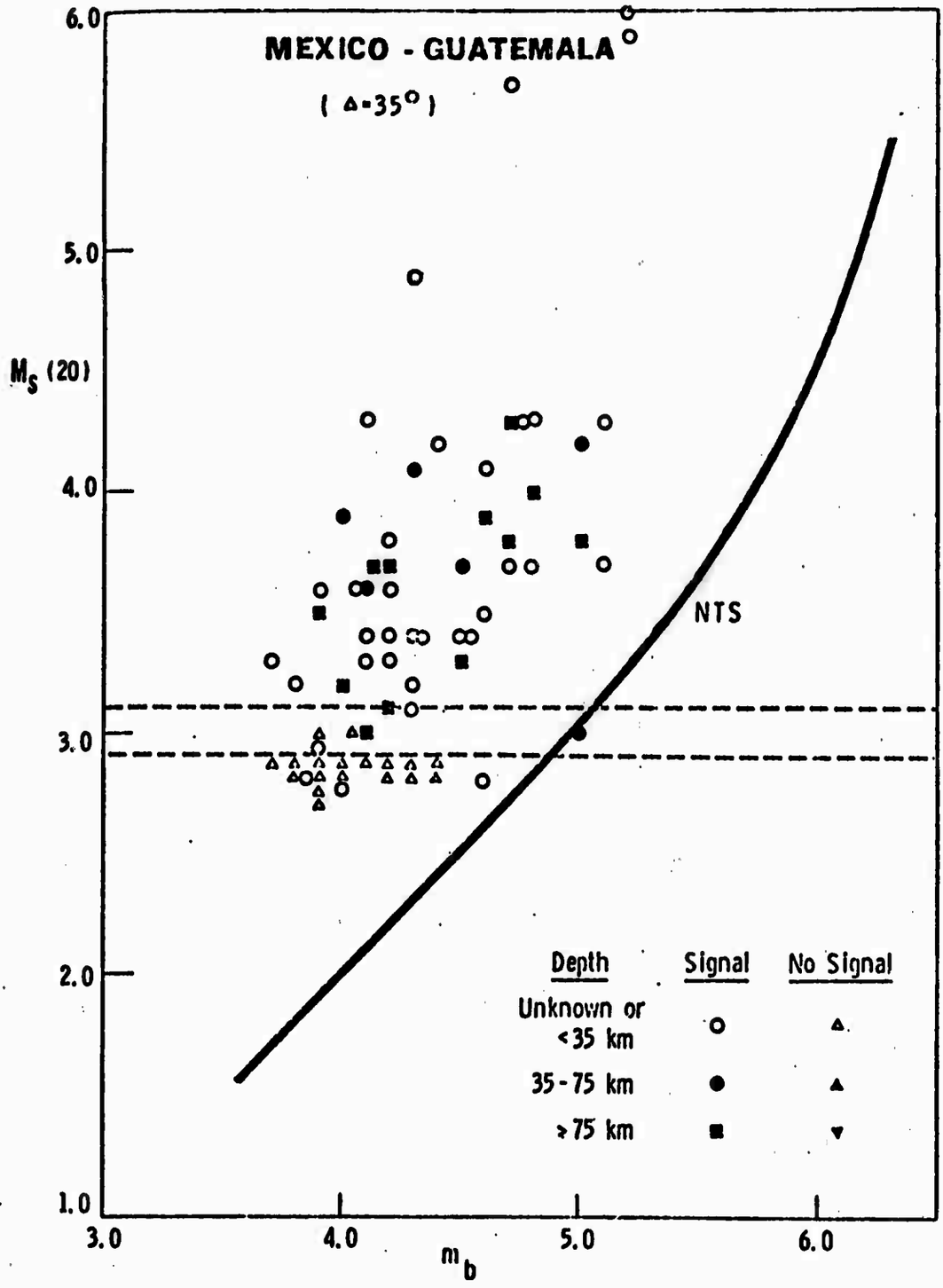
MEXICO - GUATEMALA
(Δ-35°)
NTS
Depth
Signal
No Signal
Unknown or <35 km
35-75 km
≥75 km
M_S (20)
m_b
6.0
5.0
4.0
3.0
2.0
1.0
3.0
4.0
5.0
6.0

Figure 27.

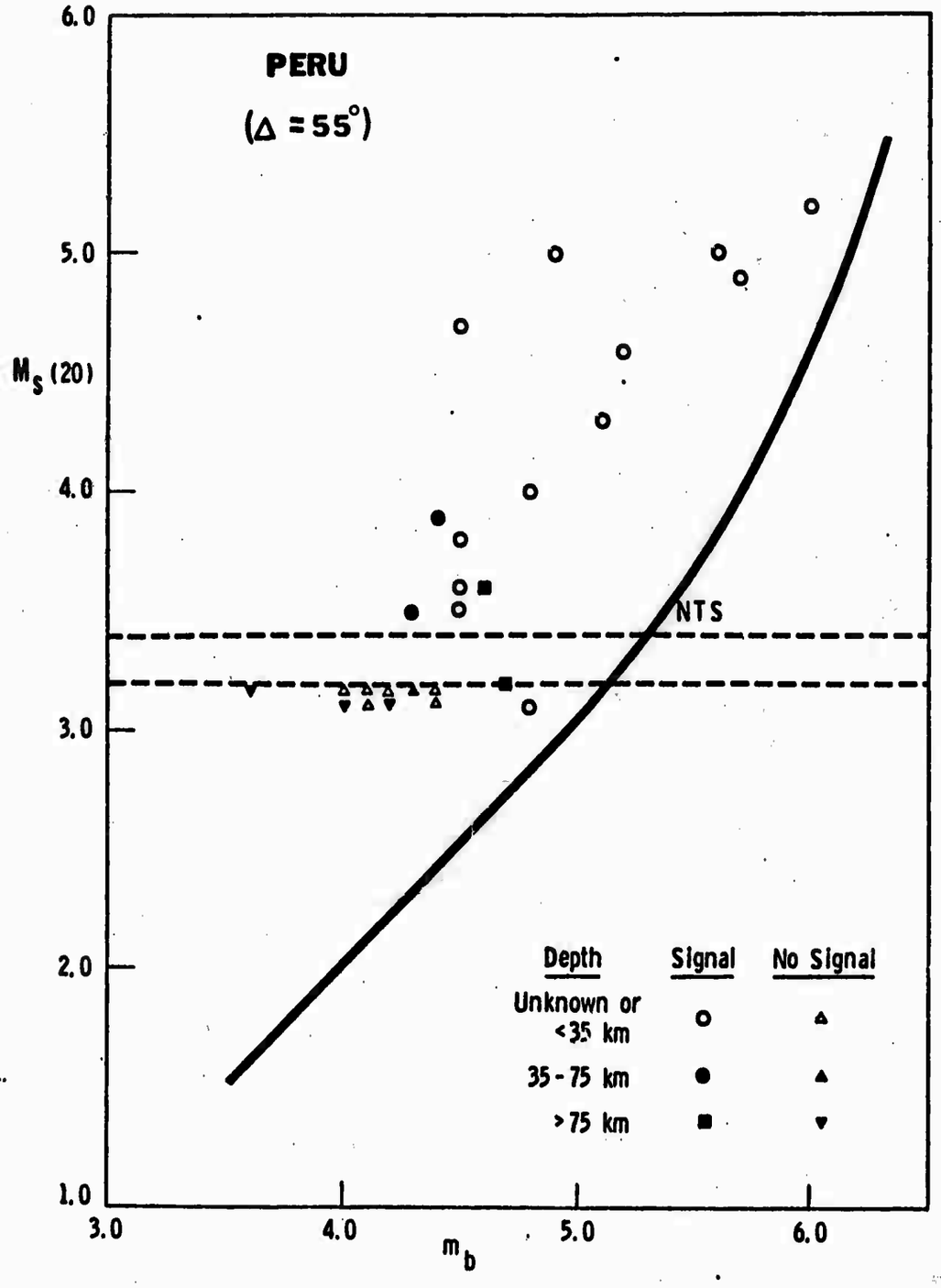
PERU
(Δ = 55°)
6.0
5.0
4.0
3.0
2.0
1.0
M_S (20)
NTS
Depth
Signal
No Signal
Unknown or <35 km
35 - 75 km
>75 km
3.0
4.0
5.0
6.0
m_b

Figure 28.

RAYLEIGH WAVE DETECTION CAPABILITY AT OGDENSBURG (Visual Analysis)

Region	Δ	Threshold	db for m_b 4
HONSHU	95°	4.5	10
KURILES	90°	4.5	10
HOKKAIDO	90°	4.5	10
ALEUTIANS	70°	4.4	8
ALEUTIANS	60°	4.4	8
SINKIANG	85°	4.5	10
GREECE/BALKANS/ TURKEY	80°	4.4	7
NEW HEBRIDES BIS/SOL	120°	4.5	10
MEXICO/GUATEMALA	35°	4.4	8
MINDANAO	130°	4.5	10
PERU	55°	4.4	8
GALAPAGOS	50°	4.0	0
KAMCHATKA	80°	4.4	8
C. AMERICA	35°	3.9	-2

Figure 29.

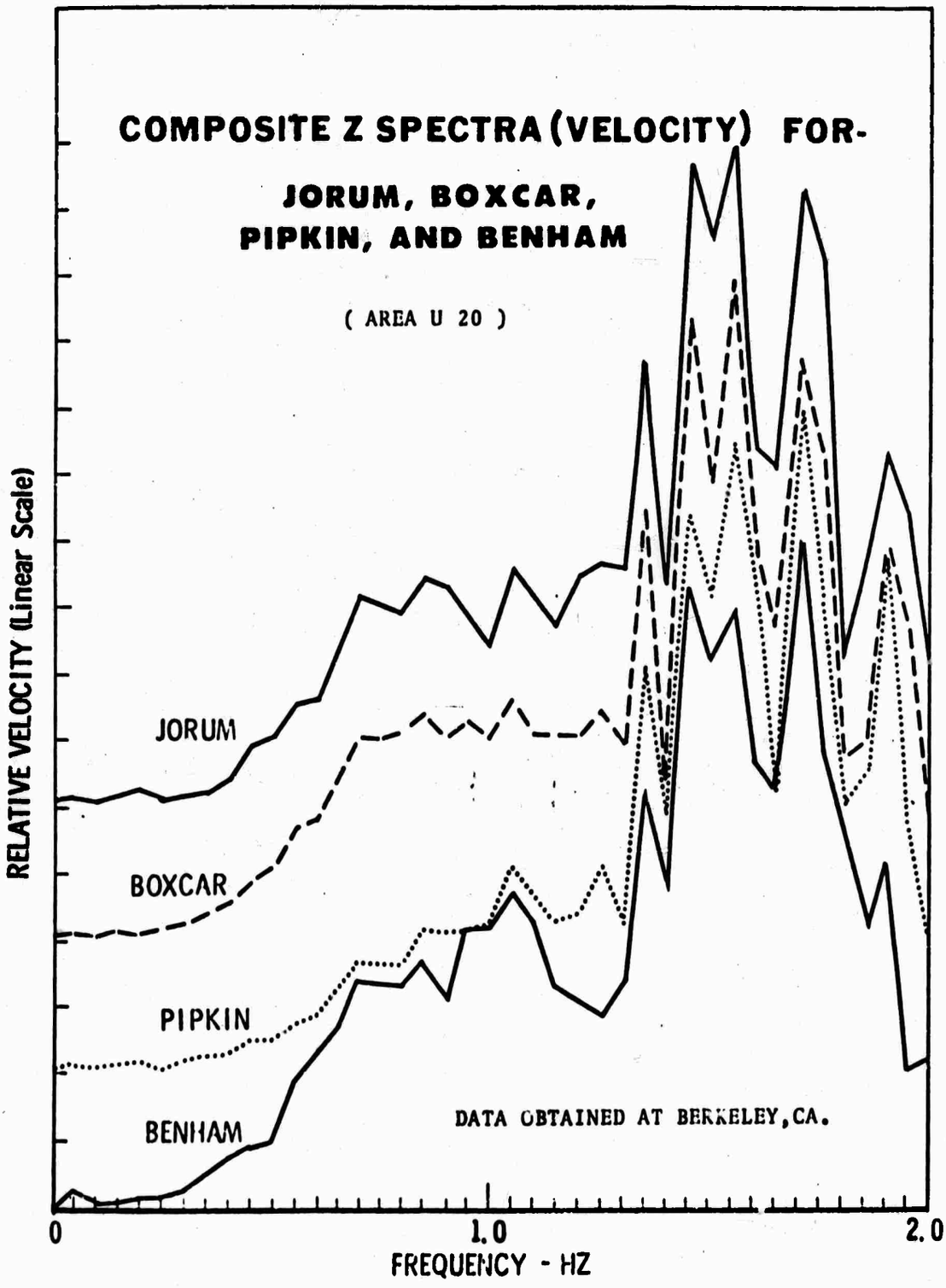
COMPOSITE Z SPECTRA (VELOCITY) FOR-
JORUM, BOXCAR,
PIPKIN, AND BENHAM
(AREA U 20)
RELATIVE VELOCITY (Linear Scale)
JORUM
BOXCAR
PIPKIN
BENHAM
DATA OBTAINED AT BERKELEY, CA.
0
1.0
2.0
FREQUENCY - HZ

Figure 30.

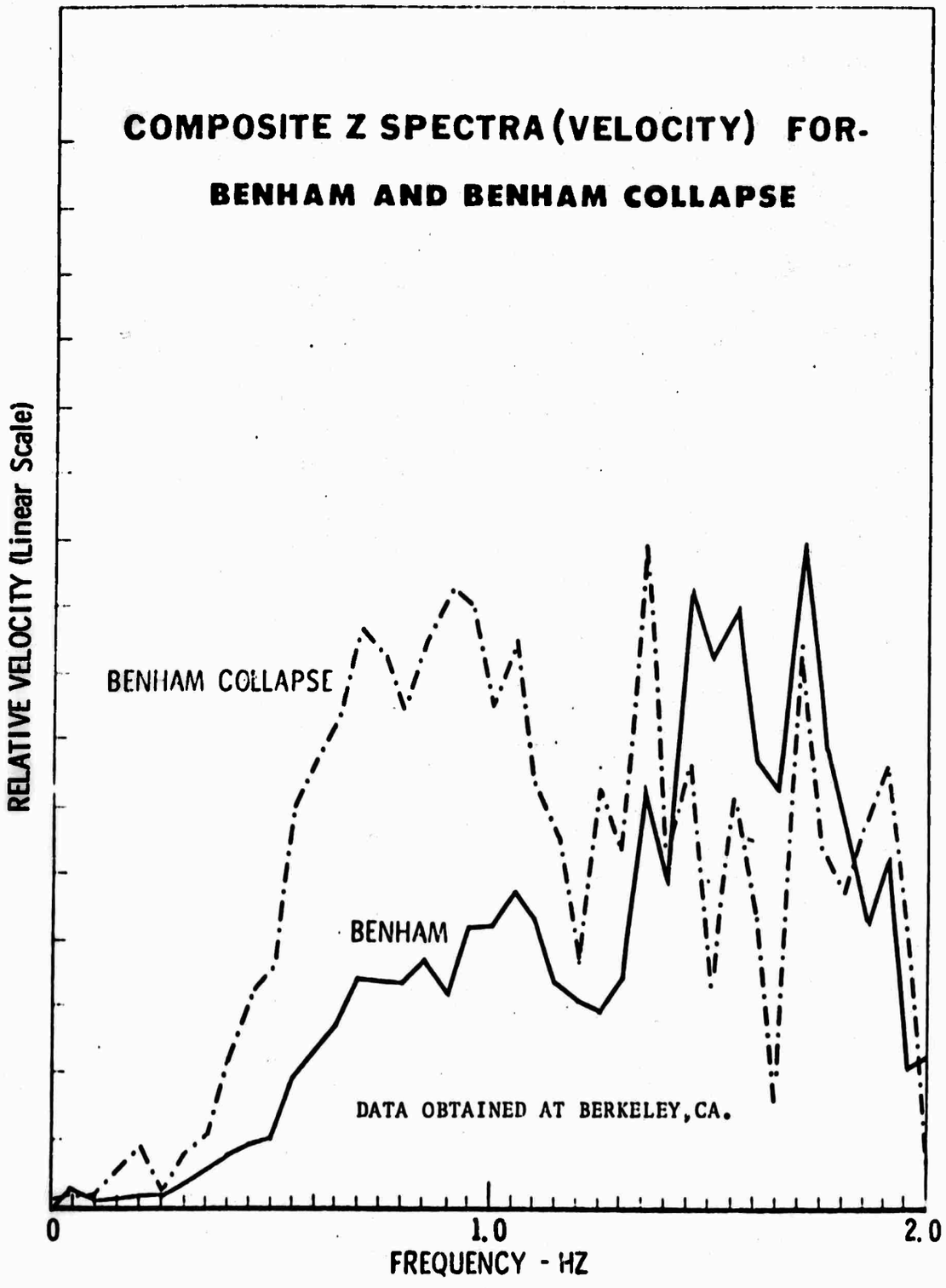
COMPOSITE Z SPECTRA (VELOCITY) FOR-
BENHAM AND BENHAM COLLAPSE
RELATIVE VELOCITY (Linear Scale)
BENHAM COLLAPSE
BENHAM
DATA OBTAINED AT BERKELEY, CA.
0
1.0
2.0
FREQUENCY - HZ

Figure 31.

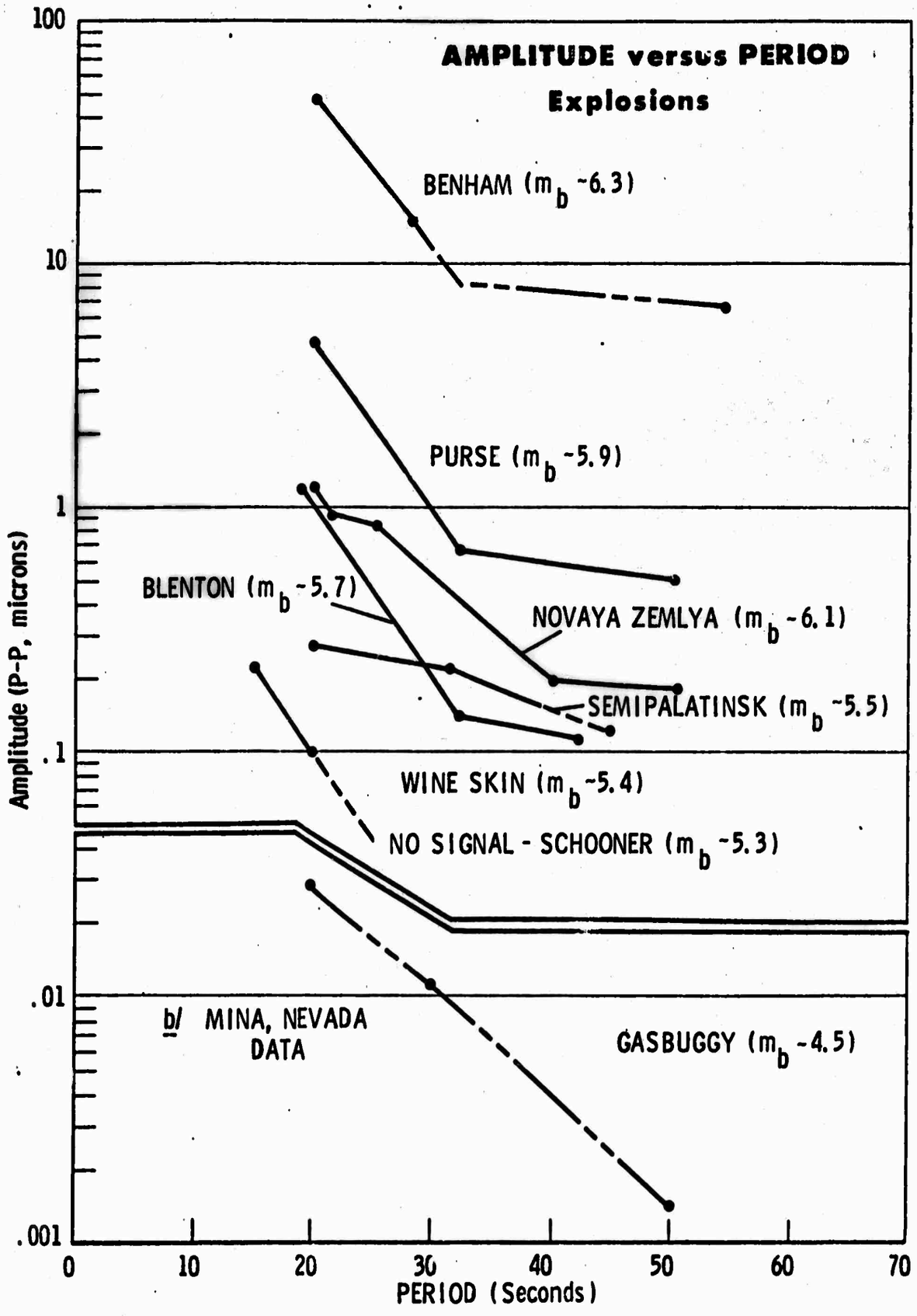
AMPLITUDE versus PERIOD
Explosions
BENHAM (m_b -6.3)
PURSE (m_b -5.9)
BLENTON (m_b -5.7)
NOVAYA ZEMLYA (m_b -6.1)
SEMIPALATINSK (m_b -5.5)
WINE SKIN (m_b -5.4)
NO SIGNAL - SCHOONER (m_b -5.3)
b/ MINA, NEVADA DATA
GASBUGGY (m_b -4.5)
Amplitude (P-P, microns)
100
10
1
.1
.01
.001
0
10
20
30
40
50
60
70
PERIOD (Seconds)

Figure 32.

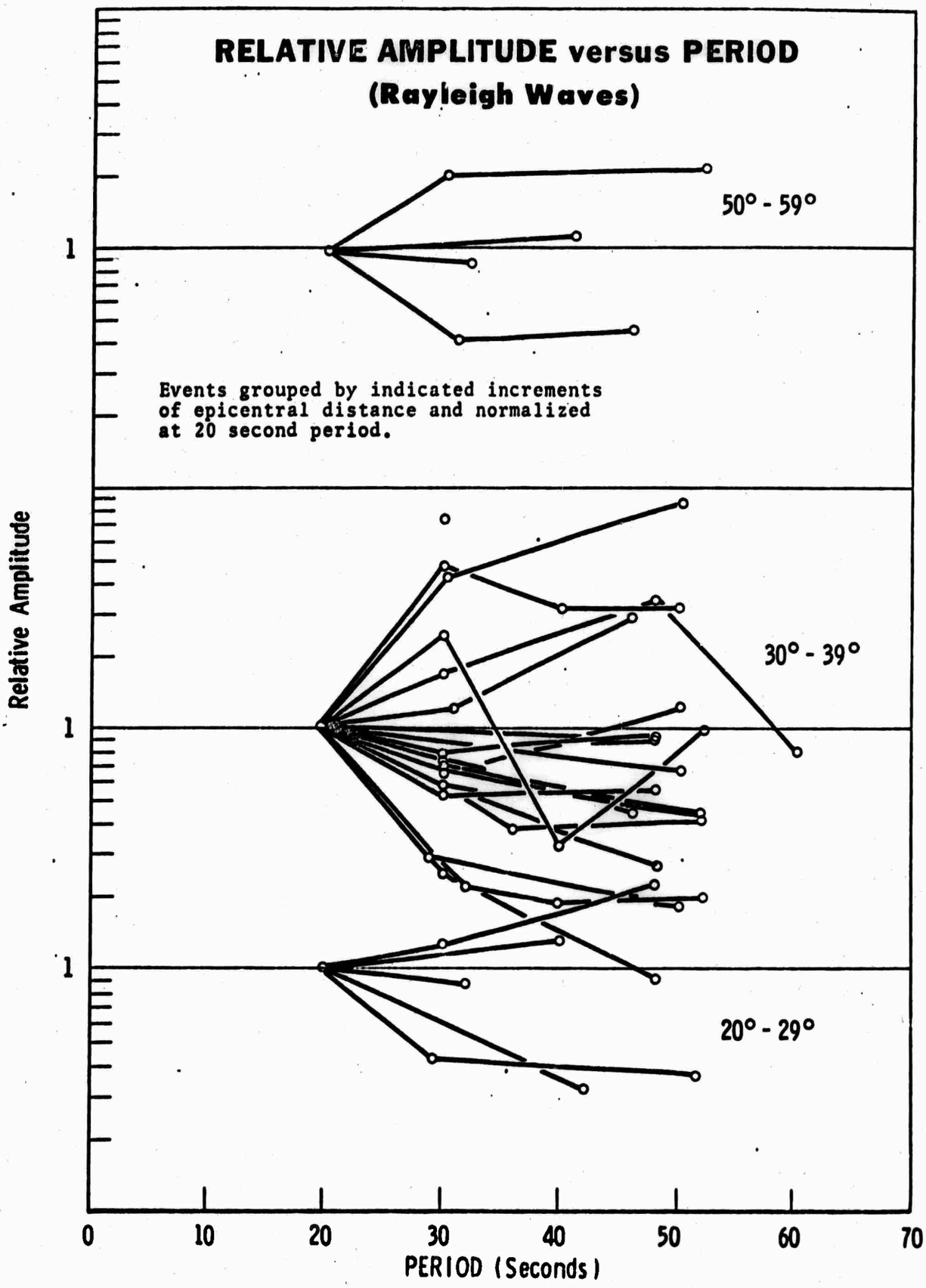
RELATIVE AMPLITUDE versus PERIOD
(Rayleigh Waves)
50° - 59°
Events grouped by indicated increments
of epicentral distance and normalized
at 20 second period.
30° - 39°
20° - 29°
1
1
1
Relative Amplitude
0
10
20
30
40
50
60
70
PERIOD (Seconds)

Figure 33.

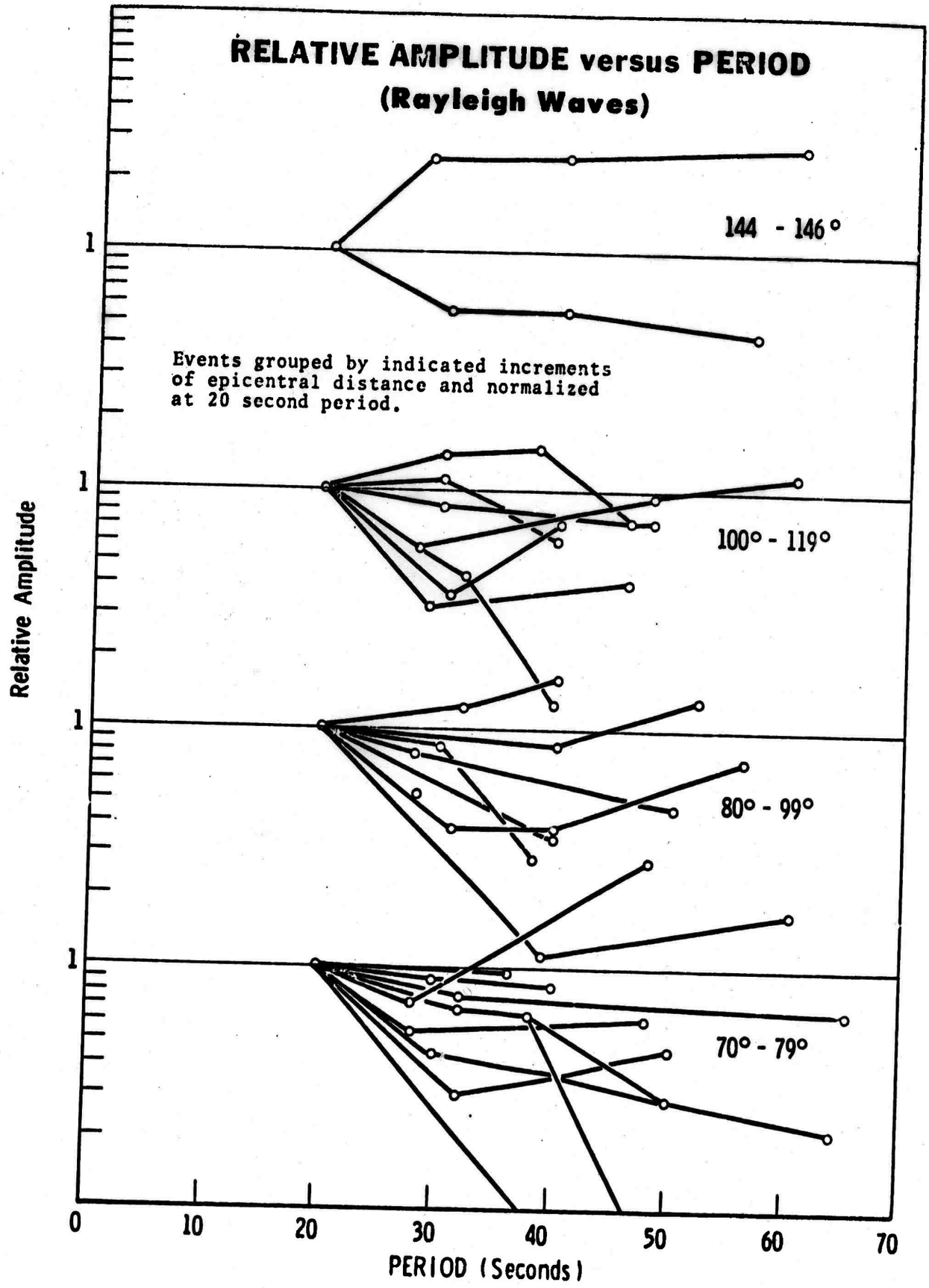
RELATIVE AMPLITUDE versus PERIOD
(Rayleigh Waves)
144 - 146°
Events grouped by indicated increments of epicentral distance and normalized at 20 second period.
100° - 119°
80° - 99°
70° - 79°
Relative Amplitude
1
1
1
1
0
10
20
30
40
50
60
70
PERIOD (Seconds)

Figure 34.

LOG A_{100} VERSUS M_S

A_{100} = AMPLITUDE OF 100 SEC. RAYLEIGH WAVES NORMALIZED TO 90°

M_S BASED ON 20 SEC. RAYLEIGH WAVES

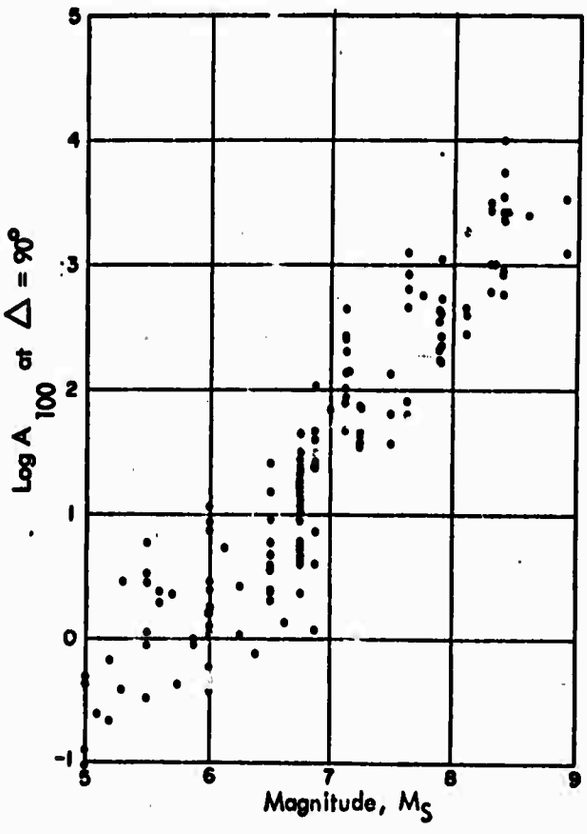

REF. BRUNE, J.N., AND CHI-YU KING, 1967

Figure 35.

Amplitude ratios of Rayleigh wave spectra from GASBUGGY and the comparison earthquake

REFERENCE: Rasmussen and Laude, 1968

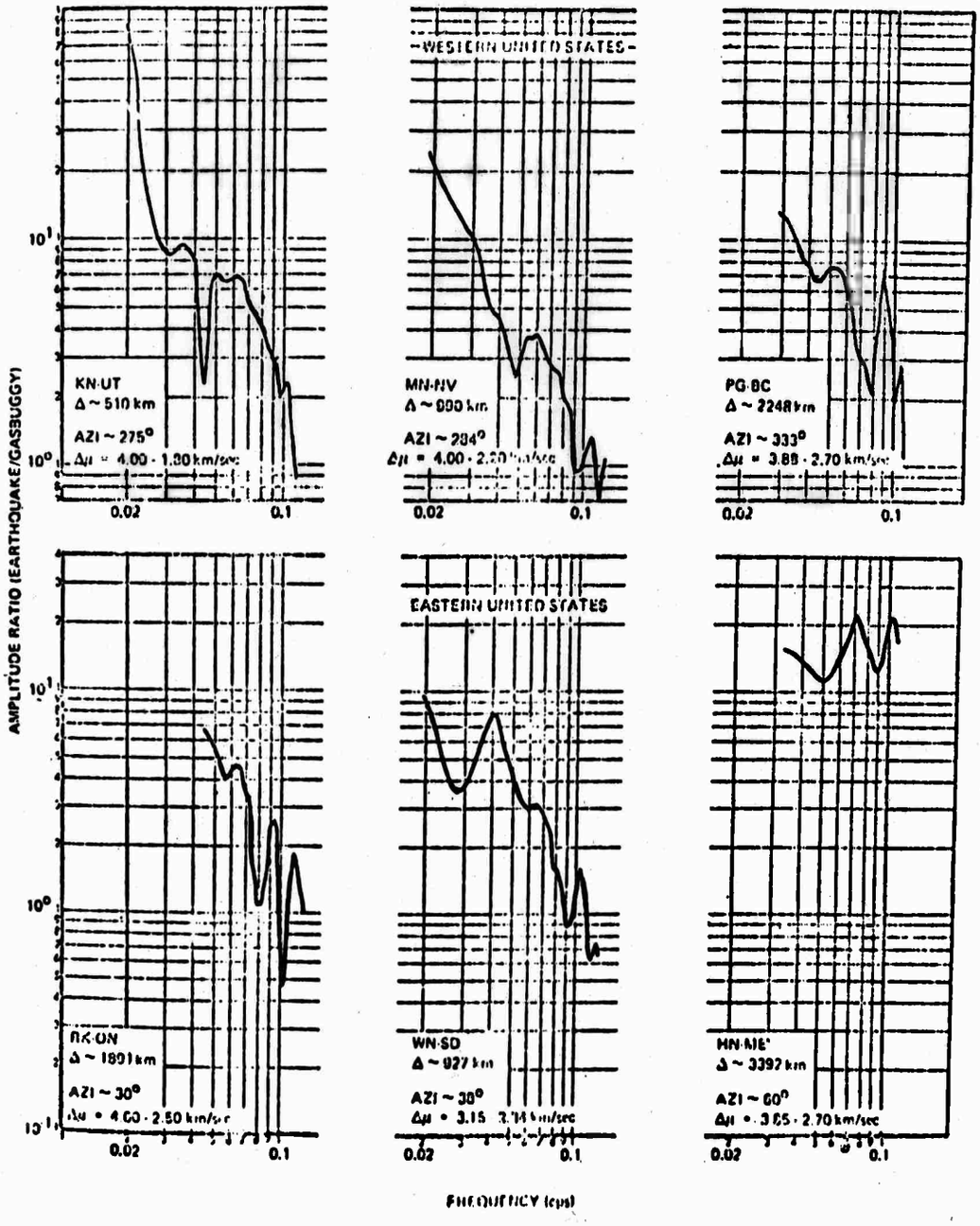

Figure 36.

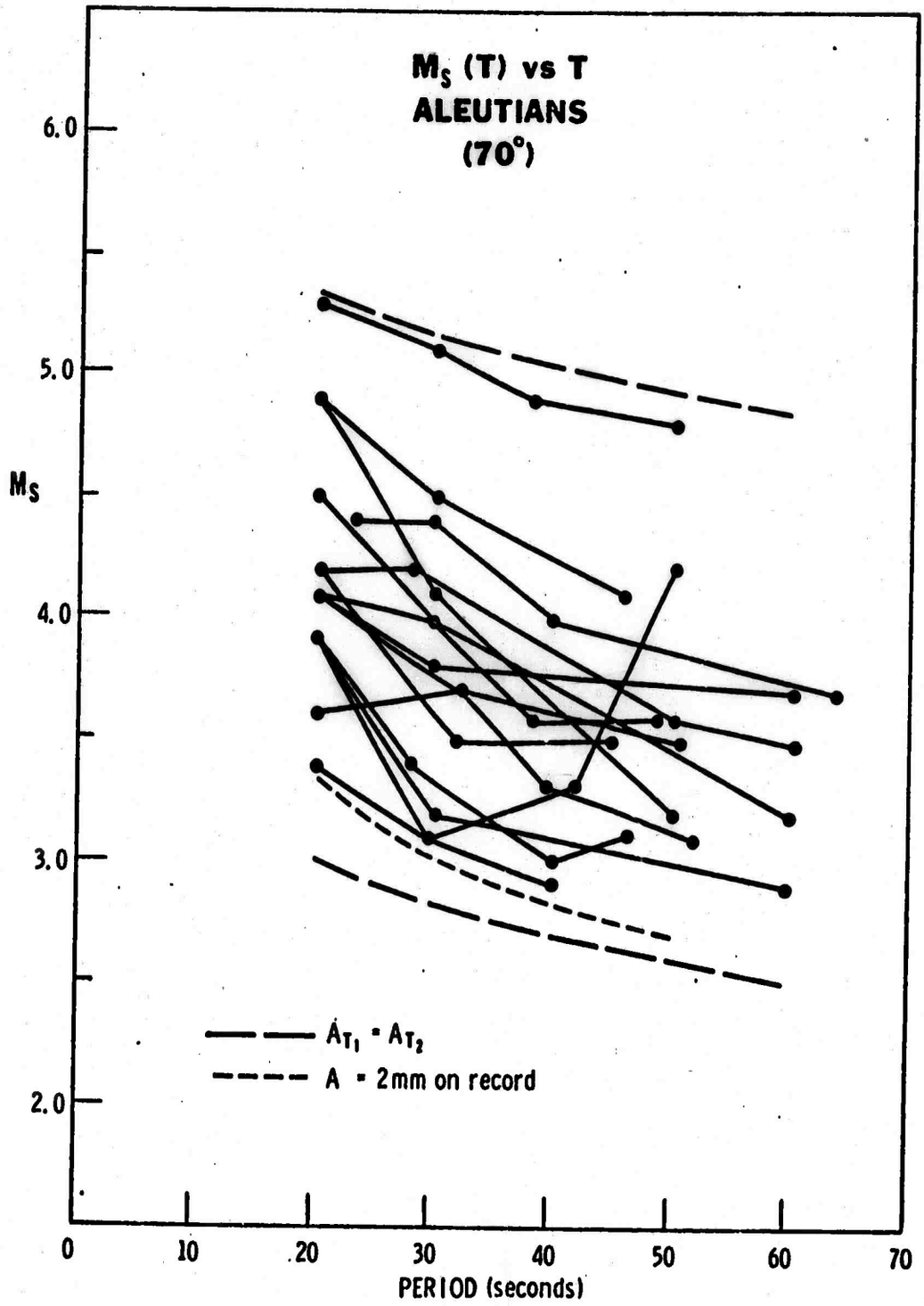
M_S (T) vs T
ALEUTIANS
(70°)
6.0
5.0
4.0
3.0
2.0
M_S
$A_{T_1} = A_{T_2}$
A = 2mm on record
0
10
20
30
40
50
60
70
PERIOD (seconds)

Figure 37.

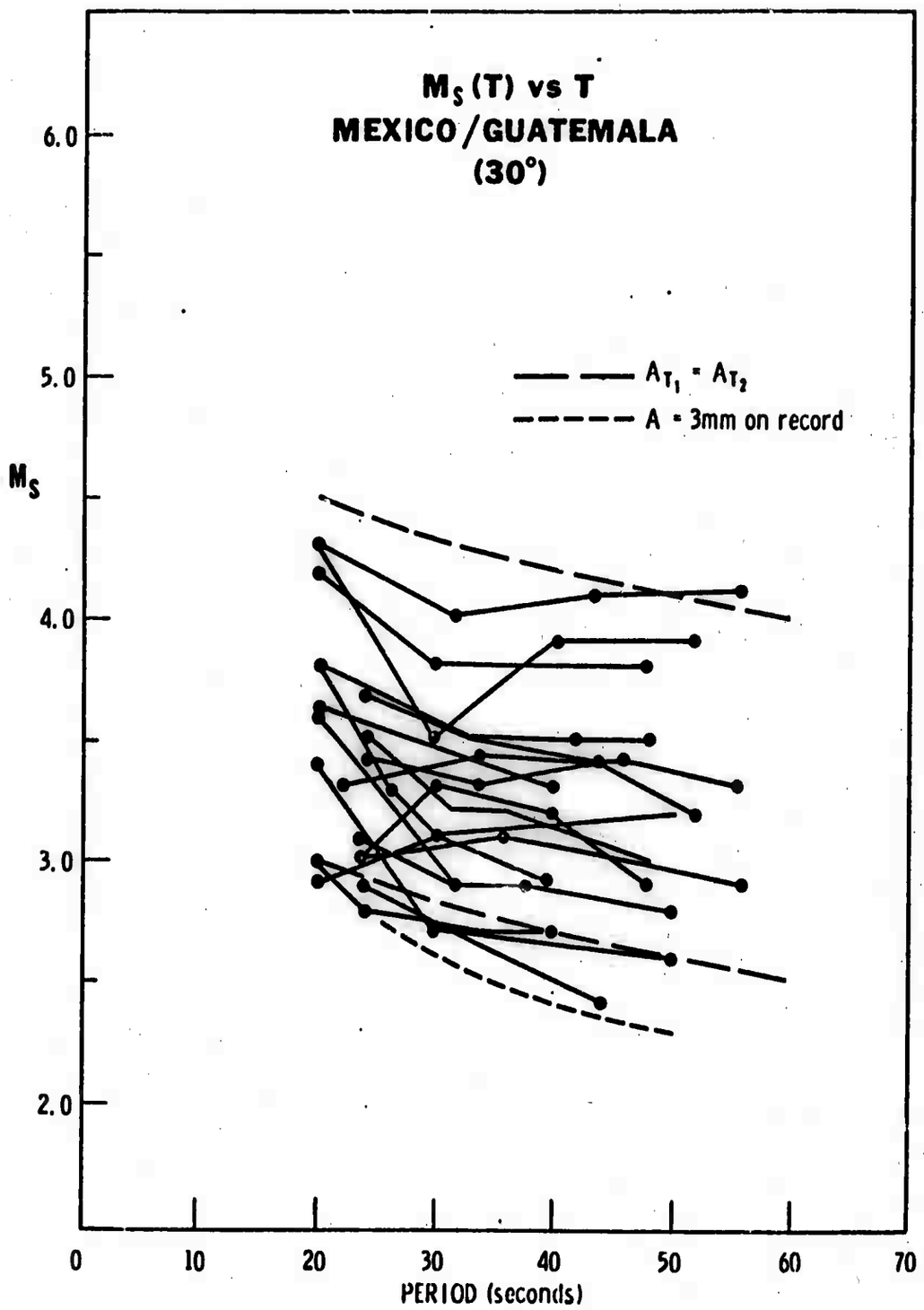
M_S (T) vs T
MEXICO/GUATEMALA
(30°)
$A_{T_1} = A_{T_2}$
A = 3mm on record
M_S
6.0
5.0
4.0
3.0
2.0
0
10
20
30
40
50
60
70
PERIOD (seconds)

Figure 38.

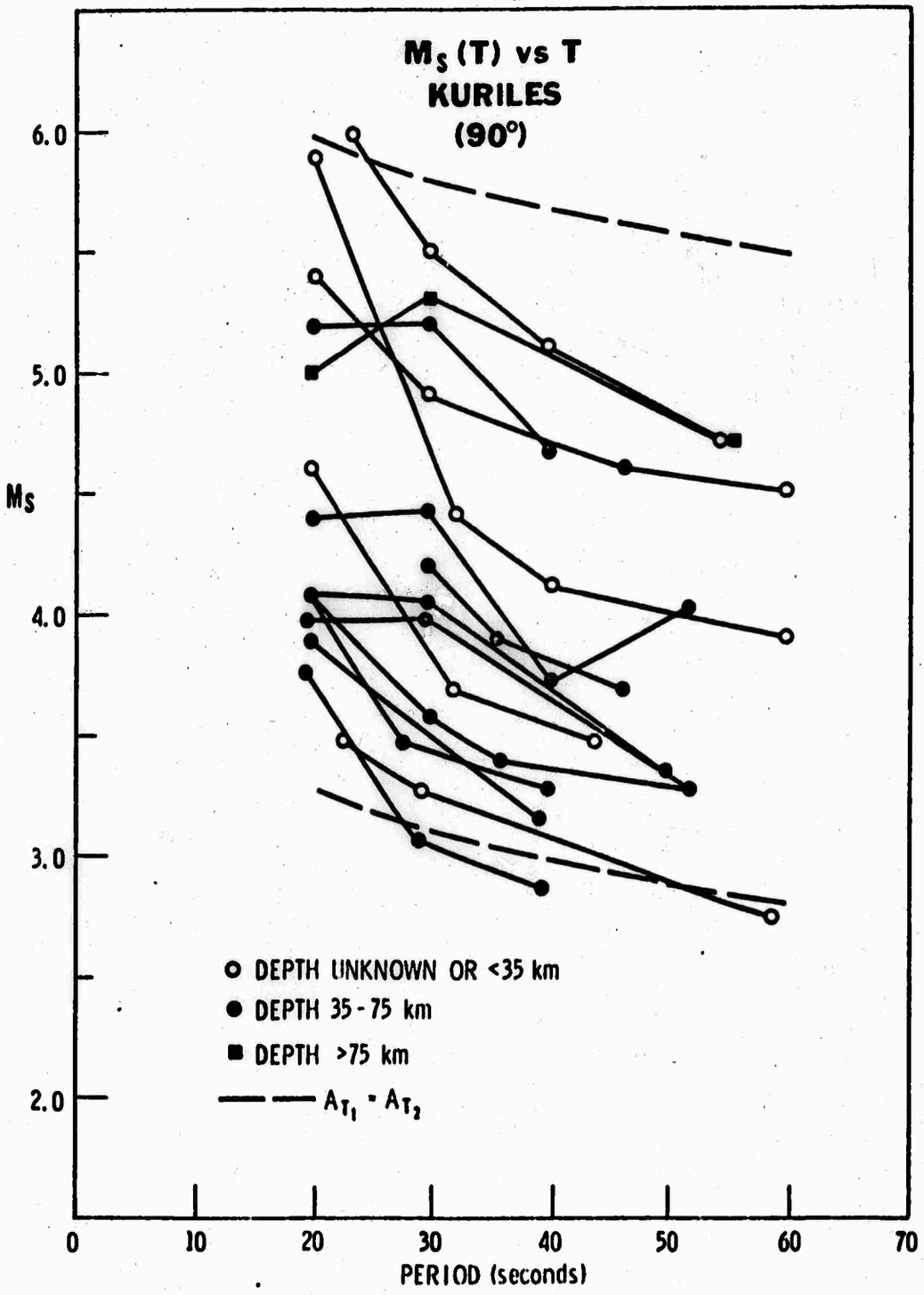
M_S (T) vs T
KURILES
(90°)
6.0
5.0
4.0
3.0
2.0
M_S
0
10
20
30
40
50
60
70
PERIOD (seconds)
DEPTH UNKNOWN OR <35 km
DEPTH 35 - 75 km
DEPTH >75 km
$A_{T_1} = A_{T_2}$

Figure 39.

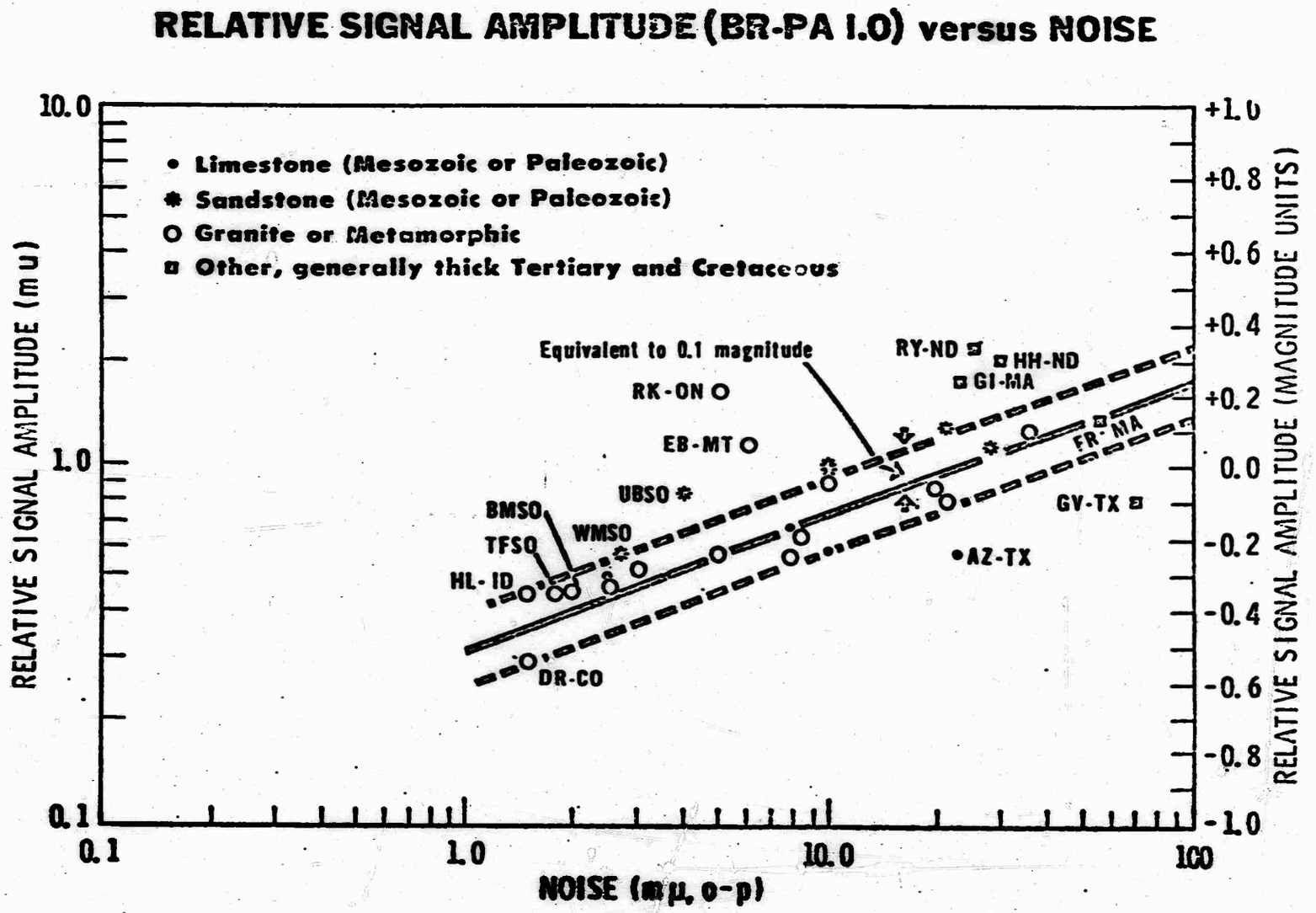

Detailed discussion of this figure can be found in Evernden and Clark, 1970

Figure 40.

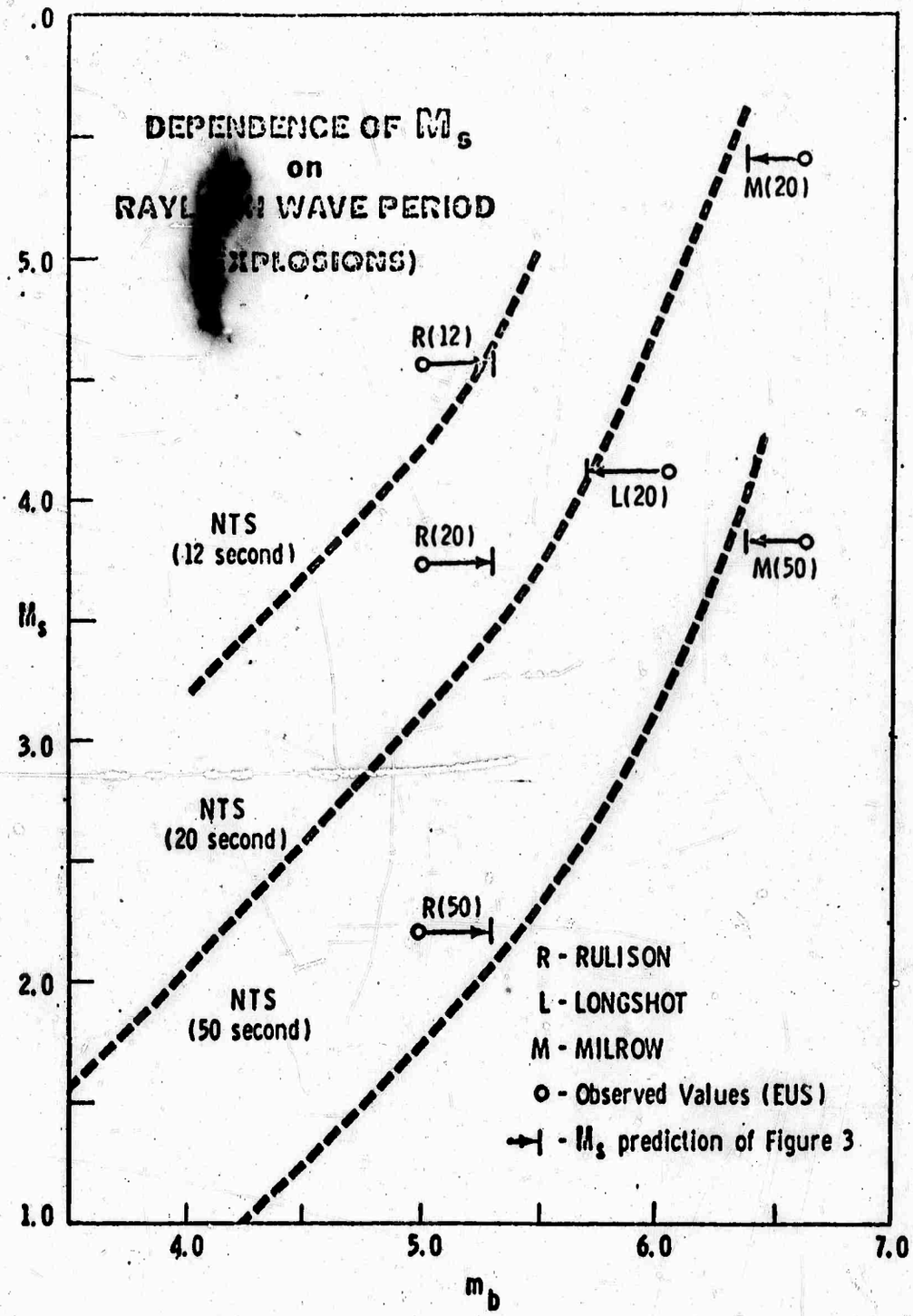
DEPENDENCE OF M_s
on
RAYL[illegible] WAVE PERIOD
[illegible]XPLOSIONS)
R(12)
R(20)
R(50)
L(20)
M(20)
M(50)
NTS
(12 second)
NTS
(20 second)
NTS
(50 second)
R - RULISON
L - LONGSHOT
M - MILROW
o - Observed Values (EUS)
- M_s prediction of Figure 3
M_s
m_b
.0
5.0
4.0
3.0
2.0
1.0
4.0
5.0
6.0
7.0

Figure 41.

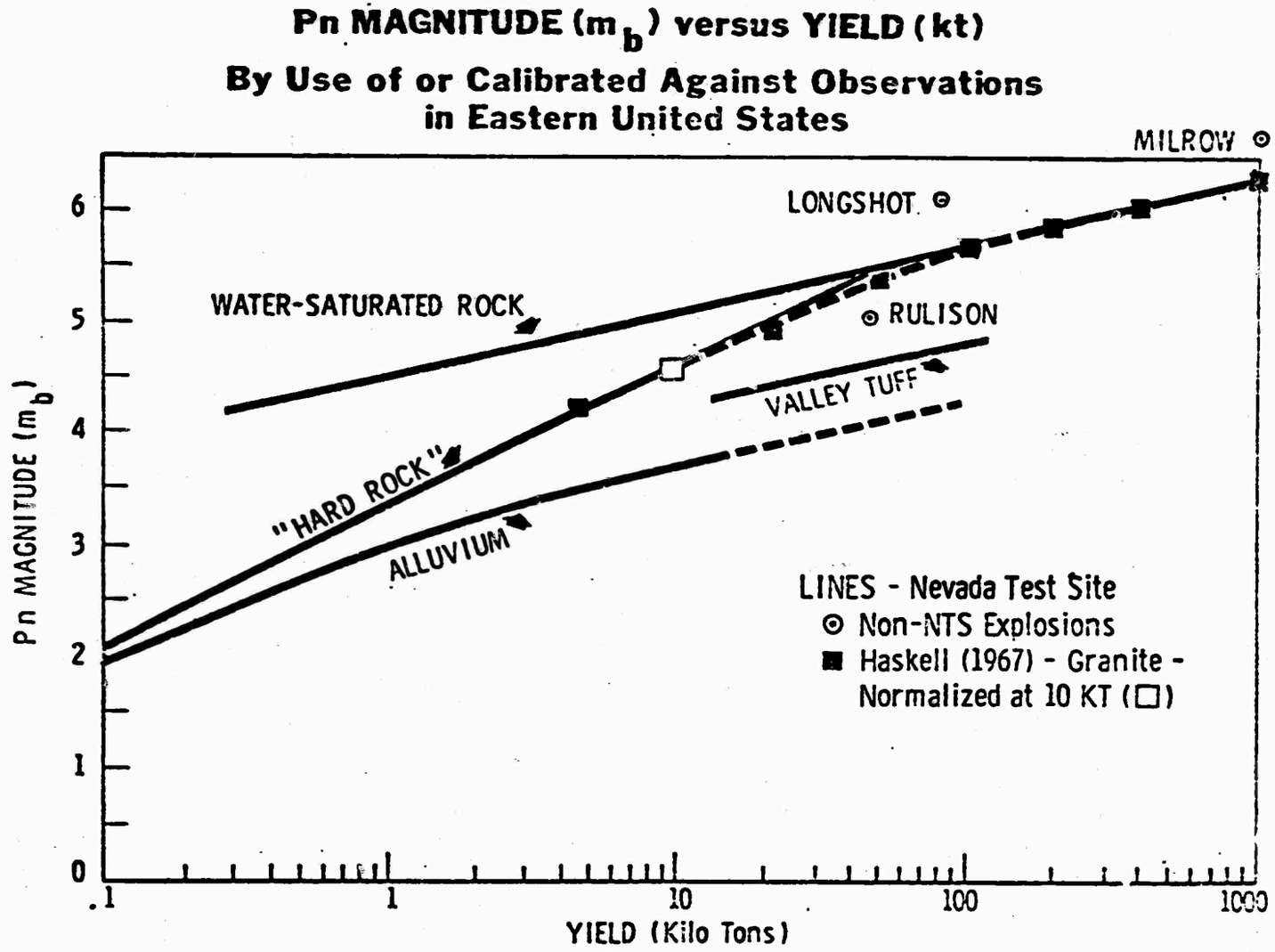
Pn MAGNITUDE (m_b) versus YIELD (kt)
By Use of or Calibrated Against Observations
in Eastern United States
MILROW
LONGSHOT
WATER-SATURATED ROCK
RULISON
VALLEY TUFF
"HARD ROCK"
ALLUVIUM
LINES - Nevada Test Site
Non-NTS Explosions
Haskell (1967) - Granite - Normalized at 10 KT
Pn MAGNITUDE (m_b)
YIELD (Kilo Tons)
0
1
2
3
4
5
6
.1
1
10
100
1000

Figure 42.

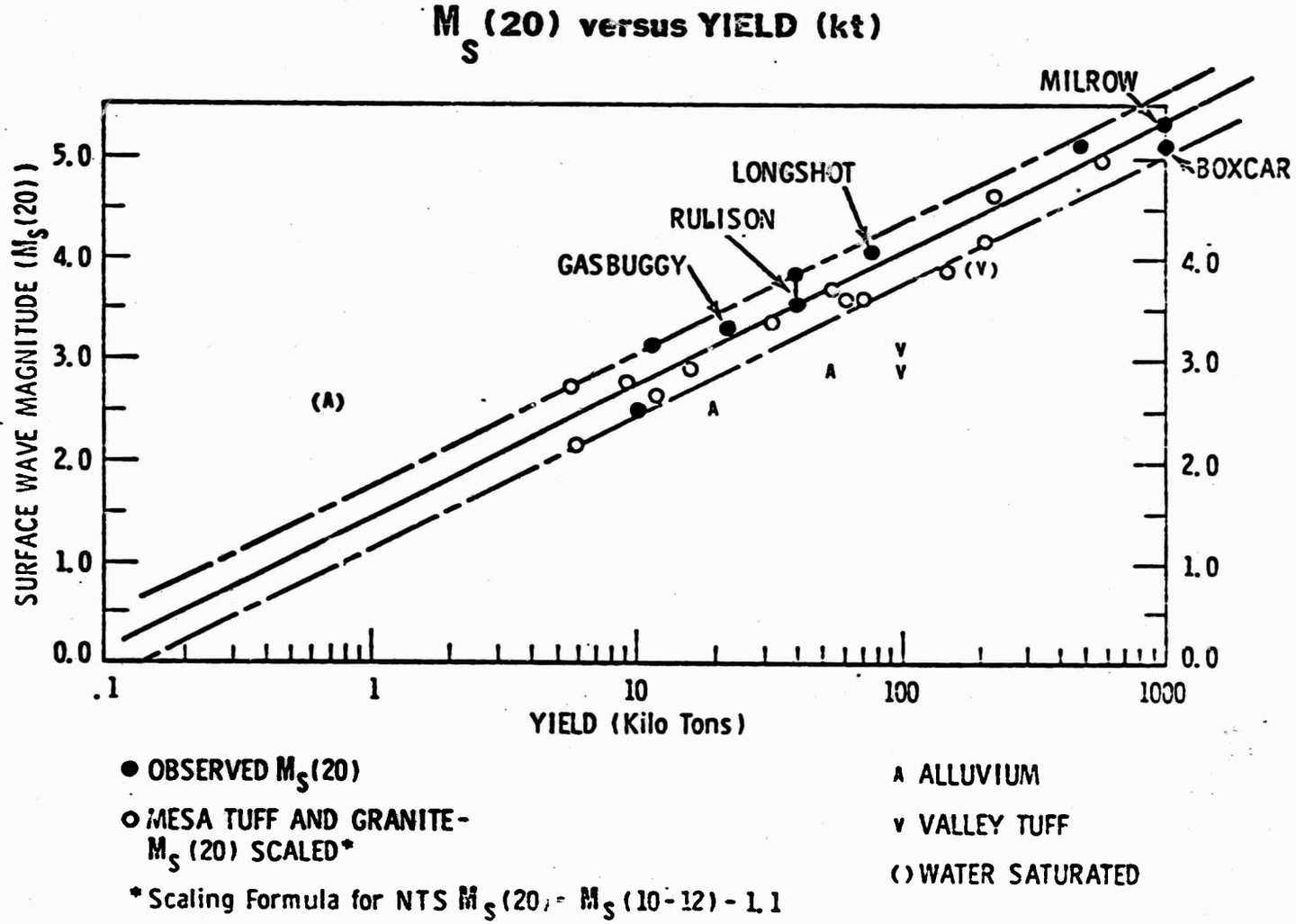
M_S (20) versus YIELD (kt)
MILROW
BOXCAR
LONGSHOT
RULISON
GASBUGGY
(V)
(A)
A
V
V
A
SURFACE WAVE MAGNITUDE (M_S(20))
5.0
4.0
3.0
2.0
1.0
0.0
.1
1
10
100
1000
YIELD (Kilo Tons)
● OBSERVED M_S(20)
o MESA TUFF AND GRANITE- M_S (20) SCALED*
* Scaling Formula for NTS M_S(20) = M_S (10-12) - 1.1
A ALLUVIUM
v VALLEY TUFF
( ) WATER SATURATED

Figure 43.

THEORETICAL M_s - m_b RELATION FOR SMALL MAGNITUDES

By

Keiiti Aki

Massachusetts Institute of Technology

This brief report is concerned with the minimum magnitude for which the M_S-m_b criterion for distinguishing explosions from earthquakes may apply. If we take Haskell's formula on the reduced potential (Haskell, 1967) as the model of an explosion, and the ω -square model as that of an average earthquake (Aki, 1967), we must conclude that such a minimum exists and the M_S - m_b criterion is not applicable to events with M_S smaller than 3, as long as M_S is defined for period of 20 seconds and m_b is measured from teleseismic P waves with spectrum peaked around 1 second.

The scaling law of seismic spectrum based upon the ω -square model implies the assumption of similarity between large and small earthquakes. This assumption received objections from several authors. Therefore, I shall first review some of the criticisms on the ω -square model.

First, let us look at the relation between M_S and fault length L. Figure 1 is reproduced from Chinnery (1969) with additional theoretical curves for the ω -square model and another one by Otsuka which is based upon an argument essentially the same as Press's (1955). As shown in the figure, the ω -square model explains satisfactorily the data of Tocher and Iida. The bending of the curve for the ω -square model is due to the inefficiency of M_S to measure the earthquake size for large events. Because of the scaling law as shown in Figure 2, the spacing between the spectral amplitude curves at long periods (which is proprotional to the product of fault length, width and dislocation) become increasingly larger for $M_S > 6$ for a unit increment in M_S. It is not necessary to invoke a violation of similarity, such as relatively thinner shape for larger earthquakes implied in Press and Otsuka's models, in order to explain the data of Tocher and Iida. Furthermore, unusually long earthquakes with small magnitudes have been discovered. Examples are the Parkfield earthquake and the Imperial earthquake (Aki, 1970, Brune and Allen 1967). They are, however, exceptional in their own groups. I believe that the shape of fault plane for an average earthquake does not vary systematically with the earthquake size.

The data shown in Figure 1 includes the Parkfield earthquake and the Imperial earthquake. Except for these two, I do not believe that the data for small events ($M < 6$) are reliable. These data are from Wyss and Brune (1968), and their epicenters are shown in Figure 3. The evidences used by them for determining fault length are the offset observed on the surface which appeared to be associated with the earthquake. For example, they detected a small offset across highway 46 after the shock N° 2, and concluded that the fault length must be at least as long as 30 km which is the distance between the epicenter and highway 46. Two of these shocks are recorded at Berkeley and included in an analysis by Filson and McEvilly (1967).

Figure 4 shows a comparison of the Love wave spectra from the main shock and several aftershocks. The mainshock, which was unusually long and thin as mentioned before, shows spectral nulls at points expected from the rupture velocity and fault length directly observed in the epicentral region. However, none of the aftershocks show such

nulls. For example, the curve designated as 5.0 corresponds to the shock N° 2 of Wyss and Brune. If their conclusion is correct, this shock must have generated the seismic waves with spectral nulls nearly at the same points as the mainshock. But there are no such nulls, except at about 7 seconds, which I suspect is due to the path effect because it shows up independent of magnitudes. Therefore, we must conclude that, at least for shock N° 2, their fault length is not associated with the seismic wave generation. The length of faulting which was responsible for Love wave generation must have been shorter than 30 km.

Since a similar technique was used for determining fault lengths of other earthquakes, I suspect that the data of Wyss and Brune given in Figure 1 may not be reliable, except for the Parkfield main - shock and the Imperial earthquake. Since these two are known to have an exceptionally long, thin fault shape, I regard the departure of these two from the theoretical curve for ω -square model as acceptable.

Once we accept the ω -square model, both 1 and 20 seconds periods lie on the flat portion of spectra for $M_S < 2$, as shown in Figure 2. In other words, an earthquake with $M_S < 2$ looks like a point source with dislocation varying as step -- function for these periods. For the same magnitude and frequency range, Haskell's scaling law for explosion predicts that an explosion will look like a point source with pressure varying as step -- function. We normalized an earthquake to an explosion in such a way that the maximum amplitude of P waves from the earthquake became equal to the P wave amplitude from explosion at the same distance when both sources are placed in an infinite, homogeneous, isotropic, elastic body. Then we put these two sources in a layered earth-model at various depths, and compared the excitation of Rayleigh waves at the period of 20 seconds. The result is shown in the report by Tsai and Aki in this conference. The Rayleigh wave amplitude from earthquakes scatter around that of an explosion placed at a very shallow depth.

The range of variability is optimistically estimated as $\pm$ 0.5 M_S unit. From this, we must conclude that if an earthquake is a point source with dislocation varying as step - function, and if an explosion is a point source with pressure varying as step -- function, then we cannot discriminate them on the basis of M_S - m_b criterion. Therefore, if the ω -square model and Haskell model apply to earthquakes and explosions respectively, we cannot use this discriminant for $M_S < 2$. Because of the variability of $\pm$ 0.5 M_S unit, the discrimination should not be reliable at $M_S = 3$. For $M_S > 3$, the effect of source size appears on earthquake spectra and will be separated from explosions by the M_S - m_b criterion.

The above conclusion is derived assuming that M_S is proportional to surface wave excitation at the period 20 seconds, and m_b is proportional to body wave excitation at about 1 second. We can lower the limiting magnitude by redefining M_S and m_b at shorter periods.

THEORY OF SEISMIC SOURCES

Introduction

In this session, we shall discuss mathematical models of seismic sources relevant to the identification problem. The identification is an inverse problem, in which we wish to find the property of source from observed seismic waves. Not only the non-uniqueness intrinsic to this type of inversion, but also the complexity due to the transmission in the heterogeneous Earth make the problem very difficult. Such difficulties in practice will be the subject of the next two sessions, one on the effect of crust, the other on the determination of source parameters.

What we must do in this session is make the job of the next sessions easier by finding good mathematical models of earthquakes and explosions, which may be described by the minimum number of source parameters.

Following my talk, Dr. Archambeau will talk on his theory of tectonic source, Dr. Harkrider will comment on the ω-square model and discuss the determination of source depth from surface wave spectra. Then, Dr. Douglas will report on theoretical seismograms for earthquakes and explosions.

There are essentially two types of earthquake models. One is the dislocation model, and the other is the stress-relaxation model. The comparison of these two models will be the main subject of my talk.

In the AGU meeting in Washington, this spring, Linde and Sacks of the Carnegie Institution, discussed the spectral analysis of long period body waves. They showed an observed spectrum which was strikingly different from what had been familiar to us working on the source mechanism study using long period waves. I was shocked because, if their observation is true, the dislocation model used in the last ten years was entirely inadequate as the earthquake model. Furthermore, they stated that their observations agreed with Archambeau's "stress-relaxation" model.

The difference in spectrum between the two was described by Dr. Archambeau on last Monday. The striking difference is at the low frequency. The dislocation model gives constant spectral density for far-field body waves in an infinite homogeneous medium, while the Archambeau model predicts a sharp drop toward zero frequency.

Dislocation models

Let us first look at the dislocation models. In a dislocation model, we give a displacement discontinuity $\Delta u(\xi,t)$ with motion direction $\vec{n}$, across the fault plane Σ with normal $\vec{\nu}$. Then, the elastic displacement components generated from this time-varying dislocation may be written as

$$u_n(\vec{x},t) = \int_{-\infty}^{\infty} dt' \int_{\Sigma} n_i \, \Delta u(\vec{\xi},t') \nu_j \, C_{ijpq} \frac{\partial}{\partial \xi_q} G_{np}(\vec{x},t;\vec{\xi},t')$$

where C_{ijpq} is the elastic constant, relating stress component τ_{ij} with displacement derivative $u_{p,q}$ and G_{np} $(\vec{x},t;\vec{\xi},t')$ is the Green's function which is defined as the nth component displacement at observation point $\vec{x}$ and time t caused by an impulsive point force directed in xp-direction exerted at point $\vec{\xi}$ and time t'. i, j, p, q, and n take the values 1, 2, and 3, and repeated index means the summation over that index. This equation can be obtained directly from the Betti's reciprocal theorem as shown by Burridge and Knopoff (1964). Earlier, solutions for special cases have been given by Knopoff and Gilbert, Maruyama, Haskell and others.

From here, we have only two problems. One is to find the Green's function, the other is to find the dislocation function Δu $(\vec{\xi},t')$ on Σ. The Green's functions have been known for varieties of wave medium models. The simplest of them is the P waves in the far-field (only the term attenuating with distance as 1/4) in an infinite, homogeneous isotropic body. The radial component of such P waves may be written as

$$\gamma_n \, U_n^P(\vec{x},t) = (4\pi\rho\alpha^3 r)^{-1} \cdot (C_{ijpq} \, n_i \nu_j \gamma_p \gamma_q) \cdot \int_\Sigma \Delta\dot{u}(\vec{\xi},t-r/\alpha)d\Sigma$$

where $\vec{\gamma}$ is the unit vector pointing from the source to the station, and $\Delta\dot{u}$ represents the time derivative of Δu. The right hand of the above equation is composed by 3 factors. The first factor shows the distance dependence and the second the radiation pattern. The third factor

$$\int_\Sigma \Delta\dot{u} \, (\vec{\xi},t-r/\alpha)d\Sigma$$

describes the wave form, and is the most important for today's discussion. Since this term is essentially smoothing of $\Delta\dot{u}$ over Σ, it is obvious that for wave lengths much longer than the linear dimension of Σ, the smoothing effect is negligible and therefore the wave form will look like the time derivative of dislocation function. If dislocation takes place like step-function, the P wave displacement wave-form should look like delta-function. Thus, the corresponding spectral density must be constant at such low frequencies.

There are several dislocation models proposed by many investigators such as Savage, Hirasawa, Stauder, Berkehemer, Jacobs, and others. The simplest and yet good dislocation model may be the one proposed by Ben-Menahem (1961) and later studied by Haskell (1964, 1966). This model is described by the following 8 parameters

1. Strike direction
2. Dip angle

3. Slip angle
4. Fault length
5. Fault width
6. Amount of dislocation
7. Rupture velocity
8. Rise time

The rise time is loosely defined as the time needed for the completion of step-wise offset between the two sides of the fault plane. The finite rise time is needed for a realistic earthquake model because the seismic energy becomes infinite if the rise time is zero. The effect of finite rupture propagation and finite rise time introduce the ω^{-2} attenuation for frequencies much higher than the "Corner frequency" as discussed by Dr. Wyss. Now I would like to enumerate some of the observations which support this "Ben-Menahem-Haskell" model.

1. The first convincing example is the Kamtchatka earthquake (M = 8.25)studied by Ben-Menahem and Toksöz, later by Haskell. The dislocation was determined as a step function with rise-time of about 22 seconds. This conclusion was obtained by surface waves travelled around the Earth many times, both Love and Rayleigh waves. It is very difficult to dispute these conclusions.

2. The second example is the Niigata earthquake (M = 7.5), for which I have determined the seismic moment, which gave the value consistent with the near-source observations. The seismic moment will have no meaning, if the dislocation does not behave like a step function because it is related to the height of step. Similar mechanical consistency of the value of seismic moment and the near source observations has been obtained for Parkfield earthquake, Imperial earthquake, Good-Friday Alaskan earthquake and others by Brune, Kanamori, Allen, Wyss, Tsai, myself and others. Hirasawa determined the rise-time of the Niigata earthquake (M = 7.5) as 2 to 4 seconds from far-field P waves.

3. The most convincing evidence for the "Ben-Menahem-Haskell" model comes from the strong-motion record obtained by Coast and Geodetic Survey at a distance of only 80 meters from the San-Andreas fault in the case of the Parkfield earthquake. This is, in fact, measuring directly the dislocation on the fault. Unfortunately, the parallel component accelerograph was not working, but the perpendicular component showed a simple spike-shape displacement, which should be associated with a step-function like dislocation (Aki, 1968). A classic work by Eshelby has shown that the two components are related by the Hilbert transform for uniformly gliding edge dislocation. Haskell (1969) and myself (Aki, 1968) studied independently these accelerograms and obtained the rise time of 0.4 to 0.9 seconds.

Another example I remember well is the Hindu-Kush earthquake studied by Brune and his colleagues. They showed that the long-period P wave record looked like the response of instrument to impulsive

ground displacement for long periods supporting the Ben-Menahem Haskell model.

4. These examples are individual events, the ω-square model (Aki, 1967) which I discussed on Monday is a simplest extension of the Ben-Menahem-Haskell model to an ensemble of earthquakes.

This model explains the following observations.

1. Magnitude (in particular by Berkhemer) dependence of seismic spectra.
2. M_s vs m_b relation (by Gutenberg and Richter)
3. M_s vs fault length relation (by Tocher and Iida)

There are arguments against the similarity assumption (King and Knopoff, Press, Wyss and Brune, Jacobs and others). But, it seems to me that some of these arguments are based on the unjustified assumption that the earthquake magnitude should be proportional to a constant times the logarithm of seismic energy. Others seem to regard exceptions as a rule. I believe, at this moment, that the similarity assumptions apply to an average earthquake, which implies that there are no magnitude dependence of stress drop, shape of the fault, rupture and slip velocities.

5. Based on the ω-square scaling law we believe that the earthquake with magnitude less than 6 may be regarded as a point source with step-function dislocation for periods longer than about 10 seconds.

Under this assumption, Ben Tsai studied Rayleigh and Love waves from many earthquakes with known fault plane solutions and known depths, and obtained consistent agreement between observed and theoretical spectra for periods 10 to 50 seconds. He will give his recent result later in this conference.

In addition to the above mentioned observational support, it is very appealing to one's intuition, that the rupture process which leaves a permanent offset is approximated by a step-function with a finite risetime.

However, nobody has yet proved that the dislocation must take place in the form of such a step-function. And I know it is very dangerous to rely upon one's intuition in the elasto-dynamics. We have seen several examples of incorrect intuitive reasonning in important seismological problems.

Stress relaxation models

Let us now look at the stress relaxation models. Honda (1960) considered a stress relaxation model of earthquake, which is a formation of spherical region of vanishing shear stress in various

pre-stressed elastic media. This model may not be a realistic one for shallow earthquakes, which sometimes take a long thin shape, but may be useful as a model of tectonic stress release by underground explosions. In the case of pre-existing shear stress, this source becomes equivalent to a point double couple for long waves. If the stress relaxation takes place as a step function, the spectral density of far field displacement becomes a constant at low frequencies. This constant is proportional to the product of the stress relaxation and the volume of the spherical region. Thus, the relaxation model of Honda with the step-function stress change shows the same feature at low frequencies, as the dislocation model with the step-function dislocation. In other words, Honda's relaxation model is just like Ben-Menahem-Haskells model for long waves. Next, let us look at Randall's work published in 1964. Randall looked at the seismic generation as an initial value problem rather than a boundary value problem. In his formulation, the initial static displacement field produced by some internal tectonic cause is released instantaneously. He states that the radiated waves are completely specified by the initial static displacement. I don't believe, however, that an instantaneous release of displacement within a finite region is physically realizable. A spontaneous release, such as an earthquake, should start at a point, then propagate to the surrounding region. The radiated seismic waves are determined not only by the initial displacement, but also by the speed of the propagating process which is controlled by elastic and non-elastic properties of earth material.

Now, finally, we must face the Archambeau model. Dr. Archambeau made a statement very much like Randall's on Monday. He said that, in his stress-relaxation model, the problem is one of the initial value, and therefore the assumption on source-time-function is not necessary. I could not understand this statement, because in his own model, he has specified the process of stress-relaxation by a rather specific process determined by a small number of source parameters.

Archambeau considered two models, one is expanding or growing rupture, the other is propagating rupture. In the former, an ellipsoidal region of vanishing stress expand its size. In the latter, a small spheroidal region, within which shear stress vanishes, propagates in the medium. In this model, the condition of shear stress vanishing does not apply to a point once the spheroid pass the point. This model was proposed to take into account the immediate welding of rupture surface after the passage of rupture front. The spectrum discussed in the introduction corresponds to a model of propagating rupture, called equilateral model, in which two such ellipsoids propagate in opposite directions.

Once the model is fixed, his method is essentially the following. First, looking at the process quasi-statically, he calculates the equilibrium elastic field at successive moments as the ellipsoid propagates. Secondly, he solves the initial value problem for each successive moments with these changes in equilibrium field as the source of waves and then superposes for all the successive moments.

Since the mathematics is involved, I could not locate exactly how the sharp drop of spectrum toward low frequency as mentioned earlier took place. It is surprising to see such a significant difference in the generation of long waves between "stress-relaxation" and "dislocation" models proposed to describe the same physical process. In the dislocation model, we cut the elastic body along a propagating surface element, moved one side relative to the other and welded.

In the stress-relaxation model, the shear stress is released in an propagating ellipsoid and then welded as the ellipsoid passed the point. I don't understand why they are different in long wave generation. I believe this puzzle is an outstanding one, because although the dislocation model has been successful in explaining seismic observations, the dislocation source function is given by rather arbitrary intuition. On the other hand the stress-relaxation model is a more realistic representative of spontaneous process like earthquakes.

REFERENCES

Aki, K., 1967, J.G.R., v. 72, p. 1217-1231.

Aki, K., 1968, J.G.R., v. 73, p. 5359-5376.

Archambeau, C.B., 1968, Rev. of Geophysics, v. 6, p. 241-288.

Ben-Menahem, A., 1961, B.S.S.A., v. 51, p. 401-435.

Brune, J.N., and Allen, C.R., 1967, BSSA, v. 57, p. 501-514.

Burridge, R. and Knopoff, L., 1964, B.S.S.A., v. 54, p. 1875-1888.

Chinnery, M., 1969, BSSA v. 59, p. 1969-1982.

Filson, J., and McEvilly, T., 1967, BSSA v. 57, p. 1245-1258.

Geyer R.L., and Martner, S.T., 1969, Geophysics, v. 34, p. 893-905.

Haskell, N.A., 1964, B.S.S.A., v. 54, p. 125-140.

Haskell, N.A., 1966, B.S.S.A., v. 56, p. 125-140.

Haskell, N.A., 1967, J.G.R. v. 72, p. 2583-2587.

Haskell, N.A., 1969, B.S.S.A., v. 59, p. 865-908.

Honda, H., 1960, Publ. Dominion Obs., Ottawa, v. 24, No. 10.

Press, F., 1965, VESIAC Conference on source mechanism.

Randall, M.J., 1964, B.S.S.A., v. 54, p. 1283-1289.

Wyss and Brune, 1968, J.G.R., v. 73, p. 4681-4694.

6t

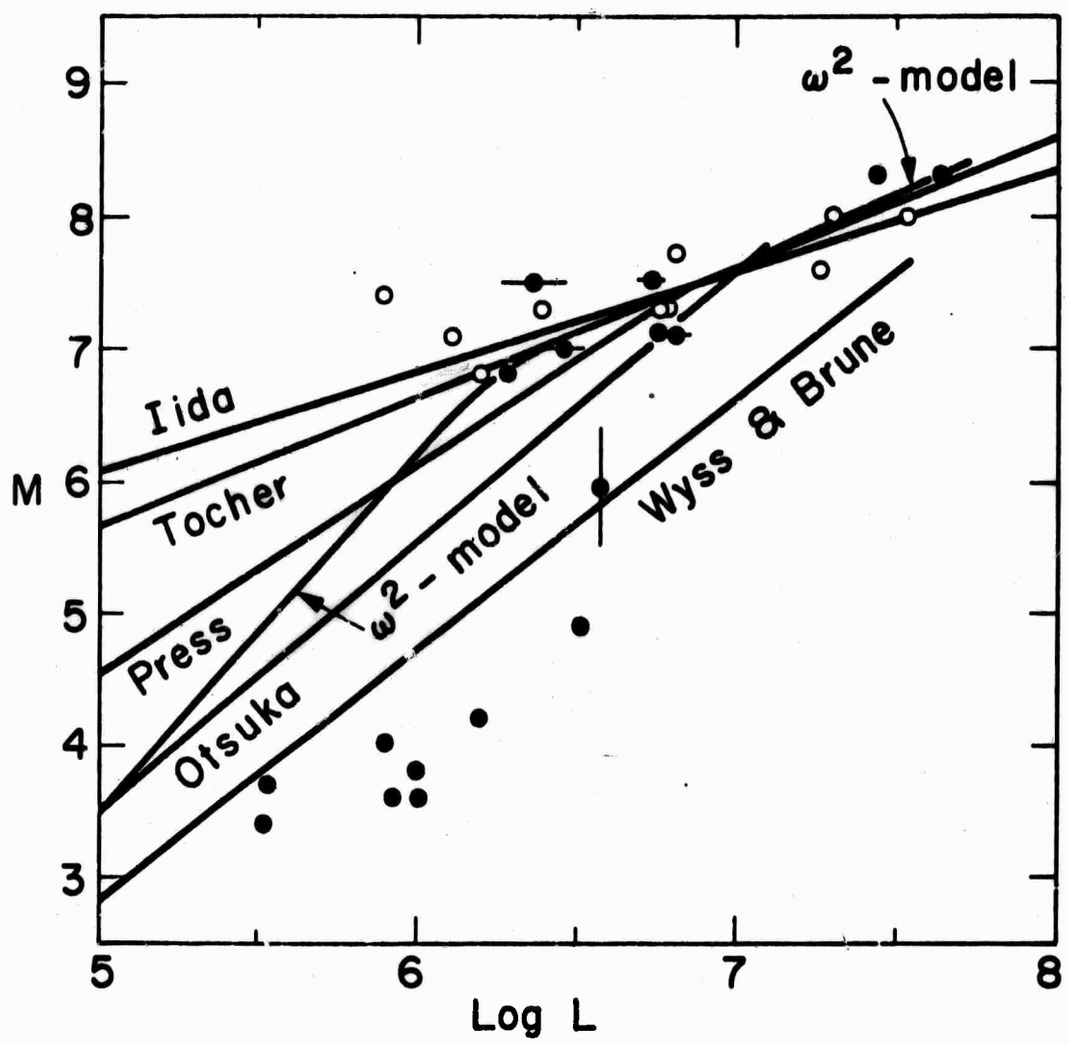

Figure 1. The relation between magnitude M and fault length L reproduced from Chinnery (1969). The theoretical curve of Otsuka was not included in Chinnery. Otsuka's curve is derived from an argument similar to Press's, both of which assume that M is proportional to the logarithm of seismic energy and invoke non-similar shapes of fault plane for large and small earthquakes. Also added is the theoretical M_S vs L curve based on the ω-squared model (Aki, 1967) derived on the assumption of similarity. The curve explains very well the data of Tocker and Iida. The bending of curve is due to the inefficiency of M_S as a measure of larger earthquakes.

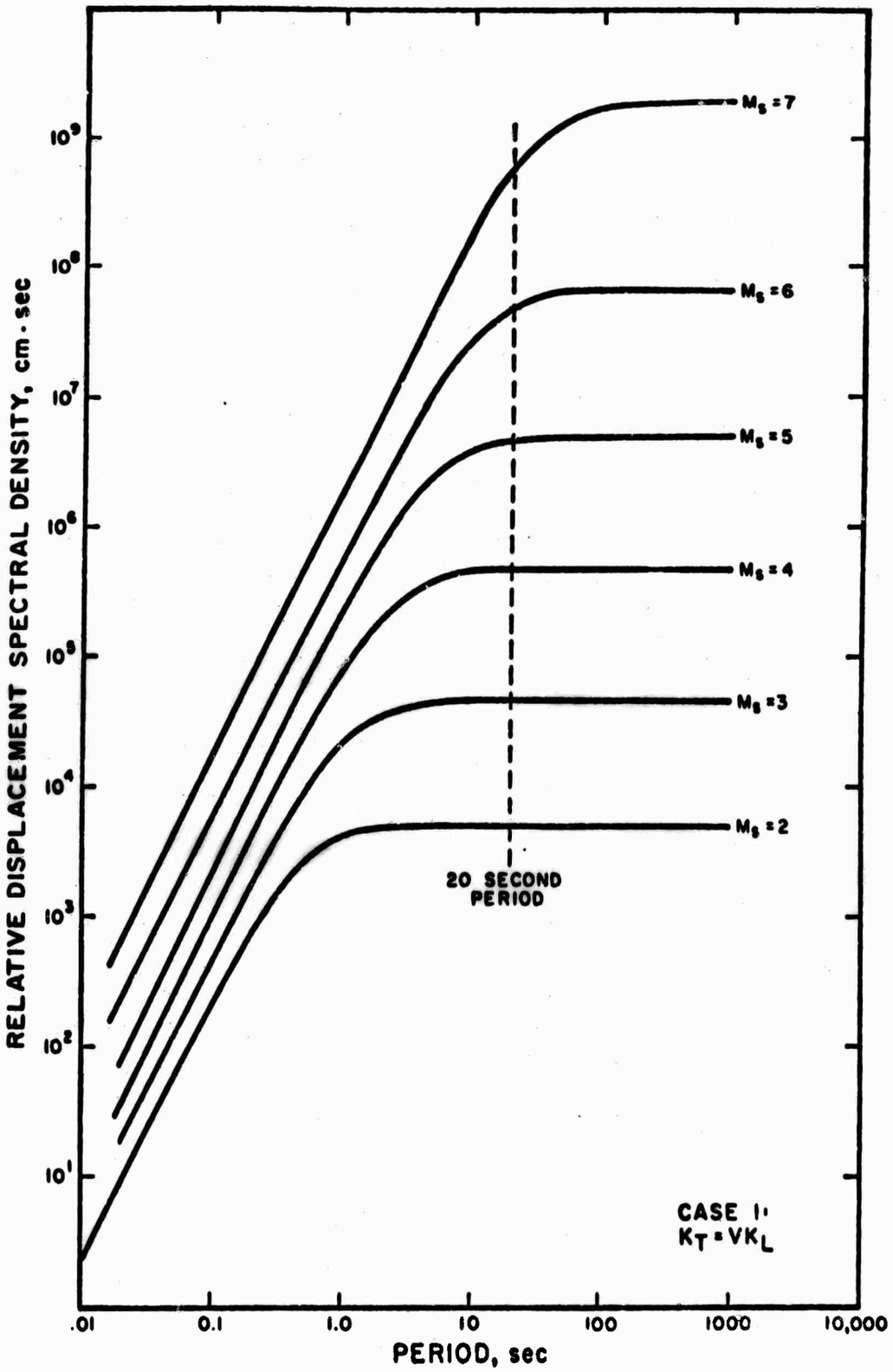

Figure 2. Scaling law of seismic spectrum based upon the ω-square model (Aki, 1967).

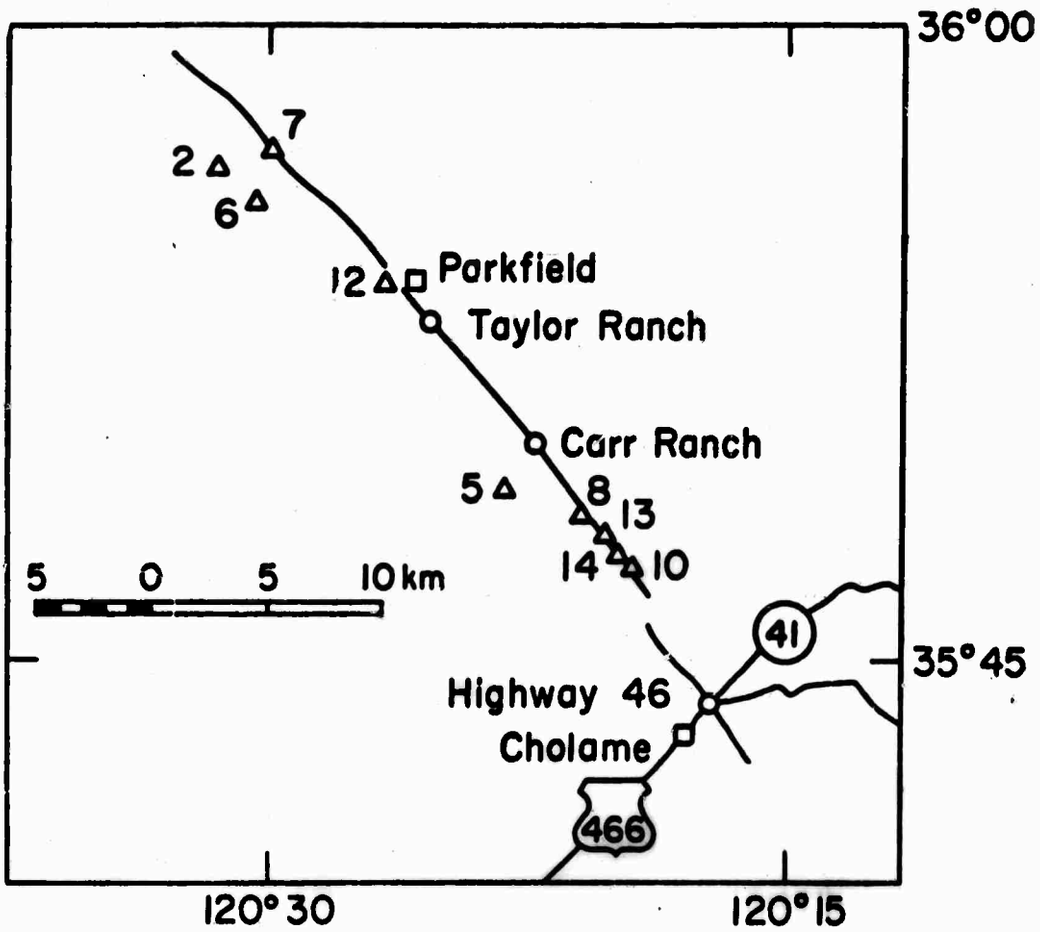

Figure 3. Map of epicenters of small earthquakes used in Figure 1. This figure is reproduced from Wyss and Brune (1968).

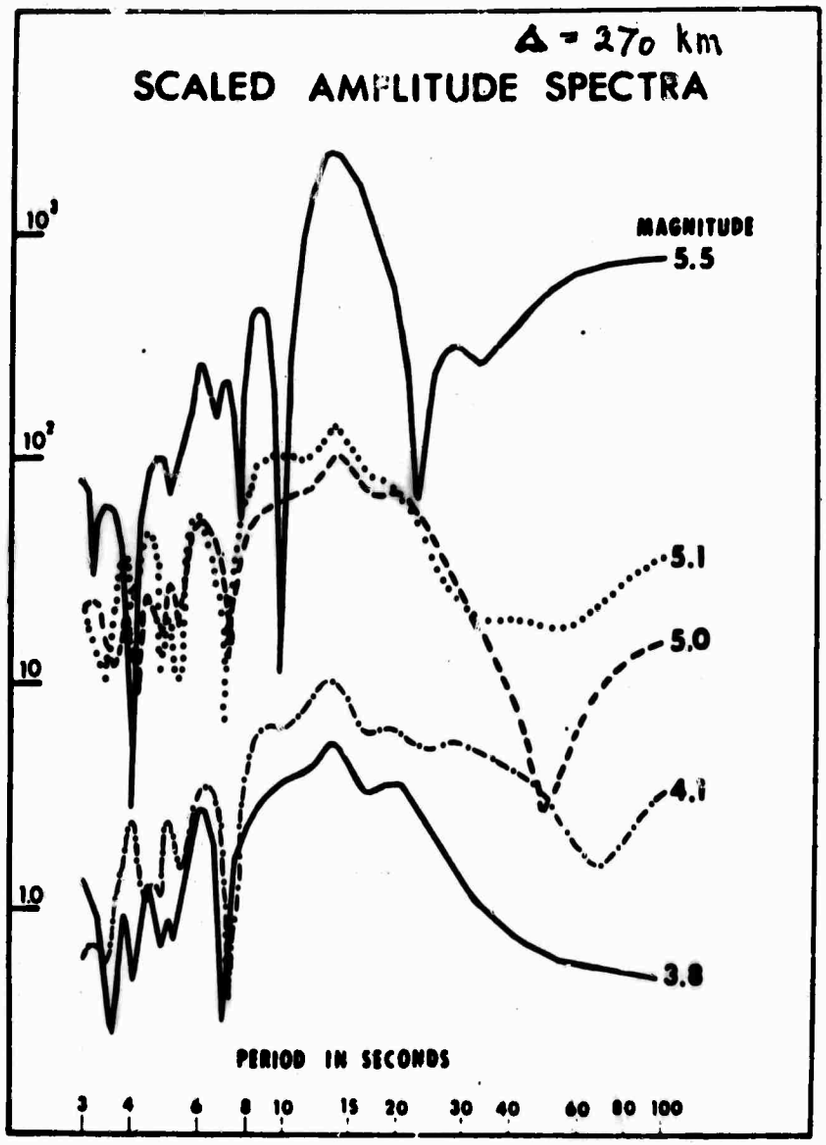

Figure 4. The spectra of Love waves computed by Filson and McEvilly (1967) for some of the earthquakes used in Figure 1. The curve M = 5.5 is from the Parkfield mainshock, the curves M = 5.0 and M = 3.8 are from the shock N° 2 and N° 6 of Figure 3 respectively. If the fault length determined by Wyss and Brune is correct, the curves M = 5.5 and M = 5.0 must share nulls at nearly the same points.

EARTHQUAKE AND EXPLOSION MAGNITUDES: THE EFFECT OF LATERAL VARIATION OF SEISMIC ATTENUATION

By

Sean C. Solomon
Ronald W. Ward
M. Nafi Toksöz

Department of Earth and Planetary Sciences
Massachusetts Institute of Technology
Cambridge, Massachusetts 02139

ABSTRACT

The relationship between surface wave and body wave magnitudes, used to discriminate underground nuclear explosions from earthquakes, can be appreciably altered by lateral variation of seismic wave attenuation, or Q^{-1}, in the upper mantle. For events in certain tectonic regions, such as western North America, body wave magnitudes measured at teleseismic distances are considerably less than magnitudes of events of comparable surface wave magnitude in other areas of the world. Amplitudes of surface waves with periods less than about 25 seconds are much less affected by lateral changes in Q^{-1} than are body-wave amplitudes. This means that if explosions are compared only with earthquakes from the same tectonic province, the separation between the two populations on the basis of the $M_S - m_b$ criterion is better defined than if events from several provinces are combined. Differences in the relative amplitudes of body waves at long periods and at short periods imply that Q^{-1} is frequency dependent. This is in qualitative agreement with current ideas of the mechanism of dissipation in the upper mantle.

INTRODUCTION

The relative excitation of long-period waves (as measured by the surface wave magnitude M_S) to short-period waves (as measured by the body wave magnitude m_b) is a positive criterion for discriminating between earthquakes and underground nuclear explosions of body wave magnitude greater than 5 (Davies, 1968). For a given m_b, earthquakes generate significantly larger surface waves than do explosions. The precise relationship between M_S and m_b for both earthquakes and explosions varies regionally, however. In particular, M_S for events in western North America is systematically greater, at a given m_b, than for events in all other areas studied (Liebermann and Pomeroy, 1969; Basham, 1969; Ward and Toksöz, 1970).

Several reasons for this unusual M_S - m_b pattern in western North America have been advanced: (1) Values of M_S, as a function of m_b, are larger than elsewhere for earthquakes because earthquake focal depths in this region are less than for typical shallow earthquakes in the rest of the world; while larger M_S values observed for explosions might be due to the source medium at NTS (tuff) behaving differently from those at other underground explosion sites (e.g. granite) (Liebermann and Pomeroy, 1969). (2) The Rayleigh waves used by Liebermann and Pomeroy (1969) and Basham (1969) in determining M_S for North American events traversed purely continental paths, while those used for other events crossed one or more continent-ocean boundaries where the wave amplitudes might be expected to be sharply attenuated (Basham, 1969). (3) Values of m_b, for a given M_S, are lower than elsewhere because of abnormally high seismic attenuation in the upper mantle of western North America (Ward and Toksöz, 1970). A combination of any of the above or other causes may of course be acting simultaneously. It is the purpose of this paper, however, to discuss the influence of propagation path on magnitude and to demonstrate that reason (3), lateral variation of seismic wave attenuation in the mantle, has a major effect on the M_S - m_b relationship.

Surface wave attenuation

The best determinations of seismic attenuation, or Q^{-1}, are those for surface waves with period greater than 100 seconds. There is considerable uncertainty, however, in Q^{-1} for 20-second Rayleigh waves, used in the definition of M_S. Estimates of an average $Q_R(T=20)$ for the earth range from about 340 (Gutenberg, 1945) to over 5100 (Tsai and Aki, 1969). In Figure 1 are shown several published observations of Q_R^{-1}, appropriate to an average or predominantly oceanic earth, for periods near 20 seconds. The figure also contains a recent estimate of Q_R^{-1} for the tectonically active western United States (solid line), determined from Rayleigh waves travelling (both directions) between WWSSN stations at Tucson, Arizona, and Longmire, Washington.

To the values of Q_R^{-1} for western United States must be attached considerable uncertainty, particularly at the shorter periods.

Nonetheless, comparison with Q_R^{-1} for the whole earth leads to several conclusions: (1) A minimum in $Q_R^{-1}(T)$ between periods of 20 and 25 seconds appears to be a world-wide phenomenon. (2) For periods less than 25 seconds, $Q_R^{-1}(T)$ in western North America does not appear to be substantially different from $Q_R^{-1}(T)$ in the rest of the world. Thus Rayleigh waves from North American events would not be expected, on the basis of surface wave attenuation alone, to have much different surface wave magnitudes from events of equal body wave magnitude in other areas. (3) $Q_R(T=20)$ is found to be 230 for western U.S. Even if we assume $Q_R = 5100$ for the rest of the world, propagation of a Rayleigh wave of period 20 seconds through the western U.S. (assumed path-length = 2000 km) amounts to an 'anomalous' decrease in M_S of only 0.2.

The attenuation measurements discussed above include the effects of scattering from inhomogeneities as well as those of anelasticity. Basham's (1969) hypothesis, however, that Rayleigh-wave propagation across a continent-ocean interface significantly lowers the surface wave magnitude, a suggestion proposed to explain the anomalously high values of M_S (as a function of m_b) observed for North American events at North American stations, is not universally valid.

Using a vertical discontinuity between two plane layered structures as a model for the ocean-continent boundary in California, McGarr (1969) showed that the energy lost by fundamental Rayleigh waves upon crossing (at normal incidence) the margin amounts to no more than 10 to 20 percent for periods near 20 seconds. This is equivalent to a decrease in amplitude of at most 10 percent. Very similar results were obtained for Love waves by Boore (1970), who used a more gradual model for the continental boundary. Ward and Toksöz (1970), furthermore, measured the magnitudes of body and surface waves, recorded at the Norwegian Seismic Array (NORSAR), from 11 western North American earthquakes and 4 NTS explosions. Their plot of M_S versus m_b, given in Figure 2, closely resembles that of Liebermann and Pomeroy (1969), whose magnitudes determined on North American LRSM and WWSSN instruments are also shown in the figure. It must be concluded that propagation across two continental margins did not measurably affect the surface wave amplitudes.

This conclusion does not preclude the possibility that at some continent-ocean boundaries or at certain angles of incidence to the boundary, Rayleigh waves are appreciably scattered. Gutenberg and Richter (1936), in fact, observed that surface waves that travel along the margin of the Pacific Ocean attenuate at approximately twice the rate of waves travelling other paths, but that the Atlantic and Indian Oceans do not display a similar phenomenon. The recent work of Capon et al (1967) supports this finding for the Pacific: earthquakes of a given body wave magnitude observed at LASA from the Aletuian and Kurile-Kamchatka arcs have smaller surface wave magnitudes than do earthquakes from central Asia or the Solomon Islands.

Body wave attenuation

The amplitude of a seismic body wave is a complicated function of the source and medium of propagation. Body wave Q^{-1}, a function of space coordinates and possibly frequency and strain amplitude, is known only roughly in the interior of the earth, often to no better than an order of magnitude. A method recently proposed by the authors, however, permits the lateral variation in attenuation to be determined with some confidence (Solomon and Toksöz, 1970).

Suppose that the attenuation characteristics of the 'average' earth, considered spherically symmetric, can be described by some function $Q^{-1}(r)$, where r is the radial distance from the earth's center. We assume losses are amplitude-independent; $Q^{-1}(r)$ may be a function of frequency, however. Then for $Q^{-2}<<1$ everywhere, the amplitude of a body wave recorded at a point $\underline{P}_0$, a distance Δ from a point source at $\underline{r}_0$, a distance Δ from a point source at $\underline{r}_0$, may be written

$$A(f) = A_0(f,\underline{r}_0, \underline{p}_0)\exp\left[-\pi f \int_{S(\underline{p}_0-\underline{r}_0)} Q^{-1}(s)V^{-1}(s)dS\right] \qquad (1)$$

where f is frequency, A_0 includes the effects of the source radiation pattern and geometric spreading, Q^{-1} is the actual attenuation along the propagation path s, and v is the wave velocity, assumed to depend only on r. Write

$$t^* = \pi \int_{S(\underline{p}_0-\underline{r}_0)} Q^{-1}(s)\, v^{-1}(s)\, ds \qquad (2)$$

$$\delta t^* = \pi \int_{S(\underline{p}_0-\underline{r}_0)} [Q^{-1}(s) - Q^{-1}(s)]\, v^{-1}(s)\, ds \qquad (3)$$

For focal depths greater than about 400 km, the largest contributions to t^* are from the upper mantle beneath the receiving station; the same may presumably be said of δt^*. For $30°<\Delta<80°$, t^* and δt^* are only weakly dependent on Δ. Then

$$\ln A(f) = c(f,\underline{r}_0,\underline{p}_0) - f(t^* + \delta t^*) \qquad (4)$$

If the same wave is observed at two stations (1 and 2, say)

equidistant from the source,

$$\ln \frac{A_1(f)}{A_2(f)} = a_{12} + f(\delta t_2^* - \delta t_1^*) \qquad (5)$$

where a_{12} is independent of frequency and equals zero if the source radiates energy uniformly in all directions and if the two stations lie on identical crusts.

Measured values of the differential attenuation δt^* (from Solomon and Toksöz, 1970) for long-period P waves from deep-focus earthquakes in South America, as recorded at WWSSN stations in the United States, are shown in Figure 3. These values were determined from P-wave spectral ratios using equation (5), assuming δt^* to be frequency independent over the frequency range studied (roughly .01 - .20 Hz). The figure clearly shows at least one large area of above-average attenuation (positive δt^*) between the Rocky Mountain front and the Sierra Nevada - Cascade ranges. From the figure one can make two important hypotheses concerning body wave magnitudes: (1) If the differences at long periods between δt^* for the Pacific Border province and that for the Basin and Range province persist at periods near 1 second, then body wave magnitudes for California earthquakes, recorded at teleseismic distances, should be greater than those for Nevada-Arizona earthquakes of comparable surface wave magnitude. (2) Because differences in m_b predicted from δt^* values obtained for long-period waves are less than those observed, attenuation appears to be frequency dependent. Each of these statements merits closer scrutiny.

As a test of the first hypothesis above, we reproduce in Figure 4 Basham's (1969) measurements at Canadian stations of m_b and M_S for earthquakes and explosions in southwestern North America, with one important distinction. The earthquake population is segregated into two groups: (i) those that occur within the zone of high attenuation (10 in the Basin and Range Province and 6 in the Gulf of California), and (ii) those that occur outside (8 in the California Border Province, 2 in western Baja California, and 1 near Denver). The earthquakes in group (ii) cluster very tightly about a straight line. With one exception, earthquakes in group (i) lie well above that line. From the fitting of straight lines, using a least squared error criterion, to the two populations, we conclude that in the m_b range 4.5 to 5.5 earthquakes of a given surface wave magnitude from the Basin and Range - Gulf of California region show apparent body wave magnitudes 0.3 to 0.4 less than do comparable earthquakes from adjacent regions (principally the San Andreas region of California). That this difference is due to lateral variations in Q^{-1} in the upper mantle is strongly suggested, though not proven. Differences in average depth of focus or source volume for earthquakes of the two areas is another possible explanation. The typically shallow depth of California

earthquakes, however, and the finding by Wyss and Brune (1968) that source dimensions of earthquakes in the Nevada-Arizona region are often much smaller than those on the San Andreas fault system are compelling arguments that the latter explanation is not valid.

Lateral variation of attenuation near the source of an event can also impose an azimuthal variation of body wave amplitude independent of the source radiation pattern. This effect is important principally for events located near mid-ocean ridges and island arcs (Ward and Toksöz, 1970; Solomon and Toksöz, 1970).

Thus the attenuative properties of a medium can significantly alter the $M_S - m_b$ relationship. The anomalous $M_S - m_b$ pattern in western North America is at least in part due to greater-than-average attenuation of P waves in the upper mantle of that region. Even more importantly, by considering in Figure 4 only those earthquakes and explosions which occur in the same tectonic region (NTS is in the Basin and Range province) a more effective separation of explosion and earthquake populations is achieved than if all earthquakes from western North America are lumped into a single category.

Consider now the difference in body wave magnitudes for earthquakes of a given M_S in California and the Basin and Range province that we might predict from Figure 3. The average δt^* for California is -3.7; for the Basin and Range province δt^* is about 2.4. Using equation (5), we find that for P waves of 10-second period the amplitude observed at California should be, on the average, a factor of 2 greater than the amplitude recorded in the Arizona-Nevada region (we assume that a_{12} in equation (5) has zero mean for a sufficiently large sample of events).

If δt^* is independent of frequency (i.e. if we make the questionable assumption that long-period spectral ratios may be extrapolated to higher frequencies), then for 1-second P waves we should predict amplitudes in California 400 times greater than in the Basin and Range area. This amounts to a magnitude difference of 2.6, clearly much larger than the difference of 0.3 to 0.4 indicated in Figure 4. Though the larger source volume of California earthquakes (Wyss and Brune, 1968) mentioned above may mask some of the effect of variations in upper mantle attenuation, the conclusion that the differences in δt^* between the two regions decreases with increasing frequency is difficult to avoid. This is consistent with recent work indicating that Q_P^{-1} decreases with increasing frequency in the upper mantle (see Solomon and Toksöz, 1970, for a summary).

Ward and Toksöz (1970) have uncovered other evidence that Q^{-1} may be frequency dependent. From observations of short-period P waves from three deep earthquakes recorded at LASA and NORSAR, they concluded

$$\delta t^*_{LASA} - \delta t^*_{NORSAR} = 0.97 \pm .60 \text{ (standard deviation of the mean).}$$

This implies (ignoring frequency-independent amplification effects) that body wave magnitudes should average 0.4 ± 0.3 units higher at NORSAR than at LASA; the observed difference is typically 0.1 to 0.3, in good agreement with the predicted value. Although the number of earthquakes well-recorded at long periods at both NORSAR and LASA is insufficient to place meaningful constraints on the frequency dependence of Q^{-1}, there is a weak indication that at long periods the upper mantle beneath NORSAR may be more dissipative than that under LASA.

That elastic wave attenuation, as given by Q^{-1}, varies with frequency is not unexpected. In the upper mantle attenuation is primarily controlled by temperature and by the possible presence of fluid phases (water or partial melt). Under such conditions attenuation typically follows a relaxation-type behavior (Walsh, 1969). Parameters of the relaxation (peak frequency, relaxation strength) depend critically on temperature and on the geometrical arrangement of any fluid zones. Thus the functional dependence of Q^{-1} on frequency will vary regionally. Beneath any particular location, Q^{-1} cannot be assumed *a priori*, but must be determined by measurement.

CONCLUSIONS

1. Lateral variation in seismic attenuation appreciably affects the M_S - m_b relationship, primarily through the decrease in amplitudes of P waves which travel through the upper mantle.

2. By comparing explosions with earthquakes from the same tectonic province, the separation between the two populations on the basis of the M_S - m_b criterion is better defined than if events from several provinces are combined.

3. Q^{-1} for P waves appears to be frequency dependent. Thus measurements of amplitudes or differential attenuation made in one frequency range cannot be applied to amplitudes in another frequency range without some care.

ACKNOWLEDGEMENTS

This research was supported by the Advanced Research Projects Agency and monitored by the Air Force Office of Scientific Research under contract AF 49(638)-1632. One of us (Solomon) was a fellow of the Fannie and John Hertz Foundation during this work.

REFERENCES

Basham, P.W., 1969, Canadian magnitudes of earthquakes and nuclear explosions in south-western North America, Geophys. J. Roy. Astr. Soc., v. 17, p. 1-13.

Boore, D.M., 1970, Love waves in nonuniform wave guides: finite difference calculations, J. Geophys. Res., v. 75, p. 1512-1527.

Capon, J., Greenfield, R.J., and Lacoss, R.T., 1967, Long-period signal processing results for Large Aperture Seismic Array, Technical Note 1967-50, Lincoln Laboratory, Massachusetts Institute of Technology.

Davies, D., 1968, editor, Seismic methods for monitoring underground explosions, An assessment of the status and outlook, Report by a Seismic Study Group, International Institute for Peace and Conflict Research (SIPRI), Stockholm, 1968.

Gutenberg, B., 1945, Amplitudes of surface waves and magnitudes of shallow earthquakes, Bull. Seism. Soc. Am., v. 35, p. 3-12.

Gutenberg, B., and Richter, C.F., 1936, On seismic waves (third paper), Gerlands Beitr. Z. Geophysik, v. 47, p. 73-131.

Gutenberg, B., and Richter, C.F., 1956, Magnitude and energy of earthquakes, Ann. Geofis., Rome, v. 9, p. 1-15.

Liebermann, R.C., and Pomeroy, P.W., 1969, Relative excitation of surface waves by earthquakes and underground explosions, J. Geophys. Res., v. 74, p. 1575-1590.

McGarr, A., 1969, Amplitude variations of Rayleigh waves - propagation across a continental margin, Bull. Seism. Soc. Am., v. 59, p. 1281-1305.

Press, F., 1964, Seismic wave attenuation in the crust, J. Geophys. Res., v. 69, p. 4417-4418.

Solomon, S.C., and Toksöz, M.N., 1970, Lateral variation of attenuation of P and S waves beneath the United States, Bull. Seism. Soc. Am. v. 60, p. 819-838.

Thirlaway, H.I.S., and Carpenter, E.W., 1966, Seismic signal anomalies, travel times, amplitudes, and pulse shapes, Proceedings of the VESIAC Special Study Conference on Seismic Signal Anomalies, Travel Times, Amplitudes and Pulse Shapes, VESIAC Rept. 4410-99-X, 119-140.

Tryggvason, E., 1965, Dissipation of Rayleigh wave energy, J. Geophys. Res., v. 70, p. 1449-1455.

Tsai, Y.-B., and Aki, K., 1969, Simultaneous determination of the seismic moment and attenuation of seismic surface waves, Bull. Seism. Soc. Am., v. 59, p. 275-287.

Walsh, J.B., 1969, A new analysis of attenuation in partially melted rock, J. Geophys. Res., v. 74, p. 4333-4337.

Ward, R.W., and Toksöz, M.N., 1970, Causes of regional variations in a long-period - short-period discriminant, to be published.

Wyss, M., and Brune, J.N., 1968, Seismic moment, stress, and source dimensions for earthquakes in the California - Nevada region, J. Geophys. Res., v. 73, p. 4681-4694.

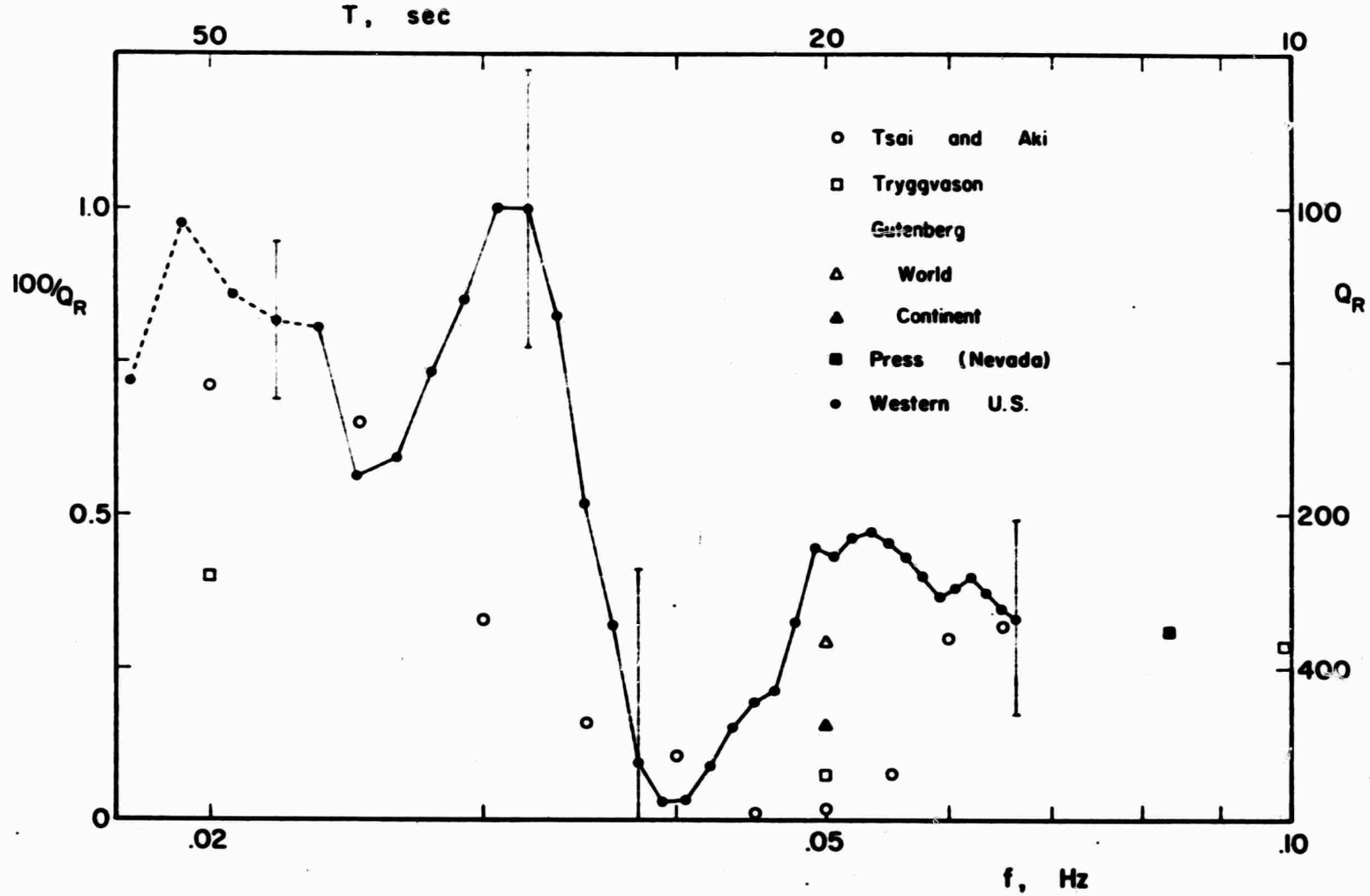

Figure 1. Rayleigh wave attenuation for the period range 10 to 50 seconds. Open symbols are averages over symbols are averages over both oceanic and continental structures (from Gutenberg, 1945; Tryggvason, 1965; Tsai and Aki, 1969); solid symbols are for purely continental paths (from Gutenberg, 1945; Press, 1964). Values of Q_R^{-1} for the western United States, as measured between WWSSN stations LON and TUC, are connected by the solid line (the line is dashed where attenuation has been determined for one direction only).

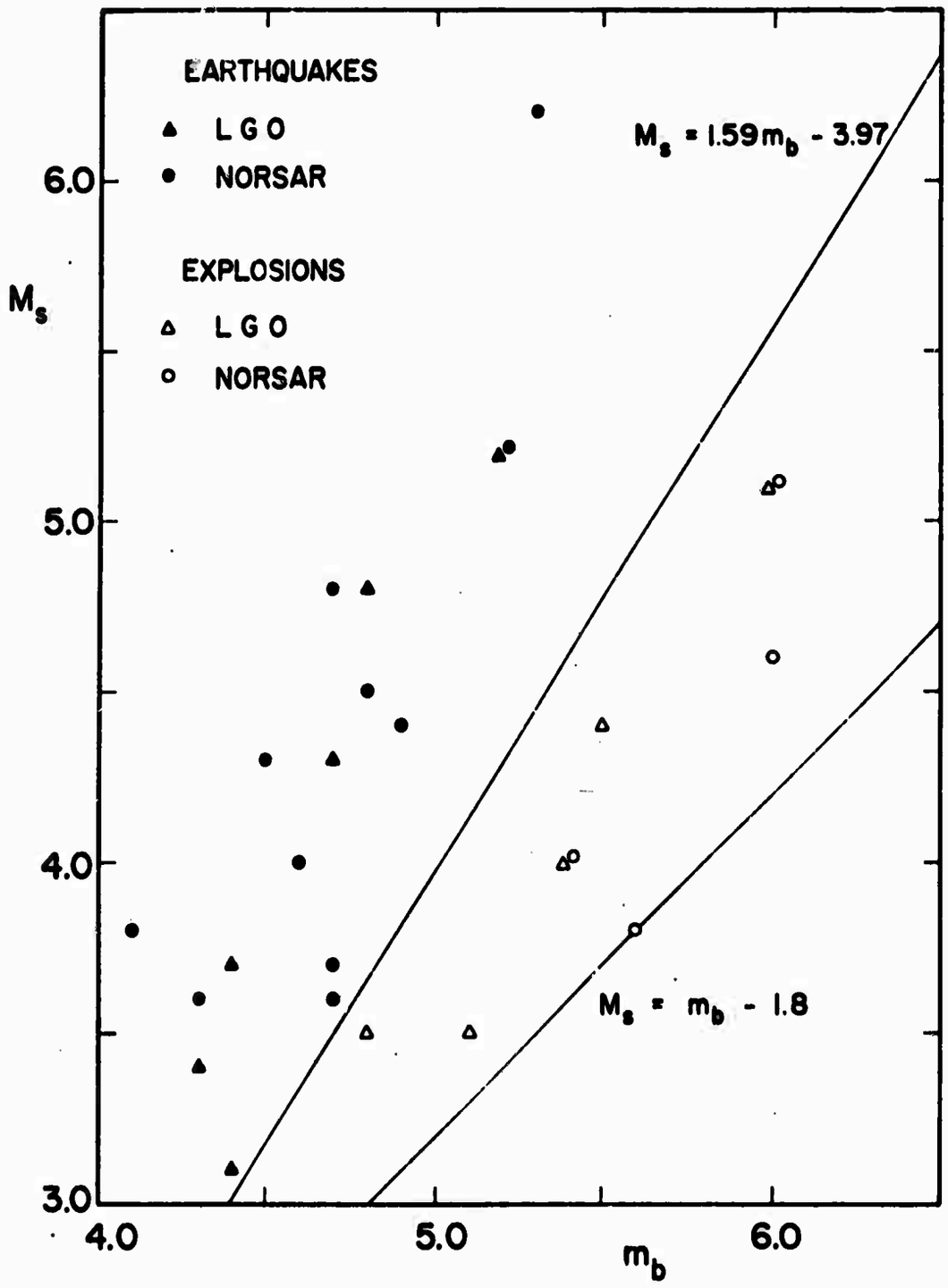

Figure 2. M_S versus m_b for events in western North America. Measurements labeled LGO were made by Liebermann and Pomeroy (1969) from records at North American stations. NORSAR measurements are from Ward and Toksoz (1970). The straight lines are an empirical relation for earthquakes (upper line, from Gutenberg and Richter, 1956) and a theoretical relationship for nuclear explosions in granite (lower line, from Thirlaway and Carpenter, 1966).

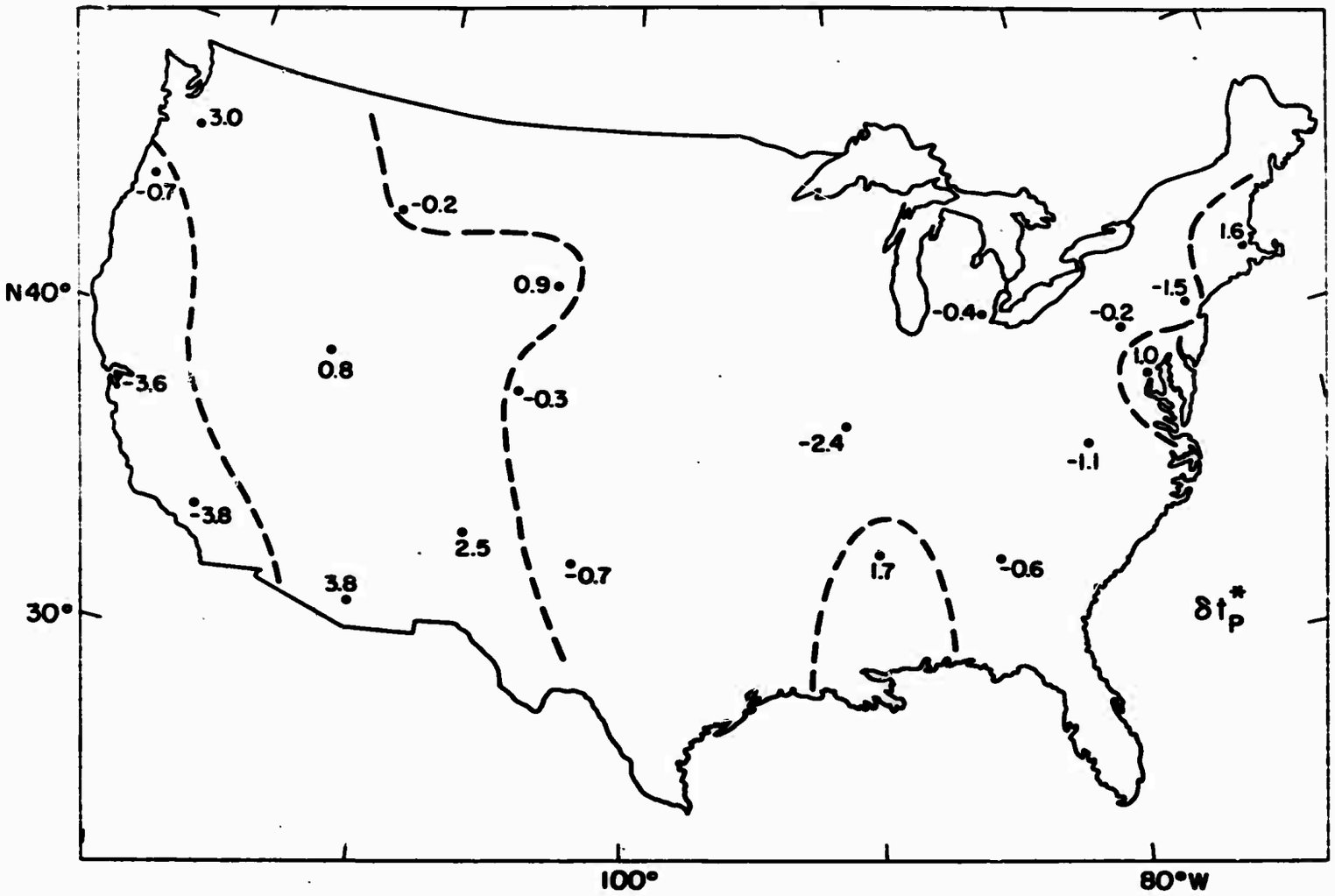

Figure 3. Differential attenuation of long-period P waves at WWSSN stations in the United States (from Solomon and Toksöz, 1970).

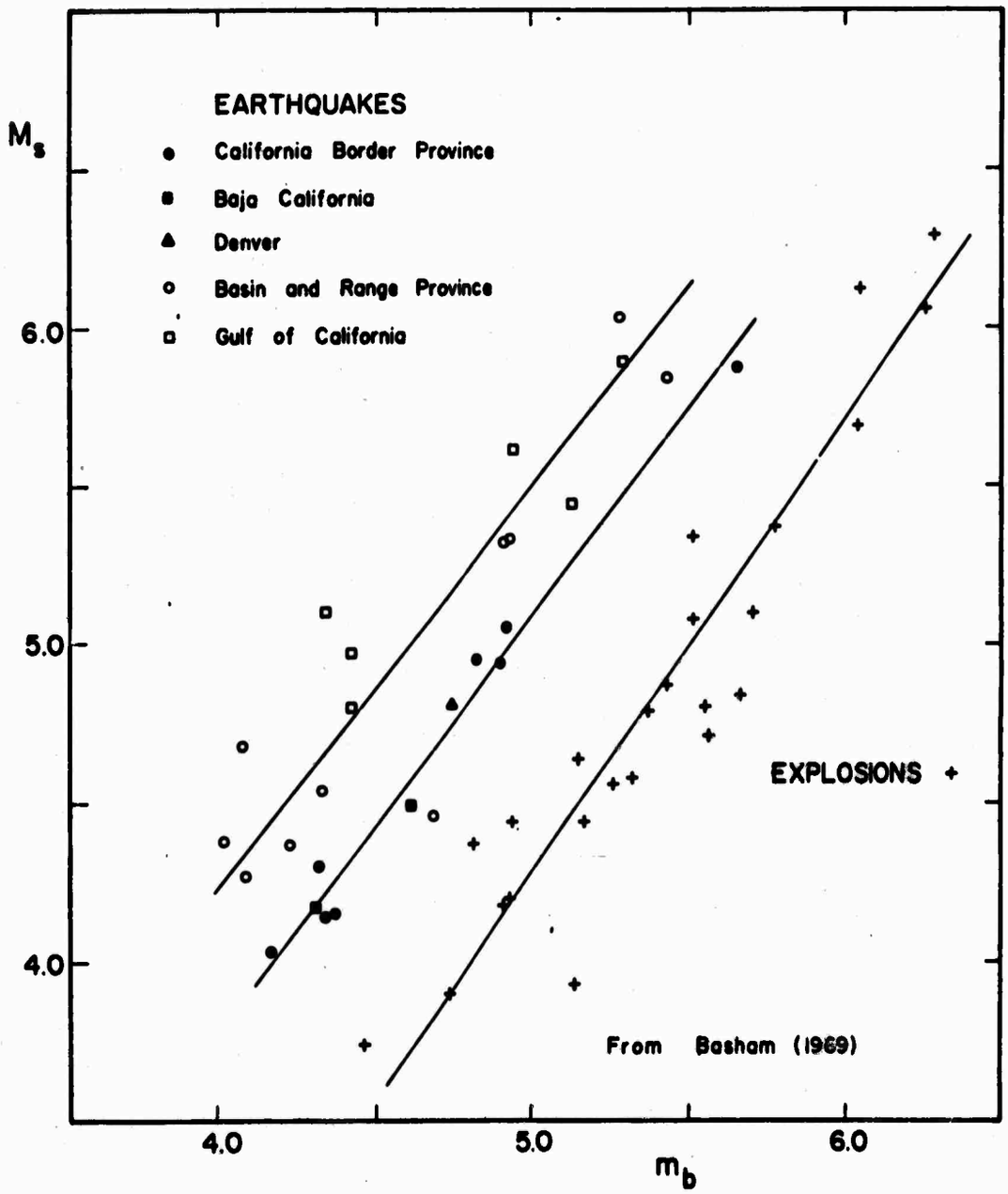

Figure 4. M_S versus m_b, measured at stations in the Canadian Network, for events in southwestern North America (from Basham, 1969). Earthquakes represented by solid symbols are located in regions of negative δt^* in Figure 3; those given by open symbols are located in areas of high attenuation (positive δt^*) in Figure 3. Straight lines are (lowest line) Basham's (1969) fit to the explosion data and (upper two lines) least-squared-error fits to the two earthquake populations.

EFFECT OF REGIONAL CORRECTION ON THE VALUE OF m_b

By

Atiq Syed

Reported By

William Stauder
Saint Louis University

Discrepancies in magnitude determination are known to result in part from the effect of the earthquake radiation pattern on the recorded wave amplitudes. The purpose of the study reported here is to obtain a quantitative estimate of the effect of the radiation pattern on P wave amplitudes and to develop a methodology for improving body wave magnitude determinations. The results of the study may also be used as an auxiliary discriminant between earthquakes and explosions.

Correction for mechanism

The P wave displacement at the surface of a focal sphere of radius R for a double couple point source is given by the expression

$$u_p = \frac{2xy}{4\pi\rho a^3 R^3} K'(t - \frac{R}{\alpha}) \qquad (1)$$

If for a given earthquake the observed P wave amplitudes are divided by the product 2xy the P amplitudes will be corrected relative to the maximum value of the P wave radiation. For magnitude calculations in keeping with the assumptions made in the definition of magnitude, a further normalization is required, a reduction of the P wave amplitude to the average value of the displacement of P over the surface of the focal sphere. This average amplitude is obtained from the relation

$$\bar{u}_p = \frac{\int 2xy\,ds}{\int ds} = 0.424$$

or

$$\bar{u}_p = 0.424\ (u_p)\ \text{max.}$$

Thus, the total reduction of P wave amplitudes to take into account includes first the application of the 2xy factor and second multiplication by 0.424 to equate the P wave radiation from a double couple to that from a spherically symmetric source of the same strength.

It has long been observed that earthquake foci located in a given region tend to have similar orientations of the focal mechanism. This observation is in keeping with the theory of plate tectonics. Plate tectonics, in turn, provides a basis for prediction of the dominant focal mechanism. On the hypothesis that characteristic foci do exist for given hypocentral regions, P wave amplitudes can be corrected for the source mechanism and thereby magnitude estimates can be obtained which have smaller standard errors.

A procedure for applying the source mechanism correction is as follows:

1. Given the source parameters for a typical earthquake in a

particular hypocentral region, compute the 2xy factor for all seismograph stations.

2. On the basis of this factor, predict which stations will record relatively large P wave amplitudes for earthquakes for the region in question, and which relatively small.

3. Select stations at which the P wave amplitudes are best suited for magnitude determinations for earthquakes from that region. For example, criteria for selection of stations might be

a. Stations should be in the epicentral distance range of 25° to 100°

b. The 2xy factor should be greater than the normalizing factor, 0.424.

The latter criterion insures that the P wave amplitude be relatively large, but also that small differences between the actual source mechanism and the average or characteristic mechanism of the region will have minimal effect on the reduced amplitudes.

4. However, if only those stations with 2xy larger than the normalizing factor are used in determining m_b, the magnitude determinations will be too small. It is possible to correct for the effect by subtracting from the initial m_b value the quantity log $(2\overline{xy}/.424)$, where $2\bar{x}\bar{y}$ is the average value of 2xy at all stations with 2xy greater than 0.424. This is a constant correction to be applied to all earthquakes in any particular geographic group. It is called the regional correction factor. In practice values of this correction in the regions studied thus far are found to vary from 0.1 to 0.25 of a magnitude unit.

5. If desirable, instead of the required correction an indiviual mechanism correction may be applied by subtracting the quantity log (2xy/.424) determined at each station. This correction is applicable even to stations at which 2xy < .424, provided the 2xy factors be not too small. That is, stations very near nodal lines should always be excluded.

Application

In order to test this suggestion and to exemplify the order of magnitude of the corrections involved, earthquakes from two regions have been studied: earthquakes of the Aleutian Islands, and ones of the North Atlantic. Earthquakes of the Aleutian Islands (Figure 1) divide into three groups on the basis of their source mechanism as determined by Stauder (1968a, b). Similarly those of the Atlantic divide into two groups (Sykes, 1967). For each group we can calculate the average or dominant source mechanism, and then apply the various corrections indicated above.

1. Earthquake of March 30, 1965.

This earthquake belongs to group 3b of the Aleutian Island

earthquakes. This group consists of earthquakes which occur along a narrow line immediately below the axis of the Aleutian trench or under the seaward slope of the trench. Foci of this group are uniformly extensional in character, with the axis of tension aligned normal to the local axis of the trench. The average focal mechanism for earthquakes in this group is characterized by two nodal planes dipping about 40° - 50°.

For m_b determinations the amplitudes and periods of the first half-cycle of the vertical component long period P waves were the basic data. The 2xy factors are determined and listed in Table 1 along with the m_b value determined the ordinary way (m_b uncorrected). One notices that for small 2xy factors the m_b values are smaller than for the larger 2xy factors. The average uncorrected magnitude using the data of all 37 stations is 7.23 ± 0.21. The average m_b value for all stations with 2xy > 0.424 is 7.34 ± 0.15. The average value for stations with 2xy < 0.424 is 7.03 ± 0.17. Applying the regional focal mechanism correction for all stations with 2xy > 0.424, m_b = 7.12 ± 0.15. Finally, correcting for individual station focal mechanism corrections we obtain for all stations m_b = 7.13 ± 0.16. These results are summarized in Table 2.

It is noteworthy that using stations with 2xy > 0.424 and applying the constant regional correction, the m_b value is very close to that from all the stations using the individual mechanism corrections. This would seem to justify using for magnitude determinations only those stations for which 2xy is > 0.424. One may, in fact, in this way define zones on the earth's surface, identifying stations (solid circles in Figure 2) favorable for m_b determinations, and others (crosses in the figure) to be avoided in magnitude determinations.

2. Earthquake of November 22, 1965.

This earthquake belongs to group 1 of the Aleutian Island earthquakes. This group consists of foci on the concave side of the island arc, in the zone immediately south of and under the island chain. Focal mechanism stations in this group have one steeply dipping nodal plane, with the other nodal plane nearly horizontal. Many stations in this case are close to the nodal plane. Consequently the number of stations suitable for P wave magnitude determination was much smaller than in group 3b. The average uncorrected magnitude using the data of all 19 stations is 6.20 ± 0.24. The average m_b for all stations with xy larger than 0.424 corrected for the regional effect is 5.99 ± 0.22. The average m_b of all stations whose amplitudes have been corrected for the source mechanism is 6.00 ± 0.26.

3. Earthquake of August 3, 1963.

This earthquake belongs to group 1 of the North Atlantic earthquakes. The events in this group are located on the equatorial fracture zone of the mid-Atlantic ridge. The mechanism of these earthquakes correspond to two near vertical nodal planes. Consequently,

the 2xy factors calculated for a typical earthquake in this group at all the stations at a distance of 25-100 degrees are smaller than 0.424, which is the normalizing factor. Consequently it is not possible to satisfy the second criterion in selecting the stations suitable for P wave magnitude determination. Departing from this criterion, we have selected those stations whose 2xy factors calculated for the average focal mechanism solution are larger than 0.2 and established the appropriate regional corrections. Since the uncorrected P wave magnitudes using the data from these stations will be too low, the regional correction has to be added to the average magnitude value. The results of the m_b calculation for this earthquake show that the average uncorrected magnitude using the data of all 31 stations is 6.51 $\pm$ 0.29. The average m_b for 15 stations whose 2xy factors are larger than 0.2 corrected for the regional effect is 6.67 $\pm$ 0.20, the average m_b for the same stations whose amplitudes have been corrected for the source mechanism is 6.73 $\pm$ 0.18.

CONCLUSIONS

From this study it can be concluded that a significant part of the scatter in the determination of earthquake magnitudes is due to the effect of the earthquake radiation pattern on the recorded P wave amplitudes. The correction for the focal mechanism becomes more important when the focal mechanism solution is one in which one or both nodal planes are steeply dipping. In these cases the average magnitude determined by using the uncorrected P wave amplitude data may be in error by as much as a quarter of a magnitude unit.

Since the observational data here examined have shown that the average m_b for stations with smaller 2xy factors is significantly smaller than the average m_b for stations with larger 2xy factors, there exists a possibility of comparing the values of uncorrected m_b from these two sets of stations in a region where the average focal mechanism solution is known to differentiate between the earthquakes and explosions. The radiation pattern due to the explosive source being azimuthally uniform, the two sets of m_b values should be identical for explosion and different for the earthquake.

REFERENCES

Stauder, W., 1968a, Mechanism of the Rat Island earthquake sequence of February 4, 1965, with relation to island arcs and sea floor spreading, JGR, v. 73, p. 3847-3858.

Stauder, W., 1968b, Tensional character of earthquake foci beneath the Aleutian trench with relation to sea-floor spreading, JGR, v. 73, p. 7693-7701.

Sykes, L.R., 1967, Mechanism of earthquakes and nature of faulting on the mid-oceanic ridges, JGR, v. 72, p. 2131-2153.

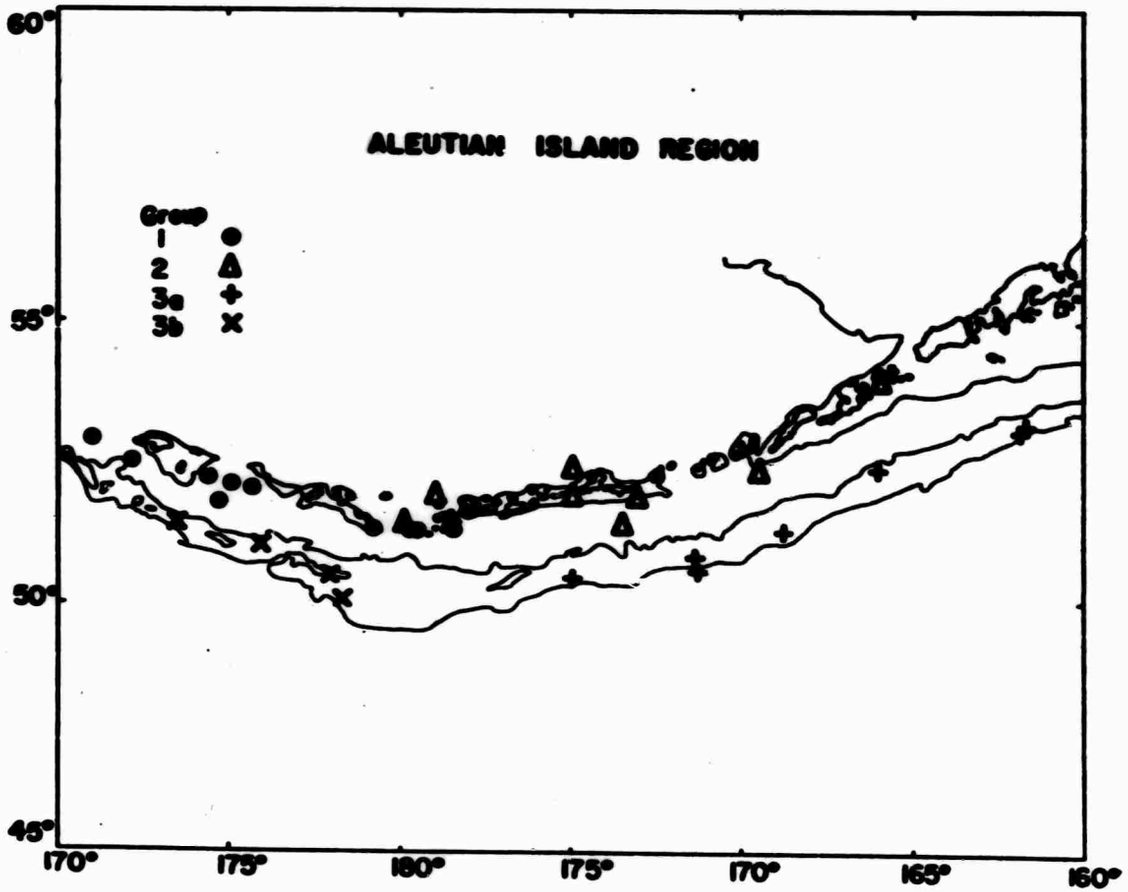

Figure 1. Earthquakes of Aleutian Island region divided into three groups: 1) earthquakes under the islands, western portion of arc, 2) earthquakes under the islands, eastern portion of arc, 3a,b) earthquakes with foci under the trench.

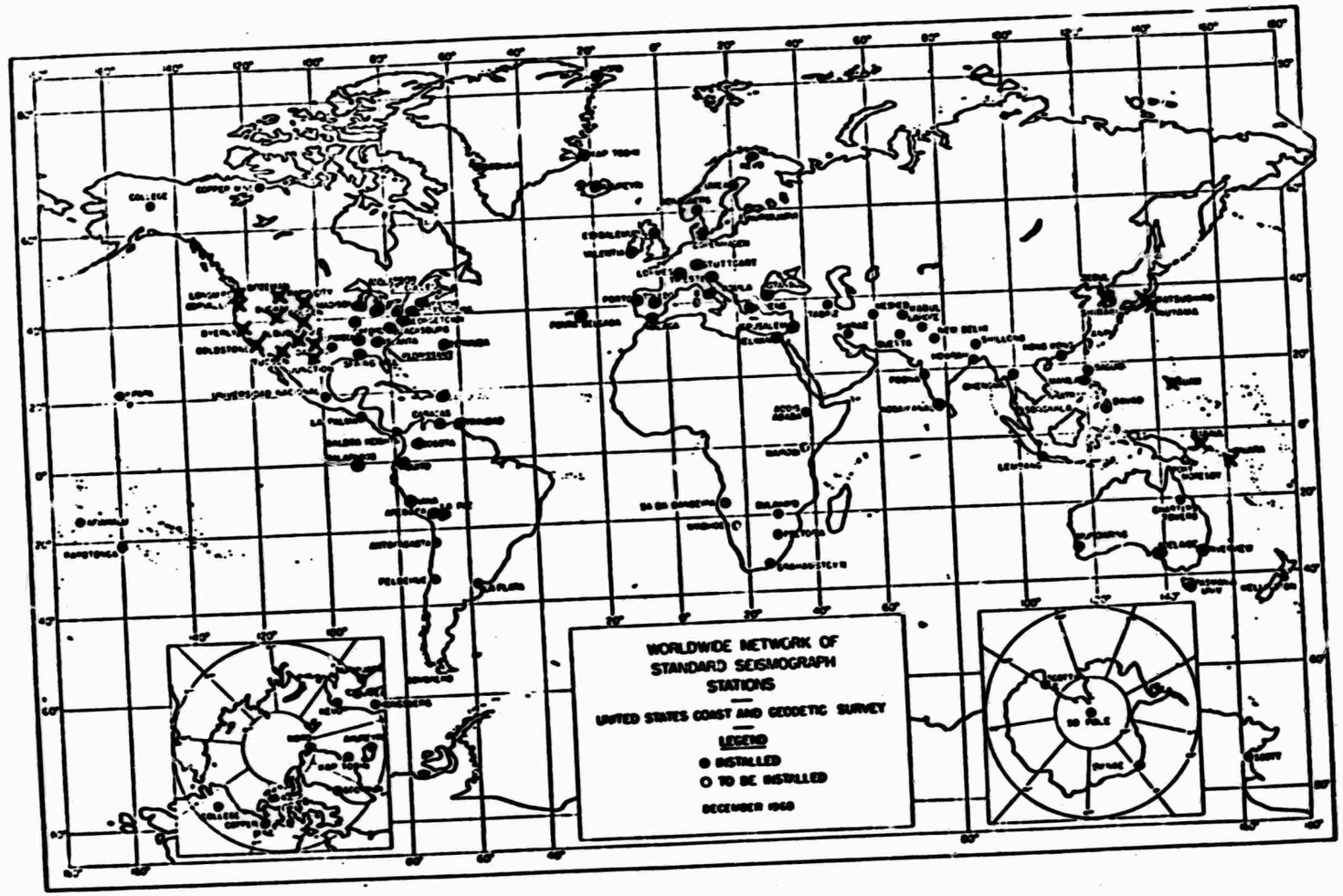

Figure 2. Map indicating stations unfavorable (x) and favorable (●) for determination of m_b for Aleutian Island earthquakes of group 3a.

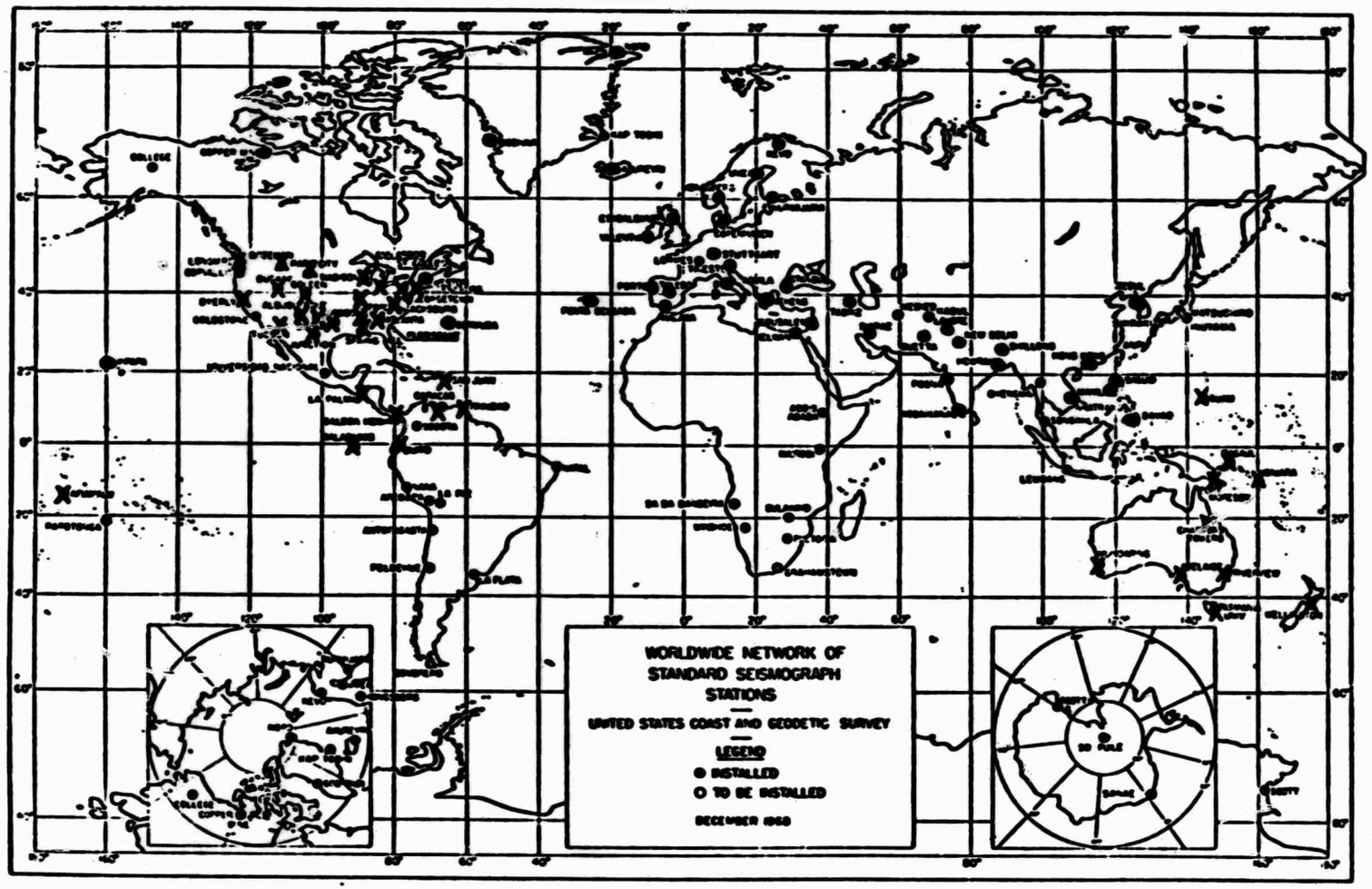

Figure 3. Map indicating stations unfavorable (x) and favorable (●) for determining m_b for Aleutian Island earthquakes of group 1.

Table 1. Earthquake of March 30, 1965.

Sta.	Dist.	2xy	m_b(uncorr)	m_b(corr)
LON	39.0	0.250	6.88	7.11
CMC	36.2	0.256	6.89	7.11
KIP	34.7	0.278	7.03	7.21
DUG	48.1	0.322	7.02	7.14
GUA	45.6	0.322	6.79	6.91
RCD	51.5	0.338	7.08	7.18
GSC	49.8	0.346	7.06	7.15
GOL	52.9	0.352	7.14	7.22
RAB	58.9	0.356	7.09	7.16
HNR	61.8	0.360	7.30	7.37
TUC	54.4	0.382	6.93	6.97
LUB	59.0	0.422	6.88	6.88
MDS	59.4	0.424	7.37	7.37
FLO	62.2	0.448	7.34	7.32
AAM	63.4	0.466	7.25	7.21
SHA	69.3	0.506	7.57	7.49
WES	69.5	0.532	7.05	6.95
RIV	87.3	0.594	7.50	7.35
TAU	96.9	0.624	7.23	7.06
KTG	58.4	0.636	7.57	7.39
ADE	91.9	0.638	7.42	7.25
BHP	91.0	0.642	7.35	7.17
QUI	98.8	0.646	7.17	6.99

Table 1. (cont'd)

Sta.	Dist.	2xy	m_b(uncorr)	m_b(corr)
CAR	97.3	0.664	7.20	7.00
TRN	100.3	0.672	7.13	6.93
VAL	77.6	0.674	7.33	7.07
MUN	98.6	0.714	7.40	7.18
HKC	56.5	0.744	7.25	7.01
KEV	58.1	0.780	7.43	7.16
KON	69.7	0.804	7.26	6.99
PTO	88.5	0.826	7.26	6.97
COP	73.4	0.834	7.28	6.99
TOL	89.9	0.844	7.52	7.22
MAL	93.0	0.850	7.17	6.87
STU	80.5	0.856	7.26	6.96
KOD	88.7	0.952	7.61	7.26
JER	91.6	0.966	7.51	7.15

Table 2. Average m_b values, March 30, 1965.

Uncorrected	
All stations (n = 37)	$m_b = 7.34 \pm 0.21$
For 2xy < 0.42 (n = 13)	$m_b = 7.03 \pm 0.17$
For 2xy > 0.42 (n = 24)	$m_b = 7.34 \pm 0.15$
Corrected	
Regional corr. (n = 24)	$m_b = 7.12 \pm 0.15$
Individual mech. corr. (n = 37)	$m_b = 7.13 \pm 0.16$

Table 3. August 3, 1963 Earthquake

Sta.	Dist.	2xy	m_b(uncorr)	m_b(corr)
NAI	36.5	0.030	6.42	7.56
BOG	38.2	0.036	5.50	6.57
KON	62.1	0.060	6.76	7.60
NUR	69.1	0.062	6.73	7.56
BUL	69.1	0.068	6.41	7.20
VAL	48.8	0.072	6.73	7.50
AAE	73.7	0.074	6.75	7.51
PRE	70.5	0.084	6.52	7.22
CAR	30.9	0.104	6.05	6.66
QUI	43.3	0.111	6.41	6.99
WIN	59.9	0.124	6.80	7.33
TRN	25.4	0.128	6.38	6.90
IST	66.0	0.154	6.75	7.19
ATU	61.4	0.180	6.93	7.30
BKS	82.5	0.194	6.17	6.51
GSC	78.4	0.198	6.32	6.66
TUC	73.3	0.212	6.33	6.63
LON	81.7	0.214	6.16	6.46
TOL	42.8	0.226	6.65	6.92
DUG	75.2	0.234	6.34	6.60
ALQ	69.8	0.242	6.53	6.77
MAL	40.6	0.252	6.70	6.92
GOL	69.4	0.260	6.45	6.66

Table 3. (Cont'd)

Sta.	Dist	2xy	m_b(uncorr)	m_b(corr)
LPA	47.3	0.266	6.97	7.17
NNA	45.3	0.268	6.61	6.81
RCD	68.5	0.276	6.39	6.58
SHA	53.9	0.312	6.70	6.83
FLO	57.9	0.322	6.45	6.55
AAM	54.4	0.366	6.61	6.67
GEO	48.4	0.398	6.67	6.69
SCP	49.8	0.398	6.69	6.72

Table 4. November 22, 1965 Earthquake

Sta.	Dist.	2xy	m_b(uncorr)	m_b(corr)
PMG	66.8	0.124	5.94	6.47
CTA	77.0	0.130	5.83	6.34
MAN	59.2	0.608	6.50	6.35
BAG	58.2	0.628	6.23	6.06
HKC	57.7	0.730	6.15	5.92
TOL	89.0	0.788	5.85	5.58
CHG	69.8	0.798	6.00	5.72
KOD	89.6	0.816	6.51	6.22
HOW	73.5	0.858	6.38	6.08
POO	85.2	0.860	6.45	5.15
KON	69.0	0.862	5.98	5.67
SHL	69.1	0.862	6.11	5.80
JER	91.5	0.886	6.14	5.82
IST	84.5	0.890	6.05	5.73
SHI	86.9	0.904	6.49	6.16
NDI	75.3	0.904	6.28	5.95
QUE	79.6	0.914	6.16	5.83
TAB	82.0	0.916	6.17	5.84
LAH	74.7	0.920	6.63	6.30

Earthquake of November 22, 1965

Av. m_b (uncorr) = 6.20 $\pm$ 0.24	n = 19
Av. m_b (uncorr) for 2xy $>$ 0.42 = 6.24 $\pm$ 0.22	n = 17
Av. m_b (corr for regional effect)for 2xy $>$ 0.42 = 5.99 $\pm$ 0.22	n = 17
Av. m_b (corr for focal mech) = 6.00 $\pm$ 0.26	n = 19

Earthquake of August 3, 1963

Av. m_b (uncorr) = 6.51 $\pm$ 0.29	n = 31
Av. m_b (uncorr) for 2xy $>$ 0.20 = 6.55 $\pm$ 0.20	n = 15
Av. m_b (corr for regional effect) for 2xy $>$ 0.20 = 6.67 $\pm$ 0.20	n = 15
Av. m_b (corr for focal mech) for 2xy $>$ 0.20 = 6.73 $\pm$ 0.18	n = 15

ANALYSIS OF LONG-PERIOD NOISE AT LASA*

By

Jack Capon

Lincoln Laboratory
Massachusetts Institute of Technology
Lexington, Massachusetts

*This work was sponsored by the Advanced Research Projects Agency of the Department of Defense.

The background noise on the long-period vertical seismometers is limiting the identification threshold at which the M_S-m_b discriminant can be applied at LASA. Thus, an investigation was made to determine the sources and properties of this noise in the 20- to 40-second period range.

The first step in the analysis was to determine how much noise was introduced by the long-period system. Power spectral density measurements taken for a locked mass test condition showed that the noise introduced by the long-period system is 10 to 30 db lower than that of the normal background noise level. Hence, the long-period system contributes a negligible amount of noise.

The frequency-wavenumber spectra for the noise were measured and two examples are shown in Figures 1 and 2. These data indicate that there is a component of the noise which propagates across the LASA as a fundamental-mode Rayleigh wave. In addition, coherence measurements show that there is a nonpropagating component of the noise which is incoherent between sensors which are 7.5 km apart. The relative amounts of each noise component, as well as the total noise, are shown in Figure 3 for thirty-one noise samples extending in time over a period of about 14 months. These results show that there is a considerable spread in the total long-period vertical noise power of about 13 db, and that a significant amount of power can be contributed by either component of the noise at any particular time.

It is important to establish the origin of the nonpropagating long-period vertical seismic noise. Thus, an effort was made to determine the coherence between the long-period vertical seismic noise and the atmospheric fluctuations as recorded on microbarograph sensors at LASA.

The long-period seismometers are located in sealed metal tanks embedded in the floor of an underground concrete structure, known as the LP vault. Each tank is sealed and tested for a leakage rate time constant of at least 8 hours.

At the time of the present experiment there were five microbarograph installations at LASA, each located near the center of a subarray and usually less than a few hundred feet from the long-period seismometers. In some cases, such as sites E3, B1, and B4, the microbarograph was actually located in the same vault as the long-period seismometers. One of the two microbarographs at site AØ had various types of wind filters and the other used a single type of wind filter, namely a linear pipe array with orifices spaced 3 meters apart. Comparable results were obtained with either of these two microbarographs.

Two examples in which coherence was measured at site AØ are given in Figure 4, where the bottom graph represents the more typical behavior of the coherence when any coherence is measured in all. In Figure 4a the coherence at 0.03 Hz is quite high,

about 0.5 and 0.4 and 0.04 and 0.05 Hz, respectively. The ratio of nonpropagating noise to the total noise, for this noise sample, was measured as 0.9 at 0.03, 0.04, and 0.05 Hz. The measured coherence is not so high at these frequencies but is the largest that was measured for the seventeen noise samples. The results in Figure 4b are more typical in that, whenever coherence is measured, it tends to be high at 0.02 Hz and then drops to the level for incoherent noise at 0.03 to 0.05 Hz. The ratio of nonpropagating to total noise for the noise sample used in Figure 4b was measured as 0.60, 0.45, and 0.35 at 0.03, 0.04, and 0.05 Hz, respectively. It is seen that the coherence never reaches a level compatible with the amount of nonpropagating noise. Thus, we may conclude that there is relatively little coherence between the long-period vertical noise and the microbarograph signals in the 20- to 40-second period range.

An attempt was made to correlate the amount of nonpropagating long-period vertical seismic noise power and the amount of microbarograph noise power in the 20- to 40-second period range. These quantities were measured at site AØ for seventeen noise samples and the results are shown in Figure 5. This figure shows that there is a definite trend for the nonpropagating seismic noise power level to increase when the power level on the microbarograph increases. Thus, we have evidence that the nonpropagating long-period vertical noise is caused by atmospheric pressure fluctuations. Unfortunately, it is not possible, on the basis of the present data, to determine whether the noise is caused by ground motion or by atmospheric buoyancy effects on the mass of the long-period seismometer, despite the pressure case, or possibly by both of these effects. There are many causes of noise in a pressure-sealed long-period seismometer, such as turbulence, convection, hinges, and flexure of the pressure case in response to atmospheric pressure changes which produce buoyancy effects on the mass of the long-period seismometer even though there is a pressure case. However, the present data do provide two significant facts about the nonpropagating noise. This noise has been found to be incoherent over spatial lags greater than 7.5 km, and this noise appears to be caused by atmospheric pressure fluctuations. A more detailed description of the measurements has been published recently.

REFERENCE

J. Capon, 1969, Investigation of long-period noise at the large aperture seismic array, J. Geophys. Res. v. 74, p. 3182-3194.

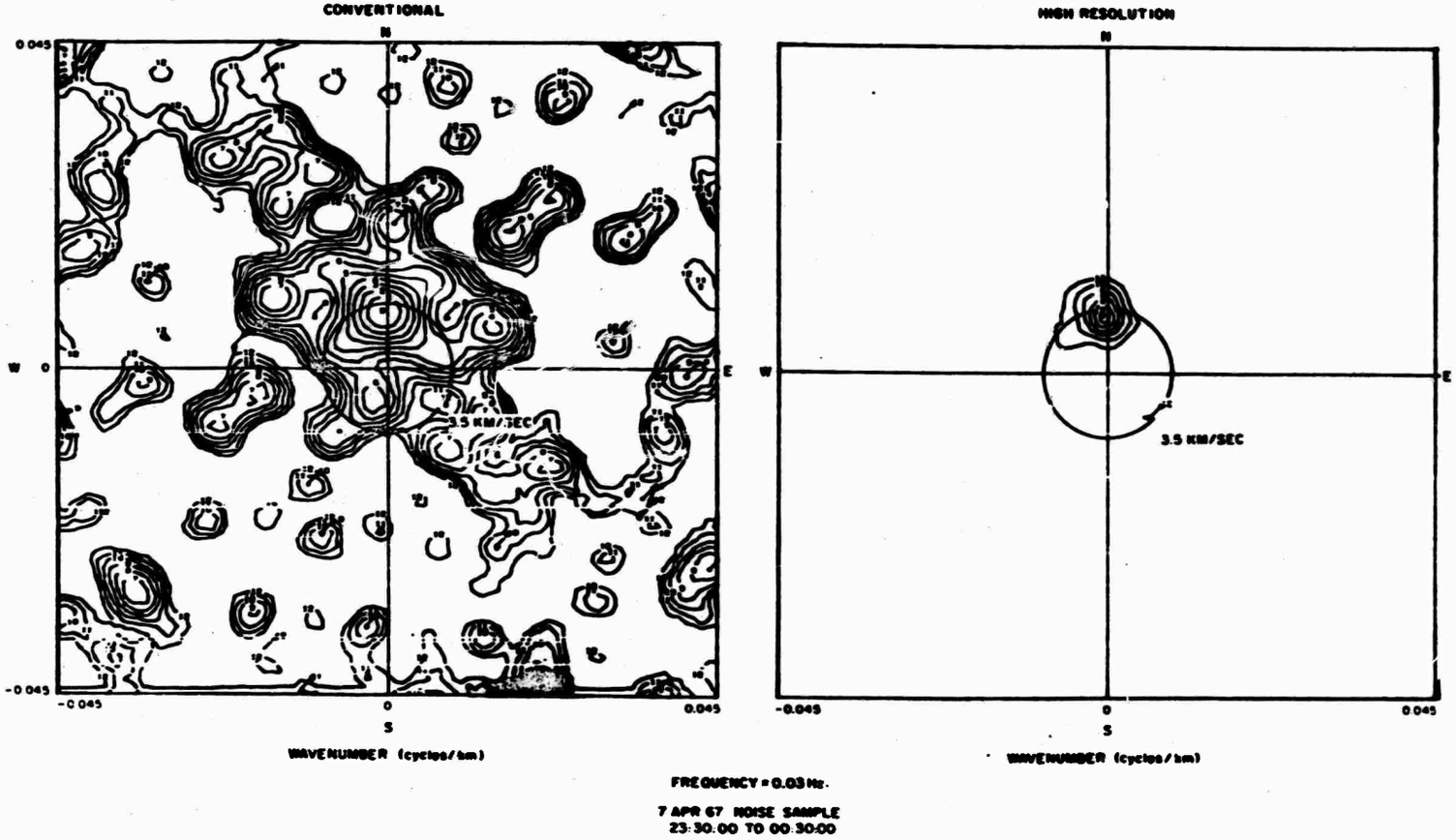
CONVENTIONAL
HIGH RESOLUTION
N
W
E
S
0.045
-0.045
0
3.5 KM/SEC
WAVENUMBER (cycles/km)
FREQUENCY = 0.03 Hz.
7 APR 67 NOISE SAMPLE
23:30.00 TO 00:30:00

Figure 1.

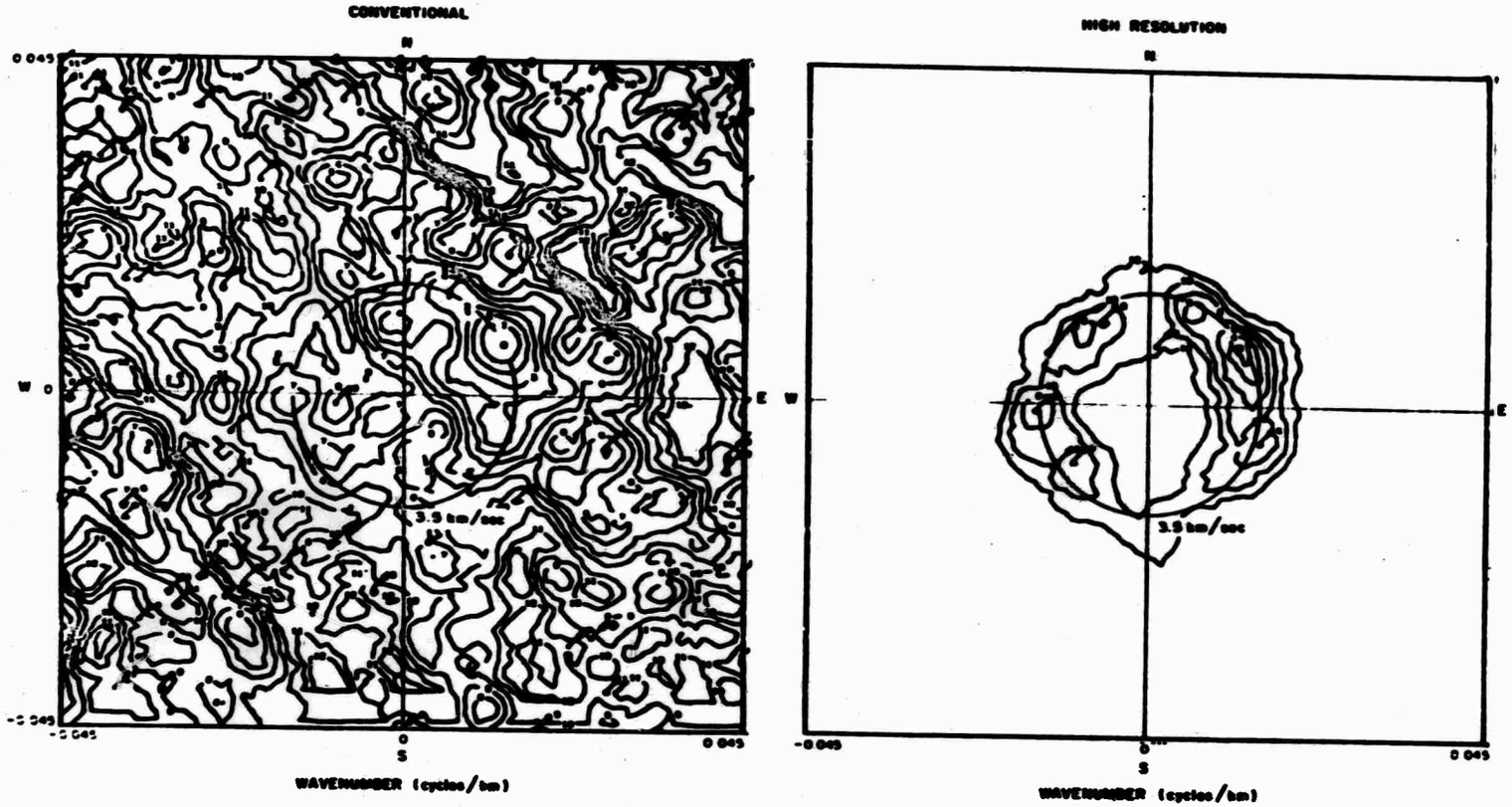
CONVENTIONAL
HIGH RESOLUTION
N
W
E
S
3.5 km/sec
WAVENUMBER (cycles/km)
FREQUENCY = 0.05 Hz
25 JAN 67 NOISE SAMPLE
00:10:00 TO 04:10:00

Figure 2.

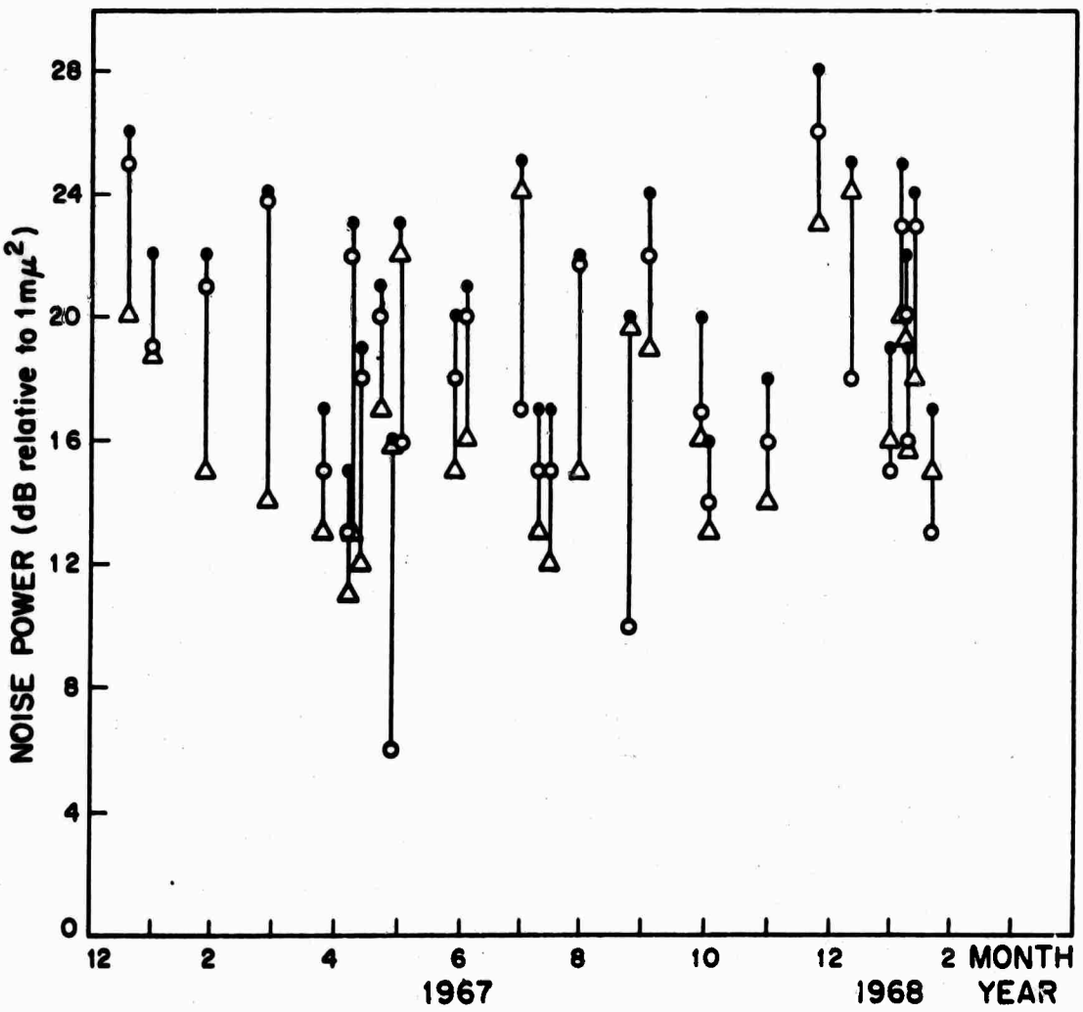

LP NOISE RESOLVED INTO TWO COMPONENTS

- • TOTAL NOISE
- o PROPAGATING NOISE
- Δ NONPROPAGATING NOISE

(20 - 40-sec period)

Figure 3.

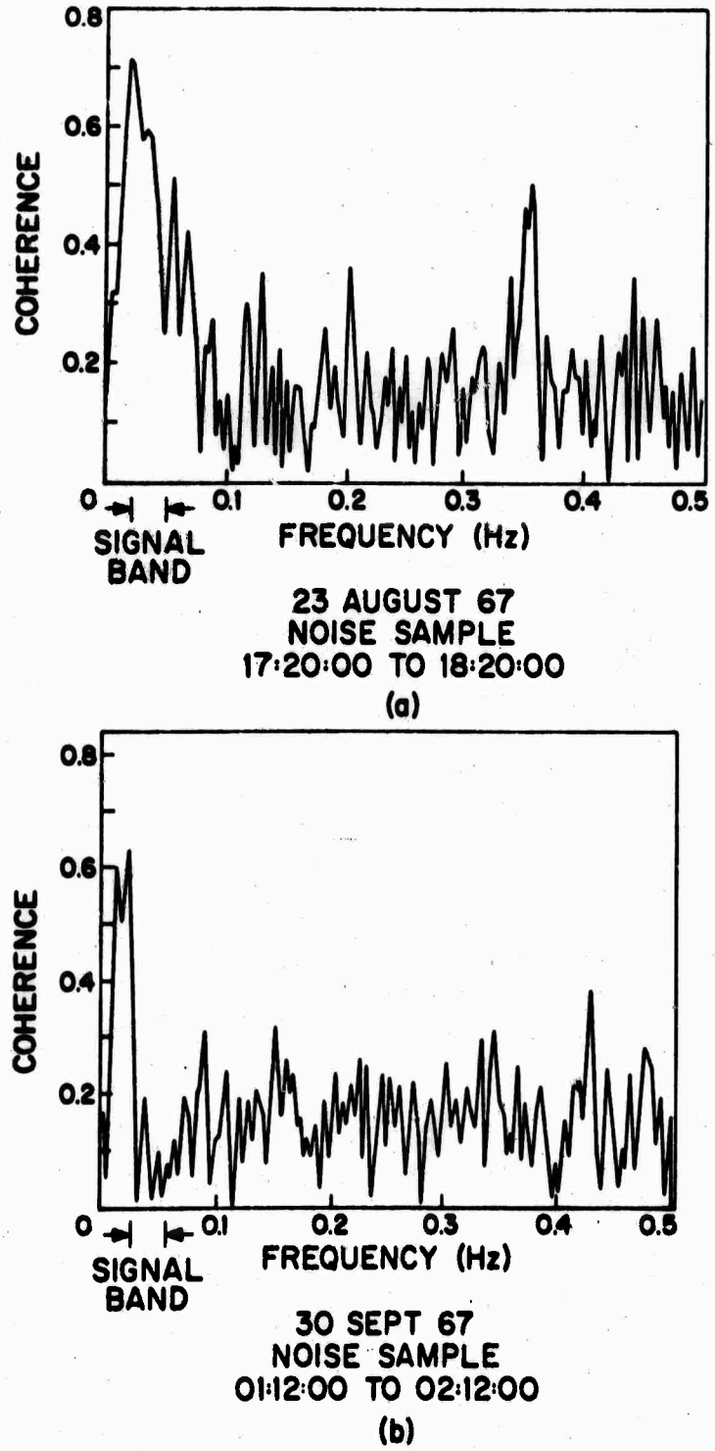
0.8
0.6
0.4
0.2
0
COHERENCE
0.1
0.2
0.3
0.4
0.5
SIGNAL BAND
FREQUENCY (Hz)
23 AUGUST 67
NOISE SAMPLE
17:20:00 TO 18:20:00
(a)
0.8
0.6
0.4
0.2
0
COHERENCE
0.1
0.2
0.3
0.4
0.5
SIGNAL BAND
FREQUENCY (Hz)
30 SEPT 67
NOISE SAMPLE
01:12:00 TO 02:12:00
(b)

Figure 4.

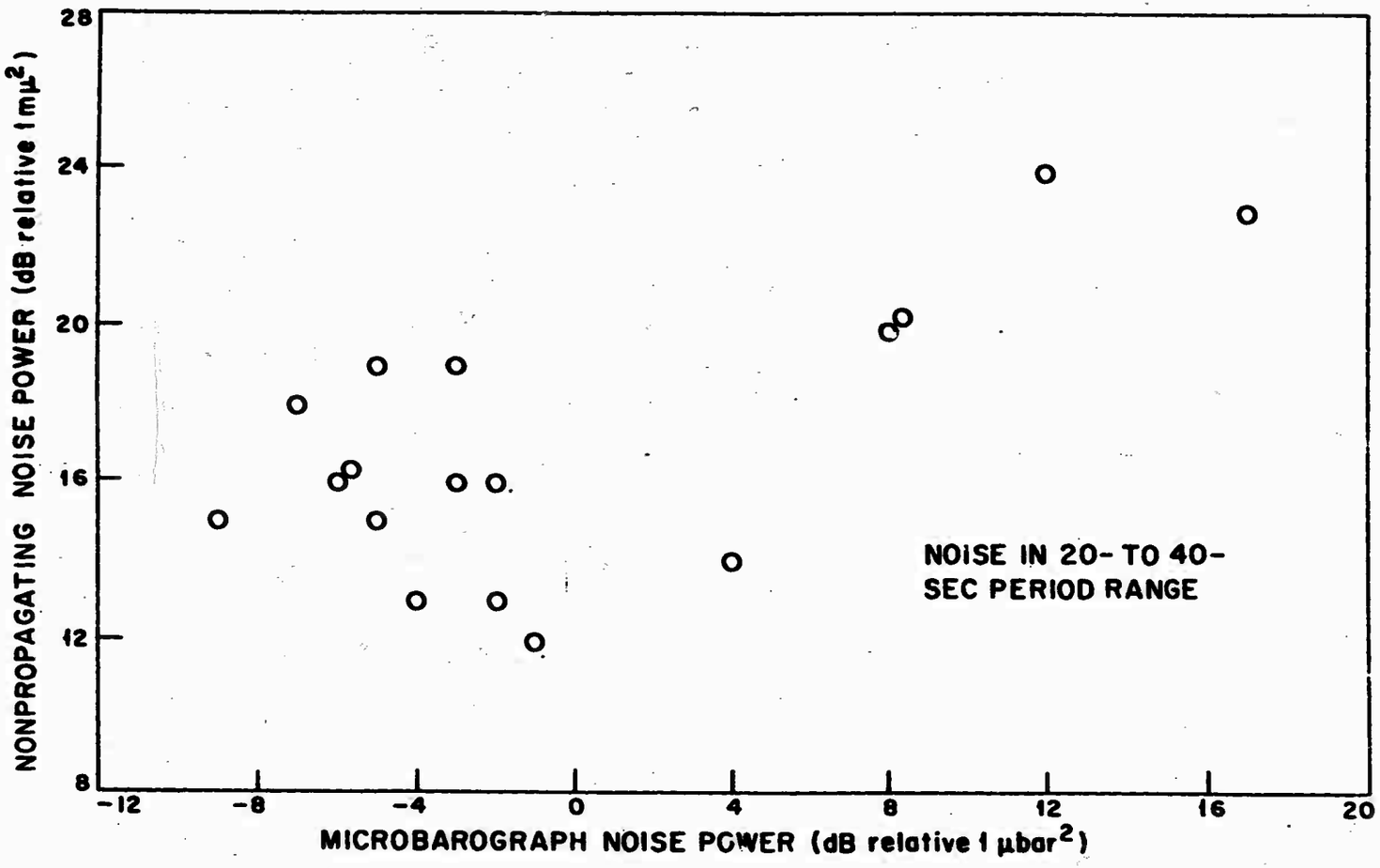
NONPROPAGATING NOISE POWER (dB relative 1 mμ²)
28
24
20
16
12
8
-12
-8
-4
0
4
8
12
16
20
MICROBAROGRAPH NOISE POWER (dB relative 1 μbar²)
NOISE IN 20- TO 40-
SEC PERIOD RANGE

Figure 5.

TWENTY- TO EIGHTY-SECOND PERIOD CHARACTERISTICS OF NUCLEAR EXPLOSIONS RECORDED AT LASA

By

Harry Mack

Teledyne Geotech
3401 Shiloh Road
Garland, Texas 75040

ABSTRACT

Surface waves recorded at LASA generated by several NTS events have been subjected to frequency-wavenumber analysis. All the spectra show a loss of signal at 0.02 Hz but there appears to exist coherent propagation at lower frequencies, producing a notch in the normalized peak wavenumber spectrum at 0.02 Hz. Several earthquakes and the deeply-buried Colorado nuclear explosion RULISON do not exhibit this notch. This may indicate that the frequency-wavenumber characteristics peculiar to NTS events is a result of shallow source depth.

The analysis procedures were designed such that frequency or wavenumber windowing could not produce a null at 0.02 Hz. Analysis of the high amplitude calibration recording rules out non-linearities in the amplitude range observed. There is still the possibility of high frequency surface waves causing spurious movements of the long-period seismometer mass (Berkhemer and Schneider, 1964). The argument is that these surface waves would propagate across the array and produce a long-period transient from each seismometer. F-K analysis of these transients would produce apparent coherent propagation at low frequencies with low phase velocity. Some measured phase velocities were low and this would agree with the above arguments. However, this is not always the case as can be seen from the velocity of 4.2 km/sec shown in Figure 1c. This higher velocity is hard to reconcile with expected phase and group velocities of short-period surface waves. Also, the short-period surface waves from the earthquakes produced no such effect.

The nuclear event RULISON, located in Colorado, produced F-K spectra similar to the earthquakes. Figure 5 shows the power and wavenumber spectrum for RULISON. Coherent propagation exists at 0.02 Hz and disappears at lower frequencies. Although RULISON had a body wave magnitude of 5.3, the surface wave displacement at LASA was greater than most of the other NTS events because the detonation site was nearer. RULISON was buried more deeply than is normal at NTS. This fact, coupled with the earthquake spectra, may indicate that the wavenumber spectra peculiar to NTS events, whether real or not, is a result of shallow source depth.

REFERENCES

Berckhemer, H., and Schneider, G., 1964, Near earthquakes recorded with long-period seismographs, Bull. Seism. Soc. Am., v. 54, p. 973-987.

Capon, J., 1969, High-resolution frequency-wavenumber spectrum analysis, Proc. I.E.E.E., v. 57, p. 1408-1418.

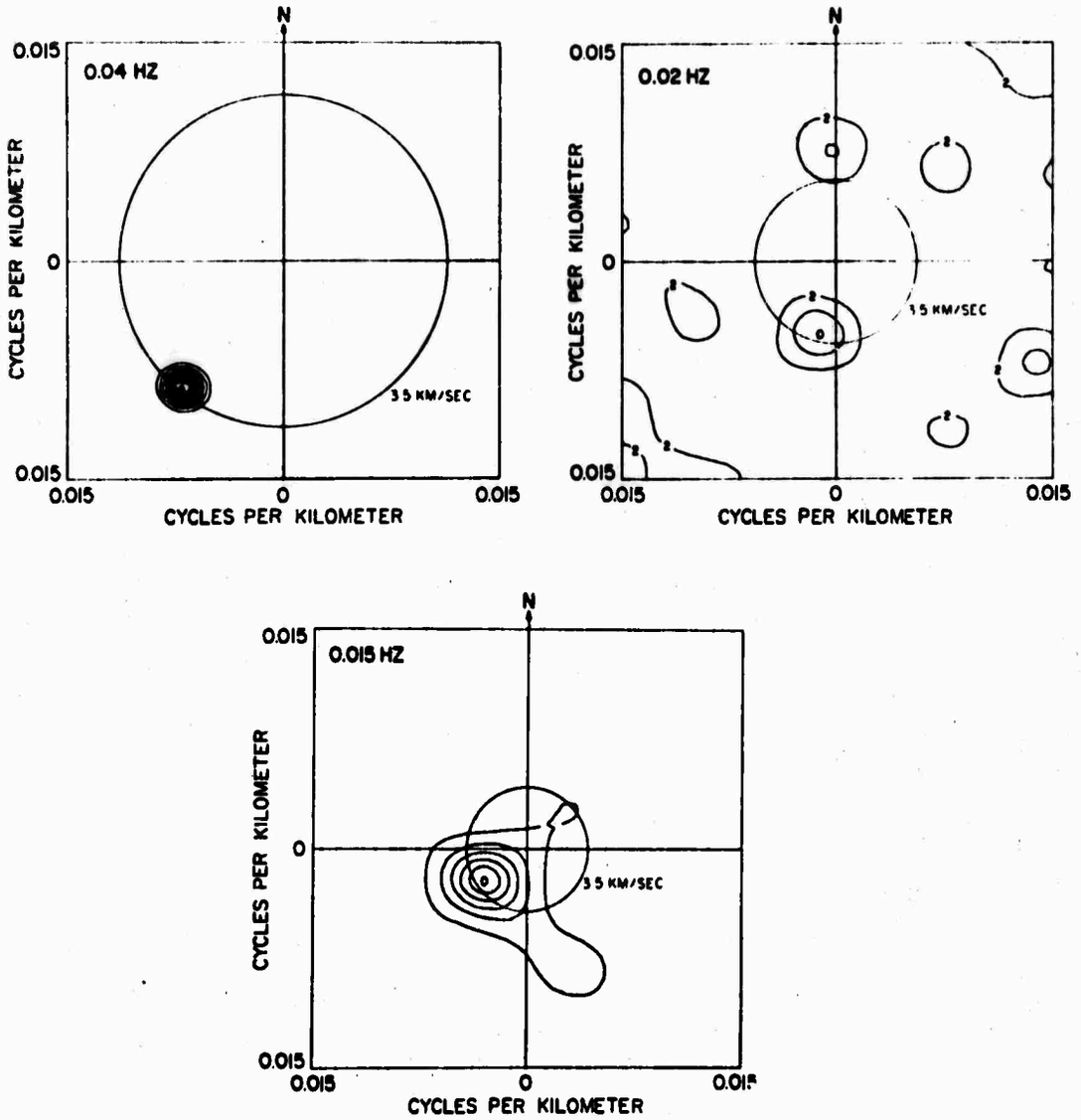

Figure 1. High resolution F-K spectra for the event LANPHER recorded at LASA at frequencies of 1a) 0.05 Hz, 1b) 0.02 Hz, and 1c) 0.015 Hz. The contours are in dB.

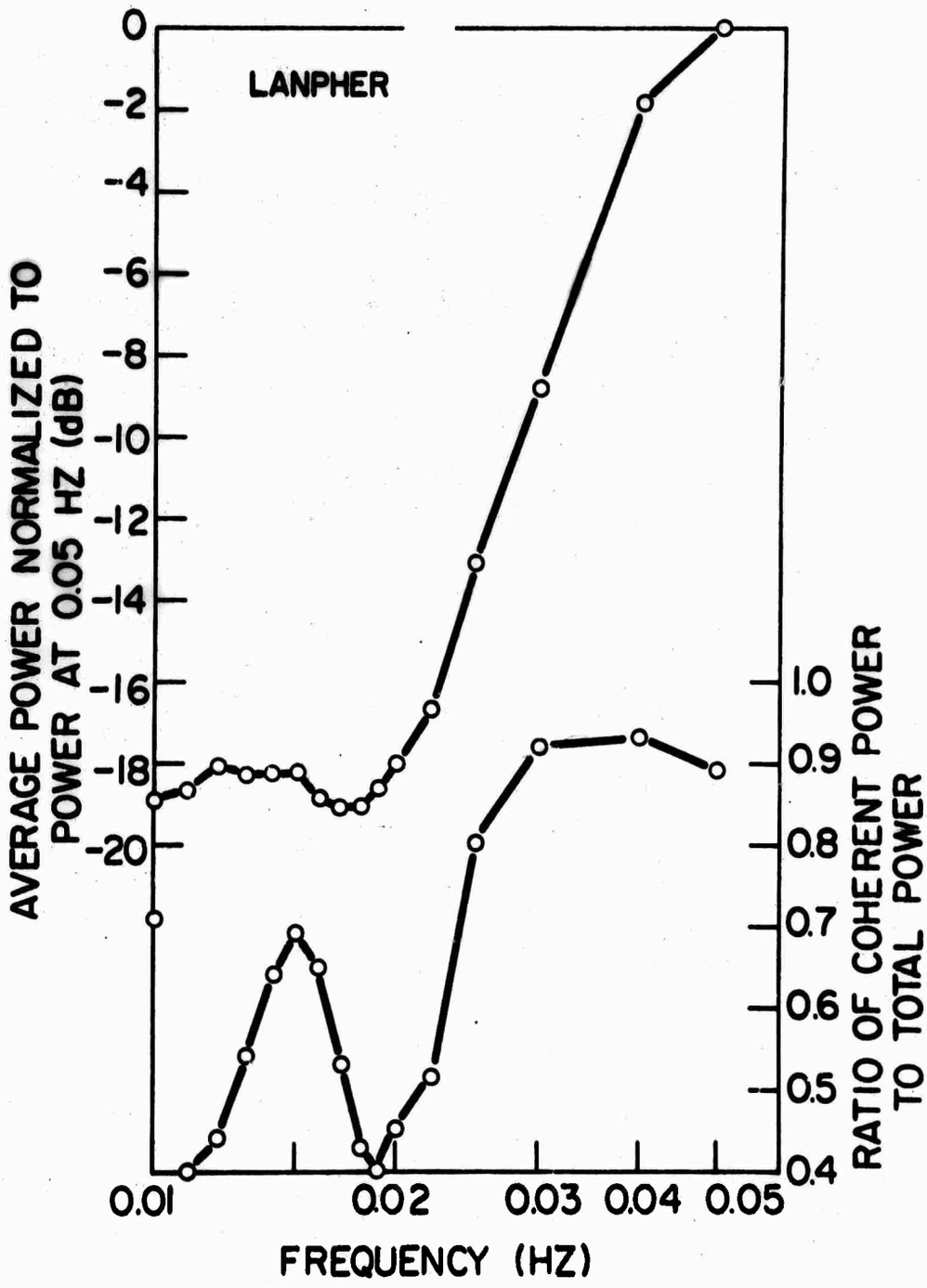

Figure 2. Average power spectrum of LANPHER recorded at LASA (upper curve and left hand scale), and normalized peak values of wavenumber spectra versus frequency (lower curve and right hand scale).

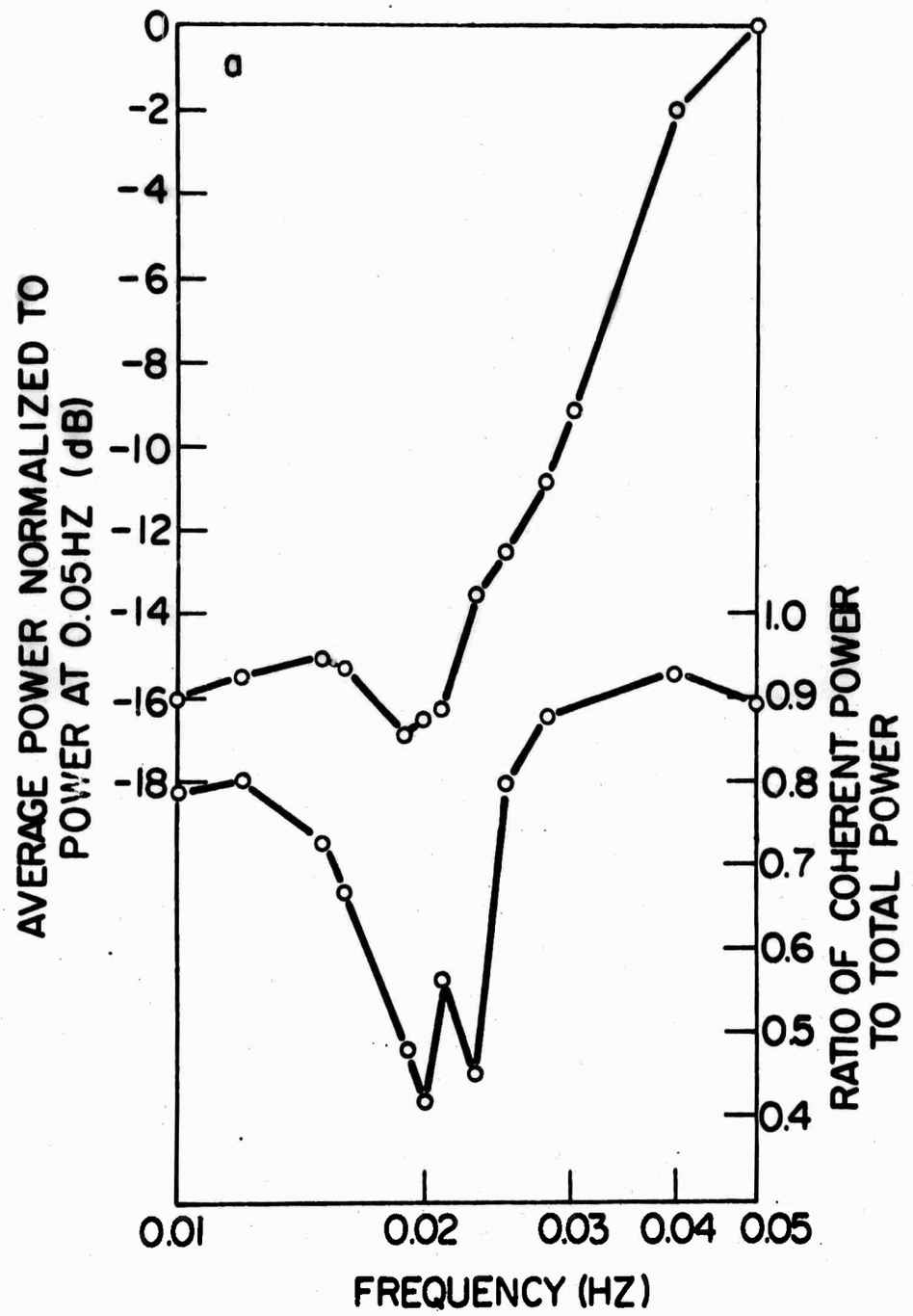

Figure 3a. Average power spectra of SLED recorded at LASA (upper curve and left hand scale), and normalized peak values of wavenumber spectra versus frequency (lower curve and right hand scale).

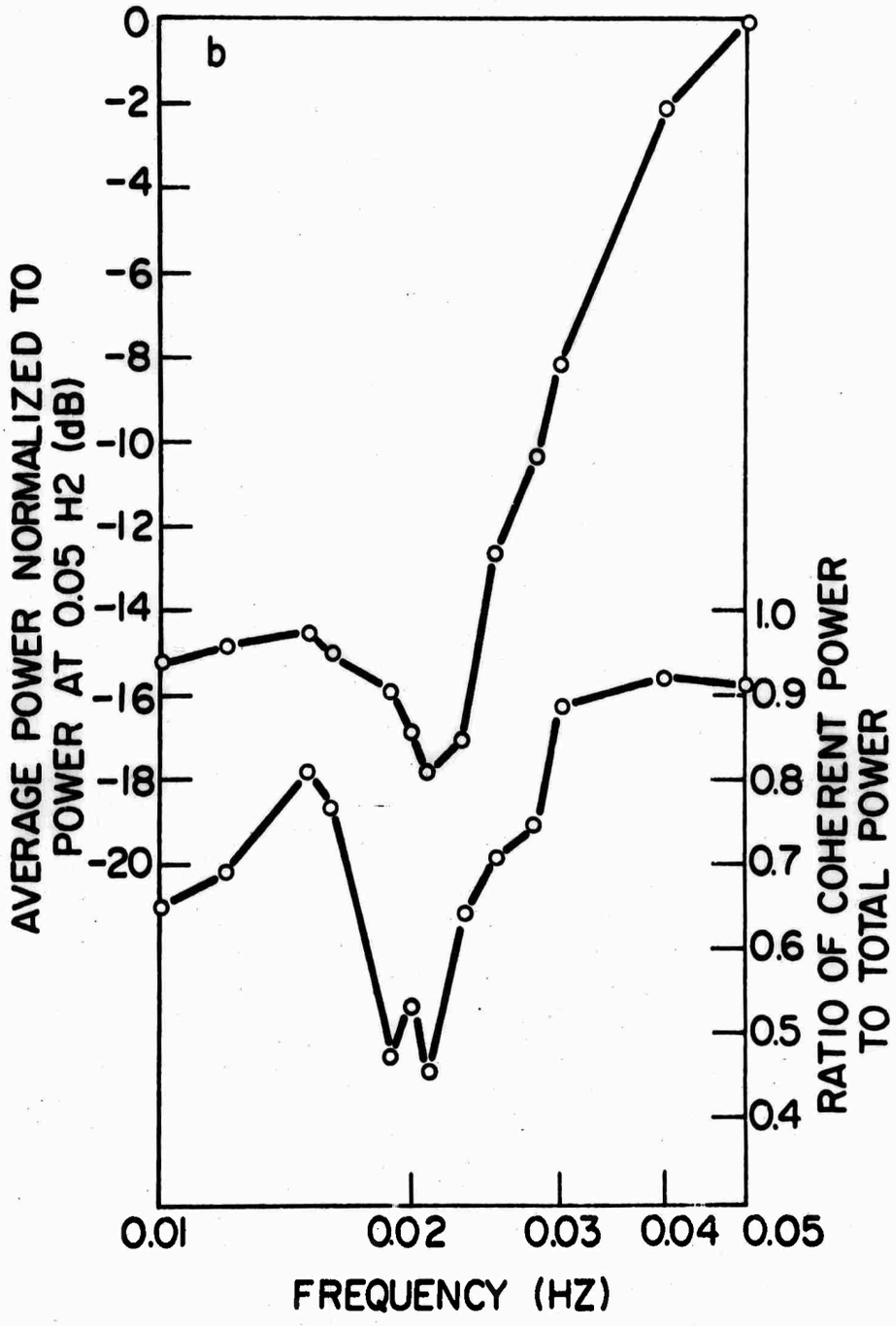

Figure 3b. Average power spectra of ZAZA recorded at LASA (upper curve and left hand scale), and normalized peak values of wavenumber spectra versus frequency (lower curve and right hand scale).

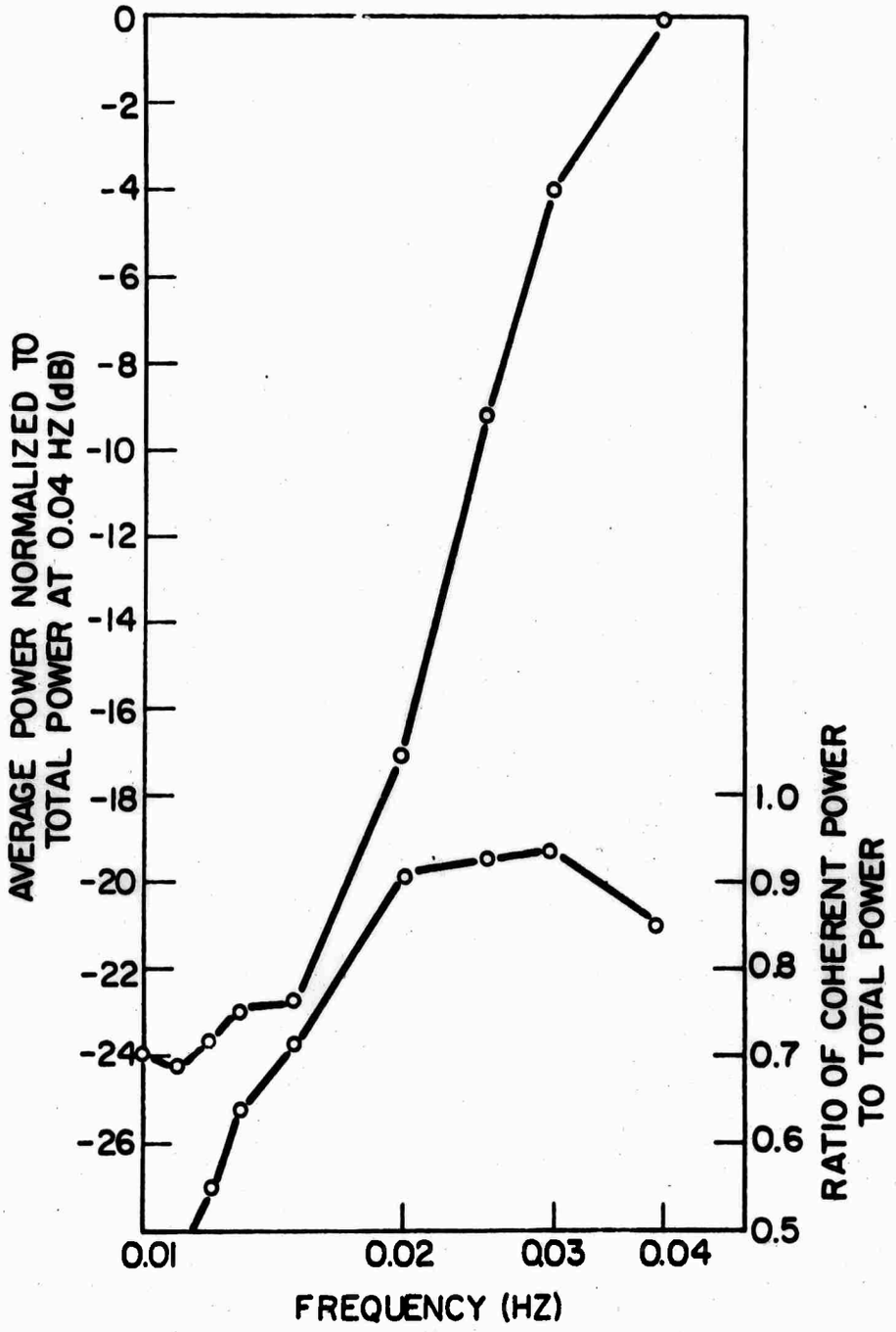

Figure 4. Average power spectrum of earthquake from Baja California recorded at LASA (upper curve and left hand scale), and normalized peak values of wavenumber spectra versus frequency (lower curve and right hand scale).

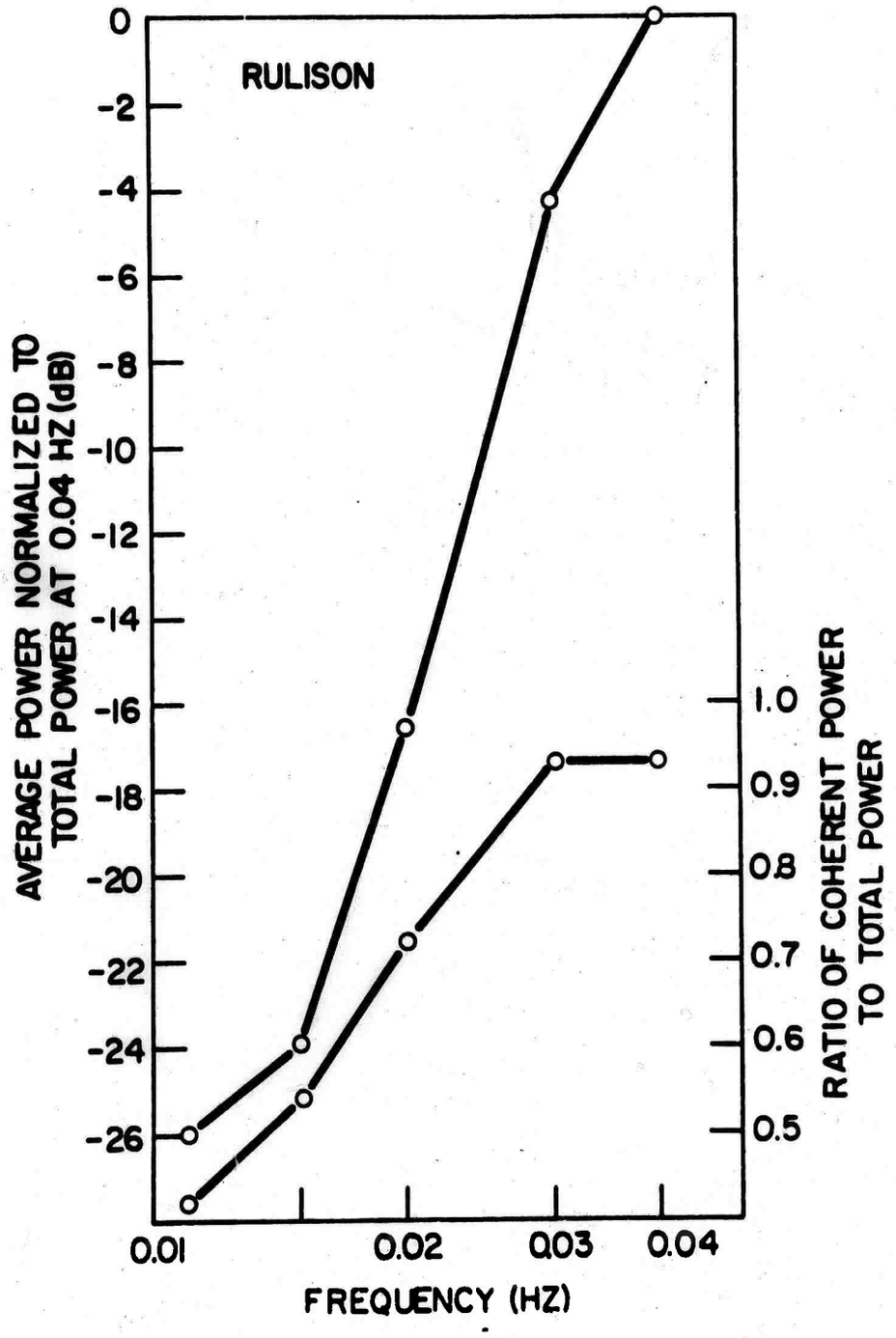

Figure 5. Average power spectrum of RULISON recorded at LASA (upper curve and left hand scale), and normalized peak values of wavenumber spectra versus frequency (lower curve and right hand scale).

LONG-PERIOD EARTH NOISE AND THE DETECTION OF THE DISCRIMINATION BETWEEN EARTHQUAKES AND UNDERGROUND EXPLOSIONS

By

John Savino

Lamont-Doherty Geological Observatory
Columbia University
Palisades, New York 10964

INTRODUCTION

In this report I will present results of two studies related to the seismic detection-discrimination problem. The first study is an investigation of the spectral, temporal, and spatial behavior of earth noise in the period range 15-130 sec. The work on earth noise was done in collaboration with George Hade and Keith McCamy. In the second study, the relative excitation of long-period (15-60 sec) surface waves from earthquakes and presumed underground explosions is analyzed for four different regions of the world: western North America, the Aleutians, the Novaya Zemlya region, and central Asia. This work was done in collaboration with Lynn Sykes, Peter Molnar, and Robert Liebermann. Event detection and discrimination at teleseismic distances (30° to 100°) are enhanced if they are based upon that portion of the surface-wave spectrum that corresponds to low earth noise levels, near a period at 40 sec.

The most important conclusion is that a relatively stable earth noise minimum exists between 30 and 40 sec. This minimum provides a new and powerful M_S at 40 sec-versus-m_b discriminant between events in all the regions investigated.

The data for these studies come from the high-gain, wide-band seismograph systems designed and described by Pomeroy et al (1969). These instruments are operated on the 1850-foot level of the Ogdensburg mine observatory in New Jersey.

LONG-PERIOD EARTH NOISE--SPECTRAL, TEMPORAL, AND SPATIAL CHARACTER

A low ambient noise level was achieved by placing the seismometers in pre-stressed, air-tight, hemispherical tanks. In addition, the tanks are located in vaults sealed off from the main observatory by a series of three bulkhead doors.

Cross spectral analysis on data from matched seismographs located in separate areas of the mine observatory and environmental noise determinations lead to the following conclusions about the observed long-period background:

1. For periods between 30 and approximately 130 sec, the noise is earth motion coherent over distance of at least 500 feet.
2. The source or sources of this noise are external to the mine observatory.

In Figure 1 amplitude spectra of the vertical and horizontal components of earth noise in the period range 15 to 130 sec are shown for a quiet three-hour time period in June 1969. These spectra were corrected for instrument displacement response. The vertical system response is indicated by the dashed curve. The most important point to note is that the spectra from all three components indicate a minimum in the earth noise between 30 and 40 sec with a rise to longer periods of approximately 12 db/oct. Similar observations on the spectrum of long-period earth noise were reported by Haubrich and MacKenzie (1965) for three surface sites in California and by Trott (1965) for an installation, 200 feet deep, in New Mexico. During this particular time period, this earth noise minimum is 6-12 db below the 16- to 20-sec peak associated with primary frequency microseismic activity. These microseisms are always present on the high-gain recordings with a mean level approximately a factor of 2 higher than that indicated in this figure.

Rigid environmental control and operation in a deep mine result in horizontal noise levels similar to that of the vertical. The importance of the successful operation of high-gain horizontals for the detection of and discrimination between events recorded at a single station can be seen in Figure 2. Here we compare the vertical component of Rayleigh waves (left-hand side) with the horizontal recordings of Love and Rayleigh waves (right-hand side) from 6 events at the Nevada Test Site. I call your attention to the Benham aftershock B2. For this event, the 20-40 sec Love waves are well recorded, whereas the 20-sec Rayleigh waves are barely above the microseismic level. Differences in focal mechanisms and radiation patterns probably give rise to the differences in Rayleigh- and Love-wave excitation between these events. Although more high-gain installations distributed in azimuth could resolve this problem, the operation of high-gain horizontal instrumentation enhances the detection-discrimination capabilities at a single station. Furthermore, on the basis of

an M_S-versus-m_b comparison using the 20- and 40-sec Love-wave amplitudes, it is seen that this event, an earthquake, separates from NTS explosions.

Extreme variations in both the 30-40 sec noise minimum and microseismic activity are shown in Figure 3. Vertical amplitude spectra, corrected for the instrument displacement response, are given for three different time periods. The April 1970 curve is based on 5 hours 14 minutes of digital magnetic tape data and because of its larger dynamic range is extended down to 8 sec. As indicated by the Brune-Oliver mean seismic noise curve, the April 1970 spectrum is more typical of the microseismic background level. During this period of time, earth motion at 20 seconds is approximately 7 times higher than the level of the 30-40 sec minimum. Depending upon the spectral decay rate of long-period surface waves, this 30-40 sec minimum should provide an important window for observations of surface waves from small teleseismic events. In fact, 40-sec surface waves from earthquakes can be seen on records when the 20-sec waves are either not detectable or masked by noise.

The March and September spectra represent relatively extreme conditions of the 15-130 sec seismic noise level. Note, however, that during the intense primary frequency microseism storm in March 1969, the 30-40 sec noise level remains unchanged as compared to the April level. The circle at 40 sec is the Brune-Oliver maximum estimate of earth noise in this period range.

In order to examine the temporal behavior of the long-period earth noise, and in particular the minimum, power spectra for the vertical component were computed for each month of the year, March 1969 through March 1970. There were no obvious or reported earthquakes during the times included in the power spectral calculations.

In Figure 4, the two lower lines show the seasonal variation of the vertical earth noise level for the two period bands centered at 40 seconds and 2 minutes. The closed circles are the mean of two spectra computed for different days of the same month plotted on the mean day. The microseismic peaks at about 6 and 18 sec vary by 1 to 2 orders of magnitude in amplitude over time spans of a week or less. In contrast the maximum amplitude variation of the 40 second and 2 minute periods is only a factor of 3 with a winter-summer dependence. This relatively small amplitude variation of the 30-40 sec minimum points up the reliability of event detection using surface waves in this period range.

The top line in Figure 4 is taken from a study by Herron et al (1969) in which a microbarograph array including the Ogdensburg vicinity was used. It represents the seasonal variation of the pressure spectrum for the period band centered at 3 minutes. The general winter-summer variation in amplitude is a recurring phenomenon dependent upon the location of the core of the jet stream. Three-minute pressure variations coherent over distances of at least 1/2 to 3/4 km were observed over this array. The vertical ground displacements recorded at a depth of 1850 feet are in approximate agreement with

those predicted by an equation for a circular load of these dimensions acting on the surface of an elastic half-space.

Haubrich and MacKenzie (1965) reported occurrences of both atmospheric and ocean loading observed with a long-period vertical (Press-Ewing) seismometer at stations within 15 km of the Pacific coast. We have not seen any indication of ocean-induced noise at Ogdensburg (100 km from the Atlantic coast). In addition, the long-period background observed on all three components at Ogdensburg is unaffected by windstorms or other micrometeorological phenomena at the surface. That the microseism storm in March 1969 did not affect the winter earth noise level for periods greater than 30 to 35 sec (shown in Figure 3) is consistent with the idea that this portion of the spectrum is primarily controlled by atmospheric loading, not by ocean-induced propagating microseisms. Thus, sites with quiet atmospheric conditions should provide ideal locations for the operation of high-gain, long-period seismic instrumentation.

The spatial dependence of the long-period earth noise was also investigated. In Figure 5 the vertical component of earth noise observed at Ogdensburg is compared with similar data from an installation 200 feet below the surface at Las Cruces, New Mexico, and with data from a surface site at Garland, Texas. The Ogdensburg and Garland data are time coincident (17 September 1969), whereas the Las Cruces spectrum covers a period of time in March 1965.

The most important point to note is that all three spectra, based on observations from these three geographically separate sites, indicate the existence of a minimum in the background noise between 30 and 40 sec with longer-period increases of approximately 12 db/oct. The approximate agreement of the absolute ground motion levels for the March, Las Cruces, spectrum and the quietest spectrum observed at Ogdensburg (September) over a period of one year would seem to indicate that sites with earth noise levels lower than that at Ogdensburg can be found at depths shallower than 1850 feet as in the Ogdensburg mine.

Primary frequency microseism storms can degrade the 20-sec detection threshold by as much as 1.0 m_b unit. Important sources of long-period waves are intermediate and deep earthquakes. Although these events supply us with important information on the structure of the earth, in the context of this meeting they are considered as sources of long-period noise. Figure 6 shows the long-period background at Ogdensburg for three conditions. All 8 traces are 1/2 hour long. The first three traces represent the background observed on the three components during an earthquake-free period in June 1969. These times were included in the spectral calculations shown in Figure 1, and are typical of the atmospherically controlled seismic background.

Traces 4 and 5 show the intense microseism storm on March 8-9, 1969. The event marked A is an m_b = 4.7 Aleutian earthquake. Rayleigh waves in the period range 25 sec to approximately 60 sec can be seen emerging from the background. Clearly the signal-to-noise ratio can

be improved by filtering the 20-sec microseisms from the record and retaining the longer-period signal.

Traces 6-8 are of particular interest. Trace 6, prior to the event marked B, shows the vertical background on February 28, 1970. At B an impulsive P wave arrives from an intermediate-depth (162 km) Aleutian earthquake. The body-wave magnitude as determined by the USC&GS PDE for this event is given as 6.1. Trace 7 starts 7 hours after the P arrival time and shows the degree to which this event controls the long-period background. Finally, at the end of trace 8, 14 hours after the P arrival, the background is nearly down to its original level. The observed amplitude decay of these waves indicates that at a site with a long-period signal/noise ratio an order of magnitude greater than that at Ogdensburg, the duration of this event would be 24-30 hours. These waves are observed after events in the depth range 70 to 650 km and m_b as small as 5.6 - 5.7. The extent to which the 20- and 40-sec detection thresholds are affected by these events is shown in Figure 7. The solid line is a low resolution power spectrum based on 1 1/2 hours of recording starting 3 hours after the beginning of this event. The total duration of this relatively small (m_b = 5.8) earthquake was 6 hours. Although the 40-sec background averages 12 db above the normal seismic background, shown by the dotted curve, the 20-sec level is unaffected.

These deep events and primary frequency microseism storms point up the complementary nature of the M_S at 40 and 20 sec-versus-m_b discriminants at a single station. For instance, during an intense microseism storm, detection and discrimination of seismic events can be performed using surface waves in the 40-sec period range, whereas during a deep earthquake, the 20-sec portion of the surface wave train can be used for discrimination. With additional high-gain installations, array processing techniques and matched filters could be employed to separate an event masked by a deep earthquake or a microseism storm.

Surface waves from events around the world

One very important application of this relatively stable earth noise minimum is the detection of and discrimination between earthquakes and underground explosions on the basis of their excitation of long-period surface waves.

A comparison of surface-wave magnitude (Ms) at 20 or 40 sec versus body-wave magnitude (m_b) from events in four different regions of the world was carried out. The results for events in the Aleutians are presented in Figures 8a and b. Along the ordinates on the left- and right-hand sides of Figure 8a, we have plotted peak-to-peak ground amplitudes in microns of the 20- and 40-sec Rayleigh waves, respectively, as a function of body-wave magnitude, m_b, as determined by the USC&GS. Since the amplitudes are plotted on a logarithmic scale and the epicentral distances are nearly the same (70° ± 5°) for all the events, surface-wave magnitude M_S is described by a linear scale

along the ordinate. The coordinates for the underground explosion Long Shot are taken from Liebermann et al (1966). These and other authors previously showed that plots of M_S at 20-sec-versus-m_b of earthquakes divide into two groups, with earthquakes yielding larger M_S values for equivalent m_b. In a recent article in Nature, Molnar et al (1969) showed that for events in western North America the M_S-versus-m_b division of earthquake and explosion populations is more distinct at 40 sec than at 20 sec; i.e., for constant m_b the difference in Rayleigh-wave amplitudes between earthquakes and explosions at 40 sec is a factor of 2 to 4 times greater than the difference at 20 sec. Although the explosion data are limited, the same result is found in the Aleutians. The relatively small amount of scatter of the earthquake data is probably due to similarity of focal mechanism and improved teleseismic m_b values.

All of the earthquakes studied are landward of the trench and probably reflect the predominant mode of faulting for this arc structure. The small scatter in the earthquake population down to $m_b = 4.3$ implies that the detection threshold at this distance (70°) is approximately $m_b = 4.4$. Thus, a shallow event assigned an m_b of 4.4 or larger that does not excite observable surface waves at Ogdensburg would be suspected of being an explosion. Similar high-gain stations distributed in azimuth could rule out the possibility of an unfavorable earthquake radiation pattern at any one site.

In Figure 8b, 40-sec Love waves are plotted as a function of m_b. As in the case of the 40-sec Rayleigh waves, the separation of the earthquake and explosion populations is approximately one m_b unit. Note that Love waves in the period range 40 to 60 sec were excited by the Milrow explosion with approximately the same amplitudes (1.5 μ at 40 sec) as the 40-sec Rayleigh waves from this event.

Rayleigh-wave amplitude spectra in the period range 18-55 sec were determined for 6 Aleutian earthquakes and the Milrow explosion and are presented in Figure 9. These amplitude measurements were corrected for instrument response and normalized to 20 sec. The long-period decay rates for 2 of the 6 earthquake spectra are as steep or steeper than that for Milrow. Although the explosion spectrum may be contaminated by the release of tectonic strain, the unusually high 20/40 sec ratios for some of the earthquakes are approximately equal to those observed for NTS explosions (thought to be nearly pure explosion ratios at Ogdensburg) by Molnar et al (1969). It is not likely that a pure explosion spectrum would exhibit a higher 20/40 sec ratio. Thus, depth of focus and possibly unfavorable radiation patterns do not always allow a simple application of the 20/40 sec Rayleigh-wave ratio test that discriminated between western United States earthquakes and NTS explosions. Nevertheless, M_S at 40 and 20 sec versus m_b remain as effective discriminants between events in this region.

Figure 10 shows plots of M_S at 20 and 40 sec versus m_b for events in central Asia and the Novaya Zemlya region. Earthquakes and presumed explosions in central Asia and the Novaya Zemlya region are denoted

by closed and open circles, and closed and open squares, respectively. These data indicate that for both of these regions discrimination is enhanced at periods of 40 sec compared with 20 sec as in the western United States and the Aleutians.

Normalized amplitude-versus-period measurements are plotted in Figure 11 for a presumed explosion and 6 earthquakes in the Novaya Zemlya region. The results in this figure indicate significant differences between the long-period decay rates of the Rayleigh-wave spectra from the presumed explosion and those from the earthquakes.

The ratio of the 20- to 40-sec surface waves from the presumed explosion compared with a similar ratio for the earthquakes is approximately 2.5. Molnar et al (1969) pointed out that this value is to be expected if the source-time function of an earthquake is approximated by a step function of displacement, and the explosion time function, by an impulse of displacement. In view of the uncertainty in the earthquake focal-depth determinations, however, we cannot rule out the effect of source depth on the Rayleigh-wave spectrum as the cause of the differences observed in Figure 11.

Nevertheless, we can conclude, on the basis of the events studied, that differences in the long-period Rayleigh-wave amplitude spectra provide an additional discriminant between earthquakes and presumed explosions in the Novaya Zemlya region.

Molnar et al (1969) plotted the maximum peak-to-peak amplitudes of ground motion for Rayleigh and Love waves in the period ranges 17 to 25 sec and 40 to 70 sec as a function of body-wave magnitude, m_b, as determined by the USC&GS. All of the events studied occurred in the western United States. We subsequently analyzed short-period ($T \approx 1$ sec) P waves recorded by WWSSN stations in the western United States for these events and some additional earthquakes and explosions from the same region. With these data and data listed by the USC&GS EDR reports, we determined the body-wave magnitude using formulas derived by Evernden (1967) for events in the western United States.

The peak-to-peak amplitudes of ground motion for Rayleigh and Love waves in the period ranges 17 to 25 sec and 40 to 70 sec recorded at Ogdensburg from these events are plotted in Figure 12 as a function of the redetermined m_b values. An average of 7 stations was used in the determination of m_b for each event. Because the epicentral distances are all about the same (35°) and the surface-wave amplitudes are plotted on a logarithmic scale, the surface-wave magnitude (M_s) is given by a linear scale along the ordinates.

The scatter in the earthquake population results from any of several effects such as radiation pattern, source dimension, focal depth, lateral variation in velocity, and attenuation. With the data plotted according to regions, however, some systematic patterns emerge. For instance, earthquakes in the Gulf of California (closed circles) excite larger surface waves than those in the other regions. Nevertheless, the earthquakes and explosions separate into two distinct populations. This separation is more pronounced for surface

waves with periods of 40 to 60 sec.

The revised body-wave magnitudes are systematically lower than those of the USC&GS (Evernden, 1967). However, the difference between the USC&GS m_b and the redetermined m_b values is greater for earthquakes than for explosions. Hence, the separation of the earthquake population from the explosion population is more distinct than that of Molnar et al (1969). Moreover, the data in Figure 12 demonstrate clearly that discrimination is more reliable when surface waves [Rayleigh (Figure 12a) and Love (Figure 12b)] with periods of about 40 sec are used rather than with 20 sec. In fact, two earthquakes plot (Figure 12a) very close to the explosion population on the basis of 20 sec surface waves, but at 40 sec they clearly separate from the explosions. That discrimination is more reliable when 40 sec Rayleigh waves are used to determine M_S, instead of 20 sec waves, is the most important result of this study.

The small Love waves observed for J2 and B1 (Figure 12b) suggest that these events are related to a cavity collapse mechanism. This interpretation is supported by the reversed polarity of the Rayleigh waves from these events as compared with Rayleigh waves from the explosions (Brune and Pomeroy, 1963), and from the depths of focus, epicenters, and character of the seismograms used to locate these events (R.M. Hamilton, personal communication).

In the distance range studied here the detection threshold for explosions is m_b approximately 4.6. However, the approximate linearity of the explosion population and its parallelism with the earthquake population suggests that the event discrimination threshold at 20 sec may be as low as the earthquake detection limit, $m_b \approx 3.8$; $M_S = 3.0$. During the intense microseism storm of March 1969, the detection limit at Ogdensburg was degraded to $M_S \approx 4.0$ at 20 sec.

The higher 40 sec detection threshold ($M_S \approx 3.6$) for NTS explosions is a result of the fast decay rate of the long-period surface-wave spectra (Figure 13) for these events. The 20/40 sec ratio for three NTS explosions determined by Fourier analysis is approximately 10. This ratio is greater for the explosions than any of the natural earthquakes occurring in the western United States, in particular, the 29 Palms event, a high-stress earthquake (Wyss and Brune, 1969). These spectra will be discussed in more detail by Molnar.

CONCLUSIONS

The existence of a minimum in seismic earth noise near 40 sec provides a new discrimination tool at 40 sec that complements the well-know M_S at 20 sec-versus-m_b discriminant. With the operation of wide-band, long-period instruments, one or the other of these discriminants can be applied in the presence of noise sources, deep earthquakes or microseism storms, thereby enhancing the detection-discrimination capabilities of a single station. In addition, the high-gain operation makes possible spectral analysis of small (m_b = 4.5) events at teleseismic distances. Spectral differences between earthquakes and presumed explosions in the western United States and the Novaya Zemlya region provide an important additional discriminant that does not require the observation of short-period P waves.

REFERENCES

Basham, P.W., Weichert, D.H., Anglin, F.M., 1970, An analysis of the 'Benham' aftershock sequence using Canadian recordings, J. Geophys. Res., v. 75, p. 1545.

Brune, J.N., and Pomeroy, P.W., 1963, Surface-wave radiation patterns for underground nuclear explosions and small-magnitude earthquakes, J. Geophys. Res., v. 68, p. 5005.

Evernden, J.F., 1967, Magnitude determination at regional and near-regional distances in the United States, Bull. Seism. Soc. Am., v. 57, p. 591.

Haubrich, R.A., and MacKenzie, G.S., 1965, Earth noise, 5 to 500 millicycles per second, 2, reaction of the earth to oceans and atmosphere, J. Geophys. Res., v. 70, p. 1429.

Herron, T.J., Tolstoy, I., and Kraft, D.W., 1969, Atmospheric pressure background fluctuations in the mesoscale range, J. Geophys. Res., v. 74, p. 1321.

Liebermann, R.C., King, C.Y., Brune, J.N., and Pomeroy, P.W., 1966, Excitation of surface waves by the underground nuclear explosion Long Shot, J. Geophys. Res., v. 71, p. 4333.

Molnar, P., Savino, J., Sykes, L.R., Liebermann, R.C., Hade, G., and Pomeroy, P.W., 1969, Small earthquakes and explosions in western North America recorded by new high gain, long period seismographs, Nature, v. 224, p. 1268.

Pomeroy, P.W., Hade, G., Savino, J., and Chander, R., 1969, Preliminary results from high-gain wide-band long-period electromagnetic seismograph systems, J. Geophys. Res., v. 74, p. 3295.

Trott, W., 1965, Investigation of noise in long-period seismographs, Geotech Div., Tech. Rept. 65-91, p. 78.

Wyss, M., and Brune, J.N., 1969, Shear stresses associated with earthquakes between 0 and 700 km depth, EOS Trans. Amer. Geophys. Union 50, p. 237.

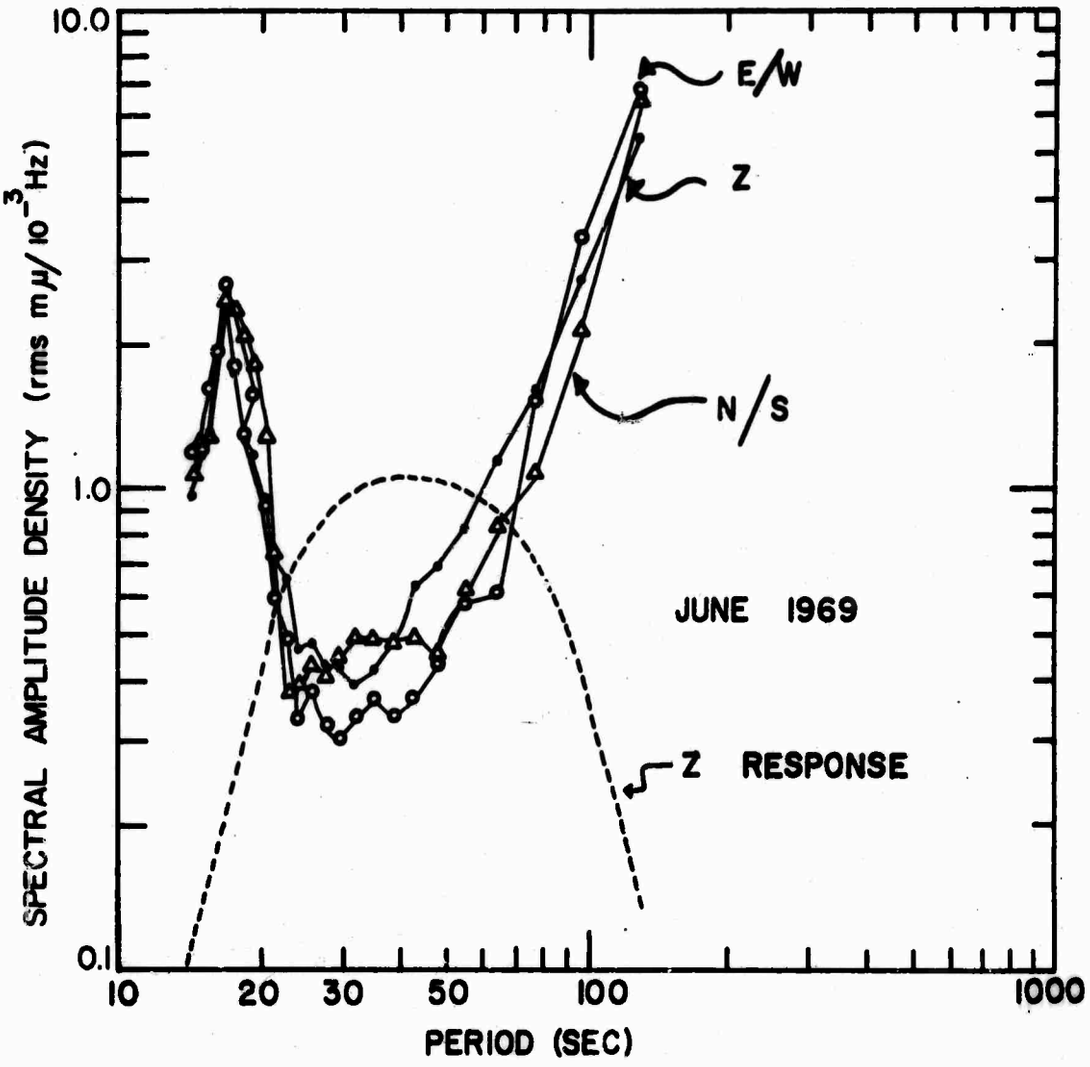

Figure 1. Spectral amplitude density for the vertical and two horizontal components of the high-gain seismograph system. Each spectrum is based on three hours of data (0500-0800 GCT 12 June 1969). The original recordings were divided into 14 equal time-length segments and power spectra were computed for each segment. The resultant amplitude spectra is the square root of the mean of 14 power spectra and is corrected for the instrument displacement response; the vertical system response is shown by the dashed curve; response curves for the horizontal components have the same shape.

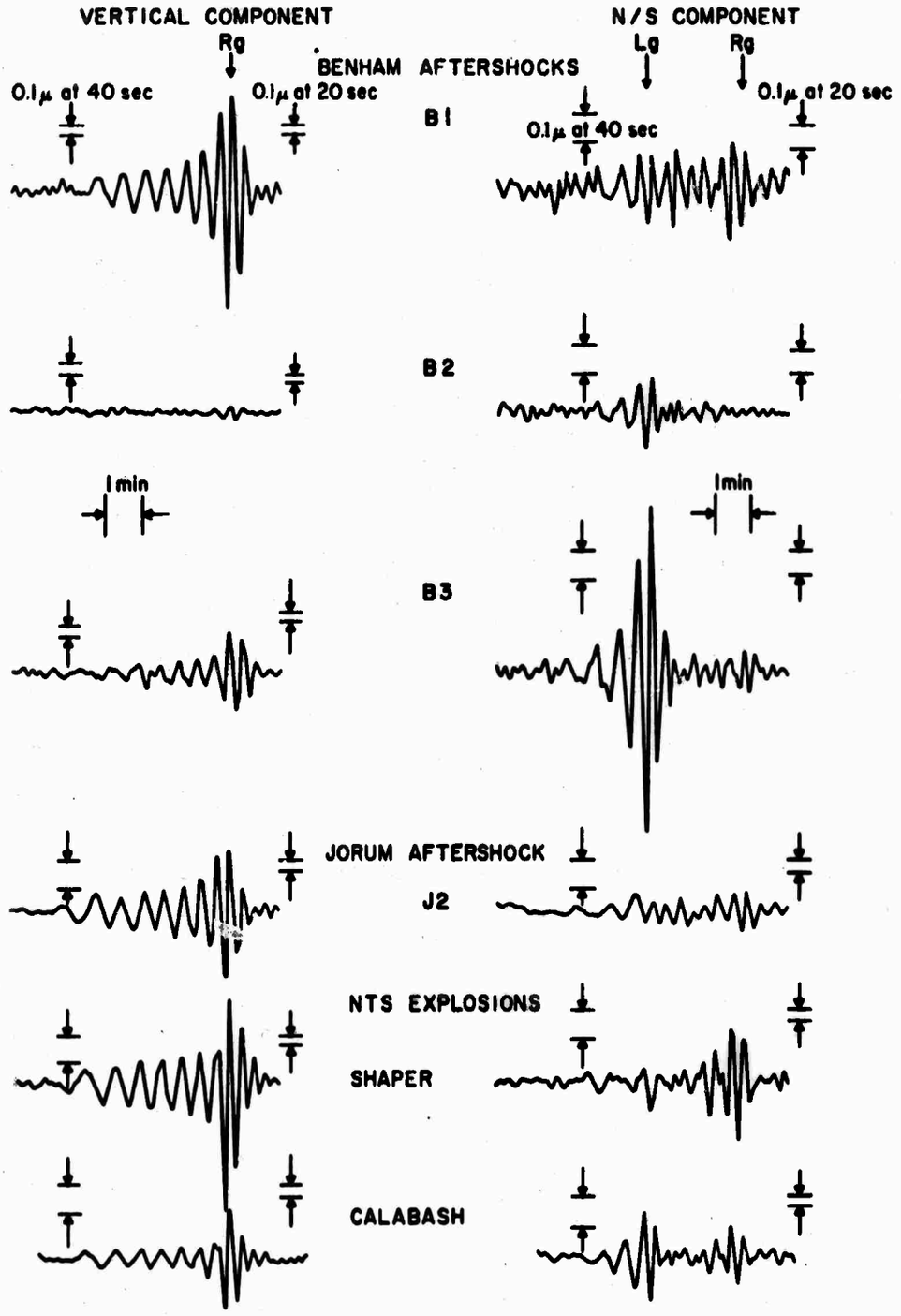

Figure 2. Vertical and horizontal (N/S) component seismograms showing Rayleigh and Love waves from 4 explosion aftershocks (B1, B2, B3, and J2) and two explosions (Shaper and Calabash). All events occurred at the Nevada Test Site. The recorded amplitude of 0.1 μ (micron) is given at 40 and 20 sec for each recording. Note the change in the response for the bottom three events. Pertinent data for events are: (B1) southern Nevada, 37.2N, 116.5W, 22h 23m 26.3s, 19 Dec 1968, m_b = 5.0; (B2) southern Nevada, 37.2N, 116.5W, 20h 08m 20.4s, 20 Dec 1968, m_b=4.2; (B3) southern Nevada, 37.3N, 116.5 W, 00h 14m 25.2s, 21 Dec 1968, m_b = 4.9; southern Nevada, 37.3N, 116.5W, 18h 15m 39.3s, 16 Sep 1969, m_b = 4.6; Shaper, 37.1N, 116.0W, 23h 05m 00.0s, 23 Mar 1970, m_b = 5.5; Calabash, 37.1N, 116.1W, 22h 03m 51.4s, 29 Oct 1969, m_b = 5.7. All information is from the USC&GS PDE reports.

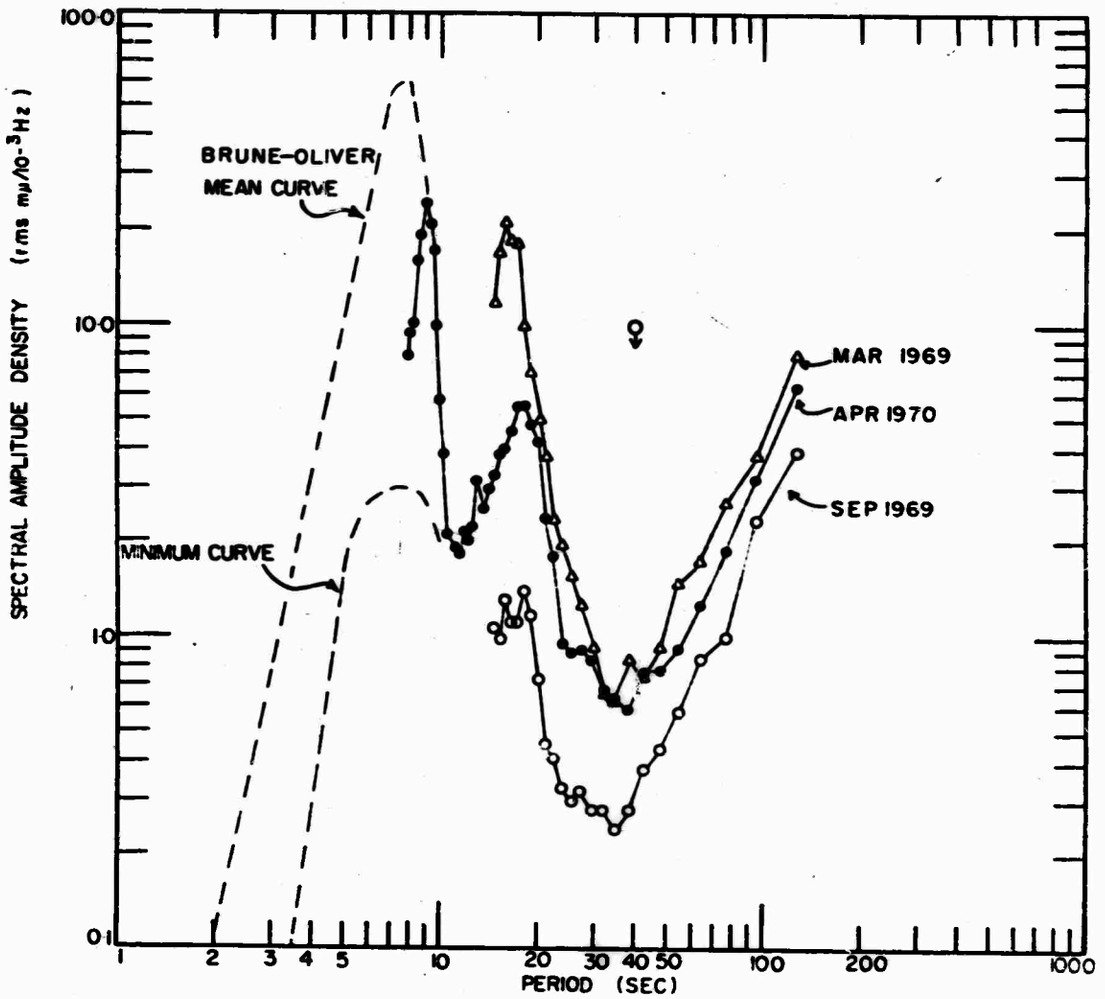

Figure 3. Spectral amplitude density for the high-gain vertical seismograph on three different occasions. The Brune-Oliver mean and minimum curves are shown for comparison The April 1970 spectrum is based on 5 hours 14 minutes of digital magnetic tape data with 88.2 degrees of freedom. The March 69 and September 69 spectra are based on three hours of data with 25.2 degrees of freedom.

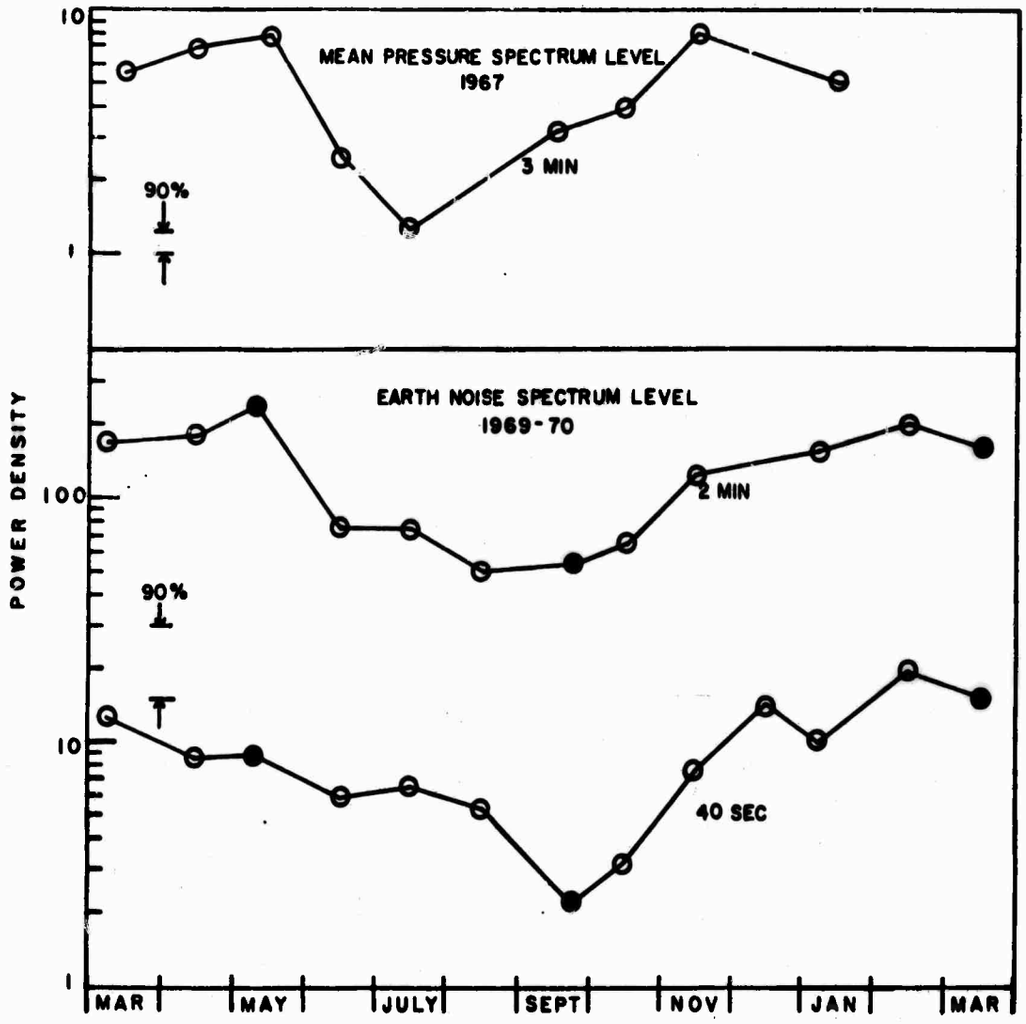

Figure 4. Seasonal variation of the long-period seismic noise in two period bands centered near 40 sec and 2 minute compared with pressure variations with 3-minute periods.

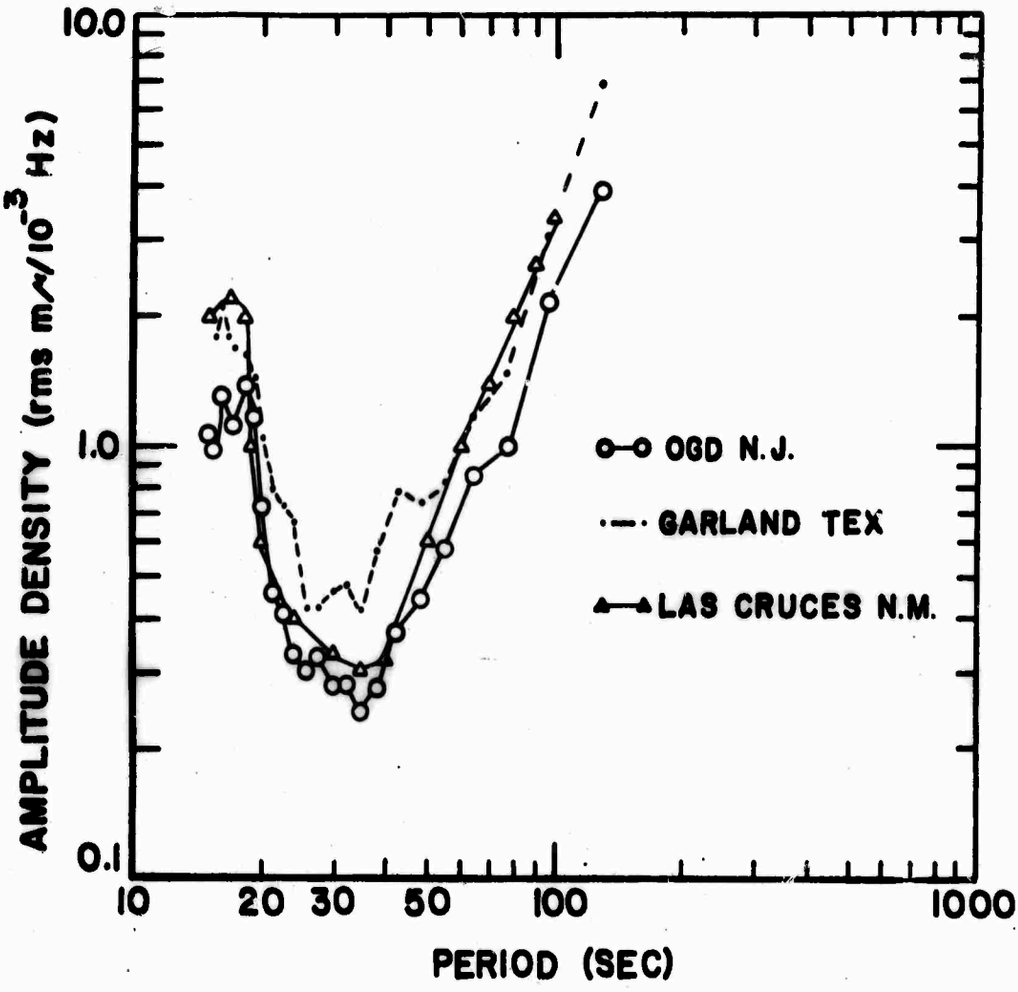

Figure 5. Vertical amplitude spectra for data from three geographically separate sites. The data for the Las Cruces, New Mexico, spectrum are taken from Trott (1965).

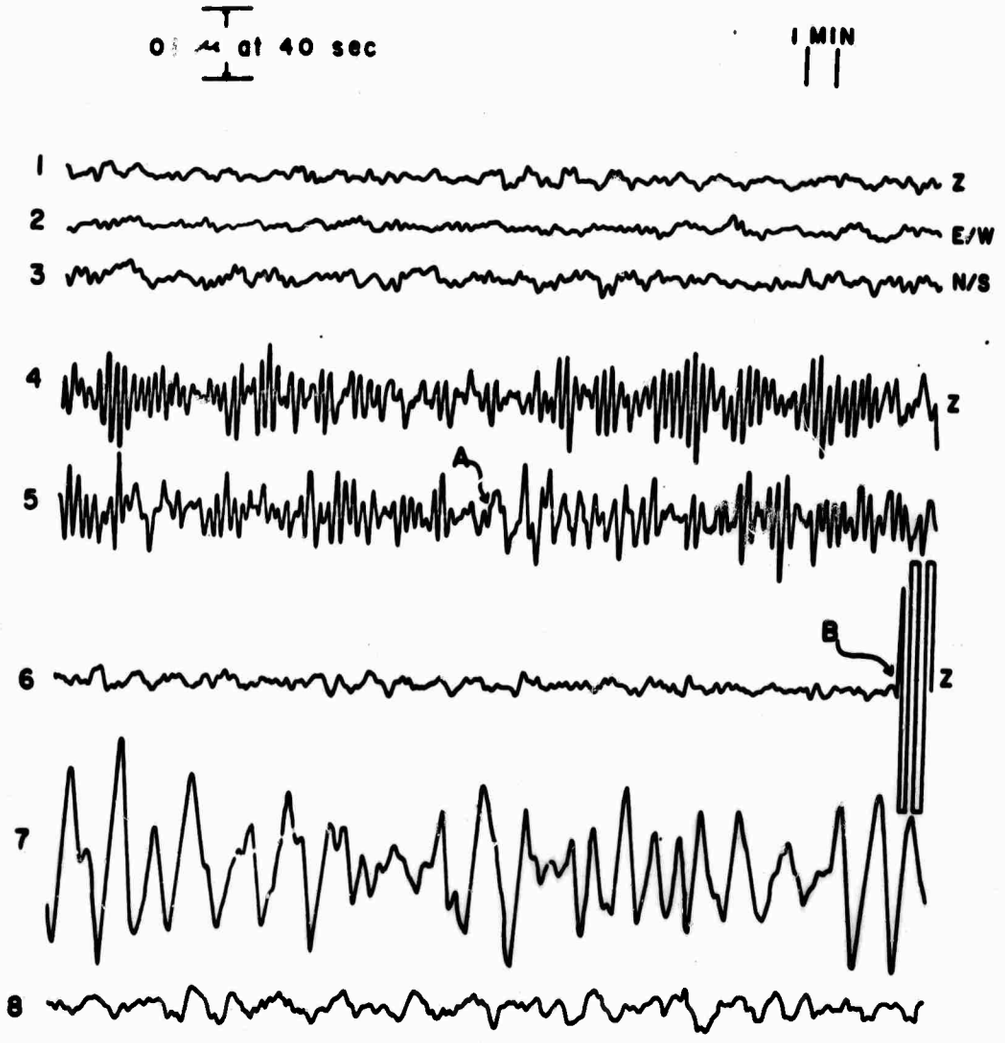

Figure 6. High-gain vertical and horizontal recordings of the long-period background. All traces are 1/2 hour in duration. Traces 1-3, 0500-0530 GCT, 12 Jun 1969; Trace 4, 0100-0130 GCT, 9 Mar 1969; Trace 5, 0430-0500 GCT, 9 Mar 1969; Trace 6, 1034-1104 GCT, 28 Feb 1970; Trace 7, 1800-1830 GCT, 28 Feb 1970; Trace 8, 0030-0100 GCT, 1 Mar 1970. Pertinent data for events A and B are: (A) Rat Islands, 51.7N, 178.9E, 04h 12m 17.3s, 9 Mar 1969, m_b = 4.7, 99 km; (B) Andreanof Islands, 52.7N, 175.1W, 10h 52m 31.2s, 28 Feb 1970, m_b = 6.1, 162 km. All information is taken from USC&GS PDE reports.

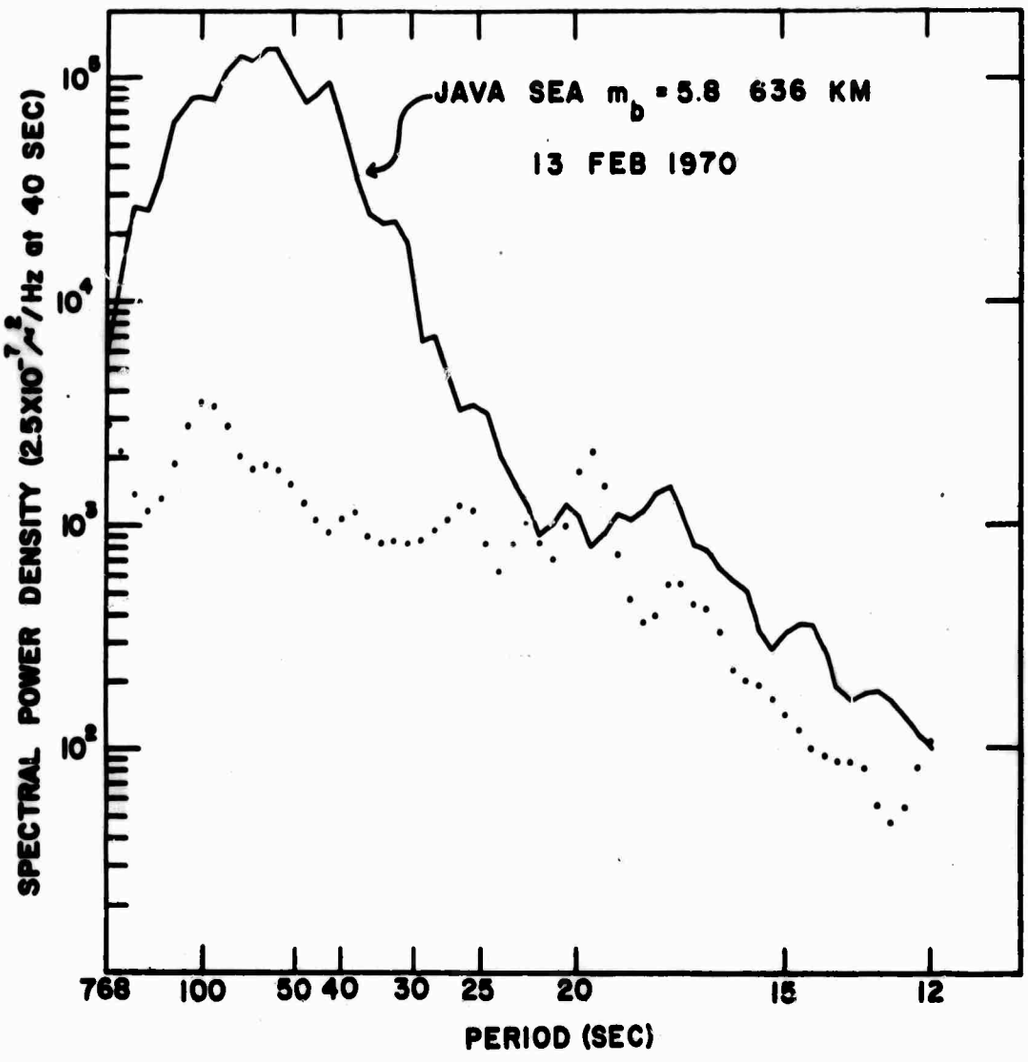

Figure 7. Comparison of vertical power spectra for data during a relatively quiet time (dotted curve) 0500-0800 GCT, 12 June 1969, and during a deep earthquake: Java Sea, 5.9S, 113.0E, 15h 43m 28.7s, 13 February 1970, m_b = 5.8 636 km. Power spectrum for Java Sea event starts at 19h 33m GCT and ends at 21h 03m GCT.

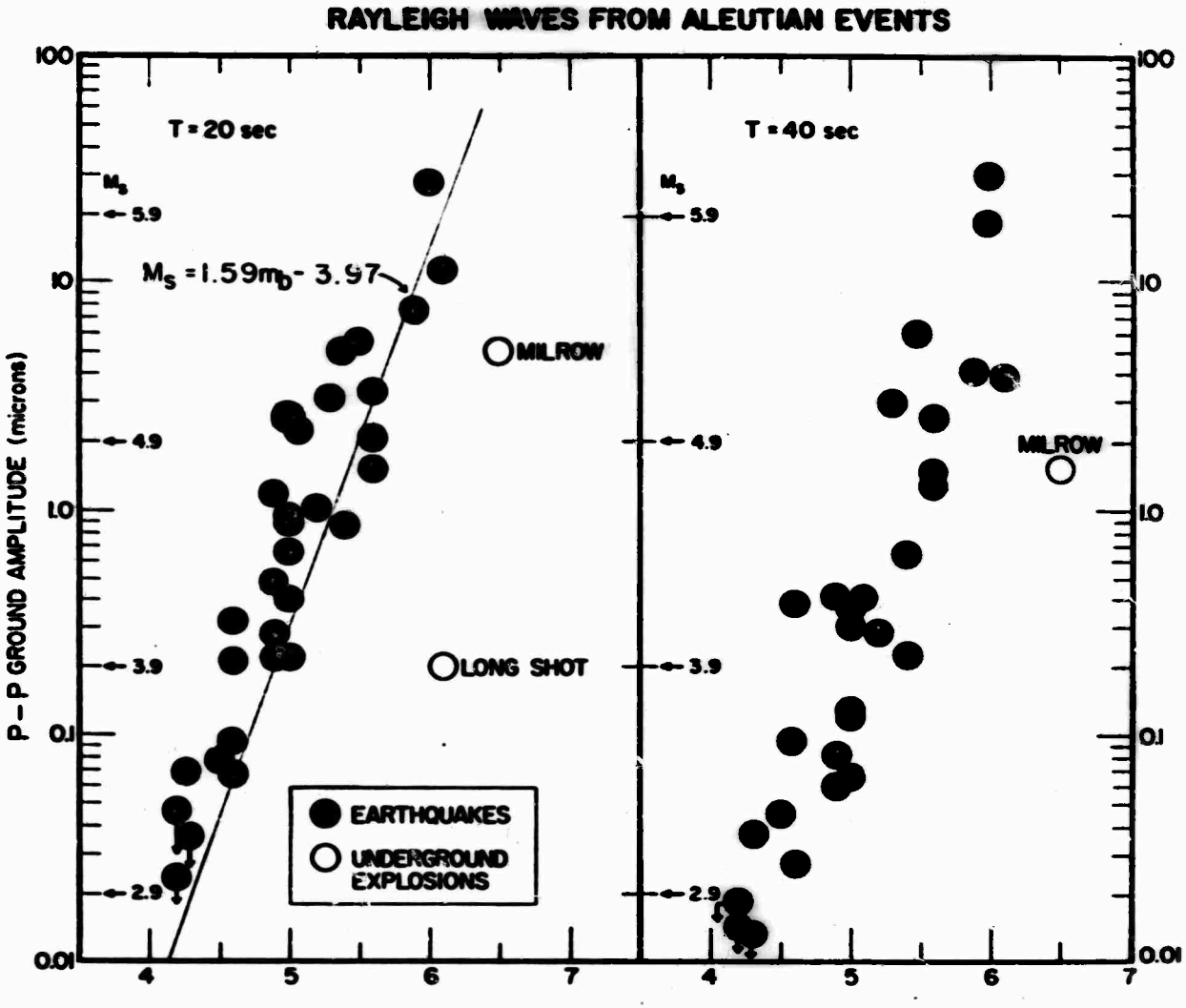

Figure 8a. Comparison of peak-to-peak ground amplitudes of the 20 sec and 40 sec Rayleigh waves from events in the Aleutians versus m_b as determined by USC&GS.

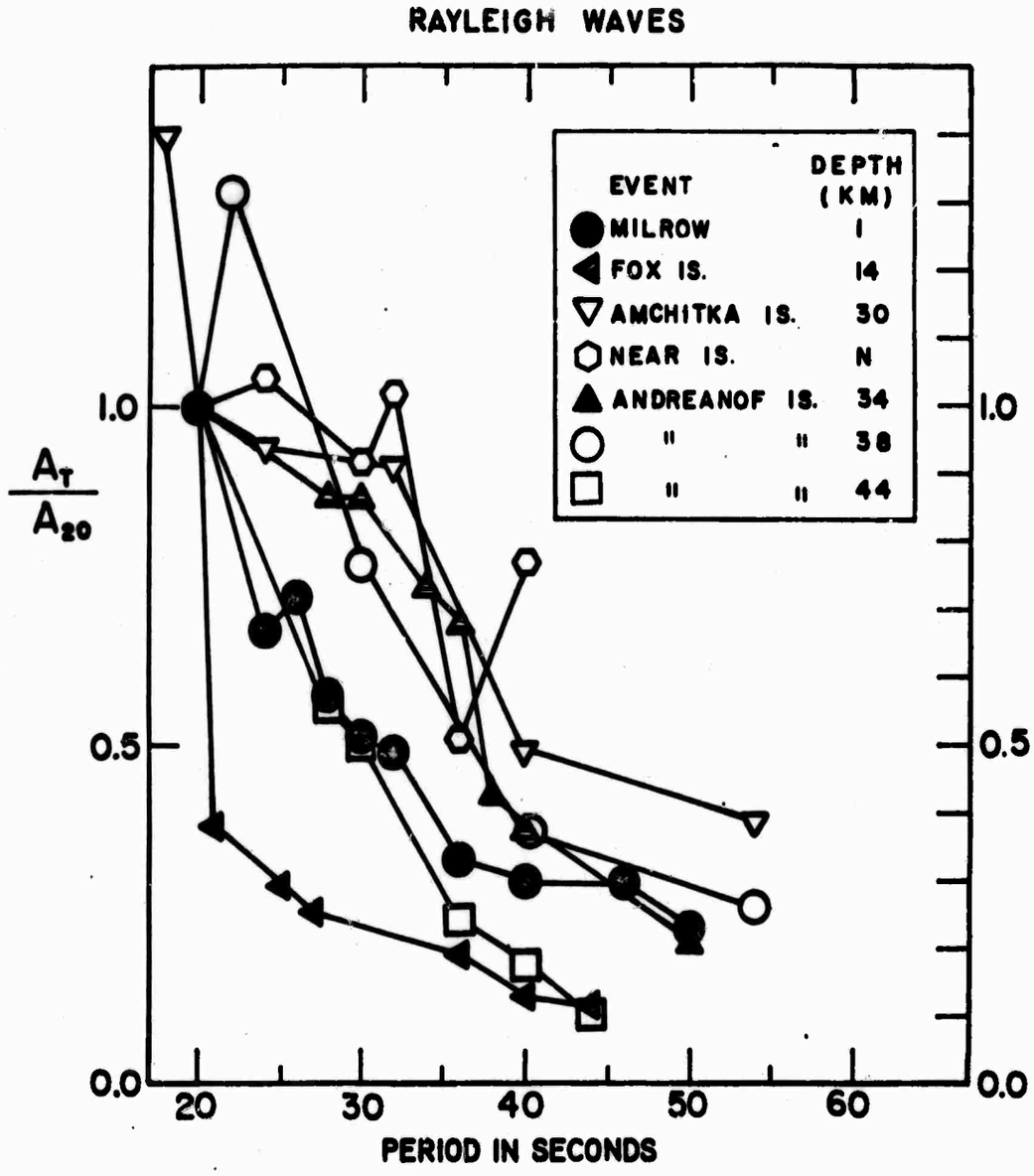

Figure 9. Amplitude spectra normalized to the peak-peak amplitude at approximately 20 sec.

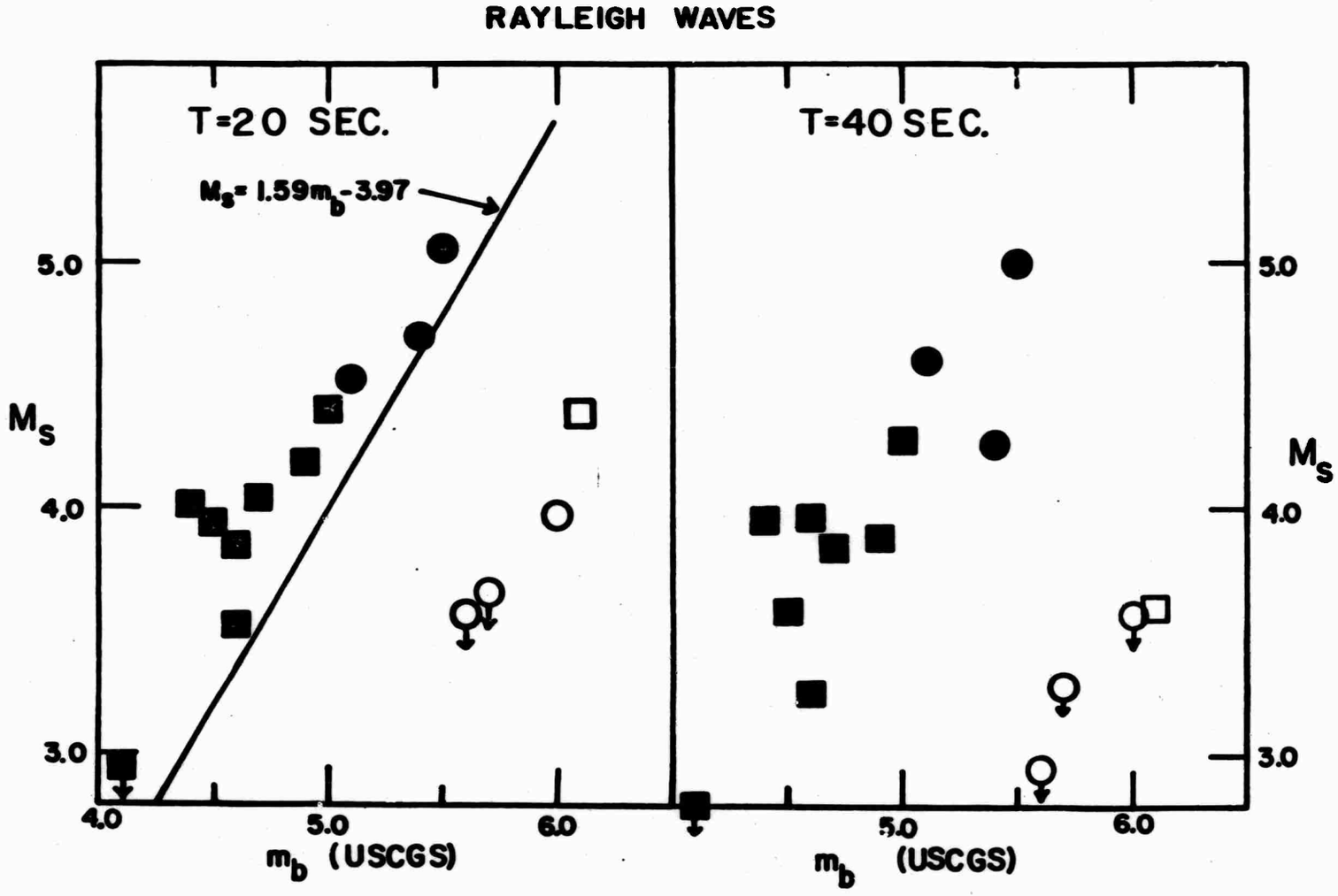

Figure 10. M_S-versus-m_b comparison of earthquakes and presumed underground explosions in the Novaya Zemlya region (squares) and central Asia (circles).

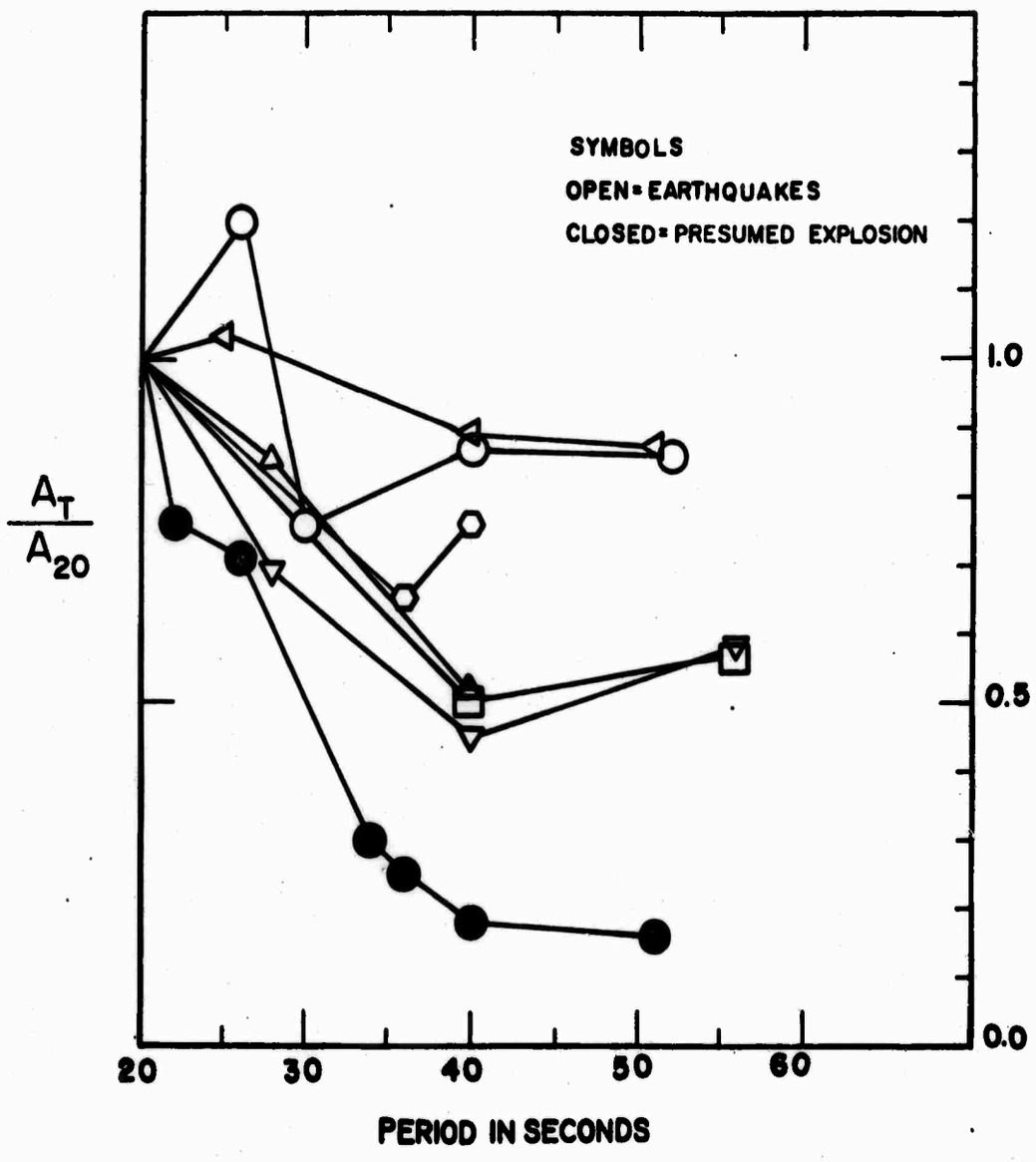

Figure 11. Amplitude spectra normalized to 20 sec for earthquakes and a presumed underground explosion occurring in the Novaya Zemlya region.

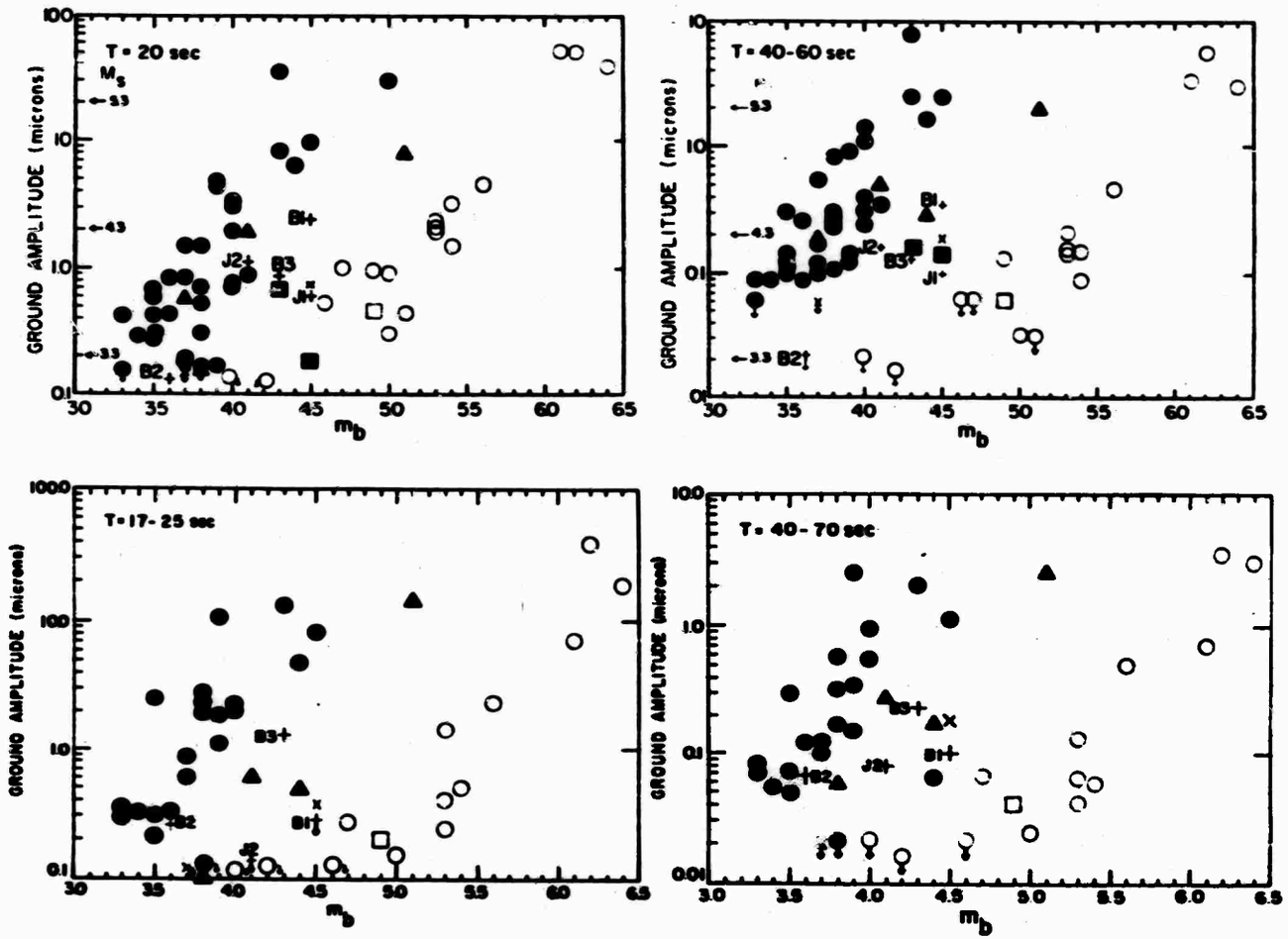

Figure 12. Comparison of peak-peak amplitudes of (a) 20-sec and 40-60-sec Rayleigh waves and (b) 17-25-sec and 40-70-sec Love waves, versus m_b determined by Evernden's formulas for western United States events. The closed circles are earthquakes in the Gulf of California; closed triangles depict events in northwestern United States; +'s depict NTS explosion aftershocks; X's depict 29 Palms earthquakes; the closed squares represent events occurring in Idaho. The open circles are NTS explosions. The open square square represents the underground explosions Rulison, 39°24'21"N, 107°56'53"W, 21h 00m 00.1s, 10 September 1969, m_b = 5.3

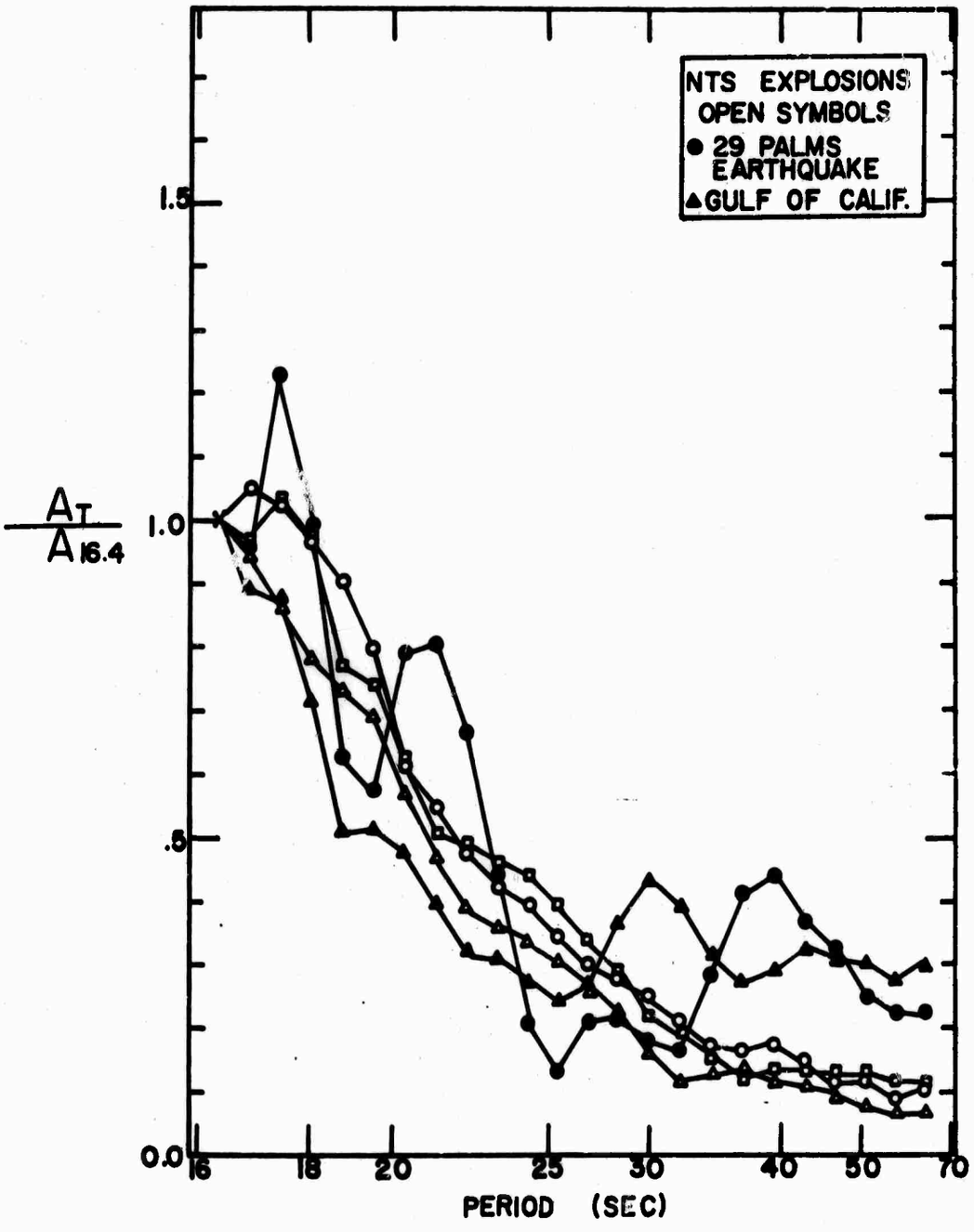

Figure 13. Amplitude spectra of events in the western United States. All spectra normalized to harmonic amplitude at 16.4 sec. Pertinent data for events not listed: 29 Palms earthquake, 33.9N, 116.0W, 23h 01m 01.0s, 23 January 1969, m_b = 4.9, 18 km; Gulf of California, 30.5N, 113.0W, 10h 23m 16.3s, 10 February 1969, m_b = 4.5, N; Pipkin, 37.3N, 116.5W, 14h 30m 00.0s, 8 October 1969, m_b = 5.5.

LONG-PERIOD EARTH NOISE

By

Stewart W. Smith*

California Institute of Technology

*Present address: Geophysics Program, University of Washington

SUMMARY AND CONCLUSIONS

Until recently, the distinctions between long-period microseisms, instrument noise, and site effects was poorly understood in the period range 30 to 3000 seconds. As a result of recent work by Pomeroy et al (1969) and by Haubrich (1970), the relative importance of instrument noise and earth noise is better understood. In an attempt to characterize long-period noise, two matched long-period pendulums were operated at Isabella, California, and compared with a microbarograph and with horizontal strain meters. The results of this study showed that virtually none of the recorded noise at periods longer than 60 seconds is propagating noise. The microbarograph showed virtually no coherence between the vertical seismometer output and the pressure variations in the tunnel. Comparison of the pendulum and strain instruments at this site confirmed that noise at periods longer than 60 seconds does not have wave lengths characteristic of propagating waves in the earth. Experimentation with a number of transducers resulted in a system with a peak magnification of 21,000 at a period of 70 seconds. This appears to be within 6 dB of the reported characteristics of the instrument described by Pomeroy et al (1969) and that described by Block and Moore (1970).

Long-period vertical seismometer.

A conventional Press-Ewing long-period seismometer with a nominal period of 30 seconds was modified by the installation of several displacement transducers and a servo controlled centering circuit, and the entire system was installed within a steel vacuum chamber. Two independent sets of coils were installed, one for the servo system and the other for damping and electrical period lengthening. Both variable-area and variable-gap capacity-type displacement transducers were installed on the boom. Figure 1 illustrates the evolution in noise spectrum of the system in several configurations. Figure 2 shows the spectrum and coherence of the two instruments in an early configuration. It can be seen that system noise predominates over ground noise at periods of 100 seconds and longer. The source of this system noise is unknown. The major drawback of the seismometer used in this experiment is the long, heavy spring used in the Lacoste geometry. That such a spring contributes serious long-period noise due to parasitic vibrations, although generally accepted, was not confirmed here. The Q of this spring in several transverse and rotational modes of vibration is approximately 1000. Two viscous dampers were attached to the spring in an attempt to damp these parasitic vibrations. The dampers were attached at the mid-point and 1/3 the distance from the end of the spring. Viscous damping was effective for transverse, rotational, and longitudinal modes of vibration of the spring. The Q of most of these higher order modes of vibration with frequencies above 3 Hz was reduced to about 50. The fundamental mode of the spring was damped such that with the

period adjusted to 60 seconds the viscous damping of the pendulum was approximately critical. Further damping of the higher order modes of the spring was not possible without over-damping the seismometer. Installation of these spring dampers did not materially affect the long-period noise spectrum of the instrument, leading us to believe that the effect of parasitic modes of vibration of the spring was not a major problem in this instrument. A series-resonant variable-capacity transducer was used initially and later replaced by a differential-capacity transducer with a lock-in amplifier. The latter system gave significantly lower noise when installed on the seismometer, although both performed comparably on the bench. Both variable-area and variable-gap sensors were used, the latter giving significantly better performance, although restricting the pendulum to a narrow range of displacements ($\pm$ 1 mm). After numerous experiments with and without the servo system, and after considerable modification to all parts of the system, including the suspension, the transducers, the spring, and the damping system, we concluded that no further improvement in system noise at periods longer than 100 seconds could be expected from this conventional instrument. Although the sources of the noise are unknown, the most likely candidates are the spring and the suspension. The spring is an isoelastic alloy and exhibits some non-linear creep. The suspension is either a flat spring or a Bendix flexural pivot, neither of which is noted for its mechanical stability. For further improvement at long period, it would appear that complete redesign, using more stable materials such as quartz (Block and Moore, 1970), would be a preferable approach.

Pendulum barograph strain coherence.

Coherence studies were run between a microbarograph and the pendulum instruments. The microbarograph sensor was located in the tunnel with the other instruments. Low coherence was noted at long period, indicating that the instruments themselves were not directly pressure sensitive. Coherence between the microbarograph and the strain instruments was also low at long periods. These results do not mean that the long-period nonpropagating noise is unrelated to pressure effects. It simply means they are not strongly correlated with the local pressure variations in the tunnel. A microbarograph array covering a larger region might well show a higher degree of coherence with the strain and pendulum instruments. Coherence between the vertical instrument and the strain seismometers was also low. This was an unexpected result. If the long-period noise were propagating, then one should see a high degree of coherence between the vertical instrument and the strain seismometers, and further, at a given frequency the ratio between strain and pendulum outputs should be proportional to the phase velocity of the particular mode of propagation in which the noise was excited. If the noise were nonpropagating, one would still expect high coherence, but inconsistent or highly varying apparent phase velocities would

be determined from the ratio of strain to pendulum. The fact that the coherence was low means that the principal part of the power we are seeing at long periods is dominated by very local effects near the instruments and by system noise. This result is consistent with the equivalent ground noise spectrums shown in Figure 2, in which it can be seen that most of the power at periods of 100 seconds and longer is due to the instrument.

Excitation of long-period waves by small earthquakes.

The vertical seismometer previously described was operated at a peak gain of 21,000 at a period of 70 seconds starting on June 24, 1970. Figure 3 shows the response and Figures 4 and 5 show typical seismograms produced by this system. They illustrate that events with surface-wave magnitudes of around 5 at distances in excess of 40° produce 100-second mantle Rayleigh waves that are easily detectable. Although the sample of events is small, one would infer from these few examples that the threshold of detection of 100-second mantle waves at distances of 40° would be about M_S = 4.6. Comparison of these records with seismograms written by the Block-Moore instrument at Camp Elliot, California, indicate that their threshold of detection would be about .3 magnitude units less than that of the system described here. Considerably more data will be collected in the next few months and the detection threshold for long-period waves can be defined with more certainty.

Free oscillations.

A number of spectra from large earthquakes (M_S>6 3/4) have been calculated. Spheroidal modes of order number 10 and greater can usually be seen in these spectra. In general, it is not useful to talk of the threshold level for excitation of free oscillations without at the same time specifying the order number at which one is detecting such oscillations. Any earthquake large enough to excite mantle waves such that one can see multiple Rayleigh waves, R_3 and R_4 for example, will, upon frequency analysis, reveal spectral lines corresponding to spheroidal modes of oscillation. It is not surprising, therefore, that earthquakes of the same body-wave magnitude will show widely varying excitation of free oscillations. Earthquakes with the same surface-wave magnitude show perhaps slightly less variation, and, comparing earthquakes with the same mantle-wave magnitude, one finds comparable free oscillation excitation. Consistent studies of excitation of free oscillations as a function of source mechanism and magnitude are clearly of importance, but they have not yet been undertaken.

Strain-pendulum combinations. It now appears that there is a window in earth noise at around 30 to 40 seconds in period. This is caused by the peak in the propagating noise spectrum at around 20 seconds, falling off quite steeply going to longer period, and by the rapid

rise in nonpropagating noise at longer periods starting around 30 seconds. These two effects combine to produce a narrow window in earth noise. Operation of high-gain instruments in this period range are very effective in detecting small earthquakes. Discrimination techniques also appear to be more effective in this long-period range. As more becomes known about the characteristics of nonpropagating noise, it may be possible to significantly reduce it and thus broaden the effective window in earth noise. This would be of substantial help in the discrimination problem. It can perhaps be accomplished by means of small arrays, microbarograph arrays, or by combined strain-pendulum systems. The imporant characteristic of nonpropagating noise is its short wave length and its relationship to pressure variations at the surface. The fact that it has short wave length can be capitalized on by use of a small array, and the fact that it is a direct result of barographic effects at the surface can also be utilized. One could, for example, record the pressure variations over the region near the instrument and construct an empirical operator which would determine the amount of nonpropagating noise generated by this pressure variation, and this noise could then be substracted from the signal. An alternative approach would be to use a combined strain-pendulum system. As mentioned previously, the ratio of pendulum to strain outputs at a given frequency is proportional to phase velocity, assuming the signal is a plane wave. One can easily imagine filters (nonlinear unfortunately) that would enhance that part of the pendulum output which is coherent with the strain and also has a phase velocity appropriate for propagating waves.

REFERENCES

Block, B., and Moore, R., 1970, Tidal to seismic frequency investigations with a quartz accelerometer of new geometry. J. Geophys. Res. v. 75, p. 1493-1506.

Haubrich, R., 1970, Low level earth motion, final report Contract AF49(638)-1388. Geophysics Division A.F.O.S.R. May 1.

Pomeroy, P., Hade, G., Savino, J. and Chander, R., 1969, Preliminary results from high-gain wide-band long-period electromagnetic seismograph system. J. Geophys. Res. v. 74, p. 3295-3298.

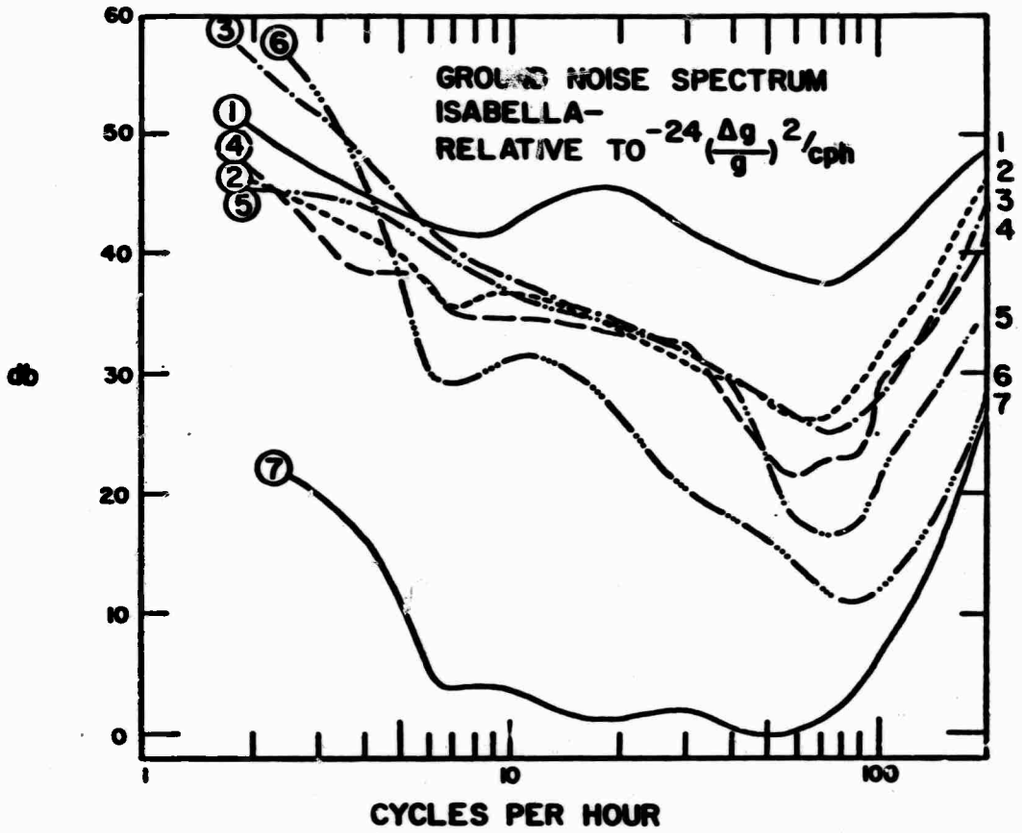

Figure 1. Ground acceleration spectrum at Isabella, California
(1) Vertical No. 1, 9 June 1970
(2) Vertical No. 2, 6 June 1970, lock-in amplifier, no servo
(3) Vertical No. 2, 16 June 1970, servo
(4) Vertical No. 2, 21 June 1970, variable gap transducer, no servo
(5) Vertical No. 2, 2 July 1970, variable gap transducer, servo
(6) Long-period seismometer, Haubrich (1970)
(7) Modified LaCoste, Haubrich (1970)

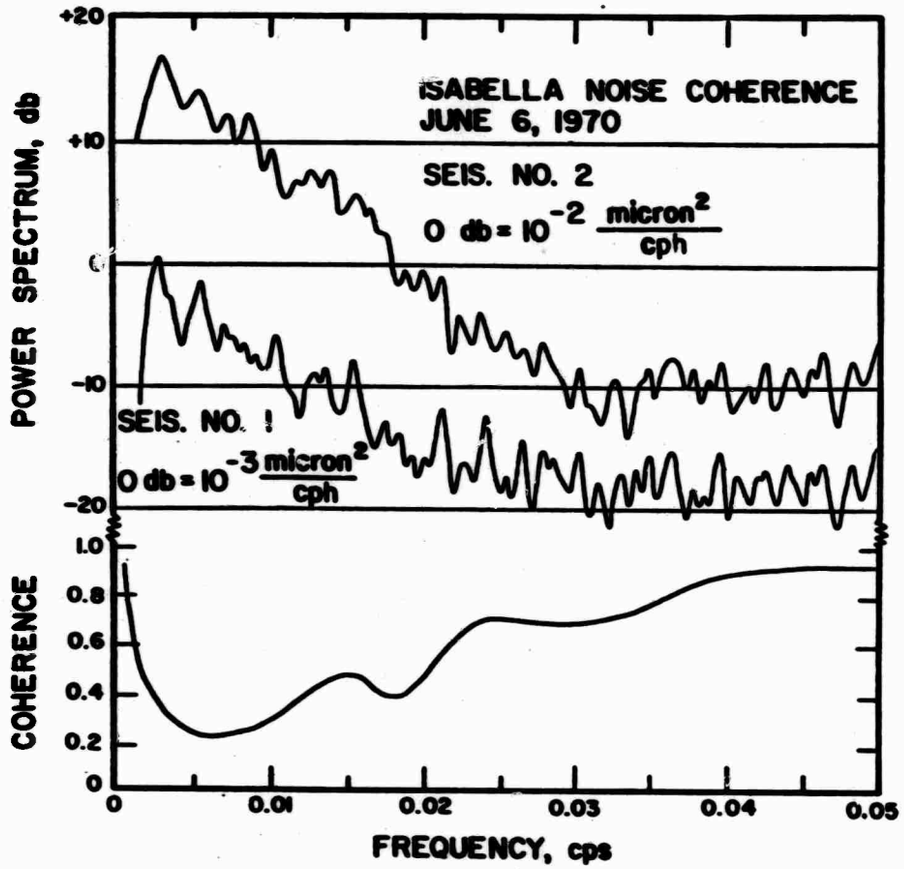

Figure 2. Ground displacement spectrum, uncorrected for instrument response. Both instruments operating at a free period of 60 seconds with variable area transducers and feedback centering. No 2 system has lock-in amplifier.

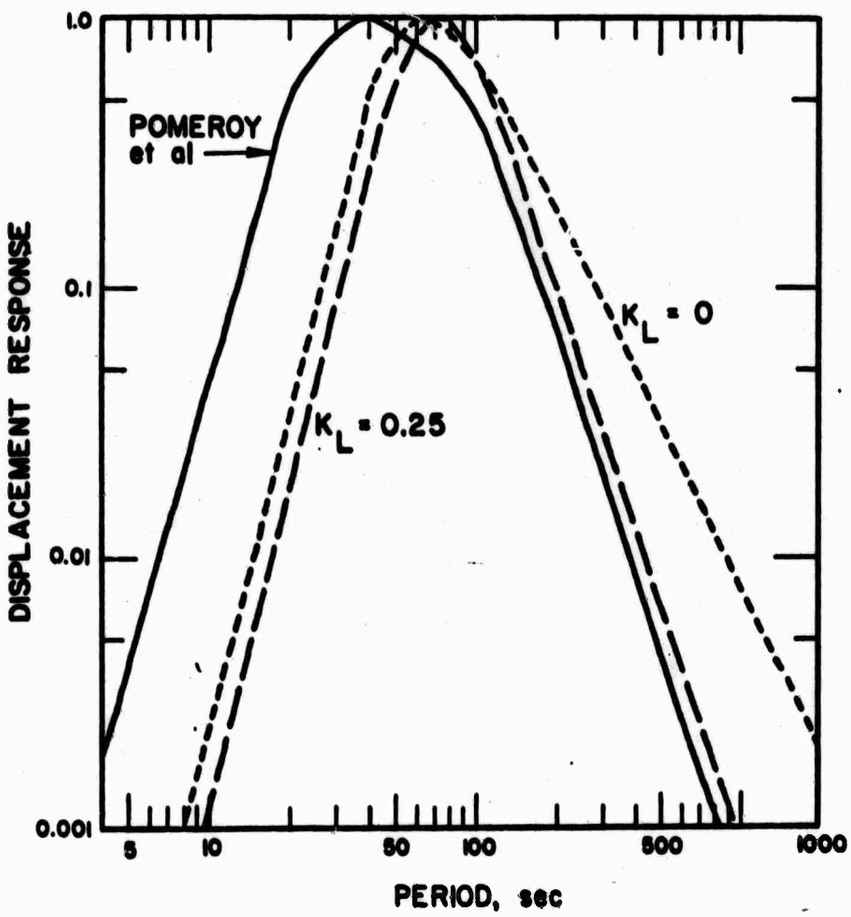

Figure 3. Displacement response without servo (K_L = 0) and with servo (K_L = .25, loop gain for optimally flat response) compared with high-gain, broad-band system described by Pomeroy et al (1969).

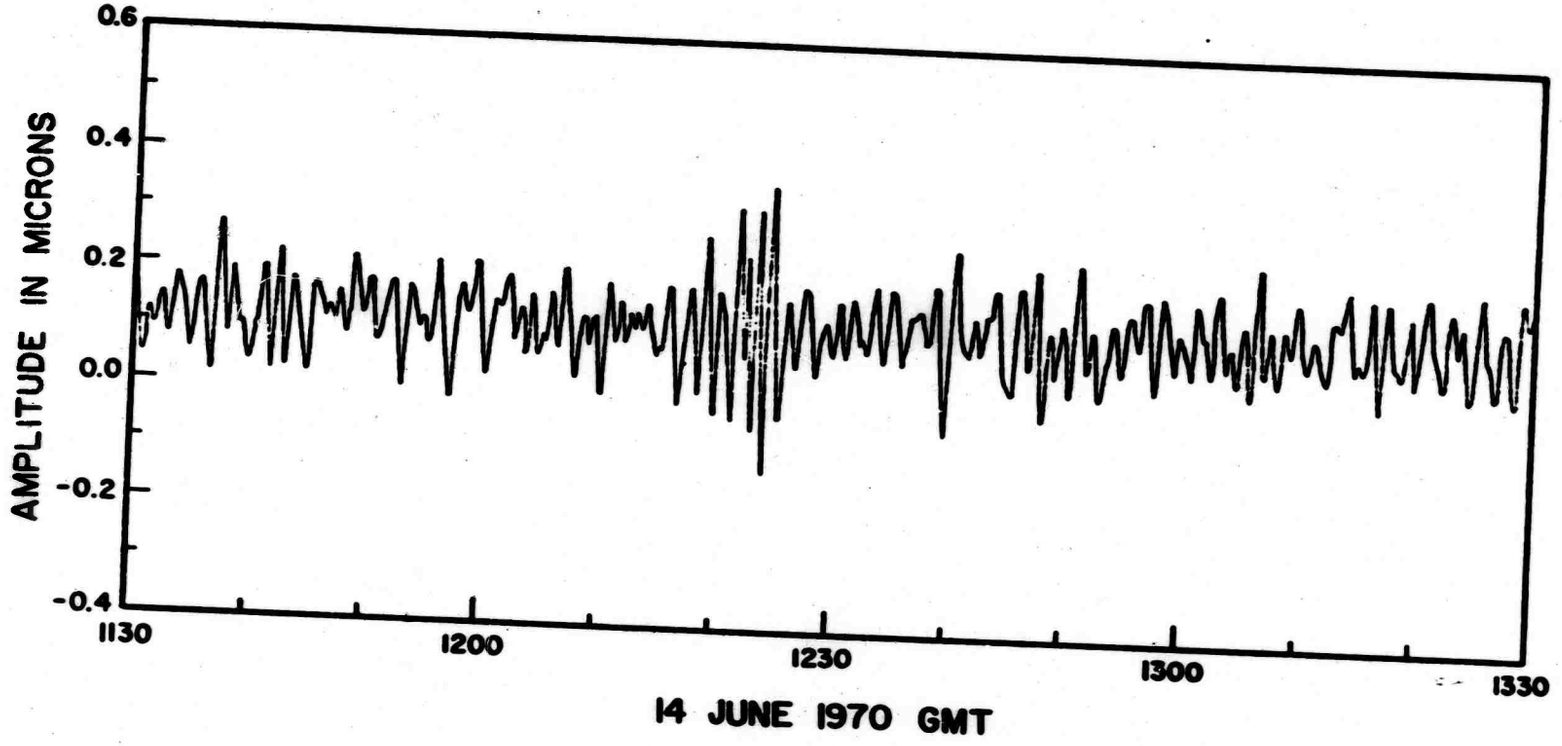

Figure 4. Seismogram showing mantle Rayleigh wave from earthquake tentatively determined to be M_b = 5.0 at 89°.

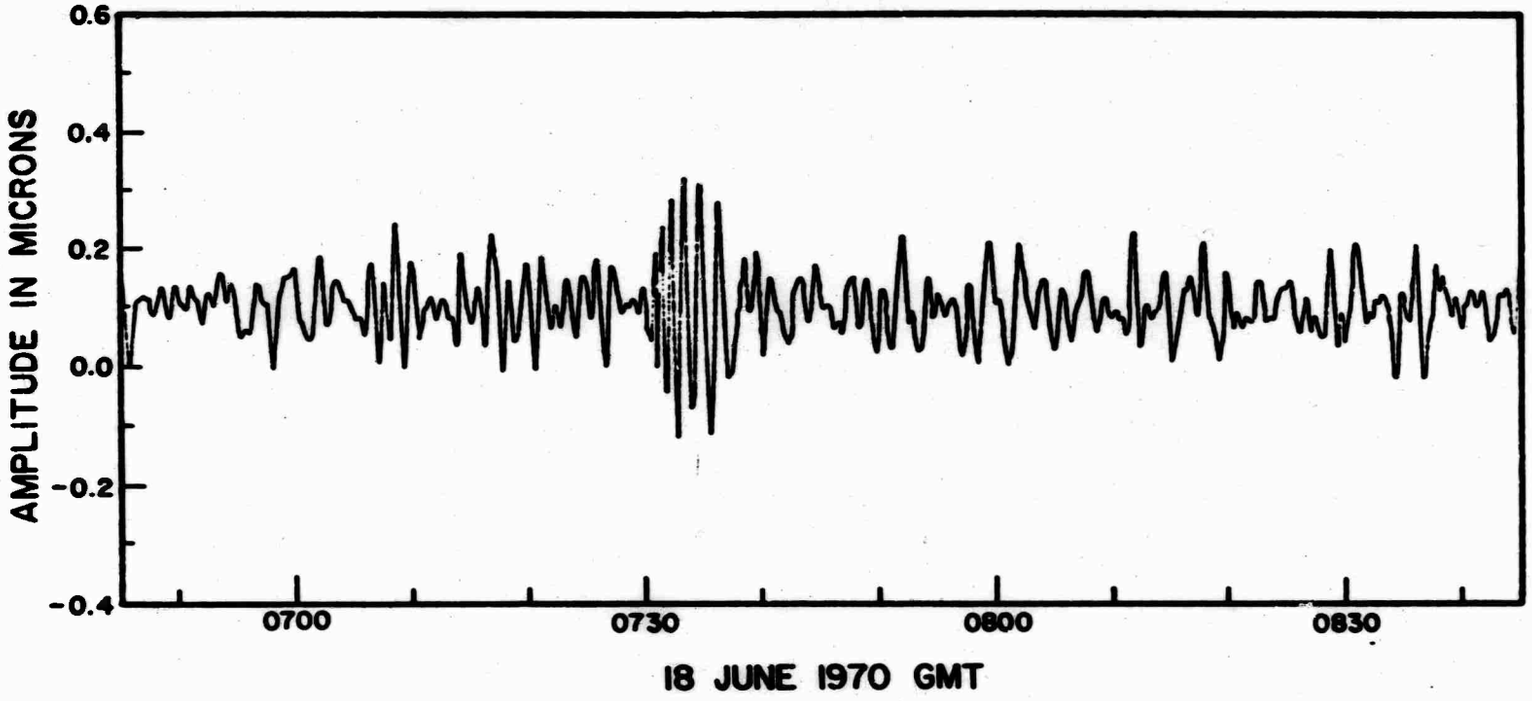

Figure 5. Seismogram showing mantle Rayleigh wave from earthquake tentatively determined to be M_s = 5.2 (Pasadena) at 35°.

CRUSTAL EFFECTS ON LONG PERIOD CHIRP FILTERS

By

M. Nafi Toksöz

Department of Earth and Planetary Sciences
Massachusetts Institute of Technology
Cambridge, Massachusetts 02139

ABSTRACT

The applicability of the linear chirp filter to seismic surface wave detection is investigated. It is found that for primarily continental paths, linear chirp filters can be synthesized to approximate the dispersion characteristics of the medium in the period range 18-50 seconds. For oceanic paths, however, a realistic filter must have a nonlinear relationship between frequency and group delay times. A simple functional form is given for such a filter. Different group velocity curves must be used to synthesize filters for different paths.

The interference of wave trains affects the performance of chirp filters. As a result, surface wave magnitudes based on chirp filtering would be lower than estimates unless these magnitudes are calibrated for each region.

INTRODUCTION

Seismic surface waves are, in general, well dispersed wave trains. The dispersion properties of these waves can be utilized for their detection and identification in the presence of seismic noise. Various techniques have been employed for this purpose. Among these are the correlation with well-recorded sample wave trains and a theoretically synthesized chirp wave form (Alexander and Rabenstine, 1967; Capon et al, 1969). For processing large amounts of data, chirp filtering is a more convenient method because of its computational adaptability. To better understand the performance of these filters, it is important that some of their properties be compared with the observed dispersion of surface waves. In this report such a study is described briefly, comparing the group delays for surface waves propagating over oceanic, continental and mixed paths, with those of linear chirps.

A desired property of chirp filters is for the filter to look exactly like the wave train to be detected. Under ideal conditions it would be possible to synthesize such a filter. In practice, however, many such filters need to be considered since the wave trains vary from one event to another. Source properties, such as focal depth and magnitude as well as laterally varying crustal and upper mantle structure, affect the Rayleigh and Love waves.

There are three main factors that must be considered in dealing with surface waves. These factors are: 1) source properties - initial spectra or time function at the source, spatial function of the source and source depth; 2) propagation (dispersion) properties - amplitude and phase response of the plane layered medium; 3) effects of heterogeneities - complications introduced because of refraction, reflection, and interference.

In sections II and III of this report, we will discuss item 2 in some detail since it is predictable and better known. In section IV source properties and interference effects are discussed briefly.

POINT SOURCE IN A PLANE LAYERED MEDIUM

To describe some of the factors that influence the seismograms, it is best to consider first the problem in the frequency domain.

Let $W(\omega)$ be the spectrum of the vertical component of the Rayleigh wave ground motion at some distance r from a point source. It can be expressed as (Toksöz, et al, 1965):

$$W(\omega) = \frac{A}{(2\pi r)^{1/2}} e^{-\gamma(\omega)\cdot r} L(\omega,h)\ S(\omega)\ T(\omega)\ e^{-i(kr+\phi_s+\phi_t-\frac{3\pi}{4})} \quad (1)$$

where

γ = attenuation coefficient

$L(\omega,h)$ = amplitude response of the layered medium

h = focal depth

$S(\omega)$ = source space function (i.e. explosion, couple, double couple)

$T(\omega)$ = source time function (e.g. step, impulse)

k = wave number = $\frac{\omega}{C(\omega)}$, C = phase velocity

ϕ_s, ϕ_t = phase factors associated with $S(\omega)$, $T(\omega)$.

If all quantities in equation (1) are known, then the wave train can be synthesized:

$$w(t) = \int_{-\infty}^{\infty} W(\omega)\ e^{i\omega t}\ d\omega \quad (2)$$

It should be noted that instrument (seismograph) response is not included in (1) and it should be included for a realistic looking seismogram. In order to determine the factors listed in (1) it is necessary to know the medium response and the source properties. The factors that are most important for the small events are: (1) source time function $T(\omega)$, and (2) propagation factor including the source depth

$$L(\omega,h)\ e^{-ikr} = L(\omega,h)\ e^{-i\frac{\omega r}{c}}$$

The propagation factor varies drastically with structure, especially between oceanic and continental regions. Although the amplitude factor needs to be computed theoretically, the velocity data are, in general, available and can be used readily.

DISPERSION DATA

A collection of measured group velocity values is given in Figures 1 and 2 for continental and oceanic regions, respectively (Data from Kovach, 1969; Press, 1961; Kuo, et al, 1962; Brune and Dorman, 1963; Santo and Bath, 1963; Dewart and Toksöz, 1965). Although the maximum group velocity contrasts occur between purely oceanic and purely continental paths, there are significant differences for paths in an oceanic or continental region (Savage, 1969). For example, certain oceanic areas such as the North Sea may have characteristics closer to a continental path than to the central basin of the Pacific Ocean. The crustal thickness and the water depth are significant parameters that control the oceanic group velocity dispersion in the period range of 10 seconds to 30 seconds.

Averaging of group velocities

In general the path between the source and the receiver is a composite of different regions and cannot be characterized as a pure path. With certain simplifications, the group velocity for such a path can be computed if the group velocity for each segment is known.

Let us assume that the surface wave train follows the great circle path when propagating over a heterogeneous region (i.e. the ray path is perpendicular to velocity boundaries and there are no lateral refractions). For this simplest case, the average group velocity $\bar{U}$ can be expressed as

$$\bar{U} = \frac{\Delta}{\sum_i t_i} = \frac{\sum_i \Delta_i}{\sum_i t_i} = \frac{\sum_i \Delta_i}{\sum \Delta_{i/u_i}} \qquad (3)$$

where Δ_i, t_i, U_i are distance, time of travel, and group velocity associated with the i^{th} segment of the path. Thus, given the dispersion curves for each of the regions, the dispersion curve for the composite path can be computed with the above relationship. Other averaging forms should be considered for a more realistic study.

For example, given the group velocities for oceanic and continental paths of equal lengths (Figures 1 and 2) the computed composite group velocity curve is given in Figure 3a. Figure 3b shows some observed group velocities over mixed paths. The shape of the curves are remarkably similar, although the observed data do not come from exactly 50-50 ocean-continent paths.

SOME LIMITATIONS OF CHIRP FILTER

A linear chirp filter given by

$$f(t) = \begin{cases} \sin\left[2\pi\left(f_0 + \frac{f_1 - f_0}{2L}\, t\right)t\right] & ; \ 0 \leq t \leq L \\ 0 & ; \text{otherwise} \end{cases}$$

is mathematically simple and its properties have been studied extensively in connection with chirp radar. As applied to seismic surface waves, however, it has certain limitations which must be considered. These include (1) the amplitude response of the surface wave trains, (2) the general shape of the group velocity curve, and (3) the interference and multi-paths effects. In this section we will discuss these properties.

Amplitude response

In chirp filtering it is assumed that the amplitudes of the peaks over a given frequency range are constant. Although this is not true, in general, it does not constitute a major problem. Variations of the amplitude spectra of surface wave trains, which are propagated over the same path, have been observed. These differences are primarily due to source spectra. Some modifications of chirp filter must be introduced to take into account the source properties. Generally, larger events generate relatively more long period surface waves. For a given magnitude, the deep focus earthquakes and the low-stress-drop earthquakes generate more long period and less short period surface waves. In these cases period limits of the filter should be shifted to longer periods.

Shape of the group velocity curve

The chirp filter given by equation (4) has a well-defined group velocity curve once the frequencies f_0, f_1 and the length L are fixed. The group delay is a linear function of the frequency. The group velocity is expressed by

$$U(f) = \frac{\Delta}{t_0 + \tau(f)} \qquad (5)$$

where Δ = epicentral distance, t_0 = initial time of the chirp = $\Delta/U_0(f_0)$, and $\tau(f) = b \cdot f$ = group delay. For a given filter (5) can be determined from the filter characteristics

$$b = \frac{L}{(f_1 - f_0)} \qquad (6)$$

The shape of the group velocity curves generated using (6) must approximate the actual group velocity curve for the path in order to obtain the theoretical signal-to-noise enhancement. If this condition is not satisfied the method will not be applicable.

Examples of frequency vs group delay times for actual paths are shown in Figures 4, 5, and 6 for three different regions. These curves are computed using observed group velocity values given in Figures 1-3. For paths which are primarily continental (Figures 4 and 5) a linear approximation to f vs τ curve in the frequency range of f = 0.025 to 0.05 cps can be justified. At lower frequencies the dispersion is greater. At frequencies above about 0.05 cps the Airy phase of crustal Rayleigh waves complicates the picture.

In the oceanic case, however, at frequencies below about 0.05 cps, which is the region of greatest interest, a linear approximation to frequency -- group delay curve is impossible (Figure 5). This implies poor performance of the linear chirp filter when applied to South Pacific events. A more realistic filter must be designed for oceanic paths. In the regions where f>0.055 cps, the group velocity curve is nearly vertical and generally the wave trains are complicated by beats and modulations which are discussed in the following section.

To summarize the above discussion, it is possible to use the linear chirp filters for paths which are primarily continental. The frequency range should be limited to 0.025 - 0.055 cps. For primarily oceanic paths (especially the Pacific Ocean) a non-linear chirp filter must be designed. A possible functional form for application in the frequency range 0.03 - 0.06 cps is

$$F(t) = \sin \left[2 \left(f_0 + \frac{f_1 - f_0}{C(L)^{1/N}} t^{1/N}\right) t\right] \qquad (7)$$

Integer N may be 2 or 3. N and the factor C must be determined to fit a given case.

Interference effects

Many of the surface wave trains show significant amplitude modulation or "beats". The presence of this modulation complicates the design and application of chirp filter. The beats can be produced by source properties or the multipath and interference effects. The observations primarily favor the latter case (Toksöz and Ben-Menahem, 1963; (Capon, 1969).

The simplest way of producing amplitude modulation is to superimpose two sinusoidal wave trains; one is delayed in time relative to the other. Based on the time delay and relative amplitudes, various beats are produced. In the earth the problem is more complicated and the interfering wave trains may be approaching from different directions.

In Figure 7, different examples of interference are shown using theoretical wave trains. In general, time delayed interference is more effective in producing beats than arrivals from different directions where the angle between wave vectors is less than about 30°. At LASA, the frequency-wavenumber spectra of Rayleigh waves show variations in the directions of approach (propagation) at different frequencies. Variations relative to great circle path can be as much as 40° (Capon, 1970).

The application of a chirp filter to a composite wave train does not produce the expected signal to noise enhancement. Both the absence of wave train, and the double-peaked correlation function contribute to this limitation. To illustrate, let us take a seismogram consisting of two similar dispersive wave trains, one delayed relative to the other by an amount Δt

$$F(t) = f(t) + a\, f(t - \Delta t) \tag{8}$$

where a is constant amplitude factor. If we choose f(t) to be

$$f(t) = Sin\ (t + 0.5t^2) \qquad 0 \leq t \leq T_{max}$$
$$= 0 \quad \text{otherwise} \tag{9}$$

a modulated wave train can be generated by

$$F(t) = Sin\ (t + 0.5t^2) + a\ Sin[(t-\Delta t)+(t-\Delta t)^2] \tag{10}$$

Values of a and Δt control the extent of modulation. The Fourier spectrum of (10) is

$$F(\omega) = T(\omega)\ [1 + a\ e^{i\omega\Delta t}] \tag{11}$$

For small a ($a \ll 1$), (11) can be approximated by

$$F(\omega) \simeq T(\omega)\ [1 + a \cos \omega\Delta t]\ e^{ia \sin \omega\Delta t} \tag{12}$$

Equation (12) shows the amplitude and phase modulation factors. Various numerical examples of the above are given by Pilant and Knopoff (1964).

In correlating (10) with a chirp filter, one would detect two peaks separated by Δt. Relative amplitudes and shapes of these peaks would depend on a, Δt, and T_{max}. When Δt is small, the peaks may interfere. If Δt is large, the chirp filter will provide only limited S/N because of excessive modulation. Beamforming reduces interference effects to some extent.

The magnitudes (M_S) computed from the correlation of the chirp with the wave train will be a lower estimate. Thus it is necessary to determine empirical corrections to chirp magnitudes based on path types and extent of interference.

CONCLUSIONS

The chirp filter provides a convenient method for signal-to-noise enhancement of surface waves in a limited period range. It can be generated easily and can approximate the Rayleigh wave train over different paths with relatively few parameters. Several points must be kept in mind in regard to limitations of the chirp filter.

1. The linear chirp filter could be applied only in the cases where the linear relationship between frequency and group delay are satisfied. This condition is approximately satisfied primarily for (i.e. more than 50 per cent) continental paths in the frequency range 0.025 - 0.055 cps. For small events ($M_S \leq 5$) this spectral range includes the most power because of source spectrum, instrument response, and the constant phase velocity used in forming LASA beams. In certain cases the above frequency range may be narrowed still further.

2. In designing chirp filters regional group velocities and limiting frequencies should be used based on the dispersive properties of the paths. Since the source regions are concentrated, paths to LASA and other arrays can be grouped into an appropriate number of categories.

3. For primarily oceanic paths such as South Pacific events, a non-linear chirp filter should be designed since these cannot be approximated with a linear chirp.

4. In choosing frequency limits it is advisable to utilize some of the source properties. For larger events the band should be expanded toward lower frequencies. For deep events (focal depth greater than about 60 km) the whole pass-band should be shifted to lower frequencies.

5. In processing data, it is advisable to compute a group velocity curve based on the initial time t_0 and group delay times $\tau(f)$ of the chirp filter.

$$U(f) = \frac{\Delta}{t_0 + \tau(f)}$$

This curve should be compared with the observed curves for an independent check on the parameters of the chirp filter.

6. The interference of surface waves due to multipaths strongly affects the performance of chirp filters and surface-wave magnitudes computed from the chirp results. These interference effects must be taken into account, at least empirically, in magnitude calculations.

ACKNOWLEDGEMENTS

This work was supported by the Seismic Array Analysis Center of the Federal Systems Division of the IBM Corporation, under contract No. F 19628-68-C-0400, and by the Advanced Research Projects Agency and monitored by the Air Force Office of Scientific Research under contract No. AF 49(638)-1632, at the Department of Earth and Planetary Sciences, M.I.T.

REFERENCES

Aki, K., 1960, Study of earthquake mechanism by a method of phase equalization applied to Rayleigh and Love waves, J. Geophys. Res., v. 65, p. 729-740.

Alexander, S.A., Rabenstine, D.B., 1967, Detection of surface waves from small events at teleseismic distances, Seismic Data Laboratory Report No. 175.

Boore, D.M., and Toksöz, M.N., 1969, Rayleigh wave particle motion and crustal structure, Bull. Seism. Soc. Am., v. 59, p. 331-346.

Brune, J., and Dorman, J., 1963, Seismic waves and earth structure in the Canadian shield, Bull. Seism. Soc. Am., v. 53, p. 167-210.

Capon, J., Greenfield, R.J., Lacoss, R.T., 1969, Long-period signal processing results for the large aperture seismic array, Geophysics, v. 34, p. 305-329.

Dewart, G., and Toksöz, M.N., 1965, Crustal sturcture in East Antarctica from surface wave dispersion, Geophys. J., R.A.S., v. 10, p. 127-139.

Kovach, R., 1959, Surface wave dispersion for an Asia-African and a Eurasian path, J. Geophys. Res., v. 64, p. 805-813.

Kuo, J., Brune, J., and Major, M., 1962, Rayleigh wave dispersion in the Pacific Ocean for the period range 20 to 40 seconds, Bull. Seism. Soc. Am., v. 52, p. 333-357.

Pilant, W.L., and Knopoff, L., 1964, Observations of multiple seismic events, Bull. Seism. Soc. Am., v. 54, p. 19-39.

Press, F., 1961, The earth's crust and upper mantle, Science, v. 133, p. 1455-1463.

Santo, T.A., and Bath, M., 1963, Crustal structure of Pacific Ocean area from dispersion of Rayleigh waves, Bull. Seism. Soc. Am., v. 53, p. 151-165.

Savage, J.C., 1969, A new method of analyzing the dispersion of oceanic Rayleigh waves, J. Geophys. Res., v. 74, p. 2608-2617.

Toksöz, M.N., and Ben-Menahem, A., 1964, Excitation of seismic surface waves by atmospheric nuclear explosions, J. Geophys. Res., v. 69, p. 1639-1648.

Toksöz, M.N., Harkrider, D.G., and Ben-Menahem, A., 1965, Determination of source parameters by amplitude equalization of seismic surface waves; 2. Release of tectonic strain by underground nuclear explosions and mechanisms of earthquakes, J. Geophys. Res., v. 70, p. 907-922.

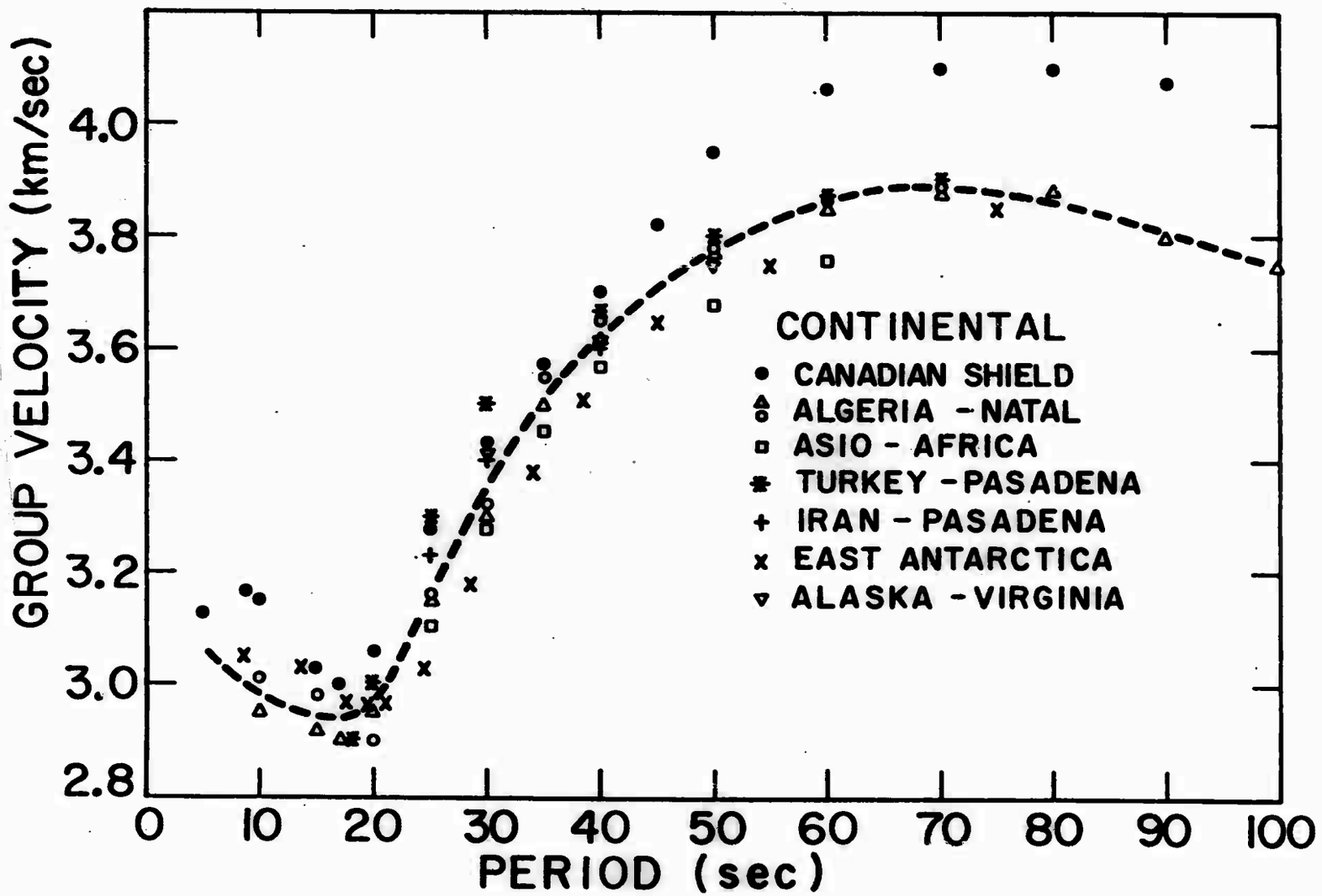

Figure 1. Phase (C) and group (U) velocities of Rayleigh waves for paths which are primarily continental.

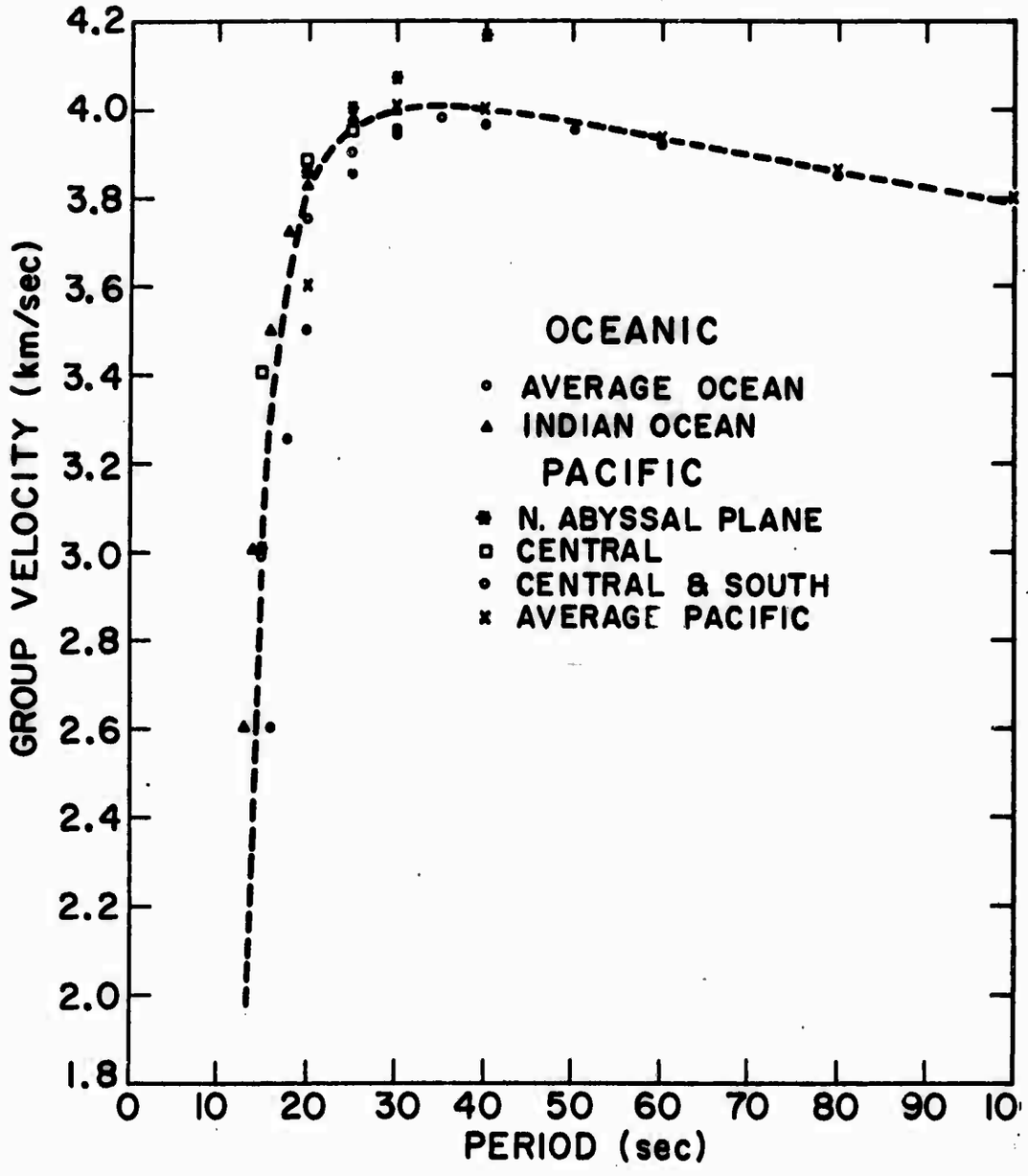

Figure 2. Phase and group velocities of Rayleigh waves for oceanic paths.

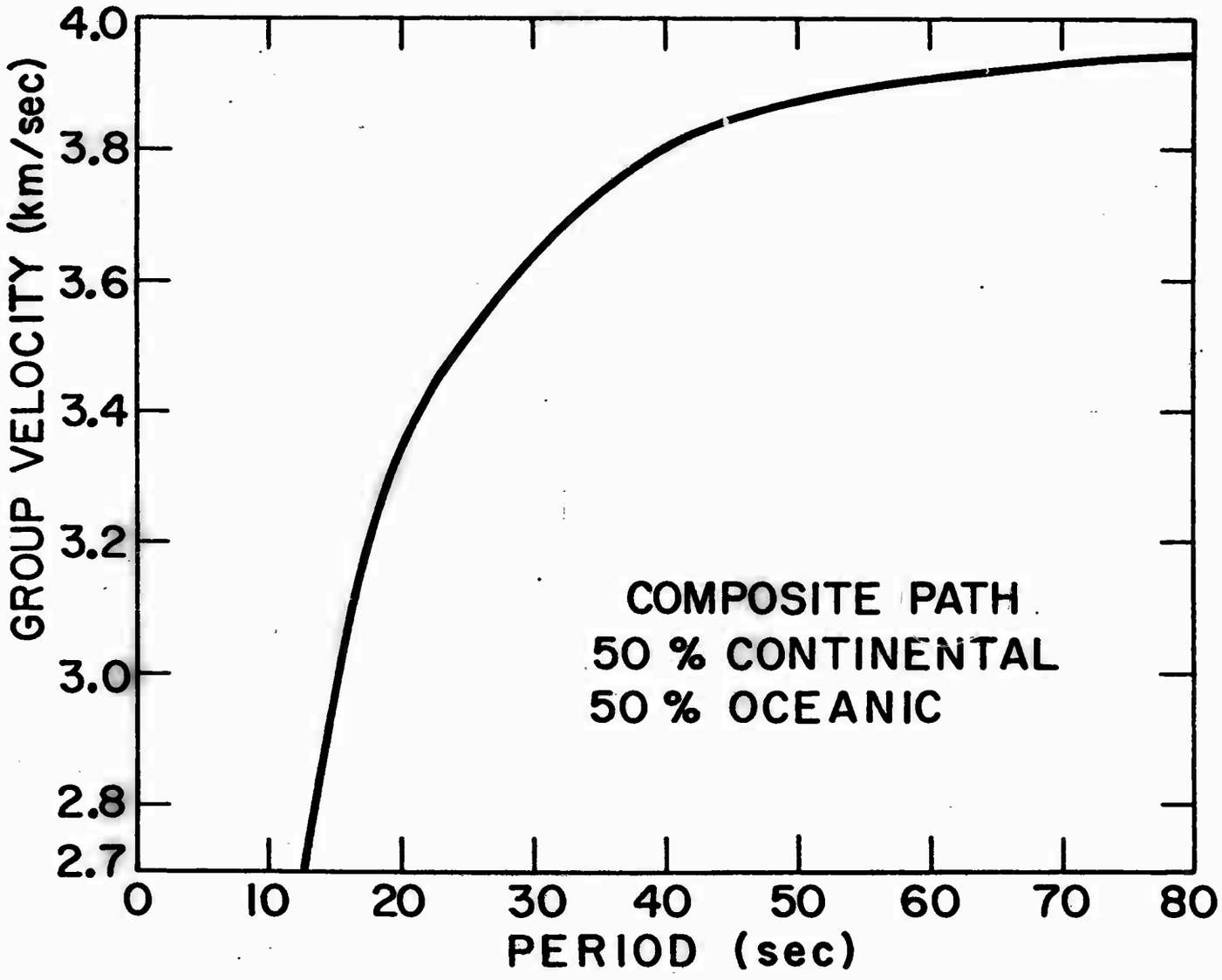

Figure 3a. Rayleigh wave group velocity curve for a composite path (50% oceanic, 50% continental). The curve is computed using the smoothed curves given in Figures 1 and 2.

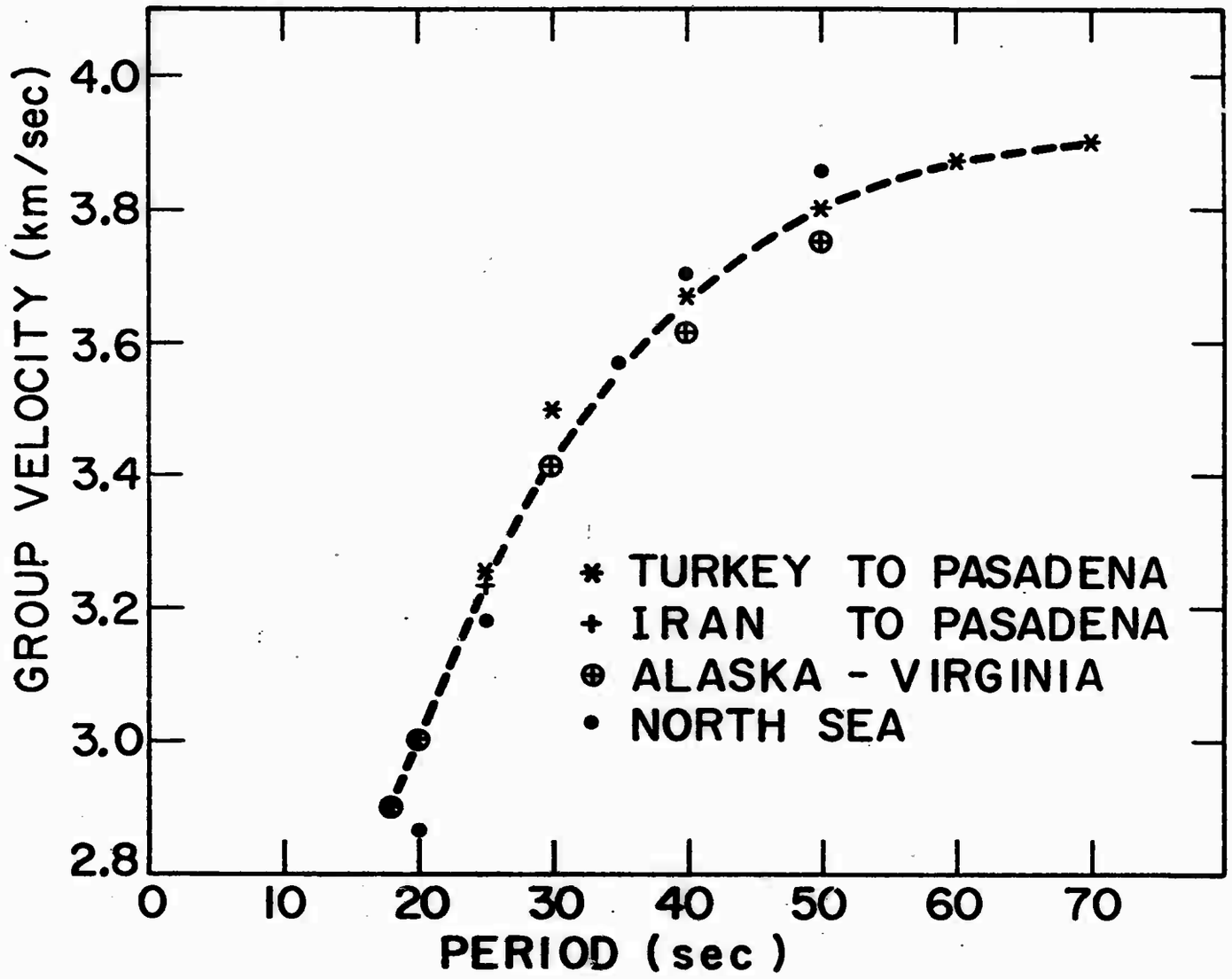

Figure 3b. Observed group velocity curve for a composite path.

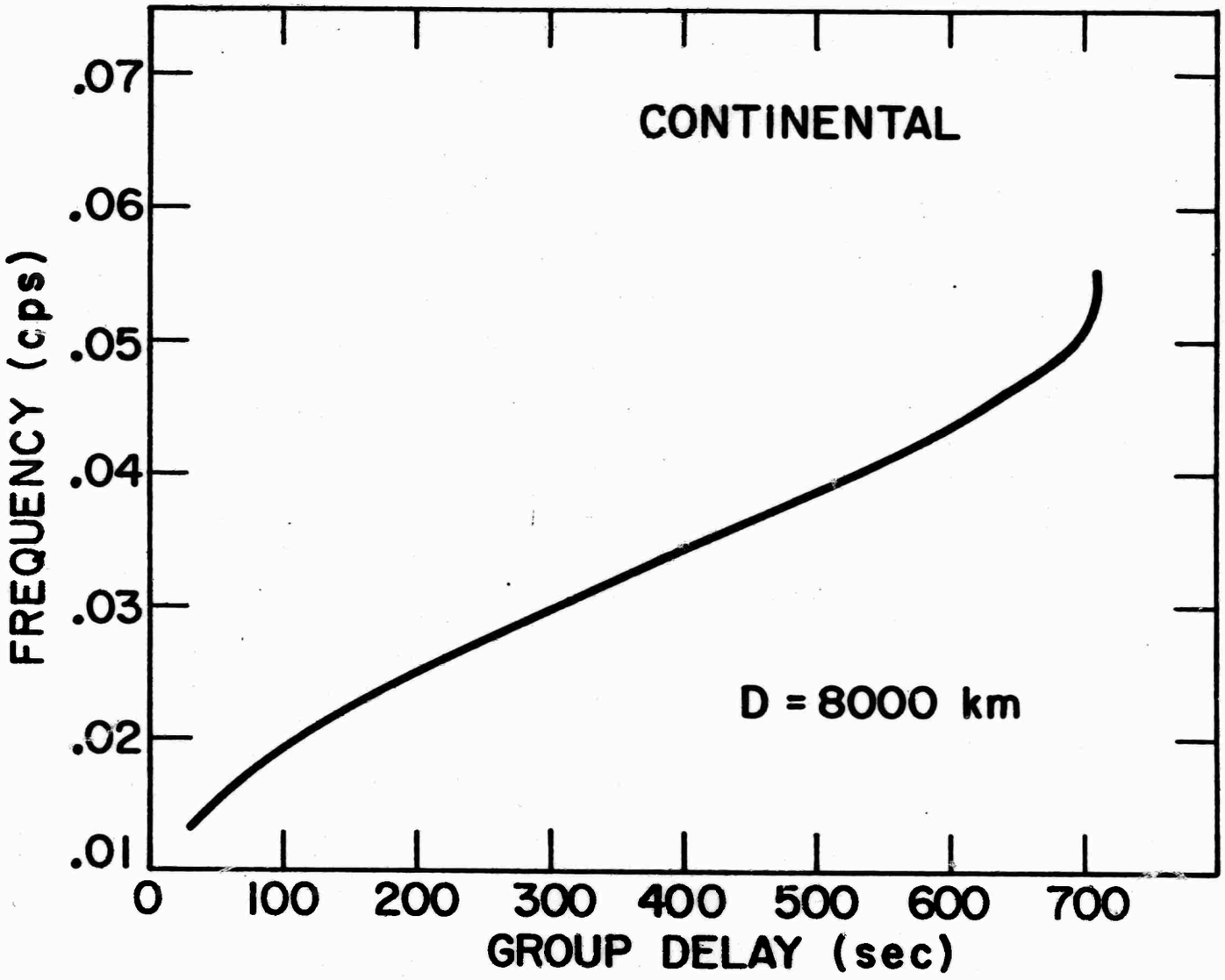

Figure 4. Frequency (f) versus group delay (τ) for a continental path computed using equation (6). Smoothed group velocities are from Figure 1. Δ = 8000 km.

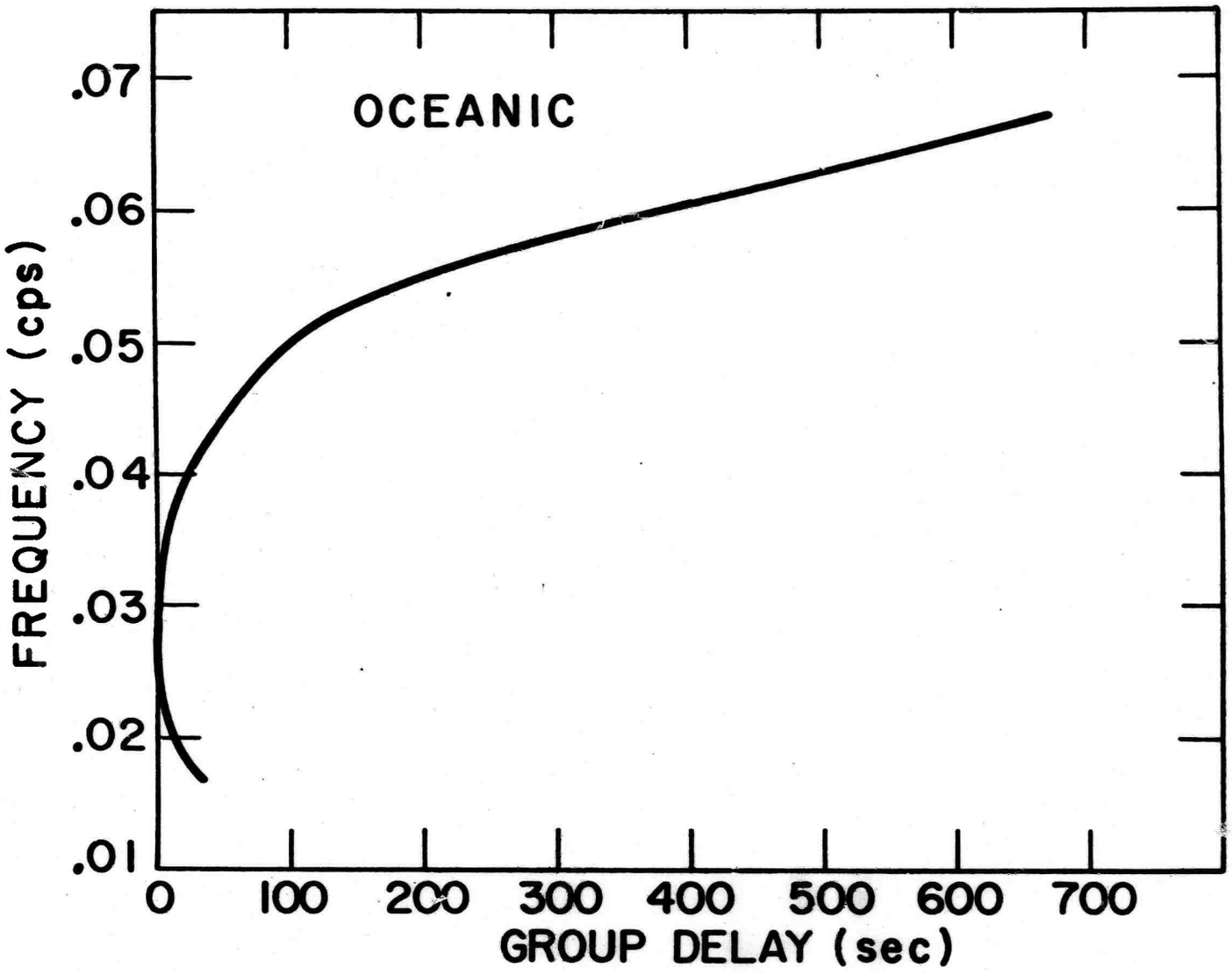

Figure 5. Frequency versus group delay for a mixed path. Δ = 8000 km. Group velocities are from Figure 3b.

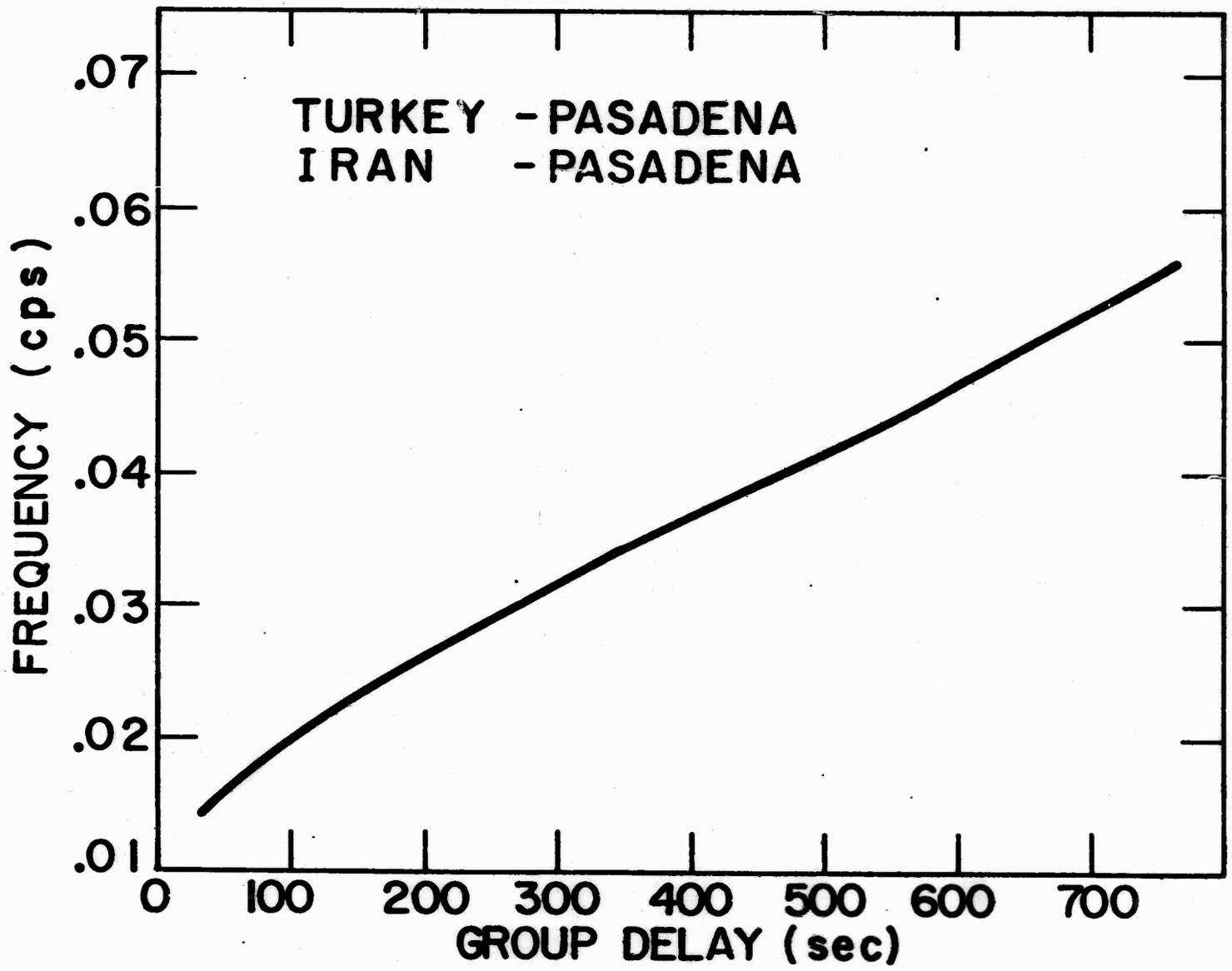

Figure 6. Frequency versus group delay for an oceanic path. Δ = 8000 km.

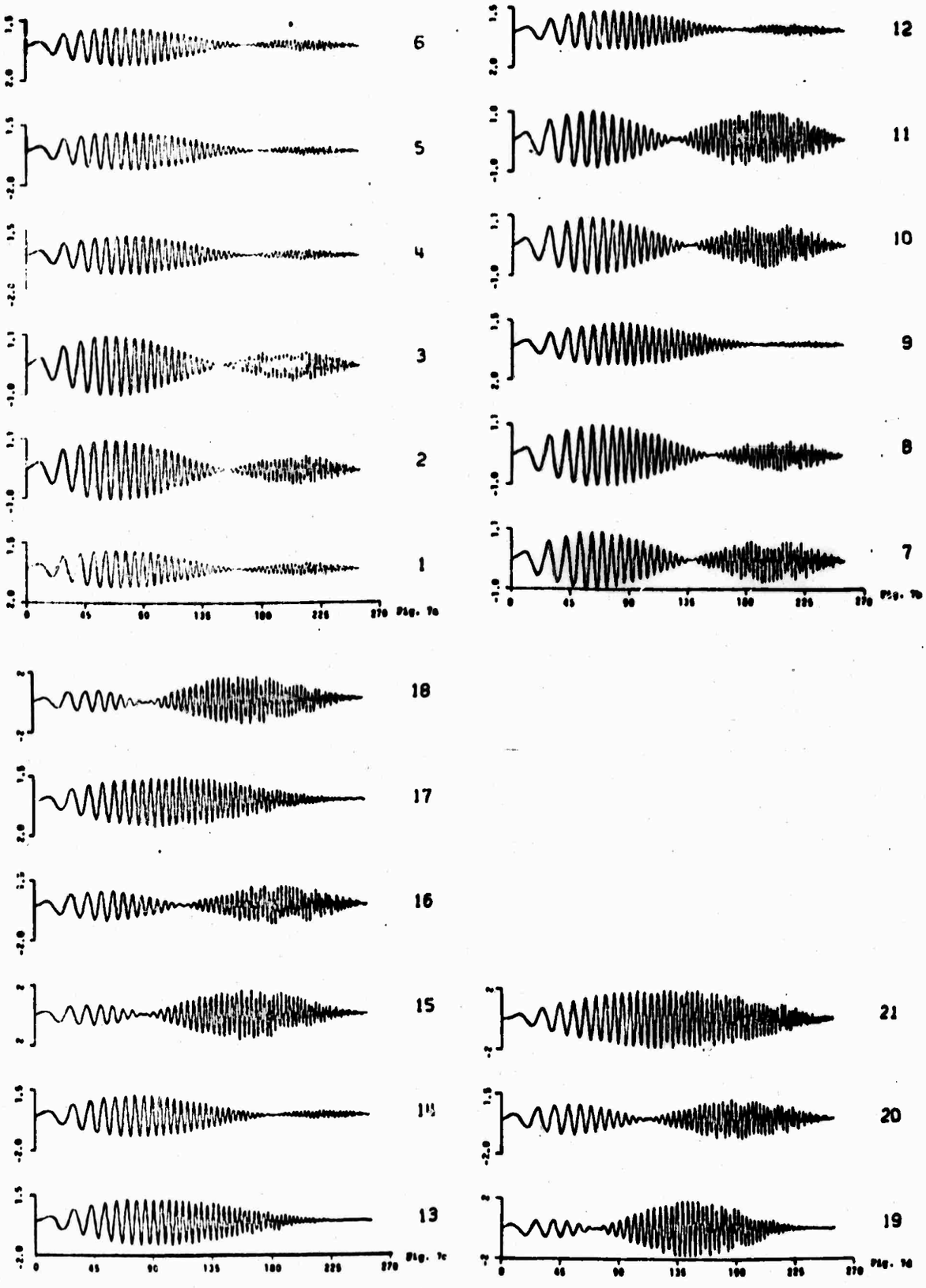

Figure 7. Theoretical seismograms showing interference effects at LASA subarrays. (7a-d) Equal amplitude waves arriving from azimuthal directions θ = 320° and 340° with no time delay (Δt = 0). (7e-h) Waves arriving from θ = 320° and 330° and Δt = 20 seconds. Numbers next to the traces indicate subarrays.

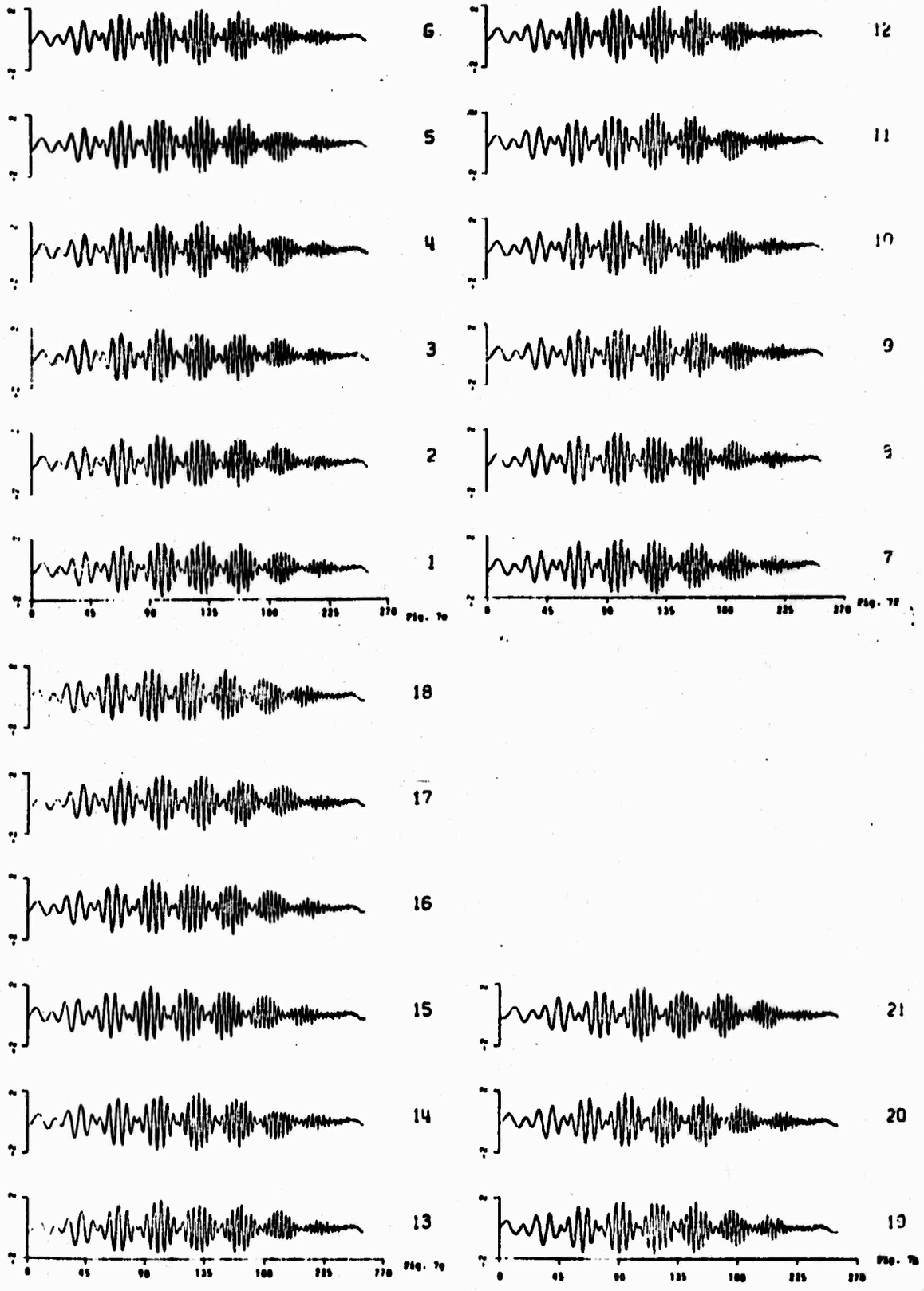

Figure 7. Theoretical seismograms showing interference effects at LASA subarrays. (7a-d) Equal amplitude waves arriving from azimuthal directions θ = 320° and 340° with no time delay (Δt = 0). (7e-h) Waves arriving from θ = 320° and 330° and Δt = 20 seconds. Numbers next to the traces indicate subarrays.

ANALYSIS OF RAYLEIGH WAVE MULTIPATH PROPAGATION AT LASA*

By
Jack Capon

M.I.T., Lincoln Laboratory
Lexington, Massachusetts 02173

*This work was sponsored by the Advanced Research Projects Agency of the Department of Defense.

An investigation has been made of the multipath propagation of Rayleigh waves by using data obtained from the large aperture seismic array (LASA). The use of the LASA in conjunction with a high-resolution analysis technique provides a greater angular resolution and accuracy than was previosuly possible for the analysis of the multipath propagation. Measurements have been made of this phenomenon for the Rayleigh waves of 26 events distributed at various azimuths and distances from LASA as shown in Figure 1. The map shown in this figure is an equidistant azimuthal projection with LASA as the projection point. Thus, on this map all great circle paths passing through LASA appear as straight lines and all points at the same distance from LASA project on a circle centered on LASA. On the basis of these measurements reasonably good conjectures can be made concerning the actual propagation paths for groups in the 20 to 40 second period range. It has been observed that in almost all cases these propagation paths can be associated with refractions and reflections at the continental margins.

The angles of approach of the 20, 25, 33, and 40 second period groups were measured, using the high-resolution method, over four successive nonoverlapping 200 second intervals, starting at the onset time of the Rayleigh wave. Thus, the group delay for the multipath arrivals will be known in multiples of 200 seconds. This information appears, in many cases, to be adequate for allowing a reasonably good conjecture to be made concerning the actual paths taken by the various group arrivals at LASA.

The propagation paths must satisfy Fermat's principle, that is, the ray path must be a stationary-time path. This means that for Rayleigh waves the paths for the initial group arrivals will be minimum-time paths, while later group arrivals propagate along paths which, while not minimum-time paths, are stationary-time paths. In addition, the propagation paths must satisfy Snell's Law for refraction and reflection at boundaries across which there is a contrast in phase velocity. In terms of propagation of Rayleigh waves in the surface layers of the earth, these boundaries usually represent the continental margins. Thus, when an angle of arrival is measured which differs from the true azimuth of an event, it is quite likely that this bending of the propagation path can be explained by the refractions and reflections which must take place at continental margins. However, in some cases the bending of the ray paths appears to be caused by other major tectonic features of the earth, such as ridges.

The initial groups will usually arrive at the true azimuth or at slight azimuthal deviations from this. Thus, initially the path will consist of the great circle path between the epicenter and LASA, or a slightly refracted version of this path. Once this initial path is known the later paths can be obtained by choosing one which fits the path length difference condition and has an angle of approach at LASA which agress with the measured angle.

Six examples of such propagation paths which were similar to or

typical of the results for the 26 events analyzed are shown in Figures 2 to 7. The timing sequence for the group arrivals is not shown in any of these figures, for simplicity. In addition, two propagation paths whose azimuthal angles of arrival at LASA are within three degrees of each other are usually merged into a single path. All propagation paths in these figures are drawn as straight line segments, again for simplicity. In addition, all refractions and reflections are depicted as taking place at the geographic boundaries for the continents although it is more likely to take place at the continental margins. The difference in positions of these two boundaries is in most cases very small and may be neglected.

The propagation paths for the 22 November 1966 Kurile Islands events are shown in Figure 2. We see that initially the longer period groups arrive at LASA along the great circle path between LASA and the epicenter, or slightly refracted versions of this path. These groups are followed by shorter period groups which are refracted and reflected at the continental margin.

In Figure 7 we see the propagation paths for the 22 September 1967 Central Mid-Atlantic Ridge. In this case the longer period groups arrive from an angle which deviates from the true azimuth by about ten degrees. It appears that these groups are guided by the mid-Atlantic ridge and then emerge from it at the point where the ridge makes a sharp turn away from the direction toward LASA. The shorter period groups do not appear to be guided by the ridge, but are refracted and reflected in the usual way.

It should be noted that reflection of a group usually takes place at a continent-to-ocean boundary and that the angle of incidence usually exceeds the critical angle for the period of the group. This result is to be expected, since it is at these angles of incidence that reflection of large amounts of energy would be expected. It should also be mentioned that the present results represent an extension of the work of Evernden, 1953 and 1954 who also measured the direction of approach of Rayleigh waves. A complete discussion of the measurements and results will be published shortly (Capon, 1970).

REFERENCES

Capon, J., 1969, High-resolution frequency-wavenumber spectrum analysis, Proc. IEEE v. 57, p. 1408-1418.

Capon, J., 1970, Analysis of Rayleigh wave multipath propagation at LASA, to be published in Bull. Seism. Soc. Am., v. 60, October.

Evernden, J.F., 1953, Direction of approach of Rayleigh waves and related problems, Part I, Bull. Seism. Soc. Am., v. 43, p. 335-374.

Evernden, J.F., 1954, Direction of approach of Rayleigh waves and related problems, Part II, Bull. Seism. Soc. Am., v. 44, p. 159-184.

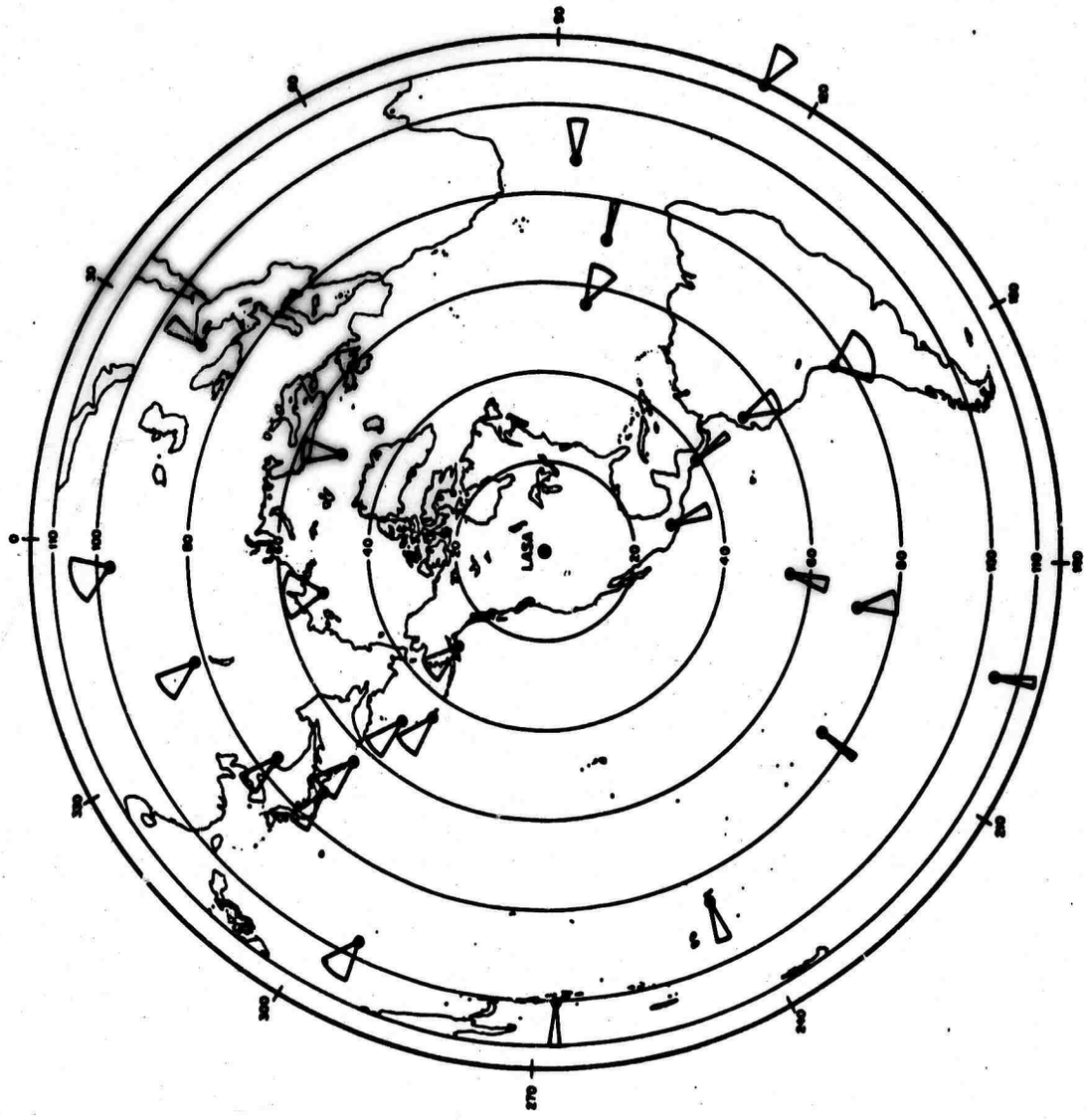

Figure 1.

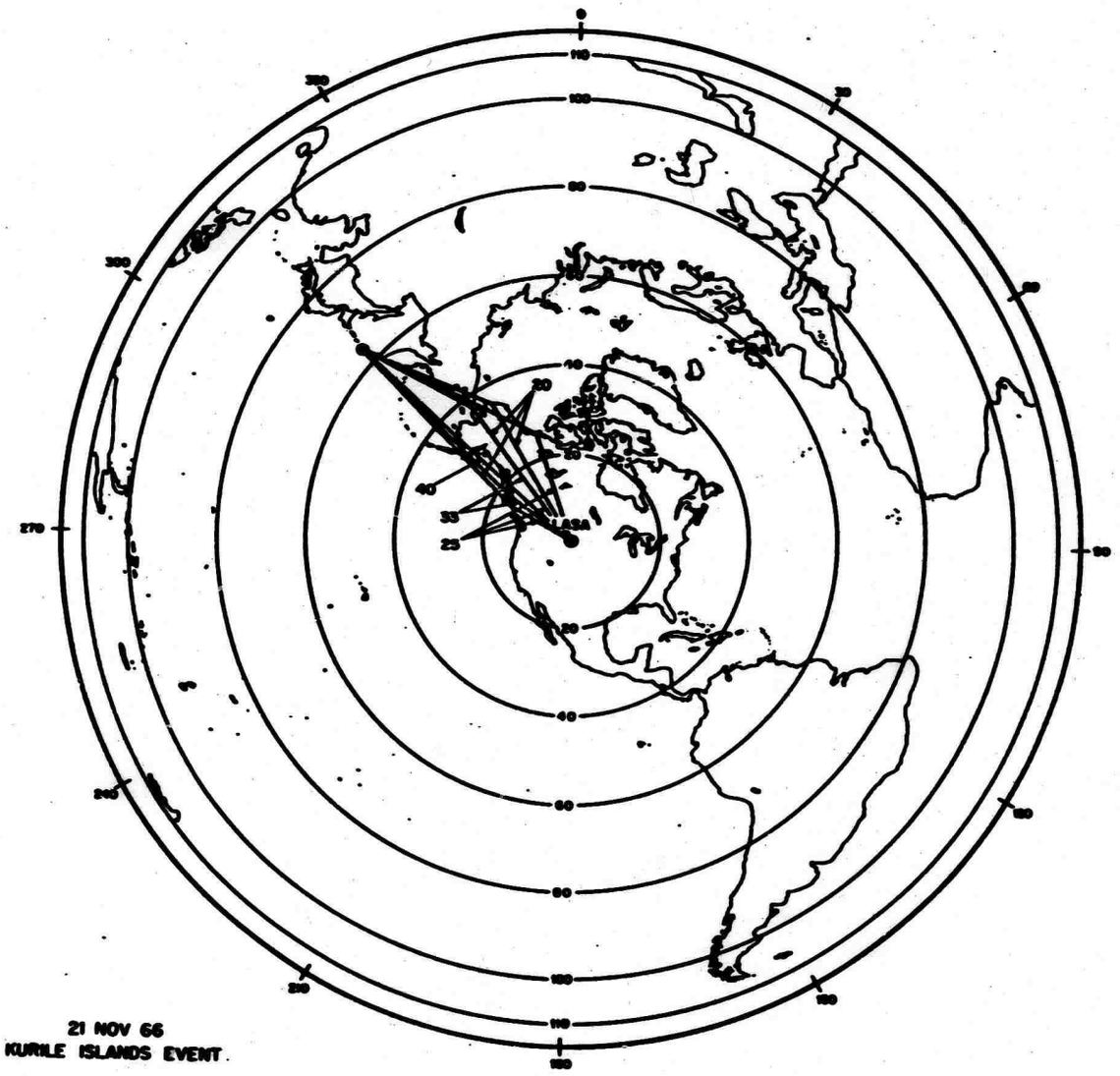

Figure 2.

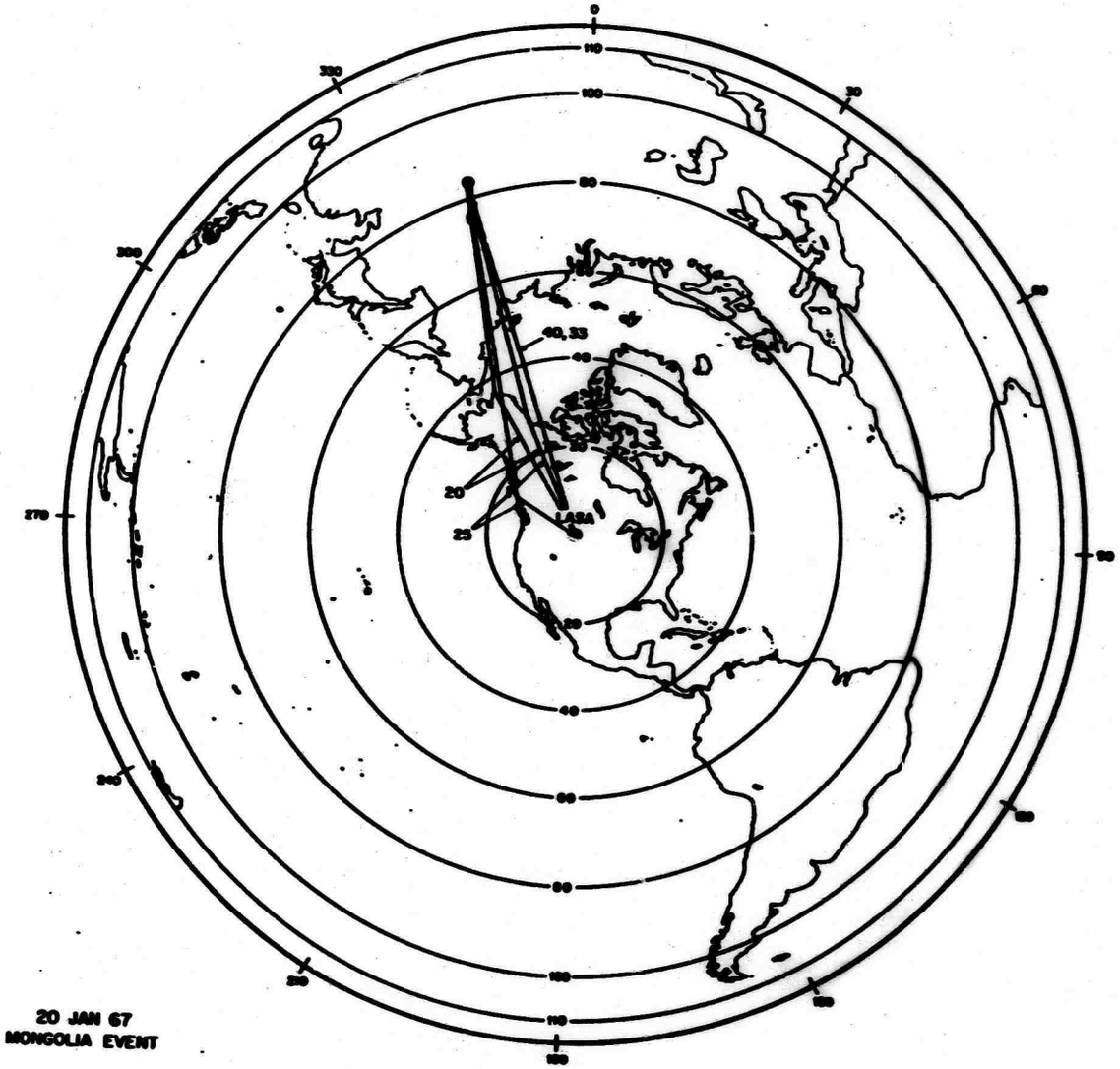

Figure 3.

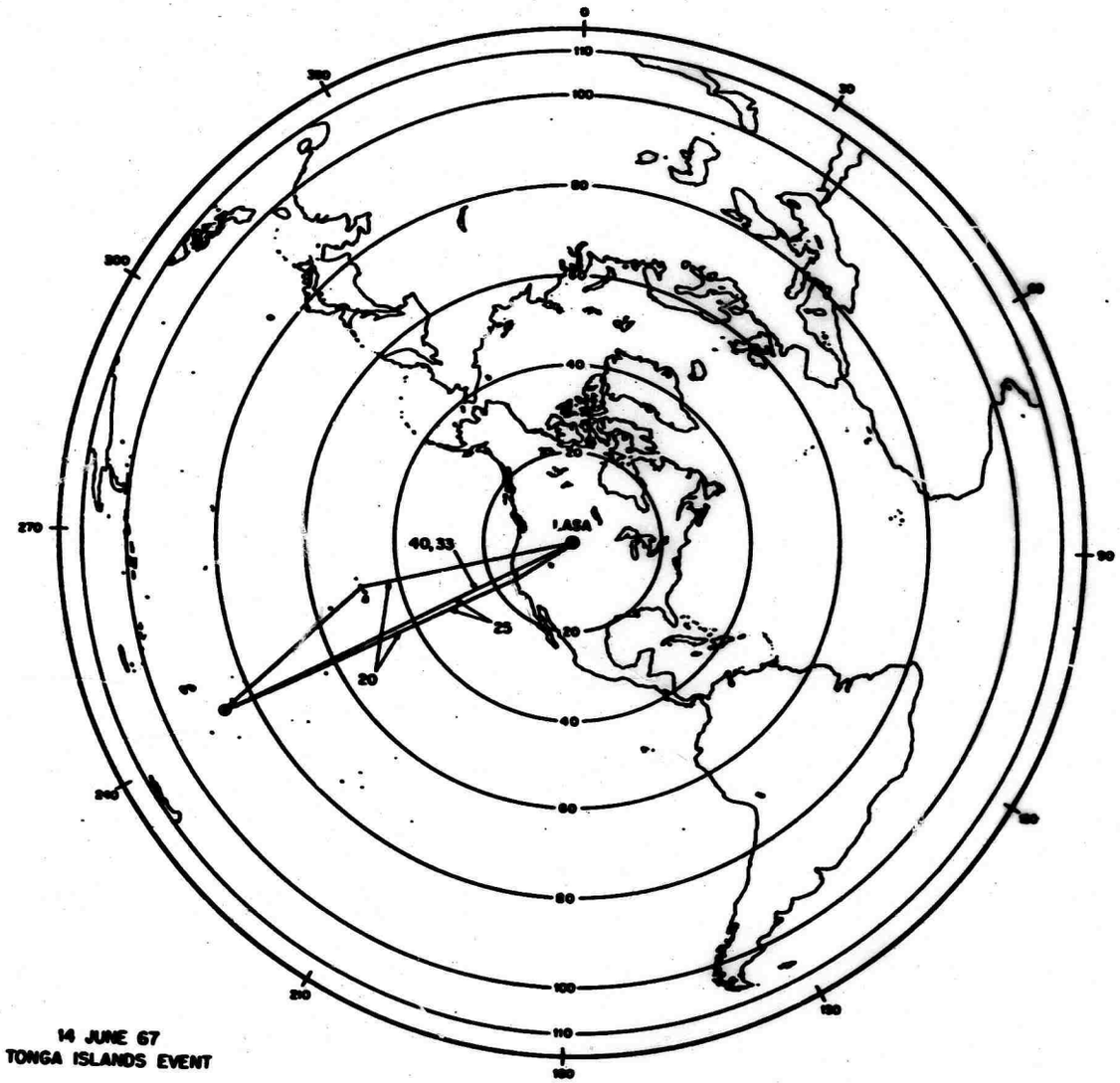

Figure 4.

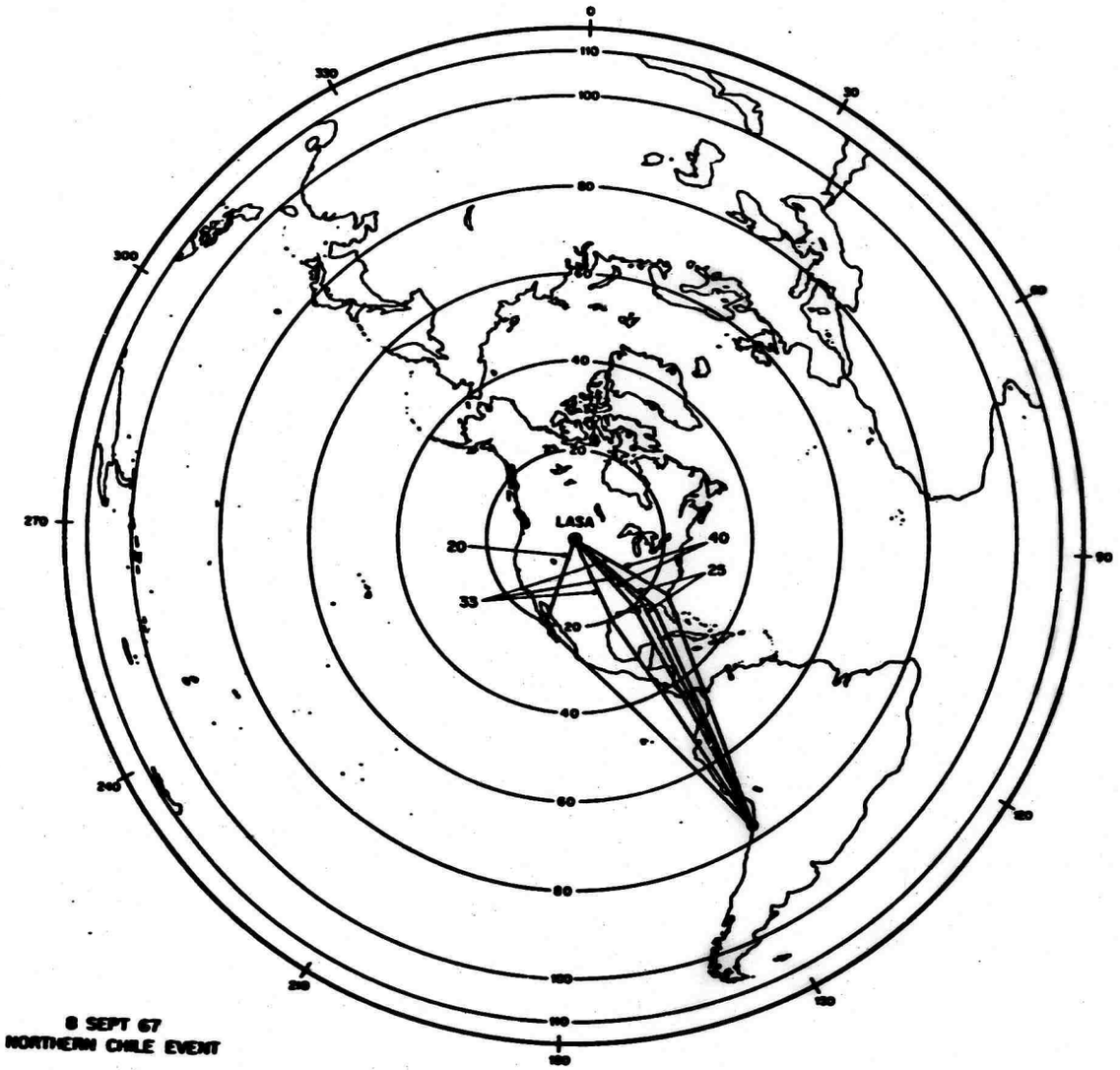

Figure 5.

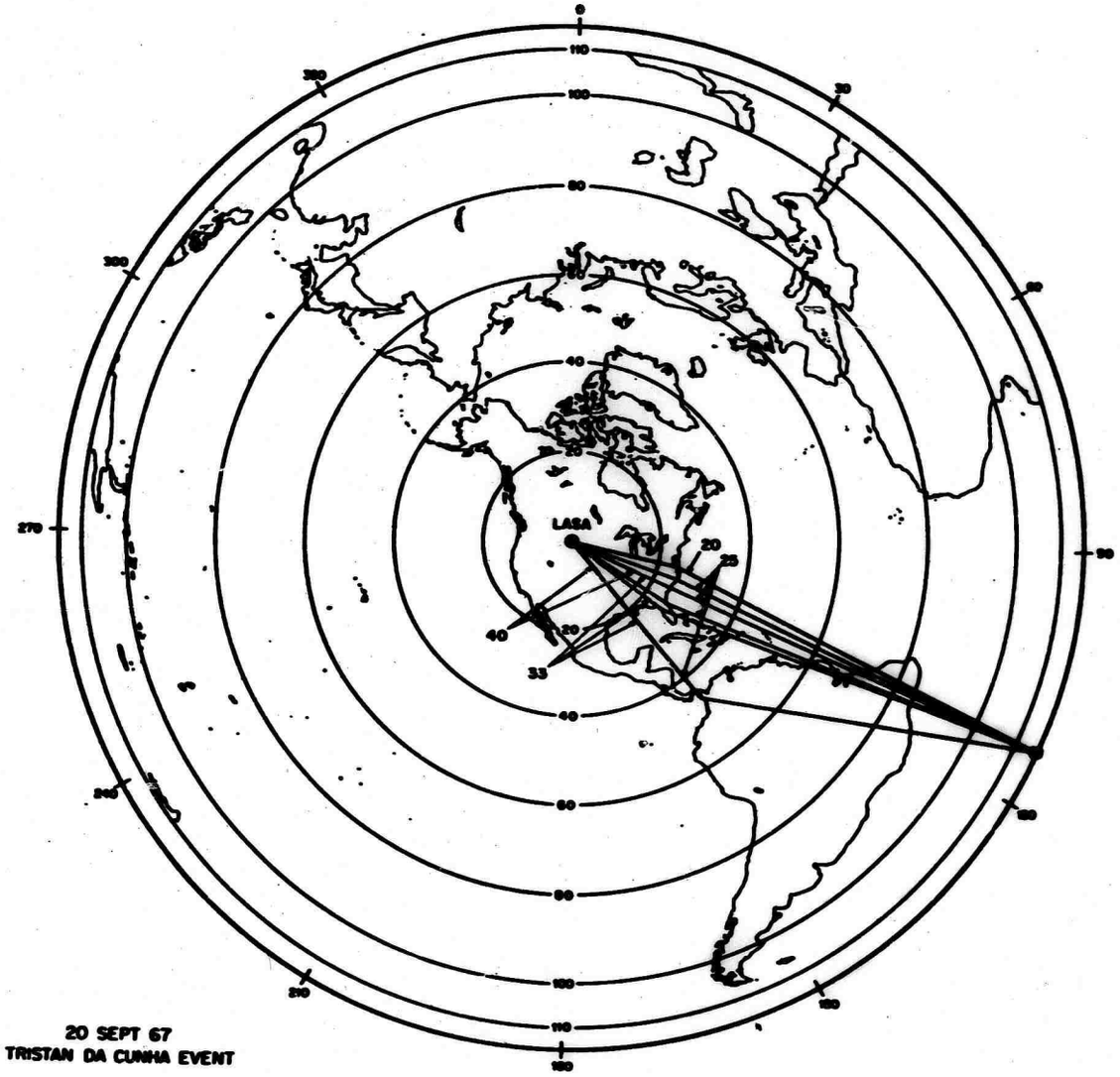

Figure 6.

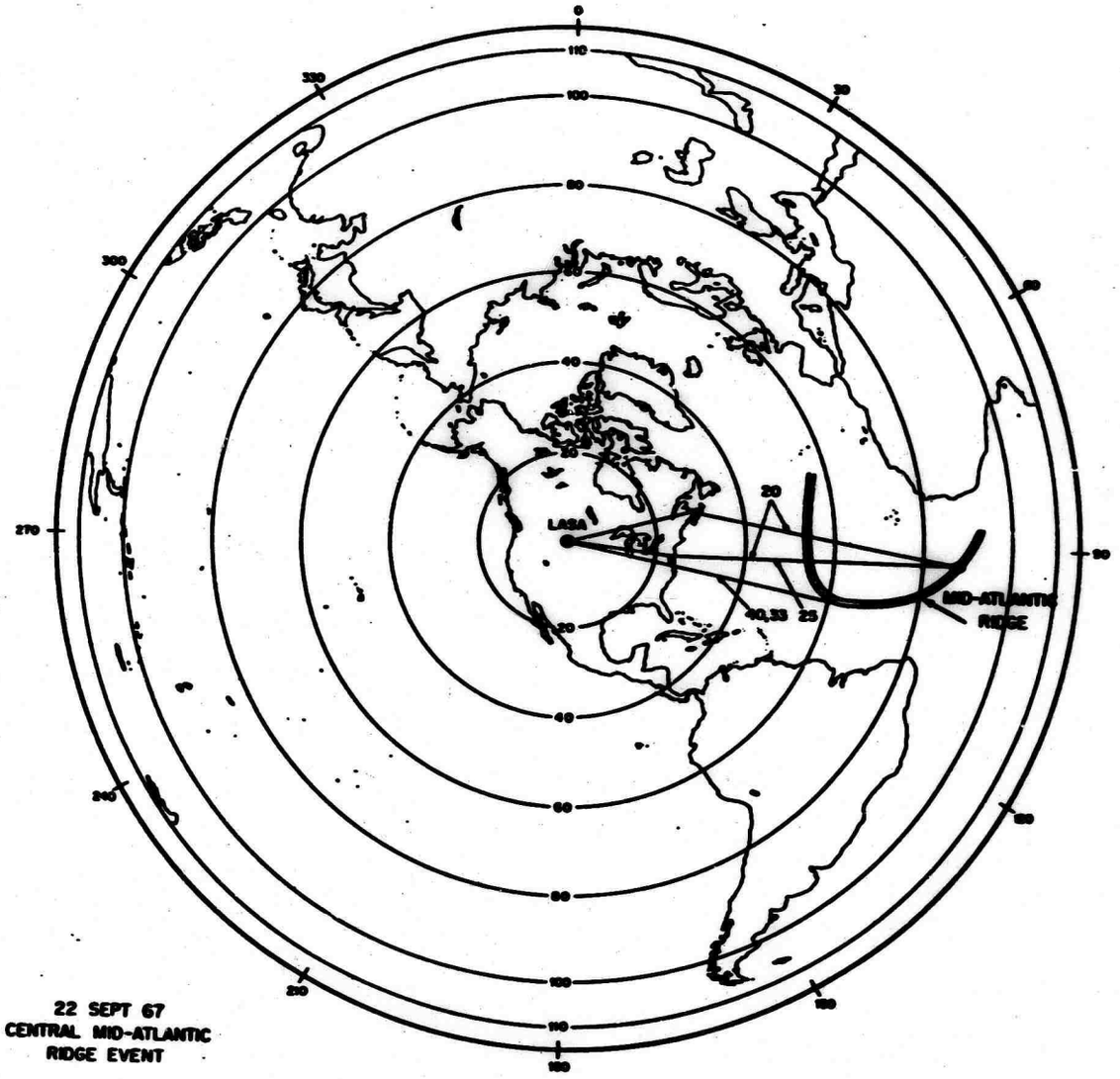
LASA
20
40,33 25
MID-ATLANTIC RIDGE
22 SEPT 67
CENTRAL MID-ATLANTIC
RIDGE EVENT

Figure 7.

A HIGH-GAIN, BROAD-BAND, LONG-PERIOD SEISMIC EXPERIMENT

By

Peter L. Ward

Lamont-Doherty Geological Observatory
Palisades, New York

The purpose of this talk is to briefly review the status of the high-gain, broad-band, long-period, seismic experiment at Lamont. I would like to review some of the important features of instrument design, the sites of the new instruments, and the types of data to be expected. In this experiment, we are installing five three-component seismograph systems around the world. These instruments will probably have gains on the order of 100,000 to 500,000 at periods of 40 to 50 sec. This high sensitivity, some 50-100 tim[illegible] greater than previously attainable at this period, should lead [illegible] a similar increase in the data now available in the long-perio[illegible] band and should particularly be of use in lowering the minimum magnitude of explosions and earthquakes that can be discriminated.

The design of these instruments is based on that developed by Pomeroy and Hade (Pomeroy et al, 1969) in the Ogdensburg Mine in New Jersey. Both vertical and horizontal components have been operating successfully for nearly two ye[illegible]rs at Ogdensburg. A block diagram of the system is shown in Figure 1. The heart of the system is a Geotech seismometer with a natural frequency of 30 sec. This is coupled to a Kinemetrics galvanometer with a natural frequency of 100 sec. The signal from the galvanometer is amplified by a phototube amplifier and recorded digitally and photographically. Both high and low gain photographic records are available. The dynamic range of the digital recordings is over 70 db and is limited by the phototube amplifiers.

The high sensitivity of these instruments is achieved by electronically filtering out 6 second microseisms and by isolating the seismometer from changes in barometric pressure. The isolation is achieved primarily by a hemispherical tank shown in Figure 2. This new design features a hemispherical top, shallow walls, prestressed bottom, and a metal to metal contact of top and base. Experiments at Ogdensburg show that tanks of this new design, unlike those used by Pomeroy and others, will perform nearly all of the necessary filtering of barometric changes. For added security and temperature stability, however, these tanks will be placed in an air-tight cement or stone vault with a bulkhead door.

High sensitivity is also achieved because the instrument pass-band has been shaped to correlate perfectly with a natural low in earth noise as discussed earlier by Savino.

The background noise observed on the test instruments at Ogdensburg appears to be true ground motion and not instrumental noise. This is most directly shown by the following experiment carried out by Savino and Hade: Two different types of seismometers were operated in two different parts of the Ogdensburg mine (Figure 3). A Sprengnether seismometer was placed in a chamber in the mine separated from the main tunnel by two bulkhead doors. A Geotech seismometer in a pressure tank was operated behind three good bulkhead doors about 500 feet from the Sprengnether instrument. The signals were recorded simultaneously on digital magnetic tape. A coherence

between the two signals was calculated digitally for a period of recording of 5 hours, 14 minutes. As can be seen in Figure 4, the coherence squared is exceptionally good and well above the 95% confidence limits in the passband of interest. This is one of the experiments that has convinced us that instrument noise does not contribute significantly to the observed seismic background.

Experiments are being carried out comparing the prototype instrument at 1850 feet below the surface with new instruments on the surface in Ogdensburg. Preliminary studies show that at best the vertical background noise at the surface is about a factor of two greater than the noise at depth. Vertical noise at the surface may at times be an order of magnitude above that at depth. Reliable numbers are not yet available for the horizontal components.

Five sets of these instruments will hopefully be installed by late November or December of this year in Fairbanks, Alaska; Charters Towers, Australia; Eilat, Israel; Toledo, Spain; and Chengmai, Thailand. Installation in Alaska and Australia is now underway and scheduled for completion in late September.

Data will consist of 6 photographic records per day (3 components of high and low gain) on 70 mm microfilm distributed by the USC&GS through the same channels as the WWSSN data. One digital tape will be filled every two weeks. The tapes will be combined and distributed by Texas Instruments. The digital tapes consist of header time data, outputs of the three velocity transducers digitized at a rate of one sample per second, and outputs of three displacement transducers digitized at rates of one sample per five seconds.

These high-gain, broad-band, long-period seismographs are expected to give unique data previously unavailable on a global scale. With good fortune, data from all these sites will be available by the end of this year.

REFERENCES

Pomeroy, P.W., Hade, G., Savino, J., and Chander, R., 1969, Preliminary results from high-gain, wide-band, long-period electromagnetic seismograph systems, J. Geophys. Res., v. 74, (12), p. 3295.

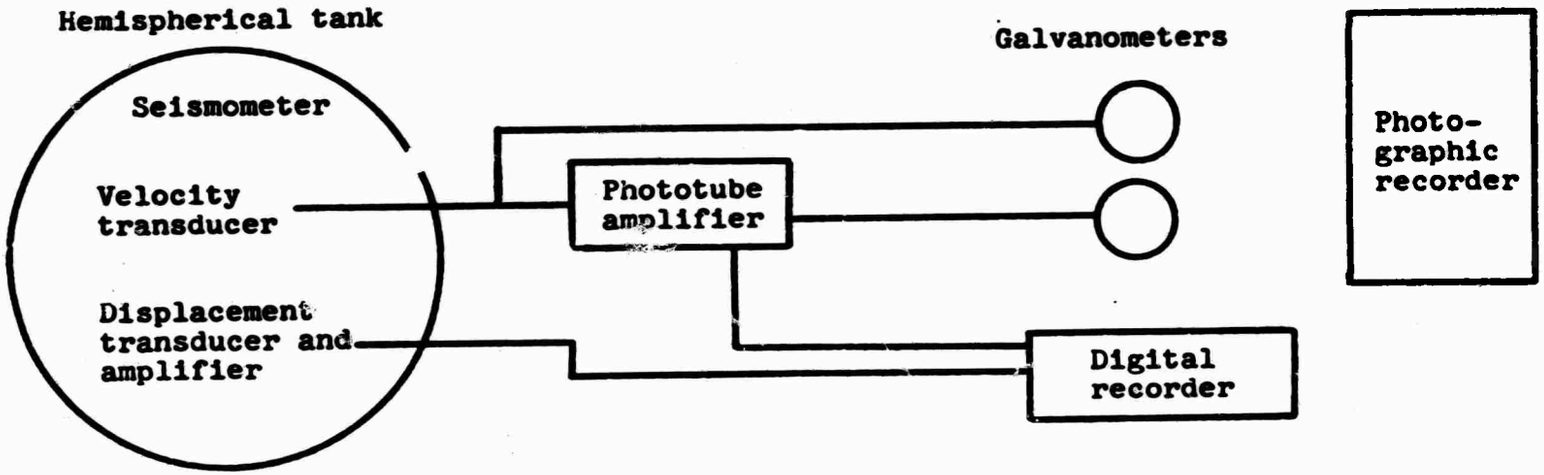

Figure 1. Block diagram of high-gain, long-period, broad-band, seismic system.

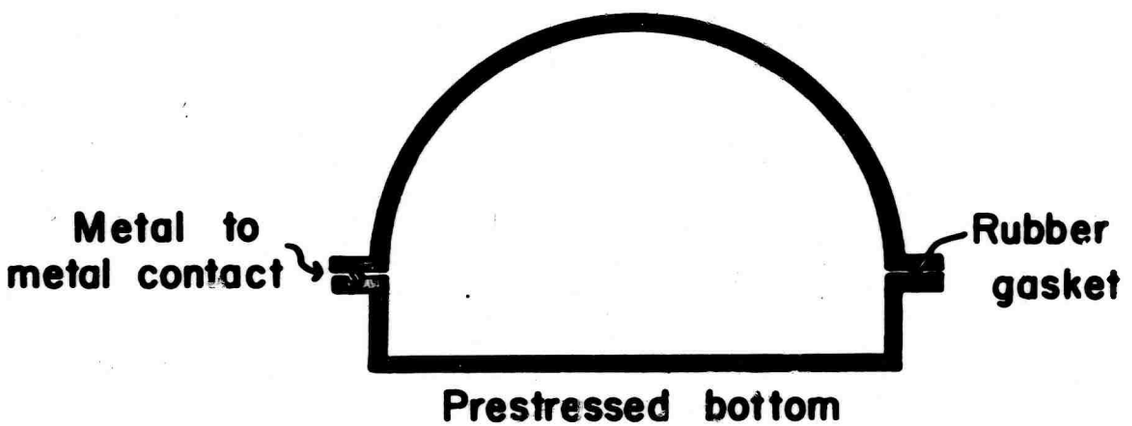

Figure 2. Schematic diagram of pressure tank.

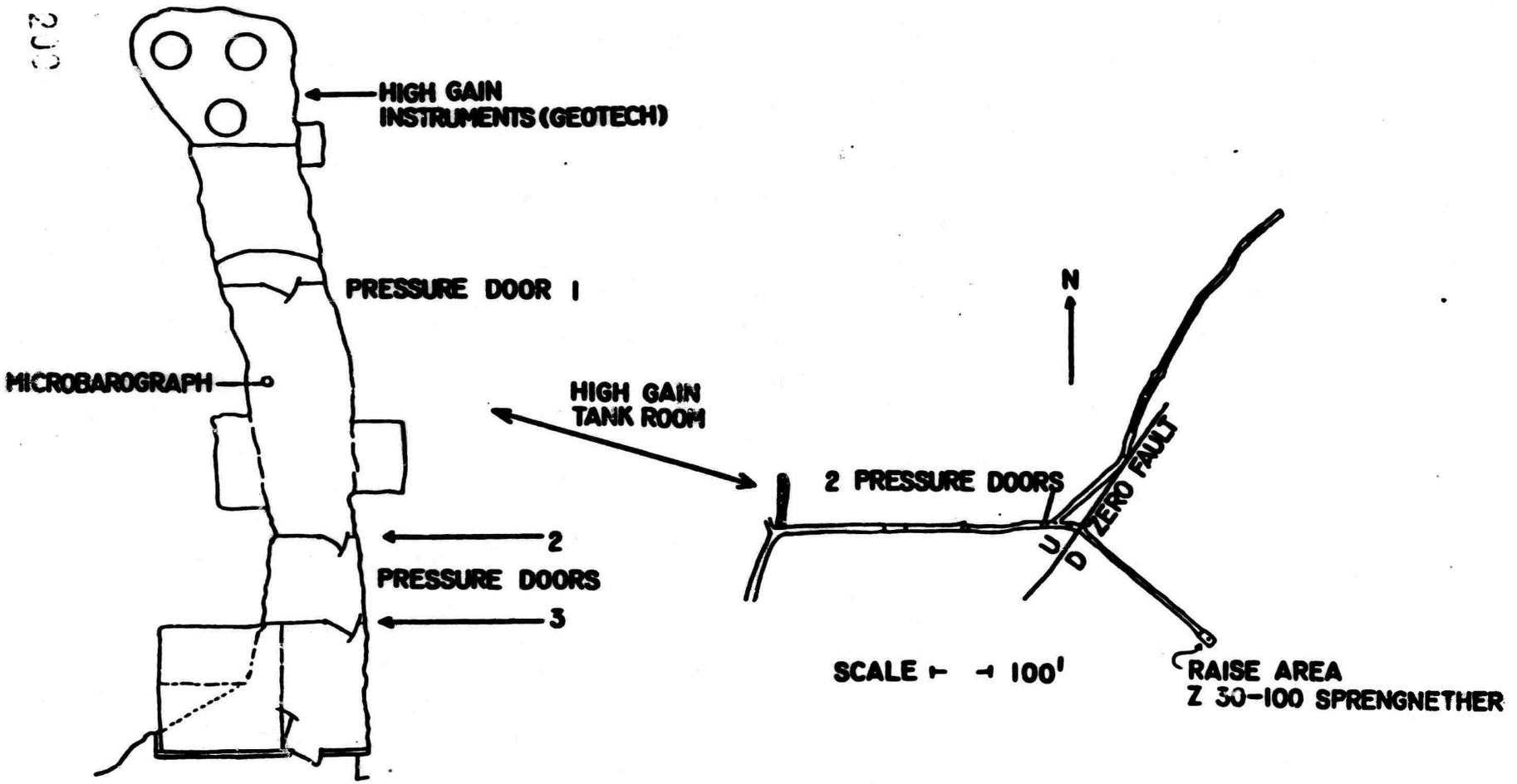

Figure 3. Map of Lamont's seismic observatory at Ogdensburg, New Jersey, 1850 feet below the surface.

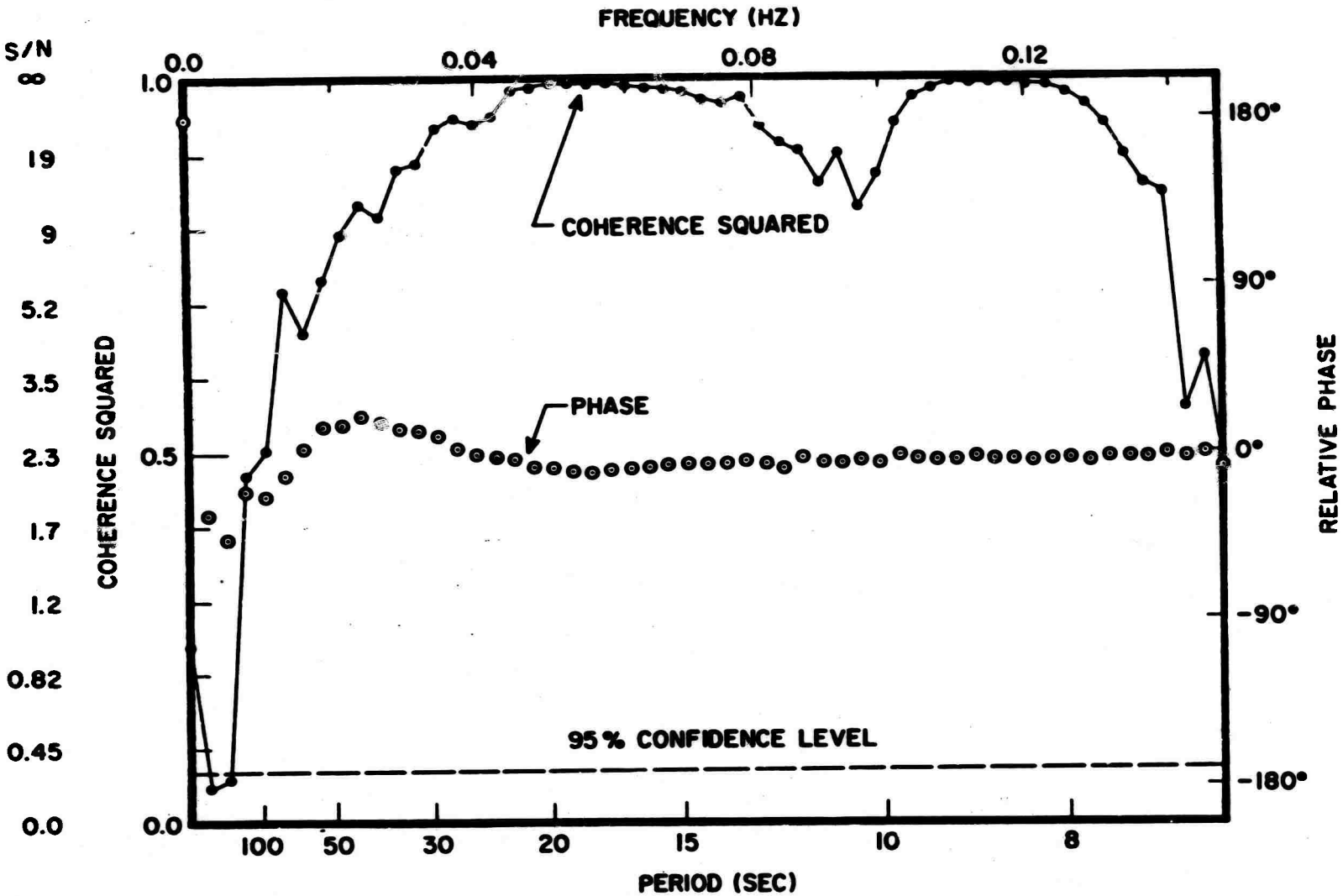

Figure 4. Coherence squared and phase relation for a 5 hour and 14 minute portion of background noise at a Sprengnether and a Geotech seismometer spaced 500 feet apart in different environments in the Ogdensburg Mine.

REPORT ON A NEW BROAD BAND VERTICAL ACCELEROMETER

By

Barry Block

Institute of Geophysics and Planetary Physics
University of California, San Diego
La Jolla, California

Several years ago at the Institute of Geophysics and Planetary Physics, La Jolla, a program was begun to build a new generation of acceleration measuring instruments. This program has as its goal the creation of broad band instruments whose noise and drift properties are understood. It was felt that the lack of broad band accelerometers was hampering the growth of some theoretical branches of geophysics and that the narrow band data gathered was preventing a clear physical picture of many phenomena from emerging. With due consideration of the design achievements made in the past, we felt that technology had progressed to the point where a fundamental review was necessary. Our basic guide lines were taken to be

1. Tidal to seismic frequencies should be measurable by the same instrumental design.

2. Drift and other noise sources should be controlled to a level where interesting geophysical information can be obtained from tidal to seismic frequencies.

3. Linear response (i.e., freedom from non-linear procecess) should be inherent in the mechanical structure of the instrument.

4. Internal calibration over frequencies from DC to seismic should be possible.

The advent of phase sensitive detection allows the use of broad-band position detectors with a sensitivity far in excess of what is needed and which have extremely low detector noise. These detectors allow a new design freedom in the choice of the mechanical system. It is now no longer necessary to make long period mass-spring systems to get the requisite overall gain of the accelerometer. In fact, there are many advantages to making a simple mechanical structure with a free period from about 1/2 to 1 second. Such a simple structure can be found which has all its higher modes well separated in frequency from the fundamental mode and which has small non-linear coupling from the higher modes to the fundamental mode. This structure is shown in Figures 1 and 2.

The mass is cantilevered on a horizontal stretched monolithic quartz fiber which is in torsion to provide the restoring torque. It should be pointed out that this design can be used as a horizontal accelerometer merely by turning it on its side and letting the mass hang down. (Figure 2). In use for the past year as a vertical accelerometer and gravimeter, one model has given an upper bound to its drift rate of 10^{-10} g/day. In other words, full scale earth tides can be run for a year without rezeroing. Several.other models have shown similar low drift. This low drift rate is achieved through processes described in a recent paper.

Instrument noise coming from temperature and barometric changes are controlled directly at the instrument and not in a large vault as has been the custom. Figure 3 shows the mechanical setup of the instrument. The mass spring system is sealed at 10^{-7} mmHg pressure in a stainless steel gold O-ring sealed tank (8 inch diameter). This inner tank is suspended from the lid of an outer (9 inch diameter)

aluminum tank sealed at 1mmHg by conventional rubber O-rings. In operation, all adjustment apparatus is removed from direct contact with the inner tank. This double container provides protection from direct barometric effects. The thermostat is wound on the outer container and a thermal feedback system has been designed to provide thermal control which in practice does not drift more than a micro-degree per day over many months of use.

It should be pointed out that no particular effort has been made to miniaturize this instrument and considerable progress is possible if a smaller version is needed. The static calibration and linearization is done by tilting the instrument about two perpendicular axes and the dynamic calibration by using an electrostatic force applied to the mass. The calibration can be carried out to the percent level in an unambiguous way. The instrument has been operated simultaneously with three outputs each of 10 V full scale.

a. Tidal channel: Operated at 2×10^{-7} g full scale. Flat from DC to 4.8 cph, 20 db/decade drop after 4.8 cph.

b. Earth normal mode channel: Gain of 1 from DC to 1 cph, gain of 100 in band 1 - 30 cph, 40 db/decade drop at frequencies higher than 30 cph; operated at 2×10^{-9} g full scale in pass band 1 - 30 cph.

c. High frequency filter channel: A variable gain channel with pass band centered at 40 second period whose response mimics the response of the Lamont long period seismometers.

With this background in mind, I would like to show you some results from the first model (with a free period of 1/2 second and Q=15) in the earth mode frequency band which we have somewhat arbitrarily called 1 - 30 cph. I will restrict my remarks to data drawn from the earth mode frequency band and leave the seismic results to be discussed by James Brune.

In the first year of operation, we have recorded about two dozen magnitude 6.0 or larger earthquakes. These earthquakes show considerable earth mode (1 - 30 cph) excitation which can extend over many hours. Figure 4 shows the earth mode filter record (channel b above) taken during the magnitude 6.5, 246 km deep earthquake in the New Hebrides on October 13, 1969. It is important to note the time scale on this figure. The background contains the earth tides and we see that the earthquake excitation lasts for nearly twelve hours in this frequency band. A number of Rayleigh waves can be seen and a detailed look at an expanded time scale shows many phenomena of interest to the seismologist. The power spectrum of the earthquake is shown in Figures 5, 6 and 7. The 0-db point is 1×10^{-24} g^2/cph. The ambient noise is also shown on these figures and is taken directly from the preceding record without any visible earthquakes. This ambient noise is the sum of the site noise and instrumental noise. This particular instrument has been found to operate at its Brownian limit by cross correlation with another instrument but this cross correlation was not carried out at this particular setup. The normal modes begin to clearly appear

REFERENCES

Block, B., and Moore, R.D., 1970, Tidal to seismic frequency investigations with a quartz accelerometer of new geometry, J. Geophys. Res., v. 75, p. 1493.

Block, B., Dratler, J., Moore, R.D., 1970, Earth normal modes from a 6.5 magnitude earthquake, Nature, v. 226, p. 343-344.

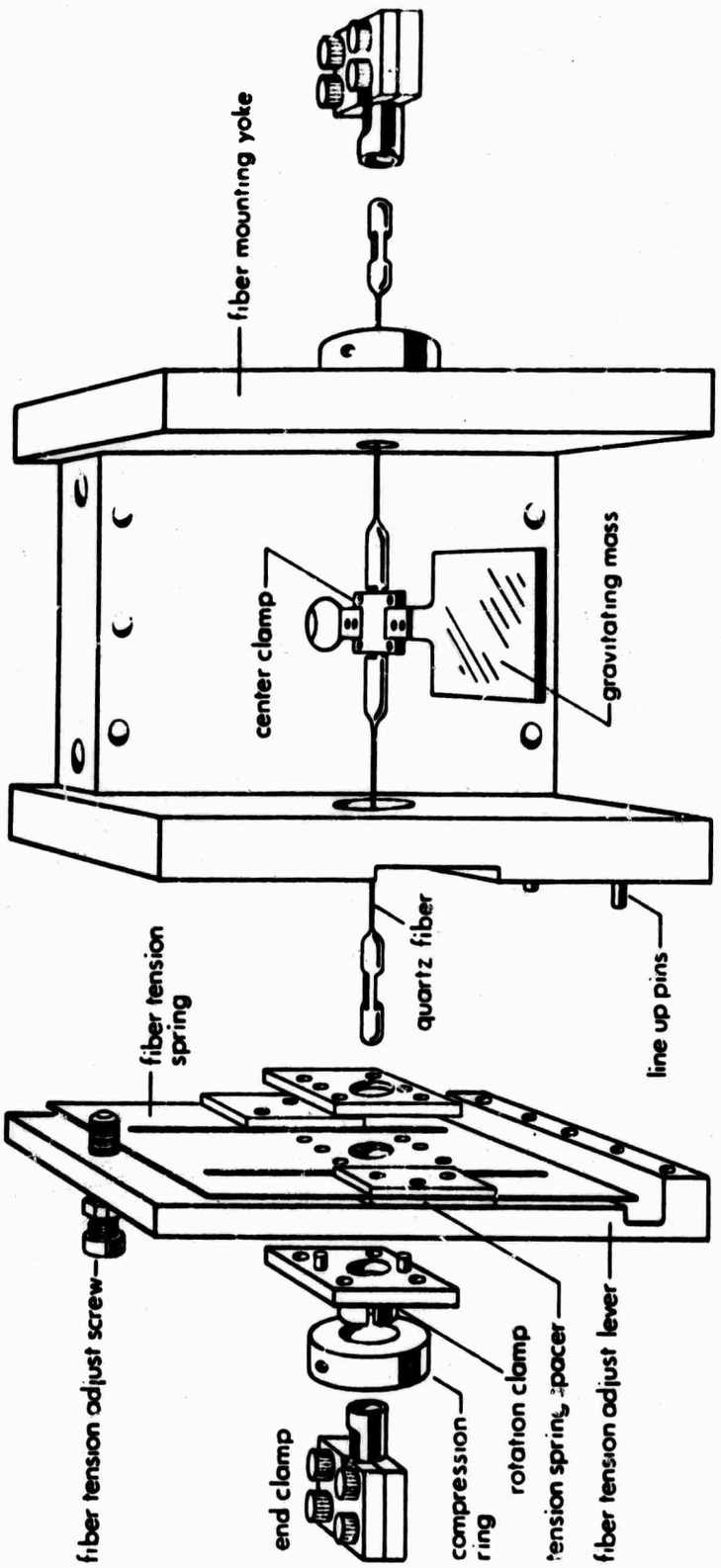

Figure 1. Exploded view of torsion spring system.

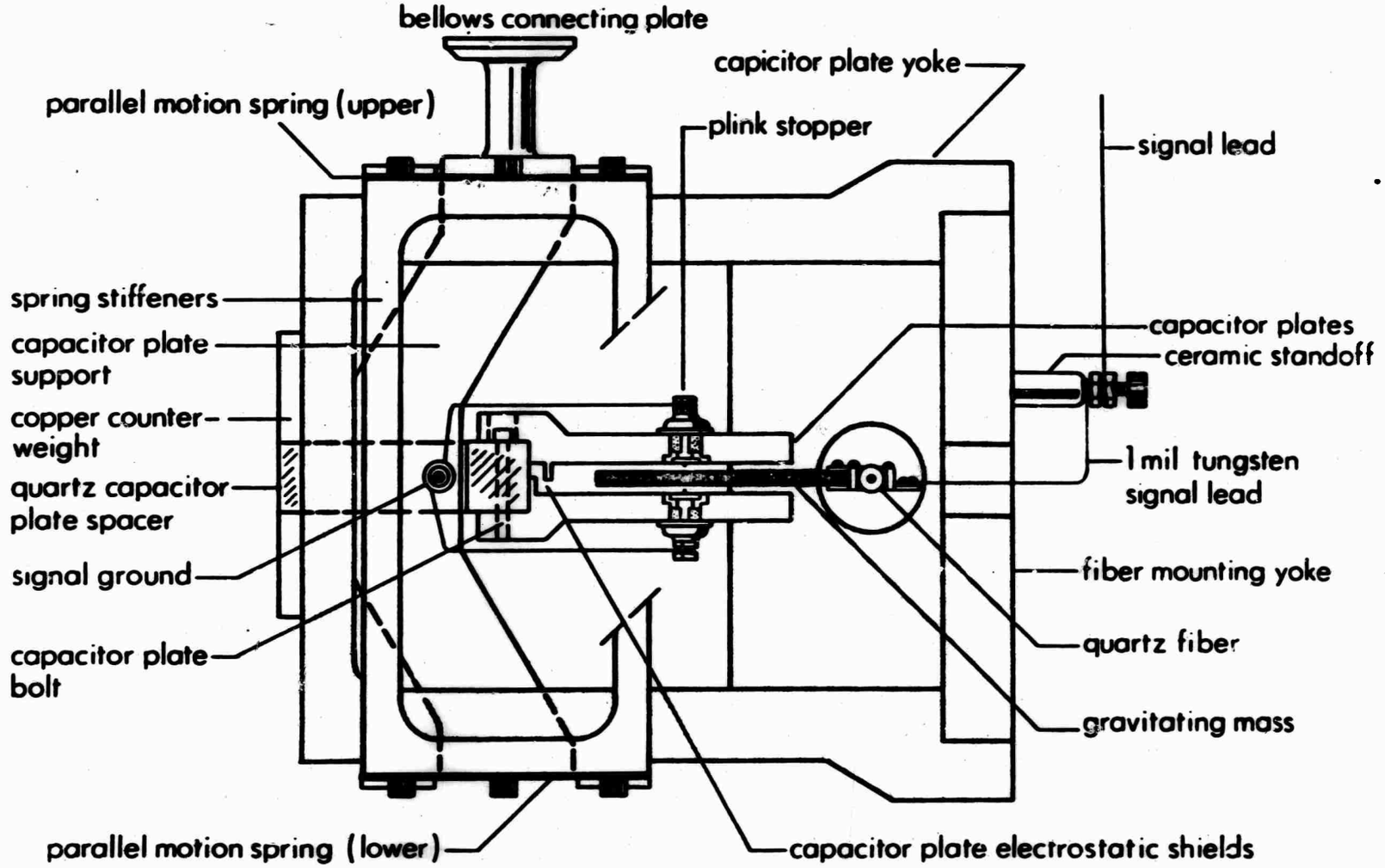

Figure 2. Side view of capacitor position sensor and torsion spring system.

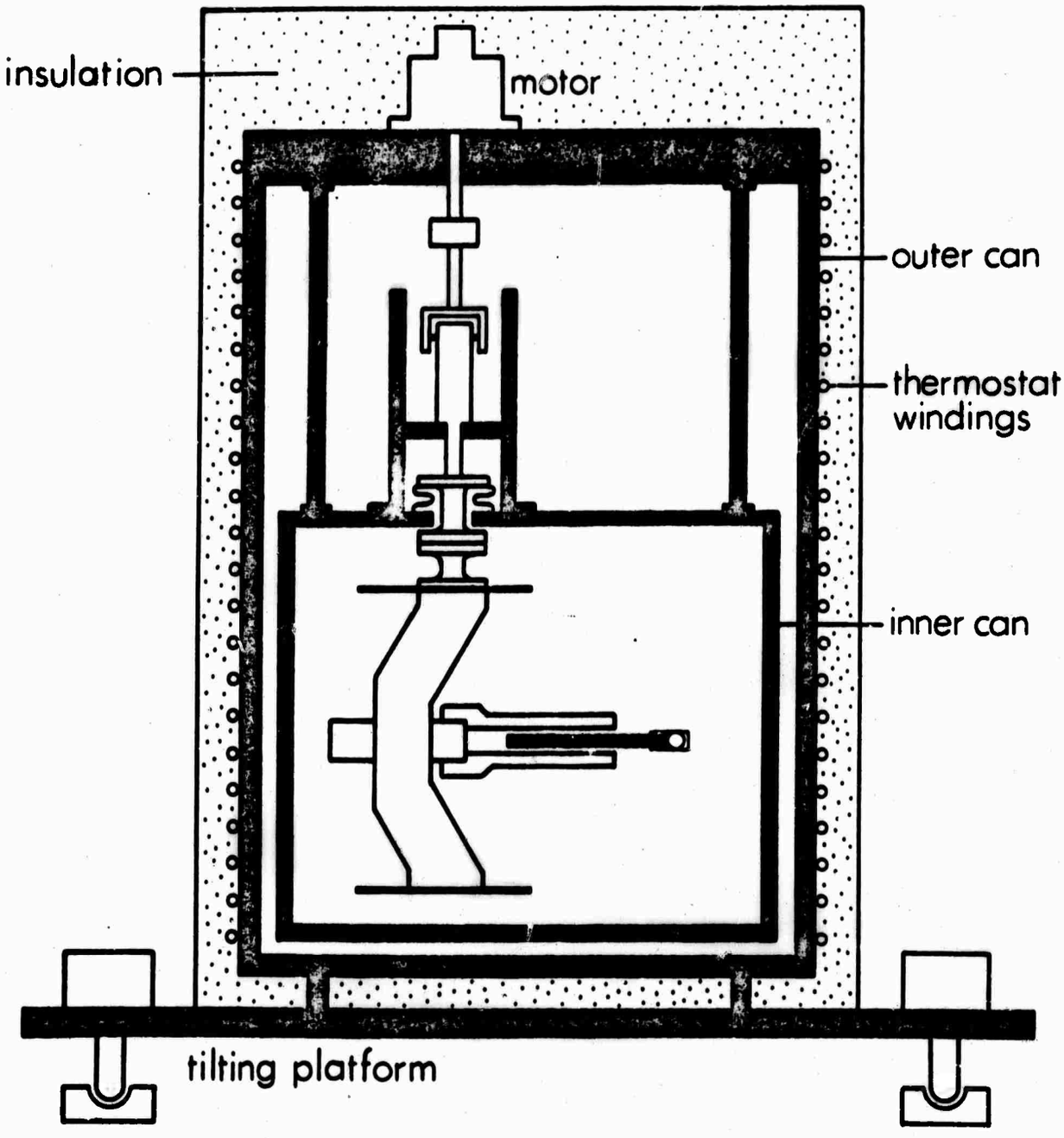

Figure 3. Double vacuum can assembly and tilting platform.

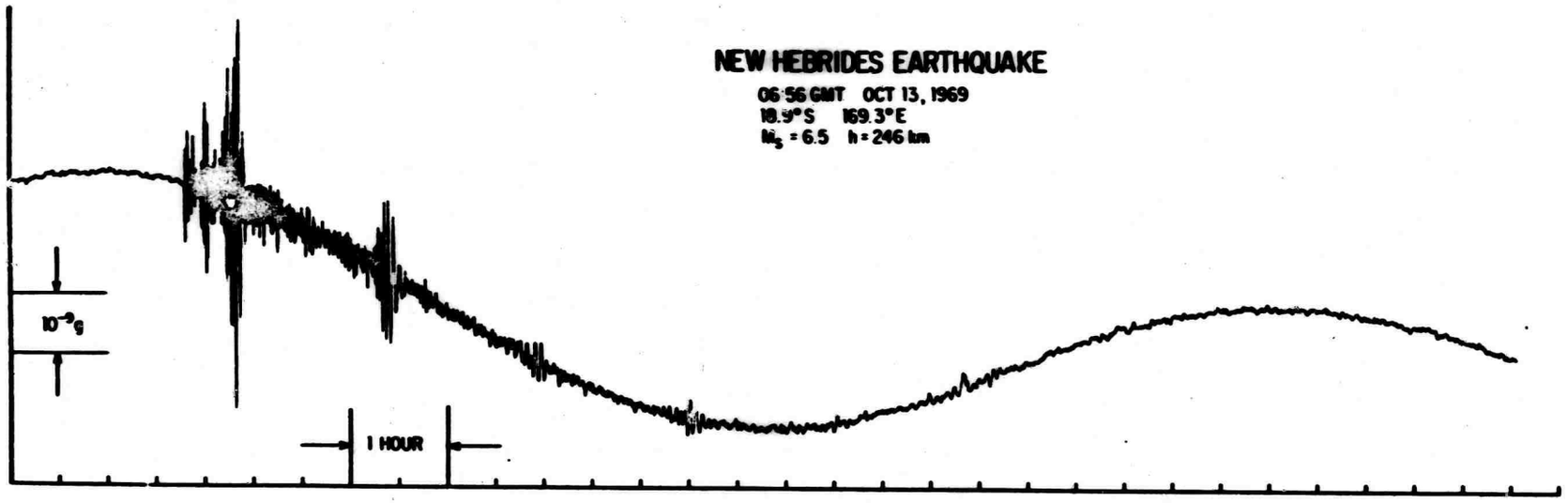

Figure 4. Filter output for New Hebrides earthquake M_S = 6.5, h = 246 km at 06:56 GMT, October 13, 1969; 18.9°S, 169.3°E.

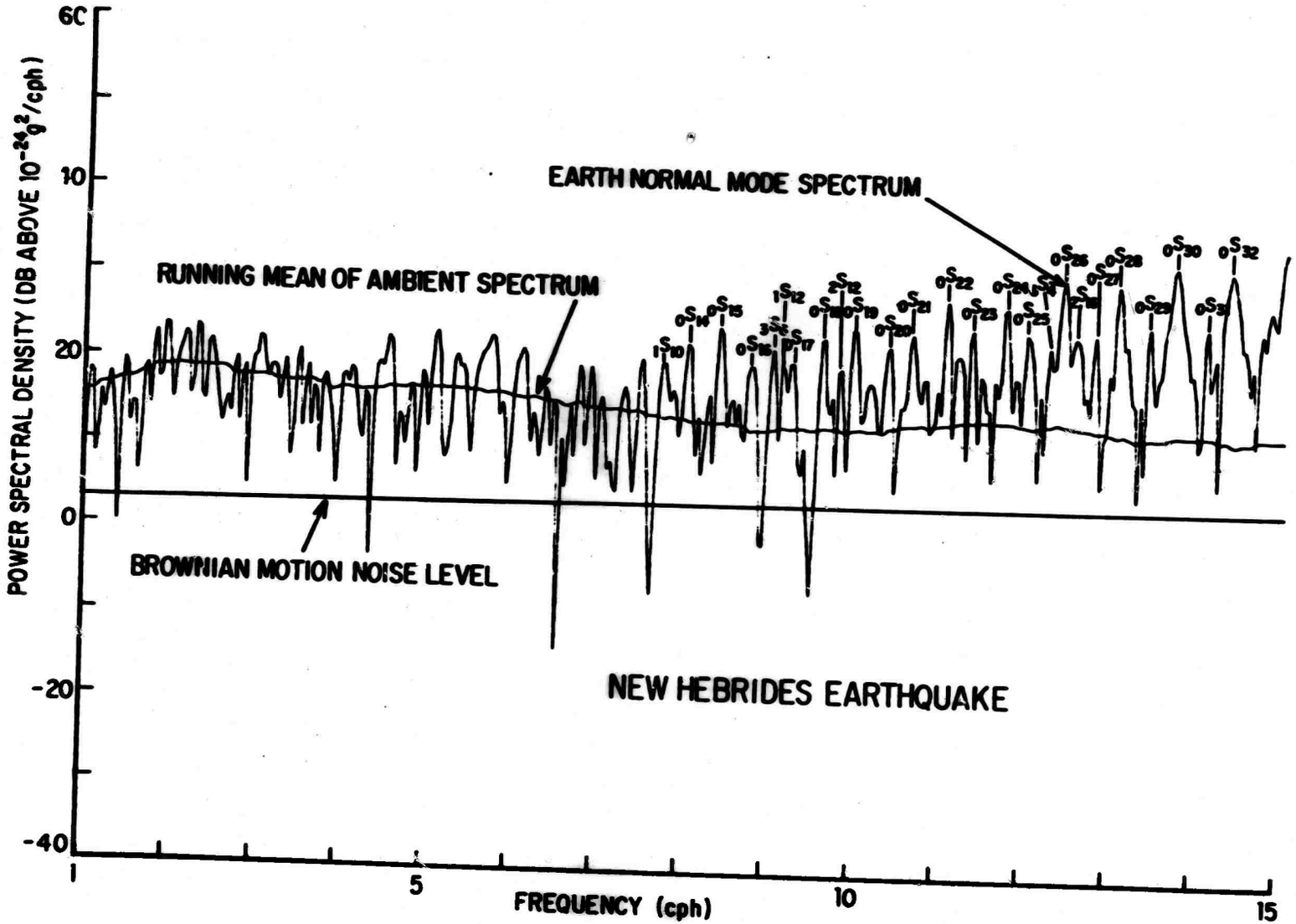

Figure 5. Power spectral density for New Hebrides earthquake of Figure 4 from 1 - 15 cph. 0 DB on Figure is 1×10^{-24} g^2/cph.

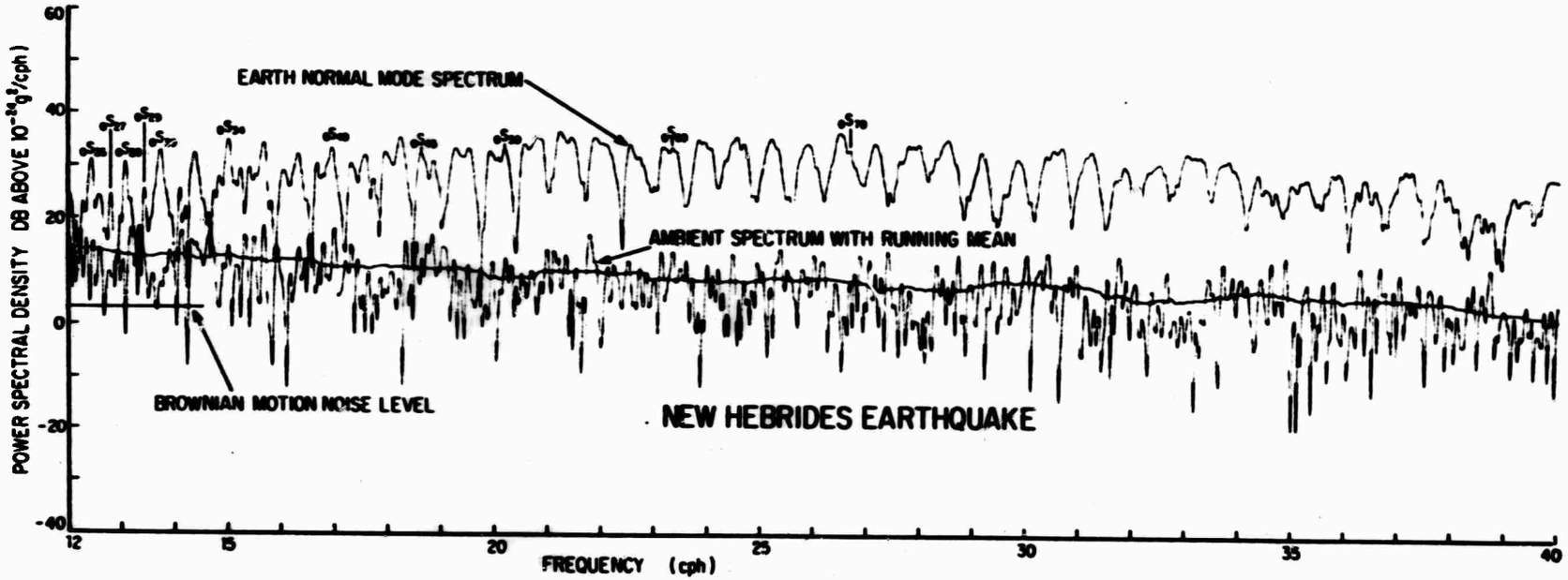

Figure 6. Continuation of Figure 5 from 12 - 40 cph.

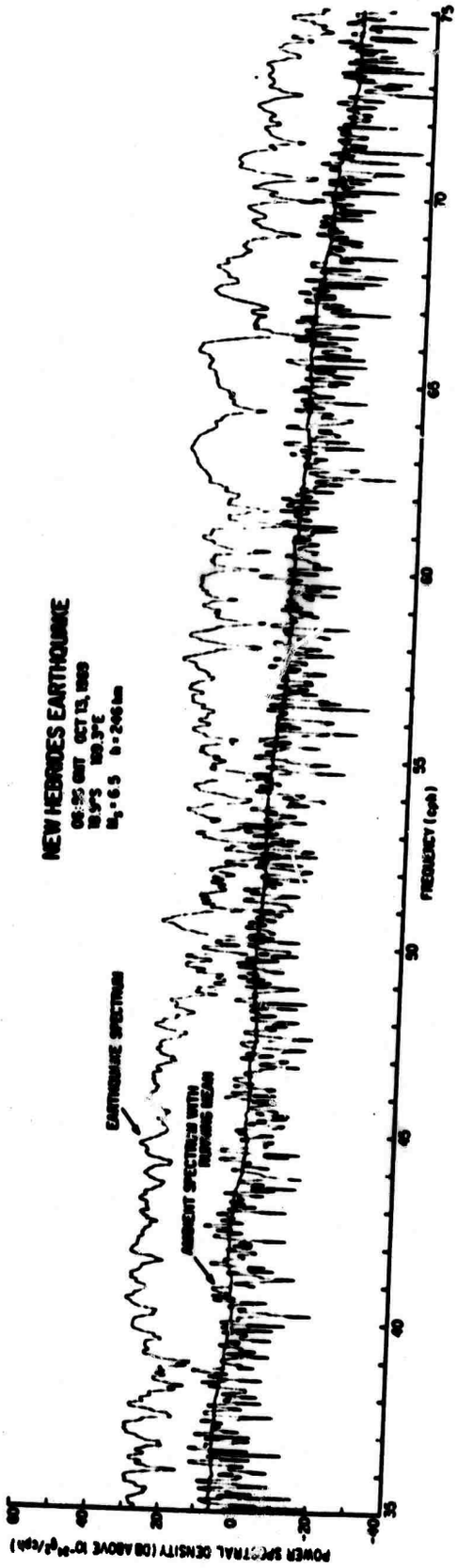

Figure 7. Continuation of Figure 6 from 35 - 75 cph.

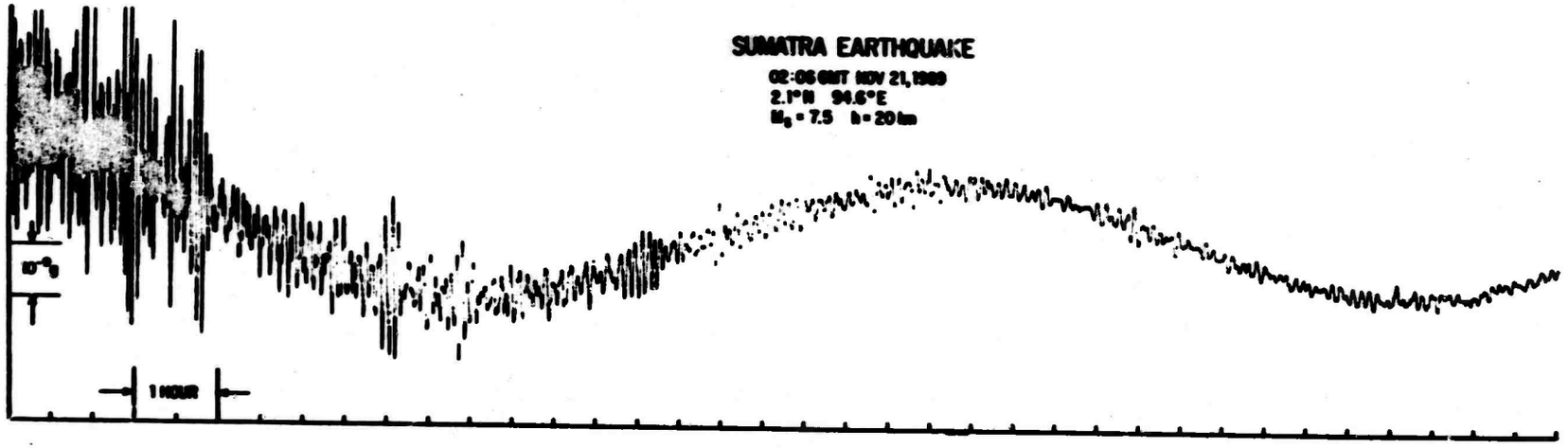

Figure 8. Filter output for Sumatra earthquake, M_s = 7.5, h = 20 km at 02:06 GMT, November 21, 1969; 2.1°N, 94.6°E.

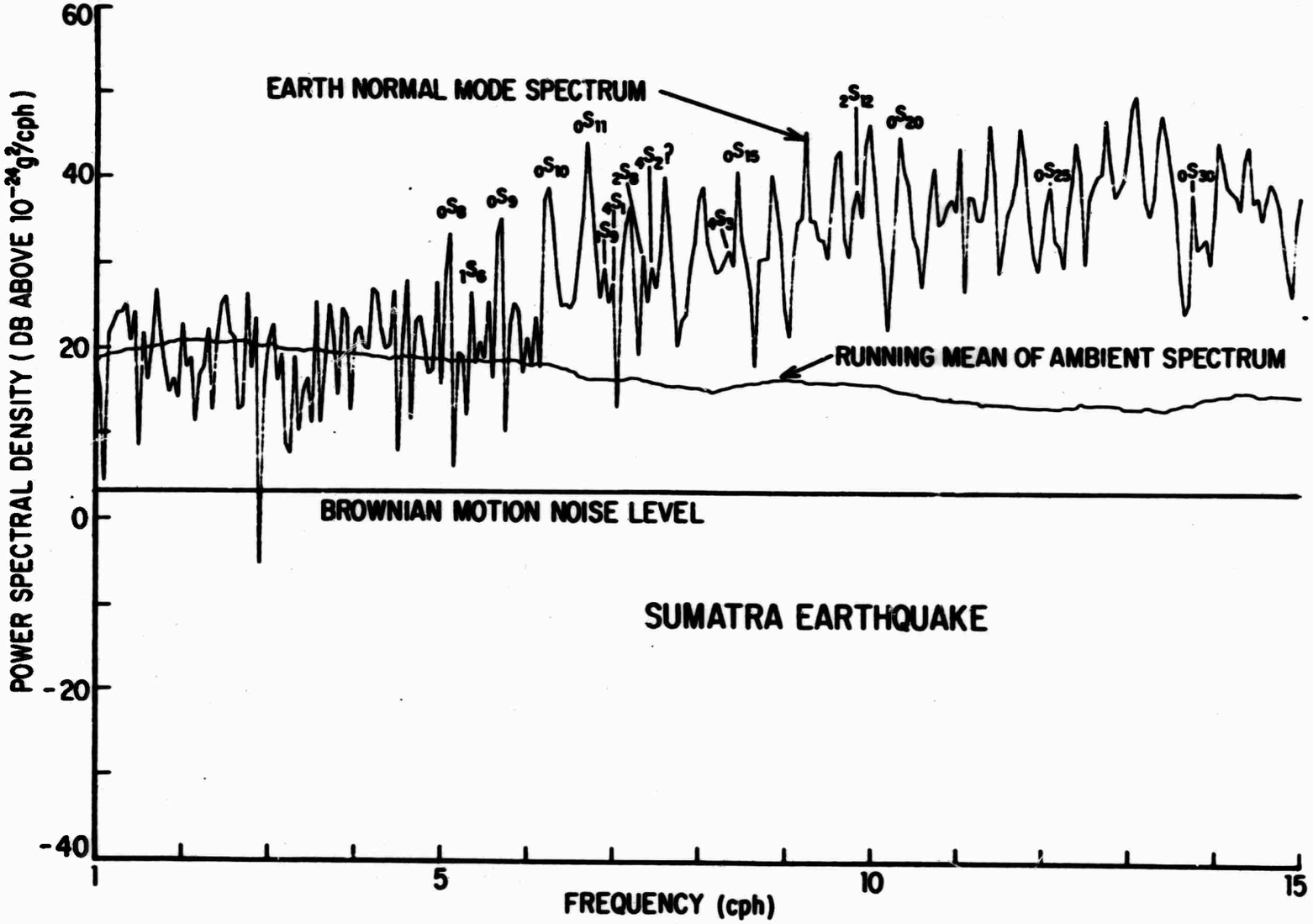

Figure 9. Power spectral density for Sumatra earthquake of Figure 8 from 1 - 15 cph. 0 DB on Figure is 1×10^{-24} g^2/cph.

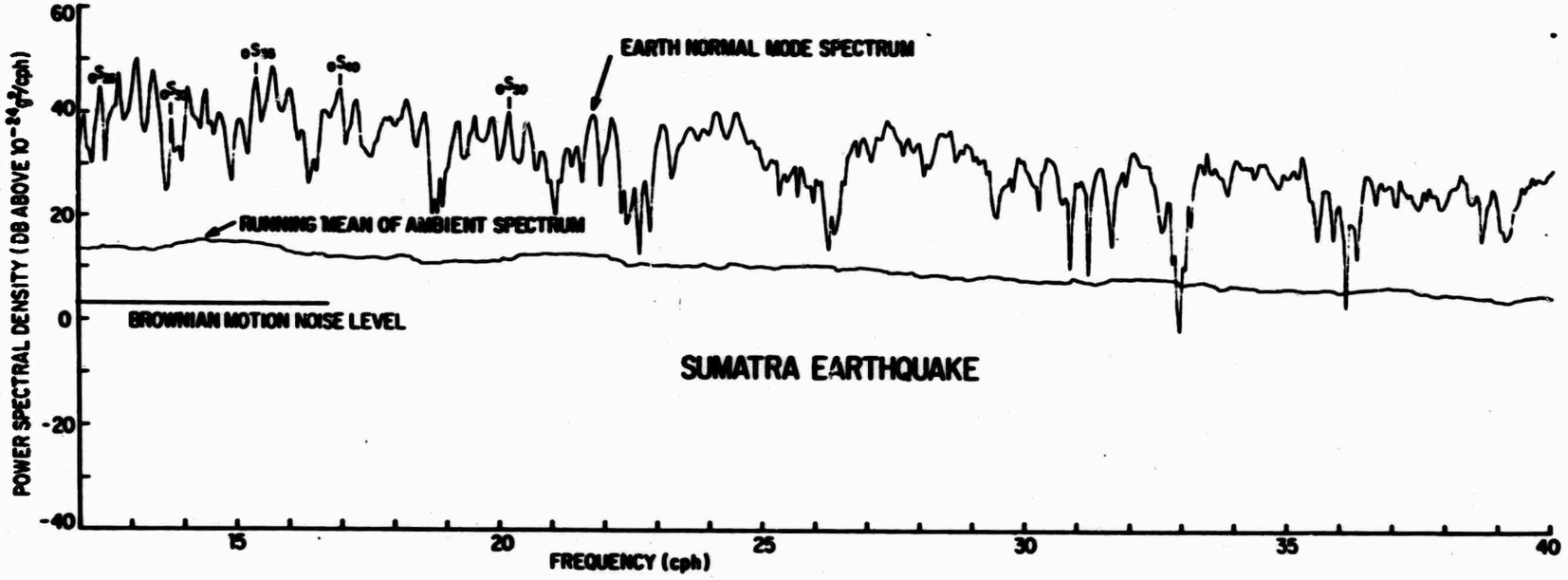

Figure 10. Continuation of Figure 8 from 12 - 40 cph.

A DIGITAL ACQUISITION SYSTEM FOR GEOPHYSICAL DATA AND SOME PRELIMINARY RESULTS

By

Eugene T. Herrin
G. G. Sorrells
John A. McDonald

Dallas Geophysical Laboratory
Southern Methodist University
Dallas, Texas

ABSTRACT

A unique digital acquisition system for geophysical data is described. The system has been operating in Grand Saline, Texas for nearly six months acquiring seismic, acoustic and meteorological information. A system of very long period seismographs at the surface and at a depth of about 200m have been used to study the relationship between long period seismic noise and local variations in the atmospheric pressure field. A 5-km triangular array of microbarographs have been used to study acoustic gravity waves generated by explosions and by natural sources. Some of the preliminary results from these data are presented.

INTRODUCTION

Since the early part of 1970 a unique digital data acquisition system has been in operation at Grand Saline, Texas. The station has been operated jointly by the Dallas Geophysical Laboratory of Southern Methodist University and by Teledyne Geotech of Garland, Texas.

Using some very long period seismograph systems, an array of microbarographs and an anemometer and a weather vane data are being collected concerning local variation in the long period seismic noise and atmospheric pressure fields. These data are being used to study:

(1) the propagation of acoustic waves in the atmosphere, and
(2) the relationship between long period seismic noise and local variations in the atmospheric pressure field.

In this paper we describe the field installations, the digital acquisition system, routine data processing techniques and some preliminary observations.

FIELD INSTALLATIONS

Acoustic program

An approximately 5 km triangular array was established with the base station near the recording trailer at the Morton Salt Mine (see Figure 1). The data from the two remote stations were transmitted by FM telemetry and recieved at the recording trailer.

Two other microbarographs were placed so as to create an approximately 0.3 km triangular array. A sixth microbarograph was placed in the mine at the location of the mine LP seismometers. The coordinates, elevations, channel designations and names of the six microbarographs are given in Table 1. Two microbarographs were moved for later tests and their locations with respect to the base station of the big array are shown in Figure 2.

The microbarographs used in the experiments are NBS model N3 designed by the National Bureau of Standards and built by NBS and by Geotech. These microphones measure pressure variations with reference to a known volume which is connected to the atmosphere by an acoustical resistance. This combination determines the long period response of the microbarograph. The short period response is controlled by an acoustical capacitance, the fore-volume, which is fixed and by an acoustical input resistance which can be varied. In these experiments the short period 3 db point was arranged to be about 2 sec. The average response of the microbarographs used in these experiments is shown in Figure 3.

The remote microbarographs were placed in small trailers with their transmitting equipment. A short hose allowed them to sample pressure fluctuations outside the trailer. Those microbarographs close to the recording trailer (Figure 2) were buried to increase the thermal stability of the backing and fore volumes. A 50 ft piece of garden hose was connected to the faucet to place the sampling point remote from the microphone body.

An anemometer and a weather vane placed at a height of 4 m at the recording trailer provided a continuous monitor of the wind speed and direction.

Seismic program

The seismograph systems are designed, built and maintained by Geotech. They consist of a seismometer with a free period of 20 seconds and a photo tube amplifier with a free period of 30 seconds. A combination of a 200 sec high pass, a 60 sec low pass filter and an operational amplifier effectly boosts the long period end of the response of the seismograph systems. An average response of such a system is shown in Figure 4. The locations of the two three component systems are shown in Figure 2, and the channel designations are given in Table 2. As can be seen in Figure 2, two of the microbarographs were moved to

the location of the surface seismometer system in order to provide more detailed information of the local atmospheric field.

Considerable care was exercised in the installation of the seismometer systems to ensure that buoyancy and temperature effects were at a minimum. Both the vertical and horizontal seismometers were housed in steel cases which, in the case of the vertical seismometers, were tightly sealed. These cases acted as low pass acoustic filters which, according to the manufacturers' specifications, had a time constant of about 4 hours. The cases for the horizontal seismometers were left unsealed in order to avoid spurious tilts.

The atmospheric pressure fluctuations were additionally attenuated by enclosing the seismometers in sealed 10 gauge steel tank vaults. The space between the instrument and the vault was filled with fiberglass. After sealing the time constants of the vaults were measured to be between 10 and 26 hours. A time constant of 10 hours indicates that at periods of less than 200 sec the pressure variations inside the vaults should be at least 3 orders of magnitude lower than the ambient pressure fluctuations. A check of these values was made by simultaneously sampling pressure variations inside and directly outside the vault. Preliminary results indicate that when the external field is 100 μbars or less the pressure variations inside the vault are at the level of system noise. Since the system noise at periods less than 200 sec is about 0.02 μbar it is suggested that the measured values of time constant are reasonably accurate. Thus the buoyancy effects can be said to have been eliminated.

DATA ACQUISITION SYSTEM

A block diagram of the microbarograph and seismograph systems and of the data acquisition system is given in Figure 5.

The microbarograph signals modulate a carrier frequency of 1550 Hz and of the eight available FM discriminators six were allocated to the microbarograph systems. The 6 seismograph systems and the anemometer and weather vane were allocated to the 8 analog channels. In addition up to 12 hours of any two seismographs could be monitored on a Helicorder.

Timing was provided by a Geotech Timing Unit. This timer was set to WWV and it outputs timing in the form; day-of-the-year; hour; minute; second, and it forms an important control in the data acquistion system.

The discriminators, timing system, tape recorder are combined in the same unit as a Raytheon Computer. This is a 16-bit, integrated circuit digital computer. Data are represented as binary numbers and processed in parallel. The basic computer consists of a central processor, 4096 words of core memory, a dc power supply, an ac controller and a teletypewriter. The teletypewriter contains a paper tape reader and punch and is the basic input-output device for the computer. Standard software for the system includes a routine diagnostic program and a program that ensures a computer compatible recording format. In addition a data acquisition system program is used which is designed to allow for two basic sampling rates called short period (4 samples/sec) and long period (2 or 1 sample/sec). The long period rate has to be some even submultiple of the short period rate.

Additional major components include an analog-to-digital converter with an input multiplexer and a binary gain-ranging amplifier, 1000 sec high pass filters for the FM channels, antialiasing filters for all input channels and a magnetic tape transport with a controller for incremental write but with a synchronous read facility.

ROUTINE DATA PROCESSING

After the data acquisition program is loaded, a tape is placed on the tape recorder, when it is advanced to a BOT marker. The tape recorder becomes ready and control can be passed to the teletypewriter. This allows the operator to input various instructions. These instructions allow options that are as follows; the short and long period sampling rates (not greater than 4 and 1 per second respectively), the allocation of short period and long period channels (not greater than 16 in all), the length of a data record (normally 60 seconds) and a four character identification (at present, A followed by the day of the year). If no parameter changes are requested the input alternatives can be circumvented and the input of the four character identification will transfer control back to the computer.

When the input data is complete from the teletypewriter a "header" record is written immediately at the beginning of the tape. This header record is written in twenty-five 18 bit words and contains the four character identification, the length of a data record, the short period sampling rate and the number of short period channels, the long period sampling rate and the number of long period channels, the number of words in a scan (determined by the number channels being scanned plus an error word), the number of words in a record (determined by the length of the data record plus three time words), and the numbers of the channels being scanned. In addition to the header record at the beginning of each tape, the day-of-the-year; hour; minute are contained in three time words written on the tape at every minute.

In all future processing of a tape this header record information has to be read by all computer programs used in this research. All programs require that the header information is always typed, printed or plotted. In this way there can never be any confusion as to the original tape, the original channel allocation or of the starting day and time of some particular data. The Raytheon Computer is programmed to start taking data at one second past any even minute and, following a command, stops taking data at any even minute. Thus any future processing periods start at one second past a minute and finish on an even minute.

The basic data format used following the original recording is called Tape IØ. Each channel is blocked into records of length 2^{10} (1024) and the channels are multiplexed. The header record is written at the beginning of each tape. Program Raytheon reads up to 16 channels of an original data tape between any given times and blocks and multiplexes the data into the Tape IØ format.

Figure 6 is a typical plot of original microbarograph data after it has been arranged in the Tape IØ format. The plot routine used (Plot Tape IØ) scans through the data within the number of blocks it is required to plot and scales all the data to the maximum excursion. An option in the program allows the data to be prescaled. The maximum excursion allowed by the Raytheon Computer is 0.8388608×10^7 which

is equivalent to +10 volts. Any excursion less than this is gain ranged. The data were originally sampled at 1 sample/sec so that a Calcomp Plotter plotting one point every 0.01 inches covers the equivalent of a 100 sec per inch. Thus a tick mark every inch gives a convenient time scale on the abscissa. The numbers on the abscissa in Figure 6 represent the end of blocks of 1024 data points. The horizontal axis in Figure 6 is 4 blocks or 4096 points or 4096 seconds or about 1 1/4 hours of microbarograph data.

The program Raytheon prints out the number of blocks of 1024 points that it writes on an output tape. This is necessary information as a two-to-three day tape can contain 200-300 blocks of data blocked 1024. For routine checking at least one microbarograph channel and the wind speed and direction channels are decimated before plotting program Filter and Decimate by thirty effectively moves the aliasing point of the data to 60 seconds and reduces the sampling rate to 0.033 samples/second. It decimates by 30 any channel but the wind speed (channel 16). The wind speed is averaged over intervals of 30 seconds. Typical plots for the data from three elements of the large array, wind speed and wind direction are shown in Figure 7. The three blocks shown now represent 3072 points at 30 seconds a point, or 1536 minutes. Thus in excess of a day of data for periods in excess of 60 seconds is conveniently displayed for a 5 km array. It should be noted that three microbarograph channels have been plotted at a prescaled amplitude.

PRELIMINARY RESULTS

Long period seismic noise

It has been possible to observe the long period seismic noise field under a variety of meteorlogical conditions. It has become apparent that at periods greater than about 20 seconds a significant fraction of the seismic noise field is directly related to local changes in the atmospheric pressure field. In particular we have found that much of the surface seismic noise in the period range 20-120 seconds is caused by the turbulent pressure field which is created by the wind.

The results presented below deal primarily with noise related to this type of source. We compare data recorded during a "calm" period, when there was no wind of a measurable speed within a three hour period, with a "turbulent" period when, over a three hour period, the wind averaged about 12 m/sec.

The methods for determining the spectra, coherence and phase are those due to Welch (1967) and have been summarized by McDonald et al (1970). As has been pointed out in the previous section the header record information is presented and it appears on the final plots.

Calm period

The first two blocks (2048 secs) of the three hours of data used in the computation are shown in Figure 8. Channel 3 is the microbarograph located at the surface seismometer (Channel 9; Figure 2); channel 12 is the seismometer in the mine. Channel 2 is a microbarograph located some 60m south south east of Channel 9 (Figure 2).

The calculated power spectra and coherences between these time series for the relevant times are shown in Figure 9.

The short period background seen on the microbarogram is of the order of a few microbars but the longer period oscillation (T = 10 minutes) has an amplitude of several hundred microbars. Both seismograms are dominated by long period noise (T = 100 secs or greater) which is higher at the surface than within the mine. Roughly speaking the background at the surface is about 100 mμ and about 30 mμ in the mine. The distribution of noise power in the frequency domain may be seen more clearly from Figure 9a and 9b. Note that the spectral densities are essentially the same beyond a period of about 10 seconds. The atmospheric noise power is seen to rise at a rate slightly greater than 6 db/octave to periods of about 100 seconds. The flattening of the power spectra in the period ranges from 50 to 100 sec is caused by the 6 db/octave cutoff of the microbarograph which starts at about 45 seconds. The increase in noise power at periods greater than 100 seconds indicates that the field increases at a rate greater than 6 db/octaves in this range. The numbers on the vertical scale refer to $(\text{counts})^2/\text{Hz}$. The conversion from $(\text{counts})^2/\text{Hz}$ to $(\mu\text{bars})^2/\text{Hz}$ is given in the figure.

The spectral estimates for the data recorded by the vertical seismographs located at the surface and in the mine are shown in Figure 9b. These spectra are uncorrected for system response but are calibrated in the sense that sine wave calibration signals with 50 second periods yield the same number of counts/mμ for both systems. Surface waves recorded by both systems indicate there is not significant difference in the response of the two systems in the period range from about 15 to 100 seconds. It is not possible to measure the relative responses at periods less than 15 seconds. It will be seen that the 6-8 microseism peak is about 4 db higher on the surface than in the mine suggesting that the responses may differ below 15 secs. Note, however, that the 18 second microseism peak is virtually the same on both systems. The consistent differences between the two curves at periods between 20 and 100 secs is not caused by differences in responses. From about 20 to 50 seconds the difference amounts to about 3 db in power and increases to about 6 db at a period of 100 seconds. At 400 seconds the difference is about 12 db. The increase in the noise observed at the surface at periods less than 100 seconds appears to be related primarily to variations in the atmospheric pressure field (Figure 9c).

Coherence computations have been made on pairs of random time series using the same processing techniques. The results indicate that the values of the square of the coherence above 0.1 are significant at the 90% confidence level.

Figure 9c (curves 3 and 9) shows the coherence between the surface vertical seismograph and a microbarograph at the same location. Note that there is a small but significant coherence from about 30-40 secs and from about 40-80 secs. Figure 9c (curves 3 and 12) shows the coherence between the surface microbarograph and the seismograph in the mine. As would be expected there is no significant coherence. Figure 9d (curves 2 and 3) show the coherence between the data from two microbarographs separated by about 60 m. It is included to give some idea of local structure of the atmosphere field in the period of time.

Figure 9d (curves 9 and 12) is the coherence between the seismic data recorded at the surface and that recorded in the mine. As expected the microseism peaks at 8 and 16 seconds are strongly coherent. What is surprising is that the coherence does not drop off sharply beyond 18 seconds suggesting the existence of long wavelength noise at the longer periods. In particular there are relatively strong peaks at 22 and 45 seconds which coincide with similar peaks in the microbarograph coherence spectrum. This suggests a relationship between the two fields and could mean that the depth at which the vertical seismometer is located (-200 meters) is insufficient to attenuate noise of this type.

The lack of coherence between the data recorded by the surface vertical seismograph and the microbarograph at periods greater than 100 seconds is somewhat unexpected. This is particularly true in view of the higher noise level at the surface and the strong correlation

between the two sets of microbarometric data recorded in the vicinity of the surface seismometer installations. The lack of coherence is not caused by a high percentage of system noise in the surface spectrum.

Spectral estimates made from data recorded while both vertical seismometers were replaced by equivalent resistances have been divided by the spectral estimates shown in Figure 9b to produce the curves shown in Figure 10. These curves give the percentage that the system noise represents of the total power as a function of period. Note that at periods greater than 100 seconds the system noise is responsible for only about 1-2% of the power seen in the surface spectrum. The contribution of the system noise to the total power in the mine is somewhat greater but is still less than 10% at periods less than 500 seconds. It can be said that both systems are recording real data up to periods on the order of 500 seconds.

One possible explanation for the high level of seismic noise and low coherence is that the noise observed at the surface is the sum of contributions from several mutually independent atmospheric sources located at distances greater than about 100 meters from the surface vaults. In this case the coherence between the microbarometric and seismic data recorded at the same point could be expected to be low, particularly if the contribution in the immediate vicinity of the sampling point was small compared to the other sources. We intend to investigate this possibility by forming small arrays around the surface vaults and computing multiple coherences between the seismic and microbarometric data.

Turbulent period

The first two blocks (2048 secs) of the three hours of data used in the computations for a turbulent period are shown in Figure 11. Channel 2 is a microbarograph located some 60m south south east of the surface seismometers (Figure 2); channel 1 is a microbarograph located in the mine (Figure 2) and channel 9 and 12 are, as before, the surface and mine seismometers.

The calculated power spectra and coherences between these time series for the relevant times are shown in Figure 12.

These data were recorded when there was no activity in the mine, and during a three hour period when a steady 12m/sec (~27 mph) wind blew from the south.

The differences between the amplitudes of the microbarometric data recorded at the surface and with the mine should be noted. The peak to peak amplitudes of the surface data is roughly 50 μbars at a period of 50 seconds while in the mine the amplitudes are about 10 microbars. A similar difference is seen in the seismograms. The peak to peak amplitude of the noise recorded at the surface is roughly 150-200 mμ. In the mine it is about 30-40 mμ.

Estimates of the microbarometric data recorded at the surface and within the mine are shown in Figure 12a. The curve shown in the inset is the ratio of the mine to the surface spectrum. The shape of

this curve at periods greater than 50 seconds indicates that the mine is acting as a low pass filter to the surface pressure fluctuations. This conclusion is further supported by the behavior of the coherence between the microbarometric data recorded at the surface and in the mine. This function is plotted as a solid curve in Figure 12d. The coherence begins to rise at periods greater than 50 seconds indicating that the two fields are linearly related within this region. The time constant of the mine appears to be about 4 minutes.

A low pass filtered surface pressure field however, is not the only contribution to the mine spectrum. Three prominent peaks at 3, 8 and 16 seconds can be seen in the mine spectrum. These are not found in the surface spectrum. The 3 second peak is caused by the blower in the mine. The peak at 8 and 16 seconds merits further comment. Their positions in the microbarometric spectrum coincides with the position of the classical microseism peaks in the long period noise spectrum. This suggests a cause and effect relationship. An initial interpretation was that the microbarographs were reacting seismically. If this was the case similar peaks should be seen in the surface spectra. They are obviously absent from the surface spectrum shown in Figure 8a and 12a. Without exception they have been found in all the mine data and are absent in all the surface data. Our tentative hypothesis is that the mine is being "squeezed" by the 8 and 16 second microseisms and that the observed pressure variations are a measure of the volumetric earth strain induced by these microseisms. The lack of coherence between the microbarometric and seismic data in the mine (Figure 12c, curves 1 and 12) would seem to preclude this hypothesis. However the absence of coherence could be caused by the presence of a significant fraction of incoherent noise in either set of data or both. Further investigation is planned in order to clarify this point.

It will be seen from Figure 12b that the surface noise power is consistently larger than the mine noise power throughout the entire period range. The maximum difference occurs at 40 seconds where the surface spectrum is 18 db greater than the mine spectrum. The coherence at the surface between the seismic and microbarametric noise (Figure 12c, curves 2 and 9) indicates that a significant fraction of the high surface noise in the period range from about 20 to 100 seconds is directly related to fluctuations in the local atmospheric pressure field. Since the surface vaults have been shown above to provide adequate insulation from external atmospheric pressure variations the high surface noise may be attributed to earth loading rather than to direct action on the seismometer.

The coherence between the data recorded by the surface and mine vertical seismographs is shown as the dotted curve in Figure 12d. The peaks at 8 and 16 seconds which were so prominent in the calm period data (Figure 9b) have now been eroded by the addition of an atmospherically generated component to the surface field.

In Figure 13 the spectral estimates of the data recorded at the surface during the calm and the turbulent period are compared. The effects of the wind generated atmospheric turbulence can be clearly seen.

During windy periods the noise can be as much as 15 db greater than during calm periods. In contrast (Figure 14) the noise field recorded within the mine shows no really significant change from calm to windy periods. This is a consistent result observed throughout the experiment.

Recording of seismic events

This section merely catalogs some events recorded by the long period seismographs and compares the signal recorded at the surface with that recorded at a depth of 200m in the mine.

In each of the Figures 15 through 18 the seismograms have been plotted using the Program Plot Tape IØ. The plots start within 1 minute of the origin time. Each pair has been scaled to the same value to ease the comparison. The information on the plots has been taken from the Preliminary Determination of Epicenter cards of the USC&GS.

Figure 15 should be compared to Figure 16 for the epicenters are located within 45 km of each other, but the magnitudes differ by almost 1 unit. The epicentral distance to Grand Saline to about 20° and crosses the Gulf of Mexico indicating that the phase Lg cannot be present.

Figure 17 shows a small event from off the coast of Northern Chile with an epicentral distance of about 67°. It would be difficult to pick this event on the surface seismogram but the surface waves are clearly evident on the mine seismogram.

Figure 18 shows the two channels compared for the NTS shot Cornice, at an epicentral distance of about 20°. The reason for the very long period oscillation is not known but it is believed to be instrumental. It has been shown that a pulse of 1μ produces a similar long period oscillation; the Lg phase should have been present on the continental path. The small later signal could be a cavity collapse.

Array processing of acoustic signals

Recently an array beam steering program has been adapted for use on the XDS 925 computer. This program is a modification of one described in Henning (1970). Signals are brought into coincidence by time shifting and the relative increase in the amplitude of the summed channels is detected when coincidence is achieved. The average power in a beam is compared with the sum of the power of the individual channels. If the ratio of these powers increases above the value for uncorrelated noise a signal is said to have been detected. The particular advantage of this program is that the time is averaged by means of a recursive filter (Shanks, 1967).

The present version of this program is called Array Beam Steer. It will form up to 18 beams from up to 10 elements of an array, and will increment through a series of propagation velocities. It is planned to use this program to detect acoustic waves from explosive and natural sources.

The program has been used on the data shown in a decimated form in Figure 19. This shows an acoustic signal from a French hydrogen bomb exploded in the atmosphere in the South Pacific on 3 July 1970, as it appears at three elements of the 5 km array. The plots represent 120 minutes of data starting at 0100 GMT on 4 July 1970, which have been filtered and decimated by 10, effectively moving the alias period to 20 sec. The three plots have been prescaled to the same amplitude.

The expected arrival time and azimuth of this event were 0125 GMT and 220 degrees (Matheson, personal communication). The beam steering program was run on data from the three elements shown in Figure 19 and the results are shown in Figures 20 and 21. The contoured output from the program is shown in Figure 20 for the full circle 0-360 degrees, and in Figure 21, giving better definition, for the quadrant 180-270 degrees. The event can be clearly seen at about 0140 GMT at an azimuth of 220 degrees.

Ground motion associated with acoustic waves

A most interesting consequence of the passage of the acoustic waves from the French test can be seen in Figure 22. This shows the spectra, the coherence and the phase relationship between the surface vertical seismograph and a microbargoraph located 60 meters away. Note the high coherence between these two channels in the period range 20-100 seconds. In contrast to the wind generated pressure fields discussed earlier; a seismic disturbance associated with the passage of the acoustic waves is also observed in the mine. This disturbance is in most respects identical to that observed on the surface.

These results are in general agreement with the study by Sorrells (1970) which showed that the seismic disturbance created by plane pressure waves attenuates with depth but the rate of attenuation is critically dependent upon the rate at which the pressure wave moves. For waves which move at acoustic speeds, the predicted attenuation at 200 meters is less than 5% of that for waves with periods greater than 30 seconds. Therefore, we should expect to record essentially identical signals in the mine and on the surface. On the other hand, for pressure fields traveling on the order of 10 meters/sec the predicted attenuation at a depth of 200 meters is greater than 50 dB at periods less than 100 seconds. Therefore, this field should not be observed in the mine.

A paper is now in preparation in which these results will be discussed in more detail.

SUMMARY

This paper has described a digital system for acquiring data. The combination of hardware instrumentation and software programming has produced a system in which errors of timing, data channel allocation and calibration are unlikely. The availability of data in digital form has been shown to facilitate data processing.

The results presented are concerned largely with the contribution of the wind generated pressure field to the long period seismic noise field. It has been demonstrated that increases of as much as 16 db in the seismic noise field observed at the surface of the earth can be directly related to the wind driven pressure field. It has further been shown that this component is absent in the seismic noise field observed at a depth of 183m in the mine. In contrast, during the passage of acoustic waves, seismic signals are recorded both in the mine and at the surface at about the same level. The results of pressurization tests and direct measurements of the pressure fields inside and outside the vaults rules out buoyancy as a possible cause for the noise. It is believed therefore, that true earth motions are being observed. In this case the results are in qualitative agreement with studies of the seismic disturbances associated with slowly moving pressure waves. A more detailed discussion of these and other results obtained at Grand Saline will be contained in a paper presently in preparation.

ACKNOWLEDGEMENT

John L. Lobdell and Nancy Cunningham were responsible for the systems programming, and Karl D. Thomason provided engineering assistance and their help is greatly appreciated. S. Montoya and H. Gautreaux were members of the Geotech field team. Five of the microbarographs were on loan from the National Bureau of Standards. The research was carried out during the tenure of a National Aeronautics and Space Administration traineeship by one of us (J.A.M.), and was supported by the Air Force Office of Scientific Research under Contract No. F44620-68-C-0086.

REFERENCES

Henning, G.N., 1970, Preliminary design report infrasonic system M6, Model 34000, Teledyne Geotech Tech. Report 70-7.

McDonald, J.A., Douze, E.J., and Herrin, E., 1970, The structure of atmospheric turbulence and its application to the design of pipe arrays, submitted to Geophys. J.R. Astron. Soc.

Shanks, J.L., 1967, Recursion filters for digital processing, Geophysics, v. 32, p. 33-51.

Sorrells, G.G., 1970, A preliminary investigation into the relationship between long period seismic noise and local fluctuations in the atmospheric pressure field, in preparation.

Welch, P.D., 1967, The use of fast Fourier transforms for the estimation of power spectra: a method based on time averaging over short modified periodgrams, Trans. IEEE, AU-15, v. 2, p. 70-73.

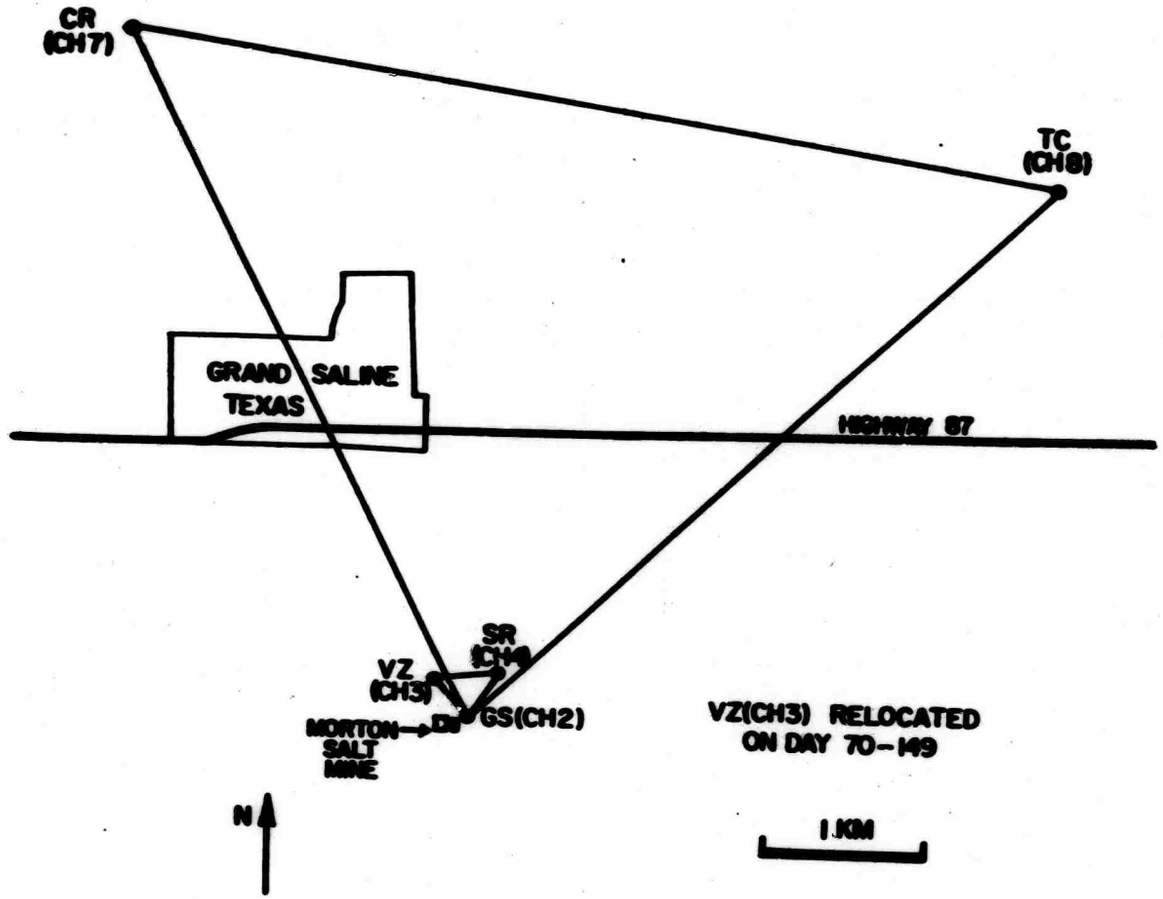

Figure 1. The microbarograph array and its relationship to Grand Saline, Texas.

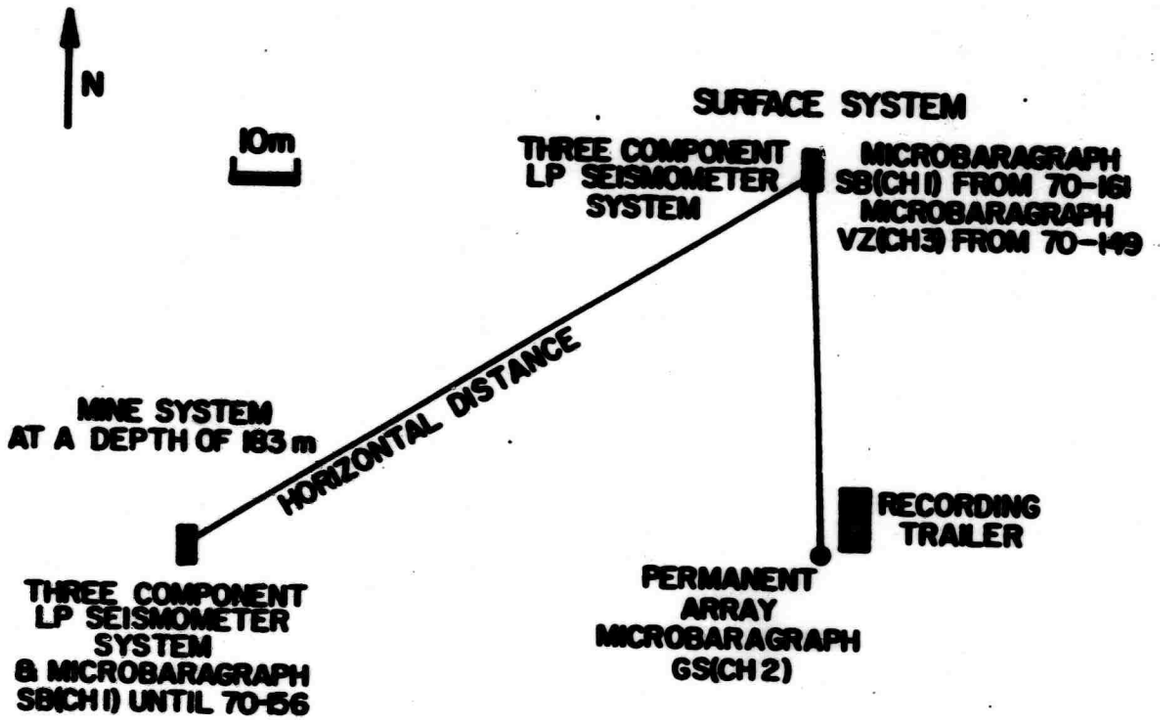

Figure 2. The microbarograph and seismograph locations at the surface and in the mine.

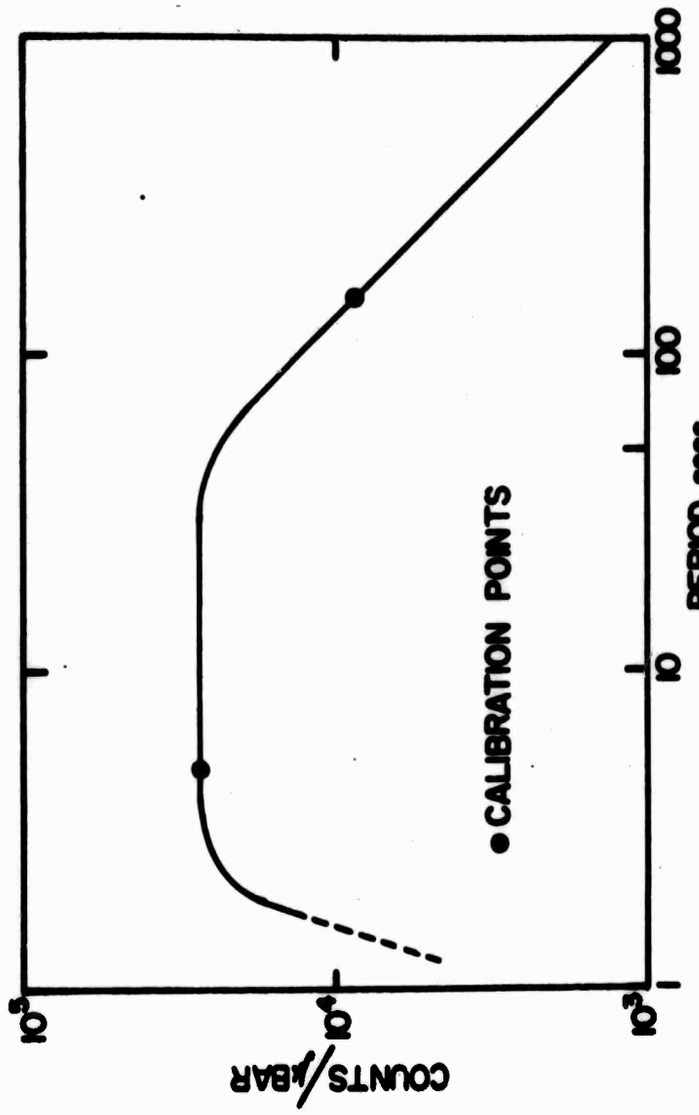

Figure 3. An average response of the microbarograph systems.

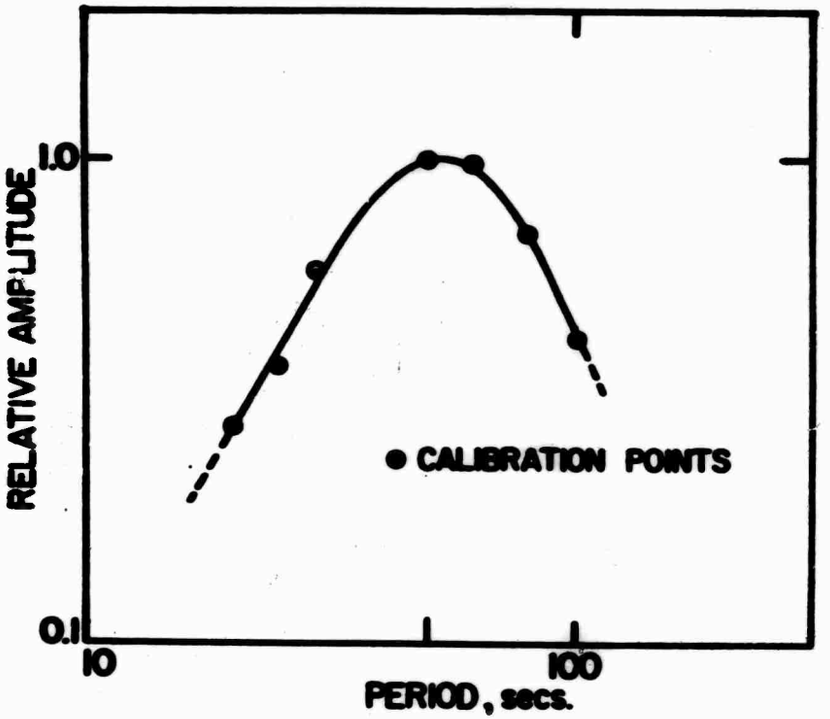

Figure 4. An average response of the seismograph systems.

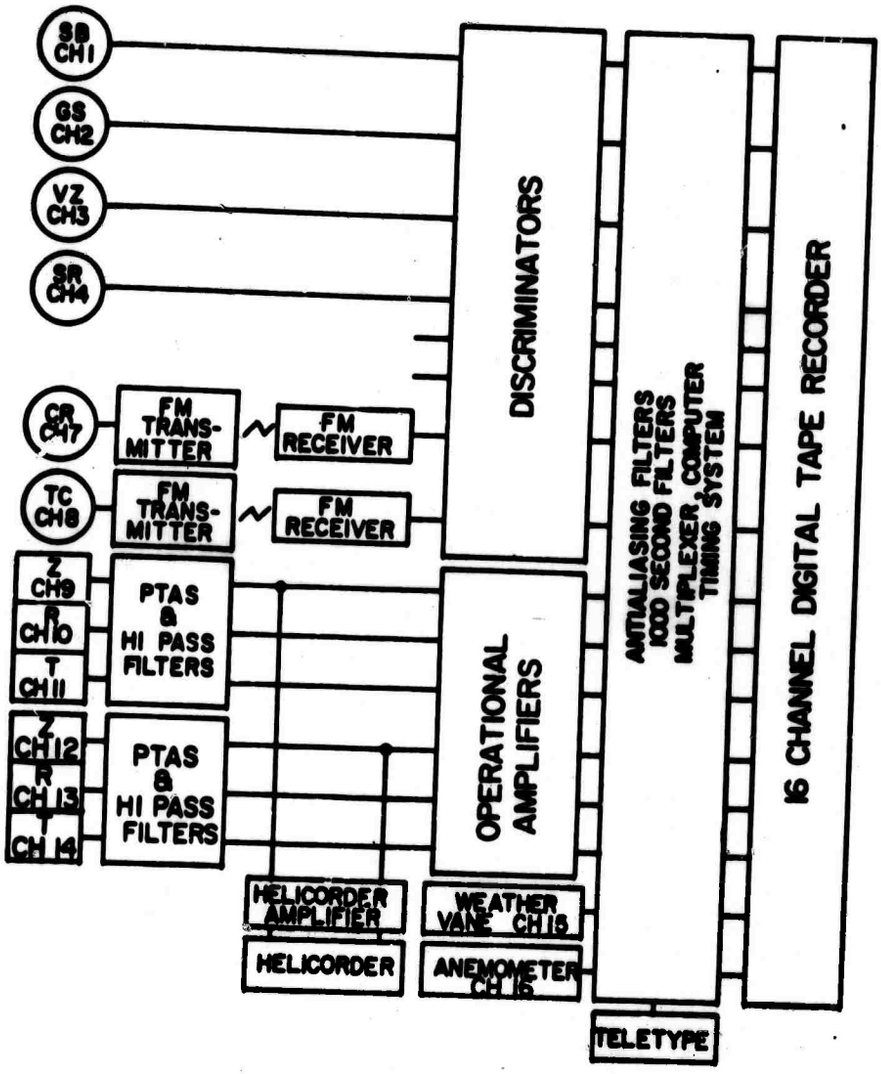

Figure 5. Block diagram of the seismograph and microbarograph systems.

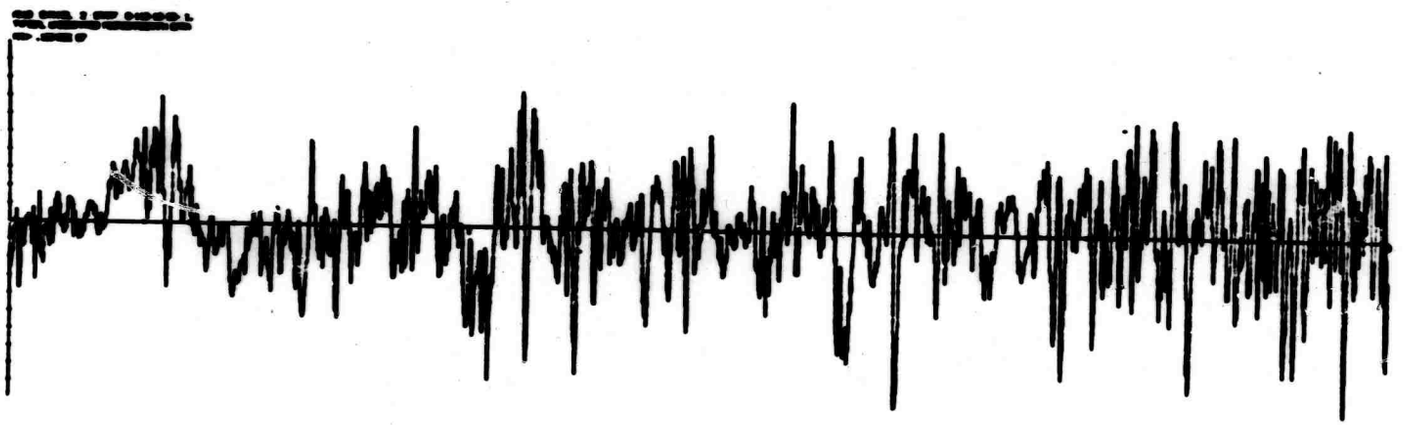

Figure 6. An example of typical undecimated microbarograph data.

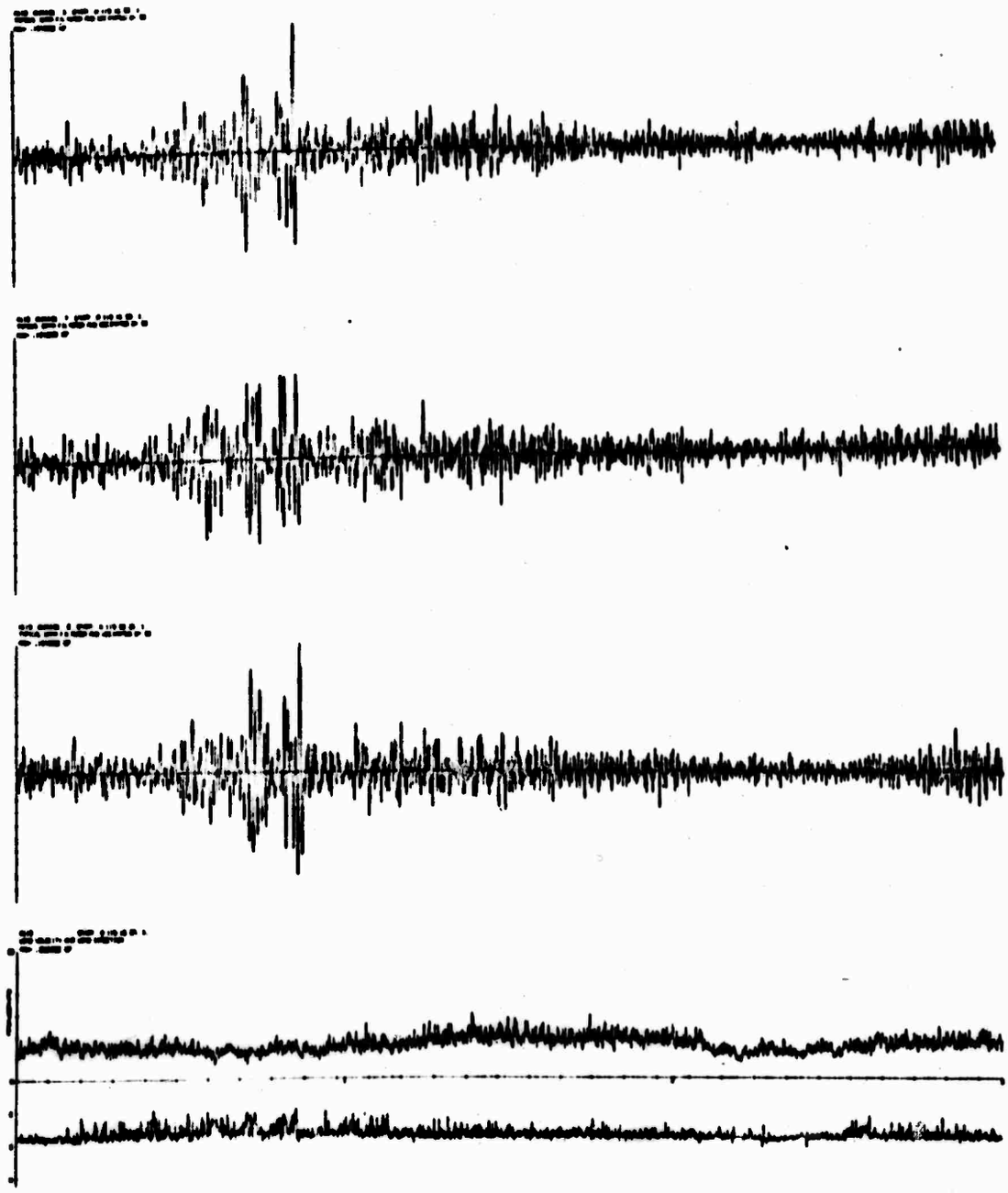

Figure 7. Examples of decimated data from the 5 km microbarograph array and the meterological instruments.

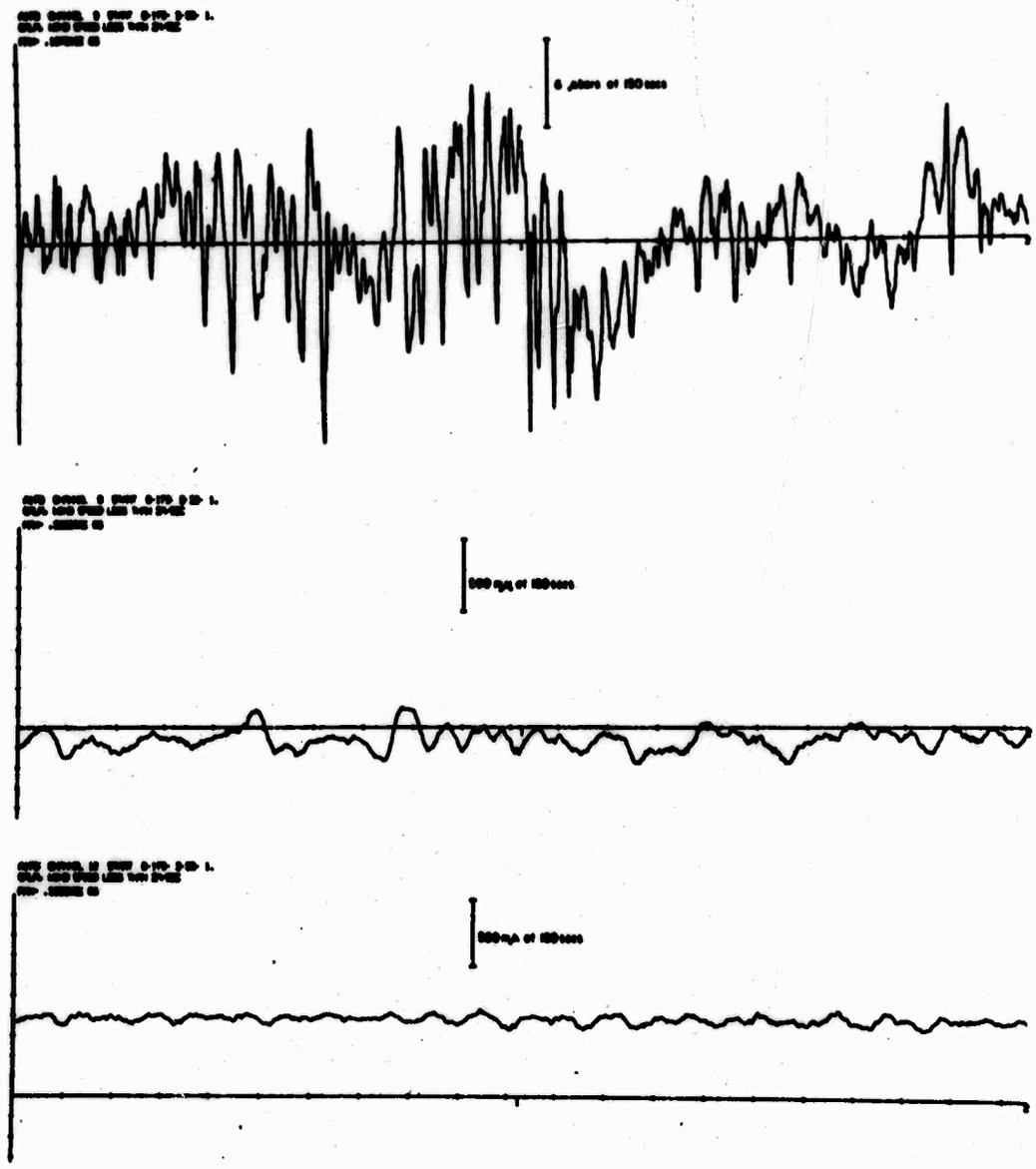

Figure 8. Data from the microbarograph on the surface (Ch. 3), the seismograph on the surface (Ch. 12) during a calm period (wind less than 2m/sec).

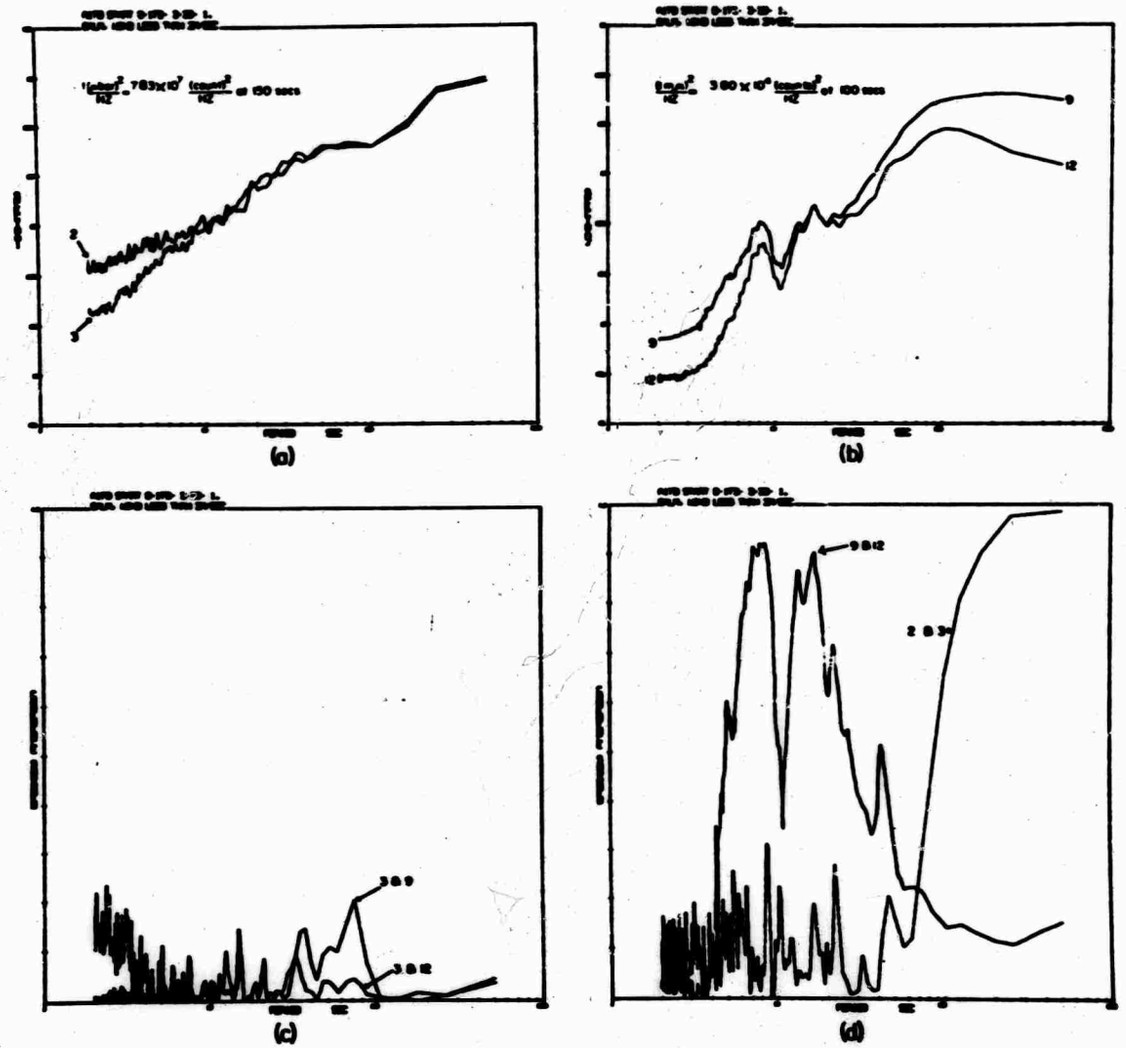

Figure 9. Spectra and coherences for data taken during a calm period (Figure 7).

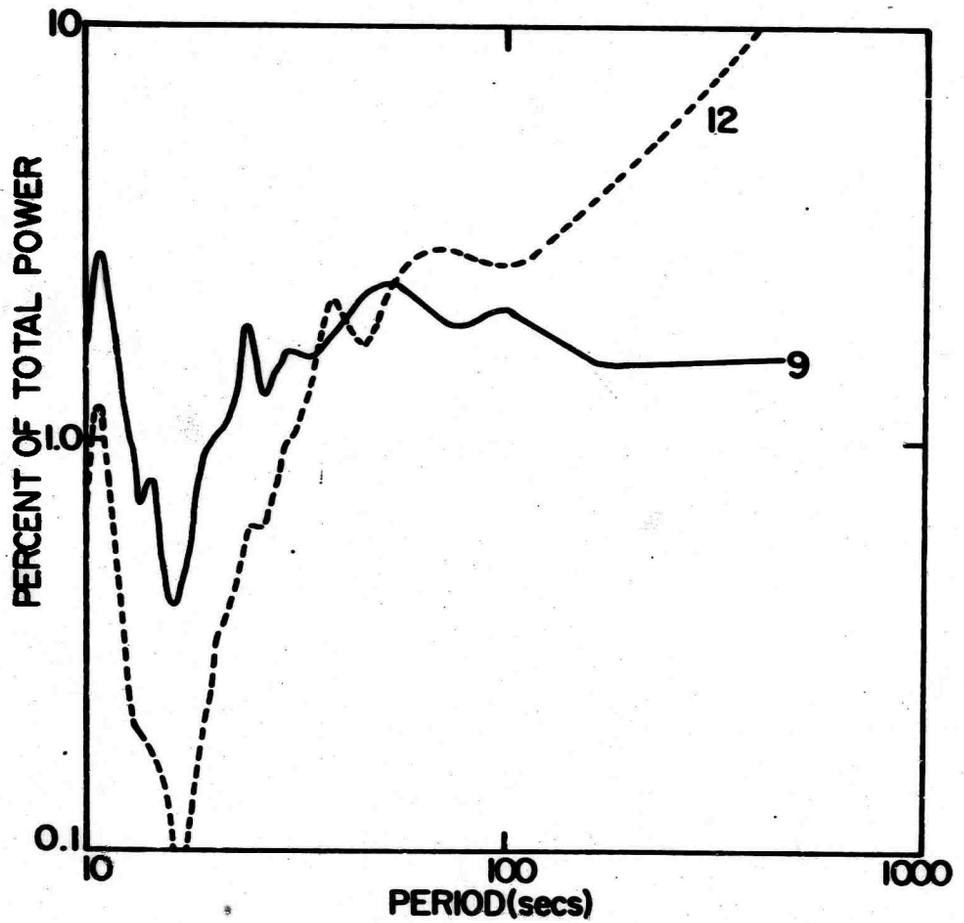

Figure 10. The relationship between the percent of system noise in the total power as a function of period during a calm period.

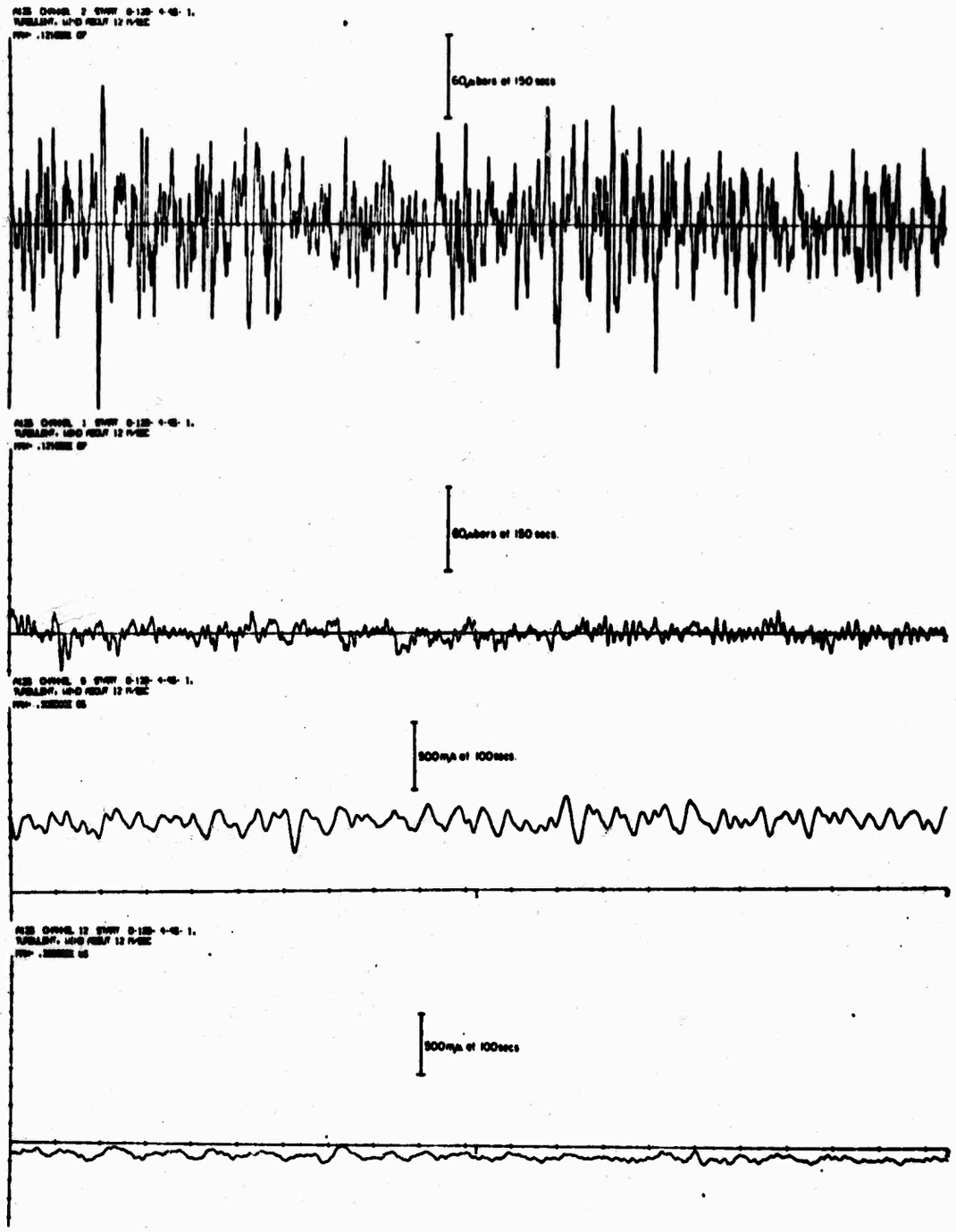

Figure 11. Data from the microbarograph at the surface (Ch. 2) and in the mine (Ch. 1), and from the seismograph at the surface (Ch. 9) and in the mine (Ch. 12) during a turbulent period (wind about 12m/sec).

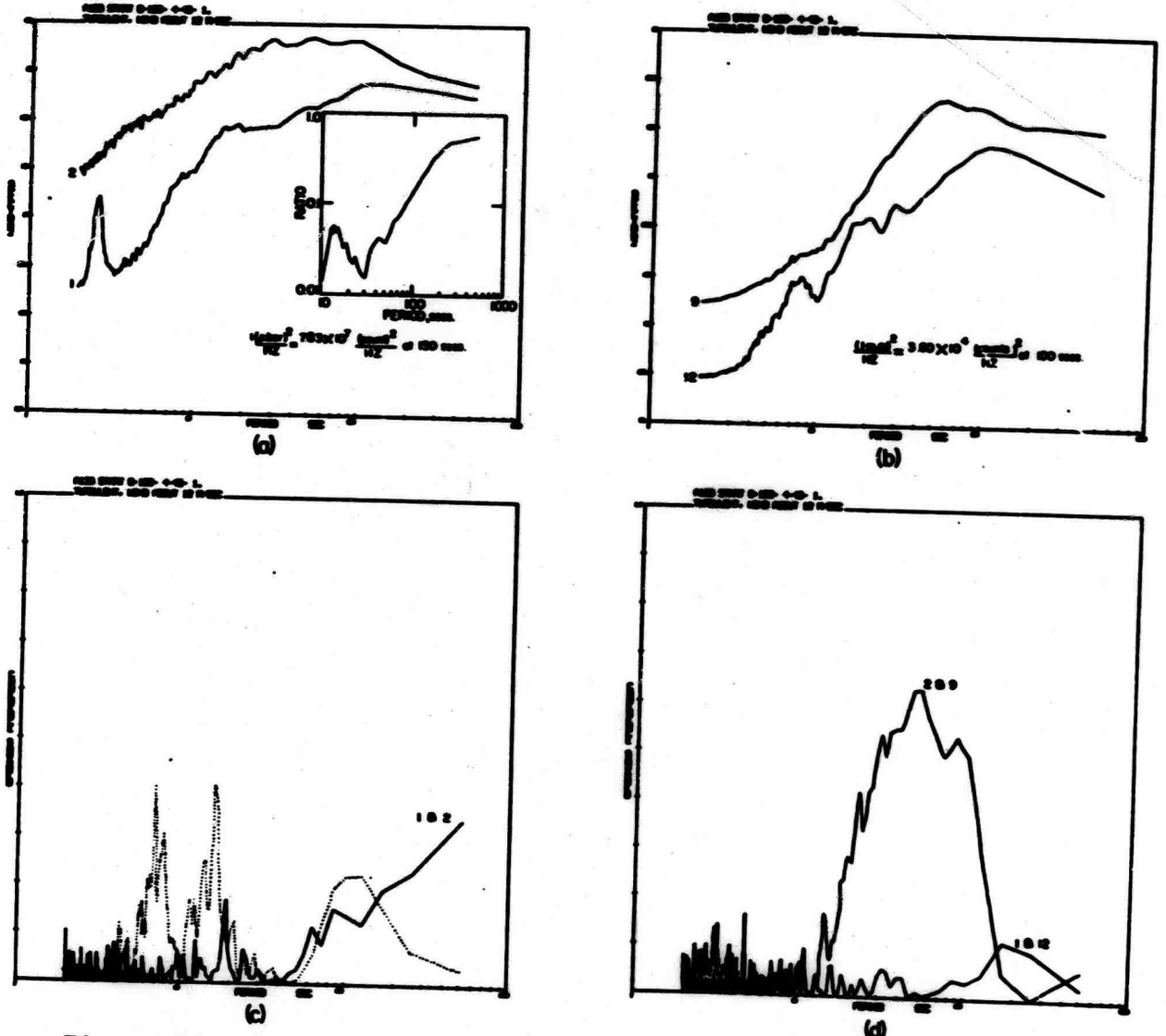

Figure 12. Spectra and coherences for data taken during a turbulent period (Figure 11).

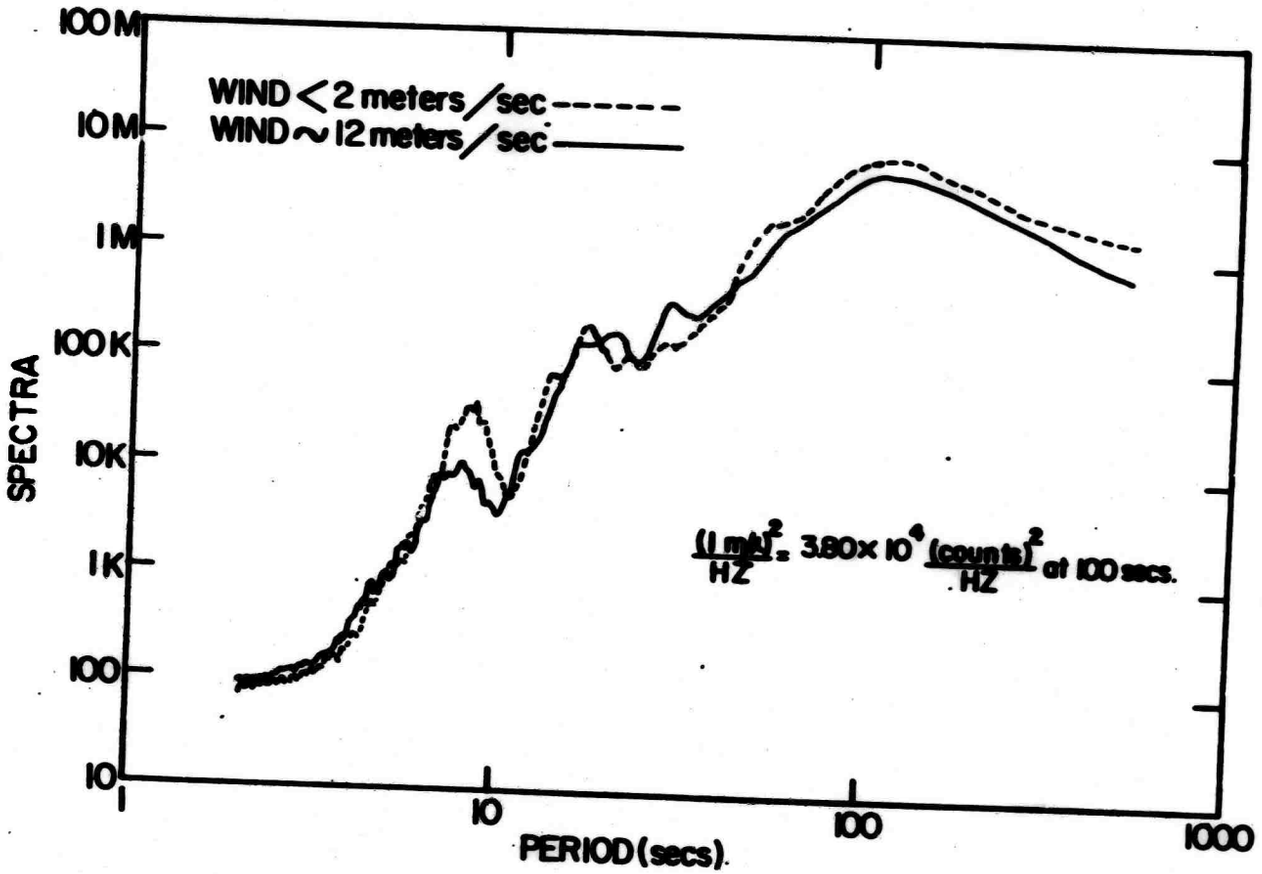

Figure 14. Comparison between the spectra for the mine seismograph during the calm and turbulent periods.

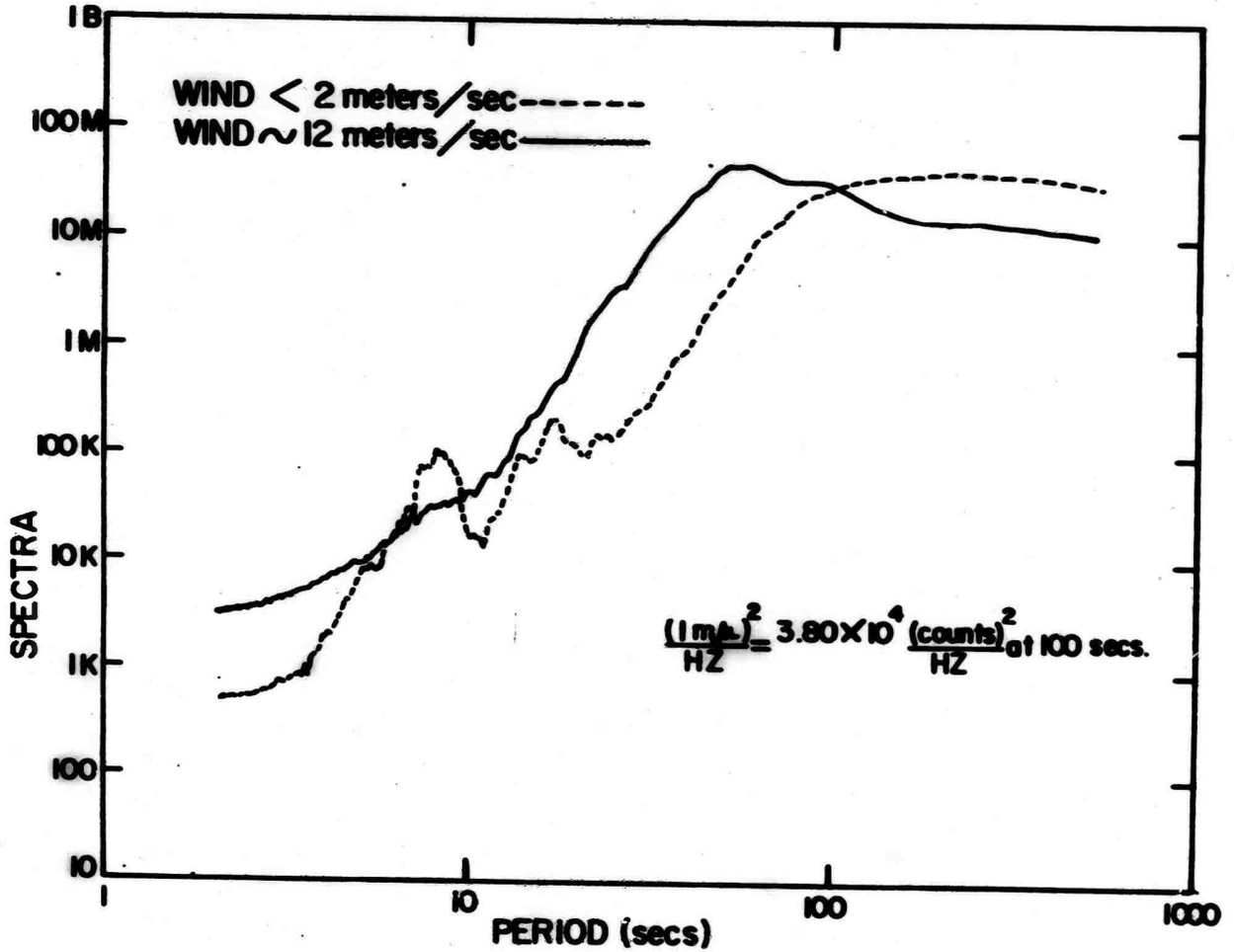

Figure 13. Comparison between the spectra for the surface seismograph during calm and turbulent periods.

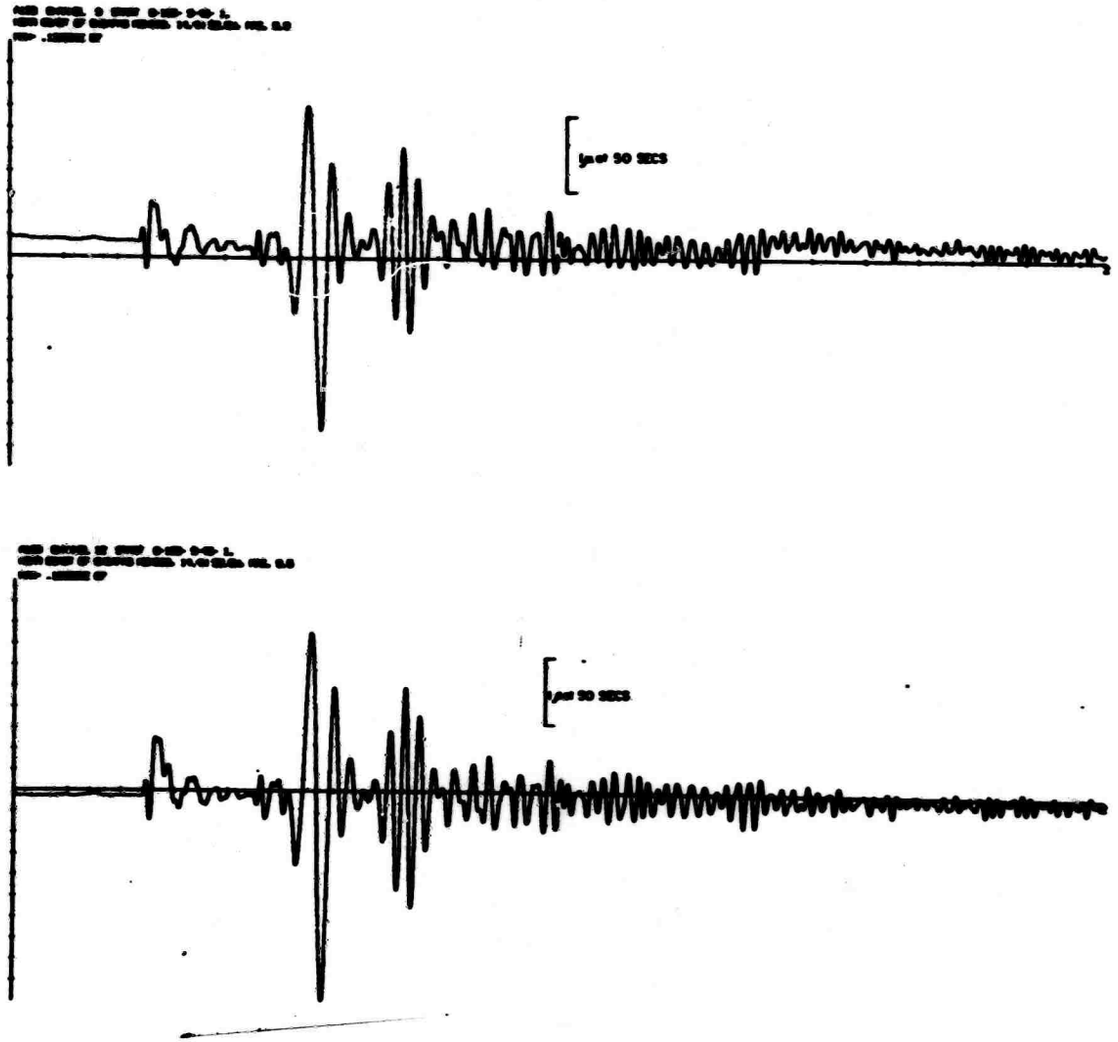

Figure 15. Seismograms recorded at the surface and in the mine for an earthquake near Chiapas, Mexico, magnitude 5.5.

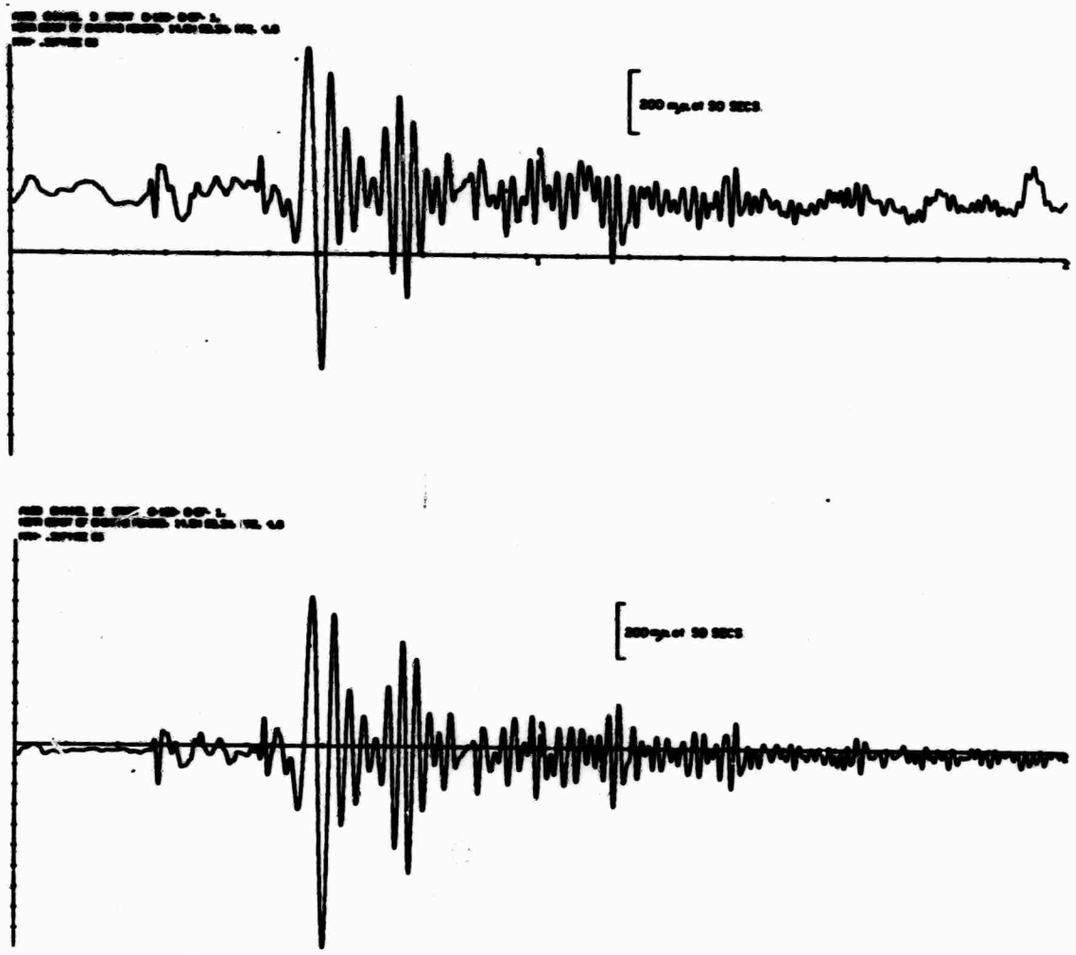

Figure 16. Seismograms recorded at the surface and in the mine for an earthquake near Chiapas, Mexico, magnitude 4.6.

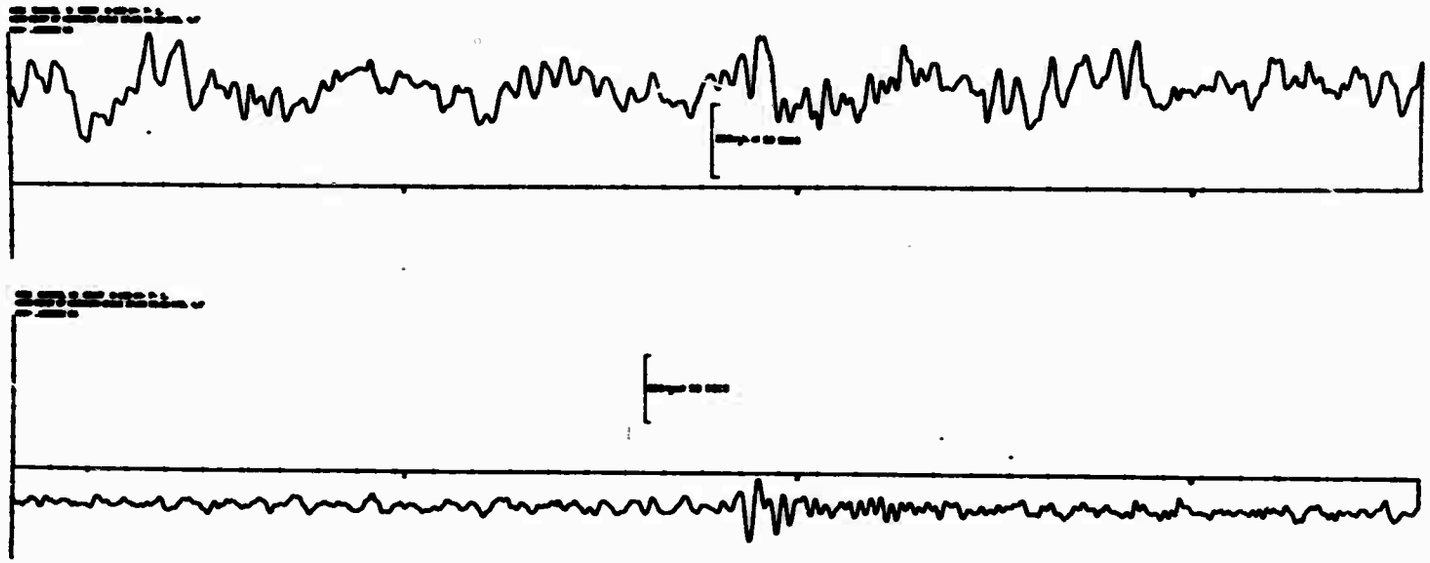

Figure 17. Seismograms recorded at the surface and in the mine for an earthquake near the coast of northern Chile, magnitude 4.7.

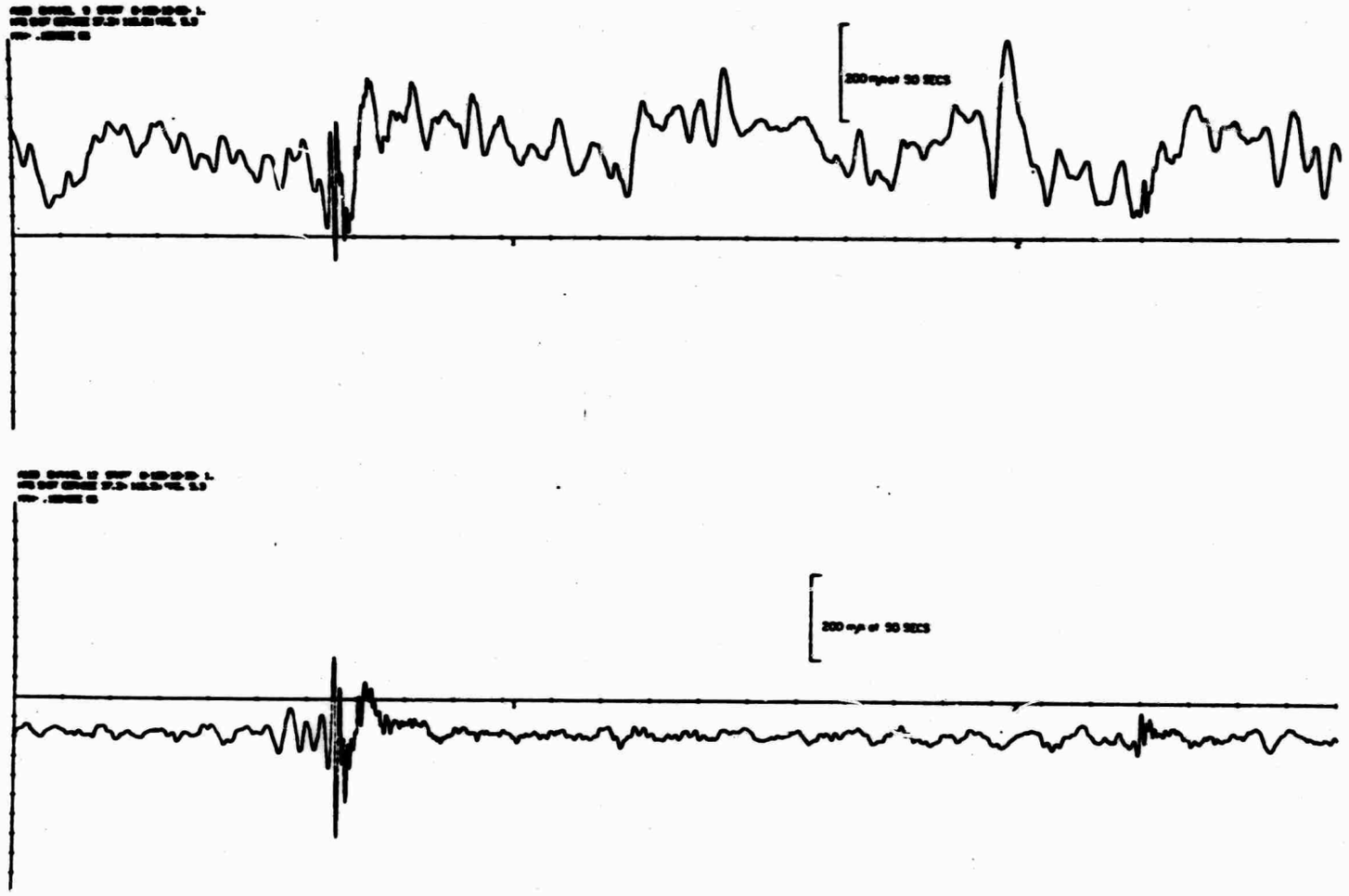

Figure 18. Seismograms recorded at the surface and in the mine for the NTS shot Cornice, magnitude 5.3.

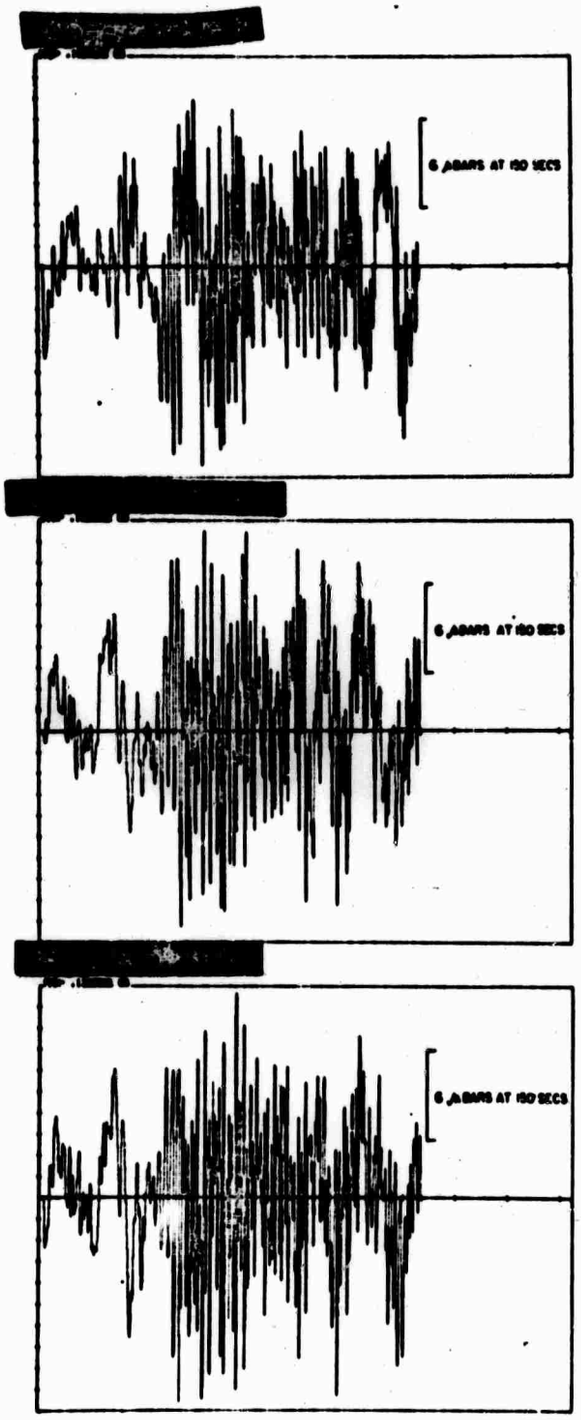

Figure 19. Microbarograms for the 3-element 5 km recorded during the passage of an acoustic wave from a French hydrogen bomb explosion.

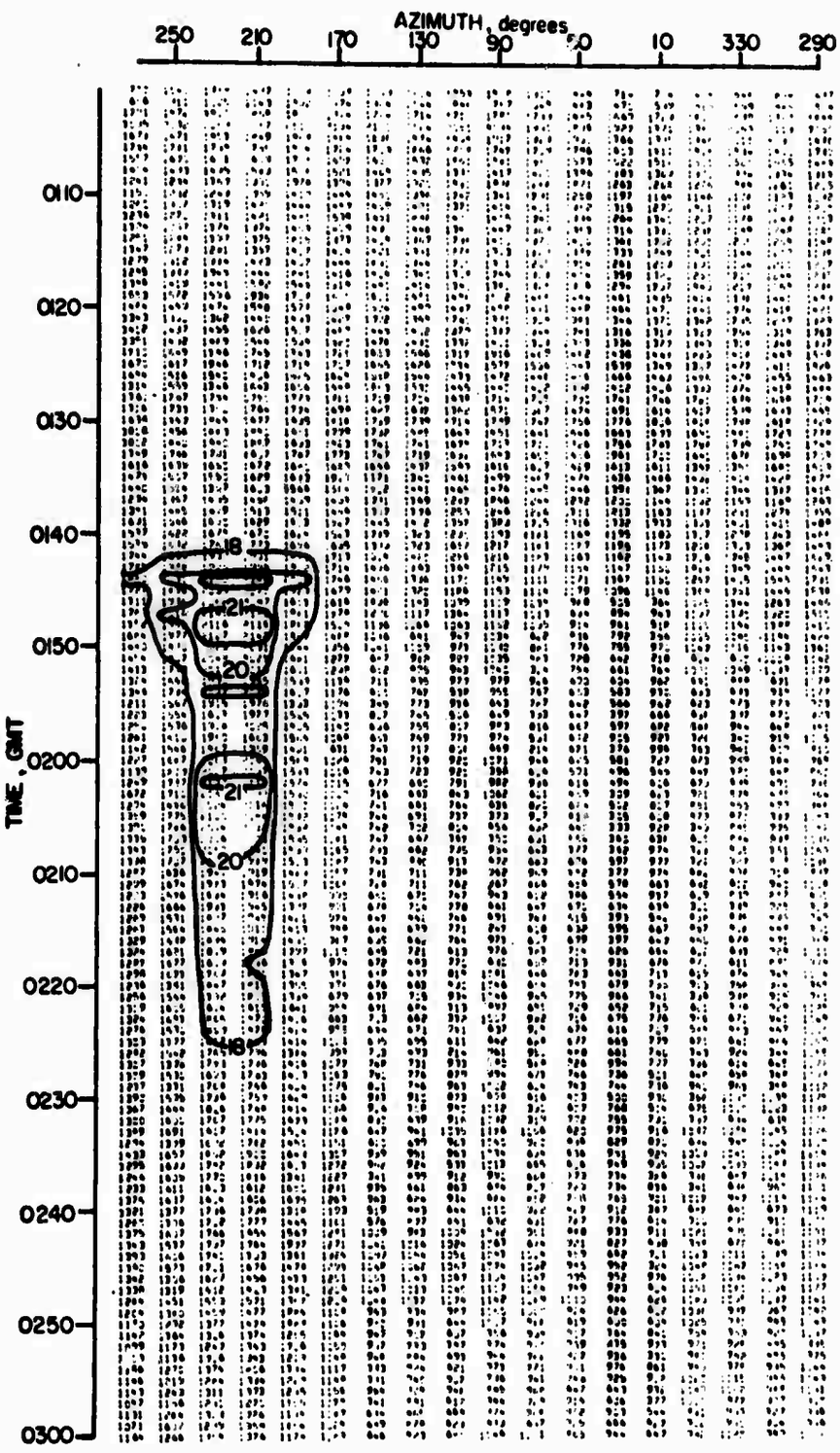

Figure 20. Output from the beam steering program operating on data shown in Figure 18, undecimated. Azimuth 0-360 degrees.

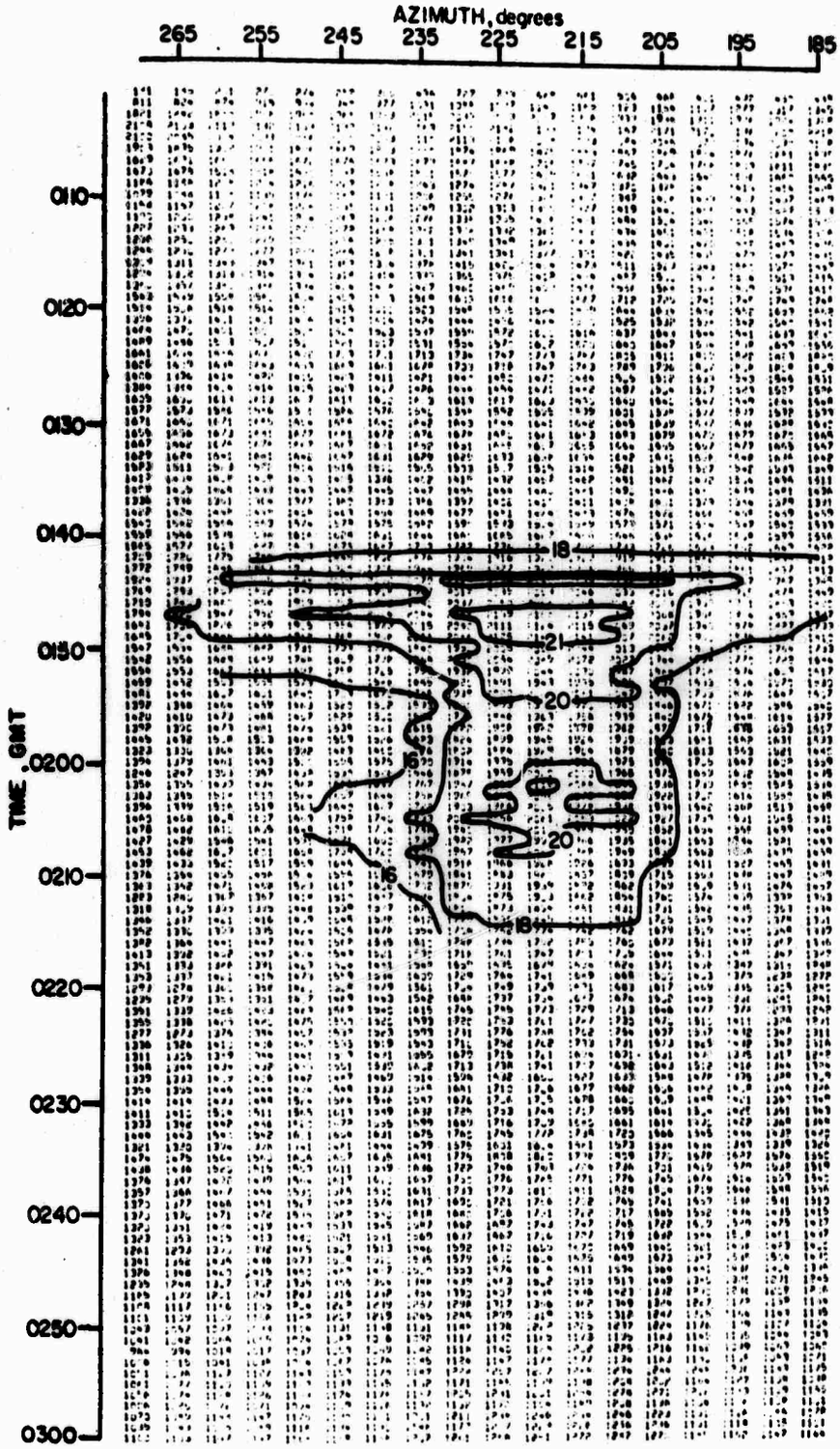

Figure 21. Output from the beam steering program operating on data shown in Figure 18, undecimated. Azimuth 180-270 degrees.

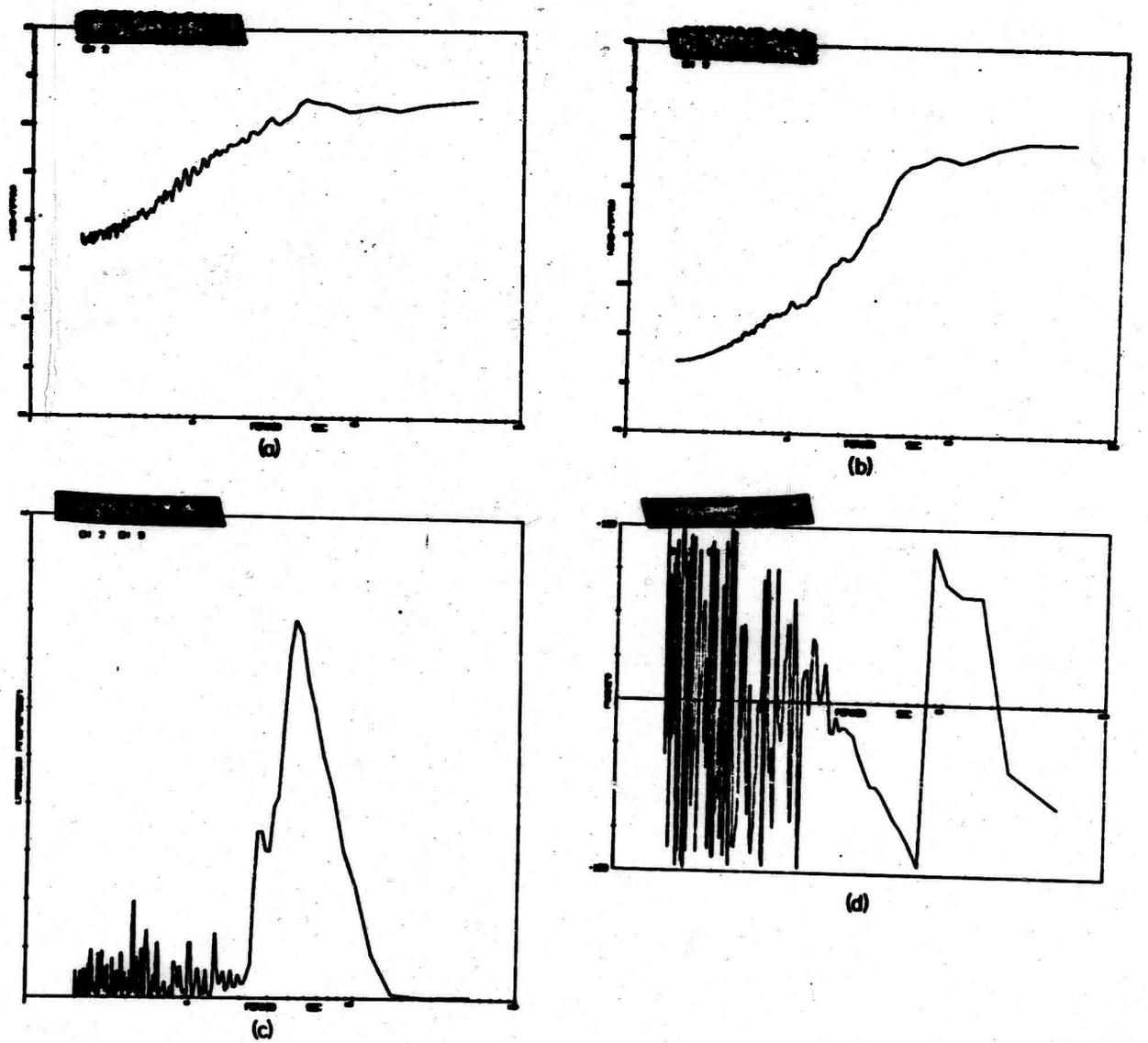

Figure 22. Spectra of microbarograms and seismograms taken during the passage of the acoustic wave and the coherences between them.

TABLE 1

Channel	Designation	Coordinates (km)	Elevation (m)
1	Study Butte (SB)	---	---
2	Grand Saline (GS)	0,0	119
3	Van Zandt (VZ)	-0.20,0.26	116
4	Sabine River (SR)	0.22,0.30	110
7	Camel Rock (CR)	-2.08,4.35	134
8	Tres Cuevas (TC)	3.65,3.37	143

TABLE 2

Channel	Designation
9	Surface vertical (SZLP)
10	*Surface radial (SRLP)
11	*Surface transverse (STLP)
12	Mine vertical (MZLP)
13	*Mine radial (MRL)
14	*Mine transverse (MTLP)

* Radial and transverse with respect to NTS

REVIEW OF RECENT RESEARCH AT COLUMBIA UNIVERSITY ON THE DISCRIMINATION OF UNDERGROUND EXPLOSIONS FROM EARTHQUAKES

By

Lynn R. Sykes

Lamont-Doherty Geological Observatory of Columbia University

Palisades, New York 10964

INTRODUCTION

This paper reviews recent work by members of the seismology group at the Lamont-Doherty Geological Observatory of Columbia University on the detection and discrimination of underground explosions from earthquakes. One of our main interests for several years has been in the field of long-period seismic waves. Various discriminants using long-period surface waves -- such as ratios of 1) 50 sec Rayleigh wave amplitudes and m_b, 2) 20 sec Rayleigh waves and m_b, 3) 20 and 50 sec Rayleigh waves, and 4) long-period Love waves and m_b -- appear to be highly reliable at teleseismic distances. The discrimination threshold using surface wave data from high-gain, long-period instruments at Ogdensburg, N.J., is $m_b = 3.8$ at 30° for events in western North America and 4.4 at 70° for two other source areas.

This paper describes the principal points of this long-period research on discrimination and discusses some of the remaining problems and the prospects for their resolution. My co-workers Savino, Molnar and Ward describe some of this research in more detail in other papers at this conference. In addition, I will discuss research on long-period body waves and on new information about the tectonic structure of island arcs as it pertains to the detection problem. These studies of arcs provide important data about the more accurate location of seismic events, the consistency of focal mechanisms of earthquakes and signal character and frequency content for various paths through the inhomogeneous structure of arcs.

1. M_s-m_b discriminants for periods greater than 20 sec

Molnar et al (1969) in a recent article in Nature and Savino and Molnar (this conference) describe our recent work on M_s-m_b for earthquakes, announced underground explosions, and presumed explosions in four areas -- 1) the western United States, 2) the Aleutians, 3) Novaya Zemlya and vicinity and 4) Central Asia. Liebermann and Pomeroy and others previously used data from the WWSSN and LRSM networks for regional studies of M_s-m_b. Our recent work has concentrated in the period range 15 to 70 sec using data from a set of low noise, high-gain instruments that have been in operation in a mine observatory at Ogdensburg, New Jersey.

For a given m_b surface waves from explosions are consistently smaller for underground explosions than for earthquakes for all of the more than 500 events we studied. This difference or discriminant is nearly always more pronounced for 50 sec waves than for those of shorter periods.

Table 1 illustrates the detection threshold for surface waves from underground explosions and the discrimination threshold for the four regions we investigated. Since the surface waves from

earthquakes and explosions are so different in size for a given m_b, it is important to distinguish the detection threshold of surface waves from underground explosions from the discrimination threshold of explosions and earthquakes. The discrimination threshold is taken as the body-wave magnitude at which surface waves are detected and measured for all earthquakes of that size. At Ogdensburg the discrimination threshold is m_b = 3.8 at 30° and 4.4 at 70°.

The lower boundary of the earthquake population is very sharp for many regions, especially for the Aleutians (Figure 1). Hence, the ability to discriminate between explosions and earthquakes is much better than merely the capability to detect surface waves from explosions. The absence of a surface wave for a detected body-wave signal places a suspected event in the explosion population.

The earthquake population scatters very little on an M_s-m_b plot for the Aleutians. The small scatter probably can be attributed to the consistency of the focal mechanisms of earthquakes. Studies of other regions indicate that focal mechanism solutions are extremely consistent for events as large as magnitude 8 and even for those as small as micro-earthquakes, i.e. magnitudes 0 to 3. The value of focal mechanism investigations to the discrimination problem has often been overlooked since first motions of P waves were difficult to determine for magnitudes below 5 1/2. The consistency of focal mechanisms in a given region, however, appears to contribute significantly to the small scatter in M_s-m_b for earthquakes. Using only the Ogdensburg station, some of the lowest values of M_s from earthquakes in the western United States correspond to azimuths near a node in the radiation pattern for Rayleigh waves. The much larger Love waves at these azimuths, and focal mechanism solutions confirm this for some of the aftershocks of underground explosions.

A knowledge of the consistency and type of focal mechanism permits a choice of optimum azimuths for the detection of Rayleigh waves. Additional stations and the use of long-period Love waves can provide good discrimination when the Rayleigh waves for a single station are near a node.

2. Functional relationship of M_s-m_b and usefullness of criteria for m_b less than 5.

Plots of M_s (40 sec) vs. m_b and M_s (20 sec) vs. m_b for underground explosions recorded at Ogdensburg define an extremely narrow band or line that is very nearly parallel to the earthquake population. In our studies there is no indication of any convergence in the two populations at teleseismic distances down to the smaller explosions for which surface waves were detected. Thus, finite source size can be ruled out as a major physical cause at long-periods of the observed discrimination between explosions and earthquakes.

Discrimination of earthquakes and explosions is improved when M_S is determined for 40 to 70 sec Rayleigh waves instead of 20 sec waves. Surface waves of 40 sec period can often be seen at teleseismic distances when the 20 sec waves either are not detectable or are masked by 20 sec microseisms.

M_S determinations for 20 sec waves, and especially those for 16 sec waves, scatter considerably. This scatter is probably caused by differences in attenuation and by multipath effects at these shorter periods. Waves of 40 sec and larger periods are not nearly as sensitive to these variations, and, hence, are not as subject to significant regional variations.

A major problem for m_b less than 5 exists if m_b determinations are not consistent or if only one or two stations are used to determine an average m_b. For events in western North America m_b determinations by the USC&GS are usually subject to these problems. Their m_b values often contribute significantly to scatter in M_S-m_b plots for $m_b < 5.5$. This problem can easily be overcome with sufficient short-period measurements of m_b and by using more appropriate formulas for magnitude determinations.

3. Long-period noise and the masking of small events by larger earthquake signals.

The minimum in the earth's seismic noise near 40 sec reported by Savino is obviously very important to the detection of long-period seismic waves. The utilization of this noise minimum, of course, necessitates the elimination of instrumental and environmental noise at long periods as was done for the Ogdensburg installation. An important feature of the earth noise at periods greater than 35 sec is its very small temporal variation. In contrast, microseismic noise near 20 sec can vary by a factor of 10 to 100. Unlike long-period microseisms, which can propagate great distances, noise with periods greater than 35 sec appears to be of atmospheric origin and to be uncorrelated on three orthogonally oriented seismographs. Hence, quiet sites for periods of 35 sec or greater should be sought with the nature of the noise source in mind -- i.e., quiet atmospheric conditions. Sites that are noisy at 20 sec, for example, may be quiet at 40 sec. It may be possible to find sites where the noise continues to drop for periods greater than 40 sec. Since the very long-period noise is not correlatable, it probably can be significantly reduced with arrays and with matched filters. In addition to verticals, horizontal components should be very valuable in noise supression. Microseisms with periods of 20 to 35 sec are very uniform in wave character and could be supressed relatively easily.

One of the main problems with long-period discriminants is the masking of small surface waves by wave trains of large earthquakes. Although matched filters and multiple stations can reduce this

problem, regional variations in attenuation, dispersion and multipath effects make this difficult for 16 to 20 sec surface waves. These three effects are probably much smaller for 40 to 70 sec waves. Thus, it should be much easier to detect a characteristic 40 to 70 sec signal than a 16 to 20 sec one in the coda of a large shallow earthquake. We intend to verify this hypothesis as soon as possible.

4. Long-period discriminants - surface waves.

Our investigations (Figure 2) revealed a systematic difference in the ratio of 20 to 50 sec Rayleigh waves for explosions and earthquakes. In the Aleutians the depth of focus and possibly certain unfavorable orientations of the focal mechanism appear to make this ratio look 'explosion-like' for some earthquakes. In that region this discriminant appears to work for shallow earthquakes, but not for those as deep as about 40 km. This is understandable from calculated excitation functions such as those of Tsai. This requires further experimental verification using sources with well determined depths. It should be noted nonetheless that M_s-m_b discriminants still work for all of these events.

One of the main virtues of using solely long-period discriminants, such as the ratio of 20 to 50 sec Rayleigh waves, is that it would be very difficult to generate signals from multiple explosions that look similar to those of earthquakes over a broad frequency range.

The 20 to 50 second ratio is regionally dependent. Hence, it must be used cautiously when different source regions are involved in an intercomparison. A 16 to 50 sec ratio for Rayleigh waves provides greater discrimination than the 20 to 50 ratio for nearby events, but it is also more regionally dependent.

These discriminants appear to work for earthquakes and explosions of comparable depths and for so-called 'high stress' earthquakes. Although triggered tectonic strain added to the explosion signal could degrade M_s-m_b and 20 to 50 sec discriminants, this had not been a serious problem for any of the announced underground explosions or presumed explosions we examined.

5. Long-period discriminants - P and S waves.

First motions can be determined with nearly 100% reliability when long-period rather than short-period P waves are employed (Figure 3). This technique is limited to about $m_b > 5.5$ for WWSSN long-period instruments, but might be lowered to 5.0 or less with long-period arrays or instruments peaked between 2 and 10 sec. Although microseisms are large at these periods, their phase velocity is different enough from that of teleseismic P waves to permit separation with arrays.

Long-period S and SS are the most conspicuous body phases on the Ogdensburg high-gain records. Figure 4 illustrates long-period P, S and surface waves from three earthquakes of magnitude m_b = 4.3 to 4.4 It is important to recognize that long-period body waves are prominent on records of many earthquakes. Chander successfully synthesized long-period wave trains following S and SS and explained them as S - coupled PL waves. Since these waves are probably not subject to large multipath effects, they could be used with matched filters for the detection of events buried either in noise or in the surface waves of a larger event.

6. Cause of long-period and M_S-m_b discriminants.

Several mechanisms have been proposed to account for the great differences in the spectra on underground explosions and earthquakes -- differences in 1) source size, 2) source time functions, and 3) depth of focus.

The large consistent differences in the ratio of 20 to 50 sec Rayleigh waves for explosions and earthquakes cannot be ascribed to differences in source size for the magnitude range we studied. Most of these events may be considered point sources for these longer periods. Also, no evidence was found of any convergence in the earthquake and explosion populations as would be expected for a finite source size for earthquakes.

Likewise, depth of focus does not appear to be major controlling factor, but this result is not as well tested as finite source size. More close in measurements of the long-period spectrum of underground explosions are needed to verify that the main factor responsible for discrimination is a difference in source time function. These measurements should be made in the elastic region outside the region of permanent deformation to confirm if the source time function for explosions differs from that for earthquakes. As discussed by Molnar, the spectra of long-period P waves can be used to decide whether the source time function is different for earthquakes and underground explosions.

7. Short-period discriminants and effects of non-uniform structures in Arcs.

The recognition that large cold slabs of lithospehere are underthrust to great depths in island arch and arc-like regions is of great importance to the detection-discrimination problem. The velocity and attenuation structure in these regions is decidedly asymetrical. Hence, errors in the calculated locations of earthquakes can occur unless the velocity structure is modeled adequately. As will be shown, seismic waves traversing certain parts of arcs are highly attenuated while others are of very large amplitude and can be rich in high frequencies.

Seismic experiments in several arcs reveal that the main dipping

seismic zone is very thin and that it does not outcrop on the island chain but outcrops within the deep-sea trench. Figures 5 and 6 illustrate this for sections through the Tonga and Kuril arcs. Thus, it would be extremely difficult to place and hide an explosion within the main seismic zone. Since only a relatively few shallow earthquakes occur on or near the island chain, the search for suspected events is relatively easy. Also, Katsumata and Sykes found that focal mechanisms of several earthquakes near island chains are of the normal-fault type. Hence, most seismic stations detect dilatational first motions at teleseismic distances. This is a positive discriminant for earthquakes larger than about m_b = 5.5.

K. Jacob developed a computer program for the 3-dimensional tracing of seismic rays through the inhomogeneous velocity structures of arcs. Seismic velocities in the downgoing slab of lithosphere (Figure 7) are as much as 7% higher than those in adjacent parts of the mantle. The energy content of the P and S waves may differ by a factor of 100. These anomalies drastically affect computed locations of earthquakes, $dT/d\Delta$ as measured by seismic arrays, the complexity of the P wave, and its frequency content. The next two figures from Jacob's study illustrate different types of P waves for the Long Shot explosion in the Aleutians.

The relatively simple P wave at ESK (Figure 8) probably travelled only a short path through the downgoing slab. At BRW (Figure 8) the presence of two separate P waves is attributed to propagation as a refracted wave off the top of the downgoing lithospheric plate and to propagation through the more normal mantle. The signal of long duration at KDC may have propagated along the slab almost its entire length. Dipping plates of lithosphere near the receiving ends of a ray path can also act as natural amplifiers. Figure 9 shows a fairly simple P wave at GUA for a path that does not ascend a dipping seismic zone and a complex P wave at HNR that travels either in the dipping seismic zone of the Solomon arc or between the seismic zone and the free surface. The P-wave signal at HNR is much longer in duration and contains a greater amount of energy than that at GUA. Both rays, however, have nearly the same path near the source in the Aleutian arc, and thus they mainly differ at the receiving end.

Thus, realistic seismic models of arcs can be used to predict the signal character, amplitude, and first motion for a proposed station or for a proposed network. We can predict, for example, which stations will have a simple short-period P wave. Advantage can be taken of the high Q zones for the location of stations.

8. Attenuation of seismic waves

Molnar and Oliver (1969) (Figure 10) made a world map showing paths for which high-frequency S waves (Sn) are propagated very

efficiently and paths with inefficient transmission. The Basin and Range province, including the Nevada Test Site, is a region of high attenuation. Shield and platform areas exhibit efficient propagation of high frequencies in the lithosphere. Current work at Lamont involves a more careful mapping of the zones of high attenuation behind most island arcs.

9. Summary

A comparison of long-period surface waves and body waves appears to be the most reliable method developed thus far for the discrimination of underground explosions and earthquakes. In particular, M_S at 40 sec vs. m_b nearly always provides greater discrimination than M_S at 20 sec vs. m_b. This better discrimination at 40 sec or greater periods is attributed to 1) a minimum in earth noise near 40 sec, 2) smaller variation in 40 sec amplitudes from region to region and 3) the very small temporal variation in earth noise at these longer periods. The ratio of 20 to 40 sec Rayleigh waves also provides good discrimination, but proper account must be taken of the effects of depth of focus upon the excitation of these waves. Love waves and data from additional stations can provide discrimination when Rayleigh waves from a single station are near a nodal plane.

There is no indication of any convergence in the earthquake and explosion populations in our M_S - m_b studies. Discrimination, particularly at long periods, seems to be attributed mainly to a difference in the source time function of explosions and earthquakes.

Probably the most serious problem in the use of long-period waves is the masking of small signals by those of large earthquakes. Waves of periods greater than 40 sec may be easier to detect within these large signals than 20 sec waves.

Many of the complexities in P wave signals are caused by the non-radially symmetric structure of island arcs. Three-dimensional ray tracing can be used to model these effects, to provide accurate epicentral locations in arcs, to compute the effect of these structures on $dT/d\Delta$ as measured by arrays, and to estimate the attenuation of body waves.

REFERENCES

Fedotov, S.A., 1965, Upper mantle properties of the southern part of the Kuril Island arc according to detailed seismological investigations, Tectonophysics, v. 2, p. 219-225.

Mitronovas, W., Isacks, B. and Seeker, L., 1969, Earthquake locations and seismic wave propagation in the upper 250 km of the Tonga island arc, Bull. Seismol. Soc. Amer., v. 59, p. 1115-1135, 1969.

Molnar, P., and Oliver, J., 1969, Lateral variations of attenuation in the upper mantle and discontinuities in the lithosphere, J. Geophys. Res., v. 74, p. 2648-2682.

Molnar, P., Savino, Sykes, L.R., Liebermann, R.C., Hade, G., and Pomeroy, P.W., 1969, Small earthquakes and explosions in western North America recorded by new high-gain, long-period seismographs, Nature, v. 224, p. 1268-1273.

Oliver, J., and Isacks, B., 1967, Deep earthquake zones, anomalous structures in the upper mantle, and the lithosphere, J. Geophys. Res., v. 72, p. 4259-4275.

Sykes, L.R., 1967, Mechanism of earthquakes and nature of faulting on the mid-oceanic ridges, J. Geophys. Res., v. 72, p. 2131-2153.

Sykes, L.R., Isacks, B., and Oliver, J., 1969, Spatial distribution of deep and shallow earthquakes of small magnitudes in the Fiji-Tonga region, Bull. Seismol. Soc. Amer., v. 59, p. 1093-1113.

TABLE I

Detection and Discrimination Capabilities of Long-Period, High-Gain Instruments at Ogdensburg, N. J. For Four Source Regions

	REGION	DISTANCE IN DEGREES	m_b DETECTION THRESHOLD TO OBSERVE 20-70 SEC SURFACE WAVES FOR ALL EARTHQUAKES, i.e., DISCRIMINATION THRESHOLD	m_b DETECTION THRESHOLD FOR SURFACE WAVES, FROM UNDERGROUND EXPLOSIONS
1.	Western United States, Gulf of California and offshore areas	30°-35°	3.8*	4.7*
2.	Aleutian Islands	70°	4.4	(5.5)**
3.	Novaya Zemlya	55°-65°	4.2-4.4	(5.3)**
4.	Central Asia	85°-100°	not enough data	5.7-5.9

*Using the magnitude formulas of Evernden. Larger m_b's are usually obtained by the USC&GS for events in western North America from different magnitude formulas.

**extrapolated

(after Savino et al, in preparation, 1970)

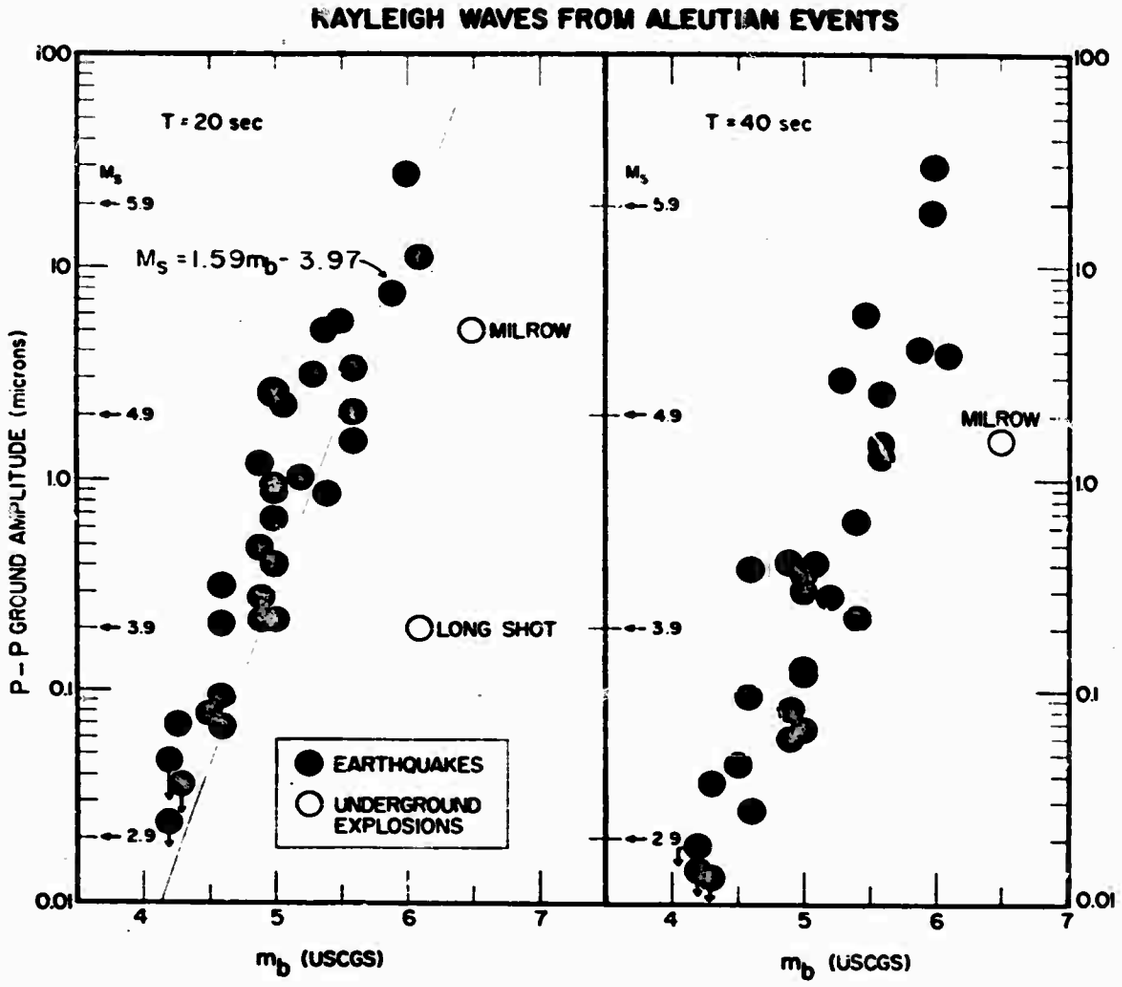

Figure 1. M_S determined from Rayleigh waves as function of m_b for earthquakes and underground explosions in the Aleutians. After Savino et al (in preparation). Note distinct gap between earthquake and explosion populations, the distinct lower limit of the earthquake population, and the small scatter of the earthquake data.

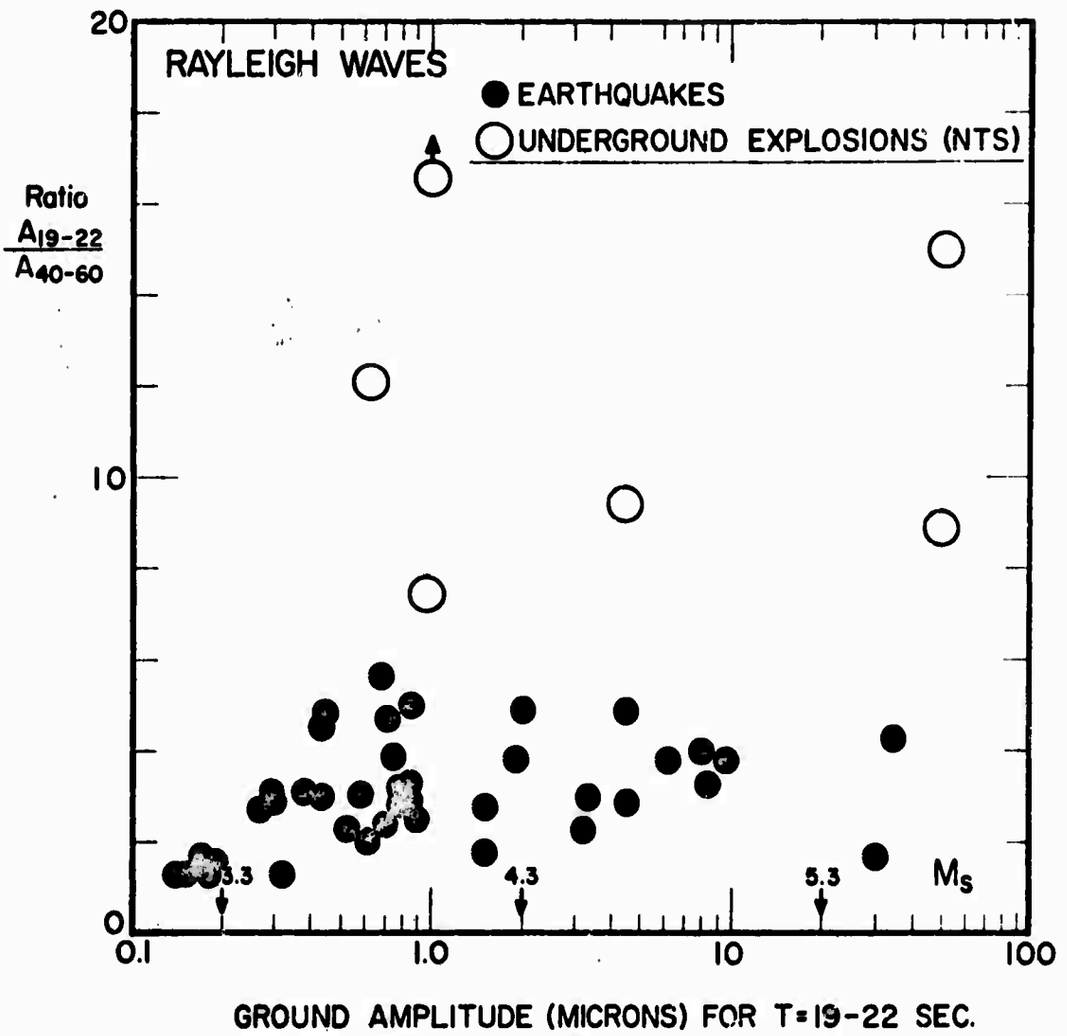

Figure 2. Ratio of 20 to 50 sec Rayleigh waves for underground explosions (open symbols) and earthquakes in the western United States, the Gulf of California and adjacent offshore areas. After Molnar et al (1969).

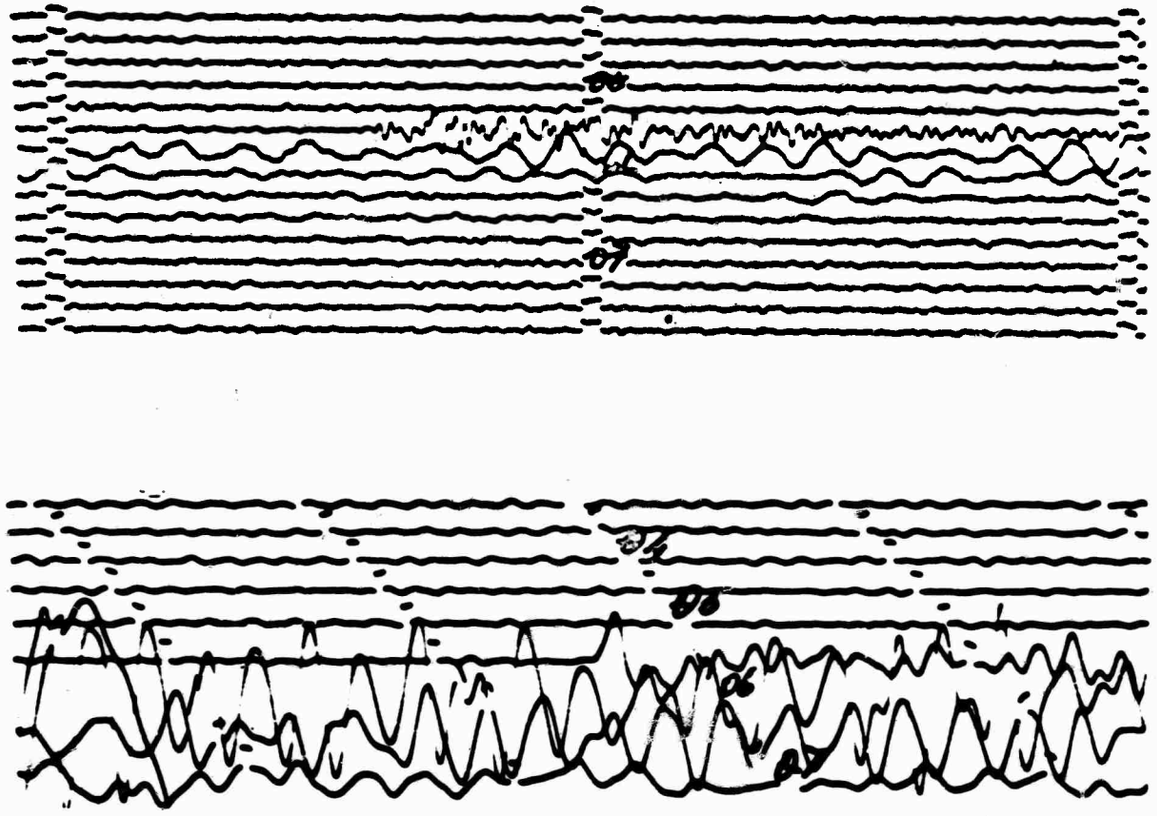

Figure 3. Comparison P wave first motions on vertical short-period instrumetns (above) and long-period (below) at Arequipa, Peru, for earthquake on East Pacific rise on March 7, 1963. Deflections represent minute marks. P wave arrives at 05h 59m. First motion is uncertain on short-period record but is clearly compressional on the long-period record. m_b = 5.5 - 6.0. After Sykes (1967).

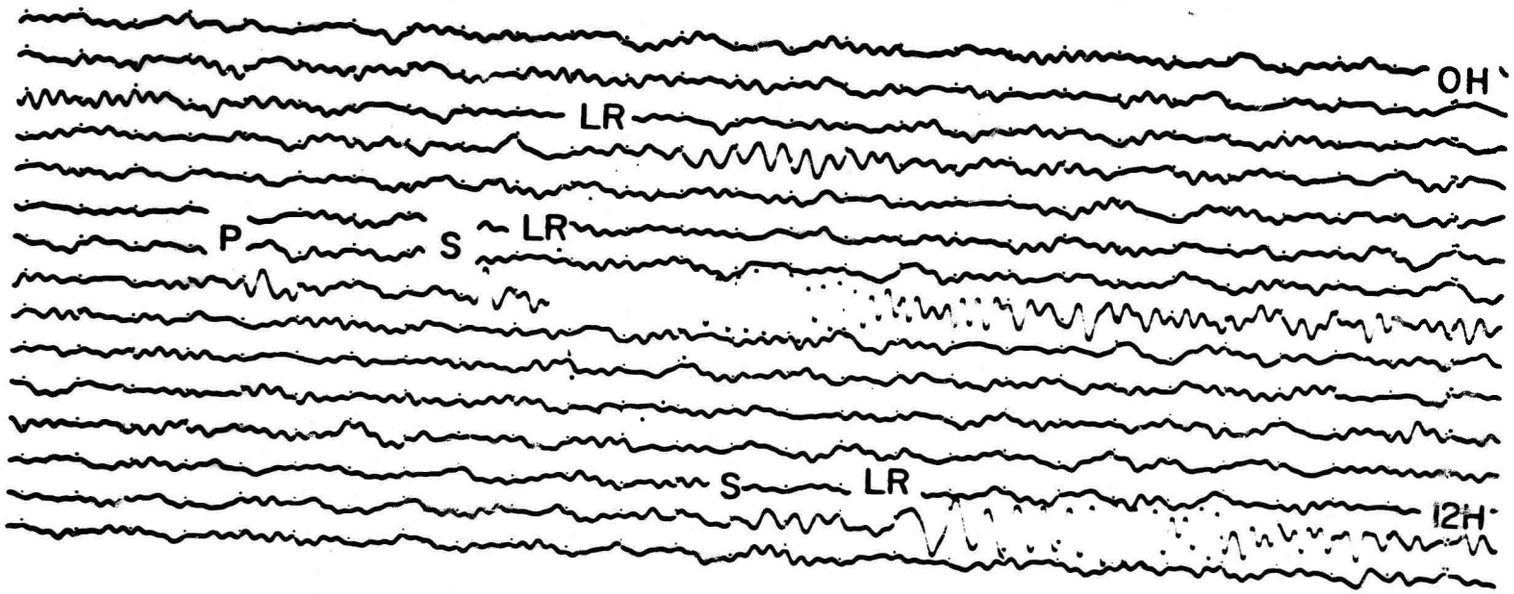

Figure 4. Long-period body waves and surface waves for three earthquakes as recorded on vertical component, high-gain seismograph in mine at Ogdensburg, N.J. 0 and 12 hour marks are indicated above trace; deflections denote minute marks. Earthquakes on June 17, 1969 with phase identified are from top to bottom: 1) South America, 24.3°S, 68.6°W, depth = 99 km, 01h 16m 22s, m_b = 4.3, Δ = 64°; 2) Puerto Rico, 19.0°N, 66.5°W, depth = 54 km, 05h 32m 57s, m_b = 4.4, Δ = 23°; 3) Mexico, 14.4°N, 93.7°W, depth normal, 11h 35m 13s, m_b = 4.3, Δ = 32°. Δ = distance. Locations and magnitudes from USC&GS.

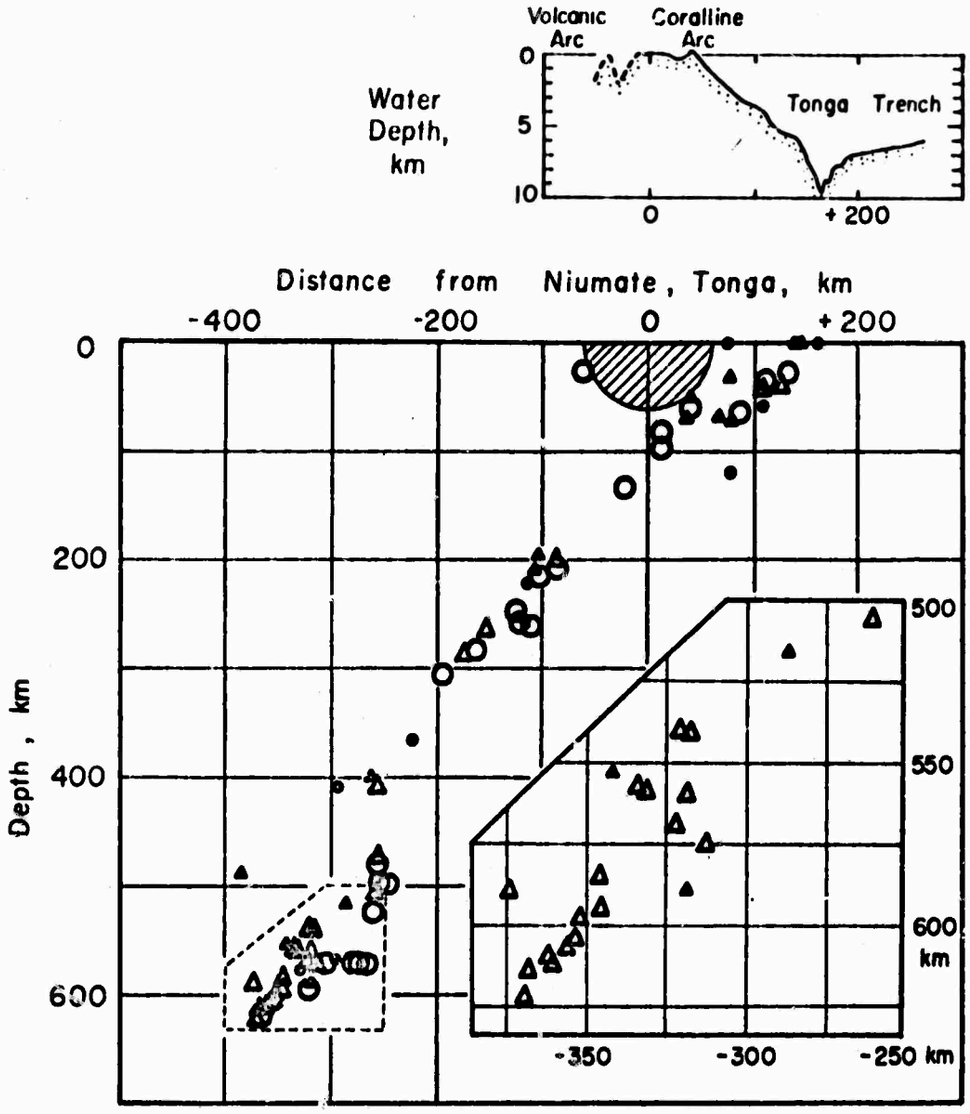

Figure 5. Hypocenters projected on to a vertical section through Tonga island arc of southwest Pacific. Insert at right shows enlarged view of dotted region for depths greater than 500 km. No small events out of a sample of 747 were detected from hatched region near the station on the coralline (non-volcanic) arc. Profile of Tonga trench shown (above) with vertical exageration 13 times. Note extreme thinness of seismic zone and that it outcrops in trench in deep water and not near islands. After Sykes et al (1969).

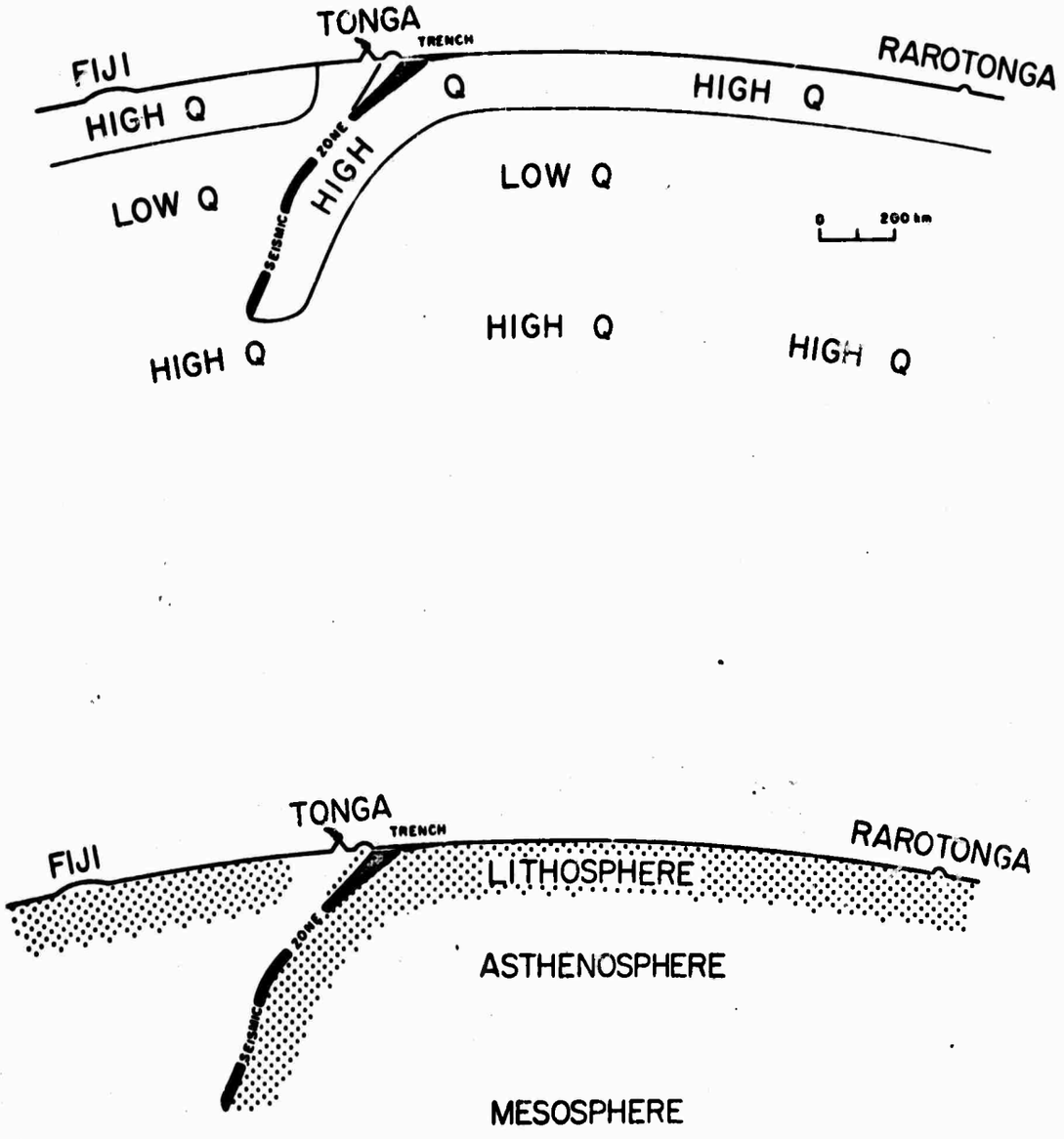

Figure 7. Vertical sections through Tonga arc showing high Q and low Q regions as determined from short-period S waves. Seismic velocities in the downgoing (high Q) slab are about 7% higher (Mitronovas et al, 1969) than in the surrounding mantle. After Oliver and Isacks (1967).

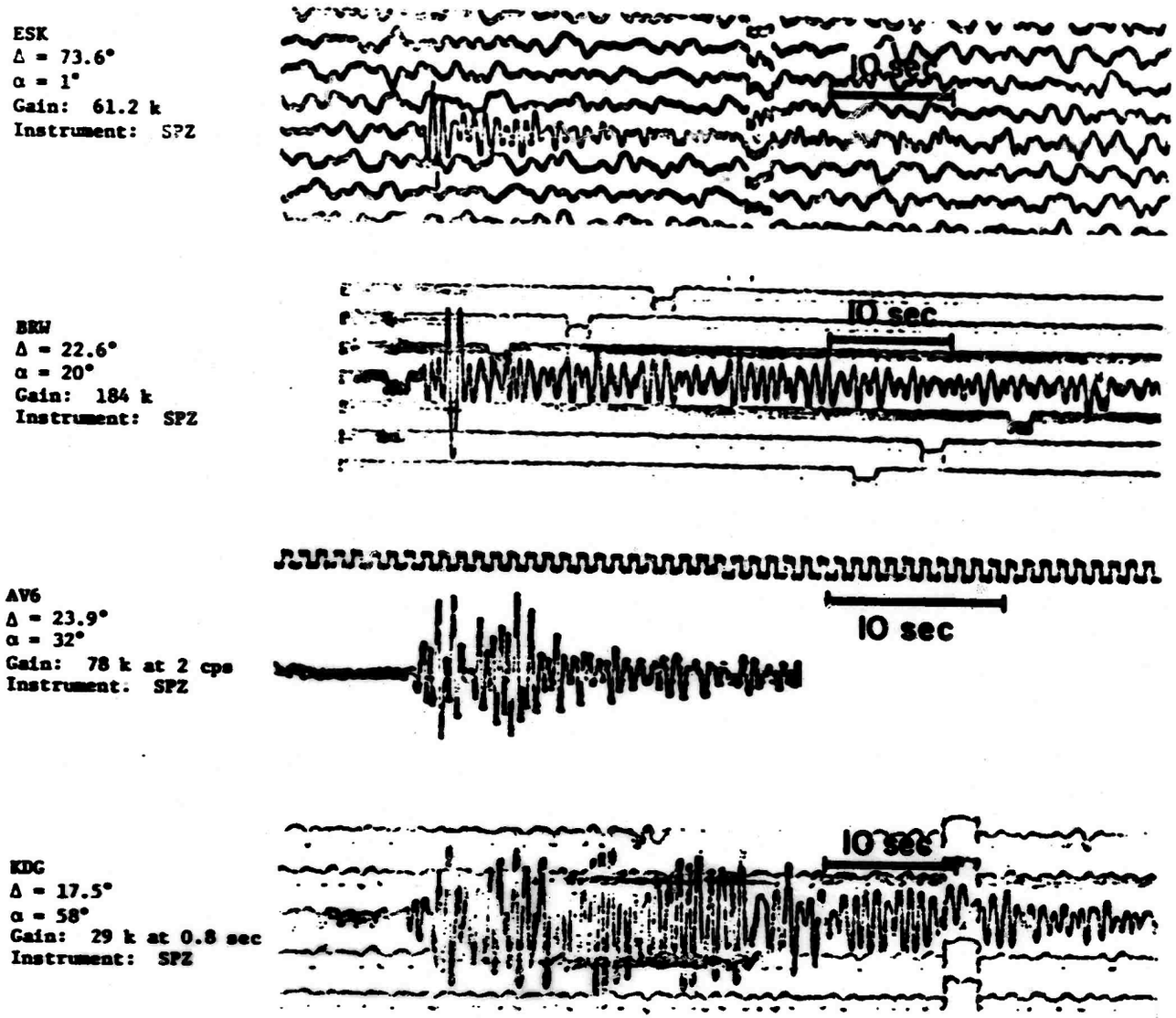

Figure 8. Short-period recordings of P waves from the Long Shot explosion in the Aleutians. After Jacob (in preparation).

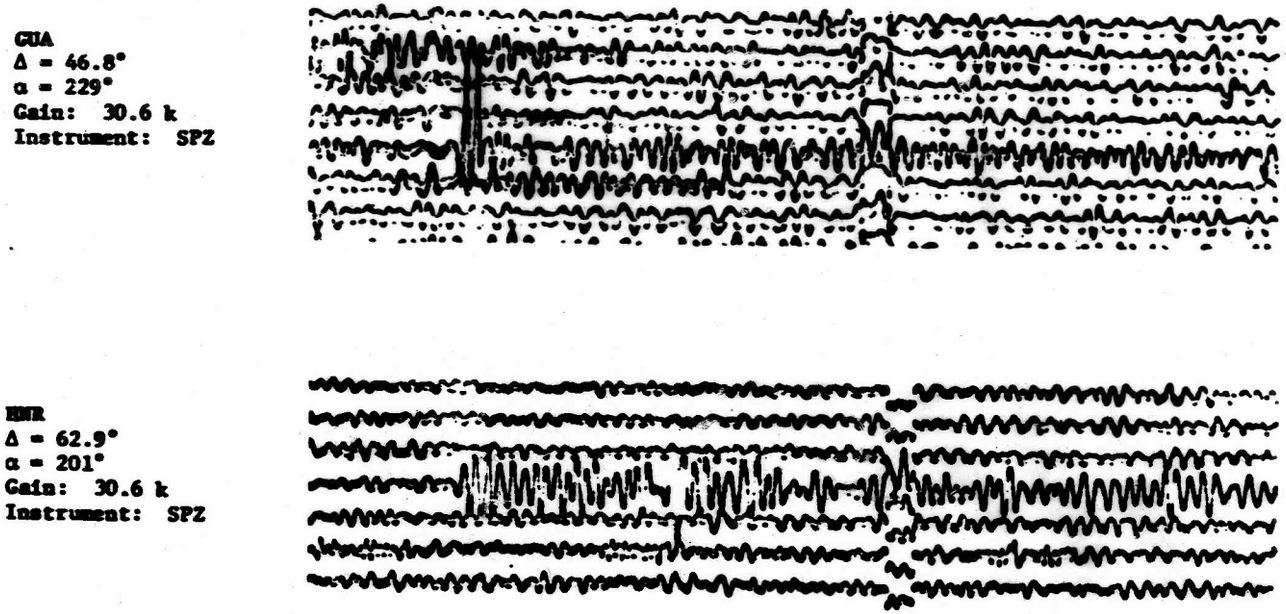

Figure 9. Short-period recordings of P waves from the Long Shot explosion in the Aleutians. After Jacob (in preparation).

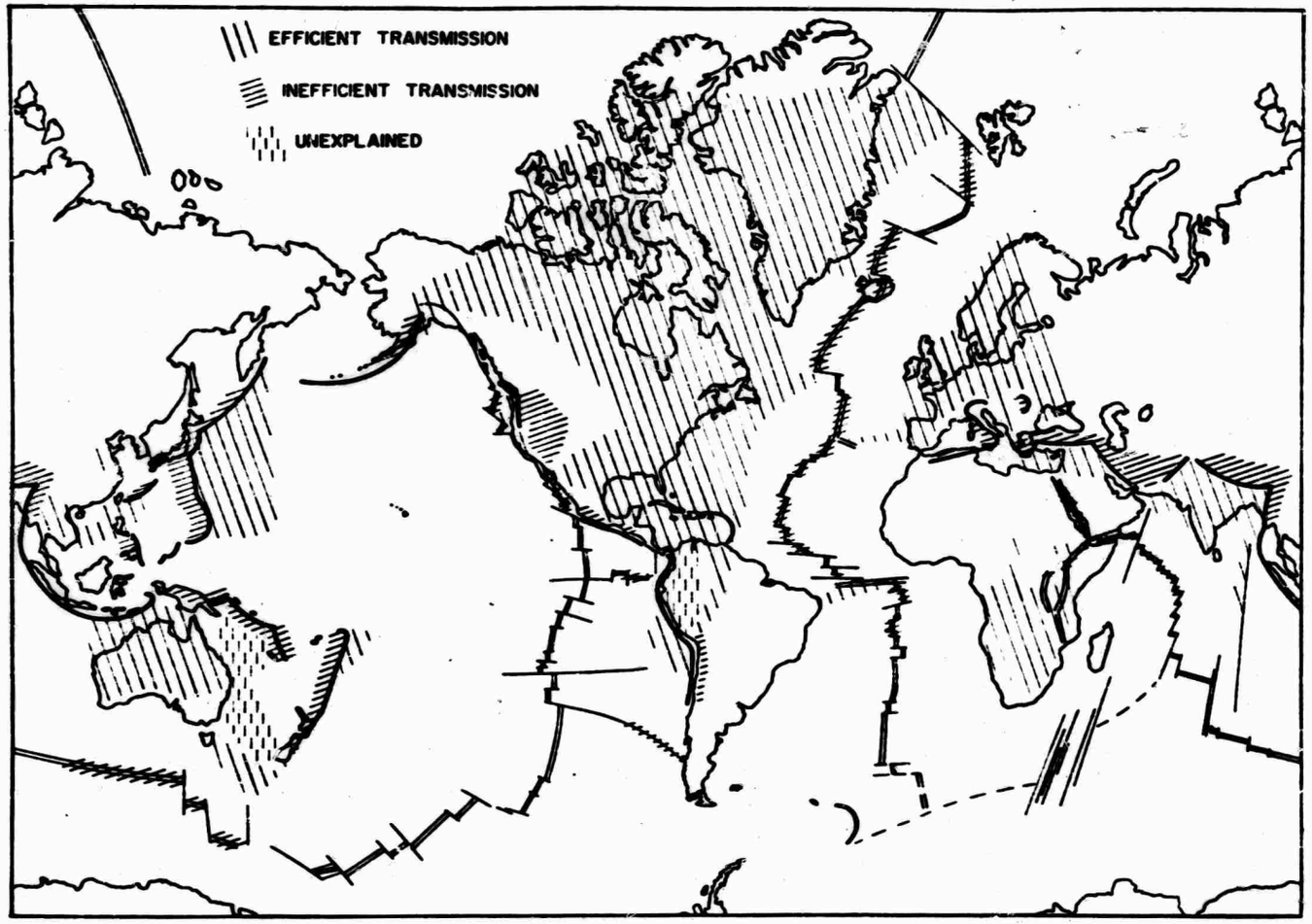

Figure 10. Paths with efficient (high Q) and inefficient (low Q) transmission of high-frequency S waves in the lithosphere. After Molnar and Oliver (1969).

COMPARISON OF SH WAVES FROM LARGE AND SMALL EXPLOSIONS

By

Keiiti Aki
Yi-Ben Tsai

Massachusetts Institute of Technology

Recently, Geyer and Martner (1969) reported a strong excitation of SH waves from small explosions, when the shot point depth was near a horizontal high-contrast interface. They suggested the possibility of disguising an underground nuclear test as an earthquake by placing the shot-point near a high-contrast interface. In order to test the validity of the above suggestion, we have compared the excitation of long period Love waves from many underground nuclear tests in Yucca Flat as a function of shot depth and depths of some high contrast interfaces. The seismic data used were the WWSS records and the readings of LQ and LR amplitudes at LRSM stations. The lithologic and hydrologic information were supplied from Dr. Frank McKeown of U.S. Geological Survey. Our data includes 8 explosions with strong Love waves. We have compared their shot depths with the alluvium-basement interface and also with the water table which may be an interface of some contrast in compressional wave velocity. We found that there were no obvious concentration of shocks with strong Love waves near any of these two interfaces. However, there is a tendency that more events with strong Love waves are found when the shot point depth is located deeper within the tuff or closer to the tuff-pleozoic interface. We don't know whether this is an interface effect or simply a depth effect.

REFERENCE

Geyer, R.L., and Martner, S.T., 1969, Geophysics, v. 34, p. 893-905.

SPECTRAL DIFFERENCES OF SEISMIC WAVES FROM EARTHQUAKES AND UNDERGROUND NUCLEAR EXPLOSIONS

By
Peter Molnar

Lamont-Doherty Geological Observatory
Columbia University
Palisades, New York 10964

INTRODUCTION

This paper discusses marked spectral differences of Rayleigh waves and P waves from earthquakes and underground nuclear explosions. For both waves, there is an enrichment of the short-period portion of the spectrum for explosions. These differences provide additional diagnostic aids for discrimination. Differences in P-wave spectra are particularly important, because discrimination should be possible even when long-period seismograms are disturbed by other earthquakes and surface waves from the events in question are masked. The spectral differences suggest that the source-time functions of pressure in the elastic region near the explosion or stress on the fault at the earthquake hypocenter are very different for earthquakes and explosions. Specifically, the stress on the fault at the time of an earthquake follows approximately a step function in time, but the pressure in the elastic region surrounding an explosion is better represented by an impulse.

I will first discuss the Rayleigh-wave spectral differences; a more detailed discussion of this work will be published later by Savino, Liebermann, Sykes, and Molnar (1970). Then I will consider P-wave spectra. This work is nearly completed and will be published later by Molnar, Matumoto, and Savino (1970). In the last section I will discuss the relevance of these observations for discrimination.

SURFACE-WAVE SPECTRA

Savino (this meeting) showed that discrimination between earthquakes and underground nuclear explosions is enhanced if surface-wave magnitudes are determined between 40 and 60 seconds instead of 20 seconds. This observation implies that spectral differences for earthquakes and explosions exist in the band from 20 to 60 seconds. We have measured the ratios of Rayleigh waves with periods between 19 and 22 seconds to those between 40 and 60 seconds for many explosions in NTS and earthquakes in western North America (Figure 1). For Rayleigh waves, but not Love waves, the ratios clearly separate into two separate populations, one for explosions and one for earthquakes.

To examine this phenomenon further, using recordings at Ogdensburg we determined Fourier spectra for Rayleigh waves of several earthquakes and explosions in the band from 15 to 70 seconds and normalized them at 15.4 sec period (Figure 2). Three explosions are shown: Shaper, Calabash, and Pipkin; their spectra are very similar to one another and very smoothly varying. In Figure 2a spectra of two aftershocks, one following Benham, and another following Jorum that is probably a cavity collapse, are compared with these explosions. Because all of these events occurred close to one another, differences in propagation paths to Ogdensburg do not have an important effect on the spectra.

The collapse spectrum is parallel to those for explosions between about 20 and 50 seconds, but is very different at shorter periods. The Benham aftershock spectrum (B3 in Figure 2a) is more complicated than those for explosions, but differs markedly at periods longer than about 20 seconds. This event was well located and occurred at 3.5 km depth (R.M. Hamilton, personal communication).

In Figure 2b, the same three explosions are compared with two other earthquakes -- one from the Gulf of California and the other, the 29 Palms earthquake of 23 January 1969. The 29 Palms earthquake is noted for being especially rich in shorter periods. Both earthquake spectra are much more complicated than those for the explosions, and both are much larger at long periods. These data suggest important differences in Rayleigh-wave spectra for earthquakes and explosions, and that these differences provide an auxiliary diagnostic aid. Similar differences are observed for a presumed explosion in Novaya Zemlaya compared with nearby earthquakes.

Figure 2c compares the spectrum from the explosion Rulison, detonated in Rifle, Colorado, with the three explosions in NTS. The spectrum for Rulison, however, is very different from those of the NTS events and demonstrates a limitation of a criterion for discrimination based on Rayleigh-wave spectra of some Aleutian earthquakes with that of Milrow does not reveal important differences. Thus, for certain regions Rayleigh-wave spectra for explosions differ from those of earthquakes, but not in all regions.

Neglecting propagation effects, surface-wave spectra are determined by spatial dimensions of the source, by the time function at the source, by the depth of focus, and by the focal mechanism or equivalent force system at the source. Tsai (1969) has shown that, for earthquakes with magnitudes less than 5, source dimensions probably do not affect the spectra much in the period range greater than 15 seconds. The effects of depth of focus and focal mechanism cannot be separated from one another and must be considered together rather than independently. We have studied earthquakes in western North America with many different focal mechanisms and with depths as shallow as 3.5 km, and these earthquakes are consistently richer in long periods than explosions. Thus, these factors are not likely to be the only cause of the spectral differences, and these data suggest that the source-time function for earthquakes and explosions may be different.

P-WAVE SPECTRA

To investigate the source-time function further we analyzed P waves, because the depth of focus and focal mechanism will not affect them very much. Figure 3 shows P waves from earthquakes and from explosions in NTS recorded by long-period seismographs of the WWSSN. The South American earthquake in Figure 3 is noted for being especially rich in higher frequencies (Wyss, 1970). It is obvious upon looking at the seismograms that P waves from explosions are very different in the long-period portion of the spectrum compared with those from earthquakes. In fact, these differences are so obvious that it should be possible to discriminate earthquakes and explosions from P waves alone. More will be said of this in a later section.

Predominant periods of P waves on long period instruments from explosions are consistently between 1 1/2 and 4 seconds, but those from earthquakes are always larger than 6 seconds. We determined spectra for two of these recordings of explosions and for the three earthquakes. Figure 4 shows these spectra corrected for instrument response. The earthquake spectra rise to a maximum value between 6 and 12 seconds. At longer periods there is inadequate resolution to determine whether the spectra become independent of period. The explosion spectra are a maximum between 1 1/2 and 4 seconds and decrease with increasing period.

If the source-time function for pressure in the elastic region or for stress on a fault is given by a step function, then in the far field and in the long-period limit the P-wave spectra will be independent of period. Effects of source dimension and rupture velocity will affect the spectrum, but not the long-period limit. For the far-field spectrum to decrease with period as it does for explosions, it is necessary for the time function to have impulsive component; i.e., a time function similar to that given by Toksoz et al (1964)

$$P(t) = 0, \quad t<0$$

$$P(t) = P_0 nte^{-nt} \quad t\geq 0$$

is more likely to exist for underground nuclear explosions than that often assumed

$$P(t) = 0, \quad t<0$$

$$P(t) = P_0(1 - d^{-t/\tau}) \quad t\geq 0$$

IMPLICATIONS FOR DISCRIMINATION OF EARTHQUAKES FROM EXPLOSIONS

Spectral differences of waves from earthquakes and explosions provide additional diagnostic aids for discrimination. The absence of longer-period Rayleigh waves from explosions compared with earthquakes may provide an auxiliary diagnostic aid that is applicable for events with surface-wave magnitude as low as 3 and epicentral distances of 30-40°. These differences are not observed for events in all regions, however, and thus this technique is not as reliable as other discrimination criteria. Differences in Love-wave spectra do not exist for earthquakes and explosions, probably because Love waves are a measure of tectonic release from explosions and not of the size of the explosion itself. In fact, the tectonic release from explosions may be the reason for the failure of the Rayleigh-wave spectra from all explosions to be different from those of all earthquakes. A more complete network of stations surrounding an explosion should provide data that would allow an estimate of the relative contributions of the explosions and the tectonic release.

Another limitation of a diagnostic aid based on surface-wave spectra is the effect of masking of one event by the surface waves of another. This effect will also limit the usefulness of the m_b=M_S criteria. A criterion that utilizes periods much less than those carried by surface waves would be useful, because the ground motion is large at periods less than 5 sec for only a short time following a large earthquake compared with that at longer periods. Analysis of P waves may provide an additional technique that will be applicable during such times. Because spectral differences for P waves are large, they provide another diagnostic aid for discrimination that is applicable for explosions large enough to be recorded by long-period instruments. With the present instrumentation and noise levels, only very large explosions ($m_b \geq 6$) can be discriminated at teleseismic distances from P-wave spectra. With improvements, however, this threshold probably can be reduced. Nevertheless, because of the narrow band of the spectrum from an explosion-generated P wave, it should be possible to filter out longer-period surface waves from other events without eliminating the P wave. Thus, the differences in P-wave spectra for earthquakes and explosions may provide an essential technique for identifying explosions during times when seismographs are disturbed by large earthquakes.

Savino (this meeting) showed that data comparing m_b and M_S for earthquakes and explosions does not seem to converge. This observation suggests that the difference in spatial dimensions for explosions and earthquakes is not the cause of the separation. A more consistent explanation is that differences in source-time function are responsible. The spectral differences for P waves also reflect differences in the source-time functions because the source time function depends strongly on the medium in which the event is detonated, however, the criteria for discrimination discussed here may not be as effective for

explosions in different media from those studied here. This may be a serious limitation of all diagnostic aids that compare portions of the spectra waves from earthquakes and explosions. On the other hand, if the source-time function is always different for explosions and earthquakes, then discrimination should always be theoretically possible. No earthquake, no matter how small its spatial dimensions are, will generate waves with the same spectra as those from explosions.

REFERENCES

Molnar, P., Savino, J., Sykes, L.R., Liebermann, R.C., Hade G., and Pomeroy, P., 1969, Small earthquakes and explosions in western North America recorded by new high gain, long period seismographs, Nature v. 224, p. 1268.

Molnar, P., Matumoto, T., and Savino, J., 1970 (in preparation), The use of P-wave spectra for identification of underground nuclear explosions and for analysis of their source-time function.

Savino, J., Liebermann, R.C., Sykes, L.R., and Molnar, P., 1970 (in preparation), Long-period surface waves from earthquakes and underground explosions.

Toksoz, M.N., Ben-Menahem, A., and Harkrider, D.G., 1964, Determination of source parameters of explosions and earthquakes by amplitude equalization of seismic surface waves, 1. Underground nuclear explosions, J. Geophys. Res., v. 69, p. 4355.

Tsai, Y-B., 1969, Determination of focal depths of earthquakes in the mid-oceanic ridges from amplitude spectra of surface waves, Ph.D. thesis, Massachusetts Institute of Technology.

Wyss, M., 1970, Stress estimates for South American shallow and deep earthquakes, J. Geophys. Res. v. 75, p. 1529.

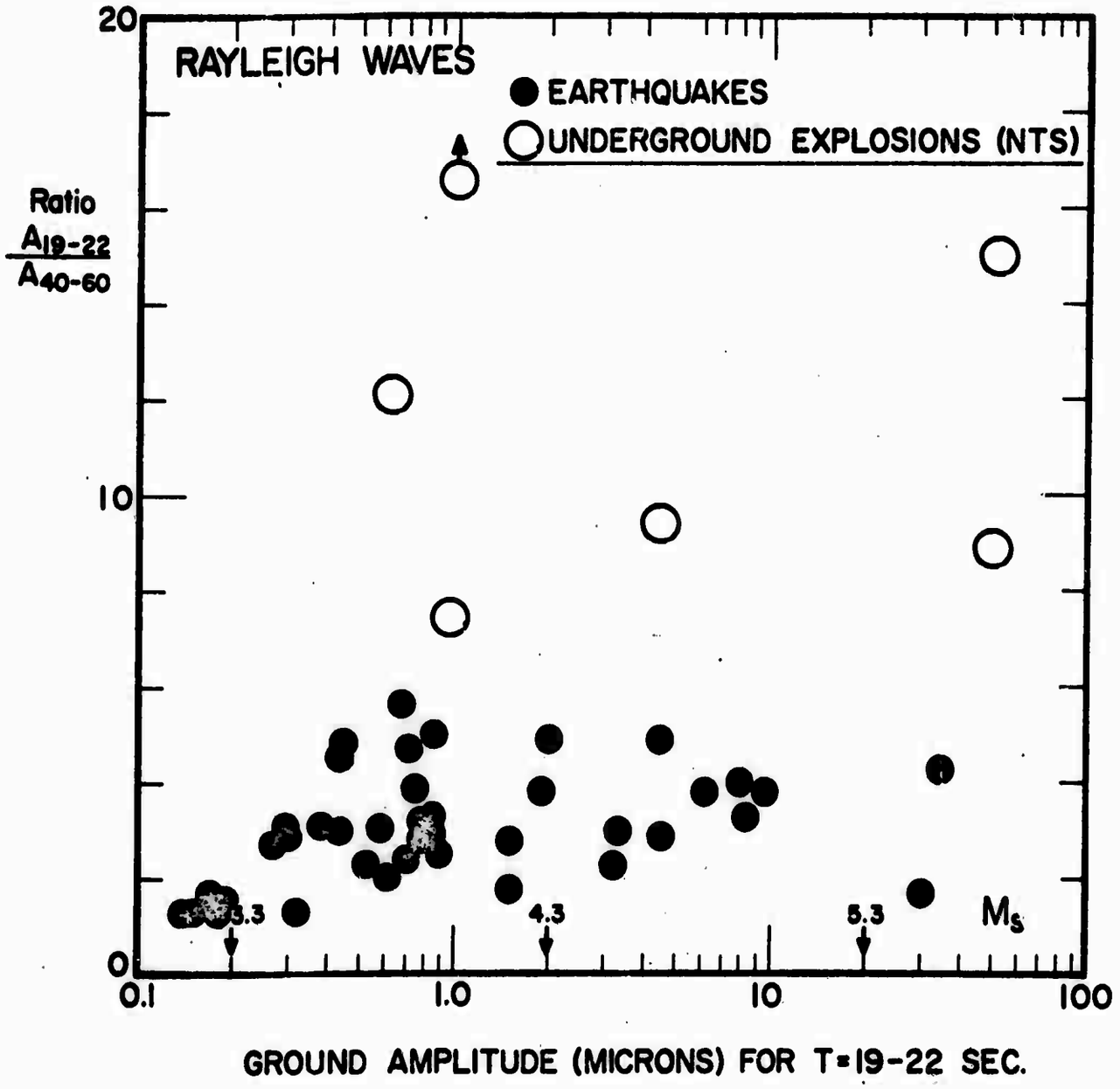

Figure 1. Ratio of ground amplitude of Rayleigh (left) and Love (right) waves in the period range near 20 sec to the amplitudes of the same waves in the period range 40 to 60 sec as a function of the amplitudes of the 20 sec waves (M_s). (After Molnar et al, 1969.)

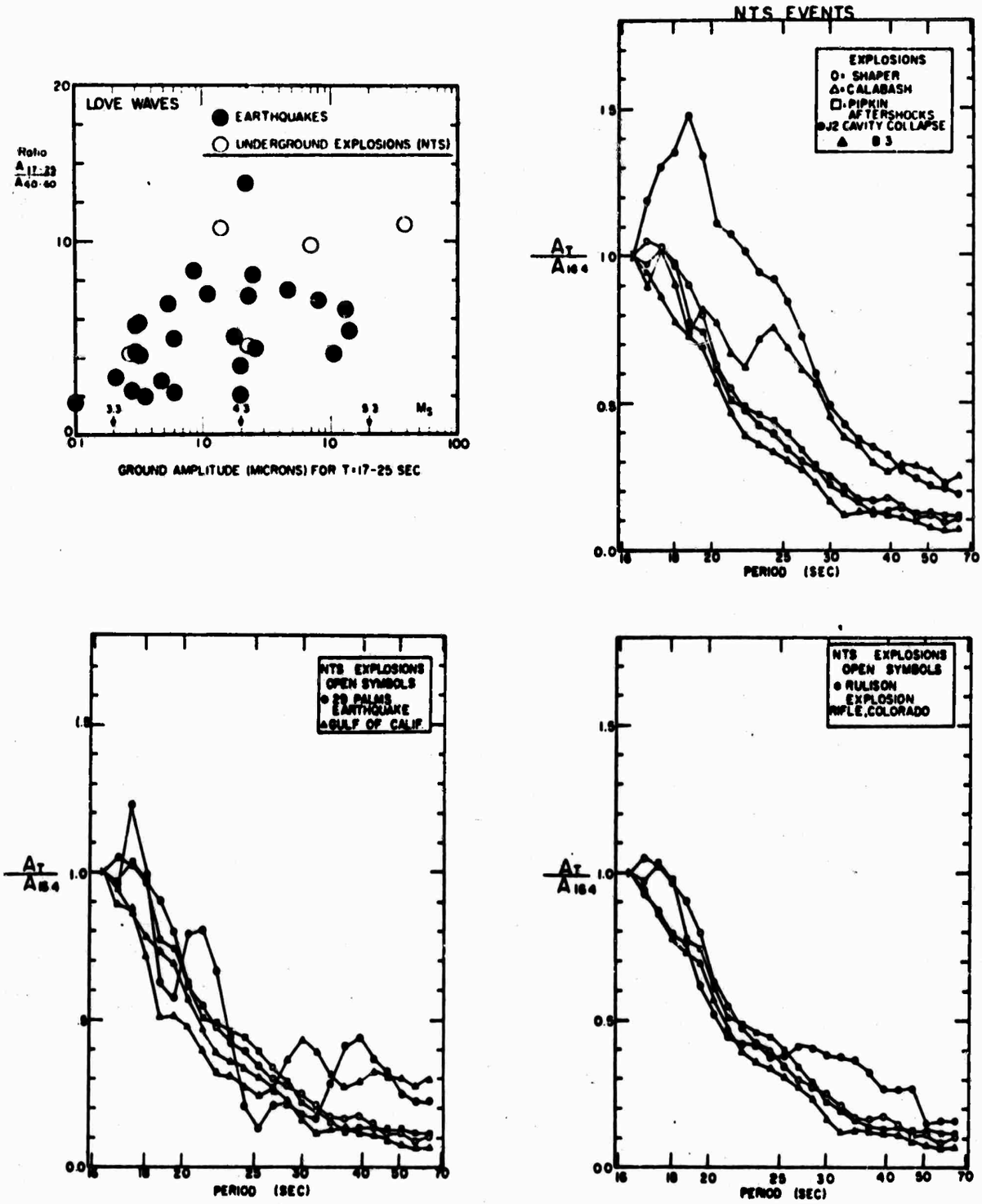

Figure 2. Spectra of Rayleigh waves from explosions and earthquakes recorded at Ogdensburg, Spectra for the explosions Shaper, Calabash, and Pipkin are compared with (a) the Benham aftershock (21 December 1968), t_o = 00 14 25.2), the Jorum aftershock (16 September 1969, t_o = 18 15 39.3), with (b) an earthquake in the Gulf of California (10 February 1969, t_o = 10 23 16.3) and the 29 Palms, California earthquake (23 January 1969, t_o = 23 01 01.0) (after Savino et al, 1970), and with (c) the explosion Rulison.

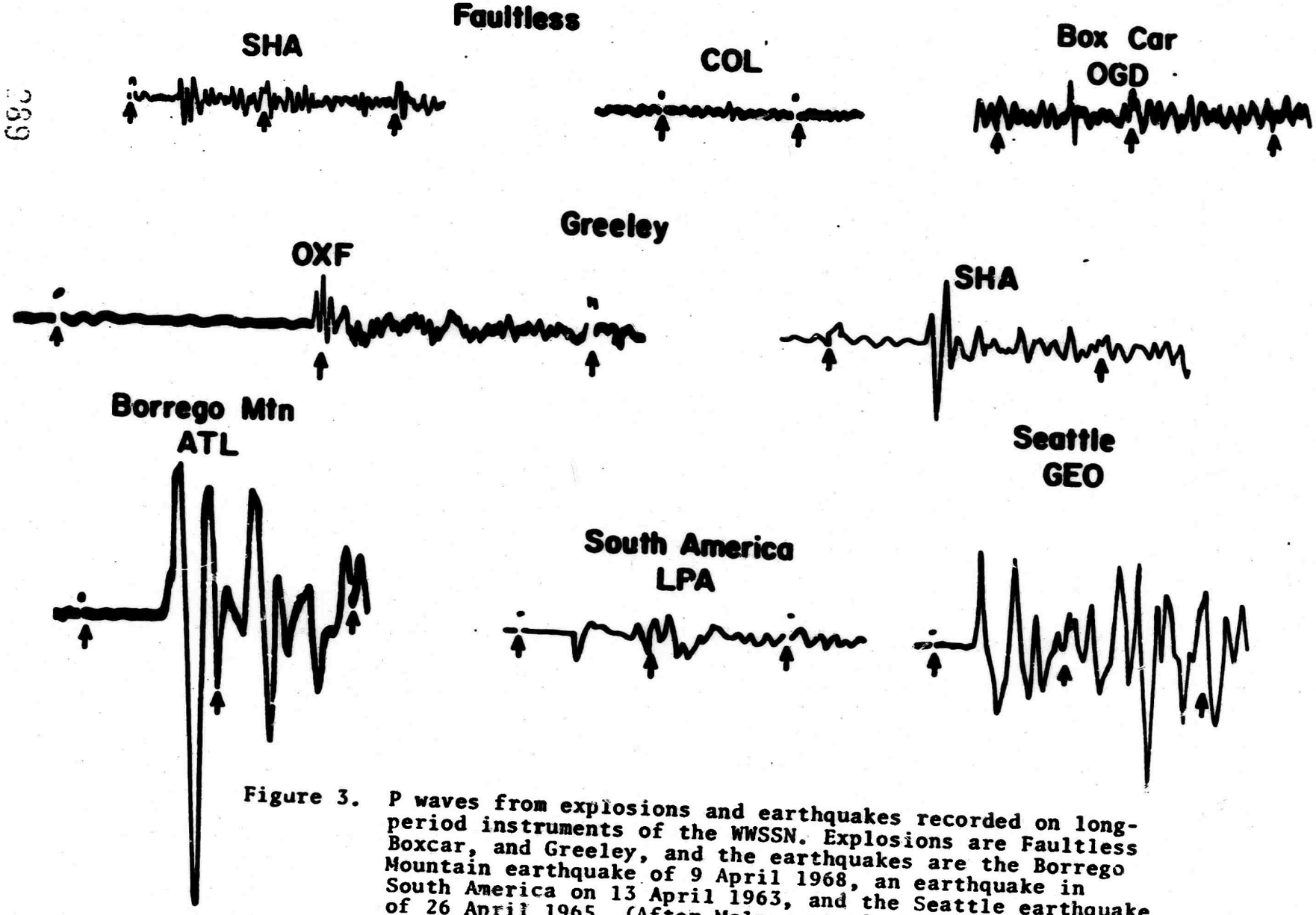

Figure 3. P waves from explosions and earthquakes recorded on long-period instruments of the WWSSN. Explosions are Faultless Boxcar, and Greeley, and the earthquakes are the Borrego Mountain earthquake of 9 April 1968, an earthquake in South America on 13 April 1963, and the Seattle earthquake of 26 April 1965. (After Molnar et al, 1970.)

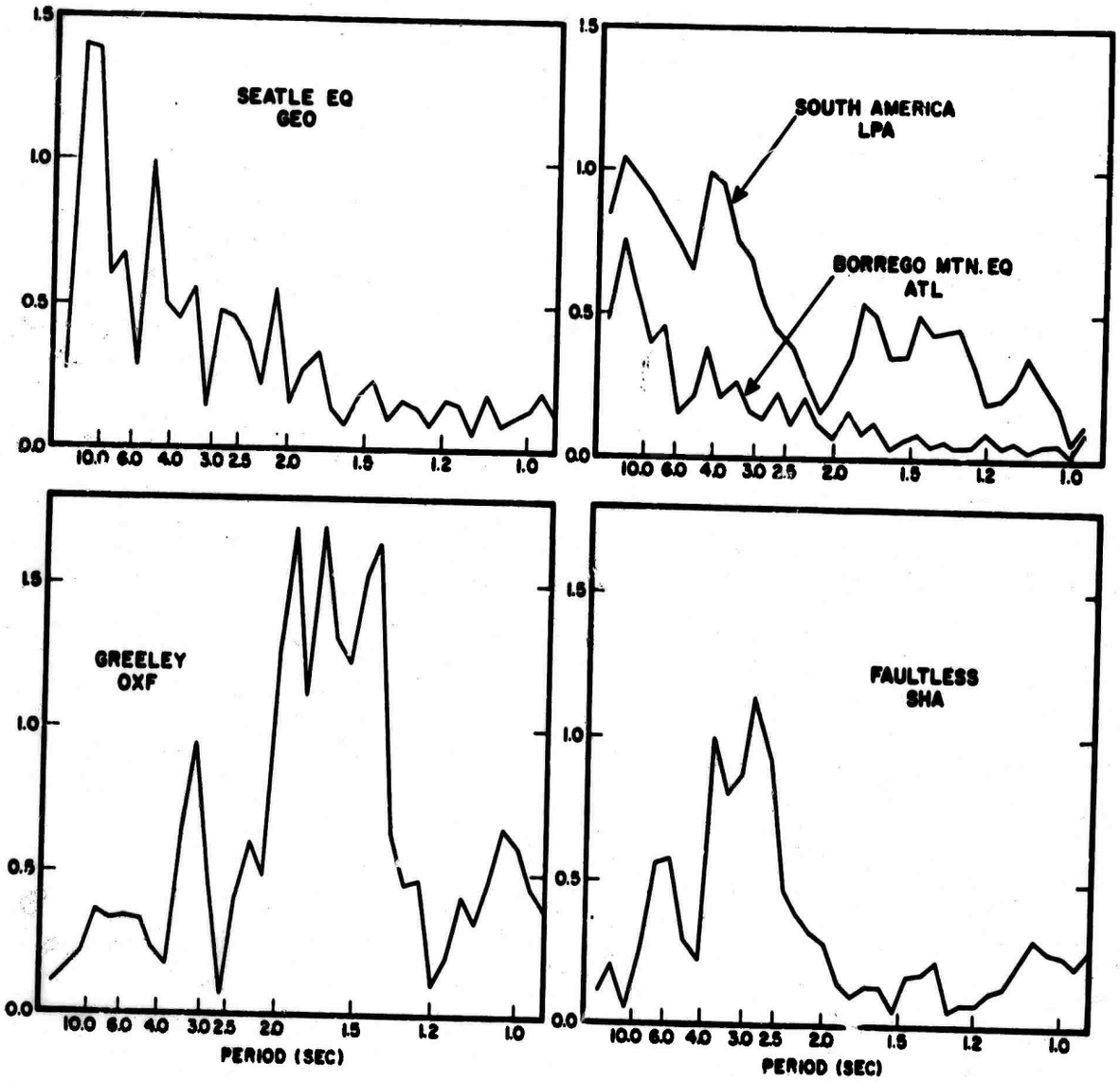

Figure 4. Spectra of P waves from selected events in Figure 3. (After Molnar et al, 1970.)

AMPLITUDE SPECTRA OF SURFACE WAVES FROM SMALL EARTHQUAKES AND UNDERGROUND NUCLEAR EXPLOSIONS

By

Yi-Ben Tsai

Keiiti Aki

Department of Earth and Planetary Sciences
Massachusetts Institute of Technology
Cambridge, Massachusetts 02139

ABSTRACT

Theoretical amplitude spectra of surface waves in a layered half-space are compared with the observed spectra for thirteen underground nuclear explosions in the Nevada Test Site and for twelve earthquakes at five localities in the Gulf of California and in the United States of America. The results are summarized below.

1. The amplitude spectral shape of Rayleigh waves for periods 10 to 50 seconds from explosions does not vary much with the shot medium and the shot yield. A linear relationship equivalent to the M_s vs m_b relationship exists for the explosions studied.

2. The earthquake triggered by the Boxcar explosion was associated with a dip-slip fault trending in N 27° E and dipping in 45° W with the downthrown side on the west. The observed Love wave amplitude spectra are used to determine a seismic moment of 0.24×10^{25} dyne-cm for this earthquake. The corresponding Rayleigh waves are relatively small as compared with Rayleigh waves from the Boxcar explosion itself.

3. Neither the source time function nor the finite source size is the primary cause for the amplitude spectral differences of Rayleigh waves between underground nuclear explosions and small earthquakes. Rather, the source mechanism and the focal depth are responsible for such differences. This finding implies that the amplitude spectra of Rayleigh waves can be used as seismic discriminants between underground nuclear explosions and small earthquakes having focal depths as shallow as a few kilometers.

INTRODUCTION

Important progress in using seismic surface waves for discriminating between small earthquakes and explosions has been made recently by Molnar et al (1969). With the aid of a new high gain, wide band, long period seismograph system, they have found pronounced differences in the amplitude spectra of Rayleigh waves from small earthquakes and underground nuclear explosions in western North America. However, the primary cause(s) of such spectral differences still needs to be positively identified before systematic applications of Rayleigh waves for seismic discrimination between explosions and small earthquakes can be made. We offer here an account of our findings with regard to this problem.

Theoretical surface wave amplitude spectra in a layered medium are calculated for explosions and earthquakes by using Saito's formulation (Saito, 1967). Data from thirteen underground nuclear explosions in the Nevada Test Site and from twelve earthquakes with known source mechanisms and, in some cases, with known small source size and focal depth, are used to test the validity of the theoretical spectra. Thus, we are able to identify the dominant factors responsible for the differences of surface wave amplitude spectra between underground nuclear explosions and small earthquakes. Implications of these results on seismic discrimination are also discussed.

AMPLITUDE SPECTRA OF SURFACE WAVES
FROM UNDERGROUND NUCLEAR EXPLOSIONS

Rayleigh waves

We first calculate the theoretical Fourier spectrum of Rayleigh waves from an underground nuclear explosion by representing the source with a "center of dilatation" (Love, 1944) which consists of three double forces without moment, having their axes perpendicular to each other. According to Saito (1967), the Fourier spectrum of Rayleigh wave displacement from such a source at depth h in a layered half-space is given by the equation

$$R_z(\omega,h) = \frac{P(\omega)\, y_1(0)}{4CUI_1(\lambda+2\mu)} \left(\frac{2C}{\pi\omega r}\right)^{1/2} \left[\frac{2\mu\omega\, y_3(h)}{C} - y_2(h)\right] \cdot e^{-i\left(\frac{\omega r}{C} - \frac{3\pi}{4}\right)} \tag{1}$$

for the vertical component and

$$R_r(\omega,h) = \frac{y_3(0)}{y_1(0)}\, R_z(\omega,h)\, e^{-i\frac{\pi}{2}}$$

for the radial component. C and U in equation (1) are phase velocity and group velocity, respectively, at angular frequency ω. I_1 is defined as

$$I_1 = \int_{-\infty}^{0} \rho(z)\, [y_1^2(z) + y_3^2(z)]\, dz \tag{3}$$

$y_1(z)$, $y_2(z)$, $y_3(z)$, and $y_4(z)$ are the normal mode solutions

satisfying the equations

$$\begin{vmatrix} \frac{dy_1}{dz} \\ \frac{dy_2}{dz} \\ \frac{dy_3}{dz} \\ \frac{dy_4}{dz} \end{vmatrix} = \begin{vmatrix} 0 & \frac{1}{\lambda+2\mu} & \frac{\omega}{C}\left(\frac{\lambda}{\lambda+2\mu}\right) & 0 \\ -\rho\omega^2 & 0 & 0 & \frac{\omega}{C} \\ -\frac{\omega}{C} & 0 & 0 & \frac{1}{\mu} \\ 0 & -\frac{\omega}{C}\left(\frac{\lambda}{\lambda+2\mu}\right) & -\rho\omega^2+\frac{4\mu\omega^2(\lambda+\mu)}{C^2(\lambda+2\mu)} & 0 \end{vmatrix} \begin{vmatrix} y_1 \\ y_2 \\ y_3 \\ y_4 \end{vmatrix} \qquad (4)$$

and the boundary conditions

$$y_2(0) = y_4(0) = y_1(-\infty) = y_2(-\infty) = y_3(-\infty) = y_4(-\infty) = 0 \qquad (5)$$

where ρ, μ, λ are density, rigidity and Lame constant, respectively, of the medium at depth z.

$P(\omega)$ in equation (1) represents the spectrum of each of the three double forces. For far field approximation it can be shown that $P(\omega)$ is directly related to the reduced displacement potential calculated from measurements of earth motion at short distances from underground nuclear explosions in various mediums by

$$P(\omega) = 4\pi(\lambda + 2\mu)\ \Psi(\omega) \qquad (6)$$

$\lambda(\omega)$ in equation (6) is the spectrum of the reduced displacement potential whose time function $\psi(t)$ is related to the radial displacement u_r at distance r and time t by

$$u_r(r,t) = -\frac{d}{dr}\left[\frac{\psi(\tau)}{r}\right] \qquad (7)$$

where $\tau = t - \frac{r}{\alpha}$ is the retarded time and α is the compressional wave velocity in the medium. The reduced displacement potentials, $\psi(\tau)$, have been published by several authors (for example, Werth and Herbst, 1963; Rogers, 1966). Haskell (1967) has shown that these reduced displacement potential curves can be approximated by a family of analytic functions of the form

$$\psi(\tau) = \psi(\infty)\{1-e^{-k\tau}[1+k\tau+\frac{(k\tau)^2}{2}+\frac{(k\tau)^3}{6}-B(k\tau)^4]\}$$

where B is a dimensionless constant independent of the shot yield W, k is a time constant scaling like $W^{-1/3}$ and $\psi(\infty)$ is a constant value directly proportional to W.

Figure 1 shows the normalized reduced displacement potentials, $\psi(\tau)/\psi(\infty)$, for 5-kiloton underground nuclear explosions in tuff and granite, as given by Werth and Herbst (1963) and approximated by Haskell (1967). Owing to the existence of equation (6), we can use the Fourier spectrum of $\psi(\tau)/\psi(\infty)$ for $P(\omega)$ in equation (1) to calculate the Fourier spectrum of Rayleigh waves. Figure 2 shows the amplitude spectrum of Rayleigh wave displacement (vertical component) from explosions in tuff (top) and granite (bottom) with yields ranging from 5 to 10^3 kilotons. In computing these curves, the Gutenberg continental earth model with a 38-km crust is used and a shot depth of 0.5 km is assumed. From these curves, we find that the amplitude spectrum of Rayleigh waves for periods 10 to 50 seconds does not depend very much either on the shot medium or on the shot yield. This theoretical prediction is confirmed by the amplitude spectra of ten smaller explosions observed at ALQ (940 km from NTS),

as shown in Figures 3a, b, c, and by those of three large explosions observed at SHA (2405 km from NTS), as shown in Figure 3d. Pertinent data about these explosions are listed in Table I. It is well known that many large NTS explosions have generated considerable amounts of Love waves. However, the source associated with the radiation of Love waves apparently does not alter the spectrum of Rayleigh waves significantly from that of a pure explosion source. Further discussion on this problem will be given in this paper.

Since we are using absolute amplitudes, it is possible for us to determine from the observations the permanent dipolar strength P_o which is related to $\psi(\infty)$ by the equation

$$P_o = 4\pi(\lambda+2\mu)\ \psi(\infty) \qquad (9)$$

Thus, if we know λ and μ of the shot medium, we can estimate $\psi(\infty)$ and in turn the shot yield W from P_o. It is also evident from equation (1) that $\log_{10} P_0$ is directly proportional to the surface wave magnitude M_s. We have plotted the observed values of $\log_{10} P_o$ against the equivalent body wave magnitude m_b (LRSM) for these thirteen NTS explosions in Figure 4 and found that

$$\log_{10} P_0 = 1.43\ m_b \pm 15.3 \qquad (10)$$

This is equivalent to the well-known linear m_b versus M_s relationship for underground explosions (Marshall et al, 1966; Capon et al, 1967; Basham, 1969; Liebermann and Pomeroy, 1969).

Love waves

Many underground nuclear explosions are known to have generated large amounts of Love waves. It has been suggested that the tectonic strain release following the explosions is responsible for the generation of Love waves and a double couple can be used to represent it (Brune and Pomeroy, 1963; Aki, 1964; Toksoz et al, 1965). Following this approach, we shall study the surface-wave amplitude spectra for the Boxcar event, a megaton explosion in NTS.

Hirasawa (1969) obtained two independent fault-plane solutions for the presumed double couple source associated with the Boxcar by using the observed polarization angles of S waves based on two different assumptions:

1. Solution I: the observed S waves are purely due to double couple source and not contaminated by the reflected waves at the free surface.

2. Solution II: the observed S waves are consisted of the direct S waves from the double couple source and the reflected S waves

at the free surface originally radiated as P and S waves from the composite source of the double couple and the explosion itself.

The two solutions are shown in Figure 5. Solution II corresponds to a vertical strike-slip fault and is very similar to the one obtained by Kehrer (1969) using the ratio of maximum amplitudes of Love and Rayleigh waves. On the other hand, Solution I corresponds to a pure dip-slip fault. The one nodal plane of this solution trending in N 27° E and dipping 45° W is very consistent with the NE-SW trending of the aftershock zone (Ryall and Savage, 1969) and the predominantly vertical ground displacement with the downthrown side on the west along a north-northeasterly surface fracture zone east of the ground zone (McKeown and Dickey, 1969). Thus, this nodal plane may be regarded as the fault plane of the earthquake triggered by the Boxcar explosion. Source mechanisms very similar to Solution I were also obtained for the Benham aftershocks in the north-northeasterly trending epicentral zones by Hamilton and Healy (1969).

The amplitude spectra of Love waves observed at GOL, AAM and WES are shown in Figure 6. These three stations are located nearly on the same azimuth from the epicenter. The theoretical spectra (solid curves) in the figure correspond to either solution I or solution II, since the shape of Love wave spectrum, as shown later in Figures 9 and 10, does not vary much with focal mechanism. The observed spectra shown in Figure 6 for the Boxcar are virtually the same as those for very shallow natural earthquakes such as those shown in Figures 13b and 15.

The seismic moment for the presumed earthquake triggered by the Boxcar obtained from these Love wave data is 0.24×10^{25} dyne-cm if solution II is used. In deriving both values an attenuation coefficient of 140×10^{-6} km^{-1} has been assumed. Since the seismic moment M is related to the surface area A and the average dislocation $\bar{u}$ of the fault by the equation

$$M = \mu A \bar{u} \qquad (11)$$

where μ is rigidity, we can estimate the average dislocation $\bar{u}$ from the seismic moment provided that A is also known.

For the present case, we may take the aftershock zone of 12×6 km^2 (Ryall and Savage, 1969) as the upper limit of the surface area of the fault and assume $\mu = 3 \times 10^{11}$ dyne/cm^2. Then, from equation (11) we get the lower limit of the average dislocation

$\bar{u}_{min} \sim 10$ cm for solution I

~ 5 cm for solution II

The first value is quite consistent with the near-field observations of fault displacement following the Boxcar explosion made by McKeown and Dickey (1969).

We have pointed out earlier that the observed Rayleigh wave spectra for large explosions such as the Boxcar do not differ much from those of pure explosions even though considerable amounts of Love waves are generated, presumably, by a triggered earthquake. This seems to suggest that Rayleigh waves generated by such an earthquake are relatively small as compared with the explosion itself. We can show here that this is indeed the case for the Boxcar.

Figure 7 shows Rayleigh wave spectra for the Boxcar observed at four WWSSN stations located over a wide range of azimuth (from -33° to 97°) around the epicenter. It is noticed that both the spectral shape and the spectral level are very similar among these stations and can be explained very well with the theoretical spectrum for a pure explosion source (solid curves). It is also shown that Rayleigh waves due to a double couple source (dash curves), having its orientation defined by solution I and its strength given as 0.24×10^{25} dyne-cm from Love wave data, are substantially lower than those actually observed. If solution II is assumed, the contribution of Rayleigh waves from the double couple source is even smaller. Thus, we can state that the observed Rayleigh waves from a nuclear explosion, large or small, are primarily generated by the explosion itself, allowing for some exceptional cases such as the Hardhat explosion in granite (Toksöz, et al, 1965).

COMPARISON OF THE AMPLITUDE SPECTRA OF SURFACE WAVES FROM UNDERGROUND EXPLOSIONS AND SMALL EARTHQUAKES

Theoretical aspects

1. Source time function: Molnar et al (1969) have suggested that differences in the source time function between explosions and earthquakes may be large enough to account for the spectral differences of surface waves between these two types of seismic source.

Our results presented above do not corroborate this conjecture. The source time functions given in Figure 1 for explosions have been confirmed by the observed Rayleigh wave spectra shown in Figures 3a, 3b, 3c, 3d for thirteen explosions in tuff or granite. The amplitude spectra of these functions for periods longer than 10 seconds are not significantly different from that of a step function which has been shown to be a good representation of the time behavior of an earthquake source (Tsai and Aki, 1970). Thus, we conclude that the differences in spectral content of surface waves between explosions and earthquakes for periods longer than 10 seconds can not be explained by the differences in source time function.

2. Finite source size: the fact that small and large explosions all generate Rayleigh waves with similar spectral content, as shown in Figures 3a, 3b, 3c, 3d suggests that the finite size of these explosion sources does not distort very much observed spectra for periods longer than 10 seconds. As for earthquakes, several authors have proposed that the source size may be substantially larger than previously estimated, especially for small earthquakes (Wyss and Brune, 1968; Liebermann and Pomeroy, 1970). According to these authors, an earthquake with magnitude $m_b = 5$ will have a fault length of about 15 km which may be large enough to distort the surface wave spectra for periods as great as 20 seconds. However, Molnar et al (1969) have found it difficult to believe that finite source dimension is responsible for the systematic spectral differences of Rayleigh waves observed for many earthquakes and explosions in western North America whose magnitude (m_b) range from 3.9 to 6.3. As shown later, some earthquakes whose finite source size is known to be small still generate Rayleigh waves with spectra distinctively different from explosions. Therefore, we believe that the finite source size is not a primary factor in causing the spectral differences of Rayleigh waves from small earthquakes and explosions.

3. Source mechanism and focal depth: we have pointed out above that neither the source time function nor the finite source size is primarily responsible for causing the systematic spectral differences of the observed Rayleigh waves between explosions and small earthquakes. This naturally leads us to suspect that the source mechanism and focal depth may be the key factors responsible. We explore here the theoretical aspects of the issue. This is followed by observational evidence presented in the next section.

Figure 8 shows the Rayleigh wave amplitude spectrum from an explosion as a function of source depth. It is interesting to point out that firstly, the spectrum varies monotonically with the source depth, and secondly, it changes very slowly when the source is located in the upper few kilometers. The first feature merely reemphasizes the simplistic nature of the explosion-generated Rayleigh waves. While the second feature has some interesting implications as far as discrimination is concerned. It suggests that one will not be able to alter the Rayleigh wave spectrum noticeably by conducting an explosion a few kilometers deeper.

On the contrary, the earthquake-generated Rayleigh waves are far more varied with the source mechanism and depth as compared to explosions. As an example, Figure 9 shows the amplitude spectra of Rayleigh waves (top) and Love waves (bottom) for a vertical, pure strike-slip earthquake at various depths (in km) as expected at a point on an azimuth of 30° from the strike and 2000 km away from the epicenter. It is evident that the Rayleigh wave spectrum associated with such an earthquake depends very strongly on the focal depth and has a spectral shape very different from an explosion except when the earthquake focus is located very close to the earth's surface. In this case, one will have to rely on the azimuthal variations of the earthquake spectrum if he intends to use the Rayleigh wave spectrum to discriminate it from an explosion. On the other hand, the corresponding Love wave spectrum is very simple. The same remarks can be made for earthquakes having other types of source mechanism, such as a pure dip-slip earthquake dipping in 45° shown in Figure 10. By comparing Figures 9 and 10, we also find that the Love wave spectrum does not vary much with the source mechanism of an earthquake.

In summary, we have found that the explosion-generated Rayleigh waves have an amplitude spectrum for periods 10 to 50 seconds varying very little with the shot medium and the shot yield. The spectrum changes very slowly with the source depth in the upper few kilometers. Further down it varies monotonically with diminishing amplitudes for short periods. On the contrary, the earthquake-generated Rayleigh waves are far more dependent upon the focal depth as well as the source mechanism, and in general, have a significantly different spectral shape as compared with that of an explosion, except when the earthquake is located very close to the earth's surface. Therefore, in principle, one should be able to discriminate between explosions and small earthquakes having focal depths greater than a few kilometers by observing the Rayleigh wave amplitude spectrum for periods 10 to 50 seconds at a single station. For the case of extremely shallow earthquakes, one will have to rely on the azimuthal variations of the Rayleigh wave amplitude spectrum for discrimination purposes.

Observed Rayleigh wave amplitude spectra for earthquakes

In this section we shall attempt to verify the inference drawn from theoretical considerations discussed in the preceding paragraphs by some observational evidence. For this purpose we have analyzed Rayleigh waves from twelve earthquakes which occurred in five localities surrounding the NTS. All but two of these events were located within the United States. The remaining two events were in the Gulf of California. These earthquakes are selected because their source mechanisms have been determined and some of their focal depths are also known. Besides, their finite source sizes are believed to be not large enough to distort the surface wave amplitude spectra. Pertinent data of these earthquakes are listed in Table II.

Figure 11 shows the Rayleigh wave spectra observed at ALQ (Δ = 1533 km) for two neighboring vertical strike-slip earthquakes in the Gulf of California (Sykes, 1968). The data can be explained very well by the theoretical spectrum (solid curve) corresponding to a focal depth of 5 km for both earthquakes. These spectra are evidently flatter than those observed at the same station ALQ for explosions shown in Figures 3a, 3b, 3c, and 3d.

Figure 12 shows the Rayleigh wave spectra observed at ALQ (Δ = 1280 km) for the foreshock and the largest aftershock of the Parkfield, California, earthquake of 28 June 1966. Both were associated with righ-lateral vertical strike-slip faulting along the San Andreas fault (McEvilly et al, 1967). Filson and McEvilly (1967) and Tsai and Aki (1970) have shown that the finite source size had very little effect on the Love wave amplitude spectra observed for tnese two events. The data in Figure 12 yield a focal depth of 7 km for the foreshock and of 9 km for the aftershock. Both values fall within the focal depth range of 2 to 12 km for the whole sequence determined by McEvilly et al (1967). The Rayleigh wave spectra for these two earthquakes can also be easily distinguished from those for the NTS explosions observed at the same station ALQ.

The next earthquake we have studied is the Truckee, California, earthquake of September 12, 1966. Ryall et al (1968) determined the focal depth as 10 km. The source mechanism obtained by them was recently revised to give a left-lateral strike-slip motion on a steeply dipping plane (80° SE) trending N 44° E (Tsai and Aki, 1970). The aftershock zone of 10 km as determined by Ryall et al (1968) and by Greensfelder (1968) suggests that the fault length associated with the main shock probably did not exceed 10 km. Therefore the effect of the finite source size is negligible on the amplitude spectra of Love and Rayleigh waves observed at MDS (Δ = 2565 km) as shown in Figure 13. The data are consistent with a focal depth of 10 km. Again, the Rayleigh wave spectrum for this earthquake is clearly different from those for the NTS explosions shown earlier.

So far, we have shown that the Rayleigh wave amplitude spectra for strike-slip earthquakes with focal depths as shallow as 5 km can

TUC (Δ = 2120 km, ϕ = -101°) and DUG (Δ = 2111 km, ϕ = -76°), respectively, for this pure dip-slip earthquake. The theoretical spectra corresponding to the source mechanism mentioned above are also shown in Figure 16 for several focal depths. The data at both stations can be explained quite satisfactorily by a focal depth of 28.5 km which is very close to the value of 25 km determined from the pP-P times (Stauder and Nuttli, 1970).

The Rayleigh wave spectrum for this earthquake can be distinguished from that for an explosion too. For the earthquake the amplitude at period 20 seconds is more than ten times of that at 50 seconds, while for an explosion, it amounts to only about three times.

We have shown above that the observed Rayleigh wave amplitude spectra for earthquakes in five different localities can be explained in terms of source mechanism and focal depth. Our results imply that the differences of Rayleigh wave amplitude spectra between explosions and earthquakes will continue to exist even for very small events as long as the earthquakes are not located extremely close to the earth's surface. Thus, with the aid of new high gain, wide band, long period seismographs, explosions and small earthquakes can be discriminated by using the Rayleigh wave amplitude spectra.

be distinguished from the spectra for the NTS explosions. As pointed out earlier, if the earthquake is located extremely close to the earth's surface, its Rayleigh wave amplitude spectrum will not be different from that for explosions, regardless of its source mechanism. This appears to be confirmed by the Caliente, Nevada sequence of 16 August 1966.

Using 26 readings (23 from WWSSN L-P records and 3 from Seismological Bulletin) of P-wave polarities in North America, we obtain a fault-plane solution for the main shock of August 16, 1966. As shown in Figure 14a, it was a strike-slip type of source mechanism.

The microaftershock observations were made by Boucher et al (1967) at the epicenter 10 days after the main shock using four portable seismographs at epicentral distances not more than 10 km. The results showed that the microaftershocks were located at depths less than 9 km (Page, 1968) and along a zone 10 km long (Liebermann and Pomeroy, 1970). This suggests that the sequence was shallow and the finite size of the main shock was probably smaller than 10 km.

The Rayleigh and Love wave amplitude spectra for the main shock observed at RCD (Δ = 1186 km) are shown in Figure 14b. The theoretical spectra corresponding to the source mechanism given in Figure 14a are also shown here for two focal depths, 1 km and 10 km. Both the shape and the level of the observed spectra can be explained with a focal depth of 1 km. The exact cause of the sharp spectral nulls near 12 seconds for Rayleigh waves and 16 seconds for Love waves is not known. They were probably a result of interference due to multipath propagation. In any case, the observed Rayleigh wave spectrum for periods longer than 16 seconds is indistinguishable from that for explosions. This feature is even more clearly manifested by the aftershock spectra observed at ALQ (Δ = 748 km), as shown in Figures 15a and 15b. The spectrum for the September 22, 1966 event observed at LUB (Δ = 1195 km and almost on the same azimuth as ALQ) is also given in Figure 15b, as an example, to show the remarkable repeatability of the surface wave amplitude spectral data. The Love wave amplitude spectrum observed at this station (not shown) is very similar to that shown in Figure 14b for the main shock, also suggesting shallow focal depth. In summary, we believe that the main shock and the larger aftershocks of the Caliente, Nevada sequency of August 16, 1966 occurred at very shallow depths and consequently, generated Rayleigh waves having similar amplitude spectra as explosions.

That the Rayleigh wave amplitude spectrum for an earthquake having source mechanism other than strike-slip faulting can also be distinguished from the spectrum for an explosion is demonstrated by the south central Illinois earthquake of November 9, 1968.

According to Stauder and Nuttli (1970), the source mechanism of this earthquake consists of two nodal planes each striking approximately north-south and dipping 45° to the east and to the west, respectively. The focal depth was determined as 25 km. Figures 16 and 17 show the Rayleigh and Love wave amplitude spectra observed at

TUC (Δ = 2120 km, ϕ = -101°) and DUG (Δ = 2111 km, ϕ = -76°), respectively, for this pure dip-slip earthquake. The theoretical spectra corresponding to the source mechanism mentioned above are also shown in Figure 16 for several focal depths. The data at both stations can be explained quite satisfactorily by a focal depth of 28.5 km which is very close to the value of 25 km determined from the pP-P times (Stauder and Nuttli, 1970).

The Rayleigh wave spectrum for this earthquake can be distinguished from that for an explosion too. For the earthquake the amplitude at period 20 seconds is more than ten times of that at 50 seconds, while for an explosion, it amounts to only about three times.

We have shown above that the observed Rayleigh wave amplitude spectra for earthquakes in five different localities can be explained in terms of source mechanism and focal depth. Our results imply that the differences of Rayleigh wave amplitude spectra between explosions and earthquakes will continue to exist even for very small events as long as the earthquakes are not located extremely close to the earth's surface. Thus, with the aid of new high gain, wide band, long period seismographs, explosions and small earthquakes can be discriminated by using the Rayleigh wave amplitude spectra.

CONCLUSIONS AND DISCUSSION

The theoretical amplitude spectra of surface waves in a layered medium have been successfully used to explain the data observed for both explosions and earthquakes. Some significant results are summarized here.

1. The amplitude spectral shape of the explosion-generated Rayleigh waves for periods 10 to 50 seconds is nearly independent of the shot medium and the shot yield. A linear relationship equivalent to that of M_s vs m_b is also obtained from the observed amplitude spectra for thirteen NTS explosions. It is also shown that the reduced displacement potentials from the close-in measurements of earth motion can be used to represent the source time history of explosions as far as the generation of long period Rayleigh waves is concerned.

2. Observations of the S wave polarization angles, the aftershock locations and the ground displacements in the source zone of the Boxcar explosion suggest that the earthquake, presumably triggered by the explosion, was probably associated with a dip-slip source mechanism. A seismic moment of 0.24×10^{25} dyne-cm is obtained from the observed Love wave amplitude spectra for such an earthquake. Assuming the fault plane has an area as large as the aftershock zone, the average dip-slip dislocation is estimated at least 10 cm with downthrown side on the northwest. This value is consistent with the near-field observations of ground displacements. The contribution of Rayleigh waves from this triggered earthquake is relatively small as compared to the explosion itself.

3. It is argued that neither the source time function nor the finite source size is the primary cause for the amplitude spectral differences of Rayleigh waves between explosions and small earthquakes. Theoretical spectra are given to show that the source mechanism and the focal depth are the dominant factors in determining the amplitude spectral shape of the earthquake-generated Rayleigh waves. Because of the very simplistic nature of the explosion-generated Rayleigh waves and the heavy dependency of the earthquake-generated Rayleigh waves upon the focal depth, we believe it is possible to discriminate between explosions and earthquakes by using the Rayleigh wave amplitude spectra, except when the earthquakes are extremely shallow. This is confirmed by data for twelve earthquakes which occurred in five different localities in the United States and the Gulf of California.

Before our results can be applied for the discrimination of remote explosions and earthquakes, further knowledge on the propagation effects on the surface wave spectra, such as attenuation, scattering, interference due to lateral inhomgeneties, is urgently needed.

ACKNOWLEDGEMENTS

We wish to express our deep appreciation to Drs. Frank Press and Jack F. Evernden for their encouragement and valuable suggestions. We have also benefited by discussions with Drs. Tomowo Hirasawa, Clint W. Frasier, John R. Filson and M. Nafi Toksöz.

This study was supported by the National Science Foundation under grant GA-14812. Computations were done at the Information Processing Center, Massachusetts Institute of Technology.

REFERENCES

Aki, K., 1964, A note on surface wave generation from the Hardhat nuclear explosion, J. Geophys. Res., v. 69, p. 1131-1134.

Basham, P.W., 1969, Canadian magnitudes of earthquakes and nuclear explosions in south-western North America, Geophys. J. R. Astr. Soc., v. 17, p. 1-13.

Boucher, G., Seeber, L., Ward, P., and Oliver, J., 1967, Microaftershocks observations at the epicenter of a moderate-sized earthquake in Nevada (Abstract), Trans. Am. Geophys. Union, v. 48, p. 205.

Brune, J.N., and Pomeroy, P.W., 1963, Surface wave radiation patterns for underground nuclear explosions and small-magnitude earthquakes, J. Geophys. Res., v. 68, p. 5005-5028.

Capon, J., Greenfield, R.J., and Lacoss, R.T., 1967, Surface - vs body-wave magnitude results, in Semi-Annual Technical Summary, Lincoln Laboratory, M.I.T., 30 June.

Filson, J., and McEvilly, T.V., 1967, Love wave spectra and the mechanism of the 1966 Parkfield sequence, Bull. Seism. Soc. Am., v. 57, p. 1245-1257.

Greensfelder, R., 1968, Aftershocks of the Truckee, California earthquake of September 12, 1966, Bull. Seism. Soc. Am., v. 58, p. 1607-1620.

Hamilton, R.M. and Healy, J.H., 1969, Aftershocks of the Benham nuclear explosion, Bull. Seism. Soc. Am., v. 59, p. 2271-2281.

Haskell, N.A., 1967, Analytic approximation for the elastic radiation from a contained underground explosion, J. Geophys. Res., v. 72, p. 2583-2587.

Hirasawa, T., 1969, Radiation patterns of S waves from underground nuclear explosions, Post-doctoral program in seismology: Annual Report, 30 June 1969, p. 27-46, Massachusetts Institute of Technology.

Kehrer, H.H., 1969, Radiation patterns of seismic surface waves from nuclear explosions, M.S. Thesis, Massachusetts Institute of Technology.

Liebermann, R.C., and Pomeroy, P.W., 1969, Relative excitation of surface waves by earthquakes and explosions, J. Geophys. Res., v. 74, p. 1575-1590.

Liebermann, R.C., and Pomeroy, P.W., 1970, Source dimensions of small earthquakes as determined from the size of the aftershock zone, Bull. Seism. Soc. Am., v. 60, p. 879-890.

Love, A.E.H., 1944, A treatise on the mathematical theory of elasticity, p. 187, Dover Publications, New York.

McEvilly, T.V., Bakun, W.H., and Casaday, K.B., 1967, The Parkfield, California earthquakes of 1966, Bull. Seism. Soc. Am., v. 57, p. 1221-1244.

McKeown, F.A., and Dickey, D.D., 1969, Fault displacement and motion related to nuclear explosions, Bull. Seism. Soc. Am., v. 59, p. 2253-2269.

Marshall, P.D., Carpenter, E.W., Douglas, A., and Young, J.B., 1966, Some seismic results of the Long Shot explosion, Atomic Weapons Research Establishment, U.K.A.E.A., A.W.R.E. Report No. 0-67/66.

Molnar, P., Savino, J., Sykes, L., Liebermann, R.C., Hade, G., and Pomeroy, P.W., 1969, Small earthquakes and explosions in western North America recorded by new high gain, long period seismographs, Nature, v. 224, p. 1268-1273.

Page, R., 1968, Focal depths of aftershocks, J. Geophys. Res., v. 73, p. 3897-3903.

Rogers, L.A., 1966, Free-field motion near a nuclear explosion in salt: project Salmon, J. Geophys. Res., v. 71, p. 3415-3426.

Ryall, A., Van Wormer, J.D., and Jones, A.J., 1968, Triggering of micro-earthquakes by earth tides, and other features of the Truckee, California earthquake sequency of September, 1966, Bull. Seism. Soc. Am., v. 58, p. 215-248.

Ryall, A., and Savage, W.U., 1969, A comparison of seismological effects for the Nevada underground test Boxcar with natural earthquakes in the Nevada region, J. Geophys. Res., v. 74, p. 4281-4289.

Saito, M., 1967, Excitation of free oscillations and surface waves by a point source in a vertically heterogeneous earth, J. Geophys. Res., v. 72, p. 3689-3699.

Stauder, W., and Nuttli, O.W., 1970, Seismic studies: south central Illinois earthquake of November 9, 1968, Bull. Seism. Soc. Am., v. 60, p. 973-981.

Sykes, L.R., 1968, Seismological evidence for transform faults, sea floor spreading, and continental drift, in The History of the Earth's Crust, edited by R. Phinney, Princeton University Press, Princeton, p. 120-150.

Toksoz, M.N., Harkrider, D.G., and Ben-Menahem, A., 1965, Determination of source parameters by amplitude equalization of seismic surface waves, 2. Release of tectonic strain by underground nuclear explosions and mechanism of earthquakes, J. Geophys. Res., v. 70, p. 907-922.

Tsai, Y.B., and Aki, K., 1970, in press, Source mechanism of the Truckee, California earthquake of September 12, 1966. Bull. Seism. Soc. Am.

Tsai, Y.B., and Aki, K., 1970, in press, Precise focal depth determination from amplitude spectra of surface waves, J. Geophys. Res.

Werth , G.C., and Herbst, R.F., 1963, Comparison of amplitudes of seismic waves from nuclear explosions in four mediums, J. Geophys. Res., v. 68, p. 1463-1475.

Wyss, M., and Brune, J.W., 1968, Seismic moment, stress, and source dimensions for earthquakes in the California-Nevada region, J. Geophys. Res., v. 73, p. 3681-3694.

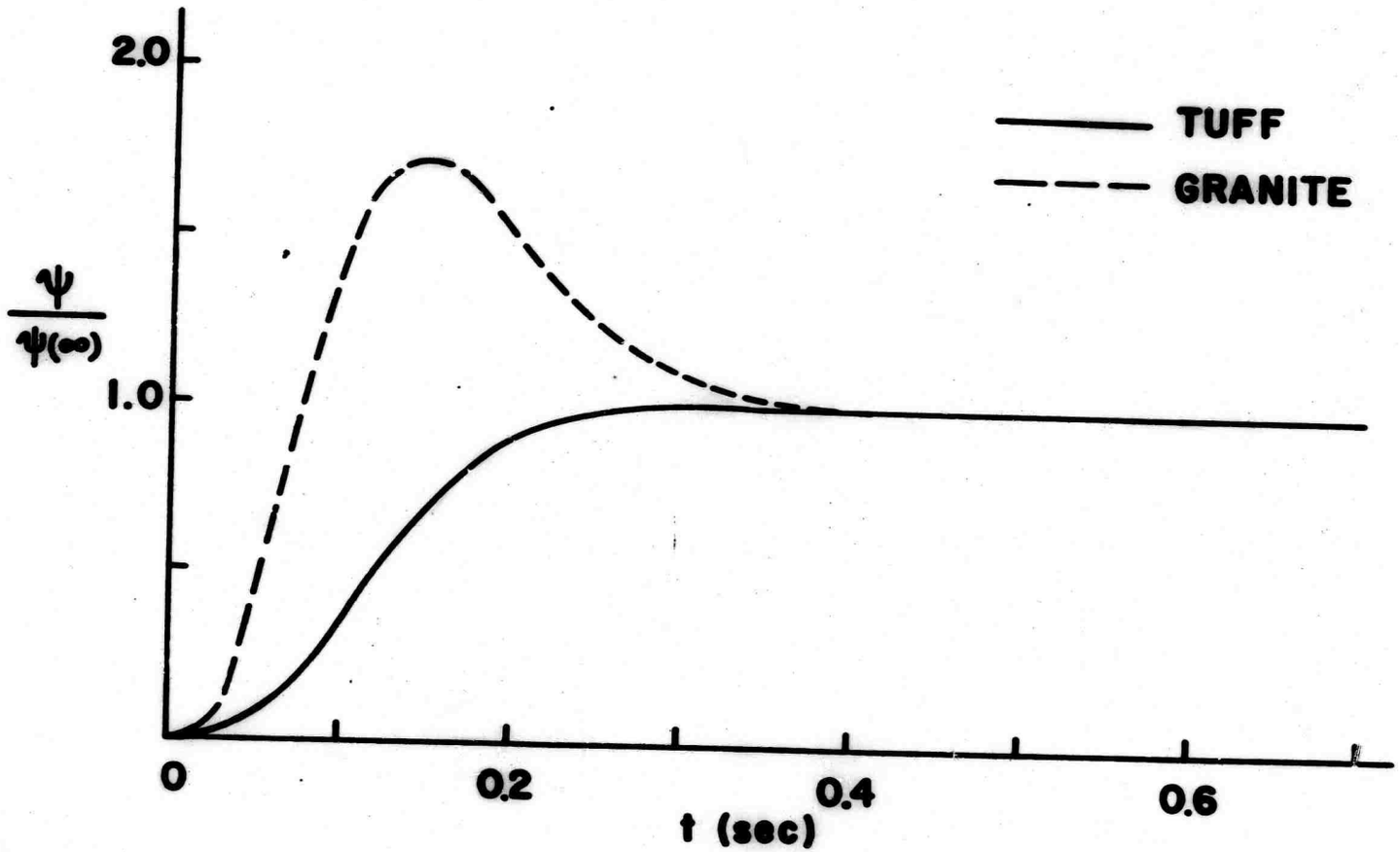

Figure 1. Reduced displacement potentials for underground nuclear explosions in tuff (solid curve) and in granite (dashed curves), having a yield of 5 kt (Werth and Herbst, 1963; Haskell, 1967).

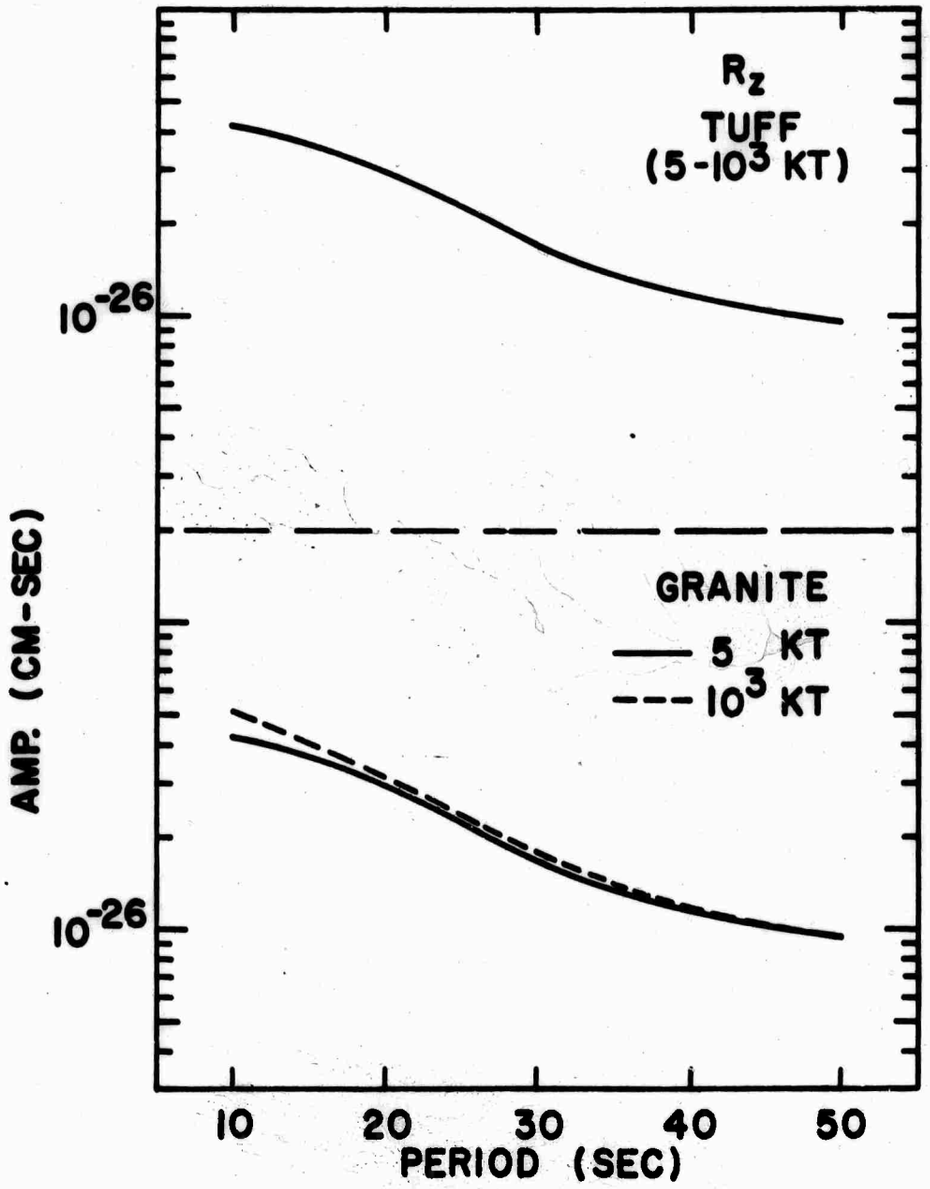

Figure 2. Vertical displacement amplitude spectra of Rayleigh waves expected at Δ = 1000 km from underground nuclear explosions in tuff (top) and in granite (bottom). The reduced displacement potentials, such as those shown in Figure 1, are used as the source time functions.

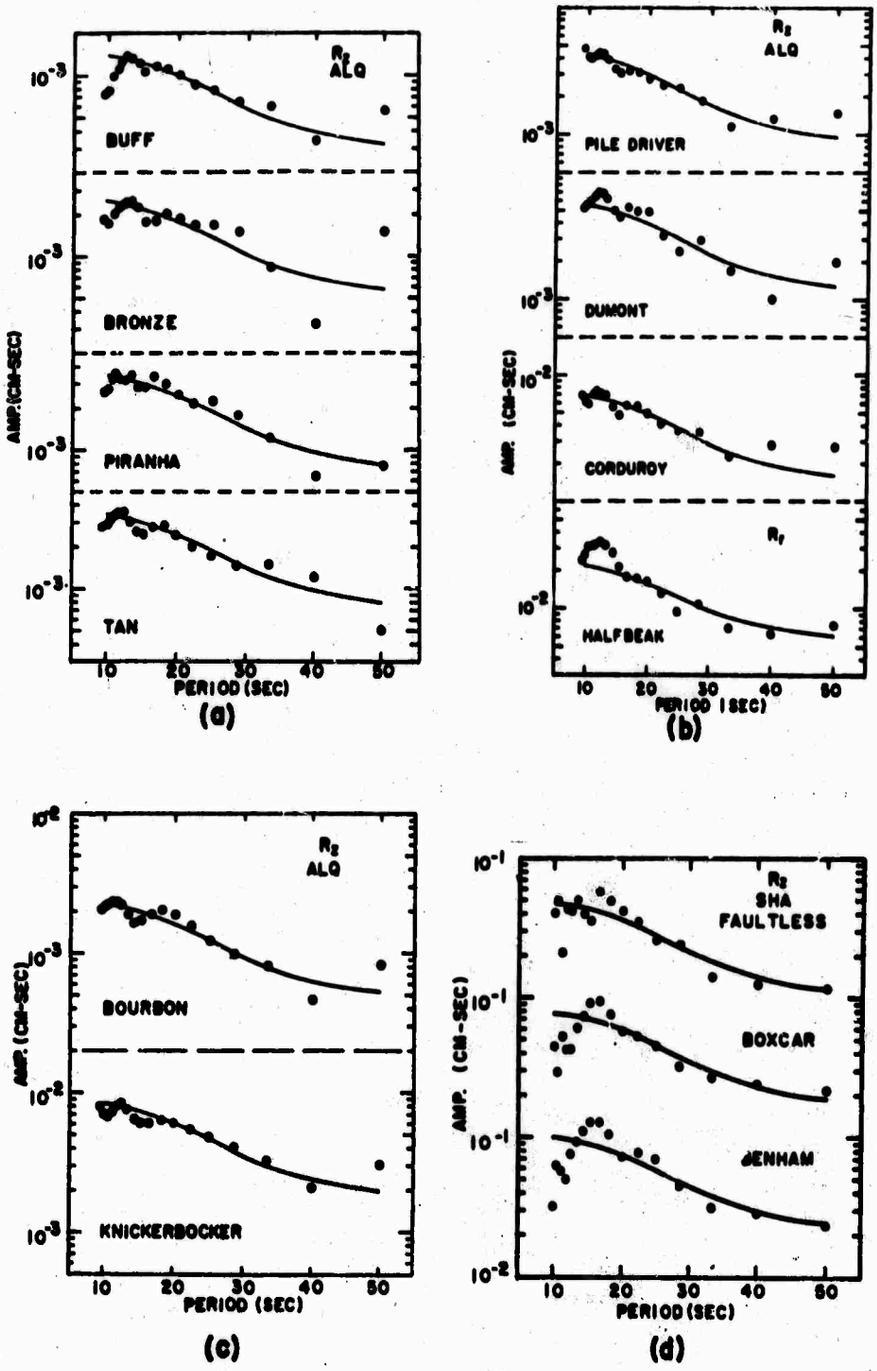

Figure 3. Observed (solid circles) and theoretical (solid curves) amplitude spectra of Rayleigh waves from underground nuclear explosions in the Nevada Test Site: (a) Buff, Bronze, Piranha and Tan; (b) Pile Driver, Dumont, Corduroy and Halfbeak; (c) Bourbon and Knickerbocker; (d) Faultless, Boxcar and Benham. Data for events in (a), (b), (c) were observed at Albuquerque, New Mexico and for events in (d) are obtained at Spring Hill, Alabama. All the data have been corrected from the instrumental response.

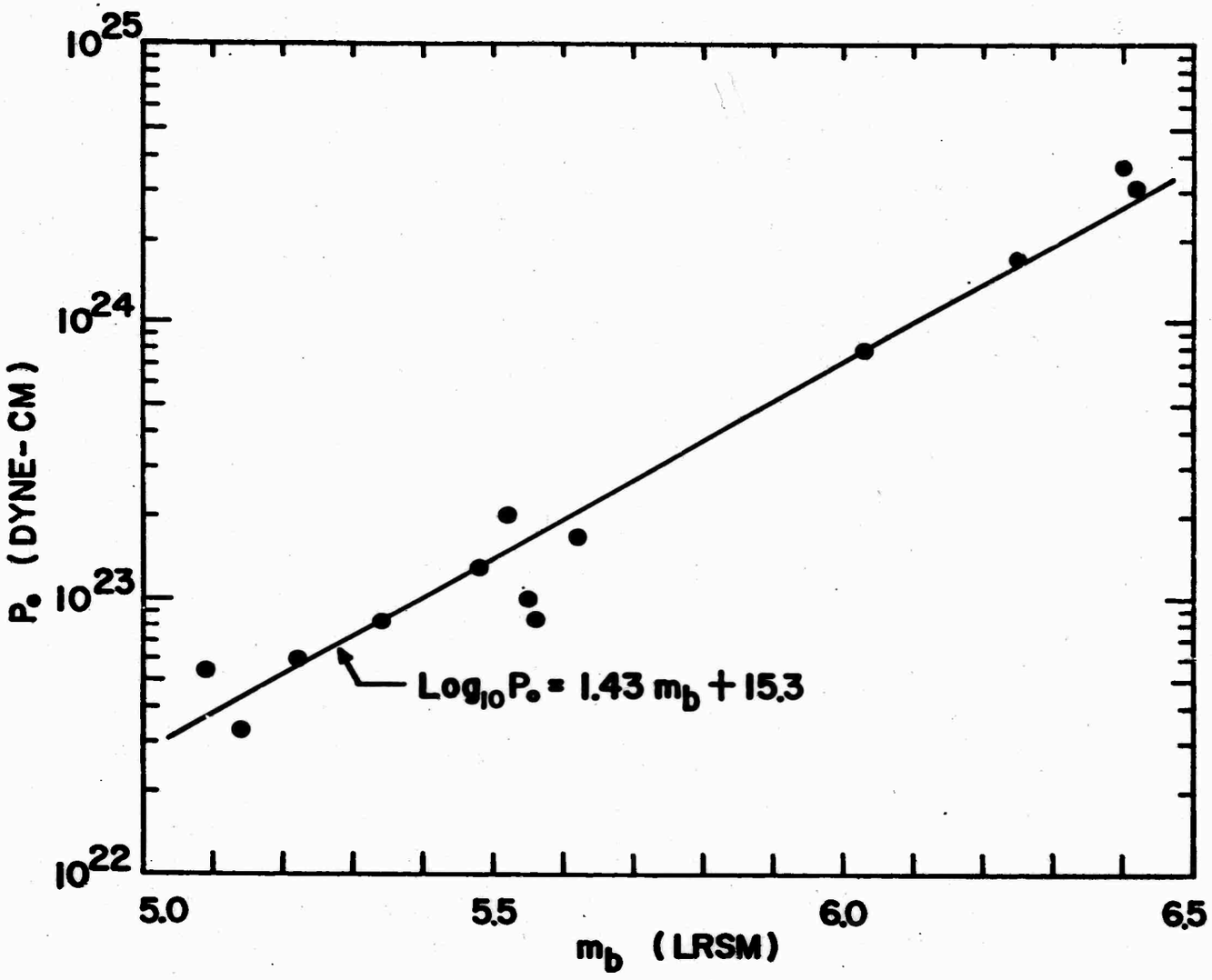

Figure 4. Relationship of P_o vs m_b for underground nuclear explosions P_o is the steady-state strength of the three orthogonal double forces used to represent an explosion source.

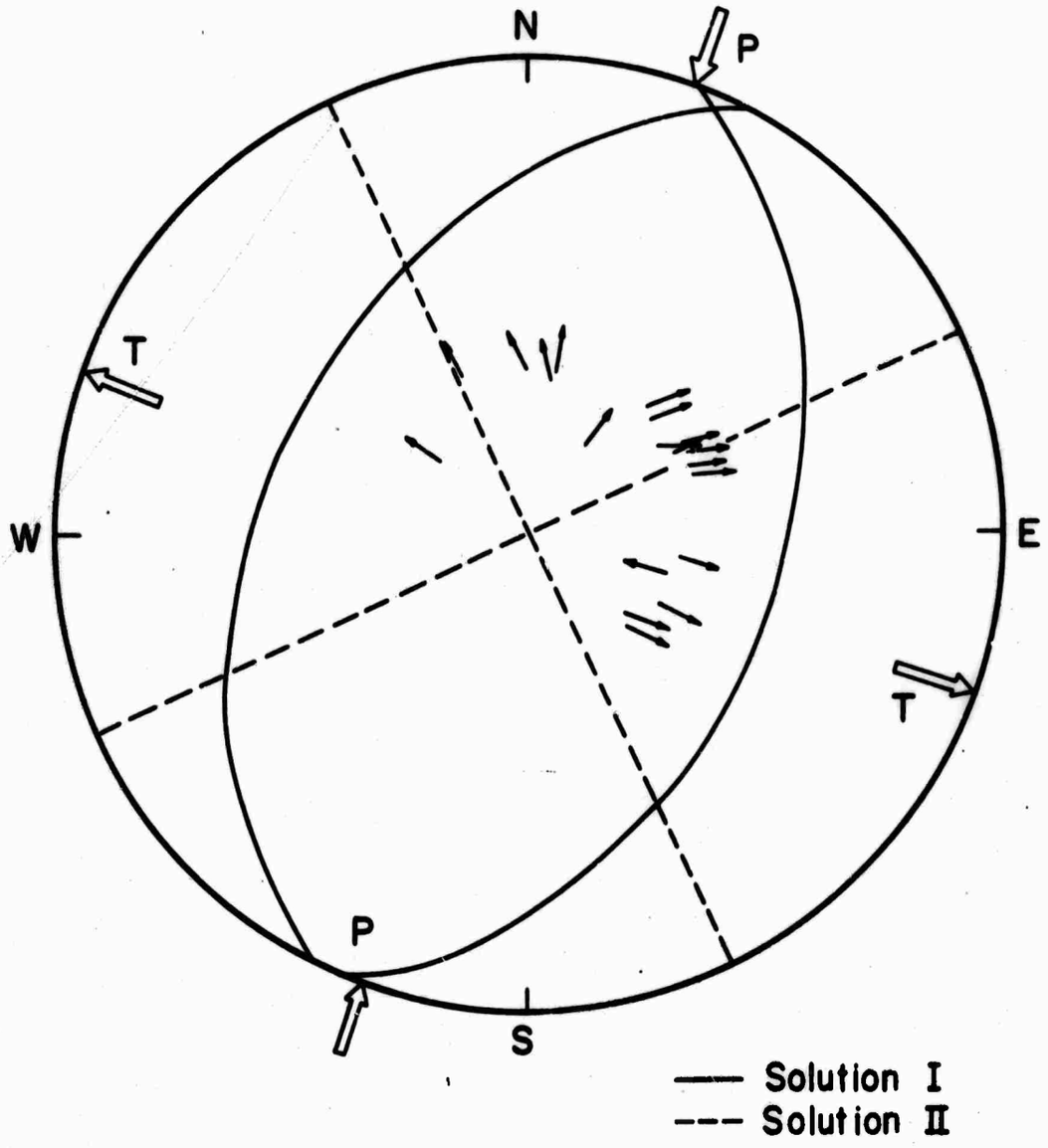

Figure 5. Fault plane solution for the earthquake triggered by the Boxcar explosion using the observed S wave polarization angles (Hirasawa, 1969). Solution I assumes that S waves are generated only by the triggered earthquake, while Solution II assumes that the observed S waves are consisted of not only direct S but also reflected pS, sS waves.

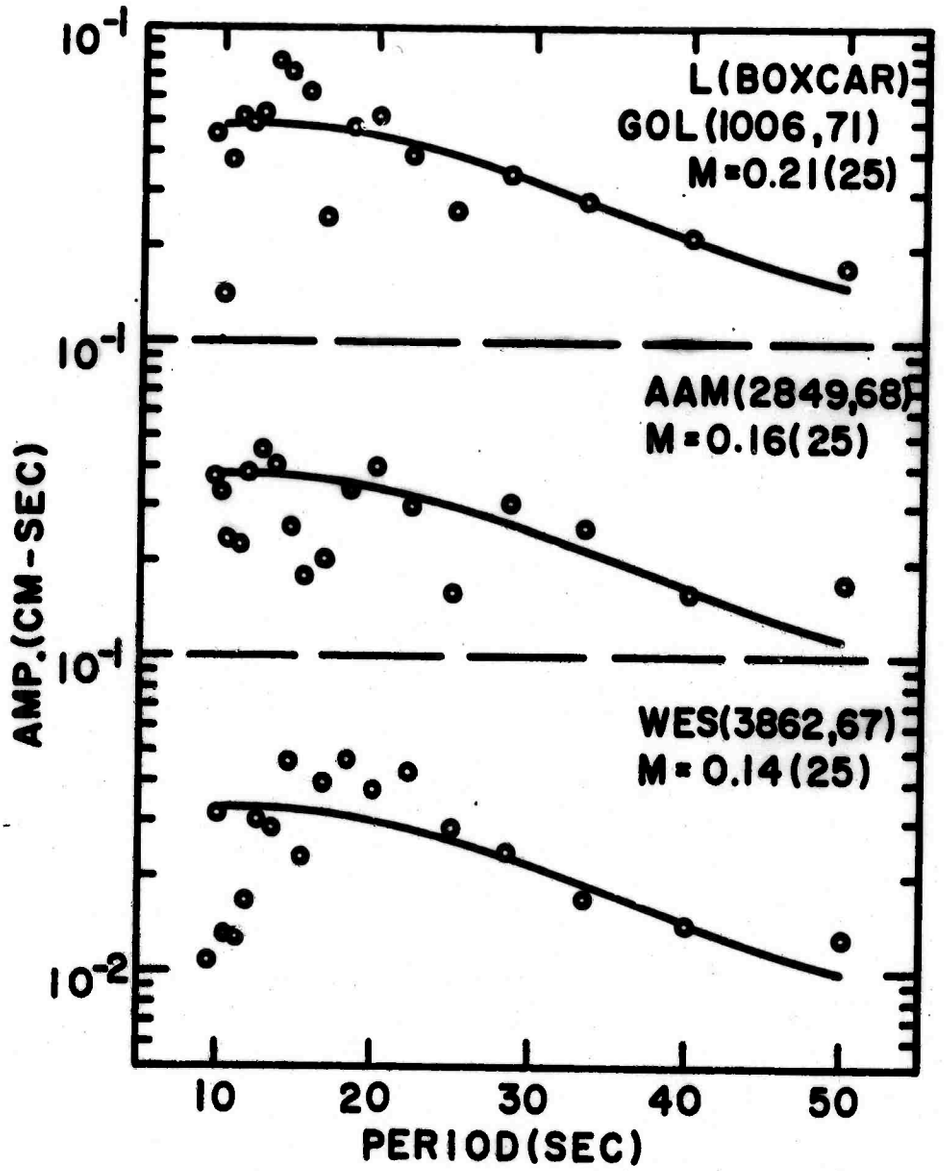

Figure 6. Observed Love wave amplitude spectra for the earthquake triggered by the Boxcar explosion. All the data shown in this and the following figures have been corrected for instrumental response and equalized to Δ = 2000 km. The solid curves represent the theoretical Love wave spectra for these stations using Solution I shown in Figure 5.

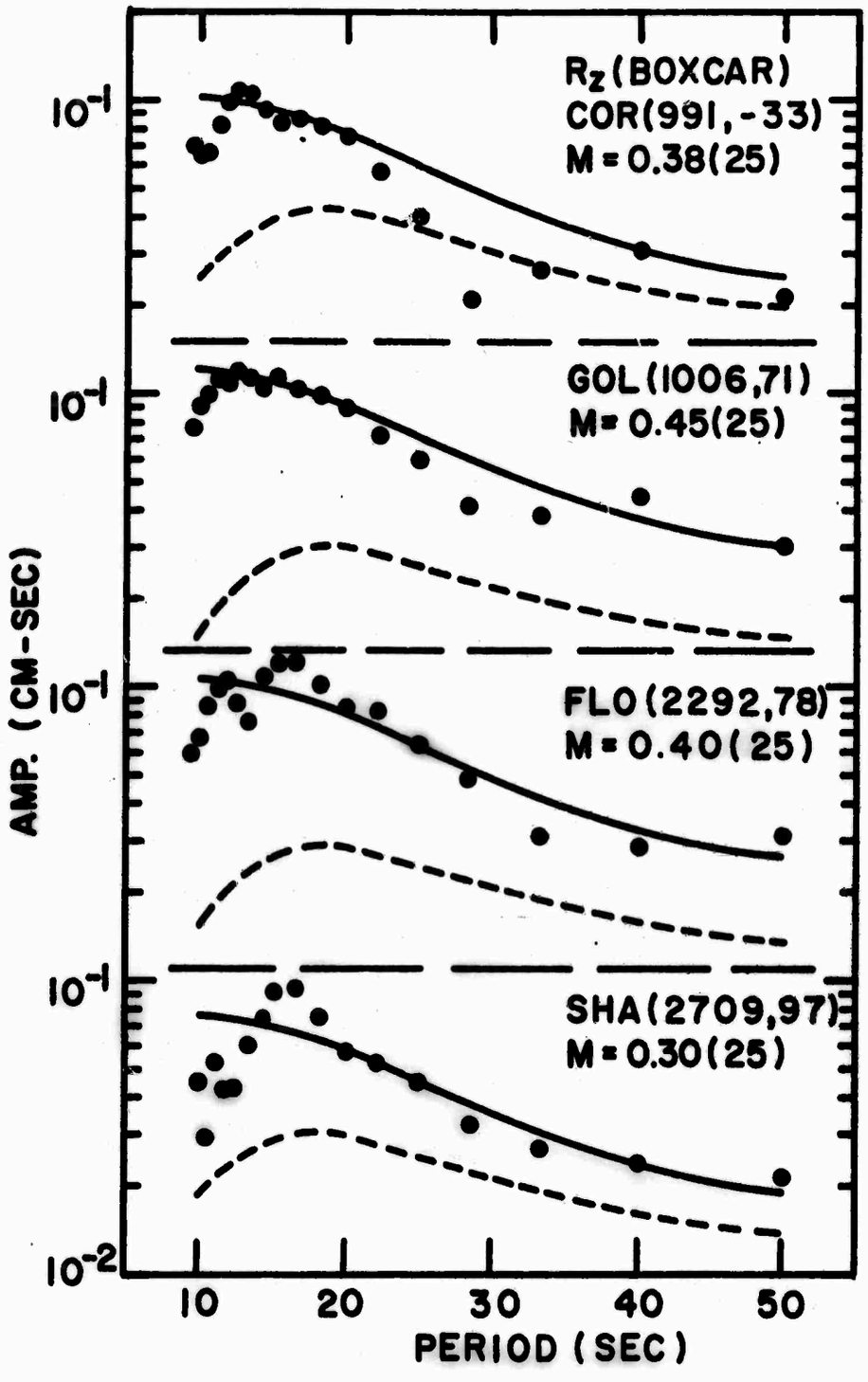

Figure 7. Observed Rayleigh wave amplitude spectra for the Boxcar explosion at four stations on different azimuths. The solid curves represent the theoretical spectra for a pure explosion source and the dashed curves show the theoretical spectra for the triggered earthquake assuming that its source mechanism is Solution I and its focal depth is 3 km. The seismic moment obtained from the observed Love wave amplitude spectra is used to give these theoretical Rayleigh wave spectra.

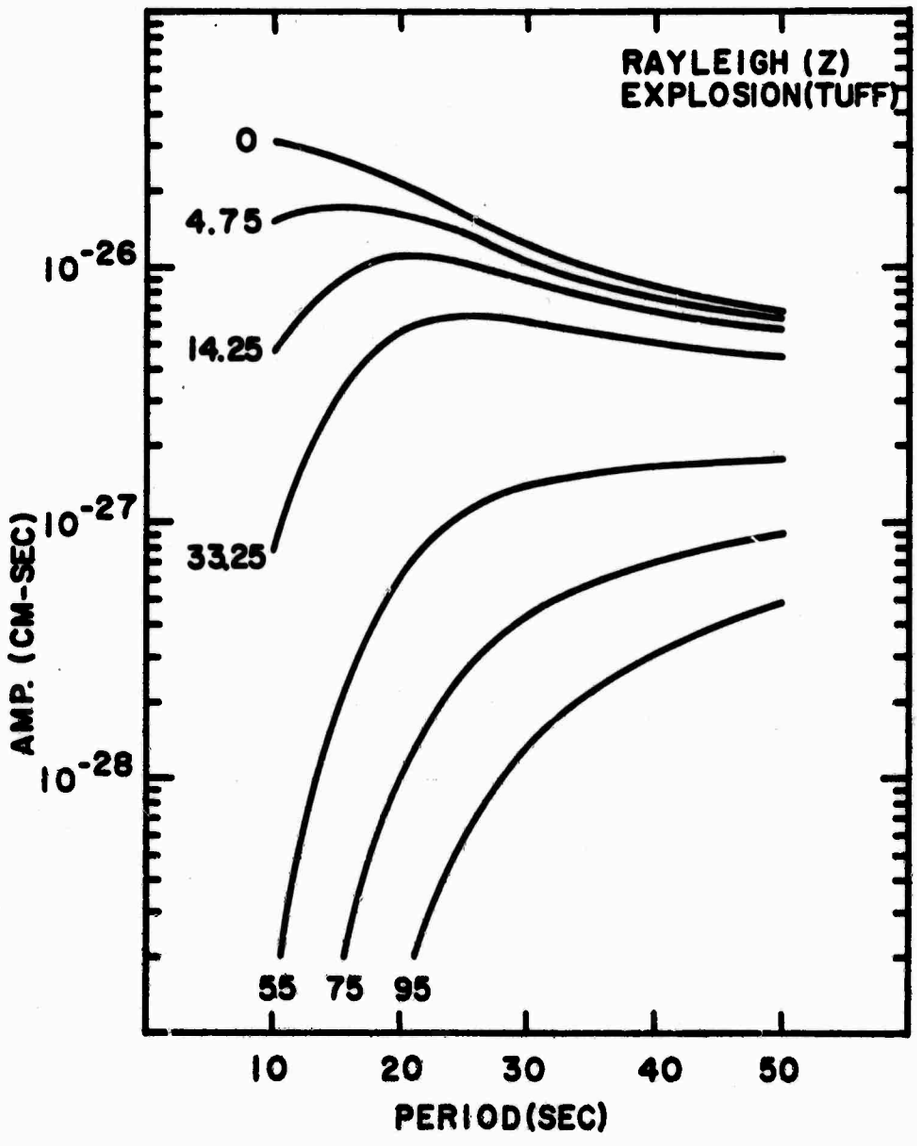

Figure 8. Theoretical Rayleigh wave amplitude spectrum for an underground nuclear explosion at various depths as expected at Δ = 2000 km.

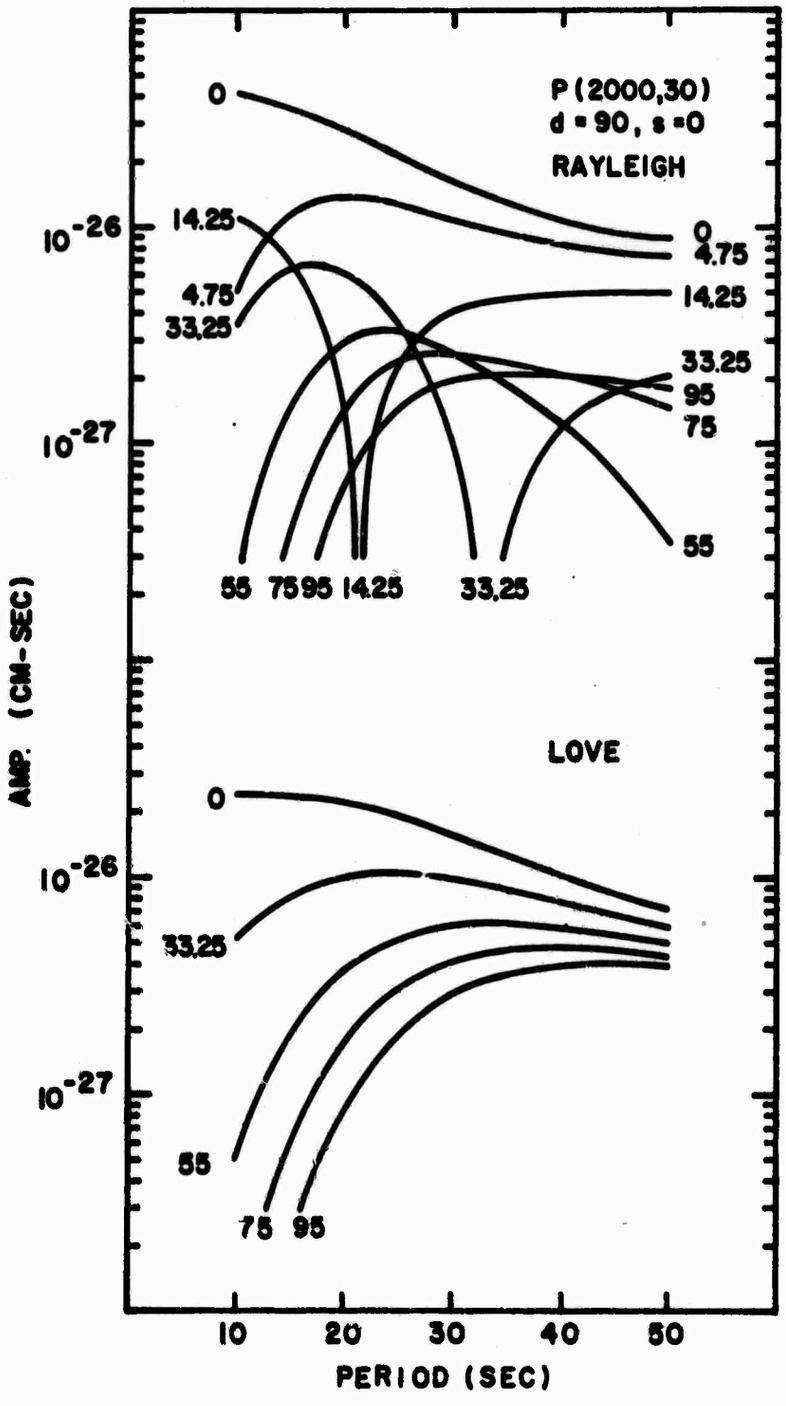

Figure 9. Theoretical Rayleigh (top) and Love (bottom) wave amplitude spectra for a vertical strike-slip earthquake at various depths as expected at Δ = 2000 km and ϕ = 30° from the fault strike. A step time function is assumed for the earthquake source.

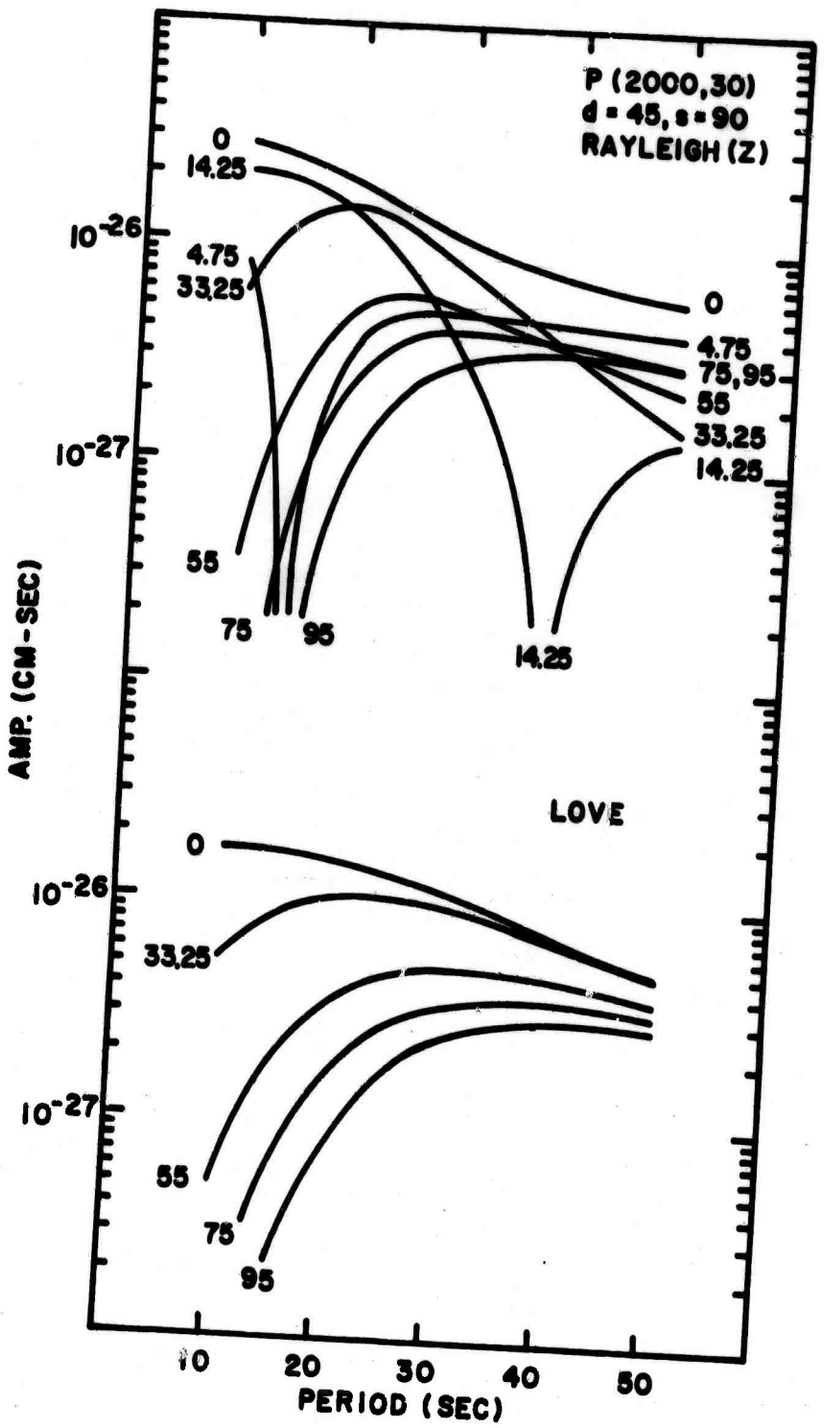

Figure 10. Theoretical Rayleigh (top) and Love (bottom) wave amplitude spectra for a pure dip-slip earthquake at various depths as expected at Δ = 2000 km and ϕ = 30° from the fault strike.

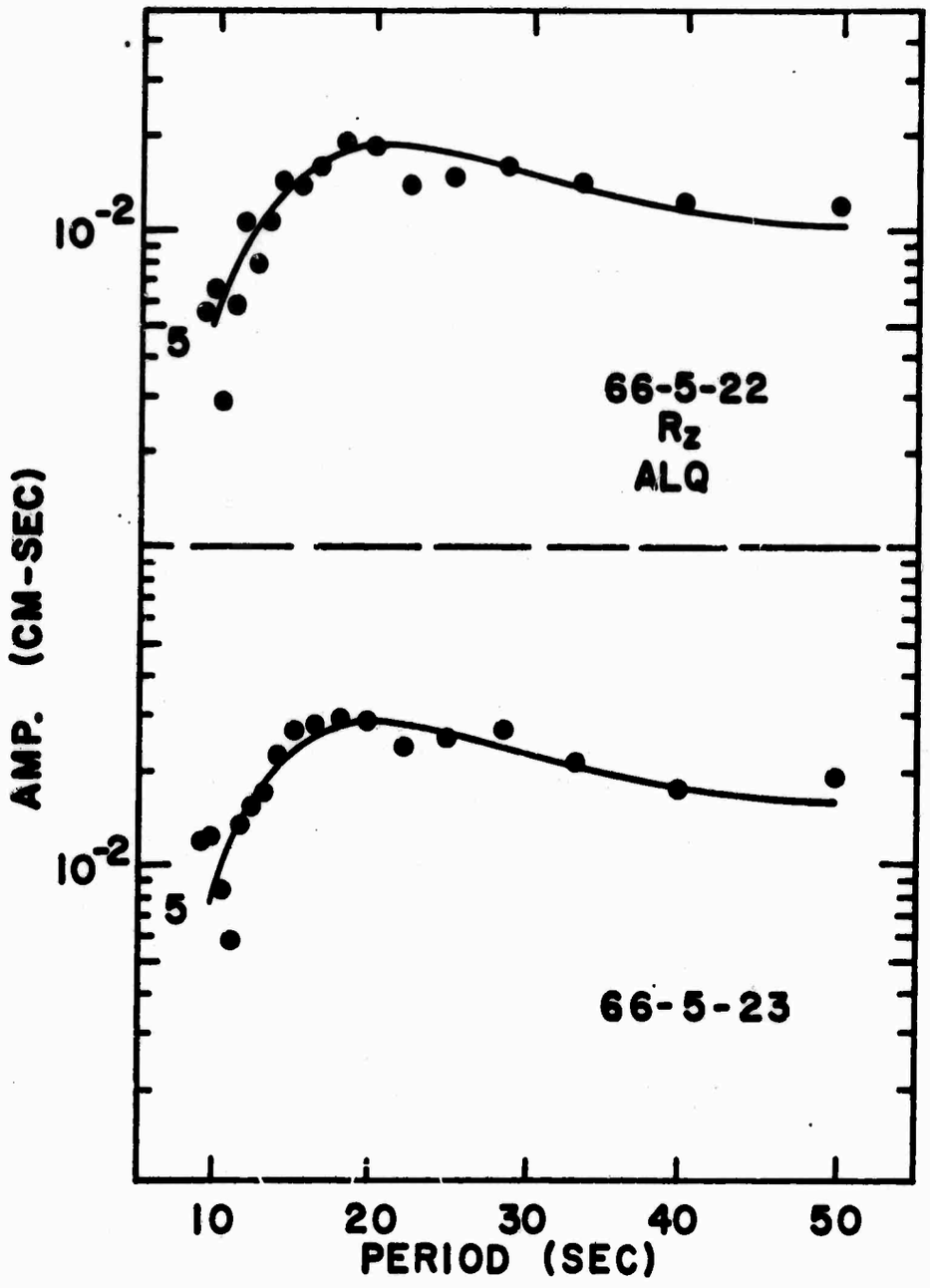

Figure 11. Observed Rayleigh wave amplitude spectra for two neighboring earthquakes in the Gulf of California.

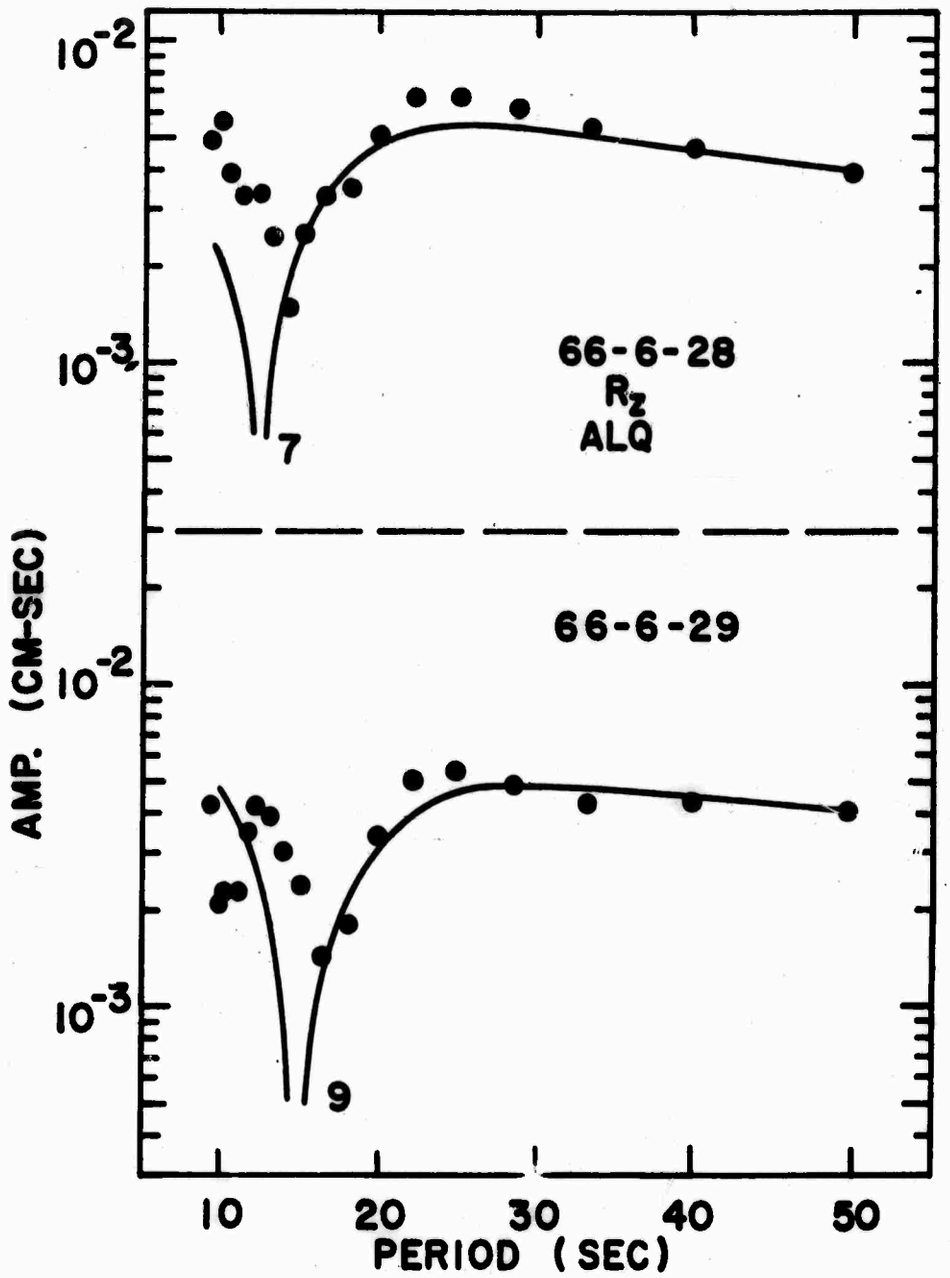

Figure 12. Observed Rayleigh wave amplitude spectra for the foreshock and the aftershock of the Parkfield, California earthquake of June 28, 1966.

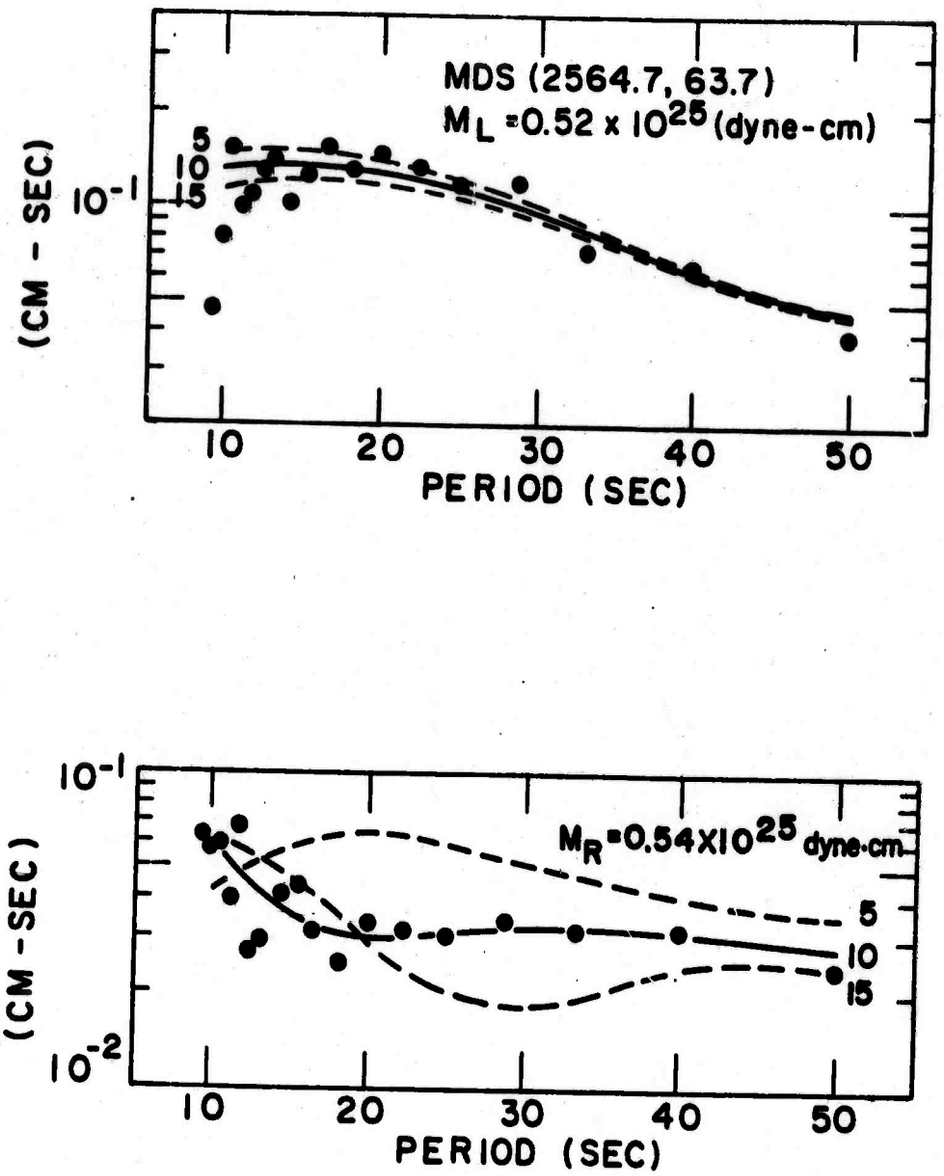

Figure 13. Observed Love (top) and Rayleigh (bottom) wave amplitude spectra for the Truckee, California, earthquake of September 12, 1966.

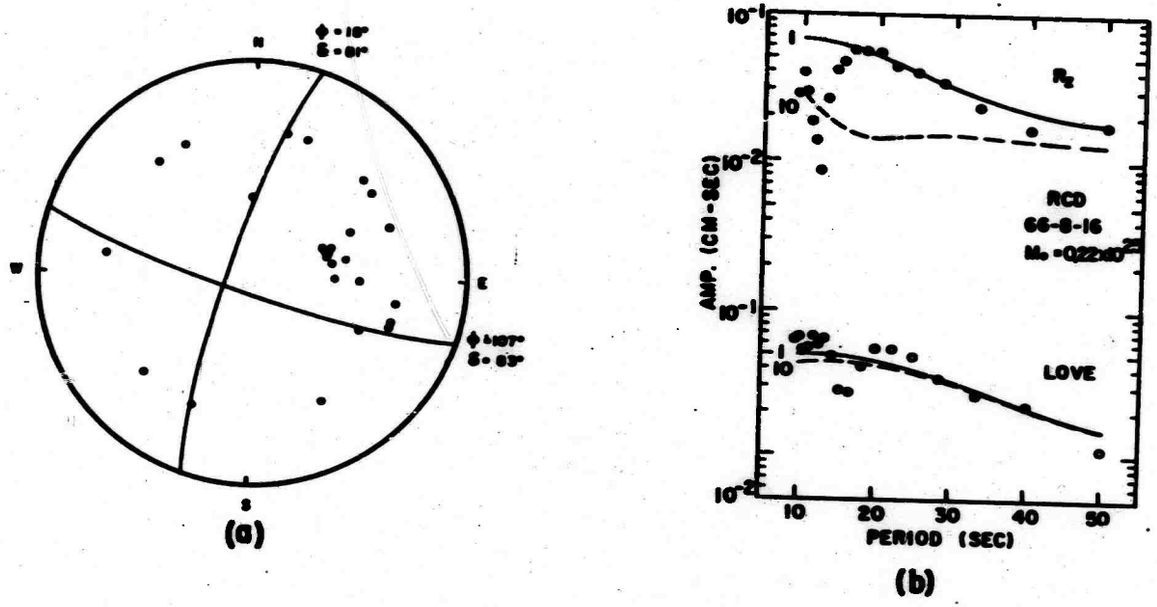

Figure 14. The Caliente, Nevada earthquake of August 16, 1966. (a) The fault plane solution from P-wave polarity data. (b) Rayleigh (top) and Love (bottom) wave amplitude spectra observed at Rapid City, South Dakota.

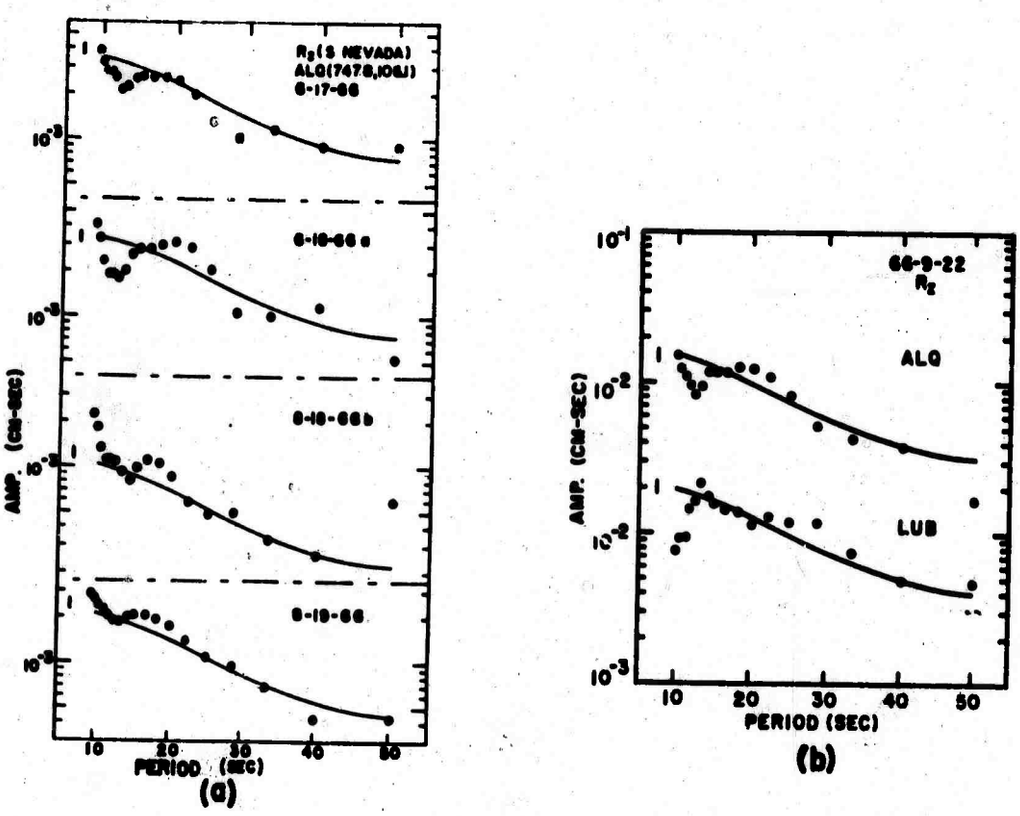

Figure 15. The Rayleigh wave amplitude spectra for (a) four aftershocks, observed at ALQ, and (b) another aftershock, observed at ALQ and LUB, of the Caliente, Nevada earthquake of August 16, 1966.

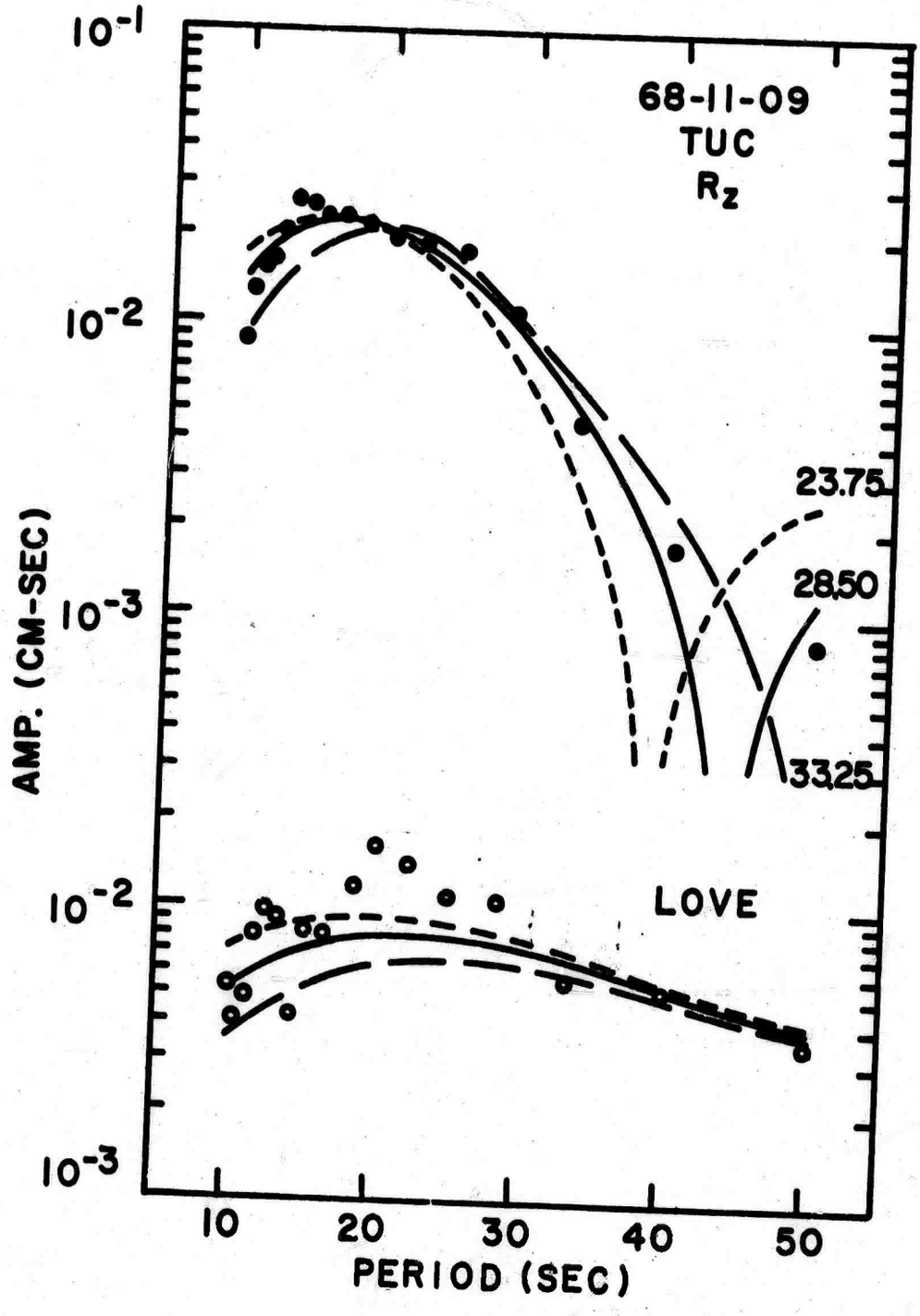

Figure 16. Rayleigh (top) and Love wave amplitude spectra for the south central Illinois earthquake of November 9, 1968 observed at Tucson, Arizona.

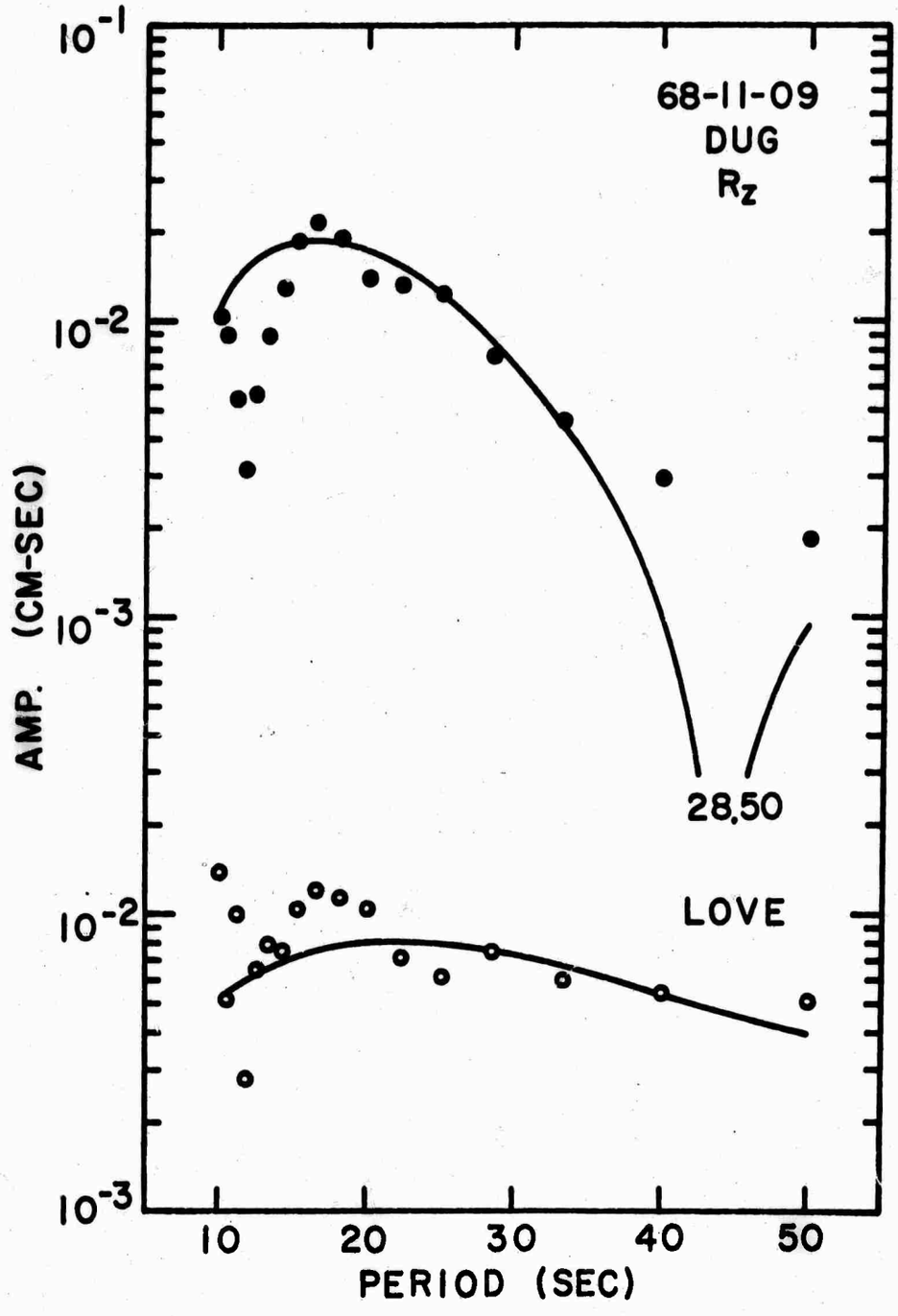

Figure 17. Rayleigh (top) and Love wave amplitude spectra for the south central Illinois earthquake of November 9, 1968 observed at Dugway, Utah.

Table 1. NTS Underground Nuclear Explosion Data

No.	Date	Name	m_b (LRSM)	Shot* medium
1	68-12-19	Benham	6.40	T
2	67-01-20	Bourbon	5.09	T
3	68-04-26	Boxcar	6.42	R
4	65-07-23	Bronze	5.22	T
5	65-12-16	Buff	5.14	T
6	65-12-03	Corduroy	5.62	T
7	66-05-19	Dumont	5.48	T
8	68-01-19	Faultless	6.21	T
9	66-06-30	Halfbeak	6.03	R
10	66-05-13	Pirahna	5.33	T
11	67-05-26	Knickerbocker	5.52	R
12	66-02-02	Piledriver	5.55	G
13	66-06-03	Tan	5.56	T

* G - Granite; R - Rhyolite; T - Tuff

Table 2. Earthquake Data

No.	Date	Time	Location	m_b (USCGS)	Source mechanism*	References
1	1966-05-22	07-42-42.9	Gulf of California	5.5	S.S.	Sykes (1968)
2	1966-05-23	11-51-27.3	Gulf of California	5.6	S.S.	Sykes (1968)
3	1966-06-28	04-08-54.7	Parkfield, Calif.	5.1	S.S.	McEvilly, et al. (1967)
4	1966-06-29	19-53-24.1	Parkfield, Calif.	5.0	S.S.	McEvilly, et al. (1967)
5	1966-09-12	16-41-01.7	Truckee, Calif.	5.4	S.S.	Greensfelder (1968) Ryall, et al. (1968) Tsai & Aki (1970)
6	1966-08-16	18-02-36.1	Caliente, Nevada	6.1	S.S.	
7	1966-08-17	23-07-58.9	Caliente, Nevada	5.2	S.S.	
8	1966-08-18a	09-15-34.9	Caliente, Nevada	5.1	S.S.	
9	1966-08-18b	17-35-06.4	Caliente, Nevada	5.2	S.S.	
10	1966-08-19	10-51-38.5	Caliente, Nevada	4.5	S.S.	
11	1966-09-22	18-57-36.5	Caliente, Nevada	5.3	S.S.	
12	1968-11-09	17-01-41.1	South Central, Ill.	5.3	D.S.	Stauder & Nuttli (1970)

* S.S. - Strike-Slip; D.S. - Dip-Slip

SOME REMARKS ON THE USE OF RELATIVE EXCITATION OF SURFACE WAVES TO DISCRIMINATE BETWEEN EARTHQUAKES AND UNDERGROUND EXPLOSIONS*

By

Robert C. Liebermann

Seismological Laboratory
California Institute of Technology
Pasadena, California

*These paragraphs are a brief summary of the work to be reported at the meeting. For details, see the figures attached and the remarks in the figure captions.

Recent work on detection and discrimination of earthquakes and underground explosions has focused on the relative excitation of body (m_b) and surface (M_s) waves by the two types of events. Such M_s vs. m_b diagrams are crude abstractions of the total information contained on the seismogram, but this technique has proven to be very useful in discriminating between events of $m_b > 5$.

A detailed comparison of M_s - m_b data for western United States events compiled by various investigators (Liebermann and Pomeroy, 1969; Basham, 1969; Evernden, 1969) indicates: a) separation of earthquake and explosion populations above $m_b = 5$; b) tendency for data population to converge below $m_b = 4\text{-}1/2$; c) better separation of event populations when M_s is based on amplitude of 20-second Rayleigh waves rather than on waves with maximum amplitude on seismogram (generally less than 20 seconds for NTS explosions recorded in continental North America). This latter observation is undoubtedly a reflection of difference in the surface-wave spectra of earthquakes and underground explosions; it has recently been demonstrated by Molnar et al (1969) that these differences are even more enhanced when periods near 40 sec are used.

It is important that such M_s - m_b studies be based on recordings at a wide range of azimuth and epicentral distances. Theoretical studies (von Seggern, 1970) have shown that variations of more than one M_s (or m_b) unit are to be expected from single-station observations as the result of radiation pattern effects. Even for presumably symmetric underground explosions, individual station values of M_s - m_b vary by more than one magnitude unit. This scatter for explosions is due to propagation effects, station bias, and, in some cases, contamination of the explosion by tectonic strain release. Contamination of the explosion surface-wave spectra by earthquake-generated Rayleigh waves leads to wide variations in the spectral ratio (amplitude of 20-sec/amplitude of 40-sec waves) observed at WWSSN stations for MILROW (Savino et al, 1970).

The observed differences in the excitation of surface waves by underground explosions and earthquakes of comparable m_b, are at least partly due to differences in the spatial dimension of the source region. Earthquakes in the western U.S. have dimensions ranging from 2 to 15 km for $m_b \approx 4$ events to 5 to 25 km for $m_b \approx 5$ events (Liebermann and Pomeroy, 1970). The wide variability in these limits presumably reflects differences between high and low stress-drop earthquakes. Explosions in the same magnitude range generally have dimensions at least one order of magnitude smaller. However, several large NTS explosions ($m_b \approx 6$) have released tectonic strain along a zone of aftershocks which extends almost 10 km (e.g., Hamilton and Healy, 1969).

REFERENCES

Basham, P.W., 1969, Canadian magnitudes of earthquakes and nuclear explosions in south-western North America, Geophys. J., v. 17, p. 1-13.

Basham, P.W., Weichert, D.H., and Anglin, F.M., 1970, An analysis of the 'BENHAM' aftershock sequence using Canadian recordings, J. Geophys. Res., v. 75, p. 1545-1556.

Capon, J., Greenfield, R.J., and Lacoss, R.T., 1967, Surface vs body-wave magnitude results, in Semiannual Technical Summary, Lincoln Laboratories, M.I.T., p. 3-5, Lexington, Mass., June 30.

Evernden, J.F., 1967, Magnitude determination at regional and near-regional distances in the United States, Bull. Seism. Soc. Am., v. 57, p. 591-639.

Evernden, J.F., 1969, Discrimination of small magnitude earthquakes and explosions, J. Geophys. Res., in press.

Gutenberg, B., 1945, Amplitudes of surface waves and magnitudes of shallow earthquakes, Bull. Seism. Soc. Am., v. 35, p. 3-12.

Gutenberg, B., and Richter, C.F., 1956, Magnitude and energy of earthquakes, Ann. di Geofis, v. 9, p. 1-15.

Hamilton, R.M., and Healy, J.H., 1969, Aftershocks of the BENHAM nuclear explosion, Bull. Seism. Soc. Am., v. 59, p. 2271-2281.

Liebermann, R.C., 1970, Excitation of surface waves by the Aleutian underground explosion MILROW (2 October 1969), J. Geophys. Res., in preparation.

Liebermann, R.C., and Pomeroy, P.W., 1969, Relative excitation of surface waves by earthquakes and underground explosions, J. Geophys. Res., v. 74, p. 1575-1590.

Liebermann, R.C., and Pomeroy, P.W., 1967, Excitation of surface waves by events in southern Algeria, Science, v. 156, p. 1098-1100.

Liebermann, R.C., and Pomeroy, P.W., 1970, Source dimensions of small earthquakes as determined by the size of the aftershock zone, Bull. Seism. Soc. Am., v. 50, p. 879-890.

Liebermann, R.C., King, C.Y., Brune, J.N., and Pomeroy, P.W., 1966, Excitation of surface waves by the underground nuclear explosion Long Shot, J. Geophys Res., v. 71, p. 4333-4339.

330-A

Molnar, P., Savino, J., Sykes, L.R., Liebermann, R.C., Hade, G., and Pomeroy, P.W., 1969, Small earthquakes and explosions in western North America recorded by new high gain, long period seismographs, Nature, v. 224, p. 1268-1273.

Richter, C.F., 1935, An instrumental earthquake magnitude scale, Bull. Seism. Soc. Am., v. 25, p. 1-32.

Ryall, A., and Savage, W.U., 1969, A comparison of seismological effects for the Nevada underground test BOXCAR with natural earthquakes in the Nevada region, J. Geophys. Res., v. 74, p. 4281-4289.

Savino, J., Sykes, L.R., Molnar, P., and Liebermann, R.C., 1970, in press.

SIPRI, Seismic Methods for Monitoring Underground Explosions, Report by a Seismic Study Group, edited by D. Davies, International Institute for Peace and Conflict Research (SIPRI), Stockholm, p. 130, August 1968.

Thirlaway, H.I.S., and Carpenter, E.W., 1964, Seismic signal anomalies travel times, amplitudes, and pulse shapes, p. 119-140 in Proceedings of the VESIAC Special Study Conference on Seismic Signal Anomalies, Travel Times, Amplitudes, and Pulse Shapes, Beaugency, France, October. VESIAC Rept. 4410-99-X, February, 1966.

Vanek, J., Zatopek, A., Karnik, V., Kondorskaya, N.V., Riznichenko, Yu. V., Savarensky, E.F., Solov'ev, S.L., and Shebalin, N.V., 1962, Standardization of magnitude scales, Bull. (Izv.) Acad. Sci. U.S.S.R., Geophys. Ser., (English Transl.) No. 2, p. 108-111.

von Seggern, D., 1970, The effects of radiation pattern on magnitude estimates, Bull. Seism. Soc. Am., v. 60, p. 503-516.

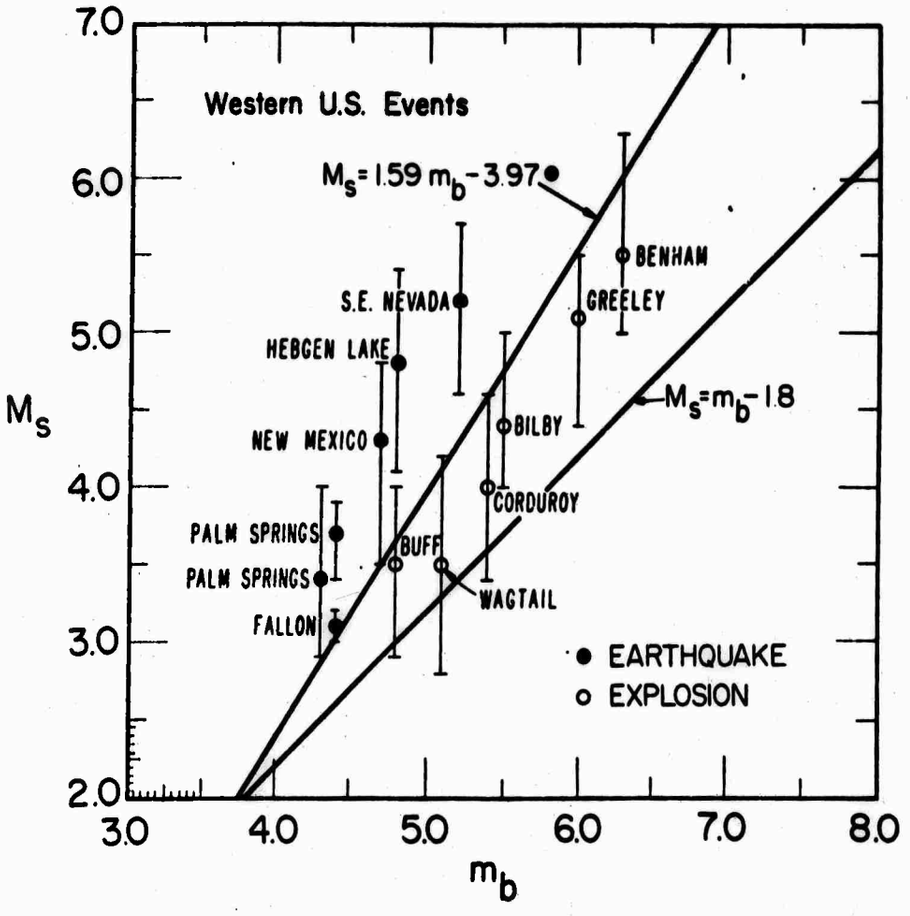

Figure 1. Data of Liebermann and Pomeroy (1969). Earthquake chosen to provide a variety of geographic and tectonic settings. For fixed m_b, the vertical bars represent the maximum scatter of individual M_s determinations. Above $m_b = \simeq 5$, the earthquakes and explosions separate into distinct populations. Separation less distinct for $m_b < 5$. Solid curves represent: (1) an empirical relationship ($M_s = 1.59\, m_b - 3.97$) determined by Gutenberg and Richter (1956) using a large number of data from earthquakes with $m_b \geq 6$; (2) a composite of the magnitude-yield relationships ($M_s = m_b - 1.8$) established by Thirlaway and Carpenter (1966; see also Marshall, 1970).

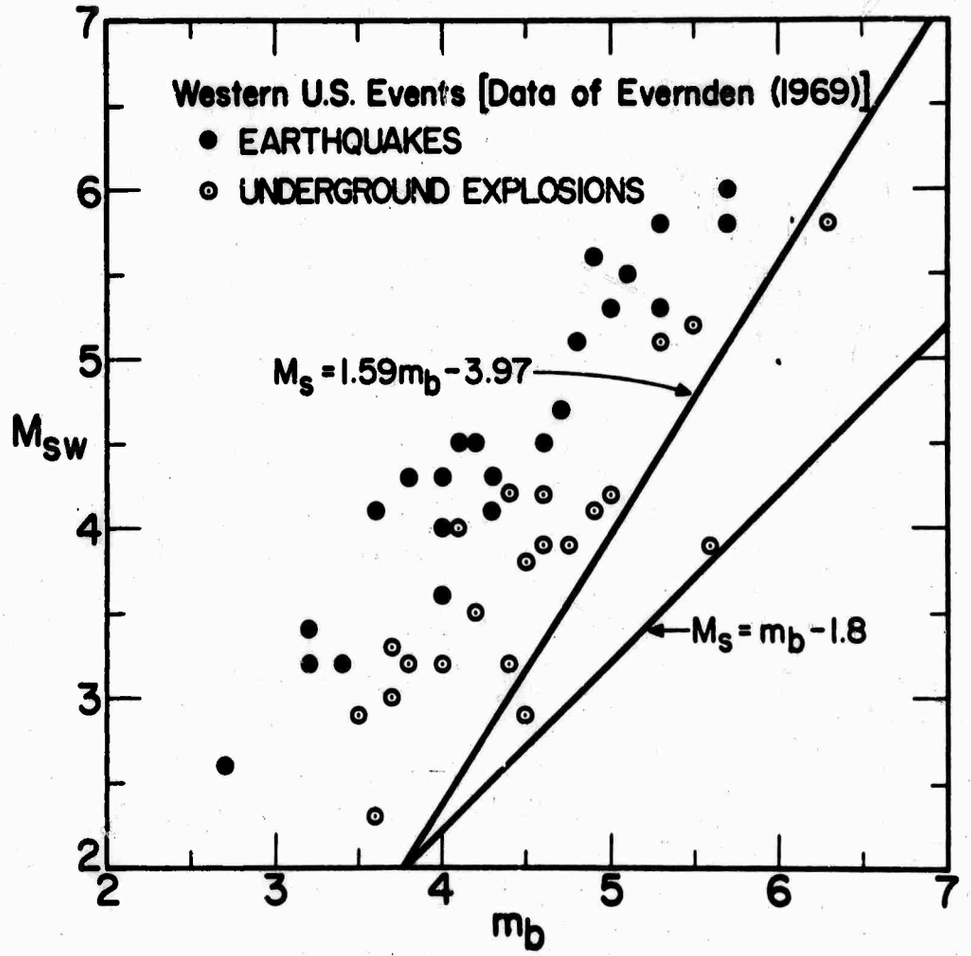

Figure 2. Data of Evernden (1969). Earthquake and explosion populations merge at m_b < 4 1/2. M_{SW} determined using maximum amplitude on seismogram (mostly LRSM stations) and $M_{SW} = M_S + 0.2$.

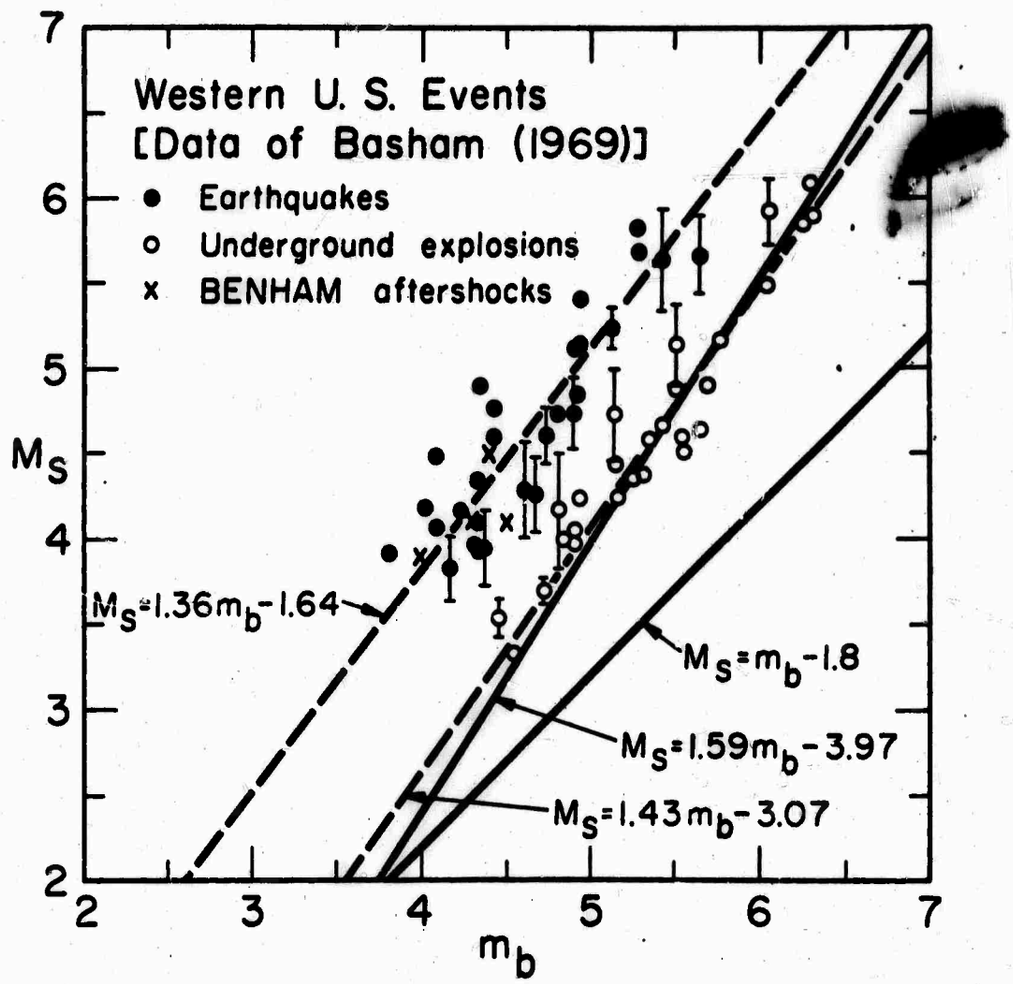

Figure 3. Data of Basham (1969, 1970). Earthquake and explosion of populations parallel to $m_b = 4.5$, but separation often less than one standard deviation of M_S determinations. Note that none of the data for the western U.S. events fit the empirical M_S vs m_b curves for earthquakes and explosions throughout the world.

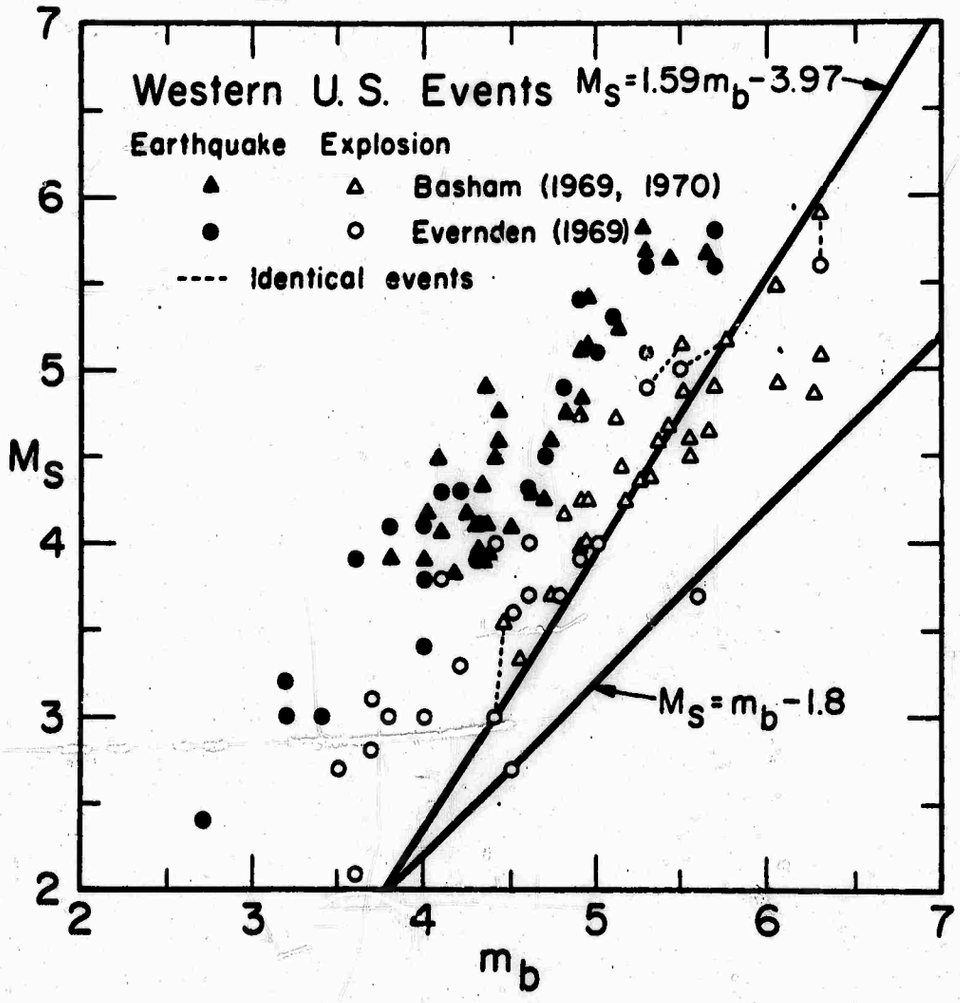

Figure 4. Comparison of data of Evernden (1969) and Basham (1969, 1970). All M_S data represent maximum amplitude of surface waves on seismogram. In general, Evernden's data is from LRSM stations while Basham's is from the Canadian network. Dashed lines connected identical events studied by both authors: BOXCAR, COMMODORE, SCOTCH, and PINSTRIPE. Consistency between two sets of data is remarkably good. Separation of earthquake and explosion populations below m_b = 4 1/2 is less distinct than at larger magnitudes.

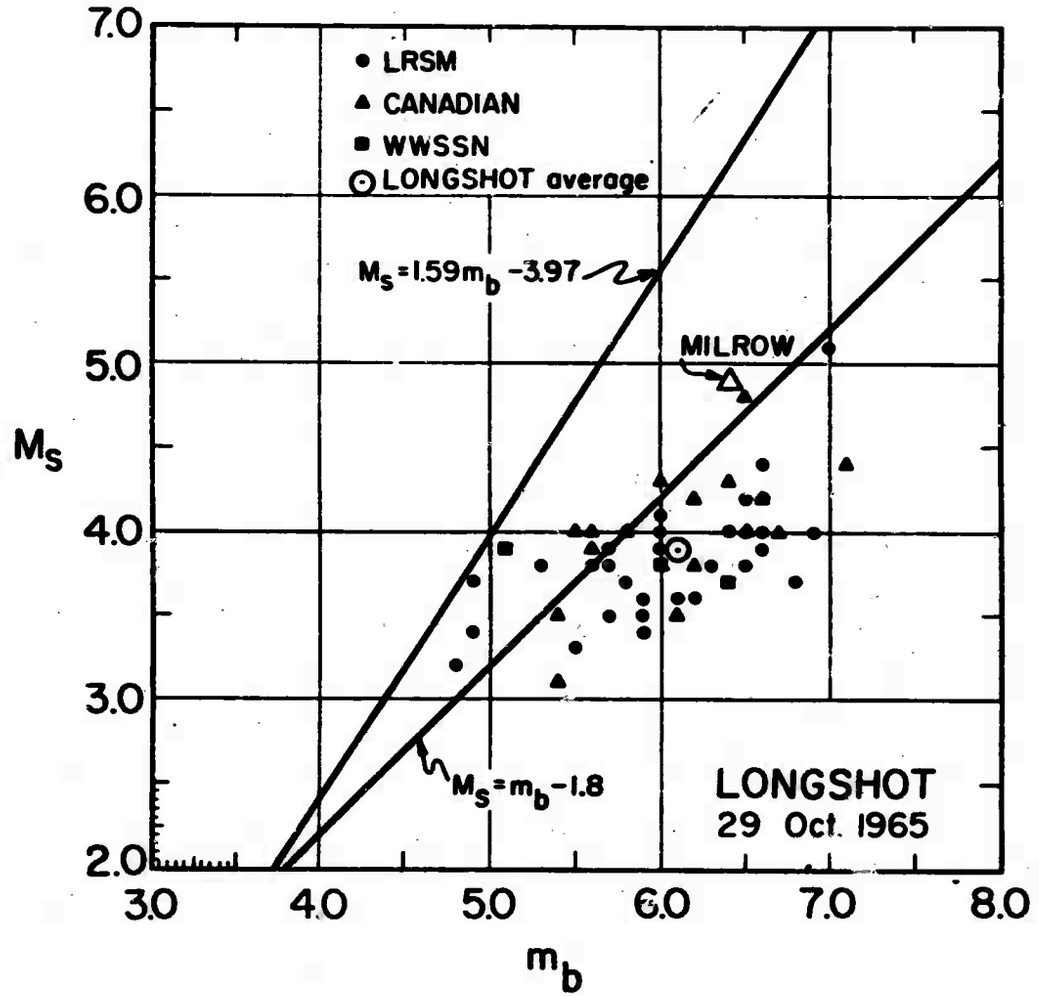

Figure 5. M_S vs m_b for individual stations for Aleutian underground explosion LONG SHOT (after Liebermann et al, 1966). Data from single-stations scatter by more than two units in both M_S and m_b. Average value for MILROW (2 October 1969) shown for comparison (Liebermann, 1970).

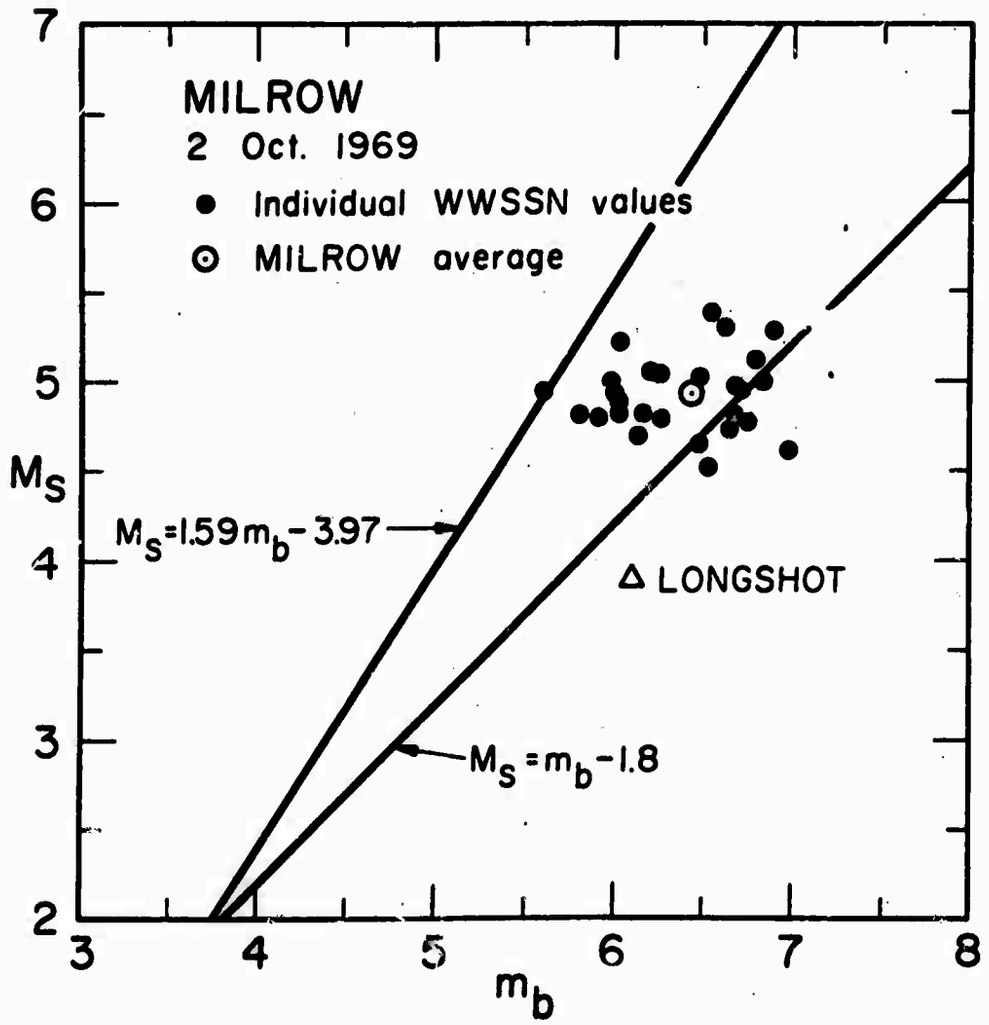

Figure 6. M_s vs m_b for individual stations for Aleutian underground explosion MILROW (Liebermann, 1970). Data from single-stations (covering all four quadrants of azimuth) scatter by 1 1/2 m_b units and 1 M_s unit. Average value for LONG SHOT (29 October 1965) shown for comparison (from Liebermann et al, 1966).

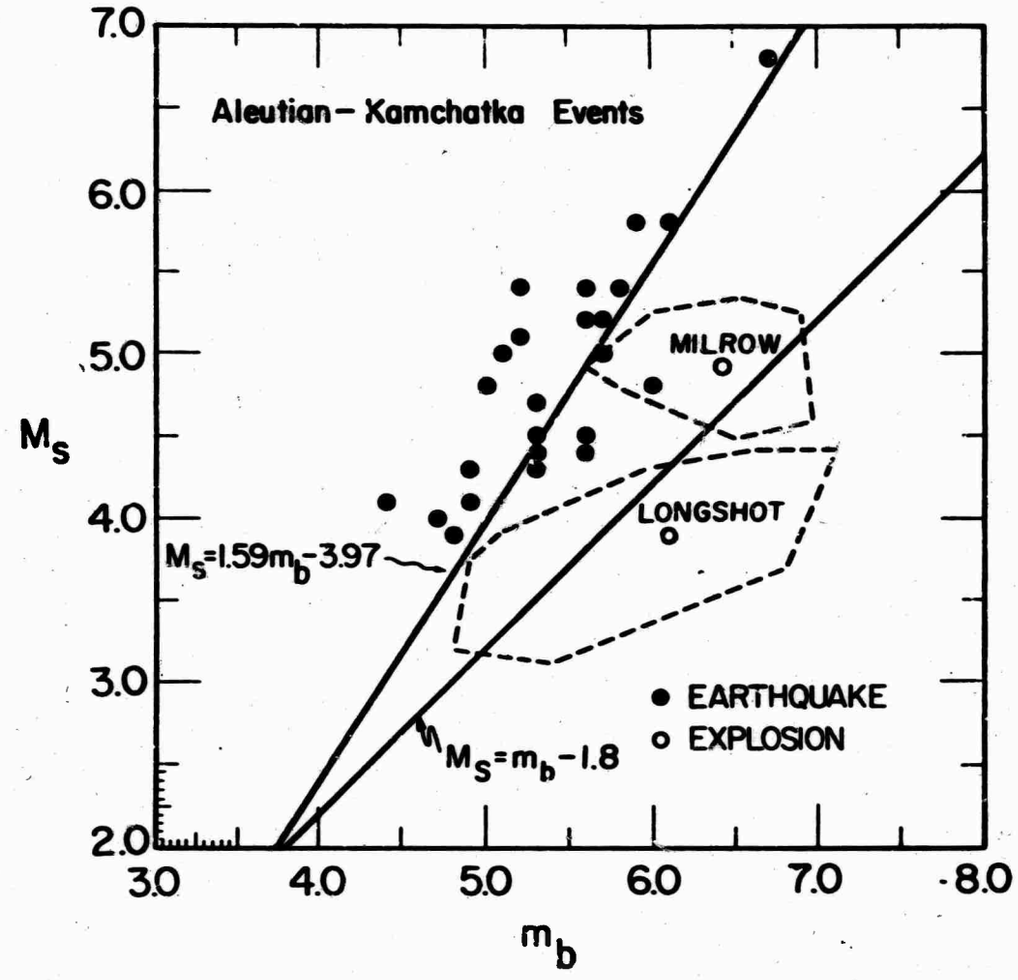

Figure 7. M_S vs m_b for Aleutian-Kamchatka earthquakes and underground explosions LONG SHOT and MILROW (Liebermann et al, 1966; Liebermann and Pomeroy, 1969; Liebermann, 1970). Dashed boxes around the LONG SHOT and MILROW averages represent scatter of the individual station values and demonstrate the pitfalls of single-station analyses of M_S and m_b and the necessity for using a large number of determinations from a range of epicentral distances and azimuths.

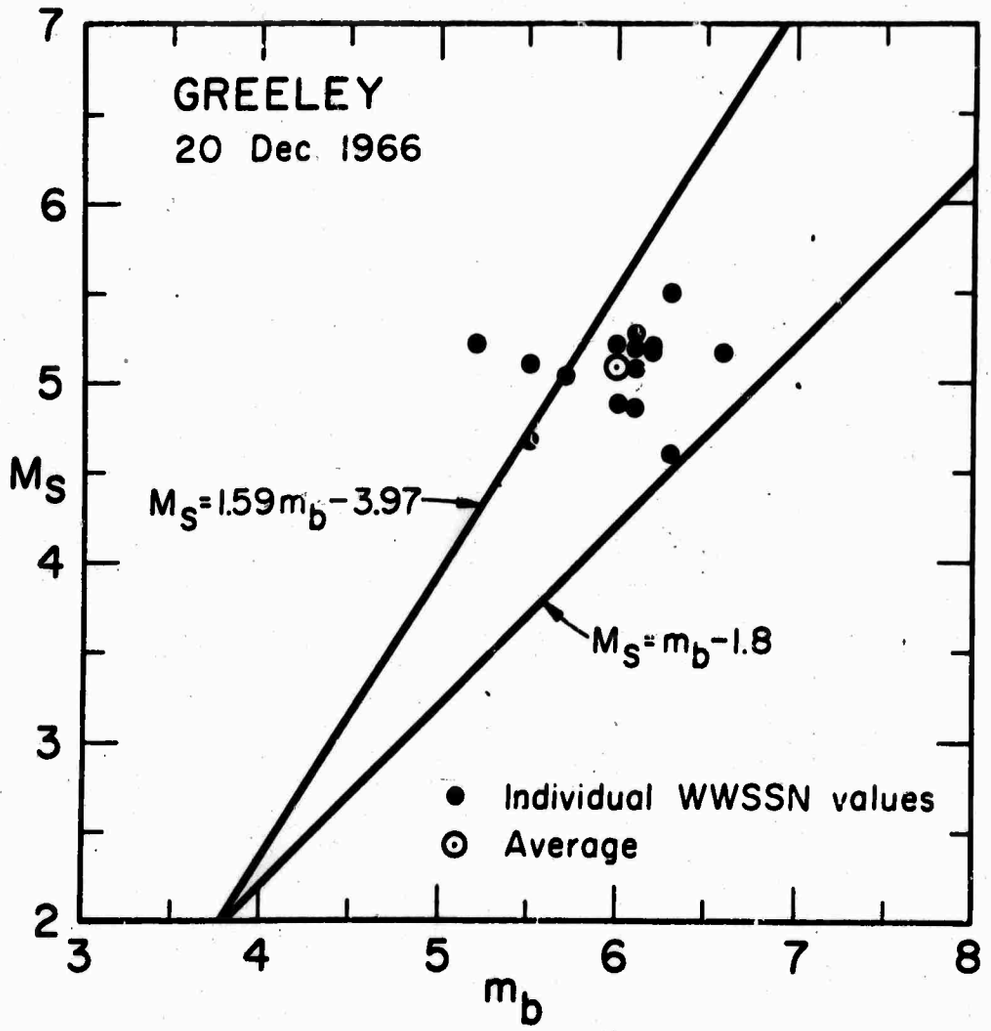

Figure 8. M_S vs m_b for individual stations for Nevada underground explosion GREELEY (data of Liebermann and Pomeroy, 1969). Data from single-stations scatter 1 1/2 m_b units and 1 M_S unit.

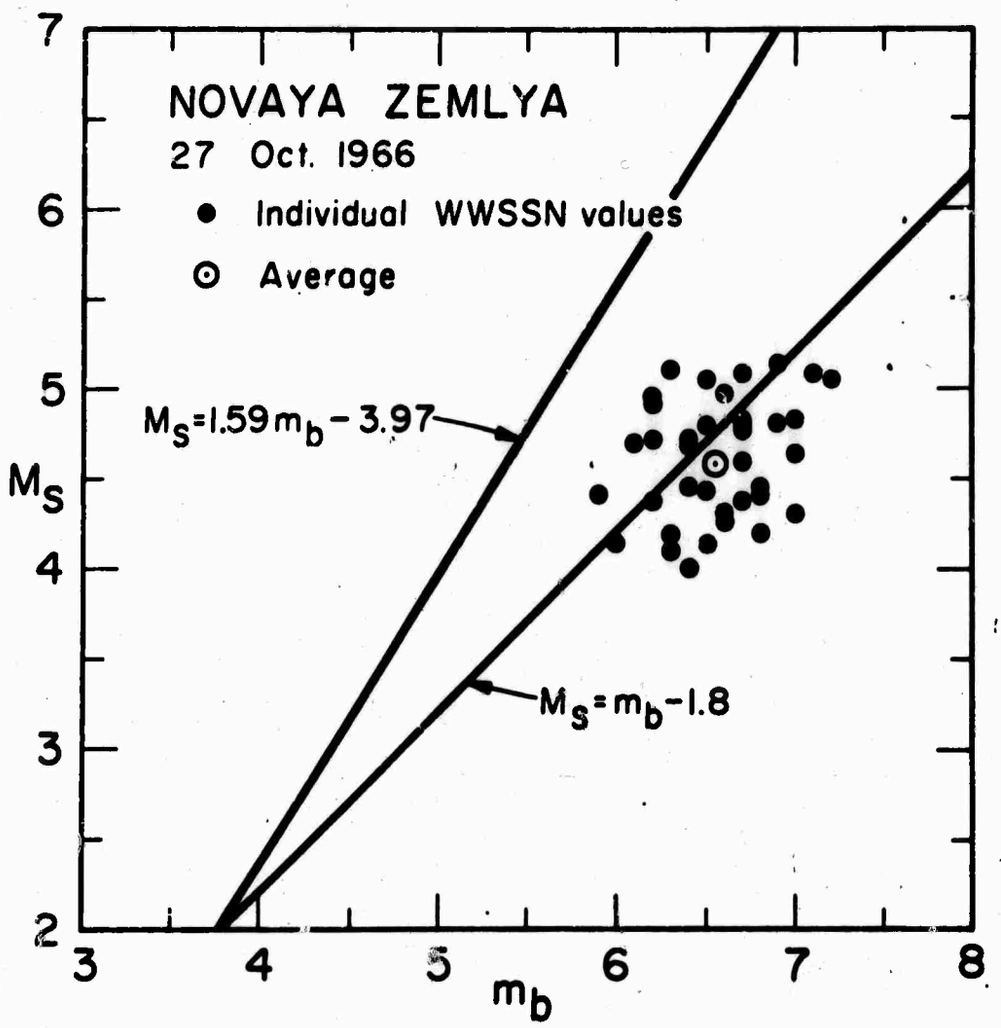

Figure 9. M_S vs m_b for individual stations for Novaya Zemlya underground explosion (see AEC press release of 27 October 1966 annpuncing Soviet test in northern testing area). Data from single-stations scatter by more than one unit for both M_S and m_b.

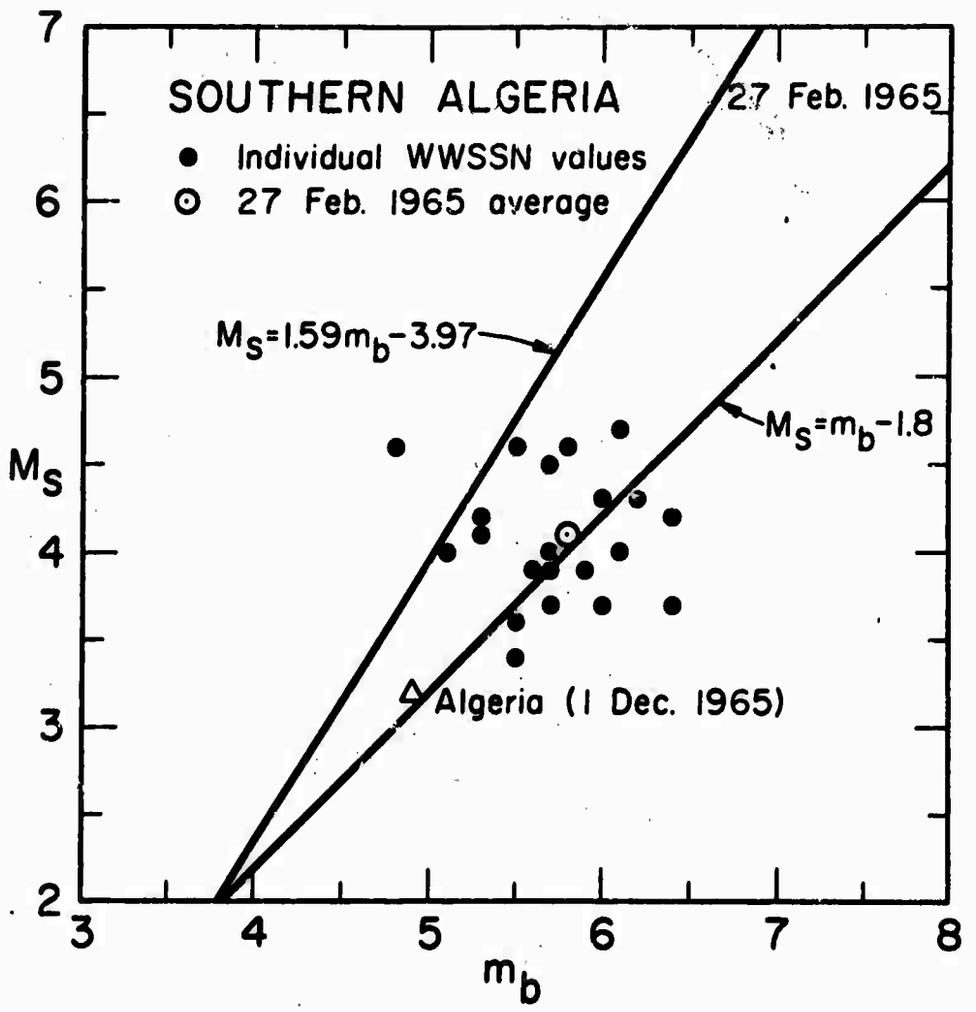

Figure 10. M_S vs m_b for individual stations for southern Algeria presumed underground explosions (data of Liebermann and Pomeroy, 1967). Data from single-stations scatter by 1 1/2 m_b units and almost 2 M_S units for the 27 February 1965 event. Average value for 1 December 1965 event shown for comparison.

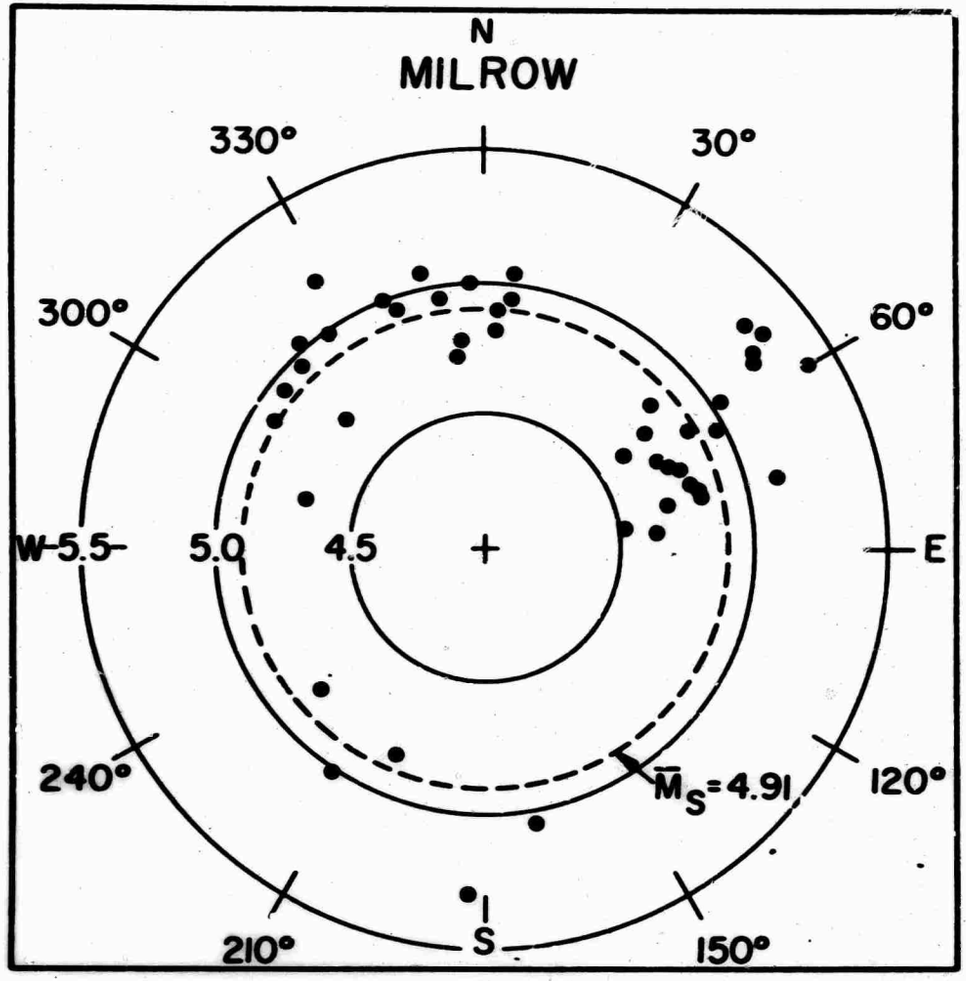

Figure 11. M_S versus azimuth for Aleutian underground explosion MILROW (Liebermann, 1970). Data cover all four quadrants of azimuth and show no clear asymmetry in the radiation pattern of 20-sec Rayleigh waves.

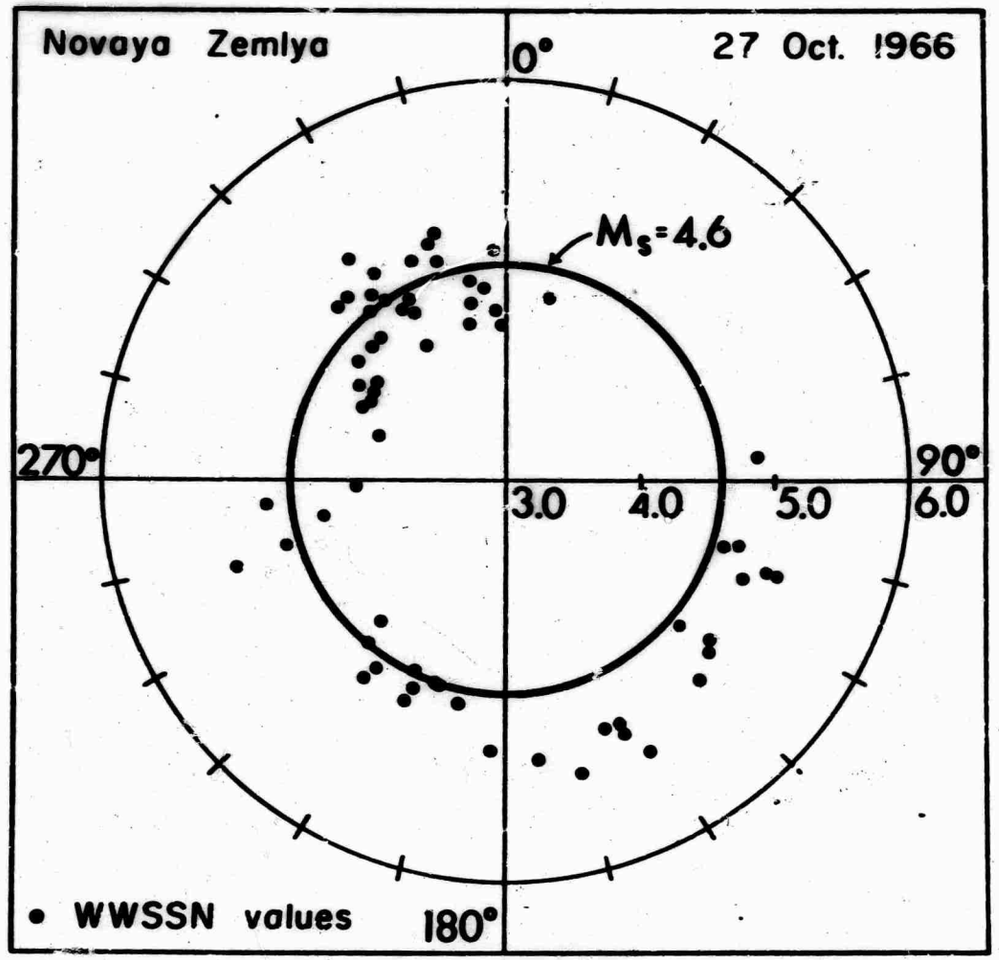

Figure 12. M_S versus azimuth for Novaya Zemlya underground explosion (27 October 1966) -- AEC press relase). Stations in NW quadrant (North America) record systematically lower M_S values than stations in the SE quadrant (southeast Asia). This asymmetry in the radiation pattern is most probably an effect of propagation path and may be a partial explanation for the low M_S values recorded at LASA for Asian explosions (Liebermann and Pomeroy, 1969).

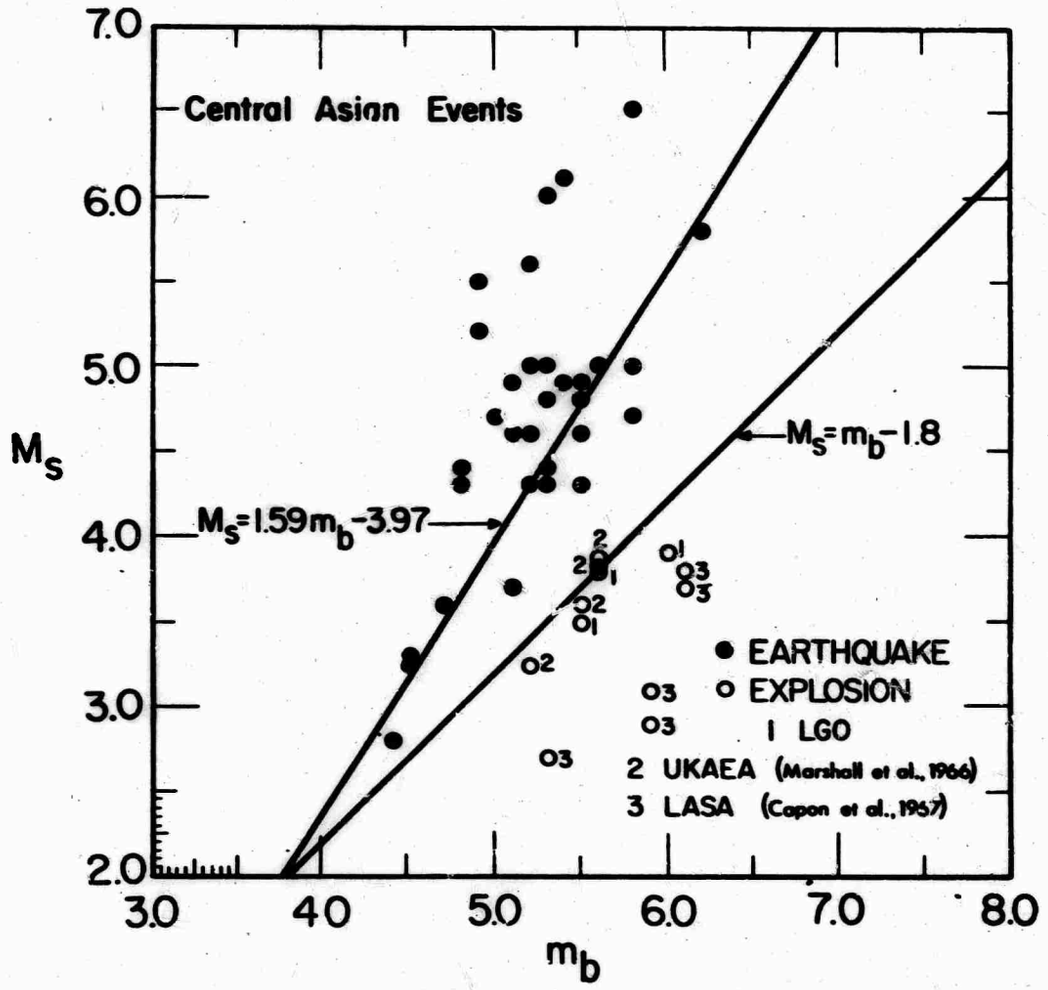

Figure 13. M_S vs m_b for central Asian events. There may be some duplication in the explosion populations treated by the various groups. Earthquake data represent evaluations at LASA (Capon et al, 1967). (After Liebermann and Pomeroy, 1969).

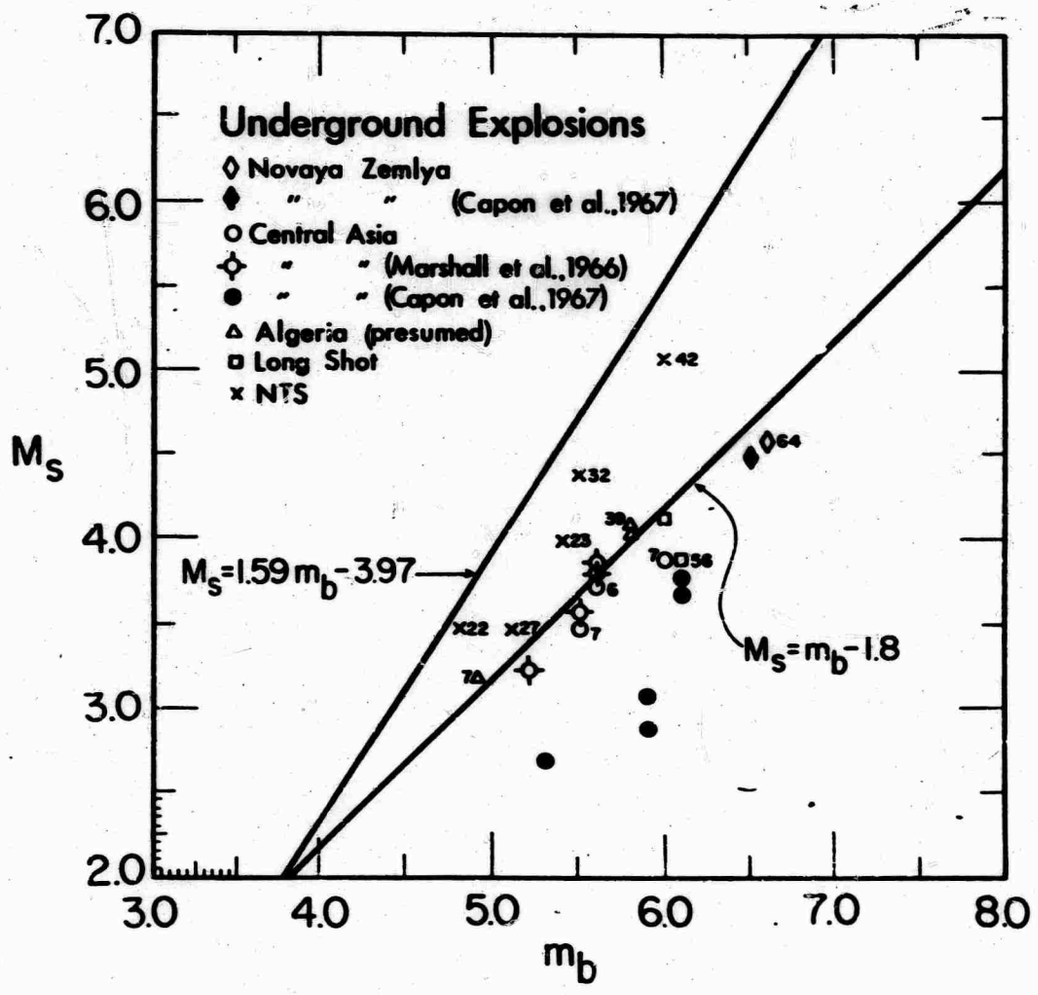

Figure 14. M_s vs m_b for underground explosions throughout the world. (After Liebermann and Pomeroy, 1969).

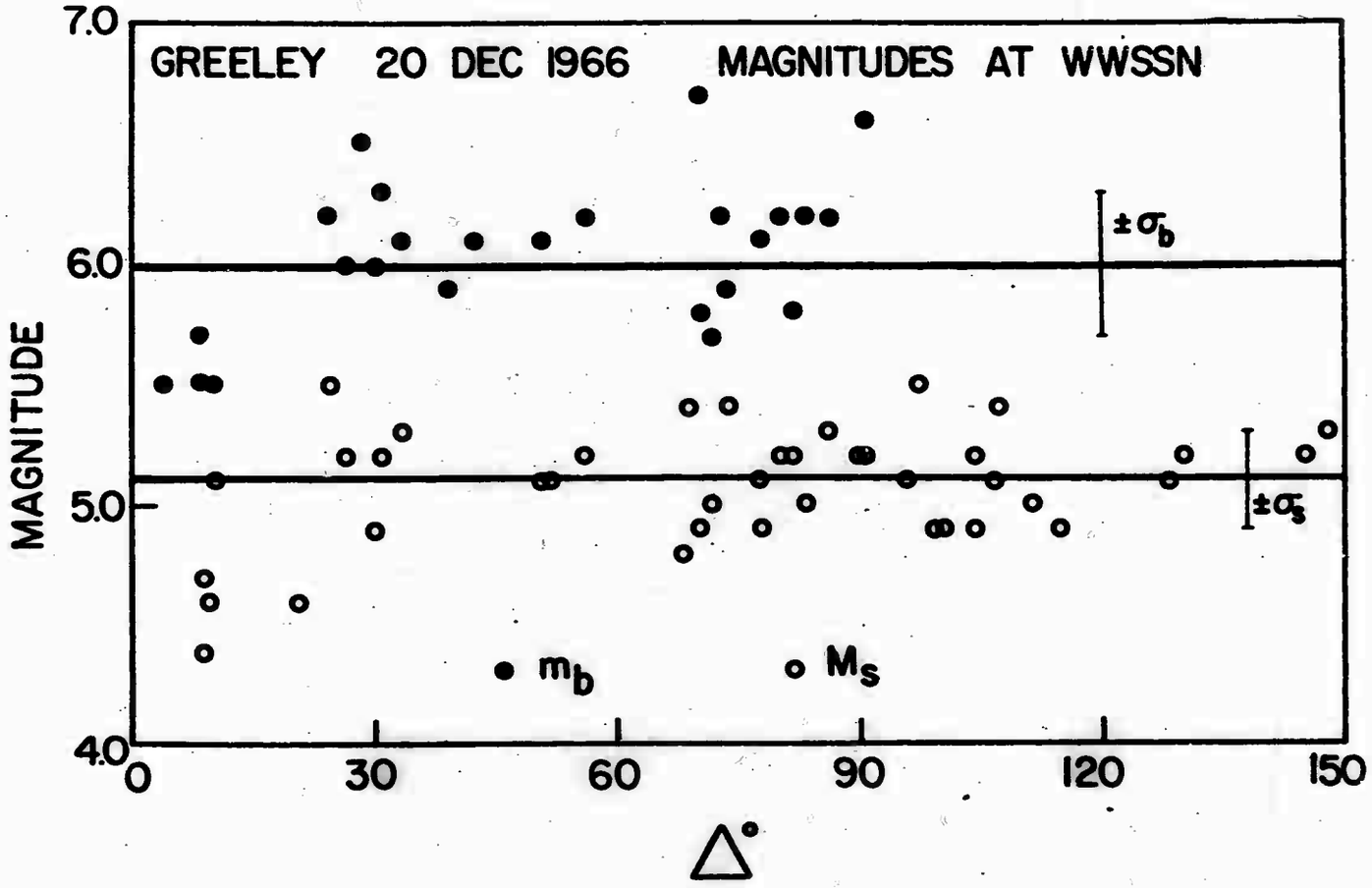

Figure 15. Magnitude vs epicentral distance for Nevada underground explosion GREELEY. Neither M_S nor m_b show any systematic dependence on epicentral distance. (Pomeroy and Liebermann, unpublished data, 1967.)

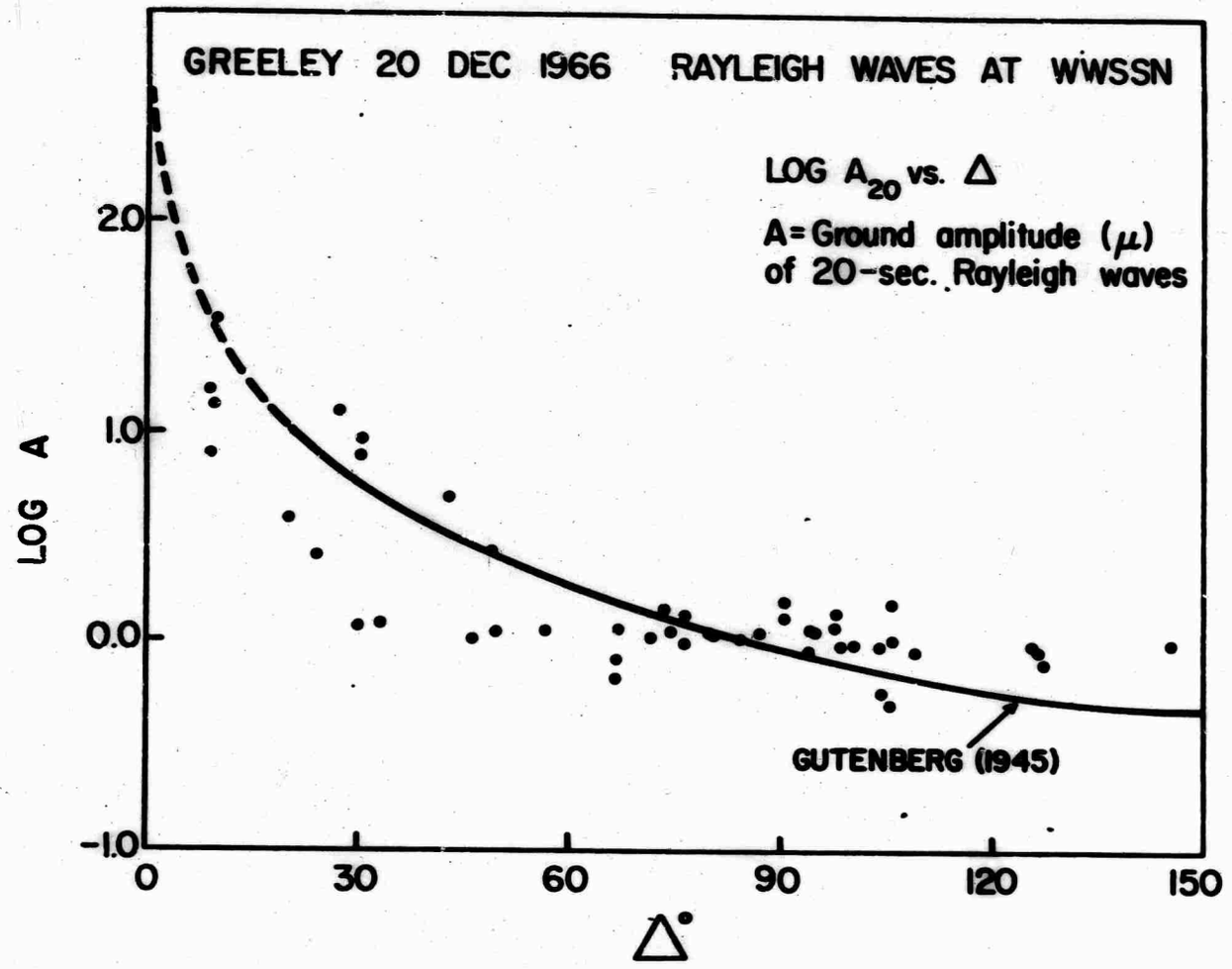

Figure 16. Ground amplitude of 20-sec Rayleigh waves versus epicentral distance for GREELEY. Solid curve is from Gutenberg (1945) and represents his - log B term in the formula for M_s = log A - log B. For Δ between 15° and 130°, Gutenberg (1945) found - log B = 1.82 + 1.66 log Δ°. Note that the Prague formula (Vanek et al, 1962) for M_S (corrected to 20-sec) = log A + 1.66 log Δ + 2.0.

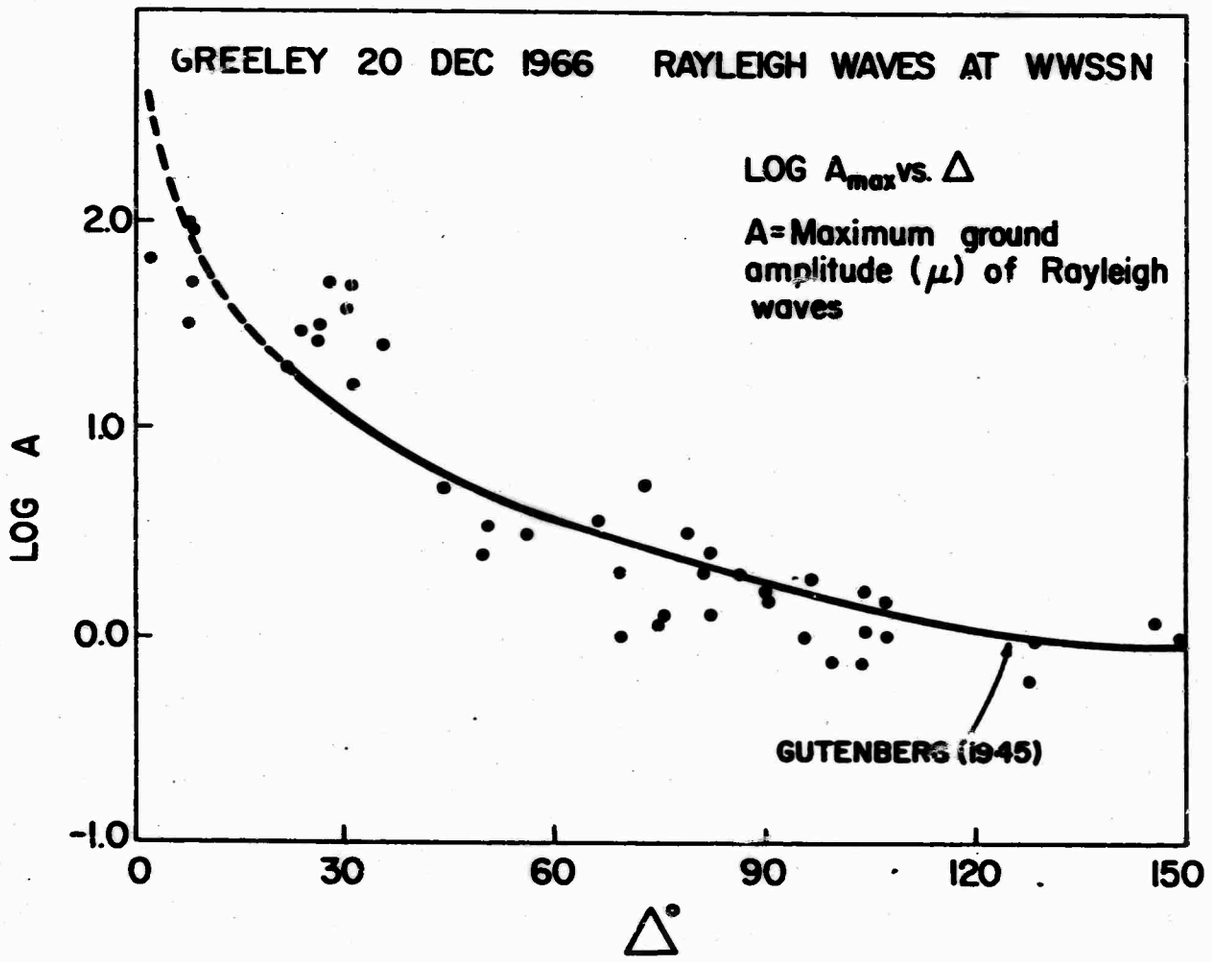

Figure 17. Maximum ground amplitude of Rayleigh waves versus epicentral distance for GREELEY. Gutenberg's (1945) curve is extended to distances less than 20° by assuming that the amplitude (A) varies as:

$$A \sim e^{-\pi X/QUT} / (X \sin\Delta)^{1/2}$$

to account for dispersion ($X^{-1/2}$), attenuation (exp ($-\pi X/QUT$), and geometrical spreading (sin $^{-1/2}\Delta$).

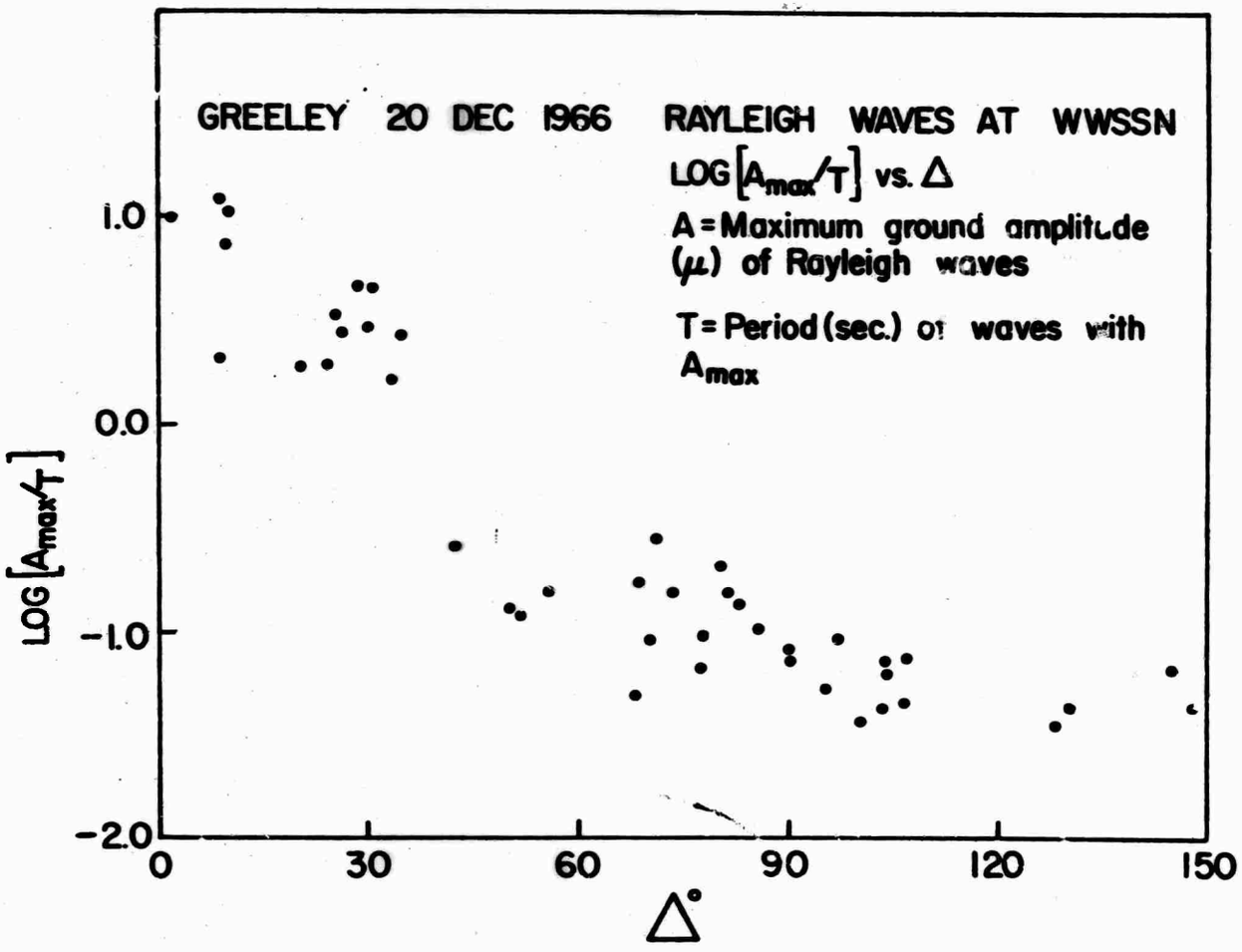

Figure 18. (A_{max}/T) versus epicentral distance for GREELEY. Data are in good agreement with 1.66 log Δ° distance term in Prague formula for M_s (Vanek et al, 1962).

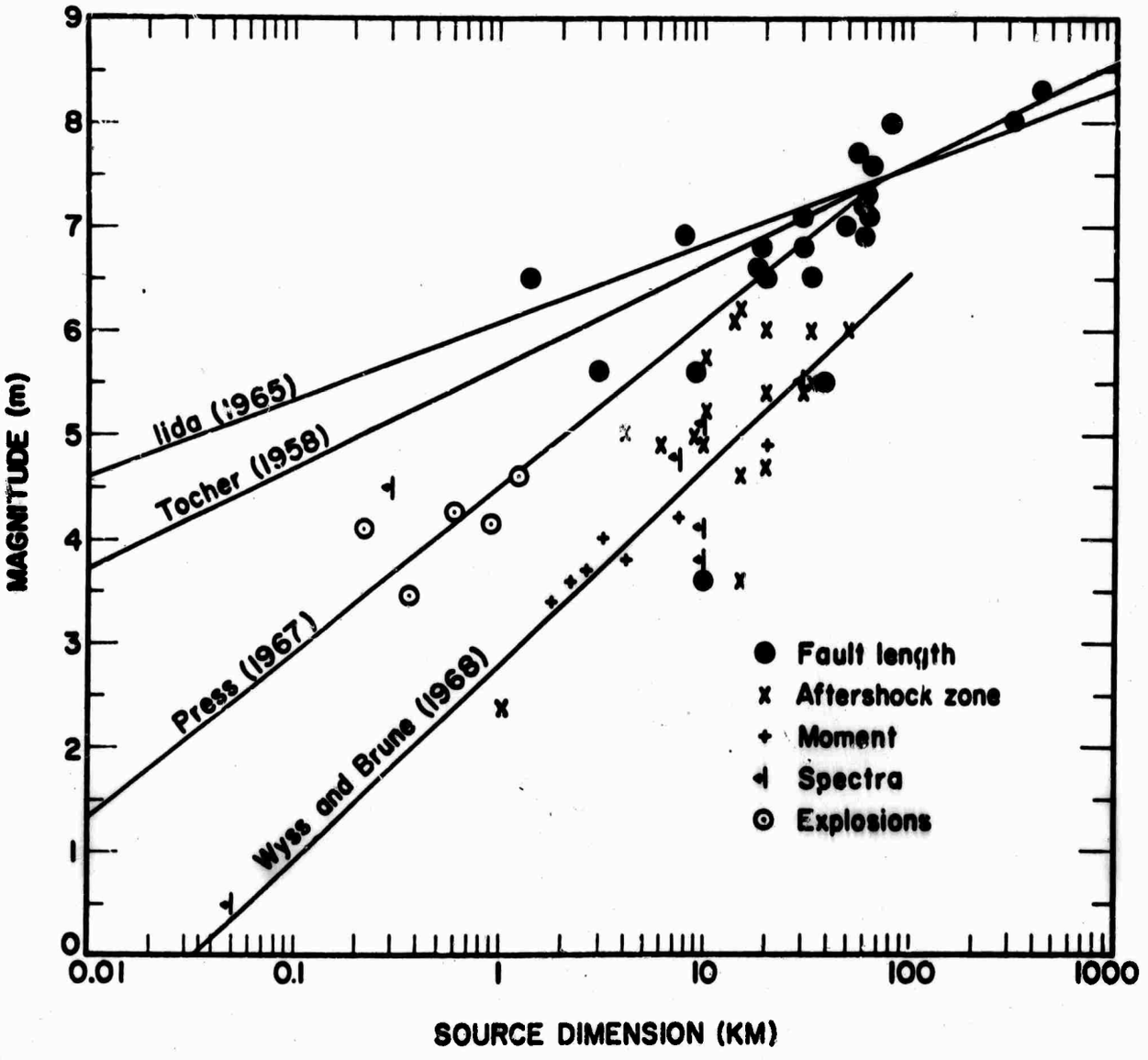

Figure 19. Source dimension as a function of body-wave magnitude (m) for earthquakes and underground explosions in the western United States (Liebermann and Pomeroy, 1970). Data for 1 km aftershock zone from 4 December 1968 Hollister earthquake (Zanetti and McEvilly, 1970).

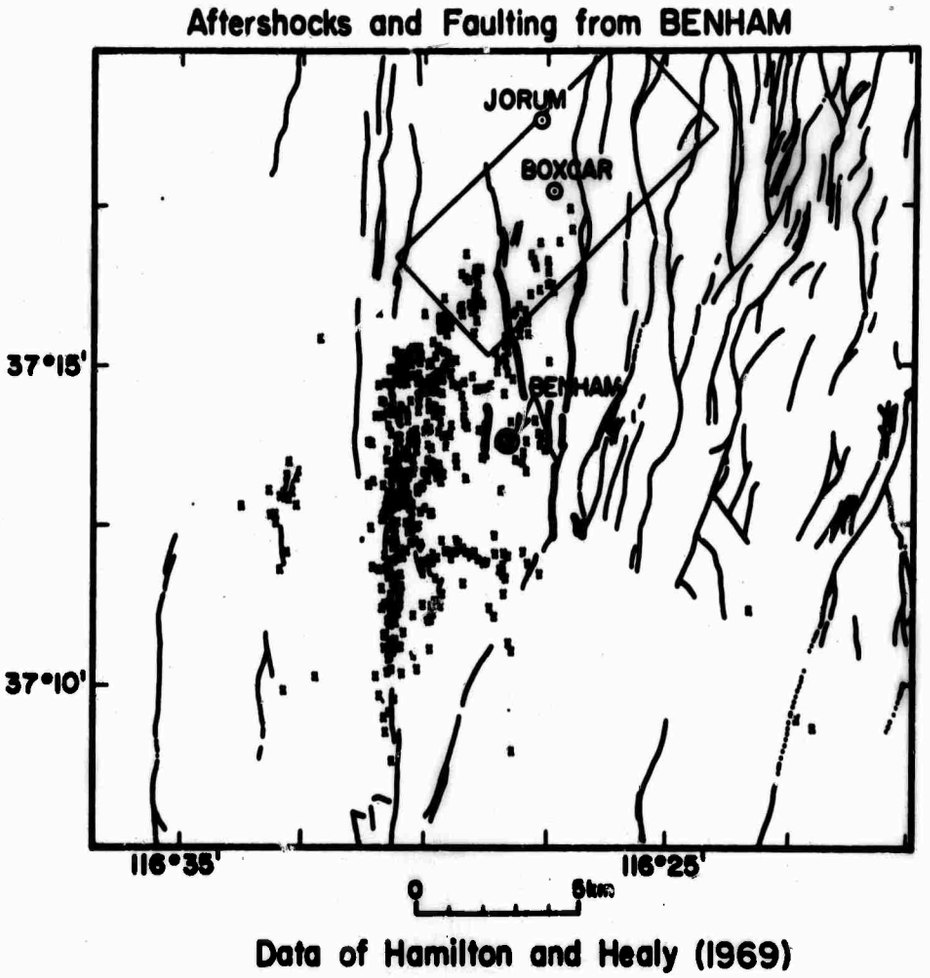

Figure 20. BOXCAR shot point located just outside of BENHAM aftershock area. Aftershock areas of BOXCAR (26 April 1968) and BENHAM (19 December 1968) overlap. Rectangular box represents aftershock zone of BOXCAR. (After Savino et al, 1969).

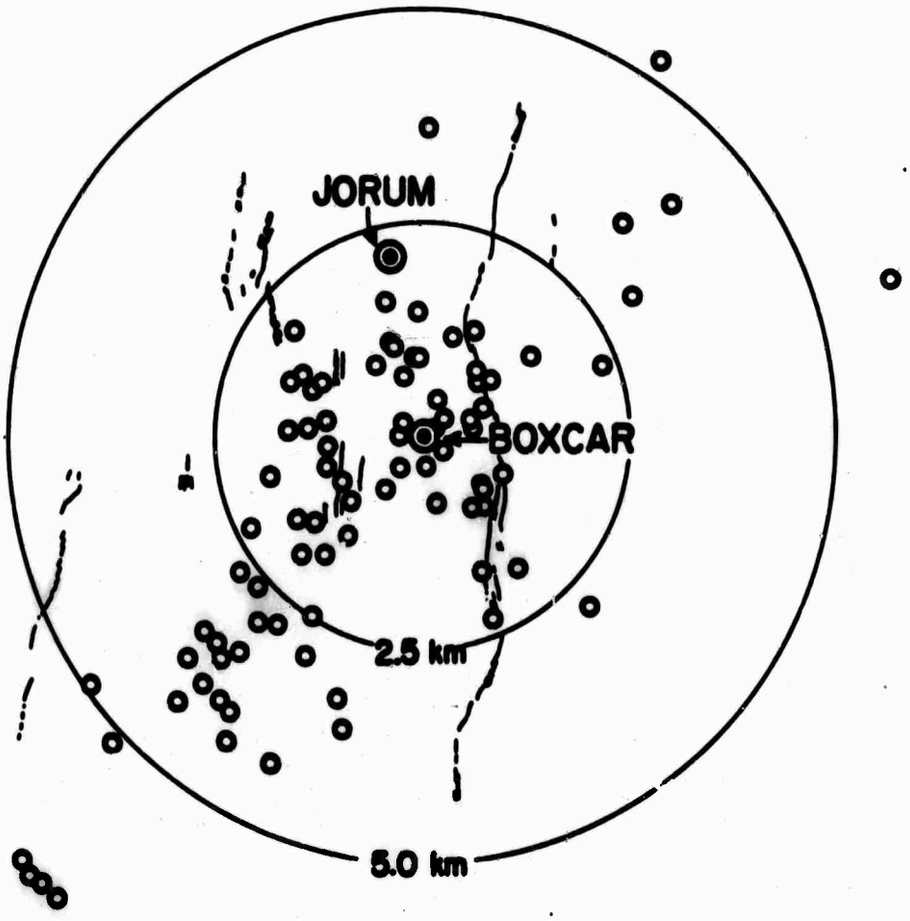

Figure 21. JORUM (16 September 1969) shot point located within aftershock zone of BOXCAR (26 April 1968). GREELEY (20 December 1966) was detonated just outside the aftershock zone of BOXCAR to northeast. (After Savino et al, 1969).

R. C. Liebermann
July, 1970

Additional Data on Source Dimensions of Small Earthquakes

Date	Location	M	L(km)
Aftershock zone: (Zanetti and McEvilly, 1970)			
4 Dec. 1968	Hollister, Calif.	2.3	1.0
Spectra: (Wyss, 1970)			
1968	Borrego Mountain	1.09	0.6
		1.09	0.6
		1.09	0.6
		0.92	0.8
		1.68	0.64
		1.25	1.0
		1.25	1.0
		2.6	1.2
		1.48	0.9
		1.63	0.48
		0.56	0.64
		2.26	0.5
		1.22	0.56
		1.31	1.0
		1.66	0.76
		1.1	0.44
		1.54	0.64
		1.68	0.62
		1.51	0.92
		0.92	0.52
		1.68	0.86
		1.25	0.4
		1.25	0.4
(Hanks, 1970)			
1969	San Gorgonio Pass	2.75	0.24
		2.8	0.21
		2.15	0.27
		2.3	0.49
		2.5	0.15

Hanks, T. C., personal communication, 1970

Wyss, M., Observations and Interpretation of Tectonic Strain Release Mechanisms, Ph. D. Thesis, California Inst. Tech., 1970

Zanetti, J., and T. V. McEvilly, Analysis of a microearthquake aftershock sequence (abstract), Program of Cordilleran Sect. of Geol. Soc. Am., Annual Meeting, Feb., 1970

TELESEISMIC SURFACE WAVE DETECTION AND UTILIZATION WITH A SINGLE LARGE ARRAY

By

R. Lacoss

Lincoln has completed a significant amount of investigation of LP signal processing possibilities at LASA and has evaluated the detection capabilities for one viable mode of operation. We wish to briefly review the results and mention some of the activity in progress to improve the array capability. Most of this work is in the 20 sec area.

Extensive analysis of LP noise properties at LASA and optimal processing of events led us to the conclusion that routine processing at that site should consist of LP beamforming for Rayleigh waves followed by chirp filtering. Figure 1 shows one reason why optimal processing (FS) was discarded in favor of simple delay and sum (DS). The plot shows the db noise reduction by the two processing methods as a function of azimuth during a particular time interval. The optimal processing tends to achieve 2 to 3 db more noise reduction than DS. However, this does not take into account potential signal degradation or sensitivity to bad data. It should be noted that the potential gain of FS over DS depends very much upon the percent of propagating noise crossing the array. At LASA this is typically 50% and thus limits the FS gain to about 3 db more than DS. This could well be different at other sites if instrument and other incoherent noise between sensors can be reduced.

Figure 2 shows an example of a situation where optimal processing can be of value. This is when the "noise" involved is actually an interfering signal. In the case shown a small Argentinean signal has been hidden in a Kuril Islands event. We see that an optimum processor can be used to detect and measure the smaller signal whereas DS cannot. No chirp filtering has been done in this example. We are now seriously considering this hidden event problem using our high resolution frequency-wavenumber methods. However we do not wish to go into depth on this point here but rather wish to review our capabilities using only DS and chirp.

Figure 3 is a summary of results obtained at LASA for one random population of Eurasian earthquakes. Presumably the interfering event population could have been reduced by utilizing optimal processing.

The data are rather limited but an attempt has been made to estimate the probability of teleseismic surface wave detection by LASA for earthquakes. The solid line on Figure 4 shows that probability as a function of m_b assuming no interfering events. Although that curve was estimated using the data of the previous Figure it has been essentially corroborated using information about LP noise and the general trend and scatter of earthquake surface noise.

The situation is somewhat different for explosions. One need not see the surface wave to determine an event is an explosion. It is sufficient simply to bound the surface wave so the event will be in the explosion region of the M_s-m_b plane. Figure 5 shows our estimate that M_s-m_b can be applied to teleseismic explosions at LASA.

This completes our brief review of LASA LP capabilities.

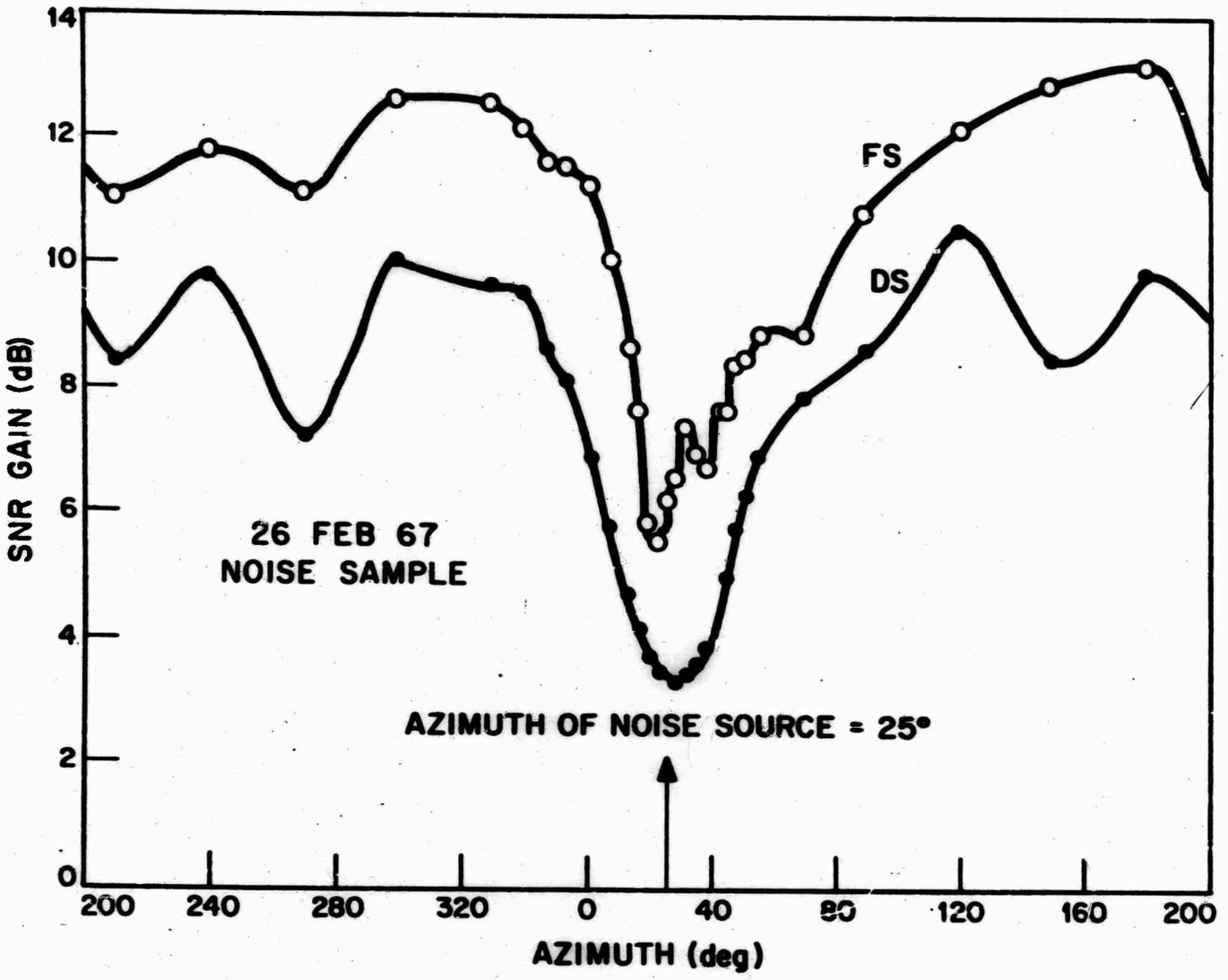
14
12
10
8
6
4
2
0
SNR GAIN (dB)
FS
DS
26 FEB 67
NOISE SAMPLE
AZIMUTH OF NOISE SOURCE = 25°
200
240
280
320
0
40
80
120
160
200
AZIMUTH (deg)

Figure 1.

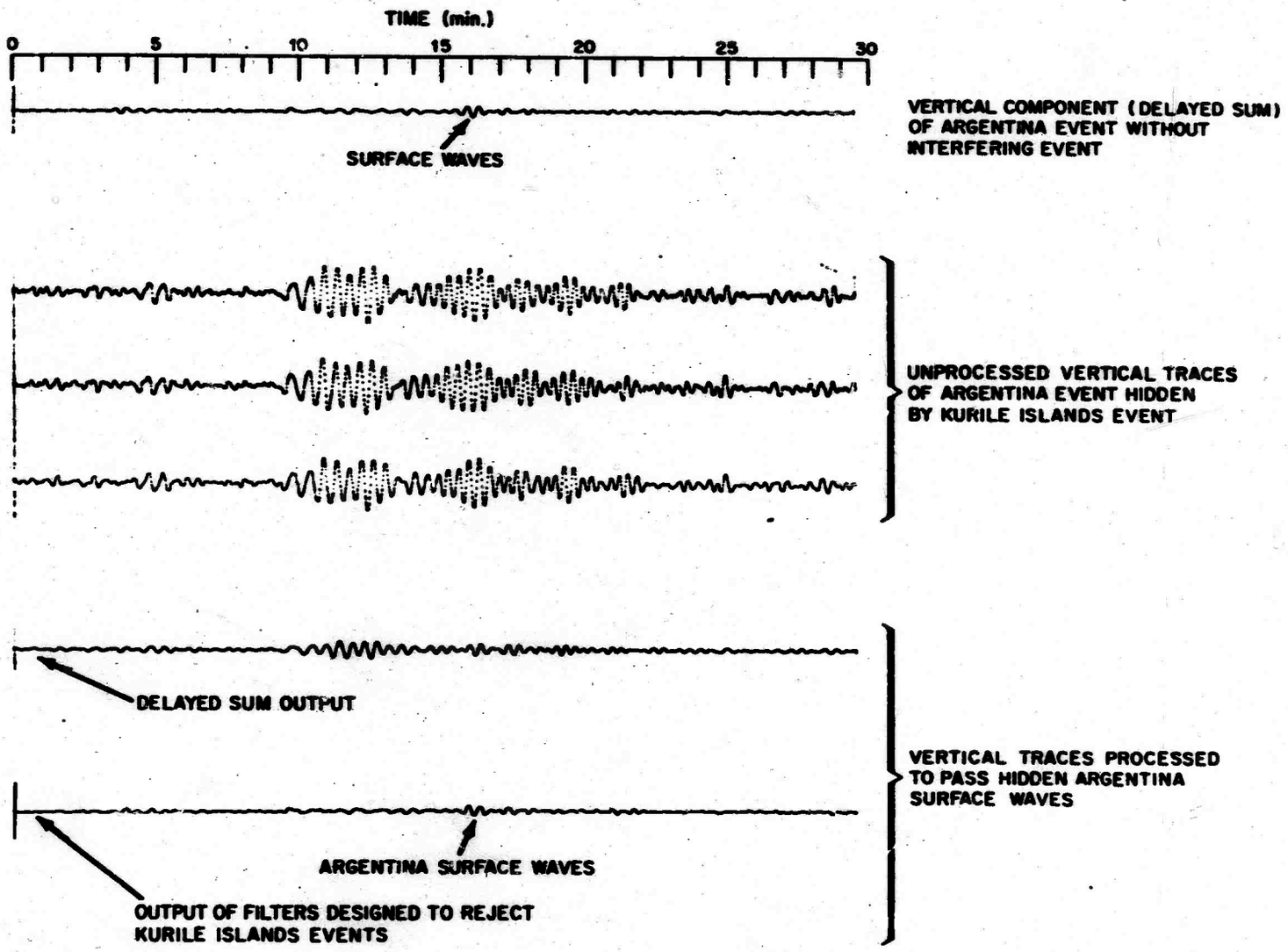
TIME (min.)
0
5
10
15
20
25
30
SURFACE WAVES
VERTICAL COMPONENT (DELAYED SUM) OF ARGENTINA EVENT WITHOUT INTERFERING EVENT
UNPROCESSED VERTICAL TRACES OF ARGENTINA EVENT HIDDEN BY KURILE ISLANDS EVENT
DELAYED SUM OUTPUT
ARGENTINA SURFACE WAVES
OUTPUT OF FILTERS DESIGNED TO REJECT KURILE ISLANDS EVENTS
VERTICAL TRACES PROCESSED TO PASS HIDDEN ARGENTINA SURFACE WAVES

Figure 2.

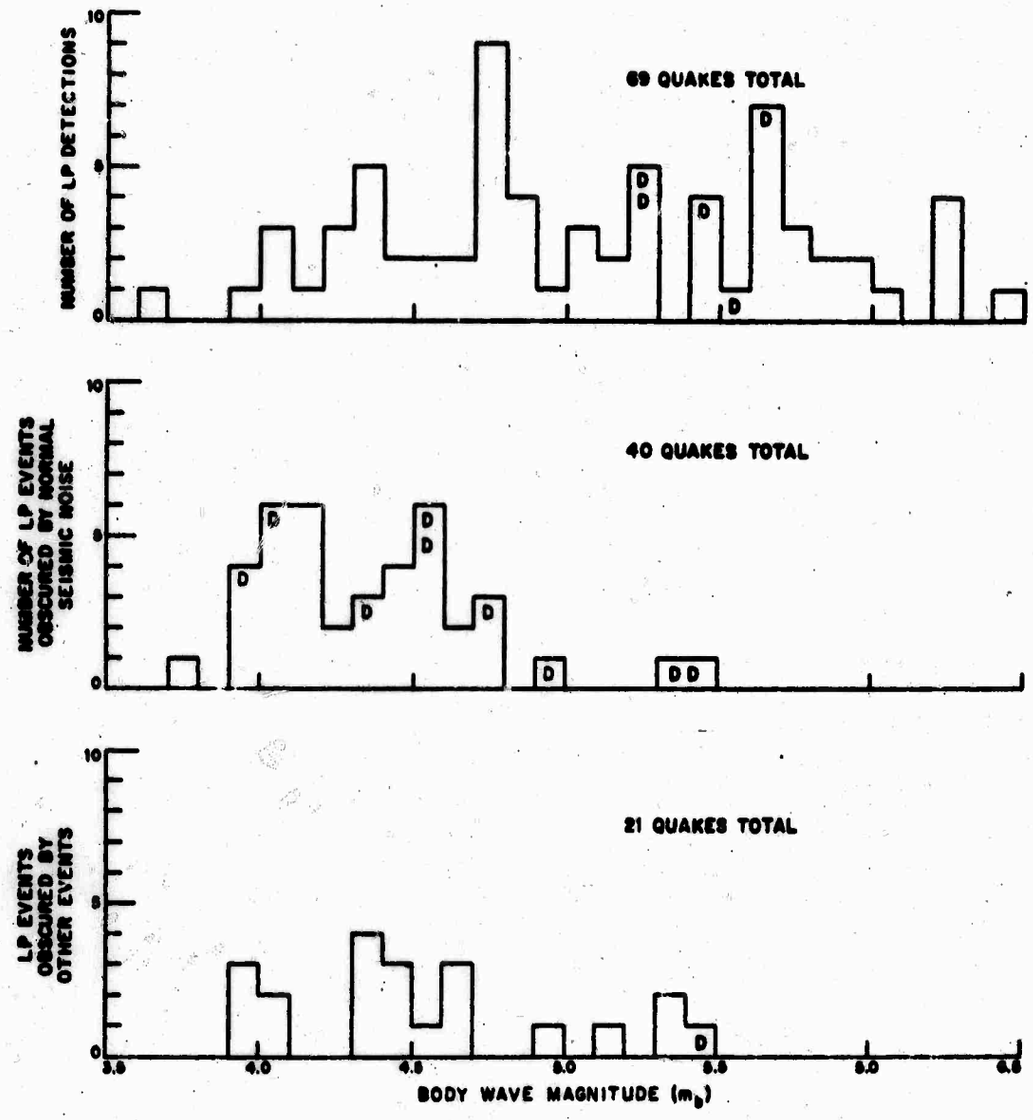

NOTE: D INDICATES DEPTH GREATER THAN 100 KM

Figure 3.

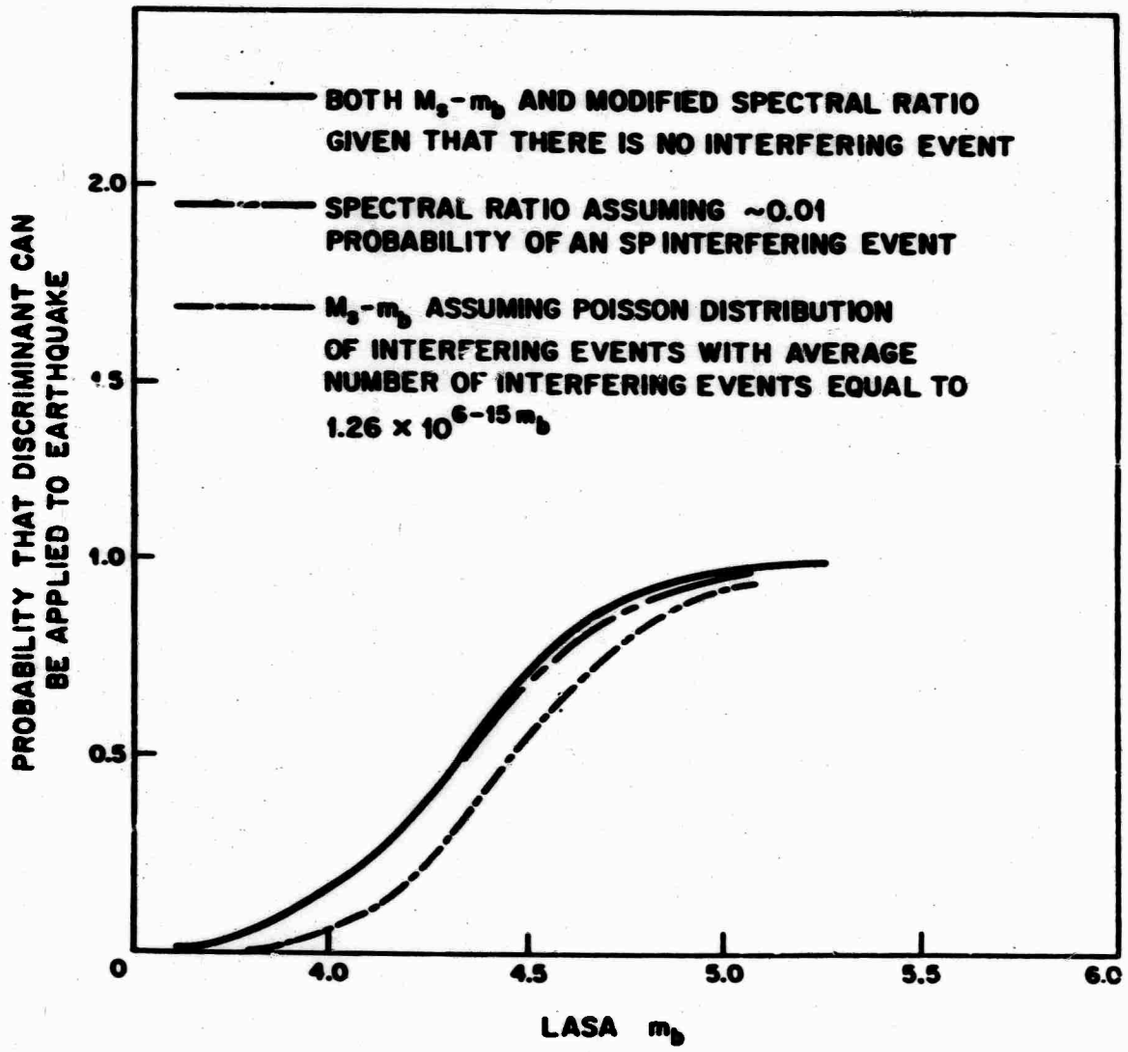
BOTH M_s-m_b AND MODIFIED SPECTRAL RATIO GIVEN THAT THERE IS NO INTERFERING EVENT
SPECTRAL RATIO ASSUMING ~0.01 PROBABILITY OF AN SP INTERFERING EVENT
M_s-m_b ASSUMING POISSON DISTRIBUTION OF INTERFERING EVENTS WITH AVERAGE NUMBER OF INTERFERING EVENTS EQUAL TO $1.26 \times 10^{6-15 m_b}$
PROBABILITY THAT DISCRIMINANT CAN BE APPLIED TO EARTHQUAKE
2.0
1.5
1.0
0.5
0
4.0
4.5
5.0
5.5
6.0
LASA m_b

Figure 4.

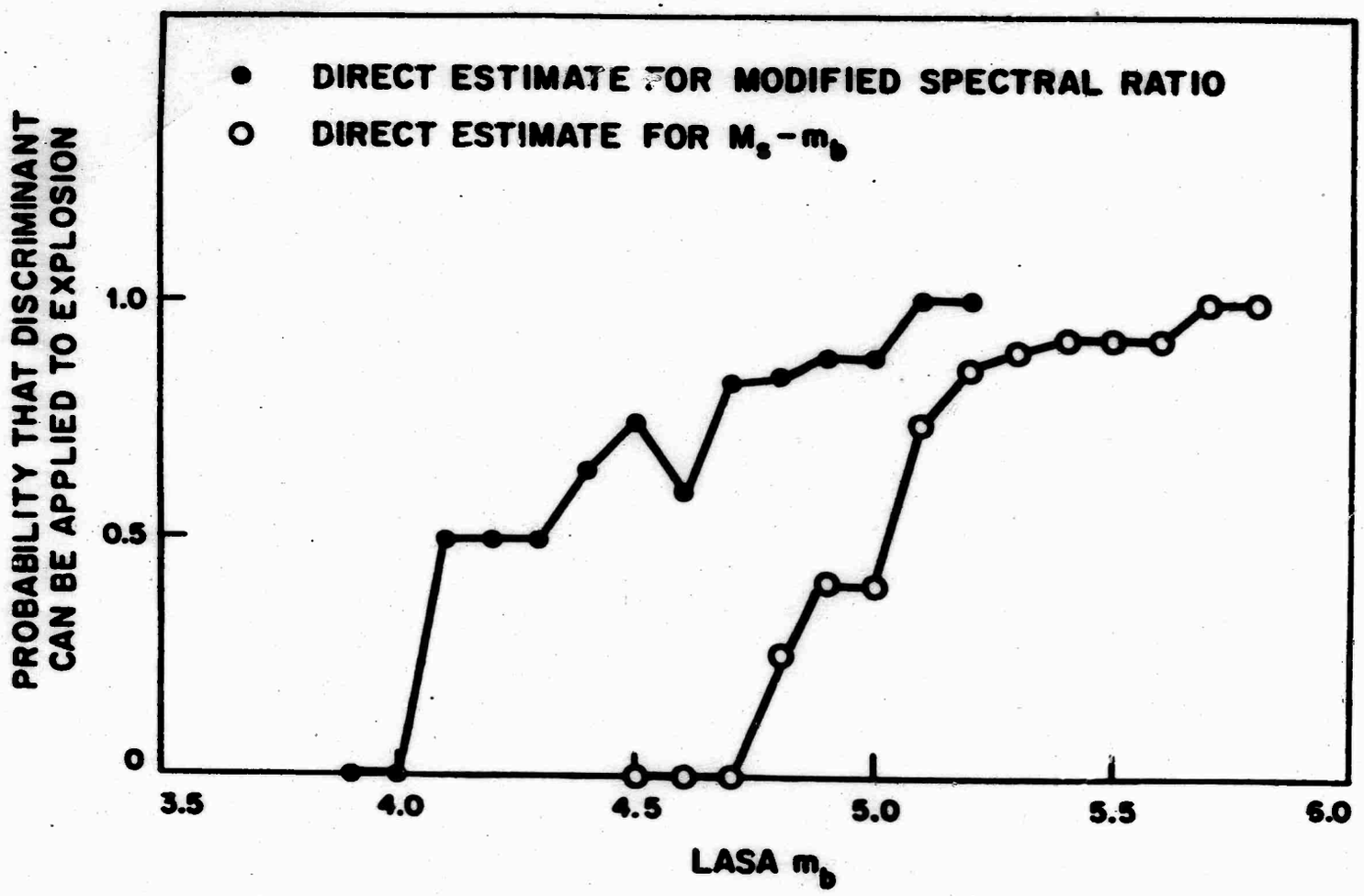
DIRECT ESTIMATE FOR MODIFIED SPECTRAL RATIO
DIRECT ESTIMATE FOR $M_s - m_b$
PROBABILITY THAT DISCRIMINANT CAN BE APPLIED TO EXPLOSION
1.0
0.5
0
3.5
4.0
4.5
5.0
5.5
6.0
LASA m_b

Figure 5.

ED-72-267

Frequency-wavenumber (F-K) spectra have been calculated for the vertical components of several NTS events recorded at LASA. For explosions in the low-intermediate yield range the wavenumber spectra exhibit common features. There is a loss of coherent signal at 0.02 Hz but there is apparent coherent propagation at lower frequencies.

Figures 1a, 1b, and 1c show high-resolution F-K spectra (Capon, 1969) for the event LANPHER at frequencies of 0.05 Hz, 0.02 Hz, and 0.015 Hz. The loss of signal at 0.02 Hz is obvious from the lack of a coherent peak in the wavenumber plane (Figure 1b). The return of coherent propagation at an apparently lower frequency is illustrated by the peak in Figure 1c which has a phase velocity of 4.2 km/sec which is about right for Rayleigh waves at this period. The apparent direction of propagation is further west than the true back azimuth. However, the resolution of the array is poor at these low frequencies and there may be quite a large error in velocity and azimuth estimation. A plot of average power versus frequency is shown in Figure 2 for LANPHER. The average power is the power spectrum averaged over the individual sensors of LASA and has contributions from both coherent and incoherent disturbances. The values are normalized to the power at a frequency of 0.05 Hz.

There is an increase in power at frequencies lower than 0.02 Hz. The lower curve in the same figure, associated with the right-hand scale, is the normalized peak value of the wavenumber spectrum at each frequency and is a measure of the ratio of coherent power to total power as determined by F-K analysis. A distinct drop is seen in this value at frequencies around 0.02 Hz corresponding to the absence of coherent propagation illustrated in Figure 1b. The curve then rises again towards the lower frequencies and is maximum at a frequency of 0.015 Hz agreeing with the coherent peak in Figure 1c.

The frequency-wavenumber characteristics of LANPHER have been found for six other events of the low-intermediate yield range. The body wave magnitude range (m_b) of these events was 5.2 to 5.8. So far, this apparent energy at long periods has not been observed at LASA for smaller events. This, however, may be a signal-to-noise problem. For illustration, Figures 3a and 3b show the average power and peak wavenumber spectra for the events SLED and ZAZA. The shapes of the wavenumber spectra are seen to be very similar, both with the notch at 0.02 Hz.

F-K analysis of earthquakes located in Nevada, California, Baja, California and off the coast of Oregon has failed to produce a wavenumber spectrum with a notch. The spread of surface wave amplitudes 0.03 Hz for the earthquakes is the same as for the NTS events. Figures shows the average power and peak wavenumber spectrum for the event from Baja, California. Both curves are smooth compared with those shown in the previous figures. The wavenumber spectrum curves for the earthquakes were not all similar but none exhibited a notch at any frequency.

115

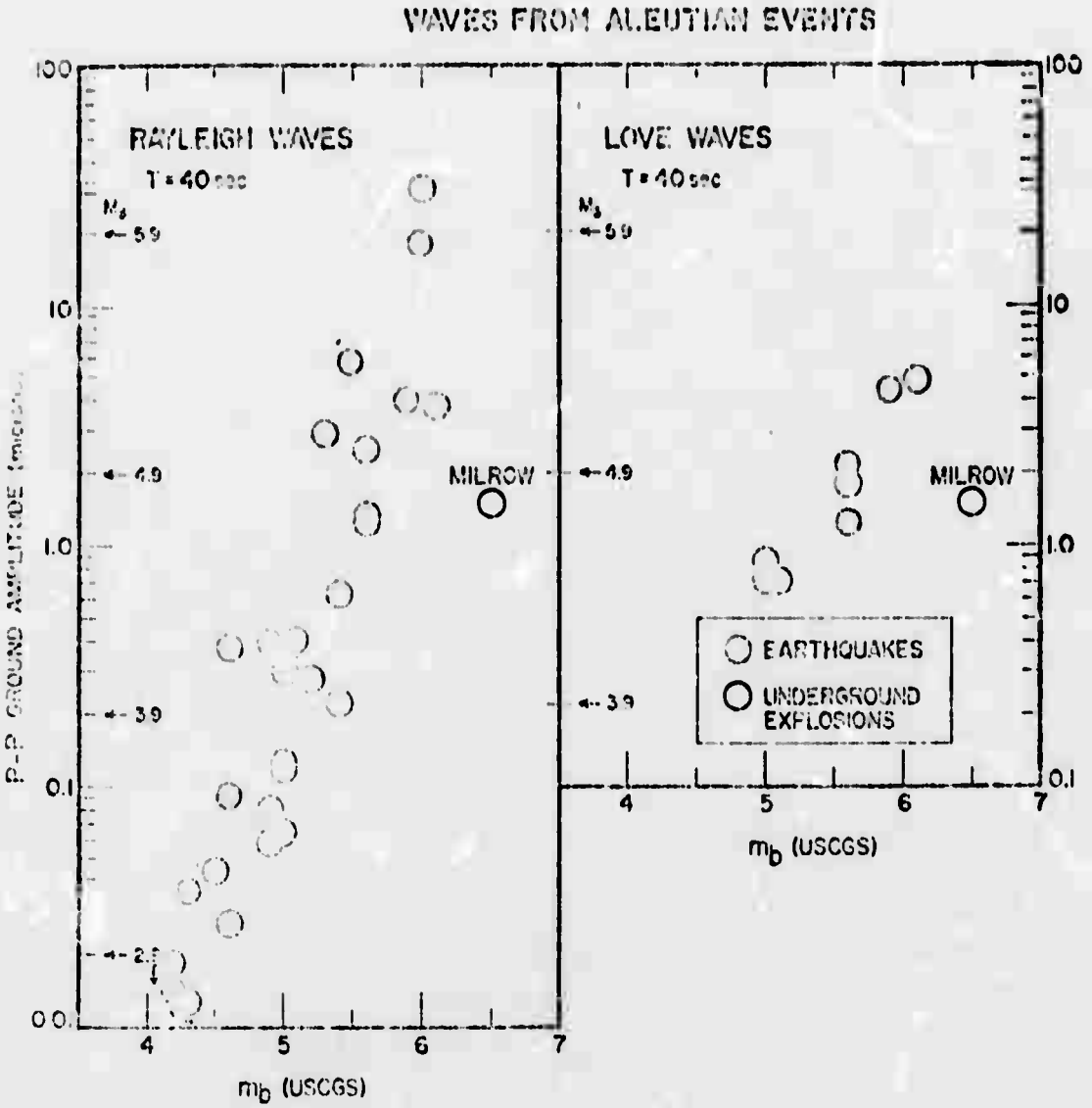

Figure 8b. Comparison of peak-to-peak ground amplitudes of the 40-sec Rayleigh and 40-sec Love waves versus m_b.

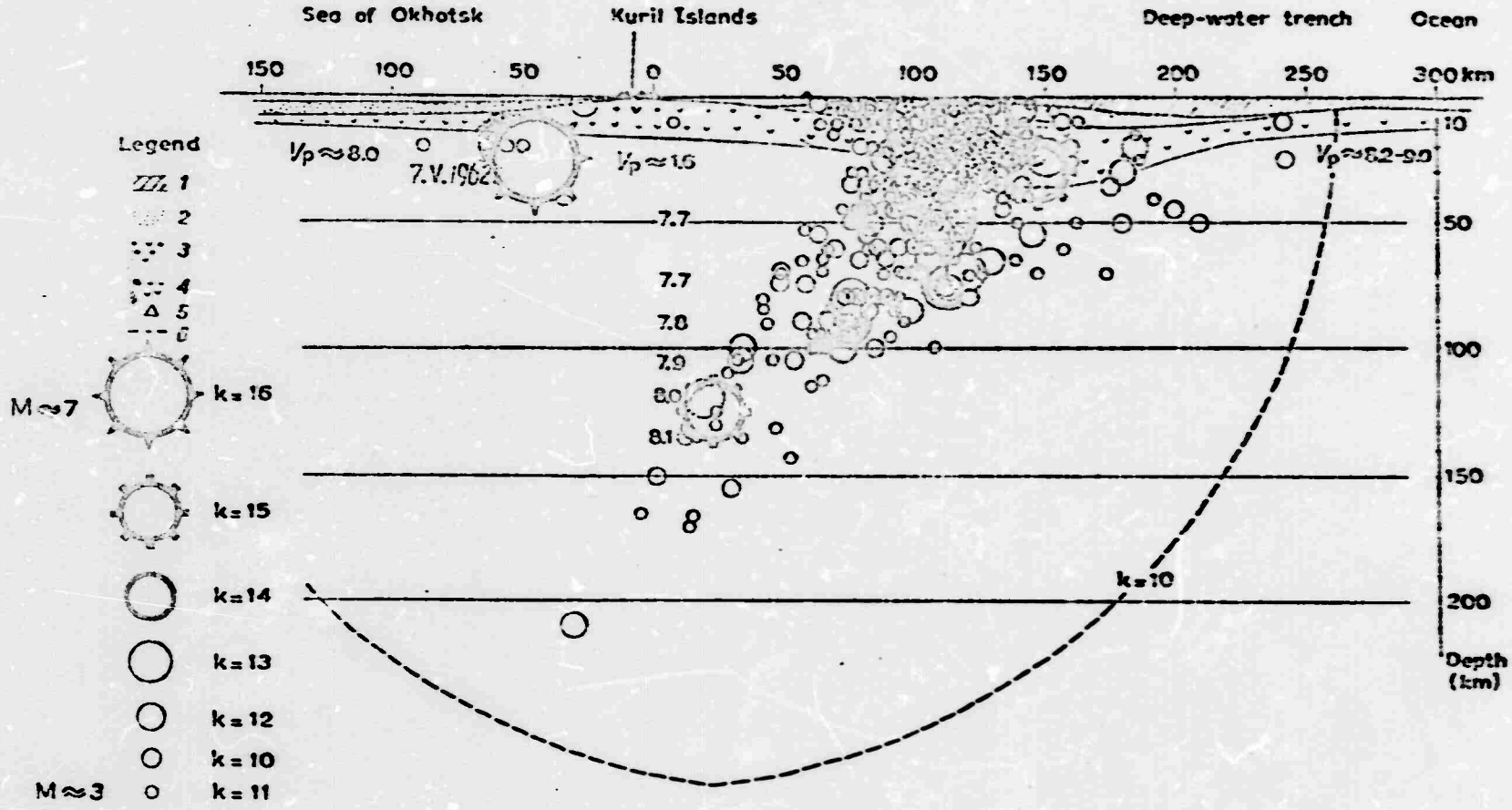

Figure 6. Similar vertical section for Kuril arc after Fedotov (1965). k is exponent of energy in joules. Note thinness of dipping seismic zone